ADVANCES IN
QUANTUM CHEMISTRY

NEW PERSPECTIVES IN QUANTUM SYSTEMS IN CHEMISTRY AND PHYSICS, PART 2

EDITORS

JOHN R. SABIN
QUANTUM THEORY PROJECT
UNIVERSITY OF FLORIDA
GAINESVILLE, FLORIDA

ERKKI BRÄNDAS
DEPARTMENT OF QUANTUM CHEMISTRY
UPPSALA UNIVERSITY
UPPSALA, SWEDEN

FOUNDING EDITOR

PER-OLOV LÖWDIN†

GUEST EDITORS

ERKKI BRÄNDAS
DEPARTMENT OF QUANTUM CHEMISTRY
UPPSALA UNIVERSITY
UPPSALA, SWEDEN

JEAN MARUANI
LABORATOIRE DE CHIMIE PHYSIQUE
CNRS AND UPMC
PARIS, FRANCE

R. McWEENY
DIPARTIMENTO DI CHIMICA E CHIMICA INDUSTRIALE
UNIVERSITA DI PISA
PISA, ITALY

Y. G. SMEYERS
INSTITUTO DE ESTRUCTURA DE LA MATERIA, CSIC
MADRID, SPAIN

S. WILSON
RUTHERFORD APPLETON LABORATORY
CHILTON, OXFORDSHIRE
UNITED KINGDOM

†Deceased.

VOLUME 40

ACADEMIC PRESS
A Harcourt Science and Technology Company

San Diego San Francisco New York Boston London Sydney Tokyo

Contributors Volume 40

Numbers in parentheses indicate the pages on which the authors' contributions begin.

Hans Ågren (191, 213), The Royal Institute of Technology, Theoretical Chemistry, Stockholm SE-10044, Sweden

Tatyana Alferova (323), Stockholm University, Department of Physics, Molecular Physics Group, Stockholm SE-113 85, Sweden

Stefan Andersson (323), Stockholm University, Department of Physics, Molecular Physics Group, Stockholm SE-113 85, Sweden

Elena S. Apostolova (143), D. I. Mendeleev Russian University of Chemical Technology, Department of Quantum Chemistry, Moscow, Russia

O. Atabek (179), Université Paris-Sud, Laboratoire de Photophysique Moléculaire, Campus d'Orsay, Orsay 91405, France

Erkki J. Brändas (225), Uppsala University, Quantum Chemistry Group, Uppsala S-75120, Sweden

P. Chaquin (161), Université Pierre et Marie Curie, Laboratoire de Chimie Théorique, Case 137, Paris Cedex 5, 75252, France

Nick J. Clarke (37), Tessella Support Services plc, Bretby Business Park, Burton Upon Trent DE15 0YZ, United Kingdom

David L. Cooper (37), University of Liverpool, Department of Chemistry, Liverpool L69 7ZD, United Kingdom

Peter Cronstrand (213), The Royal Institute of Technology, Theoretical Chemistry, Stockholm SE-10044, Sweden

I. G. Csizmadia (49), University of Toronto, Department of Chemistry, Toronto M5S1A1, Canada

L. J. Dunne (225), South Bank University, School of Applied Science, London SE1 0AA, United Kingdom

Nils Elander (323), Stockholm University, Department of Physics, Molecular Physics Group, Stockholm SE-113 85, Sweden

Bernd Engels (133), Universität Bonn, Institut für Physikalische und Theoretische Chemie, Bonn D-53115, Germany

W. Fraessdorf (345), Brock University, Department of Chemistry, St. Catherine's, Ontario L2S3A1, Canada

Y. Girard (161), Université Pierre et Marie Curie, Laboratoire de Chimie Théorique, Case 137, Paris Cedex 5, 75252, France

Mikhail V. Ivanov (361), Russian Academy of Sciences, Institute of Precambrian Geology and Geochronology, St. Petersburg 199034, Russia

I. G. Kaplan (257), Jackson State University, The Computational Center for Molecular Structure and Interactions, Department of Chemistry, Jackson, Michigan 39217

C. Kozmutza (49), Technical University of Budapest, Department of Theoretical Physics, Institute of Physics, Budapest H-1111, Hungary

Eugene S. Kryachko (79), University of Leuven, Department of Chemistry, Leuven B3001, Belgium

A. Kuleff (279), CNRS and UPMC, Laboratoire de Chimie Physique, Paris 75005, France

R. Lefebvre (179), Université Paris-Sud, Laboratoire de Photophysique Moléculaire, Campus d'Orsay, Orsay 91405, France

Jerzy Leszczynski (257), Jackson State University, The Computational Center for Molecular Structure and Interactions, Department of Chemistry, Jackson, Michigan 39217

Sergey Levin (323), Stockholm University, Department of Physics, Molecular Physics Group, Stockholm SE-113 85, Sweden

Sten Lunell (133), University of Uppsala, Department of Quantum Chemistry, Uppsala S-75120, Sweden

J. Maruani (279), CNRS and UPMC, Laboratoire de Chimie Physique, Paris 75005, France

Roy McWeeny (1), University of Pisa, Dipartimento di Chimica e Chimica Industriale, Pisa I-56100, Italy

Boris F. Minaev (191), The Royal Institute of Technology, Stockholm SE-10044, Sweden

D. C. Moule (345), Brock University, Department of Chemistry, St. Catherine's, Ontario L2S3A1, Canada

C. Muñoz-Caro (345), Universidad de Castilla-La Mancha, E. U. Informatica de Ciudad Real, Ciudad Real 13071, Spain

Minh Tho Nguyen (79), University of Leuven, Department of Chemistry, Leuven B3001, Belgium

A. Niño (345), Universidad de Castilla-La Mancha, E. U. Informatica de Ciudad Real, Ciudad Real 13071, Spain

C. Perez del Valle (179), CSIC, Instituto de Ciencia de Materiales, Cantoblanco, Madrid 28049, Spain

P. P. Raychev (279), CNRS and UPMC, Laboratoire de Chimie Physique, Paris 75005, France

Szczepan Roszak (257), Jackson State University, The Computational Center for Molecular Structure and Interactions, Department of Chemistry, Jackson, Michigan 39217

Ulf Saalmann (305), Stockholms Universitet, Atomfysik, Stockholm 10405, Sweden

Peter Schmelcher (361), Universität Heidelberg, Theoretische Chemie, Physikalisch-Chemisches Institut, Heidelberg D-69120, Germany

Vipin Srivastava (249), University of Hyderabad, School of Physics, Hyderabad 500 046, India

Phillip C. Stancil (37), University of Georgia, Department of Physics and Astronomy, Athens, Georgia 30602-2451

Brian Sutcliffe (17), University of York, Department of Chemistry, Helsington, York YO1 5DD, England

H. U. Suter (133), Universität Bonn, Institut für Physikalische und Theoretische Chemie, Bonn D-53115, Germany

O. Tapia (103), Uppsala University, Department of Chemistry, Uppsala S-75121, Sweden

E. Tfirst (49), Hungarian Academy of Sciences, Institute of Chemistry, Chemical Research Center, Budapest H-1025, Hungary

E. Yarevsky (323), Stockholm University, Department of Physics, Molecular Physics Group, Stockholm SE-113 85, Sweden

Bernard Zygelman (37), University of Nevada, Las Vegas, Department of Physics, Las Vegas, Nevada 89154-4002

Contents Volume 40

Preface

Quantum mechanics has existed for more than 75 years and forms the basis for the fundamental description of microscopic phenomena and processes. Contemporary research on quantum systems covers a vast area, from investigations on nuclei, atoms, and molecules to complex chemical and biological systems. To foster the development of innovative theory and concepts, the first European Workshop on Quantum Systems in Chemistry and Physics (QSCP I) was organized in San Miniato, near Pisa, Italy (1996). The meeting was a great success and was followed by *QSCP II* in Oxford (1997), *QSCP III* in Granada (1998), and *QSCP VI* in Paris (1999). The *QSCP II* proceedings were published in *Advances in Quantum Chemistry*, Volumes 31 and 32.

The fifth European Workshop in the series was held in Uppsala, April 13–18, 2000, at Ihresalen, Teknikum, Uppsala University. The workshop was organized as follows:

Density Matrices and Density Functionals *(Chair: J. Maruani)*
Electron Correlation Treatments *(Chair: S. Wilson)*
Relativistic Formulations *(Chair: U. Kaldor)*
Valence Theory *(Chair: Y. G. Smeyers)*
Nuclear Motion *(Chair: O. Goscinski)*
Response Theory *(Chair: B. T. Sutcliffe)*
Condensed Matter *(Chair: H. Ågren)*
Chemical Reactions *(Chair: C. Minot)*
Computational Chemistry *(Chair: I. Hubač)*
Posters *(Chairs: R. Lefebvre, E. Brändas)*

It attracted 95 scientists from 25 different countries who gathered to give 49 talks and 40 posters.

Additionally, a special *leitmotiv* was made to run through the lectures and discussions, relating to the pioneering work and achievements of Per-Olov Löwdin. In 1982, Uppsala University created a fund through collected contributions from Per-Olov Löwdin's colleagues, collaborators, and students, with the purpose of inviting prominent lecturers to Uppsala at regular intervals. The aim of

Preface

Quantum mechanics has existed for more than 75 years and forms the basis for the fundamental description of microscopic phenomena and processes. Contemporary research on quantum systems covers a vast area, from investigations on nuclei, atoms, and molecules to complex chemical and biological systems. To foster the development of innovative theory and concepts, the first European Workshop on Quantum Systems in Chemistry and Physics (QSCP I) was organized in San Miniato, near Pisa, Italy (1996). The meeting was a great success and was followed by *QSCP II* in Oxford (1997), *QSCP III* in Granada (1998), and *QSCP VI* in Paris (1999). The *QSCP II* proceedings were published in *Advances in Quantum Chemistry*, Volumes 31 and 32.

The fifth European Workshop in the series was held in Uppsala, April 13–18, 2000, at Ihresalen, Teknikum, Uppsala University. The workshop was organized as follows:

Density Matrices and Density Functionals *(Chair: J. Maruani)*
Electron Correlation Treatments *(Chair: S. Wilson)*
Relativistic Formulations *(Chair: U. Kaldor)*
Valence Theory *(Chair: Y. G. Smeyers)*
Nuclear Motion *(Chair: O. Goscinski)*
Response Theory *(Chair: B. T. Sutcliffe)*
Condensed Matter *(Chair: H. Ågren)*
Chemical Reactions *(Chair: C. Minot)*
Computational Chemistry *(Chair: I. Hubač)*
Posters *(Chairs: R. Lefebvre, E. Brändas)*

It attracted 95 scientists from 25 different countries who gathered to give 49 talks and 40 posters.

Additionally, a special *leitmotiv* was made to run through the lectures and discussions, relating to the pioneering work and achievements of Per-Olov Löwdin. In 1982, Uppsala University created a fund through collected contributions from Per-Olov Löwdin's colleagues, collaborators, and students, with the purpose of inviting prominent lecturers to Uppsala at regular intervals. The aim of

the lectures was to stimulate interest in quantum chemistry through one general lecture for a broader audience and a more specialized lecture targeted at experts in the field. The Löwdin Lecturers during 1984–2000 were R. Zahradnik, A. Pullman, R. S. Berry, R. Pauncz, H. Shull, E. R. Davidson, P. Fulde, M. Quack, F. A. Gianturco, J. P. Dahl, and R. McWeeny.

During the year 2000, two Löwdin Lecturers were invited: *Professor Roy McWeeny,* Pisa, Italy, and *Professor Jens Peder Dahl,* Copenhagen, Denmark. They both agreed to deliver their lectures during *QSCP V.* Due to unforeseen circumstances, only one lecturer could attend *QSCP V.* The second lecture was therefore presented half a year later and then as the Löwdin Memorial Lecture. Both are published as introductory chapters of the two proceedings volumes as a joint tribute to a great leader and pioneer in quantum chemistry. We are very proud to present *QSCP V: New Perspectives in Quantum Systems in Chemistry and Physics,* in the series *Advances in Quantum Chemistry,* founded by Löwdin.

The workshop was sponsored by the *European Commission - COST D9,* the *French Embassy* in Stockholm, the *Swedish Natural Science Research Council,* the *Foundation for Strategic Research,* and *Uppsala University.* We are greatly indebted to our sponsors for their generosity. In particular, we acknowledge the help and advice offered by Gérard Rivière from the COST Chemistry Secretariat. It is a pleasure to thank the members of the scientific organizing committee, R. McWeeny, J. Maruani, Y. G. Smeyers, and S. Wilson, for their excellent support and advice, and the local organizing committee and members of the Department of Quantum Chemistry at Uppsala University for their competence and efficiency which made for the smooth running of the workshop.

E. Brändas
Chair
Organizing Committee

O. Goscinski
Chair
Löwdin Lectureship Fund

Workshop Participants

M. Agback, Department of Quantum Chemistry, Uppsala University, SE-751 20 Uppsala, Sweden

H. Ågren, Theoretical Chemistry, Royal Institute of Technology, S-10044 Stockholm, Sweden

T. Alferova, Department of Physics, Stockholm University, SE-113 85 Stockholm, Sweden

M. Andersson, Department of Quantum Chemistry, Uppsala University, SE-75120 Uppsala, Sweden

S. Andersson, Department of Physics, Stockholm University, SE-113 85, Stockholm, Sweden

V. Aquilanti, Dipartimento di Chimica, Università di Perugia, I-06123 Perugia, Italy

J. S. Avery, H.C. Ørsted Institute, University of Copenhagen, DK-2100 Copenhagen, Denmark

M.-C. Bacchus-Montabonnel, Laboratoire de Spectrometrie Ionique et Moleculaire, Université Lyon I, 69622 Villeurbanne, Cedex, France

R. J. Bartlett, Quantum Theory Project, University of Florida, Gainesville, Florida 32611

G. L. Bendazzoli, Dipartimento di Chimica Fisica ed Inorganica, Università di Bologna, I-40136 Bologna, Italy

E. J. Brändas, Department of Quantum Chemistry, Uppsala University, SE-751 20 Uppsala, Sweden

J. Caillat, Laboratoire de Chimie Physique de l'Université Pierre et Marie Curie, 75231 Paris, Cedex 05, France

N. Capron, Laboratoire de Chimie Physique de l'Université Pierre et Marie Curie, 75231 Paris, Cedex 05, France

S. Carniato, Laboratoire de Chimie Physique de l'Université Pierre et Marie Curie, 75231 Paris, Cedex 05, France

D. L. Cooper, Department of Chemistry, University of Liverpool, Liverpool L69 7ZD, United Kingdom

P. Cronstrand, Theoretical Chemistry, Royal Institute of Technology, S-10044 Stockholm, Sweden

J. P. Dahl, Department of Chemistry, Technical University of Denmark, DK-2800 Kgs. Lyngby, Denmark

Ya. Y. Delchev, Institute of Nuclear Research and Energy, Bulgarian Academy of Sciences, 1784 Sofia, Bulgaria

B. Durbeej, Department of Quantum Chemistry, Uppsala University, SE-751 20 Uppsala, Sweden

N. O. Elander, Department of Physics, Stockholm University, SE-113 85 Stockholm, Sweden

M. Engström, Theoretical Chemistry, Royal Institute of Technology, S-10044 Stockholm, Sweden

M. L. Ericsson, Department of Quantum Chemistry, Uppsala University, SE-751 20 Uppsala, Sweden

L. A. Eriksson, Department of Quantum Chemistry, Uppsala University, SE-751 20 Uppsala, Sweden

J.-S. Filhol, Ecole Normale Superieure de Lyon, 69364 Lyon, Cedex 07, France

P. Froelich, Department of Quantum Chemistry, Uppsala University, SE-751 20 Uppsala, Sweden

Y. Girard, Laboratoire de Chimie Theorique, Université Pierre et Marie Curie, 75252 Paris Cedex 05, France

A. V. Glushkov, Institute of Applied Mathematics, OHMI, Odessa-9, 65009, Ukraine

O. Goscinski, Department of Quantum Chemistry, Uppsala University, SE-751 20 Uppsala, Sweden

I. Hubač, Department of Chemical Physics, Faculty of Mathematics and Physics, Comenius University, 842 15 Bratislava, Slovakia

Y. Ishikawa, Department of Chemistry, University of Puerto Rico, San Juan, Puerto Rico 00931-3346, USA

M. Ivanov, Theoretische Chemie, Physikalisch-Chemisches Institut, Universität Heidelberg, D-69120 Heidelberg, Germany

M. Jansson, Department of Quantum Chemistry, Uppsala University, SE-751 20 Uppsala, Sweden

S. Jonsell, Department of Quantum Chemistry, Uppsala University, SE-751 20 Uppsala, Sweden

U. Kaldor, School of Chemistry, Tel Aviv University, 69978 Tel Aviv, Israel

I. G. Kaplan, Instituto de Fisica, UNAM, 01000 Mexico, D. F., Mexico

E. B. Karlsson, Department of Physics, Uppsala University, S-75121 Uppsala, Sweden

H. O. Karlsson, Department of Quantum Chemistry, Uppsala University, SE-751 20 Uppsala, Sweden

I. S. K. Kerkines, Laboratory of Physical Chemistry, Department of Chemistry, University of Athens, 157 10 Zografou, Athens, Greece

E. S. Kryachko, Department of Chemistry, University of Leuven, B-3001 Heverlee-Leuven, Belgium

A. Kuleff, Laboratoire de Chimie Physique, Université Pierre et Marie Curie, 75005 Paris Cedex, France

J. Ladik, Chair for Theoretical Chemistry, University of Erlangen-Nürnberg, D-91058 Erlangen, Germany

P. O. Lantto, University of Oulu, Department of Physical Sciences, University of Oulu, FIN-90014 Oulu, Finland

Å. Larson, Department of Physics, Stockholm University, SE-113 85 Stockholm, Sweden

B. Larsson, Department of Quantum Chemistry, Uppsala University, SE-751 20 Uppsala, Sweden

P.-E. Larsson, Department of Quantum Chemistry, Uppsala University, SE-751 20 Uppsala, Sweden

R. Lefebvre, Laboratoire de Photophysique Moleculaire, Campus d'Orsay, 91405 Orsay, France

S. B. Levin, Department of Physics, Stockholm University, SE-113 85 Stockholm, Sweden

W. Liu, Lehrstuhl für Theoretische Chemie, Ruhr-Universität Bochum, D-44780, Germany

J. Llano, Department of Quantum Chemistry, Uppsala University, SE-751 20 Uppsala, Sweden

M. J. Lundqvist, Department of Quantum Chemistry, Uppsala University, SE-751 20 Uppsala, Sweden

S. G. B. Lunell, Department of Quantum Chemistry, Uppsala University, SE-751 20 Uppsala Sweden

Y. Luo, Theoretical Chemistry, Royal Institute of Technology, S-10044 Stockholm, Sweden

P. Macak, Theoretical Chemistry, Royal Institute of Technology, S-10044 Stockholm, Sweden

S. V. Malinovskaya, NPO-Computer Centre, Odessa-9, 65009, Ukraine

A. Markovits, Laboratoire de Chimie Théorique, Université Pierre et Marie Curie, 75252 Paris Cedex 05, France

I. Martín, Departamento de Quimica Fisica, Facultad de Sciencias, Universidad de Valladolid, Valladolid, Spain

C. Martinsky, Laboratoire de Chimie Théorique, Université Pierre et Marie Curie, 75252 Paris Cedex 05, France

J. Maruani, Laboratoire de Chimie Physique, Université Pierre et Marie Curie, 75252 Paris Cedex 05, France

B. F. Minaev, Theoretical Chemistry, Royal Institute of Technology, S-10044 Stockholm, Sweden

C. Minot, Laboratoire de Chimie Théorique, Université Pierre et Marie Curie, 75252 Paris Cedex 05, France

D. C. Moule, Department of Chemistry, Brock University, St. Catharines, Ontario L2S3A1, Canada

V. Mujica, Facultad de Ciencias, Escuela de Quimica, Universidad Central de Venezuela, Caracas 1020A, Venezuela

P. K. Mukherjee, Spectroscopy Department, Indian Association for the Cultivation of Science, Calcutta 700 032, India

A. Nagy, Lajos Kossuth University, Department of Theoretical Physics, Lajos Kossuth University, H-4010 Debrecen, Hungary

J. V. Ortiz, Department of Chemistry, Kansas State University, Manhattan, Kansas 66506-3701

A. A. Palma, Instituto de Fisica, Universidad Autónomo de Puebla, Puebla, Pue. 72570, Mexico

A. Papakondylis, Laboratory of Physical Chemistry, Department of Chemistry, University of Athens, 157 10 Zografou, Athens, Greece

D. E. Parry, School of Chemistry, University of Bristol, Bristol BS8 1TS, United Kingdom

R. L. Pavlov, Institute of Nuclear Research and Energy, Bulgarian Academy of Sciences, 1784 Sofia, Bulgaria

T. B. Pedersen, Department of Physical Chemistry, University of Santiago de Compostela, E-15706 Santiago de Compostela, Spain

Å. J. Petersson, Department of Quantum Chemistry, Uppsala University, SE-751 20 Uppsala, Sweden

O. Plashkevych, Theoretical Chemistry, Royal Institute of Technology, S-10044 Stockholm, Sweden

T. Privalov, Theoretical Chemistry, Royal Institute of Technology, S-10044 Stockholm, Sweden

P. Pyykkö, Department of Chemistry, Helsinki University, FIN-00014 Helsinki, Finland

J. Raber, Department of Quantum Chemistry, Uppsala University, SE-751 20 Uppsala, Sweden

S. Rettrup, Chemical Laboratory IV, Copenhagen University, DK-2100 Copenhagen, Denmark

G. Rivière, European Commission, DG Research, B-1049 Brussels, Belgium

J. Rung, Department of Quantum Chemistry, Uppsala University, SE-751 20 Uppsala, Sweden

U. Saalmann, Atomfysik, Stockholms Universitet, S-10405 Stockholm, Sweden

P. Salek, Theoretical Chemistry, Royal Institute of Technology, S-10044 Stockholm, Sweden

N. Salhi-Benachenhou, Department of Quantum Chemistry, Uppsala University, SE-751 20 Uppsala, Sweden

B. Silvi, Laboratoire de Chimie Théorique, Université Pierre et Marie Curie, 75252 Paris Cedex 05, France

Y. G. Smeyers, Instituto de Estructura de la Materia, C.S.I.C., 28006 Madrid, Spain

V. Srivastava, School of Physics, University of Hyderabad, Hyderabad 500 046, India

B. T. Sutcliffe, Laboratoire de Chimie Physique Moléculaire, Université Libre de Bruxelles, B-1050 Bruxelles, Belgium

O. Tapia, Department of Physical Chemistry, Uppsala University, SE-751 21 Uppsala, Sweden

D. Tzeli, Laboratory of Physical Chemistry, Department of Chemistry, University of Athens, 157 10 Zografou, Athens, Greece

J. T. Vaara, Department of Chemistry, University of Helsinki, FIN-00014 Helsinki, Finland

C. Valdemoro, Instituto de Matemáticas y Física Fundamental, C.S.I.C., Madrid 28006, Spain

A. J. C. Varandas, Departamento de Quimica, Universidade de Coimbra, P-3049 Coimbra Codex, Portugal

L. Veseth, Department of Physics, University of Oslo N-0316, Oslo, Norway

M. Villa, Instituto de Estructura de la Materia, C.S.I.C., 28006 Madrid, Spain

S. Wilson, Rutherford Appleton Laboratory, Chilton, Oxon OX11 0QX, United Kingdom

P. Tz. Yotov, Institute of Nuclear Research and Energy, Bulgarian Academy of Sciences, 1784 Sofia, Bulgaria

B. P. Zapol, Department of Theoretical Physics, Institute of Chemical Physics, University of Latvia, Riga LV-1586, Latvia

SYMBOLS IN SCIENCE

The Löwdin Memorial Lecture

25 October 2000

Roy McWeeny
University of Pisa, Italy

On 6 October 2000 Per-Olov Löwdin left us .... for many of us, he had seemed immortal, a constant friend and colleague in the now vast field of Quantum Chemistry to which he had devoted so much of his creative energy.

He was one of the great leaders of the post-war era, both in teaching and research, and the debt we owe him is immeasurable. He set up two leading international research centres, one here in Uppsala, the other in Gainesville, Florida, and steered their development for decades. Through the Summer and Winter Institutes that these centres hosted almost every year since 1957, Per-Olov influenced many generations of aspiring theoreticians, both chemists and physicists. In our collective memory he will remain immortal – a great scientist and a warm and powerful personality. Others will have much to say about his life: here I want to talk about his scientific 'style' and some of the wonderful ideas and images he left in our minds.

His influence on my own development began with a paper he wrote almost half a century ago, published in 1951, which showed his extraordinary gift for combining deep insight into the 'physics' of a problem with the elegant mathematics that would lead to its solution. His subsequent work, on the foundations and applications of quantum mechanics, resulted in hundreds of publications and was marked throughout by its originality and its mathematical beauty. He moved with ease from the theoretical study of alkali halides – like common salt – to the more abstruse formulation of set theory and linear algebra in the book "Linear Algebra for Quantum Mechanics" which he published only two years ago – quite clearly still at the height of his powers. Always, it would seem, he looked for elegance in whatever he was creating. Paul Dirac, one of the great founders of Quantum Mechanics, once said

> "It seems to me that if one is working from the point of view of getting beauty into one's equations, and if one really has a sound insight, then one is on a sure line of progress".

Per-Olov quite evidently worked in this way; and it therefore seems fitting that in this Memorial Lecture I should try to explain to you (or – for those who know already – remind you of) what all this means. How on earth is it possible for mathematical equations to be 'beautiful' and how does all their symbolism relate to the world around us? Difficult as it is to define mathematical beauty, I would say that essential ingredients are simplicity, symmetry and a certain economy of expression: the underlying principles that govern the working of the universe are embodied in a few equations (for instance: Newton's laws, for classical mechanics, Maxwell's equations for

the electromagnetic field, Schrödinger's equation for quantum mechanics), containing a small number of symbols – standing for physical quantities, like mass, charge, electric and magnetic field strengths. Such equations lie at the root of physics, chemistry, and indeed the whole of science; and yet they can be written down on one or two sheets of paper – a blueprint for the universe!

Hence my title Symbols in Science. Let me start with a symbol very close to Per-Olov's heart, the Greek letter 'psi' (Ψ), which in Quantum Mechanics usually stands for the **state** of a physical system such as an atom or molecule. Even the letter itself has a certain austere beauty! It has a **symmetry**, related to the way it responds to certain **operations**: if we reflect it across the vertical plane containing the central I, the left and right 'arms' are simply interchanged and the new Ψ (call it $\bar{\Psi}$) is indistinguishable from the original. This observation is expressed mathematically in the statement

$$\mathsf{R}_v\Psi = \bar{\Psi} = \Psi,$$

where R_v denotes the **operator** that causes "reflection across the vertical plane" and the $=$ sign, as usual, means "no detectable difference between the quantities it separates".

Suppose now the Ψ is cut out of white card and we mark one of the arms with a small $+$ sign on the top surface. This 'secret' mark, barely visible, we suppose, and certainly not a part of the psi, simply allows us to see what is going on: thus, if R_h denotes reflection across the 'horizontal plane' (i.e. that of the card), then we can say $\mathsf{R}_h\Psi^+ = \Psi^\oplus$, where the $\oplus$ means that the mark $+$ is to be found on the 'underneath' surface of the card, directly below the original $+$. The effects of the operators R_v and R_h can thus be summarized as

$$\mathsf{R}_v\Psi^+ = {}^+\Psi \quad (A), \quad \mathsf{R}_h\Psi^+ = \Psi^\oplus \quad (B).$$

When we remember that the $+$ is a 'secret' mark which may be disregarded, it is clear that the letter itself is left unchanged by both operations.

Now let us try repeating the operations, remembering that doing exactly the same thing to both sides of an equation is bound to leave them still equal. Thus, using (A) and (B) above,

$$\mathsf{R}_v\mathsf{R}_v\Psi^+ = \mathsf{R}_v\,{}^+\Psi = \Psi^+,$$

$$\mathsf{R}_h\mathsf{R}_h\Psi^+ = \mathsf{R}_h\Psi^\oplus = \Psi^+,$$

and this means that R_v and R_h, each applied twice in succession, leave Ψ^+ exactly as it was in the beginning. We say they are equivalent to the *identity* or *unit* operator 1 ("do nothing") and write

$$R_v R_v = 1, \quad R_h R_h = 1.$$

If the product of two operators is equivalent to the unit operator, each is said to be the 'inverse' of the other: so here both operators are said to be 'self-inverse'.

On the other hand, application of R_v and R_h, one after the other, is equivalent to a new and non-trivial operation:

$$R_v R_h \Psi^+ = R_v \Psi^{\oplus} = {}^{\oplus}\Psi$$

and $R_h R_v$ leads to exactly the same result. The mysterious ${}^{\oplus}\Psi$ could have been obtained by the *single operation* of rotating Ψ^+ through 180° around its vertical axis. The rotation operator involved is usually denoted by C_2, where the subscript 2 means the operator has to be applied *twice in succession* to achieve a full turn through 360° – which clearly returns the Ψ^+ to its original state. Like R_v and R_h, C_2 is a self-inverse operator: $C_2 C_2 = 1$.

What have we done so far? We have found four **symmetry operators**

$$1 \qquad C_2 \qquad R_v \qquad R_h,$$

which, when applied to the letter Ψ, leave it unchanged or to use the technical term 'invariant'. They characterize the symmetry of the object (i.e. the 'operand' Ψ); but they are related not only to one particular object (Ψ) – just as the operation of counting is not related to what is being counted. Their properties can be studied without reference to the operand: C_2 applied twice in succession is equivalent to 1, i.e. "do nothing" – *whatever it is that is being rotated.* The four symbols may be regarded as the 'elements' of an **abstract group**, among which there are certain formal 'laws of combination'. Any two elements may be combined (in the example used here by 'sequential performance') to give a third, which is 'equivalent' (giving the same end result) to the 'product' of the first two. The group is 'closed' – however we combine the four symbols we never find anything new – and it contains the unit 1.

The 'point groups' (containing operations that always leave at least one point fixed in space) are of great importance for symmetrical molecules; their number is limited and they prescribe a great many observable properties of a

molecule of any given symmetry. A molecule with the same symmetry as the letter psi, for example, may vibrate in many different ways: but the frequencies will all be different. On the other hand, a molecule with higher symmetry (that of, say, a tetrahedron or a cube) will exhibit modes of vibration that fall into sets (of 2 or 3) with exactly the same frequency. Similar considerations apply to the electronic structure of a molecule: when the symmetry is low, the energies of the various 'allowed' electronic states will all be different; but when it is higher some of the distinct states will have identical energies – they are 'degenerate'. The theory of groups is vital to our understanding of such properties; and the interpretation of atomic and molecular spectra – the preferential absorption and emission of light of highly specific colour, accompanied by transitions between different energy states – would have been impossible to achieve without it. The remarkable thing is that the foundations of the theory are, as we have seen, so simple. One of the great driving forces in all such theoretical enterprises, I would say, is the sheer pleasure of creating something profound from almost nothing. On re-reading Richard Feynman's book 'Theory of Fundamental Processes' (1962) I came across the statement " - the main point of this is, that *it all came out of nothing!* Evidently he felt the same sense of wonder.

Before leaving the topic of groups we should note their great diversity. If we extend the idea of a point group to include all possible rotations in 3-dimensional space we obtain the (infinite) group $\mathcal{R}(3)$, which allows us to formulate the principle that all directions in space are 'equivalent' i.e. that there is no preferred direction and that our choice of a reference frame (a set of x, y, z axes) is arbitrary and immaterial. Thus, if we rotate a physical system (including anything that interacts with it) all our equations, and the results we obtain, must be invariant against the change. Again, this simple idea has profound consequences: it largely determines the 'commutation rules' among the operators that occur in quantum mechanics.

Another striking example of a group which leaves a physical system invariant is provided by the set of *permutations of identical particles.* If we have a molecule with 2 electrons, each of which may be found in either of 2 states, ψ_A or ψ_B, it would seem that the state of the whole system could be indicated in symbols by $\psi_A(1)\psi_B(2)$ (electron 1 in the 'A state', electron 2 in the 'B state'). But if interchanging the electrons can make no observable difference surely $\psi_A(2)\psi_B(1)$ (electron 2 in the 'A state', electron 1 in the 'B state') would be equally acceptable? – or even a combination of the two? What group theory tells us is that the 2-electron system, described as being in state $\Psi(1,2)$, must respond to an interchange of 1 and 2 by either (i) remaining

invariant, or (ii) changing sign: the quantity $\Psi(1,2)$ must be *symmetric* or *antisymmetric*. In other words the state may be represented as either

$$\Psi_s(1,2) = \psi_A(1)\psi_B(2) + \psi_A(2)\psi_B(1),$$

which is unchanged on swapping 1 and 2, or

$$\Psi_a(1,2) = \psi_A(1)\psi_B(2) - \psi_A(2)\psi_B(1),$$

which changes sign (the two products on the right changing places). The two possibilities are mutually exclusive: which one applies depends on the nature of the particles – and for electrons (and all other 'fermions') only the second is acceptable.

The fact that an electronic state must be antisymmetric under interchange of any two electrons is an expression of the Pauli Principle. It implies also that no two electrons are allowed to be in exactly the same '1-electron' state: for if we replace ψ_B by a second ψ_A the antisymmetric combination disappears! In a many-electron atom, say, the state of lowest energy (the 'ground state') must have electrons spread over *different* 1-electron states $\psi_A, \psi_B, \psi_C \ldots$, not more than one in each, even if the energy of the 'A state' is lower than all the others. Were it not for the antisymmetry restriction, the ground state would be the one in which all electrons crowded into ψ_A: atoms would show no shell structure and would collapse into dense and compact 'clouds' of electrons, in the immediate vicinity of their nuclei. It can be argued that the Pauli Principle is perhaps the most important single principle in the whole of physics: were it not valid there would be no atoms, no chemistry, no life, no universe as we know it.

Now let us leave the topic of symmetry and turn to the problems of observation and measurement in quantum mechanics. Classical physics breaks down in regions where distances, masses and velocities are immense and must then be replaced by relativistic mechanics. It also breaks down in regions of atomic dimensions where the quantities involved are *very small* and in this case it must be replaced by quantum mechanics. Relativity theory is, once again, based on an invariance principle (established experimentally): the velocity of light, as measured by different observers, is always found to be the same – even though one observer may be at rest relative to the light source and the other may be moving rapidly towards it. Quantum mechanics, however, introduces even more revolutionary ideas – unacceptable even to Einstein. A classical equation, such as that which determines the orbit of a particle, becomes meaningless at the atomic level because the observer is

unable to assign precise and experimentally measurable values to the quantities it relates: he must instead learn to calculate with quantities that are essentially *uncertain* and to be content with predictions of a *statistical* nature. This point of view is embodied in Heisenberg's famous Uncertainty Principle, that in general the observer interacts with a microscopic system so strongly that measurement of one quantity is bound to disturb another. It was this aspect of quantum mechanics that Einstein was unable to accept – proclaiming with indignation that "God does not play dice". Nevertheless, the formulation of quantum mechanics proceeded, culminating in equations which worked almost perfectly and were later to give results of astonishing precision, along with interpetations (e.g. the so-called 'Copenhagen interpretation') which, after 60 years of fierce controversy, are now increasingly accepted as logically defensible.

The statistical aspect of measurement in quantum mechanics rests upon sampling observed values of a quantity and noting the frequency with which each value is recorded i.e. it involves *selection* of a particular value and counting the number of times it is found in a long series of experiments (or in one experiment on a huge number of identical systems). The mathematical machinery needed involves a remarkable blend of algebra and geometry, of which I shall try to give you a glimpse.

The simplest quantity we can observe in quantum mechanics is the 'spin' of a particle, around an axis imposed by applying a strong magnetic field. The experiment was first performed by the physicists Stern and Gerlach in 1921: its essentials are indicated in Figure 1.

Sodium atoms come streaming from a furnace and pass between the poles of a specially designed electromagnet, finally landing on a photographic plate. With no magnetic field, a single dark spot is found on the plate, showing where all the atoms land; but when the magnet is switched on there are *two* spots, separated by a distance which is bigger the stronger the field. The beam of atoms is 'split' into two, the two resultant beams arising by *selection* of atoms with two different values of a quantity now called the 'spin' which makes each atom behave like a small bar magnet. The spin is usually represented by an arrow , or better a 'corkscrew' pointing from one magnetic pole to the other, and has a certain magnitude ($+\frac{1}{2}$, in 'atomic units'). When the corkscrew points upwards, along the z axis (conventionally fixed by the field), the particles go into one beam (the top one, say) and the component of the spin along the axis is $+\frac{1}{2}$; but in the other beam the spin component is $-\frac{1}{2}$, the corkscrew pointing downwards. In this observation

the atoms have been experimentally sorted into two categories, 'up-spin' and 'down-spin', with $S_z = \pm\frac{1}{2}$ respectively. The spin component along the field direction, call it S_z, is thus an observable quantity capable of taking only two values, and selecting an atom from the top beam implies that measurement of S_z will yield the value $+\frac{1}{2}$.

To develop the symbolism for dealing mathematically with this kind of observation we can elaborate a little on 'Eddington's Zoo' – with which he entertained an audience at Cornell University in 1931, trying to convince them that mathematics could be used to describe anything!

We consider a zoo, z for short, consisting of 25 animals, 9 lions and 16 tigers. Instead of saying "the zoo consists of 9 lions and 16 tigers" let us use the mathematical shorthand

$$z = 9l + 16t.$$

The concept of selection may now be formulated in symbols by using the *operators* L and T to denote, respectively, "select the lions" and "select the tigers". Figure 2 shows the rules of the game.

On applying L to the zoo, we get only lions – let them go down the lefthand branch; while on applying T we find only tigers – and send them down the righthand branch. In symbols

$$\mathsf{L}z = 9l \quad (9 \text{ lions only}), \quad \mathsf{T}z = 16t \quad (16 \text{ tigers only}).$$

If we make a further selection, on the samples already obtained, we pass to a second level, noting that

$\mathsf{LL}z = 9l$ (still 9 lions in a sample of 9 lions)

$\mathsf{LT}z = 0$ (no lions in a sample of tigers)

$\mathsf{TL}z = 0$ (no tigers in a sample of lions)

$\mathsf{TT}z = 16t$ (still 16 tigers in the sample of tigers)

Now since, for example, $\mathsf{LL}z = \mathsf{L}z$ *however many lions were present*, the nature of the zoo is irrelevant: repeated selection of lions gives nothing but the lions from the first selection and $\mathsf{LL} = \mathsf{L}$ is an intrinsic property of the selection operator. Similarly, LT always results in the selection of *nothing* – for after selecting tigers only we can never find lions among them. Also it is clear that by adding together the results of selecting the lions and then

selecting the tigers the zoo will be reconstituted: $\mathsf{L}z+\mathsf{T}z = 1z$. On dropping the operand z, the exact composition of the zoo being irrelevant, the results may be collected in the form

$$\mathsf{LL} = \mathsf{L}, \quad \mathsf{TT}, \quad \mathsf{LT} = 0, \quad \mathsf{TL} = 0, \qquad \mathsf{L}+\mathsf{T} = 1,$$

where 0 is the 'zero operator', which empties the zoo. Mathematicians will recognize these as the properties that define a **spectral set**, each symbol being an **idempotent**. If you look in Per-Olov's book on Linear Algebra you will find countless examples of them.

Algebra provides one way of dealing with selection, geometry provides another: the different systems of description are 'isomorphic' or 'identical in structure'. When a mathematician has to deal with quantities of two different kinds, such as lions and tigers, he commonly represents them by unit steps, or displacements, in two different direction – North and East, say – starting from some fixed point or 'origin'. He adds such quantities geometrically, as in Figure 3(a), by making the displacements follow one another, their 'sum' being the single step that would reach from the origin to the end point of the last displacement. With this convention, the zoo could be represented pictorially by the arrow $\mathbf{z}$. Any lion-tiger zoo can be represented in this way by an arrow or 'vector'. The selection operators can then be given a geometrical interpretation: $\mathsf{L}\mathbf{z} = 9\mathbf{l}$ is called the 'projection' of the vector $\mathbf{z}$ on the horizontal axis (9 steps - or lions? - East), while $\mathsf{T}\mathbf{z} = 16\mathbf{t}$ is its projection on the vertical axis (16 steps North). The property $\mathsf{LL} = \mathsf{L}$ then simply means that repeated projection on a given axis can produce nothing more than a single projection; while $\mathsf{TL} = 0$ means that any projection on the horizontal axis must have zero projection on the vertical axis. How often, one wonders, have we heard Per-Olov talking about projection operators and the marvellous things one can do with them!

Before returning to the Stern-Gerlach experiment, it is useful to modify this geometrical picture slightly. If we wish to compare the characters of different zoos, it is their *relative* compositions that will be of most interest: for example, the *fractional* number of animals that are lions. The composition of a zoo might be represented in a diagram where the pointer $\mathbf{z}$ has projections representing these fractions directly (as in Figure 3(b)): but this representation is mathematically awkward, the pointer varying in length according to composition of the zoo. We therefore make a change of convention: if 9/25 of the animals are lions we shall take for the lion-component a step of length 3/5 (i.e. $\sqrt{(9/25)}$) and for the tiger-component – the remaining 16/25 of the zoo – one of length 4/5. This is the representation shown in Figure 3(c).

Thanks to Pythagoras, we can then claim that the representative vector **z** has unit length $(3/5)^2 + (4/5)^2 = 1$; so by merely rotating the pointer we can cover all possible lion-tiger zoos!

I mentioned also the statistical aspect of measurement in quantum mechanics. And this, too, can be illustrated using the zoo. If you are blindfolded and asked to select an animal at random, your chances of finding a lion will be 9 in 25: the 'probability' that random selection will return a lion is 9/25. This means simply that if you make a large number of dips into the zoo (returning the animal after each dip) the fractional number of times that you get a lion will approach closer and closer to 9/25. We are now ready to go back to physics.

The state of a physical system, representing the result of all the measurements you might have made in getting to know it, will be represented by a vector (let's call it Ψ) – though this will be in a mathematical space, with many dimensions instead of just two. And any changes produced by further attempts to obtain information will be reflected in changes in direction of the pointer. The Stern-Gerlach experiment is a beautifully simple example because the representation we need is only two-dimensional: unit step East will represent not a lion but a sodium atom with spin up and unit step North one with spin down. Instead of trying to observe one atom at a time, repeating the experiment an enormous number of times, we use the atoms streaming from the furnace and make the same experiment on all of them. If we find 16 out of every 25 atoms with spin up we shall say that an atom in the beam is in an up-spin state with a probability 16/25.

Now we have no idea what state an atom may be in when it comes from the furnace: so before making any measurements we must sort them out by means of a preliminary Stern-Gerlach experiment (extreme left in Figure 4(a)). We shall then have prepared a beam of up-spin particles, which we shall use, and another of down-spin, which we shall throw away. To confirm that the upper beam contains only up-spin particles we send it into a second Stern-Gerlach experiment, the 'analyser' on the right. There is no further splitting. Every atom comes through in the same up-spin state – there is 100% probability (certainty) that any one of them has spin up. The 'prepared' beam entering the analyser is just like a lion-only zoo, where any animal selected is sure to be a lion (in the state of being a lion!). The state vector Ψ, used to represent the state of an atom in the prepared beam, will therefore lie along the horizontal axis (extreme right in Figure 4(a)).

What happens now if we change the prepared beam by rotating the Stern-

Gerlach apparatus around the axis of the beam, so that the spins of the atoms that come out will point directly towards you – as indicated in Figure 4(b). ? The analyser (remembering the Uncertainty Principle) is likely to disturb the atoms in the prepared beam; and, in fact, the two beams that emerge contain, respectively, half the atoms in the spin-up state and half with spin down. Clearly, these new results have been 'manufactured' by the analyser! – the experimenter is interfering with what he is trying to measure. But the results still serve to identify the state of an atom in the prepared beam: it is one in which each of the two possible results has a 50% probability of being found and it will be represented by setting the pointer Ψ at 45° (extreme right in Figure 4(b)). More generally (e.g. rotating the Stern-Gerlach apparatus through 30° instead of 45°) the pointer might be set to

$$\Psi = a_1\Psi_1 + a_2\Psi_2,$$

where Ψ_1, along the horizontal axis represents the state of definite spin $s_1 = +\frac{1}{2}$ while Ψ_2, along the vertical axis, represents that with spin $s_2 = -\frac{1}{2}$. The general Ψ is a 'superposition' of the two definite spin states with numerical weights a_1, a_2 called 'amplitudes'. In the case considered above, where up-spin and down-spin states are found with equal probability $p_1 = p_2 = \frac{1}{2}$, it is evident that $a_1 = a_2 = \sqrt{\frac{1}{2}}$. But, however general the context, a probability is always the square of an amplitude.

One of the triumphs of quantum mechanics is that it allows us to deal with states of a system in which the value of some quantity is not known, in terms of states in which its value is perfectly definite.

What conclusion can be drawn from all this? In the act of measurement (i.e. in the analyser) a state vector is *rotated* until it points along the axis corresponding to one of the observable values (s_1, s_2) – which are called **'eigenvalues'**. The associated vectors themselves (Ψ_1, Ψ_2) are called the **'eigenvectors'** and characterize the 'eigenstates' of the physical system. These particular vectors have a very special property: introducing projection operators $\mathsf{P}_1, \mathsf{P}_2$, exactly parallel to those used for selecting lions and tigers, we can write $\mathsf{P}_1\Psi_1 = \Psi_1$ (state with S_z definitely equal to $s_1 = +\frac{1}{2}$), $\mathsf{P}_1\Psi_2 = 0$ (no s_1 component in a state with $S_z = s_2 = -\frac{1}{2}$, and so on.

Now let us associate with the physical quantity S_z an operator

$$\mathsf{S}_z = s_1\mathsf{P}_1 + s_2\mathsf{P}_2,$$

– expressed in Per-Olov's famous 'normal form'. This operator has the prop-

erty that the equation

$$\mathsf{S}_z\Psi = s\Psi,$$

where the vector Ψ and the number s are not known but are to be found, has only two solutions, namely $\Psi = \Psi_1$, with $s = s_1$, and $\Psi = \Psi_2$, with $s = s_2$. This key equation, which is called an **eigenvalue equation**, has solutions only when the effect of the operator is simply to multiply the vector Ψ by a number: the number is then one of the observable values of the quantity S_z, while the vector describes the corresponding eigenstate of the system. Here is the real kernel of Quantum Mechanics – all in a very small nutshell! Of course we are not quite finished yet! We must find the rules for playing with the operators; but it was discovered long long ago that these are largely prescribed by the need to respect symmetry principles (already familiar to us), together with a 'correspondence principle' – that there should be a 'continuity' in passing between classical mechanics (big systems) and quantum mechanics (small systems). So if we want to know the observable values of, say, the energy of the electrons in an atom or molecule, we can set up an operator (the 'Hamiltonian' operator), and an eigenvalue equation, with which to find them.

This completes our long excursion into fundamentals. Eigenvalue equations can be set up and solved to predict the properties of quantum systems – with increasing accuracy, but usually only at vast computational expense. Per-Olov was not greatly interested in computers – he was too fond of beautiful things to have much time for what he found less exciting. I hope that in this Memorial Lecture I have been able to touch on some of the more abstract things that he loved.

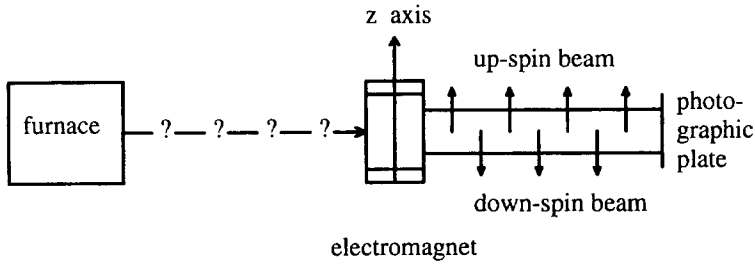

Figure 1. The Stern-Gerlach experiment (highly schematic).

A beam of sodium atoms (of unknown spin), from a 'furnace' (left), passes between the poles of a specially designed electromagnet (centre). When the magnet is switched off, the beam produces one dark spot on the photographic plate (right); but when it is on the beam is 'split' into two components, 'up-spin' and 'down-spin' (represented by the arrows).

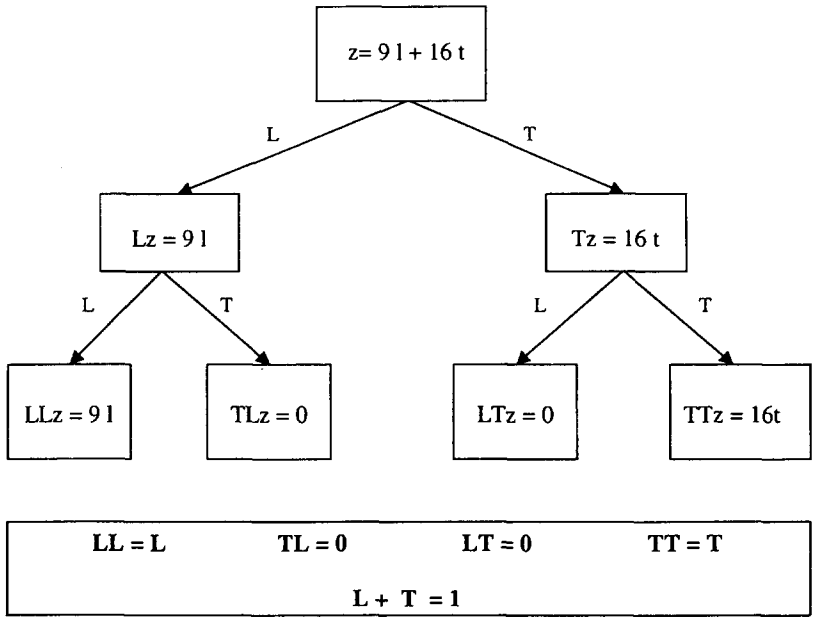

Figure 2. Eddington's Zoo: an exercise in selection.

The operators **L** and **T** select lions and tigers, respectively, results being shown in the boxes. Properties of the operators are summarized in the bottom box.

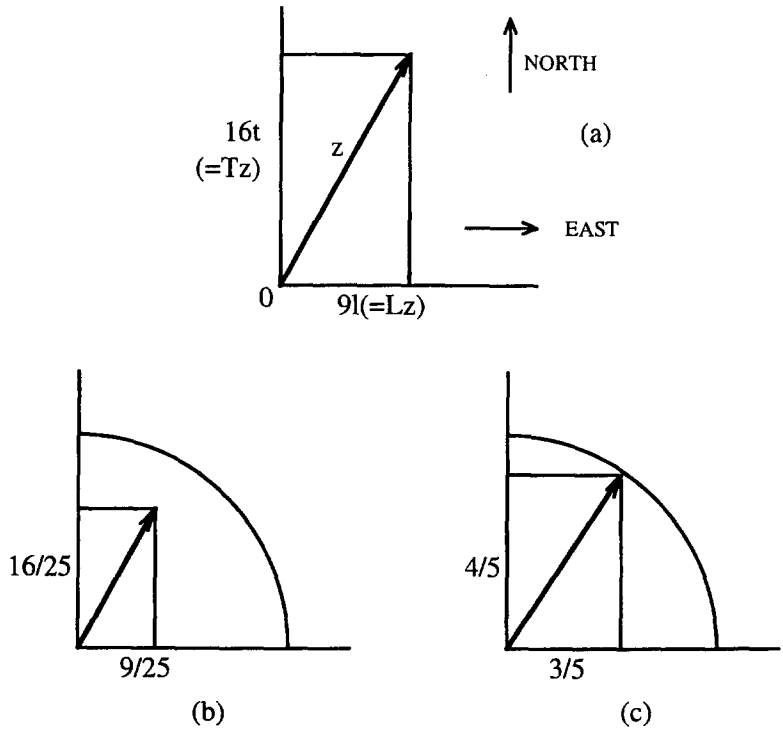

Figure 3. Vector representations of a mixture.

(a) The zoo represented by a pointer (vector), indicating 9 steps East (lions) and 16 steps North (tigers).

(b) Alternative representation, showing the *fractional* number of animals of each type as *projections*, 9/25 and 16/25, on the two axes.

(c) Projections now show the square roots, 3/5 and 4/5: the sum of the squares gives always a pointer of *unit length*, so any operation on the zoo simply rotates the pointer.

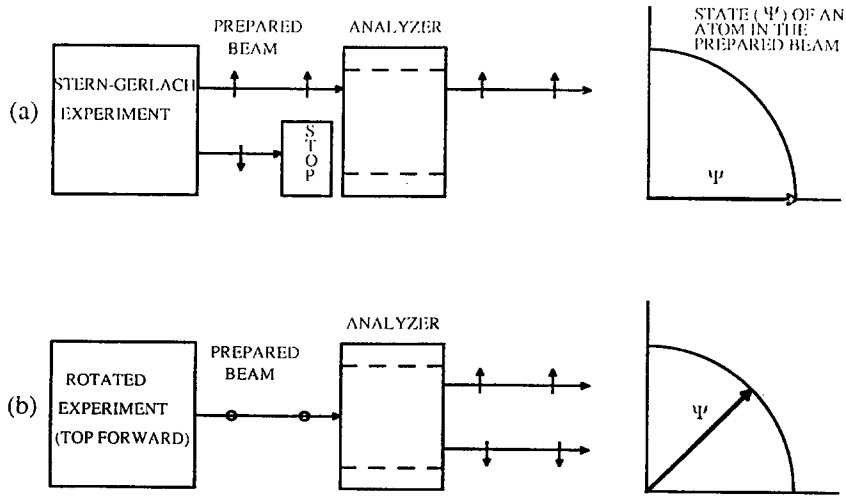

Figure 4. More Stern-Gerlach experiments.

(a) Split beam from the first apparatus (left) sent into a second magnet (the 'analyser'): the 'prepared' up-spin beam goes through unchanged.

(b) Similar experiment after rotating the first apparatus (top forwards) so that the spins of the prepared beam now point directly towards the reader: the rotated beam is split into up and down components!

In each case, the spin state of a particle in the prepared beam is indicated by a vector (extreme right), as in Fig. 3.

Some mathematical problems in the description of dissociating molecules

Brian Sutcliffe [1]

Lab. de Chimie Physique Moléculaire,
Université Libre de Bruxelles,
50 av F. D. Roosevelt, 1050-Bruxelles,
Belgium

Abstract

When separating the centre of mass motion from the Schrödinger problem for a system, some apparently reasonable choices of space fixed coordinates have transformation properties under nuclear permutations that mix variables that are formally nuclear with those that are formally electronic variables. This renders the idea of a potential surface expressed in such coordinates, problematic. The problems are discussed and some solutions suggested.

[1] bsutclif@ulb.ac.be

ADVANCES IN QUANTUM CHEMISTRY, VOLUME 40

0065-3276/01 $35.00

Contents

1. Introduction

When considering reaction dynamics it is customary to assume that the Born-Oppenheimer approximation holds to a very good approximation so that the idea of a potential energy surface is a good place to start from. An interesting collection of papers and reviews concerned with the idea has been published (1) and what follows was stimulated by remarks made by Markus Klein in his contribution, (2) entitled *The Born-Oppenheimer Expansion: Eigenvalues, Eigenfunctions and Low-Energy Scattering.* Klein offers an approach to the Born-Oppenheimer approximation not only for a bound system but also for a diatomic regarded as composed of two colliding atoms. In considering the bound system Klein finds it possible and useful to use a coordinate system in which all the electronic coordinates are referred to a common origin. (Actually the centre of nuclear mass is chosen, but other choices are possible.) When treating the colliding system however, Klein finds it "absolutely essential to use a different system of coordinates adapted to the cluster decomposition in

the separated atoms limit". What this means effectively is that the electronic coordinates of the separated atoms must be referred to separate origins, namely the nuclei of the appropriate separated atoms.

There seems to be no way round this if one wishes to follow the Klein approach (which is the strictly traditional approach) to specify the circumstances in which the Born-Oppenheimer approximation is likely to hold for scattering systems. But if we do allow different origins for the electronic coordinates, then some rather tricky problems arise, as will be seen. (An article providing a more extended context for what follows can be found in (3))

2. Removing translational motion.

Whatever way it is intended to go in specifying the electronic coordinates, they must be specifiable as translationally invariant so that the centre of mass motion can be separated from Schrödinger's equation for the system. It is only the translationally invariant part of the Hamiltonian that can have a bound state spectrum and thus be relevant to both the scattering and the bound molecule problem.

To remove the centre of mass motion from the full molecule Hamiltonian all that is needed is a coordinate transformation symbolised by

$$(\mathbf{t}\ \mathbf{X}_T) = \mathbf{x}\ \mathbf{V} \tag{1}$$

In (1) $\mathbf{t}$ is a 3 by $N-1$ matrix and $\mathbf{X}_T$ is a 3 by 1 matrix, so that the combined (bracketed) matrix on the left of (9) is 3 by N. $\mathbf{V}$ is an N by N matrix which, from the structure of the left side of (1), has a special last column whose elements are

$$V_{iN} = {M_T}^{-1} m_i, \qquad M_T = \sum_{i=1}^{N} m_i. \tag{2}$$

Hence $\mathbf{X}_T$ is the standard centre of mass coordinate.

$$\mathbf{X}_T = {M_T}^{-1} \sum_{i=1}^{N} m_i \mathbf{x}_i \tag{3}$$

As the coordinates $\mathbf{t}_j, j = 1, 2, ...N-1$ are to be translationally invariant, we require on each remaining column of $\mathbf{V}$

$$\sum_{i=1}^{N} V_{ij} = 0, \qquad j = 1, 2, ...N-1 \tag{4}$$

and it is easy to see that (4) forces $\mathbf{t}_j \rightarrow \mathbf{t}_j$ as $\mathbf{x}_i \rightarrow \mathbf{x}_i + \mathbf{a}$, all i.

The $\mathbf{t}_i$ are independent if the inverse transformation

$$\mathbf{x} = (\mathbf{t}\, \mathbf{X}_T)\mathbf{V}^{-1} \tag{5}$$

exists. The structure of the right side of (5) shows that the bottom row of $\mathbf{V}^{-1}$ is special and, without loss of generality, we may require its elements to be

$$(\mathbf{V}^{-1})_{Ni} = 1 \qquad i = 1, 2.....N \tag{6}$$

The inverse requirement on the remainder of $\mathbf{V}^{-1}$ implies that

$$\sum_{i=1}^{N} (\mathbf{V}^{-1})_{ji} m_i = 0 \qquad j = 1, 2, ...N-1 \tag{7}$$

When we write the column matrix of the cartesian components of the partial derivative operator as $\partial/\partial \mathbf{x}_i$, the coordinate change (1) gives

$$\frac{\partial}{\partial \mathbf{x}_i} = \sum_{j=1}^{N-1} V_{ij} \frac{\partial}{\partial \mathbf{t}_j} + m_i {M_T}^{-1} \frac{\partial}{\partial \mathbf{X}_T} \tag{8}$$

and when it seems more convenient this column matrix of derivative operators will also be denoted as the vector grad operator $\vec{\nabla}(\mathbf{x}_i)$.

2..1 Distinguishing electronic and nuclear motions.

Because the spectrum of the translationally invariant Hamiltonian is independent of the choice of $\mathbf{V}$, the way in which it is chosen would be immaterial if it were possible to construct exact solutions. As it is necessary in practice to use an approximation scheme, it is rational to choose a $\mathbf{V}$ adapted to the scheme. Our aim is to design the approximate wave functions so as to decouple electronic and nuclear motions as far as possible and so be good approximations in a Born-Oppenheimer sense. Ideally, the electronic part of the approximate wave function should consist of solutions of an electronic Hamiltonian which is as much like the clamped nuclei Hamiltonian as possible and whose eigenvalues can be identified with electronic energies as functions of the nuclear coordinates. The nuclear part of the approximation should, again ideally, consist of solutions to a problem composed of the nuclear motion kinetic energy operator expressed in terms of coordinates that arise from the original nuclear coordinates alone together with a potential that consists of a sum of the electronic and the potential energy of nuclear repulsion.

It seems reasonable, therefore to require that the translationally invariant nuclear coordinates be expressible entirely in terms of the original nuclear coordinates. Thus analogously to (1)

$$(\mathbf{t}^n\mathbf{X}) = \mathbf{x}^n\mathbf{V}^n \tag{9}$$

Here $\mathbf{t}^n$ is a 3 by$H-1$ matrix and $\mathbf{X}$ is a 3 by 1 matrix. $\mathbf{V}^n$ is an H by H matrix whose last column is special, with elements

$$V^n_{iH} = M^{-1}m_i, \qquad M = \sum_{i=1}^{H} m_i \tag{10}$$

so that $\mathbf{X}$ is the coordinate of the centre of nuclear mass. The elements in each of the first $H-1$ columns of $\mathbf{V}^n$ each sum to zero, precisely as in (4), to ensure translational invariance.

If the $\mathbf{t}^n$ are independent then

$$\mathbf{x}^n = (\mathbf{t}^n\mathbf{X})(\mathbf{V}^n)^{-1} \tag{11}$$

just as in (5) and, just as in (6), the bottom row of $(\mathbf{V}^n)^{-1}$ is special with elements

$$((\mathbf{V}^n)^{-1})_{Hi} = 1 \qquad i = 1, 2, ...H \tag{12}$$

while like (7) the inverse requirement on the remaining rows gives

$$\sum_{i=1}^{H}((\mathbf{V}^n)^{-1})_{ji}m_i = 0 \qquad j = 1, 2, ...H-1 \tag{13}$$

The comparable electronic coordinates will have to involve the original nuclear coordinates so that (9) becomes generalised to

$$(\mathbf{t}^e\mathbf{t}^n\mathbf{X}) = (\mathbf{x}^e\mathbf{x}^n)\begin{pmatrix} \mathbf{V}^e & \mathbf{0} \\ \mathbf{V}^{ne} & \mathbf{V}^n \end{pmatrix} \tag{14}$$

where $\mathbf{t}^e$ is a 3 by L matrix. It is not possible to choose $\mathbf{V}^{ne}$ to be a null matrix and to satisfy simultaneously the translational invariance requirements as specified by (4) while leaving the whole matrix non-singular. Given that it exists, the inverse of (14) may be written as

$$(\mathbf{x}^e\mathbf{x}^n) = (\mathbf{t}^e\mathbf{t}^n\mathbf{X})\begin{pmatrix} (\mathbf{V}^e)^{-1} & \mathbf{0} \\ \mathbf{B} & (\mathbf{V}^n)^{-1} \end{pmatrix} \tag{15}$$

where

$$\mathbf{B} = -(\mathbf{V}^n)^{-1}\mathbf{V}^{ne}(\mathbf{V}^e)^{-1} \tag{16}$$

The bottom row of $\mathbf{B}$ is special in the same way as is the bottom row of $(\mathbf{V}^n)^{-1}$ and consists of the elements

$$B_{Hi} = 1, \qquad i = 1, 2, ...L \tag{17}$$

Using (15)

$$\mathbf{x}_i^e = \mathbf{X} + \sum_{j=1}^{L} \mathbf{t}_j^e ((\mathbf{V}^e)^{-1})_{ji} + \sum_{j=1}^{H-1} \mathbf{t}_j^n B_{ji} \tag{18}$$

and

$$\mathbf{x}_i^n = \mathbf{X} + \sum_{j=1}^{H-1} \mathbf{t}_j^n ((\mathbf{V}^n)^{-1})_{ji} \tag{19}$$

A change from $\mathbf{X}$ to $\mathbf{X}_T$ has no effect on the expressions for $\mathbf{t}^e$ and $\mathbf{t}^n$ but it does affect the expression for the inverse. Using (15) and the definitions of $\mathbf{X}$ and $\mathbf{X}_T$ it follows that

$$\mathbf{X}_T = \mathbf{X} + \sum_{i=1}^{L} s_i^e \mathbf{t}_i^e + \sum_{i=1}^{H-1} s_i^n \mathbf{t}_i^n \tag{20}$$

where

$$s_i^e = {M_T}^{-1} m \sum_{j=1}^{L} ((\mathbf{V}^e)^{-1})_{ij}, \qquad s_i^n = {M_T}^{-1} m \sum_{j=1}^{L} B_{ij} \tag{21}$$

so that using (20) $\mathbf{X}$ can be eliminated in favour of $\mathbf{X}_T$ whenever necessary. In much of what follows it will be convenient to use $\mathbf{X}$ as a short-hand, but no approximation is implied.

The derivative operator (8) can now be distinguished as consisting of two parts

$$\frac{\partial}{\partial \mathbf{x}_i^e} = \sum_{j=1}^{L} V_{ij}^e \frac{\partial}{\partial \mathbf{t}_j^e} + m {M_T}^{-1} \frac{\partial}{\partial \mathbf{X}_T} \tag{22}$$

$$\frac{\partial}{\partial \mathbf{x}_i^n} = \sum_{j=1}^{L} V_{ij}^{ne} \frac{\partial}{\partial \mathbf{t}_j^e} + \sum_{j=1}^{H-1} V_{ij}^n \frac{\partial}{\partial \mathbf{t}_j^n} + m_i {M_T}^{-1} \frac{\partial}{\partial \mathbf{X}_T} \tag{23}$$

2..2 The Hamiltonian operator with electrons identified

The translationally invariant kinetic energy operator is in three parts

$$\hat{K}(\mathbf{t}) \rightarrow \hat{K}^e(\mathbf{t}^e) + \hat{K}^n(\mathbf{t}^n) + \hat{K}^{en}(\mathbf{t}^n, \mathbf{t}^e) \tag{24}$$

Here

$$\hat{K}^e(\mathbf{t}^e) = -\frac{\hbar^2}{2}\sum_{i,j=1}^{L}\frac{1}{\mu_{ij}^e}\vec{\nabla}(\mathbf{t}_i^e)\cdot\vec{\nabla}(\mathbf{t}_j^e) \tag{25}$$

with

$$1/\mu_{ij}^e = m^{-1}\sum_{k=1}^{L}V_{ki}^eV_{kj}^e + \sum_{k=1}^{H}m_k^{-1}V_{ki}^{ne}V_{kj}^{ne} \tag{26}$$

and

$$\hat{K}^n(\mathbf{t}^n) = -\frac{\hbar^2}{2}\sum_{i,j=1}^{H-1}\frac{1}{\mu_{ij}^n}\vec{\nabla}(\mathbf{t}_i^n).\vec{\nabla}(\mathbf{t}_j^n) \tag{27}$$

in which $1/\mu_{ij}^n$ is defined

$$1/\mu_{ij}^n = \sum_{k=1}^{N}{m_k}^{-1}V_{ki}^nV_{kj}^n \qquad\qquad i,j = 1,2,...N-1 \tag{28}$$

Finally

$$\hat{K}^{en}(\mathbf{t}^n,\mathbf{t}^e) = -\frac{\hbar^2}{2}\sum_{i=1}^{H-1}\sum_{j=1}^{L}\frac{1}{\mu_{ij}^{ne}}\left(\vec{\nabla}(\mathbf{t}_i^n)\cdot\vec{\nabla}(\mathbf{t}_j^e) + \vec{\nabla}(\mathbf{t}_j^e)\cdot\vec{\nabla}(\mathbf{t}_i^n)\right) \tag{29}$$

with

$$1/\mu_{ij}^{ne} = \sum_{k=1}^{H}m_k^{-1}V_{ki}^nV_{kj}^{ne} \tag{30}$$

The rather cumbersome form in which $\hat{K}^{en}$ is written is to anticipate the fact that upon a change of variables to orientation and internal coordinates, it will no longer generally be the case that the operators $\vec{\nabla}(\mathbf{t}_j^e)$ and $\vec{\nabla}(\mathbf{t}_i^n)$ commute.

The interparticle distances needed for the potential energy operator can now be written distinguishing the particle types. Using (18), $\mathbf{x}_j^e - \mathbf{x}_i^e$ becomes

$$\mathbf{x}_j^e - \mathbf{x}_i^e = \sum_{k=1}^{L}\mathbf{t}_k^e(((\mathbf{V}^e)^{-1})_{kj} - ((\mathbf{V}^e)^{-1})_{ki}) + \sum_{k=1}^{H-1}\mathbf{t}_k^n(B_{kj} - B_{ki}) \tag{31}$$

and so is not generally expressible in terms of the $\mathbf{t}_i^e$ alone. Furthermore, the form can change under permutation of identical nuclei and it does not change in the ordinary way under the permutation of electrons. Similar problems arise with $\mathbf{x}_j^n - \mathbf{x}_i^e$

$$\mathbf{x}_i^n - \mathbf{x}_j^e = \sum_{k=1}^{H-1} \mathbf{t}_k^n((\mathbf{V}^n)_{ki}^{-1} - B_{kj}) + \sum_{k=1}^{L} \mathbf{t}_k^e(\mathbf{V}^e)_{kj}^{-1} \qquad (32)$$

2..2.1 Example: translationally invariant coordinates identifying electrons and nuclei in NH_3

Suppose that we wish to treat ammonia as resulting from the collision of an H atom with the NH_2 radical. Label the electronic coordinates $\mathbf{x}_i^e$, $i = 1, 2 \ldots 10$ and the nuclear coordinates $\mathbf{x}_i^n$, $i = 1, 2, 3, 4$ with the nitrogen as 4. The translationally invariant coordinates might then reasonably be chosen as

$$\mathbf{t}_1^e = \mathbf{x}_1^e - \mathbf{x}_1^n$$

so that one electron is referred to a proton so as to constitute a hydrogen atom while the others are referred to the nitrogen nucleus

$$\mathbf{t}_i^e = \mathbf{x}_i^e - \mathbf{x}_4^n, \quad i = 2, \ldots 10$$

The translationally invariant nuclear coordinates are the three nitrogen-proton vectors.

$$\mathbf{t}_i^n = \mathbf{x}_i^n - \mathbf{x}_4^n, \quad i = 1, 2, 3$$

With this choice of coordinates we might expect to be able to extend Klein's argument for a diatomic to account in Born-Oppenheimer terms for the dissociation of NH_3 into NH_2 and H, though we pretty obviously could not do so for, say, its dissociation into NH and H_2.

The inverse of this transformation is

$$\mathbf{x}_i^n = \mathbf{t}_i^n - m_p M^{-1}(\mathbf{t}_1^n + \mathbf{t}_2^n + \mathbf{t}_3^n) + \mathbf{X}, \quad i = 1, 2, 3$$

$$\mathbf{x}_4^n = -m_p M^{-1}(\mathbf{t}_1^n + \mathbf{t}_2^n + \mathbf{t}_3^n) + \mathbf{X}$$

$$\mathbf{x}_1^e = \mathbf{t}_1^e + \mathbf{t}_1^n - m_p M^{-1}(\mathbf{t}_1^n + \mathbf{t}_2^n + \mathbf{t}_3^n) + \mathbf{X}$$

$$\mathbf{x}_i^e = \mathbf{t}_i^e - m_p M^{-1}(\mathbf{t}_1^n + \mathbf{t}_2^n + \mathbf{t}_3^n) + \mathbf{X}, \quad i = 2, 3, \ldots 10 \qquad (33)$$

Using these expressions it is seen that the inter-electronic vectors involving electronic variables labelled 2 through to 10 only are expressible entirely in terms of the $\mathbf{t}_i^e$. However all of the expressions involving the electronic variable labelled 1 involve not only the $\mathbf{t}_i^e$ but $\mathbf{t}_1^n$ too. So, for example

$$\mathbf{x}_1^e - \mathbf{x}_2^e = \mathbf{t}_1^e - \mathbf{t}_2^e + \mathbf{t}_1^n$$

and thus certain of the interelectronic variables involve what are, nominally, the nuclear variables in the transformed set.

Furthermore if the variables $\mathbf{x}_1^n$ and $\mathbf{x}_2^n$ are permuted then

$$\mathbf{t}_1^e \rightarrow \mathbf{t}_1^e + \mathbf{t}_1^n - \mathbf{t}_2^n$$

This mixing of the nominal nuclear and electronic variables that means that the separation of the Hamiltonian into electronic and nuclear parts such as is presented in the last section, is not maintained under the permutation of identical particles. In the absence of a settled division it is clearly problematic to know if the separated entities are precisely what they are claimed to be. Of course if there were some good reason for believing that the proton variables should not be permuted then there would be rather less trouble.

2..3 Permutationally restricted translationally invariant coordinates.

Now it is perfectly possible to construct coordinates that do identify electrons and nuclei in an settled way. That is, permutations of the original coordinates of one class of particle do not induce changes in the translationally invariant coordinates used

to designate the other class. But to do so means restricting the form of $\mathbf{V}^{ne}$ and of $\mathbf{V}^{e}$.

The general permutation of identical particles can be written as

$$\mathcal{P}(\mathbf{x}^e\mathbf{x}^n) = (\mathbf{x}^e\mathbf{x}^n)\begin{pmatrix} \mathbf{P}^e & \mathbf{0} \\ \mathbf{0} & \mathbf{P}^n \end{pmatrix} \tag{34}$$

where $\mathbf{P}^e$ and $\mathbf{P}^n$ are standard permutation matrices.

Using (14), (15) and (20), it follows that

$$\mathcal{P}(\mathbf{t}^e\mathbf{t}^n\mathbf{X}_T) = (\mathbf{t}^e\mathbf{t}^n\mathbf{X}_T)\begin{pmatrix} \mathbf{H}^e & \mathbf{0} \\ \mathbf{R} & \mathbf{H}^n \end{pmatrix} \tag{35}$$

with

$$\mathbf{R} = (\mathbf{V}^n)^{-1}(-\mathbf{V}^{ne}\mathbf{H}^e + \mathbf{P}^n\mathbf{V}^{ne})$$

$$\mathbf{H}^e = (\mathbf{V}^e)^{-1}\mathbf{P}^e\mathbf{V}^e, \quad \mathbf{H}^n = (V^n)^{-1}\mathbf{P}^n\mathbf{V}^n$$

It is easily established that the bottom row of $\mathbf{R}$ consists entirely of zeros and that the Hth row and column of $\mathbf{H}^n$ contain only zeros but with 1 at their intersection. The required permutational invariances of all the operators are maintained under such a transformation, but not in a settled way. That is, permutations of the original coordinates of one class of particle can induce changes in operator forms involving the translationally invariant coordinates designating the other class. This difficulty can be avoided only if $\mathbf{R}$ vanishes.

If matters are so arranged that

$$\mathbf{P}^e\mathbf{V}^e = \mathbf{V}^e\mathbf{P}^e \tag{36}$$

then the vanishing condition becomes:

$$(-\mathbf{V}^{ne}\mathbf{P}^e + \mathbf{P}^n\mathbf{V}^{ne}) = \mathbf{0}_{H,L} \tag{37}$$

and although there may be certain pairs of electronic and nuclear permutations that allow this expression to vanish, it will vanish generally only if

$$\mathbf{V}^{ne}\mathbf{P}^e = \mathbf{V}^{ne} \tag{38}$$

$$\mathbf{P}^n\mathbf{V}^{ne} = \mathbf{V}^{ne} \tag{39}$$

for arbitrary permutations.

The most general form for $\mathbf{V}^e$ that satisfies (36) is

$$(\mathbf{V}^e)_{ij} = \delta_{ij} + a \tag{40}$$

where a is a constant. The inverse has elements

$$((\mathbf{V}^e)^{-1})_{ij} = \delta_{ij} - a/(1 + La) \tag{41}$$

This shows that a can take any value (including 0) except $-1/L$.

The physical content of the requirement (38) is that any electronic variable in the problem should have exactly the same relationship to the nuclear variables as does any other electronic variable. The physical content of the requirement (39) is that every member of a set of identical nuclei must enter into the definition of $\mathbf{t}^e$ in the same way. Thus (38) is satisfied by requiring all the columns of $\mathbf{V}^{ne}$ to be identical and from now on a typical column will be denoted $\mathbf{v}$. If the entries in $\mathbf{v}$ are identical for identical nuclei then (39) is also satisfied.

Using these results in (16) it follows that the columns of $\mathbf{B}$ are identical one with another and the typical column will from now on be written as $\mathbf{b}$. Using (18) with these restrictions it follows that $\mathbf{x}^e_{ij}$ becomes $\mathbf{t}^e_{ij}$, as required. Using the results in (21) gives

$$s^e_i = \frac{m}{M_T(1 + La)}, \qquad s^n_i = M_T^{-1}Lmb_i, \qquad \mathbf{b} = -\frac{(\mathbf{V}^n)^{-1}\mathbf{v}}{(1 + La)} \tag{42}$$

With these choices the explicit forms for the translationally invariant coordinates are

$$\mathbf{t}^e_i = \mathbf{x}^e_i + a\sum_{j=1}^{L}\mathbf{x}^e_j + \sum_{j=1}^{H} v_j\mathbf{x}^n_j \tag{43}$$

$$\mathbf{t}^n_i = \sum_{j=1}^{H}\mathbf{x}^n_j\mathbf{V}^n_{ji}, \qquad i = 1, 2, \ldots, H-1 \tag{44}$$

and for translational invariance of $\mathbf{t}_i^e$, from (43),

$$(1 + La) = -\sum_{j=1}^{H} v_j$$

Their inverses are

$$\mathbf{x}_i^e = \mathbf{X} + \mathbf{t}_i^e - \frac{a}{(1+La)} \sum_{j=1}^{L} \mathbf{t}_j^e + \sum_{j=1}^{H-1} b_j \mathbf{t}_j^n \tag{45}$$

$$\mathbf{x}_i^n = \mathbf{X} + \sum_{j=1}^{H-1} \mathbf{t}_j^n ((\mathbf{V}^n)^{-1})_{ji} \tag{46}$$

If the relations (36) to (39) are satisfied then it is easy to show that (35) becomes

$$\mathcal{P}(\mathbf{t}^e \mathbf{t}^n \mathbf{X}_T) = (\mathbf{t}^e \mathbf{t}^n \mathbf{X}_T) \begin{pmatrix} \mathbf{P}^e & \mathbf{0} & \mathbf{0} \\ \mathbf{0} & \mathbf{H} & \mathbf{0} \\ \mathbf{0} & \mathbf{0} & 1 \end{pmatrix} \tag{47}$$

where

$$(\mathbf{H})_{ij} = ((\mathbf{V}^n)^{-1} \mathbf{P}^n \mathbf{V}^n)_{ij} \qquad i, j = 1, 2, ...H - 1 \tag{48}$$

The matrix $\mathbf{H}$ is not in general in standard permutational form neither is it orthogonal even though it has determinant ± 1 according to the sign of $|\mathbf{P}^n|$.

The form of the derivative operators and of the variables remains unchanged from that given in the previous section but the partition made here does enable a more specific structure to be given to them with parts attributable to the types of particle.

The derivative operator (22) can now simplified as

$$\frac{\partial}{\partial \mathbf{x}_i^e} = \sum_{j=1}^{L} (\delta_{ij} + a) \frac{\partial}{\partial \mathbf{t}_j^e} + m M_T^{-1} \frac{\partial}{\partial \mathbf{X}_T} \tag{49}$$

and (23) as

$$\frac{\partial}{\partial \mathbf{x}_i^n} = v_i \sum_{j=1}^{L} \frac{\partial}{\partial \mathbf{t}_j^e} + \sum_{j=1}^{H-1} V_{ij}^n \frac{\partial}{\partial \mathbf{t}_j^n} + m_i M_T^{-1} \frac{\partial}{\partial \mathbf{X}_T} \tag{50}$$

2..4 The permutationally restricted translationally invariant Hamiltonian identifying electrons

The electronic kinetic energy operator (25) simplifies and, adding the electron repulsion term, the electronic Hamiltonian is

$$\hat{H}^e(\mathbf{t}^e) = -\frac{\hbar^2}{2\mu}\sum_{i=1}^{L}\nabla^2(\mathbf{t}_i^e) - \frac{\hbar^2}{2\overline{\mu}}{\sum_{i,j=1}^{L}}'\vec{\nabla}(\mathbf{t}_i^e)\cdot\vec{\nabla}(\mathbf{t}_j^e) + \frac{e^2}{8\pi\epsilon_0}{\sum_{i,j=1}^{L}}'\frac{1}{|\mathbf{t}_j^e - \mathbf{t}_i^e|} \tag{51}$$

with

$$1/\mu = 1/m + 1/\overline{\mu} \tag{52}$$

$$1/\overline{\mu} = m^{-1}a(2 + La) + \sum_{k=1}^{H} m_k^{-1}{v_k}^2 \tag{53}$$

From (27) and the nuclear repulsion, the nuclear Hamiltonian is

$$\hat{H}^n(\mathbf{t}^n) = -\frac{\hbar^2}{2}\sum_{i,j=1}^{H-1}\frac{1}{\mu_{ij}^n}\vec{\nabla}(\mathbf{t}_i^n).\vec{\nabla}(\mathbf{t}_j^n) + \frac{e^2}{8\pi\epsilon_0}{\sum_{i,j=1}^{H}}'\frac{Z_iZ_j}{r_{ij}(\mathbf{t}^n)} \tag{54}$$

where $r_{ij}(\mathbf{t}^n)$ is the internuclear distance and so is the modulus of

$$\mathbf{x}_j^n - \mathbf{x}_i^n = \sum_{k=1}^{H-1}\mathbf{t}_k^n(((\mathbf{V}^n)^{-1})_{kj} - ((\mathbf{V}^n)^{-1})_{ki}) \tag{55}$$

and, using (29), the interaction Hamiltonian is

$$\hat{H}^{en}(\mathbf{t}^n, \mathbf{t}^e) = -\frac{\hbar^2}{2}\sum_{i=1}^{H-1}\frac{1}{\mu_i}\sum_{j=1}^{L}\left(\vec{\nabla}(\mathbf{t}_i^n)\cdot\vec{\nabla}(\mathbf{t}_j^e) + \vec{\nabla}(\mathbf{t}_j^e)\cdot\vec{\nabla}(\mathbf{t}_i^n)\right)$$

$$-\frac{e^2}{4\pi\epsilon_0}\sum_{i=1}^{H}\sum_{j=1}^{L}\frac{Z_i}{r'_{ij}(\mathbf{t}^n, \mathbf{t}^e)} \tag{56}$$

because

$$1/\mu_{ij}^{ne} \to 1/\mu_i = \sum_{k=1}^{H} m_k^{-1}v_kV_{ki}^n \tag{57}$$

while r'_{ij} is the electron-nucleus distance and so it is the modulus

$$|\mathbf{x}_i^n - \mathbf{x}_j^e| = |\sum_{k=1}^{H-1} \mathbf{t}_k^n((\mathbf{V}^n)_{ki}^{-1} - b_k) + a/(1+La)\sum_{k=1}^{L} \mathbf{t}_k^e - \mathbf{t}_j^e| \quad (58)$$

The choice of translationally invariant electronic coordinates makes $\hat{H}^e(\mathbf{t}^e)$ trivially invariant under permutations of the original electronic coordinates and independent of any particular choice of translationally invariant nuclear coordinates. Similarly $\hat{H}^n(\mathbf{t}^n)$ is independent of any particular choice of translationally invariant electronic coordinates and can be shown, after some algebra, to be invariant under any permutation of the original coordinates of identical nuclei. The interaction operator $\hat{H}^{en}(\mathbf{t}^n, \mathbf{t}^e)$ is obviously invariant under a permutation of the original electronic coordinates and, again after a little algebra, can be shown to be invariant under any permutation of the original coordinates of identical nuclei.

The coupling in the kinetic energy expression between the electronic and and nuclear coordinates as the first term in (56) can be removed if the elements of $\mathbf{v}$ are chosen as

$$v_k = -\alpha M^{-1} m_k, \qquad \alpha = (1 + La) \quad (59)$$

where the choice for α is determined by the translational invariance requirements as explained in connection with (43). Thus the $\mathbf{t}_i^e$ are the electronic coordinates referred to the centre of nuclear mass scaled by α. This choice satisfies the permutation restrictions and with it from (13) and (42) $b_i = 0$, $(i \neq H)$ so s_i^n vanishes too and substituting for v_k into (57), $1/\mu_i$ vanishes. The term (56) then simplifies to

$$\hat{H}^{en}(\mathbf{t}^n, \mathbf{t}^e) = -\frac{e^2}{4\pi\epsilon_0} \sum_{i=1}^{H} \sum_{j=1}^{L} \frac{Z_i}{r'_{ij}(\mathbf{t}^n, \mathbf{t}^e)} \quad (60)$$

and the electron-nucleus distance expression r'_{ij} becomes

$$|\mathbf{x}_i^n - \mathbf{x}_j^e| = |\sum_{k=1}^{H-1} \mathbf{t}_k^n (\mathbf{V}^n)_{ki}^{-1} + a/(1+La)\sum_{k=1}^{L} \mathbf{t}_k^e - \mathbf{t}_j^e| \quad (61)$$

and (53) simplifies to

$$1/\overline{\mu} = m^{-1}a(2 + La) + \alpha^2 M^{-1} \tag{62}$$

In the special case where the centre of nuclear mass is chosen as origin then $a = 0$ and thus $\alpha = 1$ and

$$1/\overline{\mu} = 1/M$$

while (61) simplifies further to

$$|\mathbf{x}_i^n - \mathbf{x}_j^e| = |\sum_{k=1}^{H-1} \mathbf{t}_k^n (\mathbf{V}^n)_{ki}^{-1} - \mathbf{t}_j^e|$$

It is with the form of the Hamiltonian that results from the nuclear centre of mass choice for the origin of the electronic variables that Klein is able to justify the Born-Oppenheimer approximation up to a specified order of small quantities for a bound system. In my view it is possible to justify it in the same way with the slightly less restricted choice of (56) in its general form.

2..4.1 Example: permutationally restricted translationally invariant coordinates for NH_3 with electrons identified.

It should now be clear that the coordinates chosen according to (14) and (15) in which the conditions (36) to (39) are satisfied, are a restricted choice. We can now analyse why choice of coordinates made earlier to describe ammonia as a collision complex, with (33) yielding $(\mathbf{V}^n)^{-1}$ and using (16), is not sufficiently restricted. A little algebra shows that with this choice, because not all the columns of $\mathbf{V}^{ne}$ are identical, then neither are all the columns of $\mathbf{B}$. The first column of $\mathbf{B}$ is

$$\mathbf{b}_1 = \begin{pmatrix} (M - m_p)M^{-1} \\ -m_p M^{-1} \\ -m_p M^{-1} \\ 1 \end{pmatrix}$$

while all the other columns are

$$\mathbf{b} = \begin{pmatrix} -m_p M^{-1} \\ -m_p M^{-1} \\ -m_p M^{-1} \\ 1 \end{pmatrix}$$

but this is sufficient to ensure that (37) is not true and hence that (35) is not block diagonal.

However choosing the nitrogen as origin for *all* the electronic coordinates leads to identical columns $\mathbf{b}$

$$\mathbf{b} = \begin{pmatrix} -m_p M^{-1} \\ -m_p M^{-1} \\ -m_p M^{-1} \\ 1 \end{pmatrix}$$

as required.

Another possible choice for the electronic origin is the centre of nuclear mass (scaled if required) this choice leads to a set of identical $\mathbf{b}$ of the form

$$\mathbf{b} = \begin{pmatrix} 0 \\ 0 \\ 0 \\ 1 \end{pmatrix}$$

as anticipated above.

Even with a fixed choice of electronic origin, different choices of $\mathbf{V}^n$ will lead to differing forms for $\mathbf{b}$. Thus suppose the electronic coordinates are described as above with the nitrogen nucleus as origin but that translationally invariant coordinates for the nuclei are defined as

$$\mathbf{t}_i^n = \mathbf{x}_i^n - \mathbf{x}_3^n, \quad i = 1, 2$$

$$\mathbf{t}_3^n = \mathbf{x}_4^n - M_3^{-1} m_p (\mathbf{x}_1^n + \mathbf{x}_2^n + \mathbf{x}_3^n) \tag{63}$$

where the sum of the proton masses is M_3. The vectors $\mathbf{t}_1^n$ and $\mathbf{t}_2^n$ define vectors from proton 3 to protons 1 and 2 while

$\mathbf{t}_3^n$ positions the nitrogen nucleus with respect to the centre of nuclear mass of the three protons. The inverse transformation is

$$\begin{aligned}
\mathbf{x}_1^n &= 2m_p M_3^{-1}\mathbf{t}_1^n - m_p M_3^{-1}\mathbf{t}_2^n - m_N M^{-1}\mathbf{t}_3^n + \mathbf{X}, \\
\mathbf{x}_2^n &= -m_p M_3^{-1}\mathbf{t}_1^n + 2m_p M_3^{-1}\mathbf{t}_2^n - m_N M^{-1}\mathbf{t}_3^n + \mathbf{X}, \\
\mathbf{x}_3^n &= -m_p M_3^{-1}\mathbf{t}_1^n - m_p M_3^{-1}\mathbf{t}_2^n - m_N M^{-1}\mathbf{t}_3^n + \mathbf{X}, \\
\mathbf{x}_4^n &= M_3 M^{-1}\mathbf{t}_3^n + \mathbf{X} \qquad (64) \\
\mathbf{x}_i^e &= \mathbf{t}_i^e + M_3 M^{-1}\mathbf{t}_3^n + \mathbf{X}, \quad i = 1, 2, 3, \ldots 10
\end{aligned}$$

and hence $\mathbf{b}$ is

$$\mathbf{b} = \begin{pmatrix} 0 \\ 0 \\ M_3 M^{-1} \\ 1 \end{pmatrix}$$

2..4.2 A permutationally restricted translationally invariant Hamiltonian operator for NH_3

Making the choice (63) for the translationally invariant nuclear coordinates and taking the origin for the electronic coordinates as the nitrogen nucleus (so that $a = 0$) the non-zero elements of the matrix of inverse reduced masses are

$$1/\mu_{11}^n = 1/\mu_{22}^n = 1/m_p + 1/m_N, \quad 1/\mu_{33}^n = 1/m_N + 1/M_3$$

$$1/\mu_{12}^n = 1/m_N$$

$$1/\overline{\mu} = 1/m_N, \quad 1/\mu_i = \delta_{i3}/m_N$$

and the kinetic energy operator in these coordinates is

$$-\frac{\hbar^2}{2\mu}\sum_{i=1}^{10}\nabla^2(\mathbf{t}_i^e) - \frac{\hbar^2}{2m_N}{\sum_{i,j=1}^{10}}'\vec{\nabla}(\mathbf{t}_i^e)\cdot\vec{\nabla}(\mathbf{t}_j^e)$$

$$-\frac{\hbar^2}{2}\frac{1}{m_N}\sum_{j=1}^{10}\left(\vec{\nabla}(\mathbf{t}_3^n)\cdot\vec{\nabla}(\mathbf{t}_j^e) + \vec{\nabla}(\mathbf{t}_j^e)\cdot\vec{\nabla}(\mathbf{t}_3^n)\right)$$

$$-\frac{\hbar^2}{2}\sum_{i,j=1}^{2}\frac{1}{\mu_{ij}^n}\vec{\nabla}(\mathbf{t}_i^n).\vec{\nabla}(\mathbf{t}_j^n) - \frac{\hbar^2}{2\mu_{33}^n}\nabla^2(\mathbf{t}_3^n) \qquad (65)$$

The expressions for the potential energy operators are easily written down from (64) and we shall examine only the one that will cause trouble when attempting to consider the dissociation of ammonia. This is the term describing the electron-nitrogen nucleus interactions and thus involving

$$\mathbf{x}_i^e - \mathbf{x}_4^n = \mathbf{t}_i^e$$

This vector does not decompose as the nitrogen nucleus separates from the protons. Such a coordinate choice would doubtless account for a separation into N^{3-} and $3H^+$ but that would be unlikely to be a state of interest in any molecular dynamics calculation. There would be similar difficulties had the centre of nuclear mass been chosen as the origin for the electronic variables.

3. Conclusions

In order to formulate the Born-Oppenheimer approximation correctly we must separate translational motion from internal motions in the Schrödinger problem and we must identify electronic and nuclear coordinates in the resulting translationally invariant problem. But it seems that if we do this and obtain a suitably settled form, we cannot properly consider dissociating and colliding systems. But if we construct our coordinates properly to describe dissociating or colliding forms, we lose the settled division and hence become insecure in identifying the fragments.

Of course the manifold successes of modern reaction dynamics theories encourage us to believe that we must be doing something right, but precisely what it is or how it works, seems still to elude us.

References

(1) Sax, A. F., Ed *Potential Energy Surfaces*, Lecture Notes in Chemistry, Vol 71, Springer, Berlin, 1999.

(2) Klein, M. In *op. cit*, 215-233.

(3) Sutcliffe, B. T. In *op. cit*, 61-96.

Recent Applications of Spin-Coupled Valence Bond Theory to Charge Transfer Collisions

by

David L. Cooper[†], Nick J. Clarke[†*], Phillip C. Stancil[‡], Bernard Zygelman[§],

[†] *Department of Chemistry, University of Liverpool, P.O. Box 147, Liverpool L69 7ZD, United Kingdom,*

[‡] *Department of Physics and Astronomy, University of Georgia, Athens, GA 30602-2451, USA*

[§] *Department of Physics, University of Nevada, Las Vegas, NV 89154-4002, USA*

Abstract

We survey the spin-coupled valence (SCVB) approach to the calculation of potential curves and nonadiabatic couplings for charge transfer in collisons of multiply-charged ions with neutral atomic targets. Subsequent fully-quantal close-coupling scattering calculations may be performed after transformation to a particularly convenient diabatic basis, and we outline how this is achieved. Various aspects of the SCVB methodology are illustrated by means of new calculations for the N^{2+}/He system. Target isotope effects are also discussed briefly, taking the Si(3*s*)/He system as a representative example.

Contents

* Current address: Tessella Support Services plc, Bretby Business Park, Ashby Road, Stanhope Bretby, Burton Upon Trent DE15 0YZ, United Kingdom

ADVANCES IN QUANTUM CHEMISTRY, VOLUME 40

0065-3276/01 $35.00

1 Introduction

Charge transfer collisions of multiply-charged atomic ions with atomic neutrals

$$A^{q+} + B \rightarrow A^{(q-1)+} + B^{+}$$

tend to suppress the abundances of highly-charged ions and play an important role in determining the ionization structure of a wide variety of astrophysical environments such as planetary nebulae, symbiotic stars, supernova remnants, shock-heated gases, quasars, active galactic nuclei, and so on. Electron capture typically populates excited states, the relevant line emissions (which also cool the plasma) potentially being an important diagnostic of plasma conditions. Various astrophysical models are hampered by significant uncertainties in state- and even fine-structure-level-dependent cross sections, and in the associated rate constants. Accurate charge transfer data are also essential for fusion plasma density impurity diagnostics. In addition to the information provided by emission from the decaying product ions, accurate cross sections may be important for constructing reliable models of the scrap-off and divertor regions of a modern tokamak fusion device.

We are concerned in the usual adiabatic molecular picture with avoided crossings of AB^{q+} potentials with asymptotes A^{q+}+B and $A^{(q-1)+}$+B^{+}, so that charge transfer corresponds to nonradiative transitions driven by matrix elements of $\partial/\partial R$, where R is the nuclear separation. The couplings $A_{ij}(R)=\langle\Psi_i|\partial/\partial R|\Psi_j\rangle$ typically take the form of distorted Lorentzians centred at (or near) the 'crossing' distance. In general, it proves necessary to investigate the potential curves, avoided crossings and $\partial/\partial R$ couplings for *several* states of the AB^{q+} quasimolecule. Whereas high accuracy for the asymptotic energy separations is clearly important, since these affect strongly the location and nature of the avoided crossings, we have found that it is also crucial to maintain consistent high accuracy for all the relevant states over the entire range of R. For some systems, it is also necessary to take account of rotational coupling (matrix elements of L_y) between states of different symmetry.

Spin-coupled valence bond (SCVB) calculations, when combined with a fully-quantum-mechanical close-coupling treatment of the scattering problem, have proved extremely useful for studying charge transfer collisions (1–5). In the present account, we outline the basic methodology, starting in Section 2 with the SCVB approach for the calculation of potential curves and $\partial/\partial R$ couplings. The transformation of these molecular data to a particularly convenient diabatic representation, and the resulting scattering equations, are discussed in Section 3. Various aspects of the SCVB methodology are illustrated in Section 4 by means of new calculations for the N^{2+}/He system. Target isotope effects are considered briefly in Section 5, taking the Si^{3+}(3s)/He system as a representative example, and we present some final remarks in Section 6.

2 The spin-coupled valence bond (SCVB) approach

In its simplest form (6), spin-coupled theory is based on a single product of N singly occupied nonorthogonal orbitals ϕ_μ for the N active electrons:

$$\Psi_{SC} = \mathcal{A}\left(\varphi_1^2\varphi_2^2 \ldots \varphi_n^2 \Theta_{PP}^{2n}\, \phi_1\phi_2 \ldots \phi_N \Theta_{SM}^{N}\right)$$

with $2n$ inactive electrons accommodated in doubly occupied orthonormal orbitals φ_i. The active-space spin function, Θ_{SM}^{N}, is fully optimized in a complete set of linearly independent N-electron spin functions with quantum numbers S and M. Simultaneously, the so-called spin-coupled orbitals, ϕ_μ, are optimized in an atom-centred basis set without preconceptions as to their form or restrictions on the overlaps between them. The inactive orbitals φ_i may also be simultaneously optimized in the same atomic basis set, or we may instead choose to take them, without further modification, from a previous calculation. The spins of the inactive electrons are perfectly paired, as denoted by Θ_{PP}^{2n}. To some extent, the spin-coupled configuration may be viewed as a compact, easy-to-interpret approximation to the analogous 'N electrons in N orbitals' CASSCF wave function. It is now straightforward to perform fully-variational calculations with fairly general multiconfiguration variants of the basic spin-coupled model (7,8) but, in spite of the additional configurations, the resulting modern VB wave functions do remain straightforward to interpret directly.

At convergence of a single-configuration spin-coupled calculation, the active orbitals ϕ_μ satisfy separate orbital equations based on $(N-1)$–electron operators $\hat{F}_\mu^{eff}$ from which the particular occupied orbital has been excluded (9):

$$\hat{F}_\mu^{eff}\,\phi_\mu^{(i)} = \varepsilon_\mu^{(i)}\,\phi_\mu^{(i)}\,.$$

In this way, we obtain for *each* active electron a 'stack' of fairly compact orthonormal virtual orbitals $\phi_\mu^{(i)}$ that correspond closely to the physical situation in actual excited states. Virtual orbitals in different stacks may of course overlap with one another.

Excited configurations may be constructed by single, double (*etc.*) excitations from one or more reference functions, replacing occupied orbitals with their 'own' virtual orbitals. We refer to these as 'vertical' excitations. Additionally, we include 'ionic' configurations in which a virtual orbital is doubly occupied. Typically the dominant configuration for each low-lying state is considered as a reference configuration, but it is rejected if the effect on the final energies is not significant. The final SCVB wave functions for multiple states of a given symmetry are obtained from nonorthogonal CI calculations involving the reference and excited configurations (10). In general, we achieve a uniformly high level of accuracy for many states of one or more spatial symmetries and spin multiplicities over the entire range of nuclear coordinates. The final wave functions are very compact and it is straightforward to identify dominant 'atomic' contributions. The compactness

of the SCVB wave functions is also beneficial for the numerical computation of the required couplings.

The evaluation of rotational couplings (matrix elements of L_y) is entirely trivial, being conveniently done at the same time as we generate transition dipole moments between states of different symmetries. The most straightforward approach for obtaining the required $\partial/\partial R$ couplings between states of the same symmetry is numerical differentiation using separate SCVB calculations at nuclear separations $R+\delta$ and $R-\delta$. Overlap integrals between GTOs (calculated for the mean nuclear separation, R) are then used to form the quantity

$$\frac{\langle \Psi_i(\boldsymbol{r}|R-\delta) \,|\, \Psi_j(\boldsymbol{r}|R+\delta)\rangle}{2\delta},$$

where $\boldsymbol{r}$ represents the electronic coordinates. We find that the numerator of this expression varies linearly with δ over an extended range of values, so that we may often employ the same value of δ (typically $10^{-4}\,a_0$) for all crossings. Our simple 'central difference' approximation to $A_{ij}(R)=\langle \Psi_i|\partial/\partial R|\Psi_j\rangle$ neglects changes to the basis functions between $R+\delta$ to $R-\delta$; we find that the corresponding contribution to $A_{ij}(R)$ is small, but it can make the procedure numerically unstable. One reassuring check is that the computed couplings are relatively insensitive to the substitution of the overlap integrals with those evaluated for a nuclear separation of $R+\delta$ or $R-\delta$. Additionally, we always confirm that $\mathbf{A}(R)$ is skew-symmetric.

3 Scattering calculations

In order to solve the scattering problem, it proves convenient to avoid the sharp changes in the nonadiabatic couplings by transforming to the so-called p-diabatic representation in which the matrix elements of $\partial/\partial R$ are zero. Explicitly, we carry out a unitary transformation using the matrix $\mathbf{W}(R)$ which satisfies:

$$\frac{d\mathbf{W}(R)}{dR} + \mathbf{A}(R)\mathbf{W}(R) = \mathbf{0}$$

subject to

$$lim_{R\to\infty}\, \mathbf{W}(R) \to \mathbf{I}\,.$$

In practice, we obtain $\mathbf{W}(R)$ by taking many small steps δR:

$$\mathbf{W}(R_1-\delta R) = \exp(-\mathbf{A}(R_1)\,\delta R)\;\mathbf{W}(R_1) + O(\delta R)^2\,.$$

Expanding the exponential to first order tends not to preserve sufficiently well the unitarity of $\mathbf{W}(R)$ and so we have tended to use instead a 'half-step' propagation:

$$\mathbf{W}(R_1-\delta R) = [\mathbf{I} + \tfrac{1}{2}\,\mathbf{A}(R_1-\delta R)\,\delta R]^{-1}\,[\mathbf{I} - \tfrac{1}{2}\,\mathbf{A}(R_1)\,\delta R]\;\mathbf{W}(R_1)\,.$$

More recently, we have realized that it is usually sufficiently accurate simply to expand the exponential to second order, thereby avoiding matrix inversion:

$$\mathbf{W}(R_1-\delta R) = [\mathbf{I} - \mathbf{A}(R_1)\,\delta R + \tfrac{1}{2}\,[\mathbf{A}(R_1)\,\delta R]^2]\;\mathbf{W}(R_1)\,.$$

The cross sections are calculated using a fully-quantal close-coupling formalism (1). In the p-diabatic representation, in which $\mathbf{A}(R)$ is null, electron capture is driven by off-diagonal elements of the diabatic potential matrix $\mathbf{U}(R)$, which is independent of the orientation of $\boldsymbol{R}$. Introducing a partial-wave decomposition for the corresponding wave amplitudes leads to radial coupled equations for channels γ,γ':

$$\left[\frac{d^2}{dR^2} - \frac{l(l+1)}{R^2}\right] G_\gamma^{lm}(R) - 2\mu \sum_{\gamma'} [U_{\gamma,\gamma'}(R) - E\delta_{\gamma,\gamma'}] G_{\gamma'}^{lm}(R) = 0 .$$

The asymptotic forms $lim_{R\to\infty} G_\gamma^{lm}(R)$ lead directly to the S–matrix and thus to the cross sections. In practice, the coupled scattering equations are integrated using an implementation of the log-derivative method of Johnson (11). Zygelman *et al.* (1) have shown that the resulting cross sections do not depend on the choice of electronic coordinate origin along the internuclear axis, so that a treatment without so-called electron translation factors should be a valid approximation for low energy collisions.

Our combination of SCVB computations and fully-quantal scattering calculations has been applied successfully to numerous charge transfer systems, including N^{4+}/H (1,2), Si^{4+}/He (3), Si^{2+}/H (4), Si^{3+}/He (5) and, most recently, to collisions of various multiply-charged ions of S and O with neutral H or He targets. In general, we see good agreement with reliable experiments (when available) and with other high-level theoretical studies.

4 SCVB results for the N^{2+}/He system

We report here new calculations for the N^{2+}/He system, so as to illustrate various aspects of the SCVB methodology and to give an indication of the level of accuracy that may be achieved. The processes of interest are

$$N^{2+}(2s^2 2p; {}^2P^o) + He(1s^2) \rightarrow N^+(2s^2 2p^2; {}^{2S+1}L) + He^+(1s) .$$

Butler and Dalgarno (12) obtained overall charge transfer rates at the Landau-Zener level. Nikitin and Reznikov (13) calculated Landau-Zener cross sections for collision energies of 4 eV and 12 eV, using an empirical form for the diabatic potentials and associated couplings. More recently, Lafayatis *et al.* (14) reported Landau-Zener calculations of the cross sections, for energies between 0.01 eV and 1 keV, this time using *ab initio* potentials. For the $^2\Pi$ states, low energy collisions most heavily populate $N^+(^1D)$ via an 'outer crossing' whereas higher energy collisions most heavily populate the $N^+(^3P)$ state. Only the 'outer crossing' pertains to the $^2\Sigma^+$ states. This system is a little unusual in that it involves relatively few states.

Experimental cross sections are available for collision energies ranging from a few eV up to several keV (15). The calculations of Nikitin and Reznikov (13) and of Lafayatis *et al.* (14) both considerably overestimate the population of $N^+(^3P)$

relative to $N^+(^1D)$, with the discrepancy being largest at low collision energies. Using the electronic wave functions obtained by Lafayatis *et al.* (14), Sun *et al.* (16) evaluated charge transfer cross sections using a close-coupling formalism, constructing a particular diabatic representation by diagonalizing, at each value of R, the adiabatic transition dipole matrix. There remains substantial quantitative disagreement with experiment for the $N^+(^3P)/N^+(^1D)$ ratio at collision energies of a few eV. Fang and Kwong (17) measured the overall charge transfer rate coefficient at an equivalent temperature of $\sim 3.9\times10^3$ K in an ion trap. Their value was said to be in good agreement with the corresponding calculated value of Sun *et al.* (16).

To the best of our knowledge, fully *ab initio* calculations of the potential energy curves and $\partial/\partial R$ matrix elements, combined with a fully-quantal close-coupled determination of cross sections, has not yet been performed for this system. Such a study is now underway in our group. In this preliminary account, we report an overview of the SCVB calculations for this system.

With the $N(1s^2)$ core described by the lowest canonical MO taken from a 'five electrons in five orbitals' CASSCF calculation on the $1^2\Sigma^+$ state at 20 a_0, we carried out single-configuration five-electron spin-coupled calculations for each value of R. The spherical GTO basis set was based on Dunning's correlation consistent valence triple-zeta sets (cc–pVTZ) for N/He (18,19), consisting of (10s5p2d/6s2p1d) primitives contracted to [4s3p2d/3s2p1d]. The spin-coupled calculations, and the subsequent generation of virtual orbitals, were performed for the lowest $^4\Sigma^-$ state, so as not to introduce a bias towards either the $^2\Sigma^+$ or $^2\Pi$ manifolds in the SCVB calculations.

For the $^2\Sigma^+$ states, we carefully selected a set of 21 virtual orbitals (20). Vertical plus 'ionic' excitations (as described in Section 2) generated a total of 264 spatial configurations, or 435 symmetry-adapted VB structures, after taking account of all the different modes of spin coupling. The resulting adiabatic potential energy curves are shown in Figure 1 and the asymptotic energies are compared to the corresponding experimental values in Table I. The incoming channel experiences a sharp avoided crossing with the $N^+(^1D)/He^+$ channel at ~ 8.5 a_0 with an energy gap in the region of 4×10^{-4} hartree. The corresponding diabatic curves of Nikitin and Reznikov (13) cross at 8.65 a_0, whereas Lafayatis *et al.* (14) found the avoided crossing to be at nearly 9 a_0 with an energy gap of *ca.* 4×10^{-4} hartree. Our curves show a further avoided interaction, at shorter R, between the two N^+/He^+ channels.

We followed the same recipe for the $^2\Pi$ states, using for consistency exactly the same set of virtual orbitals. This generated 141 spatial configurations, which we augmented with 4 'cross excitations' into a He(1s) virtual orbital (20), so as to refine the description of the incoming 'neutral' channel. The final VB expansion consisted of just 509 VB structures. The resulting adiabatic potential energy curves are shown in Figure 1 and the asymptotic energies are compared to the corresponding experimental values in Table II.

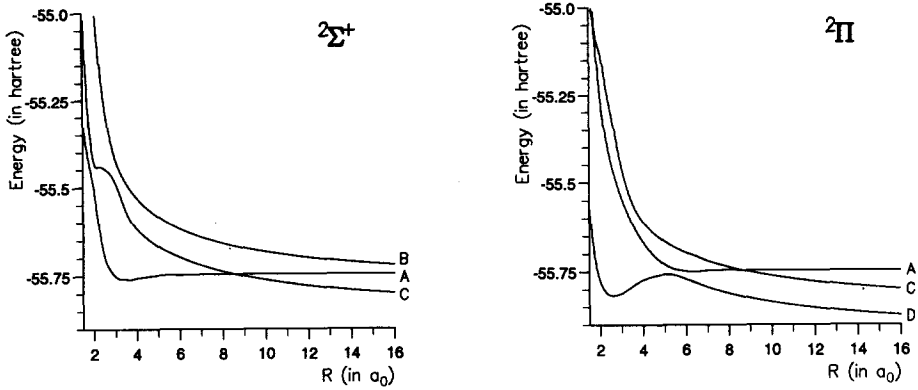

Figure 1. SCVB potential energy curves for the N^{2+}/He system. The asymptotes are labelled A=$N^{2+}(^2P^o)$/He, B=$N^+(^1S)$/He^+, C=$N^+(^1D)$/He^+ and D=$N^+(^3P)$/He^+.

TABLE I. Asymptotic energies (in eV) for $^2\Sigma^+$ states of the N^{2+}/He system.

Asymptote	Experiment	SCVB	Difference
$N^+(2s^22p^2;\,^1D) + He^+(1s)$	–3.12	–3.17	–0.05
$N^+(2s^22p^2;\,^1S) + He^+(1s)$	–0.97	–1.01	–0.04
$N^{2+}(2s^22p;\,^2P^o) + He(1s^2)$	(0)	(0)	(0)

TABLE II. Asymptotic energies (in eV) for $^2\Pi$ states of the N^{2+}/He system.

Asymptote	Experiment	SCVB	Difference
$N^+(2s^22p^2;\,^3P) + He^+(1s)$	–5.02	–5.13	–0.11
$N^+(2s^22p^2;\,^1D) + He^+(1s)$	–3.12	–3.13	–0.01
$N^{2+}(2s^22p;\,^2P^o) + He(1s^2)$	(0)	(0)	(0)

The incoming channel experiences a sharp avoided crossing with the $N^+(^1D)$/He^+ channel at ~8.6 a_0, which is again close to the Nikitin and Reznikov (13) value of 8.7 a_0 and a little less than the Lafayatis *et al.* (14) value of ~9 a_0. We find that the energy gap at this avoided crossing is on the order of 2×10^{-4} hartree. Lafayatis *et al.* (14) reported a value of 5×10^{-4} hartree, but given that their tabulated points are widely spaced, this is likely to be only a rough estimate. For our potentials, the 'inner crossing' with the $N^+(^3P)$/He^+ channel occurs near 5.5 a_0 with an energy gap

of *ca.* 1.7×10^{-2} hartree. Lafayatis *et al.* (14) report much the same values. The diabatic potentials of Nikitin and Reznikov (13) cross at 5.4 a_0.

We find that the calculated $1^2\Sigma^+$ and $2^2\Pi$ adiabatic states are asymptotically degenerate to within 0.028 eV, and that the $3^2\Sigma^+$ and $3^2\Pi$ states are asymptotically degenerate to within 0.015 eV. Taking orbitals from a prior MCSCF calculation, the sets of configurations in the CI expansions of Lafayatis *et al.* (14) consisted of all single and double excitations from a full-valence CASSCF reference. Such a procedure resulted in 14,435 configurations of $^2\Sigma^+$ symmetry and 23,169 of $^2\Pi$ symmetry, and provided asymptotic energy splittings that were not more than 0.12 eV from experiment.

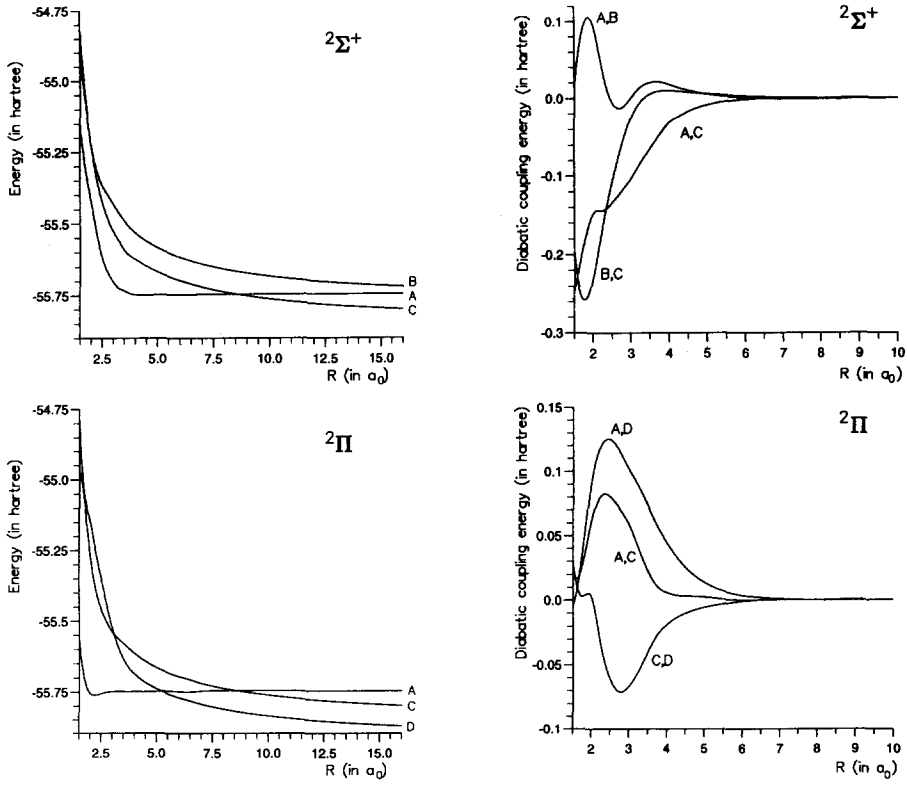

Figure 2. Diabatic potentials and couplings for the N^{2+}/He system. The channels are labelled A=$N^{2+}(^2P^o)$/He, B=$N^+(^1S)$/He^+, C=$N^+(^1D)$/He^+ and D=$N^+(^3P)$/He^+.

The required nonadiabatic couplings $A_{ij}(R)=\langle\Psi_i|\partial/\partial R|\Psi_j\rangle$ were calculated as described in Section 2 and all of the SCVB molecular data were transformed to the

p-diabatic representation according to the procedure outlined in Section 3. The resulting diabatic potentials and couplings (*i.e.* off-diagonal elements of the potential matrix) are shown in Figure 2. Fully-quantal scattering calculations are in progress; it remains to be seen whether the current potentials and couplings will lead to good agreement with experiment, especially for the $N^+(^3P)/N^+(^1D)$ ratio.

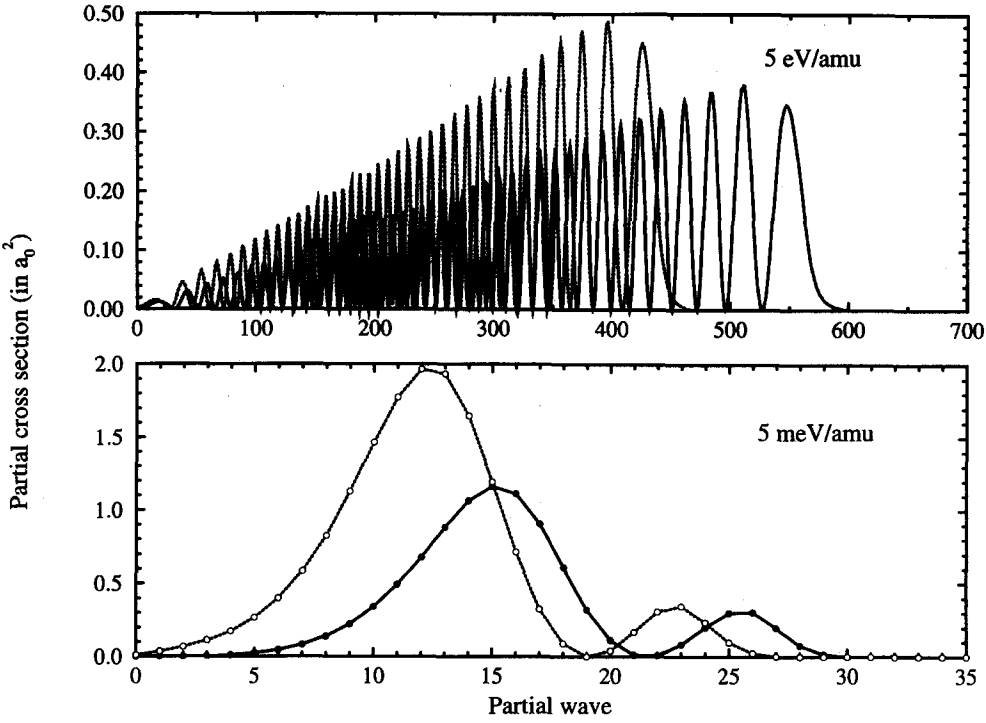

Figure 3. Partial cross sections for capture into $Si^{2+}(3s^2)$ from $Si^{3+}(3s)$ for ^4He (—) and ^3He (...) targets at collision energies of 5 eV/amu and 5 meV/amu.

5 Target isotope effects

Stancil and Zygelman (21) have derived a simple formula, based on the Landau-Zener approximation, for the influence of a kinematic isotope effect on low-energy total charge transfer cross sections. Their predictions have since been verified for various systems. Taking as a representative example the electron capture into

$Si^{2+}(3s^2)$ from $Si^{3+}(3s)$, the ratio of cross sections for ^3He and ^4He targets is given by:

$$\frac{\sigma(^3He)}{\sigma(^4He)} \approx \frac{1-2V/(\mu(^3He)v^2)}{1-2V/(\mu(^4He)v^2)}$$

where V is the diabatic potential for the entrance channel at the crossing point, v is the collision velocity in the centre-of-mass frame, and $\mu(^nHe)$ is the reduced mass of the $SiHe^{3+}$ quasimolecule based on isotope ^nHe. For this system (5), we find from the fully-quantal treatment that $\sigma(^3He)$ exceeds $\sigma(^4He)$ by 2% at ~0.5 eV/amu and by ~30% at 0.01 eV/amu. At higher collision energies (expressed in eV/amu), the ^4He target partial cross sections are ~25% smaller than those for the ^3He target, but the number of contributing partial waves is approximately 25% greater (see the top frame of Figure 3); overall, the cross section is independent of the target mass. The enhancement of $\sigma(^3He)$ over $\sigma(^4He)$ at lower collision energies can be seen to arise from an incomplete cancellation of these two factors, as shown in the bottom frame of Figure 3.

6 Final remarks

These days, our applications of the spin-coupled approach, and of its various multiconfigurational variants, tend to be concerned mostly with qualitative interpretations of the behaviour of correlated electrons in molecules. For example, a particularly fruitful area for recent work has been to examine the evolution of electronic structure that accompanies changes in geometries and total energies along a reaction coordinate. Underpinning all of this work is the ability of such modern VB approaches to provide useful accuracy with very compact wave functions that are easy to interpret directly. Our SCVB studies of charge transfer systems are of significant interest in themselves, because of their relevance to astrophysical and terrestrial plasmas, but serve also as a timely reminder of the level of accuracy that may be achieved with this type of approach.

Our future work on charge transfer collisions will concentrate on fine-structure effects and on polyatomic targets, which present a whole new range of challenges for the type of methodology presented here.

References

1 Zygelman, B.; Cooper, D.L.; Ford, M.J.; Dalgarno, A.; Gerratt, J.; Raimondi, M. *Phys. Rev. A* **1992**, *46*, 3846.

2 (a) Jamieson, M.J.; Cooper D.L.; Zygelman, B. *J. Phys. B.* **1994**, *27*, L73.
(b) Stancil, P.C.; Zygelman, B.; Clarke, N.J.; Cooper, D.L. *J. Phys. B.*

1997, *30*, 1013. (c) Zygelman, B.; Stancil, P. C.; Clarke, N. J.; Cooper, D. L. *Phys. Rev. A* **1997**, *56*, 457.

3 Stancil, P. C.; Zygelman, B.; Clarke, N. J.; Cooper, D. L. *Phys. Rev. A* **1997**, *55*, 1064.

4 Clarke, N. J.; Stancil, P. C.; Zygelman, B.; Cooper, D. L. *J. Phys. B* **1998**, *31*, 533.

5 Stancil, P. C.; Clarke, N. J.; Zygelman, B.; Cooper, D. L. *J. Phys. B* **1999**, *32*, 1523.

6 (a) Gerratt, J. *Adv. Atom. Mol. Phys.* **1971**, *7*, 141. (b) Gerratt, J.; Cooper, D. L.; Karadakov, P. B.; Raimondi, M. *Chem. Soc. Rev.* **1997**, *26*, 87.

7 (a) Thorsteinsson, T.; Cooper, D. L.; Gerratt, J.; Karadakov, P. B.; Raimondi, M. *Theor. Chim. Acta* **1996**, *93*, 343. (b) Cooper, D. L.; Thorsteinsson, T.; Gerratt, J. *Int. J. Quant. Chem.* **1997**, *65*, 439. (c) Cooper, D. L.; Thorsteinsson, T.; Gerratt, J. Adv. Quant. Chem. **1998**, *32*, 51.

8 Thorsteinsson, T.; Cooper, D. L. In "Quantum Systems in Chemistry and Physics." Hernández-Laguna, A.; Maruani, J.; McWeeny, R.; Wilson, S., Eds.; Kluwer: Dordrecht, 2000; Vol. I, 303-326.

9 Gerratt, J.; Raimondi, M. *Proc. Roy. Soc. (Lond.) A*, **1980**, *371*, 525.

10 See, for example: Cooper, D. L.; Gerratt, J.; Raimondi, M. *Chem. Rev.* **1991**, *91*, 929

11 Johnson, B. R. *J. Comput. Phys.* **1973**, *13*, 445.

12 Butler, S. E.; Dalgarno, A. *Astrophys. J.* **1980**, *241*, 838.

13 Nikitin, E. E.; Reznikov, A. I. *Mol. Phys.* **1992**, *77*, 563.

14 Lafayatis, G. P.; Kirby, K.; Dalgarno, A. *Phys. Rev. A* **1993**, *48*, 321.

15 (a) Sato, Y.; Moore, J. H. *Phys. Rev. A* **1979**, *19*, 95. (b) Sharma, S.; Awad, G. L.; Hasted, J. B.; Mather, D. *J. Phys. B* **1979**, *12*, L163. (c) Lennon, M.; McCullough, R. W.; Gilbody, H. B. *J. Phys. B* **1983**, *16*, 2119. (d) Hormis, W. G.; Kamber, E. Y.; Hasted, J. B. *Int. J. Mass Spectrom. Ion Processes* **1986**, *69*, 211. (d) Sadilek, M.; Vancura, J.; Farnik, M.; Herman, Z. *Int. J. Mass Spectrom. Ion Processes* **1990**, *100*, 197. (e) Burns, D.; Thompson, W. R.; Greenwood, J. B.; McCullough, R. W.; Geddes, J.; Gilbody, H. B. *J. Phys. B* **1997**, *30*, 4559.

16 Sun, Y.; Sadeghpour, H. R.; Kirby, K.; Dalgarno, A. *Int. Rev. Phys. Chem.* **1996**, *15*, 53.

17 Fang, Z.; Kwong, V. H. S. *Astrophys. J.* **1997**, *474*, 529.

18 Dunning, T. H., Jr. *J. Chem. Phys.* **1989**, *90*, 1007.
19 Woon, D. E.; Dunning, T. H., Jr. *J. Chem. Phys.* **1994**, *100*, 2975.
20 Clarke, N. J. Ph.D. Thesis; Liverpool University, UK, 1995.
21 Stancil, P. C.; Zygelman, B. *Phys. Rev. Lett.* **1995**, *75*, 1495.

AB INITIO PROGRAM FOR TREATMENT OF RELATED SYSTEMS. TRANSFERABLE QUANTITIES OF LOCALIZED MOLECULAR ORBITALS

C. Kozmutza[1(*)], E. Tfirst[2] and I. G. Csizmadia[3]

[1]Department of Theoretical Physics, Institute of Physics, Technical University of Budapest, Budafoki út 8. H-1111, Budapest, Hungary
[2]Institute of Chemistry, Chemical Research Center, Hungarian Academy of Sciences, Pusztaszeri út 59-67 H-1025, Budapest, Hungary
[3]Department of Chemistry, University of Toronto, M5S1A1, Toronto, Canada

ABSTRACT

It is well known that transferability is an important property for the investigation of related systems. In cases when one can define quantities for molecular parts, which are additive and transferable, certain similarities of different molecules can be simply recognized. One-electron properties, as electric moments or kinetic energy contributions derivable from transferable/localized molecular orbitals, are especially useful for the above purpose.

In this paper we demonstrate, that these quantities are convenient for studying not only extended molecules, but weakly interacting systems as well.

LIST OF CONTENTS

*Corresponding author; e-mail: kozmutza@phy.bme.hu

ADVANCES IN QUANTUM CHEMISTRY, VOLUME 40

0065-3276/01 $35.00

1. INTRODUCTION

The transferability of certain molecular properties are considered as a long established fact. The bond energies, e.g., are transferable in certain related systems (aliphatic hydrocarbons, etc.).

The transferability can be interpreted in different ways. The localized orbitals of small molecules can be used for constructing the wavefunction of related larger molecules (without further optimization). The orbitals are considered transferable if some molecular properties calculated with and without additional optimization are close together [1]. One can interpret transferability using the properties of the individual orbitals [2]. The properties of orbitals of the same type are compared in this case in different environments.

It is known, that in the framework of the independent particle model the one-electron properties of the system can be written as the sum of contributions from the individual orbitals. The transferability of the one-electron properties is implied by the transferability of the orbitals. The first and higher order electric moments determined for localized molecular orbitals (LMOs) in different systems can thus be used in comparative studies.

In this work we discuss the transferability properties of certain quantities related to the LMOs. Beside the one-electron electric moments certain one-electron energy contributions are also investigated. The actual calculations were performed on some ten- and eighteen-electron systems. The transferable quantities are investigated on a series of saturated hydrocarbons, too. The possibility of using the electric moments obtained for LMOs will also be presented.

Weakly interacting systems — as is implied by their name — are expected to change only to certain extent in the complex formation. Using some one-electron quantities (including those related to LMOs) comparative studies can thus be done by exploiting transferability.

2. LOCALIZATION OF MOLECULAR ORBITALS

2.1. Methods for localization

It was the hope that by the introduction of localized molecular orbitals (LMOs) one can come closer to chemical intuition, to understand the transferability and it will also lead to a convenient study of the electron correlation. The „localization" of electron density in many atomic system was dealt mainly by the method of the independent particle model. Most of studies refer to closed shell systems, although open shell structures were also investigated.

In order to prepare LMOs, several methods have been elaborated in the past thirty of years. The methods can be divided into two groups, depending on the

criteria used: internal and external localization methods can be distinguished. The methods of the first group arrive to LMOs by a suitable transformation of the canonical orbitals (= internal localization criterion). As to the methods which use certain external localization criterion, certain further restrictions are to be taken into consideration. The methods which transform the Hartree-Fock operator, are called direct (internal) methods. An interesting method was provided by using statistical consideration (= loge theory).

The method of Edmiston and Ruedenberg is based on the generalization of equivalent orbitals [3-5]. It is known that a one-determinant wavefunction for closed-shell system is invariant (to a phase factor of unity) to any unitary transformation of the $\{\varphi_i\}$ canonical molecular orbitals (CMOs). As both the Coulomb and the exchange interaction energy terms contain the same

$$D\{\varphi\} = \sum_i \langle \varphi_i^2 | r_{12}^{-1} | \varphi_i^2 \rangle$$

quantity, a suitable **U** transformation can be chosen for finding a maximal value for $D\{\varphi\}$. The orbitals obtained in this procedure, $\{\bar{\varphi}_i\}$, are also called energy localized molecular orbitals. The $D\{\bar{\varphi}\} = \max$ relation can be interpreted as the concentration of the molecular orbitals to certain spatial region to a maximal extent.

As to the practical consideration, the transformation procedure of the Edmiston-Ruedenberg method requires the matrix transformation of N^4 elements (in a $2N$ electron system). This tiresome work is in certain cases an obstacle to a more widely use of the above method.

The elaboration of the so-called exclusive orbitals was proposed by Foster and Boys [6]. This idea was modified by Boys whose method is often used when producing LMOs. In the procedure of Boys the criterion for finding localized molecular orbitals using a convenient unitary transformation is as follows: the $\eta = \sum_{i \neq j} |\mathbf{r}_i - \mathbf{r}_j|$, i.e. the distances of the centroids of charge vectors of the orbitals should be the maximal [7]. A maximal value for η is equivalent to the criterion that the quadratic self-repulsion of the orbitals will be the maximal:

$$\sum_i \langle \bar{\varphi}_i^2 | r_{12}^2 | \bar{\varphi}_i^2 \rangle = \max .$$

One can notify, that using the method of Boys, the matrix of N^2 elements (representing the first order moment operator) should be transformed [8]. This advantageous property is one of the reasons why the Boys' method is often used for preparing LMOs.

The method of charge-localization (or density localization) is also based on the unitary transformation of the canonical molecular orbitals [9,10]. The electron density corresponding to a one-determinant wavefunction has the form

$$\rho = 2\sum_i |\varphi_i|^2 \ .$$

In cases of LMOs, the $|\varphi_i|^2$ term is the contribution of the orbital charge density. Between localized charge densities the „charge-overlap" is small, localization criterion is, therefore, chosen to minimize the $\sum_{i\neq j}\left\langle |\varphi_i|^2 \middle| |\varphi_j|^2 \right\rangle$ expression, or (an alternative/equivalent choice) to maximize the $\sum_i \left\langle \varphi_i^2 \middle| \varphi_i^2 \right\rangle$ term, respectively. The charge localized method was used successfully also in the study of extended systems [11-15].

Localized orbitals can be obtained directly, too, as the solutions of a modified eigenvalue problem obtained by changing the HF operator. Adams' direct localization method is based on the assumption that the basis functions (which are linearly independent and normalizable) are not obligatory orthogonal to each other [16-18]. To obtain localization, the above degree of liberty is used.

The direct method of Gilbert leads to a special eigenvalue problem by the introduction of a so-called localization potential [19]. The solutions of the equation corresponding to the above problem provide directly the localized orbitals. This method is of theoretical interest, as using the formalism of the localization potential all of localization methods can be interpreted in a common way. The various localization criteria correspond to functionals of extreme value problems. These latters can be solved by using the variation method, and the solutions are the best localized orbitals (corresponding to a given localization criterion).

An external localization method was proposed by Magnasco and Perico [20,21]. The localization criterion equals the maximization of the atomic population, obtained by using the Mulliken population analysis. The number of localized orbitals as well as their association to a given atom should be defined in advance.

The method of Peters starts with approximative orbitals, and then the localized orbitals are prepared one after one, using an iterative procedure [22].

The loge theory proposes to divide the spatial region into cells. These latters are determined by maximizing the probability for that a given number of electrons be in a given cell [23-25]. One can also minimize the „missing information" about the system (containing the cells).

A recently often used practical method is that of proposed by Pipek and Mezey [26]. Their intrinsic localization is based on a special mathematical measure of localization. It uses no external criteria to define a priori orbitals. The method is similar to the Edmiston-Ruedenberg's localization method in the σ-π separation of the orbitals while it works as economically as the Boys' procedure. For the application of their localization algorithm, the knowledge of atomic overlap integrals is sufficient. This feature allows the adoption of their algorithm for both ab initio and semiempirical methods. The implementation of the procedure in existing program systems is easy, and this property makes the Pipek-Mezey's method very attractive for practical use.

One of the most carefully defined and useful method is that introduced by Saebo and Pulay [27-29]. Their local (correlation) method — as its name suggests — has been elaborated for treating electron correlation in a straightforward manner. The method is designed — as most of other localization methods — for closed shell systems. The internal, strongly occupied canonical orbitals are first localized using a standard localization technique. They apply the Boys' or the Pipek-Mezey procedure. For the external, virtual orbitals, atomic basis functions are used, projected against the occupied canonical orbitals. One of the attractive features of the localized correlation method is the significant computational saving [30-31]. It was pointed out, furthermore, that with increasing basis set the arbitrary nature of the neglect of contributions is decreasing.

The above methods were elaborated for molecules aiming a) a suitable study of systems while taking into consideration the chemical intuition and b) to promote a later, simpler investigation of more extended systems. Beside the procedures discussed in detail, the work on localization methods and their applications on various systems is continuous [32-39]. Some special use of LMOs will be presented in this review, too.

There is another field where the localization can be helpful, this is the study of weakly interacting atomic and molecular systems. In these complexes not only the localized units but especially their transferability makes possible a convenient study. In these systems, furthermore, the application of a localization procedure does not necessarily means the localization of the electron density into small spatial regions. The localizability in these cases can be interpreted as the concentration of the charge density corresponding to the spatial region of the interacting monomers. The regions in these cases are not as small as for molecules as the bond and lone pair LMO densities corresponding to the chemical intuition. The separation of the charge densities in weakly interacting systems into points from the contributing monomers, however, makes it possible that the electron densities might be compared to those obtained in the non-interacting monomers. Deviations from transferability are expected to reflect polarizational effects.

The essence of this method (separation of molecular orbitals (SMOs) [40]), as follows from the above, lies in obtaining the „closest possible" wavefunctions in

the complex as well as in the monomers. It is evident that the canonical representation offers a good choice for this purpose as the canonical molecular orbitals can be obtained directly by solving the HF equations. In some studies for a comparison of quantities obtained for the contributing monomers, further decomposition (toward more localized electron densities, e.g.) might also be required. In these cases SMOs are still obtained as unitary transforms of CMOs in the complex, these SMOs can be derived, however, by using the monomers' LMOs in the transformation. The transformation applied which aims to produce SMOs can thus be described as CMO → SMO or LMO → SMO procedure, respectively.

2.2. The localizability

The adoption of different localization criteria does not lead to equivalent orbitals, as the given procedure usually applies iterative method. The iteration is repeated until the criterion chosen is fulfilled. In spite of this, LMOs obtained by different algorithms are quite similar. This similarity increases the hope, that a) the LMOs imply a serious, general (even interpretative) significance in the study of molecular electronic structure and b) the use of LMOs (especially their transferability property) might be helpful in studying extended/weakly interacting systems.

It should be noted that the localization criteria applied do not lead to uniformly defined LMOs in each cases, in any system. It was pointed out for the molecule of F_2 and later to the C_6H_6 molecule, that the LMOs obtained belong to an infinite group of „equally localized" orbitals. This phenomenon is named continuous degeneracy, explanation was given by W. England using the group theory. It was, namely, pointed out, that the criteria of unique localization can be given by the symmetry properties and the group theory.

Another question is the degree/the extent of localization. It is well known, that although the localized orbitals describe the electron density concentrated in certain spatial region, this localization is (far) not perfect. The overlap remains and is not negligible between LMOs. It is evident that the so-called core LMOs overlap significantly with both the bond- and the lone-pair LMOs, belonging to the same atomic center. It is another question that — owing to the small „extent" of core LMOs — the core electron densities can be neglected in certain studies. The separation of the bond- and lone-pair electron densities is necessary; their study has been the subject of several works. The localizability can be measured as the magnitude of the interaction between LMOs belonging to the same (central) atom. This measure is often performed by comparing the orbital interactions between CMO and LMO densities, respectively.

Concerning the energy localized methods, their localizability can be defined by using the $J = \sum_i \langle \varphi_i^2 | r_{12}^{-1} | \varphi_i^2 \rangle$ quantities, obtained for CMOs (=J(CMO)) and LMOs (=J(LMO)). The change

$$J_{CL} = J(\text{LMO}) - J(\text{CMO}) > 0$$

or relative change $J_{CL}/J(\text{CMO})$ can be measured. The exchange interaction

$$K = 2\sum_{i \neq j} \langle \varphi_i \varphi_j | r_{12}^{-1} | \varphi_j \varphi_i \rangle$$

can also be used for the above purpose: the $K_{CL} = K(\text{CMO})/K(\text{LMO})$ ratio represent a localizability. The K_{CL} quantity in this form depends strongly on the number of electrons. The values for K_{CL} divided by the total energy (TE) or the two-electron energy (E2), represent a systematic measure for the localizability (see Table 1 and Figure 1).

Figure 1. Localizability calculated for certain ten-electron hydrides

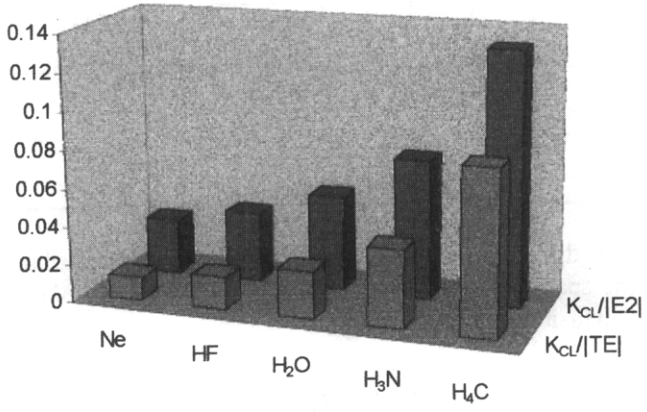

Table 1. Localizability calculated for certain ten-electron hydrides

	J_{CL}	J_{CL}/J(CMO)	K_{CL}	K_{CL}/K(CMO)	$K_{CL}/\|TE\|$	$K_{CL}/\|E2\|$
Ne	0.7486	0.0741	1.5950	1.5913	0.0124	0.0295
HF	0.6692	0.0757	1.7000	2.0933	0.0170	0.0374
H_2O	0.6260	0.0817	1.9102	2.9061	0.0251	0.0504
H_3N	0.6146	0.0931	2.3091	4.2517	0.0411	0.0733
H_4C	0.7212	0.1305	3.4301	6.7522	0.0854	0.1321

Table 2. Separability of LMO densities. Values of S''_{ij} (first entries) and S''_{ij} (second entries) (see text). c=core, b=bond, l=lone-pair

	CH_4	NH_3	H_2O	HF	Ne
c,c	1.000	1.000	1.000	1.000	1.000
	7.560	12.377	18.942	27.480	38.289
b,b	1.000	1.000	1.000	1.000	-
	0.046	0.063	0.087	0.125	-
l,l	-	1.000	1.000	1.000	1.000
	-	0.081	0.130	0.201	0.298
c,b	0.180	0.193	0.205	0.216	-
	0.023	0.042	0.074	0.122	-
c,l	-	0.227	0.240	0.250	0.262
	-	0.062	0.107	0.172	0.265
b,l	-	0.499	0.528	0.547	-
	-	0.013	0.024	0.040	-
b,b'	0.404	0.443	0.477	-	-
	0.005	0.010	0.017	-	-
l,l'	-	-	0.582	0.597	0.607
	-	-	0.031	0.052	0.082

An interesting direct measure for localizability can be obtained by the calculation of the spatial overlap of LMOs. Integrating the absolute value of the product of LMO densities

$$S'_{ij} = \int |\varphi_i^*(\mathbf{r})\varphi_j(\mathbf{r})| d\tau$$

a $0 \le S'_{ij} \le 1$ bounded quantity can be obtained, which describes the separability of the orbitals. Using the criterion of the charge localization, the localizability of orbitals can be given by comparing the

$$S''_{ij} = \int |\varphi_i(\mathbf{r})|^2 |\varphi_j(\mathbf{r})|^2 \, d\tau$$

values determined for both canonical and localized orbitals, respectively. This expression gives the matrix elements of δ-function interaction operator.

The values calculated for some ten-electron hydrides are collected in Table 2. Some S' and S'' values are also presented in Figure 2. These values show that several expectations can be affirmed concerning the spatial separation of CMO densities. For example, the increase in S' values shows the increasing atomic charge going from C to Ne. It should be emphasized that the localizability of the electron density is often worthwhile studying, especially when related systems are investigated. This conclusion holds both for extended and for weakly interacting systems, respectively.

Figure 2. Values of S'_{ij} and S''_{ij} for some ten-electron systems. c=core, b=bond, l=lone-pair

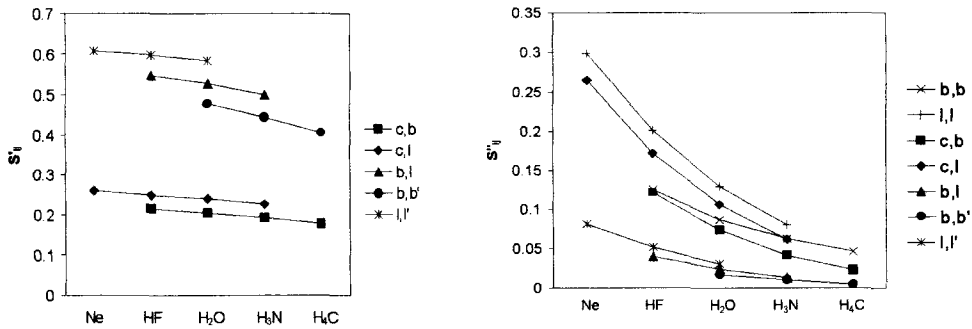

3. ELECTRIC MOMENTS FOR LMO DENSITIES

3.1. The multipole electric moments

The charge distribution of a quantum mechanical system can be expanded in terms of its multipole electric moments. The zeroth order moment is the total charge Z

$$Z = \sum_i e_i \,. \tag{1}$$

The first order electric moment is named the dipole moment μ

$$\boldsymbol{\mu} = \sum_i e_i \mathbf{r}_i \,. \tag{2}$$

The electric moments are not invariant under a shift of the origin of the coordinate system. The first non-vanishing moment is however usually independent of the choice of the coordinates. The origin of coordinate system is thus often chosen as the center of gravity or the center of the charge distribution.

In case of molecules the first order electric moments can be expressed in the following way (in atomic units):

$$\mu_u^{\mathrm{e}} = -\sum_{i=1}^{N} \langle \Phi | r_{ui} | \Phi \rangle, \qquad u = x, y, z, \tag{3}$$

where Φ denotes the eigenfunction of the system (N is the number of electrons). The contributions of the nuclei

$$\mu_u^{\mathrm{n}} = \sum_{a=1}^{n} Z_a \delta(r_u - r_{ua}) r_u \qquad u = x, y, z \tag{4}$$

are determined by the position ($\mathbf{r}_a$) and the charge (Z_a) of nuclei. The total dipole moment of a molecular system is obtained by summing (3) and (4), in all of three coordinate directions:

$$\boldsymbol{\mu} = \boldsymbol{\mu}^{\mathrm{e}} + \boldsymbol{\mu}^{\mathrm{n}} \,. \tag{5}$$

In the framework of the one-determinantal approximation of the independent particle model the first order properties can be written by summing the corresponding contributions. The electric moments can thus also be written as the sum of contributions from the individual orbitals. The first order moments will then have the following form:

$$\mu_u^{\mathrm{e}} = \sum_{k=1}^{N} \mu_u^{\mathrm{e}}(k) = -\sum_{k=1}^{N} \langle \varphi_k | r_u | \varphi_k \rangle = -\sum_{k=1}^{N} r_u(k), \qquad u = x, y, z \tag{6}$$

where φ_k denotes the k-th one-particle function. Having been subjected the orbitals to a unitary transformation (symmetry transformation, e.g.):

$$\bar{\varphi}_j = \sum_{k=1}^{N} U_{jk} \varphi_k \text{ for all } j, \qquad j = 1, N \tag{7}$$

the individual components $r_u(k)$ change but their sum μ^e remains invariant. The first order moments can be called the centroids of charge. More precisely the centroid length for $\bar{\varphi}_k$ are the scalar quantity $|\mathbf{r}(k)|$ and by the name centroid the endpoint of the vector $\mathbf{r}(k)$ is meant.

There are several different definitions for the second order electric moments. In order to be consistent with the above, the quadrupole moment is defined in a similar way:

$$\mathbf{Q} = \sum_i e_i r_i \circ r_i \,, \tag{8}$$

where $\mathbf{Q}$ is the quadrupole tensor with nine components. The definition of a traceless tensor Θ is often used:

$$\Theta = \frac{1}{2}\sum_i e_i \left(3r_i \circ r_i - r_i^2\right) \tag{9}$$

and so the sum of the diagonal elements of Θ is zero:

$$\Theta_{xx} + \Theta_{yy} + \Theta_{zz} = 0 \,. \tag{10}$$

For a cylindrically symmetric charge distribution the following relations hold:

$$-2\Theta_{xx} = -2\Theta_{yy} = \Theta_{zz} \,. \tag{11}$$

The scalar quantity Θ_{zz} ($\equiv \Theta$) is simply referred to as the quadrupole moment. $\mathbf{Q}$ and Θ are symmetric. The components of the tensor $\mathbf{Q}$ can be related to the components of Θ:

$$\Theta_{uv} = \frac{1}{2}\left(3Q_{uv} - \delta_{uv}\sum_w Q_{ww}\right). \tag{12}$$

In case of molecular systems the quadrupole moment components for the electrons as well as for the nuclei can easily be determined. The second order moment components of electrons can be defined as follows (in atomic units):

$$Q_{uv}^e = -\sum_{i=1}^{N} \langle \Phi | r_{ui} r_{vi} | \Phi \rangle \,, \qquad u,v = x,y,z \,. \tag{13}$$

The meaning of r_{ui}, r_{vi} and Φ are the same as given above. The quadrupole moment components of nuclei can be expressed as

$$Q_{uv}^{n} = \sum_{a=1}^{n} Z_a \delta(r_u - r_{ua}) \delta(r_v - r_{va}) r_u r_v , \qquad u,v = x,y,z . \tag{14}$$

The sum of (13) and (14) will yield the components of the total quadrupole moment of the system. In actual calculations a coordinate system fixed with respect to the center of charge distribution is convenient.

In case of localized densities the centroid of the individual orbitals can be taken as the center of the quadrupole tensor. Due to the shifting the values of components will change. For a given localized orbital, $\bar{\varphi}_k$, the components $\bar{Q}_{uv}(k)$ could thus be determined in the following way:

$$\bar{Q}_{uv}(k) = \left\langle \bar{\varphi}_k \left| [r_u - r_u(k)][r_v - r_v(k)] \right| \bar{\varphi}_k \right\rangle , \qquad u,v = x,y,z , \tag{15}$$

where $r_u(k)$ and $r_v(k)$ are the components of centroid vector of orbital $\bar{\varphi}_k$ and the index e is omitted for clarity. These shifted components define a quadrupole moment tensor **Q** for the individual localized orbital.

The above moments of a charge distribution can be related to the statistical moments of random variables. The orbital centroid vector is namely identical to the central first moment $M(\xi)$ of a random variable ξ with density function $p(x)$:

$$M(\xi) = \int_{-\infty}^{\infty} x p(x) dx . \tag{16}$$

Similarly, the definition of each diagonal element of the orbital second-moment tensor is formally identical to that of the statistical central second moment, m_2:

$$m_2 = D^2(\xi) = \int_{-\infty}^{\infty} p(x)[x - M(\xi)]^2 dx , \tag{17}$$

where $D(\xi)$ is the standard deviation of ξ. Hence the centroid lengths and the elements of the diagonal quadrupole tensor are often denoted by $\langle r \rangle$, $\langle x'^2 \rangle$, $\langle y'^2 \rangle$ and $\langle z'^2 \rangle$, respectively.

For the standard deviation, $D(\xi)$, the following inequality holds (Bienaymé-Chebyshev theorem):

$$P\left(\left|\xi - M(\xi)\right| > \lambda D\right) \leq \frac{1}{\lambda^2}, \qquad \lambda \geq 1. \tag{18}$$

The expression $P\left(\left|\xi - M(\xi)\right| > \lambda D\right)$ denotes the probability that $\left|\xi - M(\xi)\right|$ is larger than λ times the standard deviation. Taken $\lambda = 2$ as an example, then according to the above inequality, the probability that ξ lies within the range $-2D(\xi) \leq \xi \leq 2D(\xi)$ is at least 0.75. For $0 \leq \lambda \leq 1$ the inequality still remains valid. When the probability function is Gaussian,

$$P\left(\left|\xi - M(\xi)\right| > D\right) = 0.3174\ldots \tag{19}$$

value can be obtained.

Although the above inequality is not „sharp", it gives some limiting value of the dispersion of random variable ξ, even if its distribution function is not explicitly known. A similar relation applies to the eigenvalues $\langle x'^2 \rangle_i, \langle y'^2 \rangle_i, \langle z'^2 \rangle_i$ of the LMO second-moment tensor, hence, those are analogues of the statistical squared standard deviations. One thus can conclude that, in principle, the main features of the spatial extension of LMO's can be described by the first and second moments of their charge distribution. Hence the changes in the above moments are in relation with the change in the chemical environment of the given LMO.

We note that the first and second moments of an LMO are the coefficients of the expansion of the electrostatic potential of the studied LMO in powers of $1/R$ (see later in section 5.1).

3.2. Results obtained for some ten- and eighteen electron molecules

The first order electric moments obtained for bond and lone pair electron densities using Edmiston-Ruedenberg localization method are summarized in Table 4 and the geometry of the studied systems are presented in Table 3. The origin of $\langle r \rangle$ is taken at the corresponding heavy atom nucleus. The values presented for CH bonds are those referring to the bonds lying in the mirror plane. The results clearly show a) some regularities for bond and lone pair LMOs, b) certain transferable characteristics for LMOs in related systems. It is also remarkable that these main features are valid for both sp/s and spd/s type basis

sets, respectively. Similar relationships, thus similar conclusion holds for the second order electric moments (Table 5).

Table 3. Geometrical parameters for the studied molecules[a]

	Bond lengths (a.u.)	**Bond angles (degree)**
H_2O	OH = 1.809	HOH = 104.52
NH_3	NH = 1.912	HNH = 106.69
CH_4	CH = 2.066	HCH = tetr.
CH_3CH_3	CH = 2.066 CC = 2.890	HCH = 109.7
CH_3NH_2	CH = 2.066 CN = 2.786 NH = 1.916	HCH = 109.5 HNH = 105.8 CNH = 112.2 tilt = 3.5
CH_3OH	CH = 2.069 CO = 2.699 OH = 1.814	HCH = 109.5 COH = 109 tilt = 3.3

[a]Interatomic Distances, Special publications No. 11 and No. 18. London: The Chemical Society 1958 and 1965

Table 4. First order electric moments $\langle r \rangle$ for some selected LMO densities (given in a.u.)[a]

	Basis I.	**Basis II.**
OH / H_2O	0.9780	0.9892
NH / NH_3	1.1478	1.1615
CH / CH_4	1.3613	1.4021
CH / CH_3CH_3	1.3778	1.4093
CH / CH_3NH_2	1.4034	1.4341
	1.3727	1.4011
CH / CH_3OH	1.3933	1.4287
	1.3767	1.4065
O lone / H_2O	0.6053	0.5870
O lone / CH_3OH	0.6031	0.5823
N lone / NH_3	0.7129	0.6859
N lone / CH_3NH_2	0.7011	0.6737
CC bond in CH_3CH_3	1.4450	1.4450

[a]Basis I: sp/s type as used in Kapuy, E., Kozmutza, C., Daudel, R., Stephens, M.E.: Theoret.Chim.Acta **53**, 147 (1979)
Basis II: spd/s type (6-31G/d) Hariharan, P.C., Pople, J.A.: Theoret.Chim.Acta **28**, 211 (1973)

The values are expected not much changing when going to large extended molecules and/or weakly interacting systems. The values are, namely, so characteristic for the different types of orbitals that small geometry changes might not alter their significance.

Table 5. Second order electric moments in the main axis $\langle z'^2 \rangle^{1/2}$ (in a.u.)[a]

	Basis I.	**Basis II.**
OH / H_2O	0.9634	0.9721
NH / NH_3	1.0276	1.0436
CH / CH_4	1.1201	1.1412
CH / CH_3CH_3	1.0973	1.1188
CH / CH_3NH_2	1.1037	1.1236
	1.0898	1.1094
CH / CH_3OH	1.0975	1.1153
	1.0914	1.1098
O lone / H_2O	0.8397	0.8539
O lone / CH_3OH	0.8337	0.8511
N lone / NH_3	0.9497	0.9682
N lone / CH_3NH_2	0.9676	0.9837
CC bond in CH_3CH_3	1.2688	1.2779

[a]for basis sets see the footnote of Table 4.

3.3. Results obtained for normal saturated hydrocarbons

In order to study transferability, a series of more extended molecules was chosen. A model geometry R_{CH} = 1.094Å, R_{CC} = 1.526Å and tetrahedral angles were considered for the CH_4, C_3H_8, C_5H_{12}, C_7H_{16} and C_9H_{20} molecules, respectively. Four different basis sets were used in the calculations.

The results which are given in Table 6 suggest to draw two important conclusions. On the one hand, a transferability property unambigously can be observed, as expected, for both the first- and second order electric moments, respectively. It is also remarkable, on the other hand, that as the size of the basis set is increased, the change in the electric moments is not uniform. This is valid even for the centroid lengths which is surprising, as these are known as a rather stable quantities against the basis set variation. Although the model geometry considered ensures the similar structures, when larger basis sets are used, the transferability seems to be hold to a smaller extent. The results thus suggest that the basis sets should be chosen with caution.

Table 6. First and second order electric moments for CH bonds in a.u.[a]

molecule	basis	$\langle r \rangle$	$\langle z'^2 \rangle^{1/2}$
CH_4	I	1.3613	1.1201
	II	1.4021	1.0687
	III	1.4237	1.0432
	IV	1.4206	1.0407
C_3H_6	I	1.3821	1.1083
	II	1.4241	1.0791
	III	1.4378	1.0637
	IV	1.4352	1.0621
C_5H_{12}	I	1.3947	1.0976
	II	1.4154	1.0757
	III	1.4287	1.0681
	IV	1.4261	1.0611
C_7H_{16}	I	1.3977	1.0961
	II	1.4151	1.0743
	III	1.4229	1.0615
	IV	1.4178	1.0607
C_9H_{20}	I	1.3981	1.0959
	II	1.4149	1.0738

[a]for basis sets I and II see the footnote of Table 4. Basis III is the 6-311G/d, while basis IV is the 6-311G/d+p basis set.

3.4 Results obtained for the $(H_2O)_2$ dimer system

Using the SMO method, as pointed out above, it is possible to separate the supermolecule's molecular orbitals to a rather good extent accordingly to the contributing monomers' molecular orbitals. This is valid not only in canonical but in localized representation as well. By the use of the well known Boys' localization method [7] the canonical orbitals of the $(H_2O)_2$ dimer have been localized (no convergence problem occurred). The first order electric moments obtained in the calculations are demonstrated in Table 7. The results are significant: as the LMOs of the dimer system (having been determined in the SMO procedure) are systematically different in the electron donor and in the electron acceptor parts, this is reflected in the values of their first order electric moments as well. The charge density changes due to the weak interaction seem to be suitably characterized by the changes in the lengths of the centroid of charge vectors (compared to the value of the individual non-interacting monomers'

LMOs). It is remarkable that the same trend was found using any of the basis sets in the calculations.

These results unambiguously support the hope that electric moments can be used in the study of weakly bonded, more extended molecular structures. This possibility can be exhausted in cases when the transferability holds to a larger extent than the distorsion in geometry occur due to the weak interaction. If this is fulfilled, polarizational effect could be suitable reflected by the charge density studied using the calculated electric moments.

Table 7. First order electric moments of LMOs calculated for the studied $(H_2O)_2$ system (in a.u.). The centroid lengths are measured from the nearest oxygen[a]

Interacting H_2O monomers:

Basis sets	Bond pair LMOs			Lone pair LMOs		
	$H_2O(1)$		$H_2O(2)$	$H_2O(1)$	$H_2O(2)$	
MINI	0.825	0.863	0.849	0.567	0.561	0.602
6-31G	0.967	1.009	0.978	0.609	0.598	0.624
6-31G/d	0.950	1.000	0.980	0.588	0.582	0.613
MIDI	0.950	0.981	0.958	0.597	0.593	0.612
6-311G	0.939	0.994	0.972	0.609	0.604	0.627
6-311G/d	0.940	0.995	0.974	0.588	0.577	0.602

Non-interacting H_2O monomer:

Basis sets	Bond pair LMO	Lone pair LMO
MINI	0.857	0.565
6-31G	0.983	0.604
6-31G/d	0.992	0.585
MIDI	0.978	0.593
6-311G	0.988	0.601
6-311G/d	0.989	0.581

[a]geometry is given in ref. 48.

4. ONE-ELECTRON ENERGY TERMS CALCULATED AT THE HF LEVEL

4.1. One-electron energy quantities

The total HF energy for closed shell systems in localized representation has the following form:

$$E = E_0 + 2\sum_i T_i + 2\sum_i V_i + \sum_{i,j}\left(2J_{ij} - K_{ij}\right),$$

where T_i is the kinetic energy, V_i is the one-electron potential energy of the i-th localized orbital, J_{ij} and K_{ij} are the Coulomb and the exchange energy terms between the i-th and j-th LMOs, respectively. Particularly, J_{ii} means the self-interaction of the i-th orbital, which appear in the energy localization method of Edmiston and Ruedenberg (see Chapter 2).

4.2. Results obtained for some related molecules

According to the above expression, several energetic quantities have been calculated for the studied systems. The one-electron terms — the kinetic and potential energy ones, respectively — are tabulated in Tables 8-10.

Table 8. Kinetic energy terms for core orbitals[a]

	Basis I.	Basis II.
H_2O	30.7732	30.6572
NH_3	23.1416	23.0578
CH_4	16.6363	16.5918
CH_3OH	16.6349	16.5932
	30.7751	30.6541
CH_3NH_2	16.6363	16.5924
	23.1293	23.0389
CH_3CH_3	16.6377	16.5930
C_3H_8	16.6361	16.5917
C_5H_{12}	16.6362	16.5917
C_7H_{16}	16.6361	16.5917
C_9H_{20}	16.6362	16.5917

[a]for basis sets see the footnote of Table 4.

Table 9. Kinetic energy terms for CH bond orbitals[a]

	Basis I.	Basis II.
CH_4	0.8665	0.8651
CH_3OH	0.8984	0.8973
	0.9092	0.9037
CH_3NH_2	0.8908	0.8901
	0.8953	0.8947
CH_3CH_3	0.8801	0.8797
C_3H_8	0.8631	0.8622
C_5H_{12}	0.8647	0.8640
C_7H_{16}	0.8631	0.8611
C_9H_{20}	0.8650	0.8642

[a]for basis sets see the footnote of Table 4.

Table 10a. Potential energy terms for core orbitals[a]

	Basis I.	Basis II.
H_2O	-63.5106	-63.4006
NH_3	-48.9635	-48.8815
CH_4	-36.4118	-36.3665
CH_3OH	-38.1600	-38.0731
	-65.9491	-65.8337
CH_3NH_2	-38.9496	-38.7884
	-51.3362	-51.2350
CH_3CH_3	-38.7356	-38.5772

[a]for basis sets see the footnote of Table 4.

Table 10b. Potential energy terms for CH bond orbitals[a]

	Basis I.	Basis II.
CH_4	-5.8663	-5.8714
CH_3OH	-8.1185	-8.1241
	-8.1547	-8.1632
CH_3NH_2	-7.9511	-8.0233
	-8.0046	-8.0741
CH_3CH_3	-7.8290	-7.8496

[a]for basis sets see the footnote of Table 4.

The following main conclusions can be drawn from the results: 1) the kinetic energy terms are transferable to a very good extent both for core and bond pair LMO densities, and 2) the potential energy terms are transferable to a smaller extent, they show a larger sensitivity to the variation of the molecular environment.

The kinetic energy terms are representative one-electron quantities of molecular orbitals. Although the results are given for molecules, their transferable properties could be shown for weakly interacting systems (dimer of water, e.g.) as well.

4.3. Results obtained for some weakly interacting systems

It has also been shown that using localized representation by the so-called LMBPT method [41], the interaction energy in van der Waals (vdW) systems can be treated in a straightforward manner [40,42-52]. A large variety of atomic and molecular, dimer and more components' systems has been studied in the framework of the LMBPT procedure. It is known that the treatment of vdW systems reveals the introduction of counter-poise (CP) calculations due to the basis set superposition error [53]. The CP calculations, however, seriously increase the computational work (see, e.g. [54-56] and [57] and references therein). The introduction of separated molecular orbitals (SMOs) allows that the basis set superposition error could be taken into account without any additional (CP) calculation. The energy terms as compared at the HF level for several systems — resulted in the SMO as well as in the CP calculations — also affirmed this conclusion [43,49].

The quantities of the kinetic energy terms, could also be used in the above study. The transferability of the kinetic energies (obtained in a CMO $\rightarrow$ SMO procedure) has been studied for some vdW systems as well. The kinetic energy terms of each of the contributing monomers in a weakly interacting molecular system can be simply calculated using the SMO procedure. When SMOs are considered in canonical representation, it is straightforward, to compare the kinetic energy values to those calculated for the individual, noninteracting molecules. Several dimer and trimer systems have been investigated. The results are significant: they are summarized in Table 11. The transferability is obvious, using any of the basis sets. The results show a convenient separability of the kinetic energy terms.

Table 11. One-electron energy quantities: kinetic energies are given in hartree[a]

Systems	Basis set	Contributing monomers	Non-interacting monomers	Supersystem
$(H_2O)_2$	6-31G/d	$H_2O(1)$	75.7709	75.7900
		$H_2O(2)$	75.7707	75.7869
	6-311G/d	$H_2O(1)$	76.0535	76.0622
		$H_2O(2)$	76.0535	76.0527
$(HF)_2$	6-31G/d	HF(1)	99.8103	99.8135
		HF(2)	99.8093	99.8191
	6-311G/d	HF(1)	100.0895	100.0909
		HF(2)	100.0868	100.0860
$AlH_2OH + NH_3 + H_2O$	MINI	AlH_2OH	316.1345	316.1964
		NH_3	55.2969	55.4444
		H_2O	75.4796	75.5400
	6-31G/d	AlH_2OH	317.9471	317.9943
		NH_3	55.9748	56.1224
		H_2O	75.8239	75.8536
$CH_2O + NH_3 + H_2O$	MINI	CH_2O	111.8102	111.8424
		NH_3	55.1748	55.3312
		H_2O	75.4536	75.5218
	6-31G/d	CH_2O	113.4673	113.4841
		NH_3	55.9167	56.0463
		H_2O	75.7742	75.8277

[a]geometry is taken from refs. 52, 67 and 68, respectively.

5. USE OF ELECTRIC MOMENTS OF LOCALIZED ORBITALS

5.1. Study of the electrostatic interaction integrals

It is known from the classical electrodynamics that the electrostatic potential energy of charge densities can be calculated by using the multipole expansion of the charge distributions (see above). The electrostatic interaction energy between charge distributions has the following form:

$$I_{ab} = \iint \rho_a(\mathbf{r}_1)\rho_b(\mathbf{r}_2) r_{12}^{-1} dv_1 dv_2 ,$$

where ρ_a and ρ_b denote the given charge densities, $\mathbf{r}_1$ and $\mathbf{r}_2$ are usually taken from the center of gravity of ρ_a and ρ_b, respectively.

In the framework of the so called bipolar expansion of r_{12}^{-1} [58], for two cylindrically symmetric, normalized charge distributions, the expression I_{ab} can be written as:

$$I_{ab} = \frac{1}{r_{ab}} + \frac{1}{4r_{ab}^3}\left\{\Theta_b\left(3\cos^2\vartheta_b - 1\right) + \Theta_a\left(3\cos^2\vartheta_a - 1\right)\right\} +$$
$$+ \frac{3\Theta_a\Theta_b}{16 r_{ab}^5}\left\{1 - 5\cos^2\vartheta_a - 5\cos^2\vartheta_b - 15\cos^2\vartheta_a\cos^2\vartheta + \right.$$
$$\left. + 2\left[\sin\vartheta_a \sin\vartheta_b \cos(\varphi_a - \varphi_b) - 4\cos\vartheta_a \cos\vartheta_b\right]^2\right\},$$

using the moments up to quadrupole (r_{ab} is the distance between the centers of gravity of the charge densities). In this case the dipole moments vanish, so in the above expression the first term is the monopole-monopole, the second is the monopole-quadrupole and the third term is the quadrupole-quadrupole interaction energy. The z axis coincides with vector $\mathbf{r}_{ab}$, ϑ_a and ϑ_b are the angles between the common axis z and the mean axes of symmetric quadrupole tensors Θ_a and Θ_b. The scalar quantity Θ_a is the eigenvalue of Θ_a which belongs to the mean axis. Θ_b is defined in a similar way. The angles φ_a and φ_b are the rotation angles around z with respect to the axes x_a and x_b. The I_{ab} interactions between charge densities are calculated in atomic units.

The multipole expansion has already been used in certain quantum chemical calculations [59-65]. As localized orbitals are concentrated in certain spatial region, they can also be represented by their multipole moments. In the following we investigate whether the Coulomb integrals in terms of localized orbitals can be substituted by the multipole expansion of electric moments.

The idea of using the multipole expansion for the evaluation of intermolecular interactions is not new. It was found that for the moments of the entire molecules the convergence is questionable especially at smaller distances. The convergence can be improved, however, if the charge distributions of molecules are divided into small parts, and the multipole expansion takes the electric moments of these parts into consideration separately [66].

We decompose the charge distribution of the whole electron system into sum of contributions from localized orbitals. If the localized orbitals do not overlap and their electric moments can be considered as transferable, than it is expected that the Coulomb integrals can be approached by the sum of interaction energies

of the multipoles. Hence, for an extended molecule the effect of distant parts can also be taken into account by multipole potentials. It should be noted that the calculation time increase significantly when the system is increasing.

For the actual calculations we used basis sets of (13s7p/4s) Gaussians contracted to [4s2p/2s]. The geometry of the studied systems were taken at the experimental values. The multipole expansion was used for calculating of Coulomb interactions between localized orbital densities for some eighteen-electron systems. Now we present the results obtained for CH_3OH, NH_2OH and OHOH in order to compare the interactions of the same type in different molecules. The ((trans)-XH bond – OH bond) and the (O lone – O lone) interactions were calculated, as these orbitals are nearly cylindrically symmetric.

The calculated values are given in Table 12. For the localized orbitals connected to different centers the calculated multipole interactions agree well (within 2%) with the corresponding Coulomb integrals (bond-bond interactions in Table 12). For the localized orbitals connected to the same nucleus (lone-lone interactions) the deviations are rather large (>50% in some cases).

Table 12. Some contributions to the interaction energy in the studied systems[a]

		CH_3OH	NH_2OH	OHOH
bond-bond	r_{ab}	3.54	3.74	3.51
	I_{ab}	0.2633	0.2686	0.2849
	Coulomb integral	0.2588	0.2647	0.2796
lone-lone	r_{ab}	1.03	1.08	1.10
	I_{ab}	1.0652	1.0018	0.9660
	Coulomb integral	0.6783	0.6782	0.6782

[a]4s2p/2s basis set (see text), geometry at experimental values

It is evident from the above results that applicability of the multipole expansion depends strongly on the distance of the corresponding centroids. This is also demonstrated by comparing the results obtained for the CH_4 and C_2H_6 molecules, respectively. It is remarkable that the agreement between I_{ab} and the corresponding Coulomb integrals is quite satisfactory for the LMO densities in C_2H_6 (see Table 13). For the calculation of the interaction energies of two localized orbitals connected to the same center the multipole expansion, however, can not be applied. For disconnected charge distributions the method seems to be promising at least for obtaining a rough estimate of the corresponding Coulomb integrals.

As it can be seen Coulomb integrals cannot always be regularly approximated by using multipole expansion. The above values resulted in our calculations are aimed to demonstrate their transferable properties.

Table 13. Results obtained for some interaction energy quantities between LMO densities[a]

		CH_4	C_2H_6
Core self		3.5670	3.5671
Bond self		0.6700	0.6767
Core/Bond	**Coulomb integral**	0.6441	0.6461
	Exchange integral	0.0086	0.0086
Bond1/Bond2	r_{ab}	2.22	2.25
	Mono-Mono	0.4498	0.4449
	Mono-Quadru	0.0251	0.0223
	Quadru-Quadru	0.0060	0.0048
	Total I_{ab}	0.4809	0.4720
	Coulomb integral	0.4047	0.4055

for C_2H_6:

	Core1/Core2	**Bond1/Bond3**	**Bond1/Bond4**
r_{ab}	2.90	4.04	4.76
Mono-Mono	0.345060	0.247668	0.209966
Mono-Quadru	0.000090	-0.001309	-0.000566
Quadru-Quadru	0.000000	0.000098	0.000073
Total I_{ab}	0.345150	0.246456	0.209473
Coulomb integral	0.345209	0.240552	0.217541

[a]for basis sets see the footnote of Table 12.

5.3. Investigation of van der Waals systems

As described in the precedent section, the Coulomb integrals' matrix elements could be approximated by using the electric moments. This is valid for vdW systems, too. It is demonstrated in Table 14 that the matrix elements calculated are transferable. (The electric moments can be calculated as given in section 3.4.) There is another way of using electric moments of LMOs in case of weakly interacting systems. Comparing the values in the noninteracting monomers to those calculated in the dimer system, e.g., it is possible a) to get information on the charge displacement (see also 3.4) and b) to separate the significant and less important contributing LMO densities.

The charge displacement can be described by the displacement of the centroids of the LMOs. The calculations have been performed on the water dimer, using 6-31G/d basis set. The displacements of the centroids of charges for each bond and

LMO densities were calculated. The results are demonstrated for the occupied LMOs of the $(H_2O)_2$ dimer in Figures 3 A, B and C. In Figures 3A and 3B the centroids of the noninteracting monomers and the interacting supersystem are presented, respectively. In Figure 3C both types of centroids are shown. A significant displacement reflects the formation of a bond between the two water molecules. This is usually named H-bond and described as a linkage between an oxygen atom of one water molecule and a hydrogen atom of another water molecule. The term electron donor / H acceptor is often used for the first molecule, while electron acceptor / H donor is the latter molecule. It is remarkable that the displacement of the centroid of a bonding LMO of the second molecule is more than 2% of the OH distance in water molecule. The centroid of a lone pair LMO density of the second molecule shows also a displacement (to a smaller extent): it is oriented to the same direction. The charge displacements calculated for any other LMO densities in the water dimer is not significant.

Table 14. Diagonal Fock-matrix elements of LMOs calculated for the studied $(H_2O)_2$ system (in a.u.)[a]

Interacting H_2O monomers:

Basis sets	Bond pair LMOs			Lone pair LMOs		
	$H_2O(1)$		$H_2O(2)$	$H_2O(1)$	$H_2O(2)$	
MINI	0.877	0.863	0.907	0.544	0.598	0.601
6-31G	0.894	0.889	0.960	0.656	0.725	0.733
6-31G/d	0.883	0.879	0.941	0.674	0.735	0.740
MIDI	0.876	0.885	0.949	0.685	0.752	0.760
6-311G	0.891	0.895	0.966	0.670	0.736	0.749
6-311G/d	0.887	0.876	0.992	0.691	0.747	0.761

Non-interacting H_2O monomer:

Basis sets	Bond pair LMO	Lone pair LMO
MINI	0.885	0.570
6-31G	0.929	0.696
6-31G/d	0.913	0.709
MIDI	0.917	0.726
6-311G	0.929	0.702
6-311G/d	0.943	0.711

[a]geometry is given in ref. 43.

These results open the possibility toward the description of weak interactions in terms of centroid displacement of LMO densities. This seems to be straightforward in the study of large biological systems, as the Hartree-Fock level is only to be considered and one-electron properties are to be computed.

Figure 3. Centroids of the occupied LMOs of the $(H_2O)_2$ dimer. **A:** centroids of the noninteracting monomers, **B:** centroids in the supersystem, **C:** centroids of both types (red: oxygen, white: hydrogen, blue: centroids of the noninteracting monomers, gray: centroids in the supersystem)

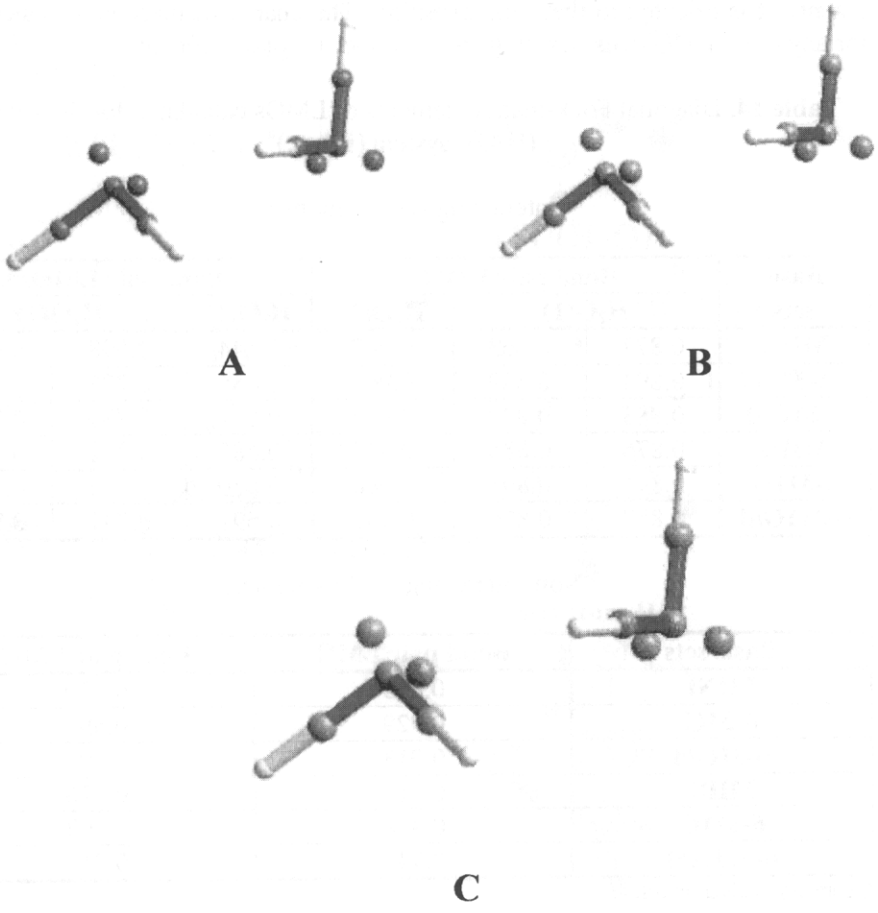

ACKNOWLEDGEMENTS

This work was initialized by Professor E. Kapuy. A careful reading of the manuscript is acknowledged to Dr. I. Nagy. We are indebted to the OTKA grants Nos. T032116 and T025622. The authors are grateful to the support No F40039 of the Ministry for Education of Hungary, Budapest.

REFERENCES

[1] O'Leary, B., Duke, B.J., Eilers, J.E.: Advan,Quantum Chem. **9**, 1 (1975)
[2] Rothenberg, S.: J.Chem.Phys. **51**, 3389 (1969)
[3] Edmiston, C., Ruedenberg,K.: Rev.Mod.Phys. **35**, 457 (1963)
[4] Edmiston, C., Ruedenberg, K.: in P.O.Lowdin (Ed.) Quantum Theory of Atoms, Molecules and Solid State, Academic Press, N.Y.p.253 (1966)
[5] Edmiston, C., Ruedenberg, K.: J.Chem.Phys. **43S**, 97 (1965)
[6] Foster, J.M., Boys, S.F.: Rev.Mod.Phys. **32**, 300 (1960)
[7] Boys, S.F.: Rev.Mod.Phys. **32**, 296 (1960)
[8] Boys, S.F.: in P.O.Löwdin (Ed.) Quantum Theory of Atoms, Molecules and Solid State, Academic Press, N,Y. p.253 (1966)
[9] von Niessen, W.: J.Chem.Phys. **56**, 4290 (1972)
[10] Amos, A.T., Crispin, R.J., Smith, R.A.: Theoret.Chim.Acta (Berl.) **39**, 7 (1975)
[11] England,W., Gordon, M.S., Ruedenberg, K.: Theoret.Chim.Acta (Berl.) **37**, 177 (1975)
[12] von Niessen, W.: Theoret.Chim.Acta (Berl.) **33**, 7 (1974)
[13] von Niessen, W.: Theoret.Chim.Acta (Berl.) **29**, 29 (1973)
[14] von Niessen, W.: Theoret.Chim.Acta (Berl.) **33**, 185 (1974)
[15] von Niessen, W.: Theoret.Chim.Acta (Berl.) **38**, 9 (1975)
[16] Adams, W.H.: J.Chem.Phys. **34**, 89 (1961)
[17] Adams, W.H.: J.Chem.Phys. **37**, 2009 (1962)
[18] Adams, W.H.: J.Chem.Phys. **42**, 4030 (1965)
[19] Gilbert, T.L.: Molecular orbitals in chemistry, physics and biology, Academic Press, N.Y. p.405 (1964)
[20] Magnesco, V., Perico, A.: J.Chem.Phys. **47**, 971 (1967)
[21] Magnesco, V., Perico, A.: J.Chem.Phys. **48**, 800 (1968)
[22] Peters, D.: J.Chem.Phys. **51**, 1559, 1566 (1969)
[23] Aslangul,C., Constenciel, R., Daudel, R., Kottis: Adv.Quant. Chem. **6**, 93 (1972)
[24] Aslangul, C., Constanciel, R., Daudel, R., Esnault, L., Ludena, E.V.: Int.J.Quant.Chem. **8**, 499 (1974)

[25] Daudel, R., Bader, R.F., Stephens, M.E., Borrett, D.S.: Can.J.Chem. **52**, 1310 (1974)
[26] Pipek, J., Mezey, P.G.: J.Chem.Phys. **90**, 4916 (1989)
[27] Pulay, P.: Chem.Phys.Letters **100**, 151 (1983)
[28] Saebo, S., Pulay, P.: Chem.Phys.Letters **113**, 13 (1985)
[29] Pulay, P., Saebo, S.: Theor.Chim.Acta **69**, 357 (1986)
[30] Kristyan, S., Pulay, P.: Chem.Phys.Letters **229**, 175 (1994)
[31] Rauhut, G., Boughton, J.W., Pulay, P.: J.Chem.Phys. **103**, 5662 (1995)
[32] Hampel, C., Werner. H.J.: J.Chem.Phys. **104**, 6286 (1996)
[33] Coffey, P.: Int.J.Quant. Chem. **8**, 777 (1974)
[34] Peeters, D., Leroy, G.: Theoret.Chim.Acta (Berl.) **50**, 135 (1978)
[35] Böhm, M.C.: Theoret.Chim.Acta (Berl.) **59**, 609 (1981)
[36] Cullen, J.M., Zerner, M.C.: Int.J.Quant.Chem. **22**, 497 (1982)
[37] Cizek, J., Förner, W., Ladik, J.: Theoret.Chim.Acta (Berl.) **64**, 107 (1983)
[38] Leonard, J.M., Luken, W.L.: Int.J.Quant.Chem. **25**, 355 (1984)
[39] Rajzmann, M., Brenier, B. Purcell, K.F.: Theor.Chim.Acta **72**, 13 (1987)
[40] Kozmutza, C., Tfirst, E.: Advances in Quantum Chemistry **31**, 231 (1998)
[41] Kapuy, E., Csépes, Z., Kozmutza, C.: Int.J.Quant.Chem. **23**, 981 (1983)
[42] Kozmutza, C., Kapuy, E.: Int.J.Quant.Chem. **38**, 665 (1990)
[43] Kapuy, E., Kozmutza, C.: J.Chem.Phys. **94**, 55 (1991)
[44] Kozmutza, C., Kapuy, E.: J.Comp.Chem. **12**, 953 (1991)
[45] Kozmutza, C., Kapuy, E., Evleth, E.M.: J.Comp.Chem. **10**, 1136 (1993)
[46] Kozmutza, C., Tfirst, E., Kapuy, E.: Mol.Phys. **80**, 1059 (1993)
[47] Kozmutza, C., Kapuy, E., Tfirst, E.: Mol.Phys. **82**, 343 (1994)
[48] Kapuy, E., Kozmutza, C.: Chem.Phys.Letters **226**, 484 (1994)
[49] Kozmutza, C., Kapuy, E., Evleth, E.M., Kassab, E.: J.Mol.Structure (Theochem) **332**, 141 (1995)
[50] Kozmutza, C., Kapuy, E., Evleth, E.M., Pipek, J., Trezl, L.: Int.J.Quant.Chem. **57**, 775 (1996)
[51] Kozmutza, C., Tfirst, E., Kapuy, E.: Mol.Phys. **87**, 569 (1996)
[52] Kapuy, E., Kozmutza, C., Ovari, L.: J.Mol.Structure (Theochem) **422**, 143 (1998)
[53] Boys, S.F., Bernardi, F.: Mol.Phys. **19**, 553 (1970)
[54] Alagona, G., Ghio, C., Cammi, R., Tomasi, J.: Int.J.Quant.Chem. **32**, 207 (1987)
[55] Alagona, G., Ghio, C., Cammi, R., Tomasi, J.: in J.Maruani (Ed.) Molecules in Physics, Chemistry, and Biology, Vol. II, Kluwer Academic Publishers, p.507 (1988)
[56] Feller, D.: J.Chem.Phys. **96**, 6104 (1992)
[57] van Duijneveldt, F.B., van Duijneveldt-van de Rijdt, J.G.C.M., van Lenthe, J.H.: Chem.Rev. **94**, 1873 (1994)

[58] Hirschfelder, J.O., Curtiss, C.F., Bird, R.B.: Molecular Theory of Gases and Liquids, J. Wiley and Sons, New York (1954)
[59] Epstein, I.R., Liscomb, W.N.: J.Chem.Phys. **53**, 4418 (1970)
[60] Epstein, I.R.: J.Chem.Phys. **53**, 4425 (1970)
[61] Levy, M., Stevens, W.J., Shull, H., Hagstrom, S.: J.Chem.Phys. **52**, 5483 (1970)
[62] Bonaccorsi, R., Cimiraglia, R., Scrocco, E., Tomasi, J.: Theoret.Chim.Acta (Berl.) **33**, 97 (1974)
[63] Joslin, C.G., Gray, C.G.: Mol.Phys. **50**, 329 (1983)
[64] Panas, I., Almlöf, J.: Int.J.Quant.Chem. **42**, 1073 (1992)
[65] Moszynski, R., Wormer, P.E.S., Heijmen, T.G.A., van der Avoird, A.: J.Chem.Phys. **108**, 579 (1998)
[66] Rabinowitz, J.R., Swissler, T.J., Rein, R.: Int.J.Quant.Chem. **6**, 353 (1972)
[67] Kozmutza, C., Tfirst, E., Udvardi, L.: THEOCHEM **455**, 261 (1998)
[68] Kapuy, E., Kozmutza, C., Evleth, E. M.: *The role of CH2O in biological systems*, Conference Proceeding, Sopron, Hungary (1994)

Thiouracils:

Structures, Tautomerism, Interaction with Water, and Functioning in RNA and Modified DNA Base Pairs

Eugene S. KRYACHKO[1,2] and Minh Tho NGUYEN[2]

[1]Bogoliubov Institute for Theoretical Physics, Kiev, 03143 Ukraine
[2]Department of Chemistry, University of Leuven
Celestijnenlaan 200 F, B-3001 Leuven, Belgium

Submitted to:

ADVANCES IN QUANTUM CHEMISTRY
Proceedings of the Fifth European Workshop on
QUANTUM SYSTEMS IN CHEMISTRY AND PHYSICS

Address for correspondence:
Department of Chemistry, University of Leuven
Celestijnenlaan 200 F, B-3001 Leuven, Belgium
Tel: +32 (16) 32 73 84; FAX: +32 (16) 32 79 92
E-mail: eugene@chem.kuleuven.ac.be

Thiouracils:

Structures, Tautomerism, Interaction with Water, and Functioning in RNA and Modified DNA Base Pairs

Eugene S. KRYACHKO[1,2] and Minh Tho NGUYEN[2]

[1]Bogoliubov Institute for Theoretical Physics, Kiev, 03143 Ukraine
[2]Department of Chemistry, University of Leuven
Celestijnenlaan 200 F, B-3001 Leuven, Belgium

Abstract

The present work discusses some properties of thiouracil nucleobases calculated at the B3LYP/6-31+G(d,p) computational level, namely, their structures, most stable tautomers, proton affinities and deprotonation enthalpies, hydrogenation, interaction with water, and base pairing, in order to shed a certain light on the problem of why their functioning in RNA and modified DNA base pairs is so unusual.

Table of Contents

1. Introduction

An understanding of the physico-chemical properties of the modified nucleic acid bases is undoubtedly of fundamental importance (see Ref. [1] for current review). Among them are thiated nucleobases whose oxygen atom is substituted by the bulkier sulphur one and which have recently attracted a great deal of attention [1a, 2] due to designing of potential antiviral and antitumor drugs [3]. One of these thiated nucleobases is thiouracil, thiated derivative of uracil, where the exocyclic oxo group(s) is (are) substituted by the heavier thio group(s) that results in 2- or 4-thiouracil or 2,4-dithiouracil (2,4DTU). Thiouracil is identified as a minor constituent of tRNA, anticancer drugs, and peptide nucleic acids PNAs [4-6]. Crystallographic [6a] and NMR [6b] data demonstrate that 4-thiouracil (4TU) forms the hydrogen (H-) bond with adenine in the position 14 that is actually the reversed Hoogsteen pair where the oxygen atom O_4 accepts the H-bond [4a-b]. 2-thiouracil (2TU) performs also a pairing with adenine and diaminopurine in PNAs [4c]. Thiouracils have been well studied experimentally [7] because of its considerable importance in biophysics, biochemistry, and pharmacology (see Refs. [8, 9] and references therein). It is known that while 2-thiouracil [7d] acts as a cancerogen agent [9a-b], 4TU behave as a cross-linked agent in RNA transcriptional regulation [9d]. The substitution of uracil by 2TU can be responsible for misrecognition in mRNA [6c] and also decreases its interaction energy with adenine [7g]. It is also known that in the codon-anticodon complex, adenine forms a rather strong H-bond with 2TU although the thio group is not involved there [8d].

What makes the thiated nucleobases so markedly different from the normal ones? Put in the other words, what is a key effect of the thio substitution which, in turn, causes a variety of bizarre effects in the interaction of thiouracils with water, in proton migration, recognition patterns, biological and pharmacological activities, etc., etc. There are actually two key effects underlying the thio substitution and certainly inter-related. One is that such substitution dramatically changes the structural features of nucleic acids whereas the other is due to the drastic change of their functional ones expressed in terms of intermolecular interactions.

The structural changes are mainly caused by the C=S bond(s) appearing longer than the C=O one(s) although the thio substitution significantly alters many other structural parameters of nucleobases. The other implications of the thio substitution such as, e. g., a resistance to N-glycosidic bond hydrolysis by nucleoside phosphorylases [3d] and perturbation in the electronic environment of the heterocyclic ring due to the lower electronegativity of sulfur compared to oxygen are well documented. However, the thio substitution, as we will show in the present work, increases the polarizability of nucleobases by a factor of nearly 2, that in turn influences the induction and dispersion contributions to the stabilization energy of base pairs. This likely underlies the suggestion expressed in Ref. [10] that the modified biochemical activity of thiobases arises from their altered molecular interactions.

Besides, the analysis of comparable molecular compounds with oxygen or sulphur electron-pair donor atoms show consistently that the oxygen atom is a better acceptor of hydrogen bonds than the sulphur atom of the corresponding thio-compound [11]. Thus, such pair of related compounds provides a clear-

cut example of the hard-soft acid-base principle [12]: *the softer sulphur atom is the stronger Lewis base towards soft electron-pair acceptors and the harder oxygen atom is the stronger Lewis base in the harder hydrogen-bonded interactions.* Also, comparing oxygen and thio-compounds, we should expect that the former one is less acidic than the latter [13]. A recent review analyzing N-H···S=C and O-H···S=C hydrogen bonds [14] shows a stronger hydrogen bonding to terminal oxygen atoms than to sulfur. That is, the sulphur atom is a weaker acceptor of H-bond than the oxygen one [15a-b]. This is in fact the case, e. g., with the thio substitution of uracil in the adenine-uracil A·U base pair which, as demonstrated via simple electrostatic estimations by Geller et al. [16], decreases the stabilization energy by 3.9 kcal/mol. It is well known that in weak hydrogen bonds, the long-range electrostatic attraction predominates. Although, and we will demonstrate this in the present work as well, in the case of the thiobase pairs there might appear rather strong contributions of dispersion and exchange interactions which, on the one hand, diminish the difference between the electrostatic contribution of the hydrogen bonds involved oxygen and those involved the sulphur one, and, on the other hand, cause their rather spectacular departure from non-planarity.

We will also demonstrate further that there is still a noticable structural effect in the hydrogen bonding patterns of the thiobase pairs. It is related to the fact that if the sulphur atom is involved in the formation of a hydrogen bond, the latter one is longer compared to that involved the oxygen atom because, according to the phenomenological definition of the hydrogen bonding given by Pimentel and McClellan [17], the hydrogen bond length should be shorter than the sum of "classical" van der Waals radii, and the "classical" van der Waals radii of the sulphur atom (1.85 Å) exceeds that of the oxygen one (1.4 Å) by 0.45 Å [18]. This may cause a marked strain in the double helix structure of DNA.

Another aspect of the thio substitution of nucleobases and uracil in particular arises due to a highly probable link between the spontaneous point mutations developing during the RNA replication and likely describing by the Löwdin mechanism of double proton transfer [19] and the occurrence of the rare enol tautomers of uracil viewed as a major factor responsible for the formation of the nucleobase pairing mismatches (see Ref. [20] and references therein). This aspect addresses to the question of how thio substitution alters the order of stability of tautomers (see also Refs. [21, 22]).

The present work highlights some of quandaries related to the unexpected features in the structure and functioning of the thiated nucleobases and the base pairs involved them. We endeavour to offer a series of informative and entertaining answers by means of the theoretical study of thiouracils in the following directions: their structures and properties, lower-energy tautomers, interaction with water, structures of some thiobase pairs, and finally, the base pairing between adenine and thiouracils. On these grounds, the offered answers appear conceivable in explaining some unusualness of the thiated nucleobases.

2. Computational Methodology

All computations were performed at the DFT B3LYP computational level with the 6-31+G(d,p) basis set using GAUSSIAN 98 suit of programs [23]. The geometries of the thiouracils, their tautomers, and the related base pairs

were fully optimized without any constraint on a possible planarity. The harmonic vibrations were also calculated in order to distinguish the structures of the studied complexes, to analyse further their vibrational sprectra and thermodynamic properties. The harmonic frequencies and zero-point vibrational energies (ZPVE) are retained unscaled. The reported energy values are rescaled to the electronic energy + ZPVE level given in kcal/mol.

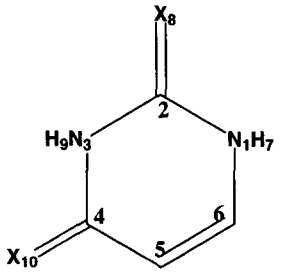

$X_8 = X_{10} = O$ - uracil
$X_8 = S, X_{10} = O$ - 2TU
$X_8 = O, X_{10} = S$ - 4TU
$X_8 = X_{10} = S$ - 2,4DTU

Figure 1. Numbering of atoms in uracil and thiouracils.

3. Structure of Thiouracils and Their Lower-Energy Tautomers

The B3LYP/6-31+G(d,p) optimized ground-state structures of uracil and thiouracils are schematically displayed in Figure 1. Their geometrical parameters are listed in Table 1. We readily see there the noticable changes in the geometry of uracil under the thio substitution. For example, the C=S bond is elongated by $\approx$ 0.44 Å with respect to the C=O bond in uracil. A variety of changes in other geometrical parameters of thiouracils compared with uracil are also occurred in the vicinity of the sulphur atom (see also Ref. [24]). The properties of thiouracils are collected in Table 2. It shows in particular that the 4TU thiouracil is more energetically favorable than 2TU by ca. 1.7 kcal/mol. The present computational level predicts the total dipole moment of the 2TU, 4TU, and 2,4DTU equal to 4.8, 5.0, and 5.0 D, respectively. Table 2 also demonstrates that the double substitution of the oxygen atoms in uracil by the sulphur ones increases the dipole polarizability by the factor of about two. Due to the fact that, as well known, the dispersion energy is an important part of the total stabilization energy of base pairs [25], we anticipate that for the base pairs involved thiouracil and 2,4DTU especially, the dispersion interaction might play a more important role in comparison with those including uracil (see Sections 8 and 9).

Table 2 reports the Mulliken charges of the ground-state thiouracils. In 2TU, the electronegativity of the sulphur atom is lowered by a factor of three after substituting the oxygen atom of uracil. The bridged carbon atom significantly loses its net positive charge and the neighboring nitrogen atom becomes also less electronegative. In 4TU, the Mulliken charge on the sulphur atom is positive. The double substitution of the oxygens in uracil by the sulphur atoms results in that the latter ones in 2,4DTU possess positive Mulliken charges. The decrease of the Mulliken charges on the sulphur atoms are mainly due to the transfer of π electrons which are shifted toward the carbon atoms C_2 and C_4.

By the analogy with uracil [20], the potential energy surfaces of tautomerization of thiouracils reveal twelve tautomeric forms. The four most stable

ones are shown in Figure 2 and some their properties are gathered in Table 3. In Figure 2, T_3 has the X_8-H bond on the N_1 side while in T_4, it resides on the N_3 side. The relative order of stability of these four most stable tautomeric

Table 1. Geometries of uracil U and thiouracil nucleobases. Bond lengths are in Å, bond angles in degrees.

Geometry	U	2TU	4TU	2,4DTU
Bond Lengths				
$r(N_1\text{-}C_2)$	1.393	1.379	1.392 (1.370; 1.388)[a]	1.379
$r(N_1\text{-}C_6)$	1.377	1.376	1.375 (1.367; 1.376)[a]	1.375
$r(N_1\text{-}H_7)$	1.010	1.011	1.011 (0.995; 1.009)[a]	1.011
$r(C_2\text{-}N_3)$	1.384	1.371	1.388 (1.375; 1.390)[a]	1.375
$r(C_2\text{-}O(S_8))$	1.220	1.664	1.219 (1.192; 1.224)[a]	1.662
$r(N_3\text{-}C_4)$	1.412	1.416	1.392 (1.367, 1.390)[a]	1.395
$r(N_3\text{-}H_9)$	1.014	1.014	1.015 (0.998; 1.014)[a]	1.015
$r(C_4\text{-}C_5)$	1.459	1.457	1.444 (1,447; 1.445)[a]	1.443
$r(C_4\text{-}O(S_{10}))$	1.223	1.222	1.662 (1.648; 1.646)[a]	1.660
$r(C_5\text{-}C_6)$	1.352	1.352	1.356 (1.334; 1.355)[a]	1.356
$r(C_5\text{-}H_{11})$	1.081	1.081	1.081 (1.069; 1.078)[a]	1.081
$r(C_6\text{-}H_{12})$	1.084	10.84	1.084 (1.073; 1.081)[a]	1.084
Bond Angles				
$\angle N_1C_2N_3$	113.2	113.3	113.2 (113.7; 112.6)[a]	113.3
$\angle N_1C_2O(S_8)$	122.7	122.5	123.0 (123.2; 124.6)[a]	122.8
$\angle N_1C_6C_5$	121.8	121.7	121.3 (121.9; 121.2)[a]	121.1
$\angle N_1C_6H_{12}$	115.4	115.3	115.8 (115.6; 115.8)[a]	115.7
$\angle C_2N_1H_7$	115.1	115.2	115.2 (115.6; 115.0)[a]	115.3
$\angle C_2N_3C_4$	127.9	128.0	127.9 (127.7; 128.8)[a]	128.1
$\angle N_3C_4C_5$	113.7	113.6	114.1 (114.5; 113.3)[a]	114.0
$\angle C_4N_3H_9$	149.2	115.7	117.1 (117.4; 116.8)[a]	115.5
$\angle C_4C_5C_6$	119.8	119.5	120.2 (121.9; 121.2)[a]	119.9
$\angle C_5C_4O(S_{10})$	126.1	126.4	125.0 (124.4; 125.2)[a]	125.3
$\angle C_6C_5H_{11}$	122.0	122.1	121.2 (121.9; 120.8)[a]	121.4

[a] Calculated geometry of 4TU at HF/6-31G(d,p) and MP2/6-31G(d,p) levels, respectively [22e].

forms is then taken the following form:

$$\mathrm{U} \overset{10.90}{>} \mathrm{T_1} \overset{0.85}{>} \mathrm{T_2} \overset{0.93}{>} \mathrm{T_3} \overset{1.11}{>} \mathrm{T_4} \tag{1}$$

$$\mathrm{2TU} \overset{9.34}{>} \mathrm{T_1} \overset{0.04}{\approx} \mathrm{T_3} \overset{0.38}{>} \mathrm{T_4} \overset{2.27}{>} \mathrm{T_2} \tag{2}$$

$$\mathrm{4TU} \overset{10.30}{>} \mathrm{T_1} \overset{1.11}{>} \mathrm{T_3} \overset{0.02}{\approx} \mathrm{T_2} \overset{0.57}{>} \mathrm{T_4} \tag{3}$$

$$\mathrm{2,4DTU} \overset{7.96}{>} \mathrm{T_3} \overset{0.28}{>} \mathrm{T_4} \overset{0.44}{>} \mathrm{T_1} \overset{2.97}{>} \mathrm{T_2} \tag{4}$$

where T_1 tautomeric form is referred to the 2-hydroxy-4-oxo form, T_2 to 2-oxo-4-hydroxy, and T_3 and T_4 to the 2,4-dihydroxy one. In Eqs.(1)-(4), the quantity above the inequality or $\approx$ sign indicates the corresponding energy difference between the right-hand complex and its left-hand one. It is worth

mentioning, first, that the tautomerization energies of the tautomers T_1 and T_4 of 4TU agree pretty well with those calculated at the second-order Møller-Plessett perturbation theory MP2/6-31G(d,p) computational level [22e], viz., 10.26 and 11.89 kcal/mol, respectively, and second, that, in comparison with the Ref. [22e], the two other most stable tautomeric forms T_2 and T_3 are reported in the present study for the first. As shown in Table 3, the 2-oxo-4-hydroxy tautomeric form T_2 always has the total dipole moment larger than its parental normal form mainly due to the formation of the X_{10}-H (X = O, S) bond dipole moment on the N_3 side which is directed almost parallel to the parental total dipole moment. The largest dipole moment pertains to the 2-oxo-4-hydroxy tautomer T_2 which reaches ca. 6 D in the case of the 2,4DTU thiouracil. Besides, this tautomer possesses the largest dipole polarizability among all studied tautomeric forms.

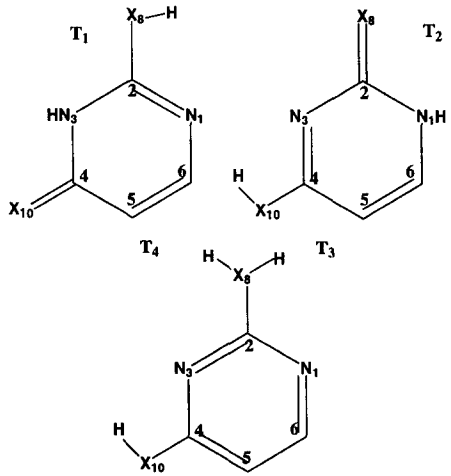

Figure 2. The four most stable tautomers of uracil and thiouracils.

It follows from Table 3 that the most stable uracil tautomer is the 2-hydroxy-4-oxo T_1 with the tautomerization energy of 10.9 kcal/mol. Despite this fact, it is unable to function as a normal nucleobase due to the absence of the N_1-H_7 bond connected to the sugar-phosphate backbone although it appears in the modified nucleobases including pseudouridine. Among the normal ones, the 2-oxo-4-hydroxy T_2 tautomer of uracil is the most stable one lying above T_1 by only 0.9 kcal/mol. Its dipole moment exceeds that of T_1 by more than 50% and, therefore, polar solvents may favor T_2 rather than T_1 (see Section 6). For these two reasons and also because it has the N_1-H_7 link to the sugar-phosphate backbone, it becomes of a major biophysical interest (see also Sections 4 and 6).

Returning to the orders of stability of the most stable tautomeric forms of uracil and thiouracil displayed by Eqs.(1)-(4), we find that the thio-substitution has two major effects. One is that it may substantially increase the stability of tautomers whereas the other is that it drastically alters their order of stability. This is vividly seen by comparing (1) with (4). We observe then that the

Table 2. Properties of thiouracils in comparison with uracil. Energy in hartree, ZPVE in kcal/mol, total dipole moment in D, Mulliken charges and dipole polarizability $\alpha = (\alpha_{xx} + \alpha_{yy} + \alpha_{zz})/3$ in atomic units.

Atom	U	2TU	4TU	2,4DTU
Energy	-414.847362	-737.796909	-737.799615	-1060.749204
ZPVE	54.57	53.22	53.24	51.87
Dipole	4.7	4.8	5.0	5.0
α	67	89	91	121
Charge				
N_1	-0.45	-0.34	-0.44	-0.34
C_2	0.67	0.15	0.65	0.11
N_3	-0.55	-0.43	-0.40	-0.28
C_4	0.29	0.23	-0.19	-0.27
C_5	0.16	0.21	0.17	0.19
C_6	-0.09	-0.14	-0.12	-0.15
S_8	-	-0.19	-	0.16
O_8	-0.52	-	-0.51	-
S_{10}	-	-	0.16	0.14
O_{10}	-0.51	-0.50	-	-

Table 3. Relative energies (in kcal/mol) of the most stable thiouracil tautomers (for the definition see text below Eqs.(1)-(4)). Their total dipole moment (D) and dipole polarizability α (a.u., in parentheses) are shown below the corresponding relative energy.

Tautomer	U	2TU	4TU	2,4DTU
T_1	10.90	9.34	10.30	8.68
	2.4 (68)	3.0 (85)	4.2 (92)	3.9 (109)
T_2	11.75	12.03	11.43	11.65
	5.1 (68)	5.8 (92)	5.4 (86)	6.0 (112)
T_3	12.68	9.38	11.41	7.96
	1.3 (67)	1.4 (84)	1.8 (84)	1.7 (102)
T_4	13.79	9.76	12.00	8.24
	2.5 (67)	2.1 (84)	2.3 (84)	2.0 (102)

double thio substitution of uracil replaces the most stable tautomer T_1 of uracil by T_3 of 2,4DTU and increases its stability by ≈ 2 kcal/mol. This has a very interesting implication on the occurrence of mismatches of the base pairs under the thio substitution (see Ref.[26] and references therein). Using the following expression for the equilibrium constant $k_{X \Leftrightarrow Y}$ of the tautomerization process X $\Leftrightarrow$ Y: $k_{X \Leftrightarrow Y} = exp[-(\Delta H - T\Delta S)/k_B T]$ where ΔH is the difference in enthalpies of X and Y, ΔS is their corresponding entropy difference, and k_B is Boltzmann constant equal to $198.72156 \cdot 10^{-2}$ cal/mol·T, we obtain that the equlibrium constant $k_{U \Leftrightarrow T_1}$ of the tautomerization U $\Leftrightarrow$ T_1 becomes equal to $1.0 \cdot 10^{-8}$ that is within the interval of the estimated frequency of the spontaneous point mutations [26], whereas the equlibrium constant $k_{2,4DTU \Leftrightarrow T_3}$ of the tautomerization 2,4DTU $\Leftrightarrow$ T_3 is equal to $1.45 \cdot 10^{-6}$. The latter one is larger by two orders than $k_{U \Leftrightarrow T_1}$. In the other words, the occurrence of the

spontaneous point mutations caused by the 2DTU tautomer T_1 increases by a factor of nearly 100.

4. Adiabatic Protonation and Deprotonation of Thiouracil

Table 4 presents the proton affinities PA and deprotonation enthalpies DPE of thiouracils calculated at the B3LYP/6-31+G(d,p) computational level. Inspecting this Table, we find that first, the thio substitution of uracil systematically increases its PAs by 3-6 kcal/mol and second, it decreases the DPEs of uracil by 6-13 kcal/mol. As far as the base pair A·thioU is considered, it particularly implies a lowering, on the one hand, of the potential well at the S_{10} atom of thiouracil corresponding to the proton transfer from the N_6 atom of adenine to the S_{10} of thiouracil and, on the other one, a raising of the potential well at the N_3 atom of thiouracil involved in the proton transfer from the N_3-H bond to the N_1 atom of adenine. Therefore, summarizing, the thio substitution of uracil is in a favor to the double proton transfer mechanism of the occurrence of the spontaneous point mutations proposed by Löwdin [19]. Table 4 also includes the PAs of the T_2 tautomer of uracil and thiouracils. A comparison with the corresponding PAs of the parental normal nucleobases shows that their tautomerization to the T_2 form is accompanied by an increase of the proton affinity by 20-23 kcal/mol.

Table 4. Proton affinities (PA) and deprotonation enthalpies (DPE) of uracil and thiouracils in kcal/mol.

	PA				DPE	
	X_8 (N_1)	X_8 (N_3)	X_{10} (N_3)	X_{10} (C_5)	N_1-H	N_3-H
U	195.0	196.0 (218.5)[a]	202.9	205.5	332.5	345.9
2TU	200.9	201.5 (220.7)[a]	202.1	205.2	326.1	334.9
4TU	194.7	195.8 (218.6)[a]	208.4	209.0	325.0	339.0
2,4DTU	201.0	201.5 (220.7)[a]	207.9	208.5	320.0	332.8

[a]Proton affinities for the T_2 tautomer.

5. Hydrogenation of Thiouracil

This Section briefly outlines the possible hydrogenation products of thiouracils under radiation effects (see Ref. [27] for review). As shown in Ref. [28], uracil has two most preferential sites for its hydrogenation, viz., on its C_5 and C_6 carbon atoms, with the energy difference of 2.2 kcal/mol at the B3LYP/6-311G(2df,p) computational level in favor to the uracil C_5-hydrogenated radical with the binding energy of 31.6 kcal/mol. This energy difference agrees rather satisfactorily with the value of 2.0 kcal/mol predicted by the present calculation. The thio substitution of the O_{10} oxygen atom of uracil results, first, in that the most preferential site of the hydrogenation of 4TU changes to the C_6 carbon atom with the binding energy of 35.2 kcal/mol and, second, in that the sulphur atom becomes more favorable for the hydrogenation than the C_5 atom by 4.9 kcal/mol and less favorable by $\approx$ 2 kcal/mol compared to the C_6 site. It is interesting to notice that in the 4TU S_{10}-hydrogenated radical, the

excess hydrogen atom distances from the corresponding sulphur atom by 1.360 Å which is larger by ca. 0.25 Å compared to the analogous bond length in the carbon-hydrogenated radicals of uracil and thiouracils and is pointed nearly perpendicular (98.9°) out of the molecular plane. Reminding that the sulphur atom S_{10} forms a hydrogen bond with another base (see, e. g., Sections 8 and 9), we anticipate that the base pairing with the 4TU S_{10}-hydrogenated radical may substantially rupture this pairing and influence a stacking as well.

6. Interaction of Thiouracils and Their Tautomers with Water

The B3LYP/6-31+G(d,p) optimized structures of the most stable complexes of thiouracils with three water molecules residing at the w_1, w_2, and w_3 sites and composing the first hydration shell are displayed in Figure 3. Interacting with $(H_2O)_3$, the 2,4DTU thiouracil possesses two nearly isoenergetic complexes I and II having the binding energies of 18.5 and 19.2 kcal/mol and total dipole moments of 4.9 and 3.6 D, respectively. The latter one is a little stronger likely due, first, to that two water molecules donate hydrogen bonds to different sulphur atoms and, second, to that the formed water dimer has a shorter hydrogen bond and, thus, it is more stable than that in the complex II. As shown in Figure 3, the O_w- $H'_w \cdots S_{10}$ hydrogen bond between the water molecule w_3 in the complex II and the lone-pair of the sulphur atom S_{10} is shrinked by 0.05 Å compared to that formed between the water molecule w_1 and S_8 and it markedly lies out of plane. The latter feature has not been revealed for the uracil-water (see Ref. [29] and references therein) and $2TU(H_2O)_3$ and $4TU(H_2O)_3$ complexes. The lengths of all O_w-$H'_w \cdots S$ hydrogen bonds vary in the interval from 2.366 to 2.458 Å that is shorter than the sum of 3.05 Å of "classical" van der Waals radii of hydrogen and sulphur.

The binding energies of the $2TU(H_2O)_3$ and $4TU(H_2O)_3$ complexes are equal to 21.2 and 18.9 kcal/mol, respectively. Bearing in mind that in the gas phase, 4TU thiouracil is more stable by 1.67 kcal/mol than 2TU, we find that their first-coordination-shell hydration reverses the order, or, in other words, water slightly favors, by 0.7 kcal/mol, the stabilization of 2TU via forming the $2TU(H_2O)_3$ complex than 4TU. This is likely due to the quite similar reasons noticed above for the complexes I and II of $2,4DTU(H_2O)_3$ corrected by that, in the case of the $2TU(H_2O)_3$ complex, the functioning of the O_8 as a bidonor of hydrogen bond is preferential compared to the functioning of both O_8 and S_{10} as single donors.

We have demonstrated in Section 3 that the double thio substitution of uracil enhances by two orders an occurrence of possible mismatches. It has been shown there that the T_2 tautomer as the most polar one with the largest dipole polarizability compared to the other most stable tautomers of 2,4DTU has the stabilization energy of 11.7 kcal/mol. Examining the complexes of the most stable tautomers of 2,4DTU with $(H_2O)_3$, we reveal that water favors to lower the stabilization energy of T_2 one by 2.3 kcal/mol and to keep the stabilization energy of the T_1 one nearly ($\approx$ -0.2 kcal/mol) at the same level. The $T_2(H_2O)_3$ complex is particularly formed by means of the sulphur atom S_8 acting as the biacceptor of hydrogen bonds with the bond lengths of 2.359 and

2.383 Å and the corresponding bond angles of 174.5° and 142.3°. All hydrogen bonds in both these complexes lie in the molecular plane. It is highly worth noticing an appearance of a rather short S_{10}-H···O_w bond with the length of 1.807 Å that is by only 0.052 Å longer than the adjacent hydrogen bond in the water dimer.

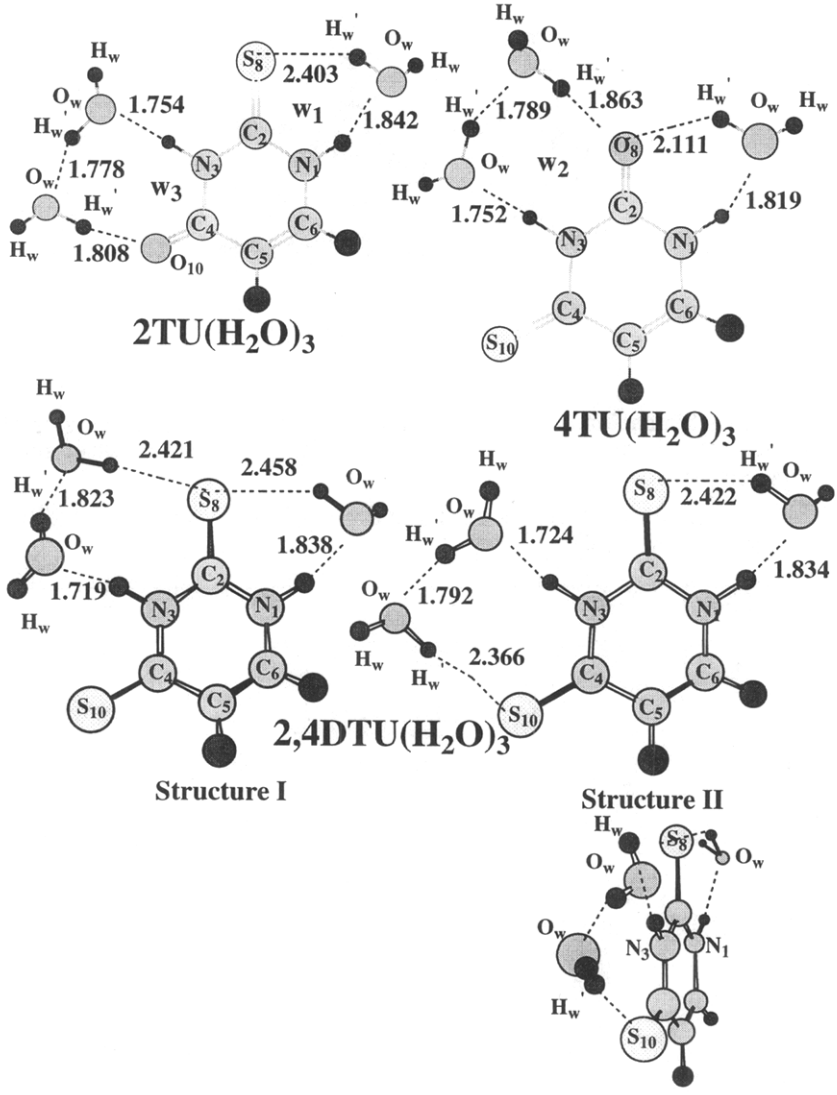

Figure 3. The complexes of thiouracils with three water molecules.

7. Tautomerism and Double Proton Transfer Mediated by Water

The present Section addresses the following question: how water molecule facilitates the tautomeric proton transfer. The tautomer T_2 is chosen for this

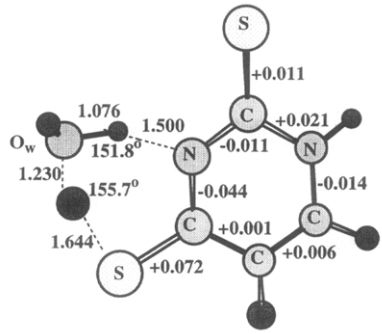

Figure 4. The transition state of the concerted double proton transfer of the tautomerization process 2,4DTU-w_3 $\Leftrightarrow$ T_2-w_3 mediated by a water molecule at the w_3 position.

Table 5. Interaction features of the hydrogen bonded uracil and 2TU base pairs (values in kcal/mol).

Base pair	$-\Delta E_{HB}$ ΔE_{def}	ΔE_T	ΔZPVE	ΔE
U·U_a	-17.35 1.80	-15.55 (-15.9)[a]	1.16	-14.39
U·U_c	-11.24 1.20	-10.42 (-10.5)[a]	0.82	-9.60
U·U_d	-10.66 1.07	-9.59 (-10.4)[a]	0.82	-8.77
2TU·2TU_a	-12.80 1.62	-11.18	0.61	-10.57
2TU·2TU_b	-12.01 1.79	-10.22	0.58	-9.64
2TU·2TU_c	-10.43 (-10.2)[b] 1.11 (0.6)[b]	-9.32 (-9.6)[b]	0.77 (0.9)[b]	-8.55 (-8.7)[b]
2TU·2TU_d	-8.23 (-9.3)[b] 0.95 (0.5)[b]	-7.28 (-8.8)[b]	0.56 (0.7)[b]	-6.72 (8.1)[b]

[a]Interaction energies calculated at the MP2/6-31G(d)(0.25)//HF/6-31G(d,p) computational level [10c].

[b]The optimization of the base pairs at the HF/6-31G(d) level and their interaction energies are evaluated at the MP2/6-31G(d)(0.25) level [10a].

purpose. We deal here with a concerted double proton transfer of the tautomerization process 2,4DTU-$w_3 \Leftrightarrow T_2$-w_3 in the presence of a bridging water molecule. The transition structure [2,4DTU-$w_3 \Leftrightarrow T_2$-w_3]^{tr} governing this process is displayed in Figure 4 where the changes of its intraring geometrical parameters compared to 2,4DTU are also indicated. This transition structure possesses the imaginary frequency $1056i$ cm^{-1} assigned to the simultaneous double proton transfer of H'_w and H_9. The double proton transfer is thus described by the asymmetric double well potential possessing two minima which correspond to the 2,4DTU-w_3 and T_2-w_3 complexes separated by an activation barrier. The energies of these complexes are equal to 15.4 and 4.3 kcal/mol relative to the barrier height. It implies particularly that a water molecule placed on the minor groove side of the Watson-Crick adenine-2,4DTU base pair substantially facilitates the aforementioned tautomerization process. It is interesting to compare the present activation barrier of 15.4 kcal/mol with the similar one governing the tautomerization of guanine (14.7 kcal/mol) [30a], cytosine (14-15 kcal/mol) [30b], and uracil (14.7 kcal/mol) [29] mediated by a water molecule. In the present case, the proton transfer from the lower well to the transition structure is accompanied by the excess entropy which, at T = 298.15 K, lowers the activation free energy of the double proton transfer to 12.3 kcal/mol.

Table 6. Characteristic vibrational frequencies in cm^{-1} of the 2TU thiobase and its pairs 2TU·2TU$_{a,b}$ characterized by pairs of the corresponding monomer vibrational modes (see text and Figure 5). IR intensities in km/mol are shown in parentheses.

ν	2-TU			
	Present work	Expt[a]	B3LYP/ 6-31G(d,p)[a]	MP2/ 6-31G(d,p)[a]
$\nu(N_1H)$	3636 (93)	3457 (151)	3570 (67)	3556 (108)
$\nu(N_3H)$	3599 (65)	3415 (79)	3537 (67)	3514 (71)
$\beta(N_1H)$	1572 (698)	1534 (623)	1545 (648)	1550 (821)
$\beta(N_3H)$	1455 (28)	1336 (22)	1431 (34)	1431 (36)
$\nu(C_2{=}S)$	1160 (146)	1148 (192)	1140 (120)	1165 (162)
$\gamma(N_3H)$	705 (83)	727 (4)	730 (31)	720 (90)
$\gamma(N_1H)$	612 (34)	604 (31)	608 (32)	589 (56)
	2TU·2TU			
	2TU·2TU$_a$		2TU·2TU$_b$	
$\nu(N_1H)$	3247 (0)	3283 (3070)	3270 (194)	3307 (2590)
$\nu(N_3H)$	3597.7 (122)	3594.9 (1)	3594.8 (96)	3595.0 (28)
$\beta(N_1H)$	1609 (1028)	1428 (310)	1608 (996)	1428 (297)
$\beta(N_3H)$	1462 (0)	1463 (46)	1461 (2)	1462 (44)
$\nu(C_2{=}S)$	908.9 (0)	909.5 (14)	1162 (3)	1173 (147)
$\gamma(N_3H)$	719 (21)	720 (0)	718 (22)	720 (1)
$\gamma(N_1H)$	825 (0)	836 (28)	786 (96)	812 (167)

[a] Experimental and theoretical frequencies [15b]. Theoretical frequencies are scaled by the factors of 0.98 and 0.96 for B3LYP/6-31G(d,p) and MP2/6-31G(d,p) computational levels, respectively.

8. Thiobase Pairs

In this Section we analyze the minimum energy structures of the H-bonded thiobase pair 2TU·2TU shown in Figure 5 and compare them with the analogous structures of the uracil U·U pairs [10]. Figure 5 displays four different minimum-energy structures of the 2TU·2TU thiobase pair. Despite the fact that the N_1 position is inaccessible in all canonically based pairs, the interest in such study steams out from from the importance to understand the interactions of nucleic acid bases and to accurately parametrize molecular mechanical force fields for a further modelling of nucleic acids. The global minimum is attained at the perfectly planar, symmetrical, and, thus, non-polar structure $2TU{\cdot}2TU_a$ whose binding energy defined as ΔE_{HB} + $\Delta ZPVE$ is equal to 12.2 kcal/mol (see Table 5). It is smaller by 4 kcal/mol than the analogous uracil base pair $U{\cdot}U_a$. This binding energy is largely attributed to the formation of the two symmetrical N_1-H$\cdots$$S_8$=$C_2$ hydrogen bonds with the bond length of 2.324 Å and the bond angle of 168.0°. The stabilization energy ΔE_T = - ΔE_{HB} + ΔE_{def} of such the complex is equal to -11.2 kcal/mol. It partly consists of the deformation energy ΔE_{def} of 1.6 kcal/mol related to the deformation of the constituent thiobases under the formation of the base pair $2TU{\cdot}2TU_a$ with respect to the optimized isolated thiobase 2TU. The corresponding changes in the thiobase geometry are mainly manifested in the elongation of the C_2=S_8 and N_1-H bonds by $\approx$ 0.02 Å and the compression of the N_1-C_2 bonds by $\approx$ 0.015 Å.

Spectroscopically, the formation of the $2TU{\cdot}2TU_a$ base pair manifests in the appearance of two pairs of vibrational modes, each composing of the symmetric and asymmetric ones. One pair describing the $\beta(N_3H)$ vibrational mode is splitted in the two vibrations at 1463 cm^{-1} (46 km/mol) and 1462 cm^{-1} (0 km/mol). The other one, assigned to the $\beta(N_1H)$ mode, is predicted at 1609 cm^{-1} (1028 km/mol) and 1428 cm^{-1} (310 km/mol). IR intensities are indicated in parentheses. Comparison with the analogous vibrations of 2TU predicted at 1455 cm^{-1} (28 km/mol) and 1572 cm^{-1} (698 km/mol) shows that the former pair of modes in the base pair is blue shifted by ca. 8 cm^{-1} and the latter pair of modes is blue shifted by 37 cm^{-1} and red shifted by 144 cm^{-1}, respectively. The other pair of vibrational modes is associated with the symmetric at 3247 cm^{-1} (0 km/mol) and asymmetric at 3283 cm^{-1} (3070 km/mol) stretches of the N_1-H bonds. They are both shifted to lower wavenumbers by 389 and 353 cm^{-1}, respectively, and IR of the asymmetric stretch is spectacularly enhanced by a factor of 33.

The buckled base pair $2TU{\cdot}2TU_b$ with the same type of bonding as the $2TU{\cdot}2TU_a$ base pair although with a broken symmetry lies by 0.8 kcal/mol above it. It is characterized by the total dipole moment of 1.0 D. A symmetry pertained to the $2TU{\cdot}2TU_a$ thiobase pair and related to the symmetrically disposed N_1-H$\cdots$$S_8$ hydrogen bonds is broken in the $2TU{\cdot}2TU_b$ pair resulting in a slightly different lengths of these H-bonds of 2.337 and 2.342 Å and the corresponding bond angles equal to 165.7° and 159.0°, respectively. This results in the two N-H stretching vibrations, viz., the symmetric one peaked at 3270 cm^{-1} with the IR intensity of 194 km/mol and the corresponding redshift of 366 cm^{-1} and the asymmetric vibration shifted to the red by 329 cm^{-1} and enhanced in IR by the factor of ca. 28. A similar structure has not been

found for the U·U base pair and we suggest that this is only due to presence of the sulphur atom resulting in the increase of the contribution of the second-order exchange and dispersion interactions (see Ref. [31] for review) into its stabilization. A symmetry breakdown in the $2TU{\cdot}2TU_b$ pair compared to the $2TU{\cdot}2TU_a$ one causes an excess of entropy of ca. 3.5 cal/mol·T. This turns out that at the ambient temperature T = 298.15 K, the buckled thiobase pair becomes somewhat more favorable than the planar one, with the corresponding free energy difference of 0.2 kcal/mol. Summarizing, there are two highly stable structures of the 2-thiouracil base pair which lie very close to each other and, therefore, at ambient temperature there might exist some 'averaged' base pair with rather large amplitude of bending and bugling.

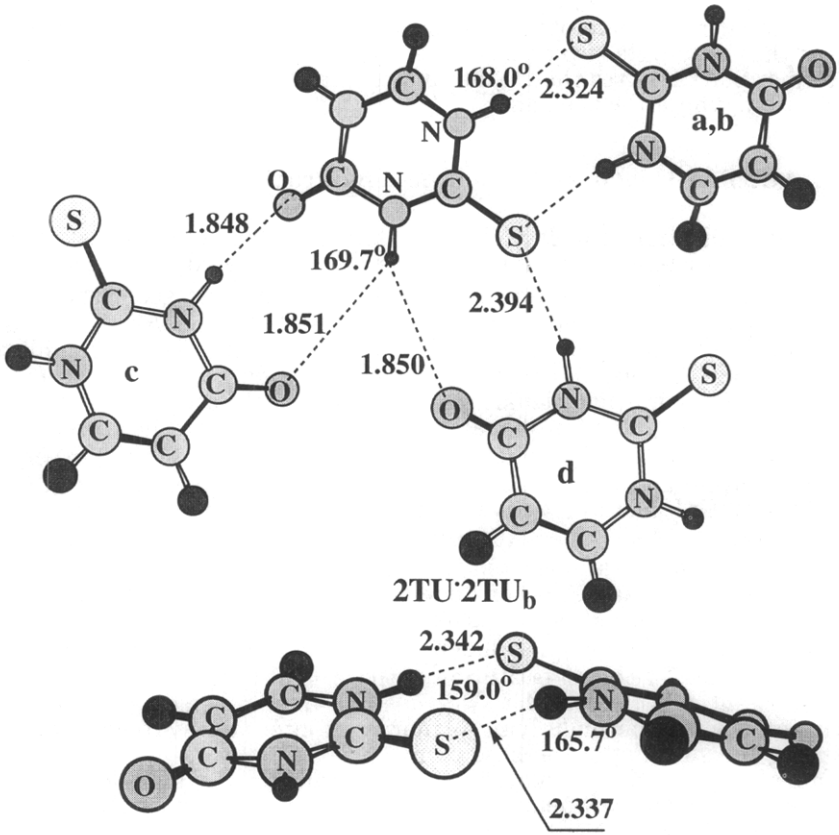

Figure 5. Thiobase pairs.

The buckled thiobase pair is separated by ca. 0.8 kcal/mol from the less stable planar structure $2TU{\cdot}2TU_c$ with the symmetrical $N_3\text{-}H\cdots O_{10}{=}C_4$ type

of hydrogen bonding and the binding energy of 9.7 kcal/mol. Both formed hydrogen bonds are characterized by bond lengths of 1.848 Å and bond angles of 169.7°. Their symmetric and asymmetric stretching vibrations are red shifted by 325 and 294 cm^{-1} and IR intensity of the latter one is enormously increased by a factor of 34. The hetero-type of bonding when the studied thiobases form two H-bonds of the N_3-H$\cdots$$O_{10}$=$C_4$ and N_3-H$\cdots$$S_8$=$C_2$ types corresponds to the less stable structure 2TU·2TU_d with the binding energy of 7.7 kcal/mol.

The order of stability of the 2TU·2TU base pairs can be easily explained in terms of the DPEs of the N-H groups of the 2TU thiobase and the PAs of its sulphur and oxygen atoms. As follows from Table 4, the DPE of the N_1-H group is lower than that of the N_3-H group by ca. 9 kcal/mol whereas the PA of the S_8 atom is lower than the PA of the O_{10} atom by only 0.6 kcal/mol. That is why the thiobase pair 2TU·2TU_a with the more acidic N_1-H bonds is more stable than 2TU·2TU_c with the less acidic N_3-H bonds. On the other hand, comparing the two other thiobase pairs, 2TU·2TU_c and 2TU·2TU_d, one notices that they differ from each other by a single hydrogen bond which, for the former pair, involves the O_{10} atom as the acceptor, and, for the latter one, the S_8 atom whose PA is smaller.

9. Adenine-Uracil and Adenine-Thiouracil Base Pairing

We have mentioned in Introduction that the adenine-uracil A·U Watson-Crick (WC) pair base is one of major base pair in RNA codon-anticodon complex and in modified DNA and PNA [5a]. Its optimized geometry, together with the optimized geometries of the A·2TU, A·4TU, and A·2,4DTU, is displayed in Figures 6 and 7. Except the geometry of the latter pair, all other base pairs have the planar structures. As seen in Figure 7, the structure of the A·2,4DTU WC pair is not planar, viz., the constituent base pairs are twisted to each other by 26.4°. Its non-planarity is completely due to the correlation because at the HF/6-31+G(d,p) level, it is perfectly planar. On the other hand, in order to avoid an interpretation of this non-planarity as a sort of shortcomings of the B3LYP method, we have performed an additional optimization with the second-order Møller-Plessett perturbation theory MP2/3-21+G(d,p). The latter clearly demonstrates the tendency to the non-planarity of the A·2,4DTU WC base pair. We may thus conclude that the origin of this non-planarity is likely due to the second-order exchange interactions because the dispersion interactions are mainly angular independent [30]. Therefore, summarizing, we suggest that the 2,4-thio-substitution of the A·U in RNA, modified DNA, and PNA substantially distorts the Watson-Crick double helix architectural motif via influencing the underlying planarity of interbase hydrogen bonds and rupturing the stacking of the base pairs.

Table 7 reports the calculated value of parameter R which determines the distance between the carbon atoms of the sugar rings linked by glycosidic bond to the nucleic bases at N_9(A) and N_1(U) and replaced by the hydrogen atoms in the present study and the angles α_1 and α_2 measuring the inclination of the glycosidic links to the **R** direction (see Figure 6) [5a]. Inspecting this Table, we reveal that the present value of R = 10.12 Å for the A·U WC base pair is in a rather good agreement with its experimental value of 10.44 Å for the A·U crystal [32]. The values of the angles α_1 and α_2 of this base pair equal to 54.4°

(57.4°) and 55.5° (56.2°) also match rather well the crystallographic

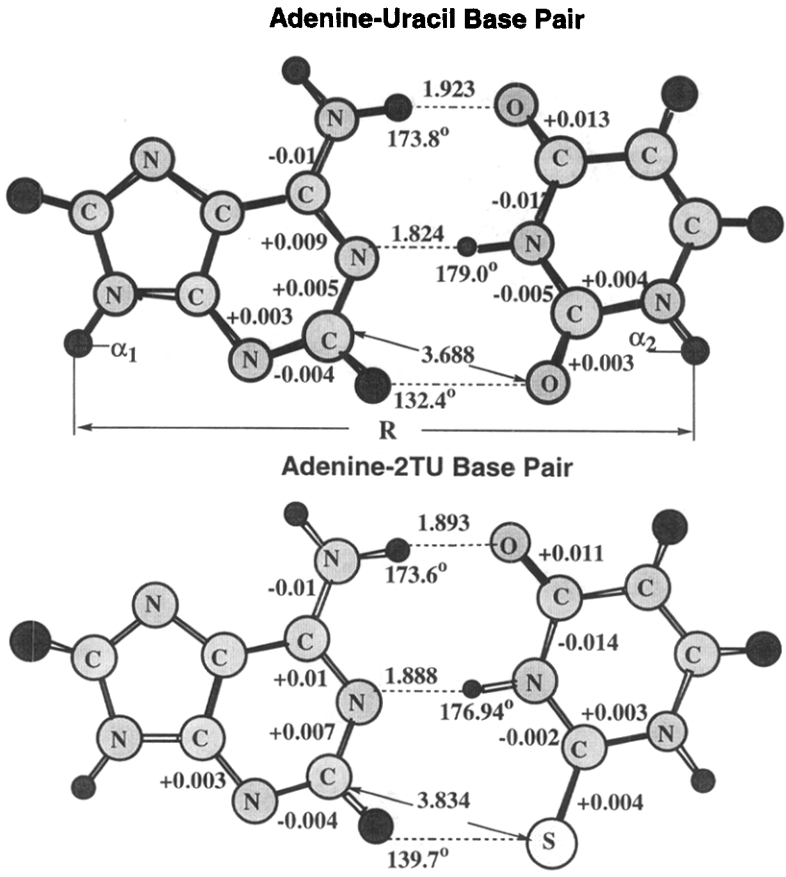

Figure 6. A·U and A·2TU base pairs.

experimental values [32] given in the parentheses. We also find that R(A·2TU) exceeds R(A·2TU) by 0.14 Å whereas the others R(A·4TU) and R(A·2,4DTU) are smaller by 0.37 and 0.05 Å compared to R(A·U), respectively. On the other hand, the angles α_1(A·4TU) and α_2(A·4TU) are larger than the corresponding ones of the A·U base pair by 5.2° and 8.7°, respectively. In this regard, it is worth mentioning that, according to Spencer estimations for the A·T WC pair [33], if the parameter R varies from 10.5 and 12.1 Å and the angles α_1 and α_2 from 36° and 59°, the accompanied variations of the bases disposition in the base pair do not significantly affect the double helix structure. Analyzing

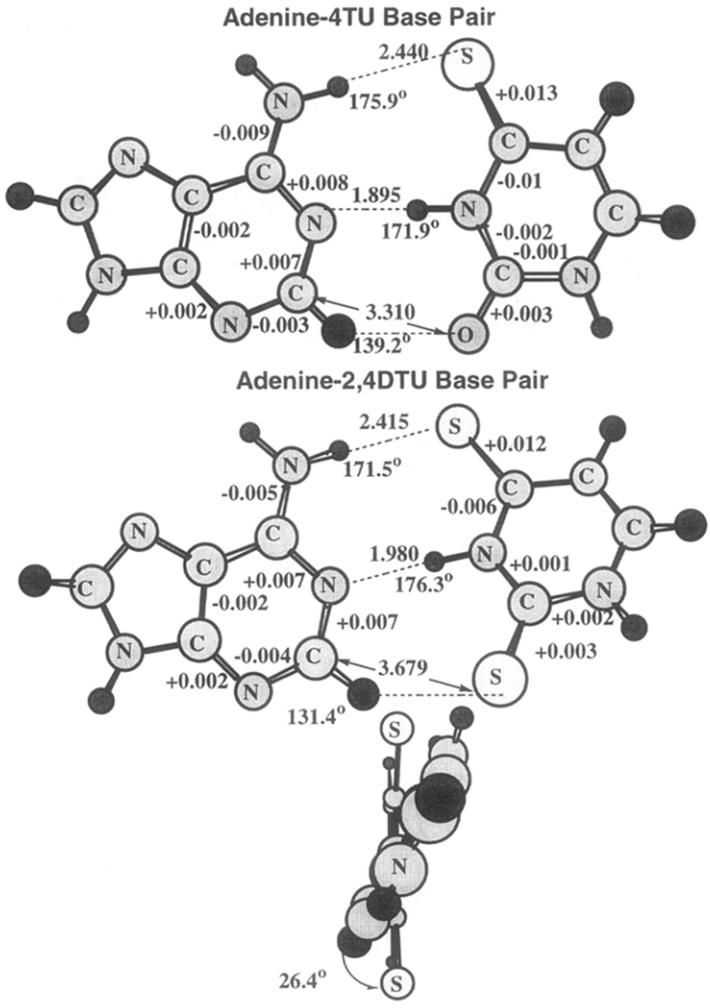

Figure 7. A·4TU and A·2,4DTU base pairs.

Table 7, we observe an opposite trend, namely, a thio substitution of uracil in the A·U WC base pair compresses R to 9.75 Å for the A·4TU WC base pair and increases the angles beyond the Spencer interval to 64.3° for the same base pair. This implies that such thio substitution causes rather substantial strain in the double helix structure which is more pronounced in the case of the A·4TU WC base pair.

Table 7 also includes the hydrogen bond lengths of the studied WC base pairs between adenine, on the one side, and uracil and its thio-derivatives, on the other one. Its analysis results in that, first, the 2-thio substitution of uracil decreases the H-bond contact by 0.032 Å on the major groove side,

second, the 4-thio substitution reduces it by 0.455 Å on the minor groove side, and finally, third, the hydrogen bond lengths r($(C_2(A))H\cdots O_8(U)$) in the normal A·U WC base pair and r($(C_2(A))H\cdots S_8$(2,4DTU)) in the modified A·2,4DTU one are nearly of the same length, with the difference of 0.004 Å, despite the fact that in the former, the oxygen atom acts as the acceptor of a rather weak H-bond because its length of 2.866 Å exceeds 2.6 Å, the sum of "classical" van der Waals radii of the hydrogen and oxygen atoms, while in the latter, it is the sulphur atom that acts as the H-bond acceptor. A slightly longer $(C_2(A))H\cdots S_8$(2TU) distance of 2.940 Å is predicted for the modified A·2TU base pair on the minor groove side. Therefore, it is likely that the thio substitution makes the C-H···S much stronger compared to the C-H···O one. We find by the comparison, for instance with the above discussion of the interaction of uracil and its thio-derivatives with water, that the difference between the hydrogen bond lengths of the $O\cdots H_w$-O_w and O···C-H H-bonds comprises of $\approx$ 1 Å, whereas that between $S\cdots H_w$-O_w and S···C-H is only 0.4 Å. It might also be interesting to notice that in the A·4TU WC base pair, the hydrogen bond $(C_2(A))H\cdots O_8$(4TU) of 2.411 Å is one of the shortest H-bond in the base pairs reported in the literature [34].

Table 7. Geometrical parameters and hydrogen bond lengths of the adenine-uracil and adenine-thiouracil Watson-Crick base pairs. Distances in Å, angles in degrees. In the distance notations, the former base belongs to adenine while the latter one to uracil or thiouracils.

Base pair	R H_6-O_{10} N_1-N_3	α_1 $\angle N_6HO_{10}$ H_6-O_8	α_2 N_1-H_3 C_2-O_8	N_6-O_{10} $\angle N_1HN_3$ $\angle C_2HO_8$
A·U	10.116	54.41	55.54	2.941(3.09)[a]
	1.923	173.8(172.2)[a]	1.824	179.0(178.8)[a]
	2.872(2.99)[a]	2.866(2.96)[a]	3.688	132.4
A·2TU	10.257	53.33	53.64	2.909(3.03)[a]
	1.893	173.6(172)[a]	1.888	176.9(174.4)[a]
	2.935(3.08)[a]	2.940(3.11)[a]	3.834	139.7
A·4TU	9.746	59.60	64.28	3.457(3.66)[a]
	2.440	175.9(173.7)[a]	1.895	171.9(170.3)[a]
	2.935(3.08)[a]	2.411(2.50)[a]	3.310	139.2
A·2,4DTU	10.072	55.92	59.60	3.426
	2.415	171.5	1.980	176.3
	3.022	2.870	3.679	131.4

[a]The geometry of the base pairs is optimized at the HF/6-31G(d) level and further evaluated at the MP2/6-31G(d)(0.25) level [10].

Table 8 collects the information on the interaction features of the Watson-Crick A·U and A·thiouracils base pairs. As follows from its last column, the total energies of the A·U and A·2TU base pairs after ZPVE correction are nearly identical and differ from each other by 0.4 kcal/mol. In this Table we separate the deformation energies of adenine and uracil or thiouracil under the corresponding base pairing. We find then that both uracil and thioracils experience more substantial deformations compared to adenine. These deformations are also indicated in Figures 6 and 7.

Table 8. Interaction of the Watson-Crick A·U and A·thiouracils base pairs.

Base pair	$-\Delta E_{HB}$ ΔE^{A}_{def} $\Delta E^{U,a}_{def}$	$-\Delta E_T$	ΔZPVE	$-\Delta E$
A·U	-12.94(-12.4)[a] 0.40 0.99(0.6)[a]	-11.55(-11.8)[a]	1.38(1.3)[a]	-10.17(-10.5)[a]
A·2TU	-12.50(-12.8)[a] 0.35 1.01(0.7)[a]	-11.14(-12.1)[a]	1.36(1.2)[a]	-9.78(-10.9)[a]
A·4TU	-10.99(-11.8)[a] 0.29 0.98(0.6)[a]	-9.72(-11.2)[a]	1.16(0.1)[a]	-8.56(-11.1)[a]
A·2,4DTU	-8.89 0.36 1.03	-7.50	1.18	-6.32

[a]The optimization of the base pairs at the HF/6-31G(d) level and their interaction energies are evaluated at the MP2/6-31G(d)(0.25) level [10]. The total deformation energy is indicated in parentheses.

10. Summary and Outlook

In the present work we juxtapose different subtle features of the thio-derivatives of uracil thus shed a certain light on why their functioning is so unusual. It is, afterall, the very electronic structure of the sulphur atom that, replacing the oxygen atom in uracil, entails the substantial changes in the uracil geometry and, due to enhancing in particular its dipole polarizability, in its interaction with water and nucleobase pairing. This is actually the major thrust of the present work toward providing a clue to the known features of thiated nucleobases and demonstrating the novel ones such as, e. g., those related to possible radiation damage of thiouracils, the increase of occurrence of the spontaneous point mutations by a factor of nearly 100 under the double thio substitution, the noticable out-of-plane position of water molecule bonded to the sulphur atom S_{10} and N_3-H bond in the 2,4DTU, the stabilization of 2TU by the first hydration shell compared to 4TU, the excess entropy effect on the double proton tautomerization mediated by water which reduces the activation barrier to 12.3 kcal/mol, the buckling of the modified 2TU·2TU base pair, and finally, the twisted non-planarity of the adenine-2,4DTU base pair and the appearance of the substantial strain in the double helix structure cased by the A·4TU base pair. Many of these features, particularly the aforementioned ones related to the functioning of thiouracils in the nucleobase pairs, are explained by the appearance of rather strong contributions of the dispersion and exchange interactions under thio substitution.

Acknowledgements

E. S. K. gratefully thanks the Organizing Committee and E. Brändas in particular for the invitation, and I. Kaplan, V. Ortiz, and B. Silvi for useful discussions. Earlier discussions with P.-O. Löwdin on the mechanism of base pair mismatches are also appreciated. Support of the University Leuven within Fellowship Grant is acknowledged. M. T. N. thanks the Fund for Scientific Research FWO - Vlaanderen for financial support. The authors also appreciate Th. Zeegers-Huyskens for stimulating discussions and L. A. Eriksson for providing the work [26b] prior to its publication.

References

[1] (a) M. J. Novak, L. Lapinski, J. S. Kwiatkowski, and J. Leszczynski, in "Computational Chemistry: Reviews of Current Trends", vol. 2, ch. 4 (Eds. J. Leszczynski, World Scientific, Singapore, 1997); (b) P. Hobza and J. Šponer, Chem. Rev. 99, 3247 (1999).

[2] (a) V. Martinez-Merino and M. J. Gill, J. Chem. Soc., Perkin Trans. 2 33 (1999); (b) M. Črnugelj, D. Dukhan, J.-L. Barascut, J.-L. Limbach, and J. Plavec, *Ibid.* 255 (2000).

[3] (a) N. A. Van Draanen, G. A. Freeman, S. A. Short, R. Harvey, R. Jansen, G. Szczech, and G. W. Koszalka, J. Med. Chem. 39, 538 (1996); (b) S. G. Rahim, N. Trivedi, M. V. Bogunivich-Batchelor, G. W. Hardy, G. Mills, J. W. T. Sellway, W. Snowden, E. Liiler, P. L. Coe, I. Basnak, R. F. Whale, and R. T. Walker, *Ibid.* 39, 789 (1996); (c) M. A. Clement and S. H. Berger, Med. Chem. Res. 2, 154 (1992); (d) M. I. Elzagheid, M. Oivanen, R. T. Walker, and J. A. Secrist, Nucleosides Nucleotides 18, 181 (1999); (e) E. R. T. Tiekink, P. D. Cookson, B. M. Linaham, and L. K. Webster, Met. Based Drugs 299 (1994) and references therein.

[4] (a) W. Saenger and D. Suck, J. Mol. Biol. 50, 153 (1970); (b) E. M. Gotschalk, E. Kopp, and A. G. Lezius, Eur. J. Biochem. 24, 168 (1971); (c) P. E. Nielsen, Acc. Chem. Res. 32, 624 (1999).

[5] (a) W. Saenger, "Principles of Nucleic Acid Structure" (Springer, New York, 1984), ch. 7; (b) U. Thewald and C. E. Bugg, J. Am. Chem. Soc. 94, 8892 (1972); (c) K. H. Scheit and E. Gartner, Biochim. Biophys. Acta 182, 10 (1969).

[6] (a) S. H. Kim, J. L. Sussman, F. L. Suddath, G. J. Quigley, A. McPherson, A. H. Wang, N. C. Seeman, and A. Rich, Proc. Natl. Acad. Sci. USA 71, 4970 (1974); (b) B. R. Reid, N. S. Ribeiro, G. Gould, G. Robillard, C. W. Hilbers, and R. G. Shulman, *Ibid.* 72, 2049 (1975); (c) C. F. Beck and G. Howlett, J. Mol. Biol. 111, 1 (1977); (d) R. Vormbrock, R. Morawetz, and H. G. Gassen, Biochim. Biophys. Acta 340, 348 (1974); (e) G. H. Lin and M. Sundaralingham, Acta Crystallogr. B 27, 961 (1971); (f) G. H. Lin and M. Sundaralingham, J. Am. Chem. Soc. 93, 1235 (1971).

[7] (a) A. R. Katritzky and J. M. Lagowski, in "Adv. Heterocyclic Chem.", vol. 1, 400 (Eds. A. R. Katritzky and A. J. Boulton, Academic, New York, 1963); (b) J. S. Kwiatkowski and B. Pullman, in "Adv. Heterocyclic Chem.", vol. 8, 256 (Eds. A. R. Katritzky and A. J. Boulton, Academic, New York, 1975); (c) A. R. Katritzky, G. Baykut, S. Rachwal, M. Szafran, and K. C. Caster, J. Chem. Soc., Perkin Trans. 2 1499 (1989); (d) I. Winckelmann and E. H. Larsen, Synthesis 1041 (1986); (e) Yu. V. Rubin, F. A. Savin, and Yu. P. Blagoi, Studia Biophys. 123, 203 (1988).

[8] (a) W. H. Miller, R. O. Roblin, and E. B. Astwood, J. Am. Chem. Soc. 67, 2201 (1945); (b) R. Jeemer and J. Rossels, Biochim. Biophys. Acta 11, 438 (1953); (c) R. Hammers, *Ibid.* 21, 170 (1956); (d) J. A. Carbon, L. Hung, and D. S. Jones, Proc. Natl. Acad. Sci. USA 53, 979 (1965); (e) M. N. Lipsett and B. P. Doctor, J. Biol. Chem. 242, 4072 (1967).

[9] (a) M. Yoshida, T. Takeishi, and T. Ukida, Biochim. Biophys. Acta 228, 15 (1971); (b) C. F. Beck and G. J. Howlett, J. Mol. Biol. 111, 1 (1977); (c) N. I. Saxand R. J. Lewis, "Dangerous Properties of Industrial Materials" (Van Nostrand Reinhold, New York, 1989); (d) G. K. McEvoy, Ed., "AHFS Drug Information" (American Society of Hospital Pharmacists, Inc., Bethesda, MD, 1989); (e) Z. Wang and T. Rana, Biochemistry 35, 6491 (1996).

[10] (a) J. Šponer, J. Leszczynski, and P. Hobza, J. Phys. Chem. A 101, 9489 (1997); (b) J. Šponer and P. Hobza, Chem. Phys. Lett. 267, 263 (1997); (c) M. Kratochvil, O. Engkvist, J. Šponer, P. Jungwirth, and P. Hobza, J. Phys. Chem. A 102, 6921 (1998).

[11] (a) M. H. Abraham, P. P. Duce, D. V. Prior, D. G. Barratt, J. J. Morris, and P. J. Taylor, J. Chem. Soc., Perkin Trans. 2 1355 (1989); (b) C. Laurence, M. Berthelot, J.-Y. Le Questel, and M. J. El Ghomari, *Ibid.* 2075 (1995); (c) J.-L. M. Abboud, C. Roussel, E. Gentric, K. Straidi, J. Lauransan, G. Guihéneuf, M. Kamlet, and R. W. Taft, J. Org. Chem. 53, 1545 (1988); (d) H. Borrmann, I. Persson, M. Sandström, and C. M. V. Stålhandske, J. Chem. Soc., Perkin Trans. 2 39 (2000).

[12] (a) R. G. Pearson, "Hard and Soft Acids and Bases" (Dowden, Hutchinson and Ross, Stroudsburg, PA, 1973); (b) R. G. Pearson, "Chemical Hardness: Applications from Molecules to Solids" (Wiley-VCH, Weinheim, 1997).

[13] J. March, "Advanced Organic Chemistry" (Wiley, New York, 1992).

[14] F. H. Allen, C. M. Bird, R. S. Rowland, and P. R. Raithby, Acta Crystallogr. B 53, 680 (1997).

[15] (a) H. Rostkowska, K. Szczepaniak, M. J. Nowak, J. Leszczynski, K. KuBulat, and W. B. Person, J. Am. Chem. Soc. 112, 2147 (1990); (b) L. Lapinski, H. Rostkowska, M. J. Nowak, J. S. Kwiatkowski, and J. Leszczynski, Vibrat. Spectrosc. 13, 23 (1996).

[16] M. Geller, A. Jaworski, and A. Pohorille, Int. J. Quantum Chem. 15, 369 (1979).

[17] G. C. Pimentel and A. C. McClellan, "The Hydrogen Bond" (Freeman, San Francisco, 1960).

[18] J. Emsley, "The Elements" (Oxford University, Oxford, 1996).

[19] (a) P.-O. Löwdin, Rev. Mod. Phys. 35, 724 (1963); (b) P.-O. Löwdin, Adv. Quantum Chem. 2, 213 (1965).

[20] E. S. Kryachko, M. T. Nguyen, and Th. Zeegers-Huyskens, J. Phys. Chem. A 104 (2000).

[21] (a) H. Chojnacki and W. A. Sokalski, J. Theor. Biol. 54, 167 (1975); (b) M. Aida, C. Nagata, I. Ohmine, and K. Morokuma, *Ibid.* 99, 599 (1982); (c) J. Lipinski, J. Mol. Struct. (Theochem) 201, 87 (1989).

[22] (a) J. Leszczynski, Int. J. Quantum Chem. Quantum Biol. Symp. 18, 9 (1991); (b) J. Leszczynski and K. Lammertsma, J. Phys. Chem. 95, 3128 (1991); (c) A. Lés and L. Adamowicz, J. Am. Chem. Soc. 112, 1504 (1990); (d) J. Leszczynski, J. Phys. Chem. 96, 1649 (1992); (e) Yu. V. Rubin, Yu. Morozov, D. Venkateswarlu, and J. Leszczynski, *Ibid.* A 102, 2194 (1998).

[23] *GAUSSIAN 98* (Revision A.5); M. J. Frisch, G. W. Trucks, H. B. Schlegel, G. E. Scuseria, M. A. Robb, J. R. Cheeseman, V. G. Zakrzewski, J. A. Montgomery, Jr., R. E. Stratmann, J. C. Burant, S. Dapprich, J. Millam, A. D. Daniels, K. N. Kudin, M. C. Strain, O. Farkas, J. Tomasi, V. Barone, M. Cossi, R. Cammi, B. Mennucci, C. Pomelli, C. Adamo, S. Clifford, J. Ochterski, G. A. Petersson, P. Y. Ayala, Q. Cui, K. Morokuma, K. D. Malick, A. D. Rabuck, K. Raghavachari, J. B. Foresman, J. Cioslowski, J. V. Ortiz, B. B. Stefanov, G. Liu, A. Liashenko, P. Piskorz, I. Komaromi, R. Gomperts, R. L. Martin, D. J. Fox, T. Keith, M. A. Al-Laham, C. Y. Peng, A. Nanayakkara, C. Gonzalez, M. Challacombe, P. M. W. Gill, B. Johnson, W. Chen, M. W. Wong, J. L. Andres, C. Gonzalez, M. Head-Gordon, E. S. Replogle, and J. A. Pople (Gaussian, Inc., Pittsburgh, PA, 1998).

[24] E. S. Kryachko, M. T. Nguyen, and Th. Zeegers-Huyskens, J. Phys. Chem. A 104 (2000).

[25] (a) W. Förner, P. Otto, and J. Ladik, Chem. Phys. 86, 49 (1984); (b) P. Hobza and C. Sandorfy, J. Am. Chem. Soc. 109, 1302 (1987).

[26] (a) L. V. Mendelman, M. S. Boosalis, J. Petruska, and M. F. Goodman, J. Biol. Chem. 264, 14415 (1989); (b) see also A. Lés and L. Adamowicz, J. Phys. Chem. 93, 7078 (1989).

[27] (a) A.-O. Colson and M. D. Sevilla, Int. J. Radiat. Biol. 67, 627 (1995); (b) S. D. Wetmore, L. A. Eriksson, and R. J. Boyd, in "Theoretical Biochemistry - Processes and Properties of Biological Systems"; Theoretical and Computational Chemistry, vol. 9 (Ed. L. A. Eriksson, Elsevier, Amsterdam, 2000).

[28] S. D. Wetmore, R. J. Boyd, and L. A. Eriksson, J. Phys. Chem. B 102, 5369 (1998).

[29] E. S. Kryachko, M. T. Nguyen, and Th. Zeegers-Huyskens, J. Phys. Chem. A 104 (2000).

[30] (a) Z. Smedarchina, W. Siebrand, A. Fernández-Ramos, L. Gorb, and J. Leszczynski, J. Chem. Phys. 112, 566 (2000); (b) S. Morpurgo, M. Bossa, and G. O. Morpurgo, Adv. Quantum Chem. 36, 169 (2000).

[31] I. G. Kaplan, "Theory of Molecular Interaction" (Elsevier, Amsterdam, 1986).

[32] N. C. Seeman, J. M. Rosenberg, F. L. Suddath, J. J. P. Kim, and A. J. Rich, J. Mol. Biol. 104, 145 (1976).

[33] M. Spencer, Acta Crystallogr. 12, 66 (1959).

[34] M. Brandl, K. Lindauer, M. Meyer, and J. Sühnel, J. Theor. Chem. Acc. 101, 103 (1999).

Towards a Rigged Born-Oppenheimer Electronic Theory of Chemical Processes

O.Tapia
Department of Physical Chemistry, Uppsala University,
Box 532, S-75121 Uppsala,Sweden

Abstract

A direct relationship between chemical species and electronic quantum state is obtained with a rigged Born-Oppenheimer (R-BO) approach. The problems with the standard separation in the BO scheme are bypassed with the definition of an auxiliary electrodynamic model system, i.e. an electronic system interacting with a classical set of fixed external Coulomb sources. The electronic stationary states derive from electronic Schrödinger equations wherefrom numerical solutions are obtained. These wave functions do not parametrically depend upon arbitrary nuclear configurations. However, they determine trapping potentials in nuclear configuration space. We show that, for any value of the nuclear configuration coordinates, electronic wave functions for different attractors must be orthogonal if they are to diagonalize the molecular Hamiltonian. The nuclear stationary states are obtained from the nuclear Schrödinger equation including the kinetic energy and trapping potential. The products of electronic and nuclear wave functions are shown to render diagonal the exact total molecular Hamiltonian. The procedure permits the assignment of an electronic state to a given chemical species. This latter is labeled by the stationary geometry of the model external sources of Coulomb potential. Inertial reference frames can be introduced in a very simple manner. For chemical reactions in the gas phase, the R-BO approach naturally leads to a state-to-state description in a quantum scattering theory context. The chemical change corresponds to a change of electronic state induced by an external field (electromagnetic or/and ultrasound). The transition amplitudes permit the introduction of electronic parity rules that impose strict selection rules. Franck-Condon nuclear overlap integrals factor out the transition moment integrals; they are used to discuss mechanistic issues. For reactant and product channels having equal parity, the theory enforces the mediation of an electronic state differing in parity, termed as a quantum transition-state (QTS); for electric-dipole mediated processes, the QTS state wave function must have a negative parity component. For bimolecular mechanisms, the cross sections depend upon the FC integral between the QTS and the wave packets describing reactants or products; the cross sections are directly determined by the QTS vibration spectra.

ADVANCES IN QUANTUM CHEMISTRY, VOLUME 40

0065-3276/01 $35.00

Contents

1 Introduction

Separation of electronic and nuclear dynamics is a fundamental idea underlying the Born-Oppenheimer (BO) scheme [1]. The actual form given to the total wave function in the BO approximation is a matter of concern, especially when orbital basis sets located on the atoms are used in standard computations. The problem is the adiabatic transformation of an electronic state of a given symmetry driven by a change of "nuclear" coordinates into a different one. However, what has been overlooked is the fact that continuous transformations between different point symmetry groups, or between different electronic states, is forbidden quantum mechanically. Moreover, the continuous change of an electronic wave function in the BO scheme blurs the relationship between a chemical species and a quantum electronic state. The description based on adiabatic electronic potential energy functions is basically a classical mechanical description. This kind of adiabatic change is a key issue to be remedied before rigorous quantum mechanics can be employed to describe chemical processes. On the other hand, computing schemes based on the adiabatic idea have had enormous success [2] and the question is whether by complementing the interpretation of the BO scheme one can recover a proper quantum mechanical picture. If a one-to-one map were possible to construct between chemical species and electronic stationary wave function, thereby putting aside the adiabatic scheme, a change of electronic structure would have to be seen as a Franck-Condon process. This would entail a different way to describe chemical processes. The elementary chemical conversion would happen on time scales at or below the femtosecond range while the whole extension of the configuration space participates in the change via the transition moment integral. In this paper, a theoretical analysis is developed to help state the conditions required to formulate a new approach that is as closely related as possible to the standard quantum chemical scheme.

In section 2, the formalism behind the separation of nuclear and electronic systems is sketched. The theory leading to an approach complementing the BO scheme used hitherto is introduced. The driving idea is to eliminate the use of the dynamical coordinates in defining reference frames. A rigged BO scheme is obtained where a one-to-one mapping between chemical species and electronic

quantum state is the most salient feature. In section 3, the chemical change is described as a Franck-Condon process. The necessity of transition states is shown from a quantum mechanical analysis involving parity selection rules [3].

2. Electro-nuclear separation theory

In the quantum mechanics of a system of n_e-electrons and n_N-nuclei, neglecting relativistic effects, the fundamental energy operator is the Coulombic Hamiltonian, H(r,Q). Since the total momentum and angular momentum are constant of motion, it is customary accepted that it is convenient to separate the motion of the "center-of-mass" and the rotations of the system as a whole. Assuming such a procedure was feasible, the new Hamiltonian H´ does not define the atoms and molecules involved. Furthermore, chemistry requires the introduction of molecular structure and that is not a concept evolving from the general quantum theory [4;5]. From the very beginning, Born and Oppenheimer in their seminal paper [6] used the nuclear framework to define a reference system and introduced the concept of nuclear equilibrium structure. Wooley and Sutcliffe [1;5;7], Goscinski and Mujica [8] and Klein [9] have shown the drawbacks with such a procedure.

2.1 Electronic system in external Coulomb potentials

In this work we bypass this problem by considering first a more general class of electronic systems. The electronic systems included here are those interacting via static classical external sources of Coulomb potentials. These sources have no connection to the mass distribution. This approach departs from the standard clamped nuclei picture [1], although for all practical purposes the numerical results obtained for equivalent cases would be indistinguishable. A second aspect to the new approach is based on a simple remark. It is not the Hamiltonian H or H´ that define the state of system but the electronic eigenstates, if they exist. Two isomers, having the same global Hamiltonian H, but different electronic spectra, must be related to different boundary conditions. These will be expressed via auxiliary electronic Hamiltonians wherefrom the electronic eigenfunction should

be derived.

Let us first define the general problem, namely, to find solutions to the Schrödinger equation for the global system

$$H(r,Q)\,\Psi(r,Q) = E\,\Psi(r,Q) \qquad (1)$$

H(r,Q) is the Hamiltonian of the interacting electrons and nuclei. The configuration variables of n_e electrons, $r=(r_1,\ldots,r_{ne})$, and n_N nuclei, $Q=(Q_1,\ldots,Q_{nN})$ are defined with respect to a coordinate frame fixed in the laboratory. The nuclei are identified by their nuclear charges, $Z=(eZ_1,\ldots,eZ_{nN})$, where e is the electron charge, and the mass vector (or block diagonal $3n_N x 3n_N$ matrix) $M=(m_1,\ldots,m_{nN})$.

In general, H(r,Q) is invariant to a translation of origin of the laboratory frame, not to be mixed up with the space fixed frame which moves with the center-of-mass commonly used [1]. Let us select a particular (arbitrary for the time being) origin with real space coordinates **u**. Applying the corresponding translation operator H(r,Q) changes into:

$$H \dashrightarrow H' = K_u + H_m(\Gamma) - \mathbf{P}_{Ku}\cdot\mathbf{p} \qquad (2)$$

K_u is the kinetic energy operator for the global system. If the reference frame attached to **u** is moving with uniform motion (inertial frame), then eq.(2) describes this situation. There is no "center-of-mass" involved, just a new inertial frame. The wave functions are delta-normalized (they do not belong to the square integrable function domain). The coupling operator between global and internal dynamics is given by $V_u = -\mathbf{P}_{Ku}\cdot\mathbf{p}$. The operator **p** is related to the linear momentum operator for the molecular system ($\mathbf{p}_e+\mathbf{p}_N$) and $\mathbf{P}_{Ku}$ is related to the global linear momentum operator (mass factor involved are not relevant at this stage of analysis). The solution of eq.(1) requires of well defined boundary conditions. In a basis of the global momentum eigenstates, the transformed operator is diagonal. The result is only natural. If there are solutions to eq.(1) with appropriate boundary conditions written in an arbitrary laboratory inertial frame, it does not matter where we select the origin.

The molecular Hamiltonian, $H_m(\Gamma)$, in the fixed frame with origin **u**, is given

by the sum of nuclear and electronic operators,

$$H_m(\Gamma) = K_N(R; M)+H_e(\Gamma;Z) = K_N+K_e+V_{ee}(\rho)+V_{eN}(\rho,R;Z)+V_{NN}(R;Z) \quad (3)$$

The configuration coordinates of electrons (ρ) and nuclei (R) in the new frame are related to the laboratory one by $r_k = \mathbf{u} + \rho_k$, $Q_{k'} = \mathbf{u} + R_k$, symbolically written as $r = \mathbf{u}+\rho$, $Q=\mathbf{u}+R$, and $\Gamma=(\rho,R)$. K_e represents the electrons kinetic energy operators; $V_{ee}(\rho)$, $V_{eN}(\rho, R)$ and $V_{NN}(R)$ are the standard Coulomb interaction potentials; they are invariant to origin translation. The vector $\mathbf{u}$ is just a vector in real space R^3. K_N is the kinetic energy operator of the nuclei, and in this work the electronic Hamiltonian $H_e(\Gamma; Z)$ includes all Coulomb interactions. This Hamiltonian would represent a general electronic system submitted to arbitrary sources of external Coulomb potential.

In principle, most physical and all chemical process will be represented as a change among the exact solutions of the molecular Schrödinger equation:

$$H_m(\Gamma)\, \Phi_j(\rho, R) = \{K_N(R; M) + H_e(\rho,R;Z)\}\, \Phi_j(\rho, R) = \varepsilon_j\, \Phi_j(\rho, R) \quad (4)$$

Following Hunter [10] an eigenstate of this equation can be written rigorously as a product of the form:

$$\Phi_i(\rho, R) = X_i(R)\, \vartheta_i(\rho,R) \quad (5)$$

$\vartheta_i(\rho,R)$ is a solution of the Schrödinger equation with the electronic Hamiltonian $H_e(\Gamma;Z)$. The analysis using a $\mathbf{u}$-vector defined in terms of the configuration coordinates and the masses has been thoroughly discussed by Sutcliffe [1]. It is at this point that we depart for a second time from the standard approach.

Let us consider first the general dynamics of the electrons in the field of a set of Coulomb sources, Z. To differentiate this problem from our initial one, we will represent the position coordinates of the Coulomb sources with the symbol $\alpha=(\alpha_1,\ldots,\alpha_{nN})$. And the electronic Hamiltonian is given as $H_e(\rho,\alpha;Z)$. By analogy with the BO scheme we can write

$$H_e(\rho,\alpha;Z)\ \vartheta_i(\rho,\alpha) = E_i\ (\alpha)\ \vartheta_i(\rho,\alpha) \qquad (6)$$

This equation is isomorphic to the clamped-nuclei equation [1,6]. We contend that the wave functions $\{\vartheta_i(\rho,\alpha)\}$ with α continuously varying are not adequate to describe a number of physical processes. For, as α can be continuously changed from one external source configuration transforming according to a given point symmetry group into a different one, the electronic state characteristic to each symmetry cannot be physically changed in such a manner. This is a constraint imposed by quantum mechanics. The electronic wave function of these species must be different and independent from arbitrary values of α [11].

In order to distinguish the point symmetry group in the electronic wave function one must be able to relate this wave function to a unique external framework (yet to be defined) transforming according to the given group in α-space. When a diatomic is continuously dissociated in the BO framework, it moves from a well-defined molecule into the state of two atoms. But the electronic state of two (non-interacting) atoms is totally different from the electronic state of the diatomic molecule and consequently they cannot be transformed into each other by using a continuous transformation with an adiabatic parameter. This is also true for any bond breaking/making process in which the fragments have well defined electronic properties that are different from those of the bonded system. This unphysical behavior must be corrected. One thing is certain, a solution to this problem cannot be found by taking the dynamical variables of the nuclei to define a reference frame [1;7]. The question is to find a framework able to provide relief from the constraints derived from the standard BO scheme without throwing away the computation algorithms developed for the calculation of electronic wave functions [12].

2.2 Model electronic Schrödinger equations

The next task is to introduce model electronic systems. One seeks to establish a direct connection between a particular chemical species defined in the first instance with the help of a rigid classical source of Coulomb potential α_{oi} and a unique associated electronic wave function: $Y_i(\rho;\alpha_{oi})$. Consider the energy

expectation value:

$$E_i(\alpha; \alpha_{oi}) = < Y_i(\rho;\alpha_{oi})|H_e (\rho , \alpha)| Y_i(\rho ; \alpha_{oi}) > \quad (7)$$

The parametric Z-dependence is implicitly assumed now. For the exact model electronic wave function, any variation in a neighborhood of the geometric coordinates around α_{oi}, the energy $E_i(\alpha; \alpha_{oi})$ must be a local minimum at $\alpha = \alpha_{oi}$. Following the same line of argument than in the BO approach, one would obtain a Schrödinger equation for this special arrangement:

$$\{K_e + V_{ee} + V_{eN}(\rho , \alpha_{oi}) + V_{NN}(\alpha_{oi})\} Y_i(\rho;\alpha_{oi}) = E_i (\alpha_{oi}) Y_i(\rho;\alpha_{oi}) \quad (8)$$

The equation generates a complete set of model electronic eigenfunctions at α_{oi}. The point is that the wave function Y_i should determine the stationary geometry α_{oi} in the sense that the energy expectation value $E_i(\alpha; \alpha_{oi})$ has a minimum for any variation of the external sources around α_{oi}. The model wave function leads to zero gradient, $\delta E_i(\alpha; \alpha_{oi})/ \delta\alpha|_{\alpha oi} = \mathbf{0}$. This is the necessary condition imposed to the model wave function. Here resides the fundamental difference with the clamped-nuclei approximation. The model introduced here is assumed to go beyond the clamped-nuclei model. If eq.(8) is fulfilled, the repulsive forces compensate the attractive forces originated by the exact electronic wave function. The Hellman-Feynman theorem holds with this class of wave functions. Note that asymptotic systems can also be defined and treated under similar premises. Let us search for the conditions relating the general model system to the solutions of the molecular Hamiltonian.

Two isomers can have now a well-defined stationary arrangement of external Coulomb sources, say α_{oi} and α_{ok}, respectively. Each one has a different Schrödinger equation (8) wherefrom the electronic wave function can be determined with modern analytical gradient techniques. The problem now is to find solutions for the molecular problem, eq(4).

2.3 Rigged BO scheme

The functions belonging to the set $\{Y_i(\rho;\alpha_{oi})\}_j$ must fulfill definite orthogonality requirements with respect to the electronic Hamiltonian $H_e(\rho, R)$ that must be valid for any value of R.

The electronic wave function for the i-th stationary state is only tied to the external sources of the potential α_{oi}, namely, it is independent of the point chosen in the nuclear configuration space. Using the completeness of the solutions to eq.(8) one can write:

$$H_e(\rho,R)\ Y_i(\rho\ ;\ \alpha_{oi}) = \Sigma_j\ C_{ij}(R)\ Y_j(\rho;\alpha_{oi}) \qquad (9)$$

Multiplying from the left by $Y_k(\rho;\alpha_{ok})^*$ and integrating over the electronic coordinates

$$< Y_k(\rho;\alpha_{ok})|H_e\ (\rho\ ,R)|Y_j(\rho;\alpha_{oi})> = \Sigma_j C_{ij}(R)< Y_k(\rho;\alpha_{ok})|Y_j(\rho;\alpha_{oi})> \qquad (10)$$

For k=i one recovers eq.(7) by replacing α by R and one obtains $C_{ij}(R) = \delta_{ij}$ $E_i(R;\alpha_{oi})$ as an exact result (δ_{ij} is Kronecker delta). This is an exact potential energy function in R-space. It acts as an attractor for the nuclei.

For $k\neq j$, and $k\neq i$, it is necessary and sufficient that $<Y_k(\rho;\alpha_{ok})|Y_j(\rho;\alpha_{oi})> = \delta_{kj}$, namely, the electronic wave functions characterizing electronic states from different attractors must be normalized and orthogonal independently of R. The orthogonality property defines suitable electronic wave functions diagonalizing the electronic Hamiltonian.

Let us now take the product $X_i(R)Y_i(\rho;\alpha_{oi})$ to represent the molecular wave function $\Phi_i(\rho,R)$. This substitution defines the rigged BO scheme.

The electronic Hamiltonian is diagonal in the rigged-BO basis and it remains now to study eq.(4). The equivalence: $E_i(\alpha;\alpha_{oi})= E_i(R;\alpha_{oi})= E_i(R)$ is fulfilled by the wave functions derived from the auxiliary model. By multiplying eq.(4) from the left by $Y_i^*(\rho;\alpha_{oi})$ and integrate over the electronic coordinates we obtain

$$\{K_N + E_i\ (R)\}\ X_{ik}(R) = \varepsilon_{ik}\ X_{ik}(R) \qquad (11)$$

This is an eigenvalue equation for the nuclei degrees of freedom submitted to the model potential generated by the exact electronic wave function $Y_i(\rho;\alpha_{oi})$. Depending upon the particular mass vector, the electronic potential may sustain bound nuclear dynamical states of diverse frequencies. The nuclear stationary states $X_{ik}(R)$ in the inertial frame are obtained as functions relative to the electronic attractor potential $E_i(R)$.

To sense the difference between the BO and the R-BO schemes consider the solution to eq.(11). For a stretching mode in the R-BO scheme, whatever the energy one puts on it, the bond by itself will never dissociate. In The BO scheme, adiabatic dissociation processes are allowed.

Note that the electronic wave functions in the R-BO scheme have the parameter set α_{oi} only as labels to remind us of the existence of an attractor related to the electronic wave function. It is the attractor (trapping potential) which acts on the nuclear dynamics. The α_{oi}'s are not dynamic coordinates in themselves. Thus, eq.(8) simply says that the set of all electronic wave functions in the R-BO scheme are orthogonal. The electronic Hamiltonian being diagonal for all R means that eq.(4) is consistent with eq.(8) and (11).

2.4 Reference frames

At this point it is possible to discuss the way the origin vector **u** could be defined and to introduce molecular reference frames. For each electronic state associated to a particular stationary arrangement of external Coulomb sources, α_{oi}, these coordinates can be used to define an appropriate origin, say $\mathbf{u}_i$. In fact, the origin is the same for all electronic attractors since the stationary geometry defines distances and angle constraints for the Coulomb sources only. A reference frame parallel to the laboratory one can be defined at the tip of **u**.

The nuclear dynamics is derived once the stationary states are extracted from the Schrödinger equation (11). There is no nuclear degree of freedom eliminated from this equation. For a particular electronic state, that defines an α_{oi}, the Taylor expansion around this geometry permits calculating a Hessian or matrix containing the second derivatives of the energy with respect to the geometric

parameters. This Hessian will show for non-linear systems three zero eigenvalues related to the origin displacement and three zero eigenvalues related to free rotations. The remaining degrees of freedom correspond to vibration-rotation dynamics. The elimination of redundant degrees of freedom is automatically performed by the electronic wave function.

For a given stationary state, the idea of nuclear "positions" does not make sense; this is a classical mechanical description. One can take α_{oi} as a surrogate of the "equilibrium" position of the nuclei if we retain the rigid molecule model only.

A body-fixed frame can easily be defined without the introduction of constraints among the dynamical coordinates of the problem. Observe that the system is invariant to the O(3), the orthogonal rotation group. And, as α_{oi} "rotates" so does the stationary model electronic state function. The electron-nucleus separation problem is hence solved in a manner differing radically from the standard approach.

Goscinski and Palma have carefully examined the formulation of the BO or adiabatic formulation and explored alternative formulations based on density matrix methods [13]. They obtained an optimal electronic wave function, in their notation $\Phi_1(q)$, as an integral over the diagonal of a nuclear density kernel $\chi(Q)\chi^*(Q')$ multiplied by the BO wave function $\psi^{el}(q;Q)$

$$\Phi_1(q) = \int \chi(Q)\chi^*(Q)\, \psi^{el}(q;Q)dQ \qquad (12)$$

in the early days of molecular quantum mechnaics, Herzberg and Teller [14] introduced the "crude BO" approximation to help introduce point symmetry rules. The electronic wave function is given by $\Phi_1(q) \approx \psi^{el}(q;Q_o)$ for some value Q_o. Scaled and unscaled crude-BO wave functions have been discussed by Siebrand [15] and R.Lefebvre and coworkers [16]. There is a fundamental difference between the crude-BO approach and ours. Let us take eq.(12) and reinterpret it formally by introducing the electronic wave function) $\psi^{el}(q;\alpha_i^o)$, where α_i^o is the stationary geometry for the external sources derived from Schrödinger eq.(8). Transforming to a new origin $\mathbf{u}(\alpha_i^o)$, $\chi(Q)\chi^*(Q)$ can be formally written as a product $\chi(Q-\mathbf{u}(\alpha_i^o))\, \chi^*(Q-\mathbf{u}(\alpha_i^o))$ so that one can define a

$$\Phi_1'(q; \alpha_i^o) = \int \chi(Q-\mathbf{u}(\alpha_i^o))\, \chi^*(Q-\mathbf{u}(\alpha_i^o))\, \psi^{el}(q; Q- \alpha_i^o)\, dQ \qquad (13)$$

Now, if $\chi(Q-\mathbf{u}(\alpha_i^o))\ \chi^*(Q-\mathbf{u}(\alpha_i^o)) = \delta(Q-\mathbf{u}(\alpha_i^o))$ (Dirac's delta distribution) one gets $\psi^{el}(q; \mathbf{u}(\alpha_i^o)) = \Phi_1'(q; \alpha_i^o)$ as one would formally expect. The difference is now apparent. The frame α_i^o is related to the classical arrangement of sources and can be used to define frames helping describe the motion of the nuclear masses. But Q_o is defined with the nuclear framework. To use the nuclear coordinates for that task leads to problems as shown by Woolley and Sutcliffe [1;4;7;17].

In the R-BO scheme, the stationary electronic wave function drives the nuclear dynamics via the setup of a fundamental attractor acting on the sources of Coulomb field [11]. The nuclei do not have an "equilibrium configuration" as they are described as quantum systems and not as classical particles. The concept of molecular form (shape) is related to the existence of stationary nuclear state setup by the electronic attractor and their interactions with external electromagnetic fields.

In absence of external forces acting at the **u**-level, the set of $\{f_{Pui}(\mathbf{u})X_i(R)Y_i(\rho;\alpha_{oi})\}$ provides at least a subspace where the total Hamiltonian is diagonal since $f_{Pui}(\mathbf{u})$ is an eigenfunction of the momentum operator $\mathbf{P}_{ui}$. Now, we will describe physical and chemical processes with the help of this basis of orthogonal states.

The infinite number of Schrödinger's equations (6) in the BO scheme is replaced by a countable infinite set of Schrödinger equations (8) in the R-BO scheme. Whether or not the eigenstates of this latter set provide a complete basis to represent any quantum mechanical state solution to eq.(1) cannot be mathematically proven. However, we assume that subspaces of physically relevant states can be approximated in this manner.

3. Chemical change as electronic spectroscopy processes

A theoretical description of chemical reactions comports three important aspects: i) equilibrium limit; ii) rate processes; iii) mechanism(s). In the R-BO framework, a chemical reaction is described as the change of electronic state from the chemical species defining reactants into the electronic state of the species

related to products. A spectral representation of H' can be obtained by adding the set of quantum states, that are not related to those derived from the set of equations (8), but belong to an orthogonal complement. This includes the asymptotic cluster states of all kinds that conserve the total number of electrons and nuclei into which the system can be decomposed. The quantum states can be ranged according to energy from the fully ionized cluster with any pre assigned amount of relative kinetic energy down to the electronic eigenstate of the complete cluster (molecule) having the lowest energy derived from eq.(8), if it exists. The choice of molecular frames would depend upon the process to be described.

It is apparent from the above considerations that the external energy E plays a role in this approach. With respect to the eigenstates of H', the system is open. Energy conservation principle brings the description into the realm of thermodynamics. The inclusion of the kinetic energy related to the inertial frame used to unfold H' is then required by energy conservation.

3.1 Quantum basis for an elementary scattering approach

The description of a chemical process relies on a correspondence between the subset of stationary states $\{\Psi_k(r,Q)\}$ of the total H(r,Q). Once the general equation is laid down, the submatrices representing particular states are identified with those coming from the molecular Hamiltonian H' as it is obtained in the R-BO scheme. The quantum states involved are dependent upon the total energy E assigned to the system. The energy conservation principle makes those states having energy about and below E accessible. They can be populated (measured). The states having energy above E enter as usual via perturbation theory schemes. They produce "effects" but are not measurable if their energy is above E.

We assume that each $\Psi_k(r,Q)$-state can be associated either to an asymptotic α-configuration or to a full molecular species with its stationary α-configuration.

Note that by giving to the system an external energy E, excited vibration-rotation and electronic states can be activated (populated too). These states can radiate energy into the field by photon emission or can be populated by photon absorption. The electromagnetic field is considered here as a source or as a sink of energy ensuring energy conservation. The total Hamiltonian must include the

operator coupling the external electromagnetic field $\mathbf{A}(\mathbf{r},t)$ to the charge system, i.e. the operator V_{rm} and $\mathbf{r}$ is real space position vector. The time evolution is driven by the operator $[H+V_{rm}(r,Q,t)]$.

We focus attention on both the theory of rates and the electronic mechanism for generic chemical processes. An exact quantum mechanical transition state theory was early developed by Miller [18] and rate expressions were derived from quantum scattering theory [19]. That approach and subsequent developments are based upon the reactive BO potential energy surfaces where the familiar case concerns a reaction accompanied by a smooth change in the overall electronic energy surface [20]. The R-BO approach does not have such adiabatic changes of electronic states and it is of interest to see the way quantum scattering theory handles the problem in this new context.

To this end, let us analyze the equation: $(H-E)\varphi = -V_{rm}\varphi$ which, by using the stationary states of H, $\varphi = \Sigma_{ik}\, C_{ik}\, \Psi_{ik}(r,Q)$, can be cast as a matrix equation:

$$\mathbf{(H - E1)\, C = V_{RM}\, C} \qquad (14)$$

The matrix $\mathbf{H}$ is (almost) block-diagonal, where each block belongs to a particular electronic state. $\mathbf{1}$ is the unit matrix of appropriate dimension.

The R-BO scheme allows one now to use each quantum state independently of the others since, to each block we can formally apply a specific translation operator T related to the stationary external source of Coulomb potential: $\langle\Psi_{ik}(r,Q)|\, \mathrm{T}(u)\ \ \mathrm{T}(u)^{-1}\, H\, \mathrm{T}(u)\, \mathrm{T}(u)^{-1}\, |\, \Psi_{ik}(r,Q)\rangle$. The matrix element is invariant. In this manner, local frames can be introduced into the general framework to qualitatively discuss mechanistic issues. The translated Hamiltonian, $H' = \mathrm{T}(u)^{-1} H\, \mathrm{T}(u)$, is given in eq.(2). The matrix elements of the operator V_{rm} are invariant to any origin shift.

The rigged BO wave functions, $\Phi_{ik}(\rho,R) = X_{ik}(R)\, Y_i(\rho;\alpha_{oi})$, render diagonal the molecular Hamiltonian of equation (4). They cannot be used yet to expand the $\varphi(r,Q)$ functions as the R-space is limited. We can consider now the solution to the initial equation for the i-th electronic quantum state. The origin translation operator, $\mathrm{T}(u)$, applied to a function $g(x)$ is given as, $\mathrm{T}(u)^{-1}\, g(x) = g(x-u) = (\exp\{-i\, u.p_u/\hbar\}\, g(x))$, where p_u is the linear momentum conjugate to u. The stationary wave

function in the laboratory frame is given by $\Psi_{ik}(r,Q)$ so that

$$T(u)^{-1}\,\Psi_{ik}(r,Q) = \Psi_{ik}(r-u,Q-u) = (\exp(-i\,\mathbf{u}.\mathbf{P}_{Ku}/\hbar))\Phi_{ik}(\rho,R) \qquad (15)$$

The second equality completes the set $\Phi_{ik}(\rho,R)$ with the plane waves describing the **u**-dynamics. This transformed function is approximated, in the molecular frame α_{oi} by $X_{ik}(R)\ Y_i(\rho;\alpha_{oi})$ and the total wave function is naturally factored in three terms: $\exp(-i\,\mathbf{u}.\mathbf{P}_{Ku}/\hbar)\ X_{ik}(R)\ Y_i(\rho;\alpha_{oi})$. A general expansion of the exact wave function in terms of such states has to be handled with care. There is no mathematical proof that the set of all these states provides a complete basis. In practice, one always works with subspaces suggested by the physical and chemical nature of the problem.

The transformed Hamiltonian H', however, is diagonal in the base constructed with the help of the rigged BO approximation since the function $\exp(-i\,u.P_{Ku}/\hbar)$ is an eigenfunction of the momentum operator $\mathbf{P}_{Ku}$, the coupling operator V_u is diagonal. Changes of the global momentum can be produced via the coupling to external systems. In this case, chemistry can be driven with V_u and/or V_{em}. For the time being, only this latter operator is singled out in eq.(14).

3.2 Time dependent processes

The chemistry must be reflected now by the time evolution of particular quantum states $\varphi(r,Q,t)$ including appropriate initial conditions. The total time-dependent wave function is

$$\varphi(r,Q,t) = \Sigma_k\, C_k(t)\, \exp(E_k t/\hbar))\Psi_k(r,Q). \qquad (16)$$

The probability to find the system populating the f-th state is $|C_f(t)|^2$. The problem is the determination of the transition probability T_{if} per unit time that a system prepared at initial time t_o in the state i would be in state f in the future of t_o. Initial conditions for this system are assumed to be: $C_k(t_o) = 0$ for all $k \neq i$ and $C_i(t_o) = 1$. Now, by making explicit the rovibration quantum numbers (k,k') for each electronic state one gets

$$T_{fk\,ik'} = |\langle\Psi_{fk}(r,Q)\,|\varphi(r,Q,t)\rangle|^2 = |\langle\Psi_{fk}(r,Q)\,|U_I(t,t_o)|\Psi_{ik'}(r,Q)\rangle|^2 \qquad (17)$$

The time evolution operator in the interaction representation $U_I(t,t_o)$ propagates the initial state. This operator can be cast into a series:

$$U_I(t,t_o) = 1 - i/\hbar \int dt'\; V_{rmI}\, U_I(t',t_o)dt' \qquad (18)$$

In the Born approximation retained here [3], an the minimal coupling framework used for the sake of simplicity leads to

$$\langle\Psi_{fk}|U_I(t,t_o)|\Psi_{ik'}\rangle = -\int dt'\; \exp(i(E_{fk}-E_{ik'})t'/h)\; \mathbf{A}(t').\langle\Psi_{fk}(r,Q)|(\mathbf{p})|\Psi_{ik'}(r,Q)\rangle \qquad (19)$$

Where the limits of integration are t_o, t, and assume the electromagnetic field to slowly change with space coordinates. The square modulus of $\langle\Psi_{fk}|U_I(t,t_o)|\Psi_{ik'}\rangle$ gives the probability to populate the final fk-state starting from the initial ik'-th. For the electronic transition, the R-BO transition moment is given by:

$$\mathbf{p}_{ik\,i'k'} = \langle Y_i(\rho\,;\alpha_{oi})\,|\,\mathbf{p}_e(\rho)\,|\,Y_{i'}(\rho\,;\alpha_{oi'})\rangle_\rho\;\langle X_{ik}(R)\,X_{i'k'}(R)\rangle_R \qquad (20)$$

$\langle X_{ik}(R)\,X_{i'k'}(R)\rangle_R$ is the standard Franck-Condon (FC) nuclear overlap integral. The overlap integrand may be different from zero if both states have amplitudes differing from zero in common configuration ranges. In the R-BO approach, the electronic transition moment $\mathbf{p}_{ii'}=\langle Y_i(\rho;\alpha_{oi})|\mathbf{p}_e(\rho)|Y_{i'}(\rho;\alpha_{oi'})\rangle_\rho$ is <u>independent</u> of the nuclear configuration coordinates.

3.3 Chemistry as electronic spectroscopy

The one-to-one assignment between an electronic wave function and a chemical species brings the description of chemical change to a problem of electronic spectroscopy. Parity selection rules enter into a chemical description.

A chemical reaction between closed shell species is a common situation in chemistry. In this case, the parity of the reactants and products is the same.

Therefore, the matrix element of the electronic term $\mathbf{p}_{e\ ii'}=\mathbf{0}$ and there will be no direct chemical conversion. This is a somewhat surprising result when seen from the old point of view.

The previous situation would imply that for a chemical conversion to occur between species having the same parity in the reactant and product channels, a quantum state having appropriate parity is necessary to mediate the chemical process. Such a state is dubbed as a quantum transition state (QTS). This is a new result: transition states are not accidental but they appear to be a quantum mechanical necessity.

The QTS is a part of a reaction mechanism. These species may be found related to stationary arrangements of the external Coulomb sources. Solutions to eq.(8) coming as saddle points of at least index one (one imaginary frequency) are natural candidates to play the role of QTS. If the saddle point wave function has closed electronic shell structure, its electronic parity is positive. In this case one would expect a situation similar to the symmetry-forbidden electronic absorption bands. The intensity is borrowed from the excited states having the correct parity via couplings at second-order perturbation theory [21].

For simple covalent bond breaking reactions, a bound state in the R-BO scheme correlates to a diradical asymptotic state. This latter state represents in the laboratory world a collision pair. In α-space we can define an intermolecular distance. For all values of such distance, the system cannot change its electronic state in an adiabatic process. The asymptotic state must be orthogonal to the bound state. It is therefore necessary that the electronic wave function of the collision pair show one node more than the bounded system. The energy expectation values as a function of the intermolecular distance for the two states would cross above the dissociation energy limit. The corresponding FC factor can hence be different from zero. Experimentally, it is well known that most of the bond-forming processes may have a small barrier (about 1 Kcal/mol) [22].

Let us examine a simple model for chemical reactions now. The first two states define asymptotic reactants (R1+R2, represented as $|1k\rangle$) and products (P1+P2, or $|2k'\rangle$) as collision pairs. In real low energy chemistry the reactant and product channels have the same electronic parity. In particular, this is the case when partners in both systems have closed shell electronic structures. The

electronic momentum operator has negative parity (Cf.eq.(18)). The R-BO scheme requires the existence of a quantum transition state having at least a component with negative parity. In this case, the transition matrix elements can be different from zero while the direct collision conversion is parity forbidden. This state would mediate conversion between states in the reactant channel with those of the product channel. Without explicit calculations, one has at least the hint for a mechanistic path.

In a chemical interpretation, the mechanism requires first the population of a third quantum state, the QTS (state 3, |3k''>). The overlap integral <3k''|1k'> is bound to be zero if the nuclear stationary wave functions do not have overlapping regions. Since the QTS low energy vibration states are relatively bounded in the configuration space, the collision pair must be brought to a region where overlap is non-negligible. The vibration quantum k' state actually stands for the product function of the vibration states of the partners separated by the intermolecular distance R1R2. Consider three subspaces in eq.(14),

$$
\begin{aligned}
(H_{11} - E1_{11})\, C_{11} &= (V_{rm})_{13}\, C_{31} \\
(H_{22} - E1_{22})\, C_{22} &= (V_{rm})_{23}\, C_{32} \\
(H_{33} - E1_{33})\, C_{33} &= (V_{rm})_{31}\, C_{13} + (V_{rm})_{32}\, C_{23}
\end{aligned}
\qquad (21)
$$

The interaction $(V_{rm})_{13}$ will produce a finite amplitude for the QTS in the total wave function.

3.3.1 Elastic and inelastic scattering

Let us examine the processes described in the reactant channel (1) corresponding to the collision pair R1+R2. Elastic scattering effects are hidden in H_{11}. To see this, one uses with the asymptotic Hamiltonian: $(H_{R1}+H_{R2})$ to represent the 1-state. The Hamiltonian $H' = K_u + H_m$ (Γ) can be written in terms of the asymptotic system: $H_m = H_{R1} + H_{R2} + W_{R1R2}$. The term W_{R1R2} is the intermolecular interaction operator measured from the local stationary frames whose origins are $\mathbf{u}_1$ and $\mathbf{u}_2$. Taking $\mathbf{u}$ to be the center of mass of the α-colliding pair, and the distance R1R2= $\mathbf{u}_{12} = \mathbf{u}_2 - \mathbf{u}_1$, a Schrödinger equation for the $\mathbf{u}$-variables is obtained by integrating over the electronic and nuclear coordinates of the isolated

clusters so that:

$$\{K_u + K_{u12} + (\varepsilon_{ik}^{R1+R2} - E) + \langle ik|W_{R1R2}|ik\rangle\}|\, f_{Pu12}\rangle\, |f_{Pu}\rangle \qquad (22)$$

ε_{ik}^{R1+R2} is the proper energy of the asymptotic pair with internal rovibration quantum number k; $U_{ik}(\mathbf{u}_{12})=\langle ik|W_{R1R2}|ik\rangle$ is the potential energy function corresponding to the asymptotic ik-state. $|f_{Pu12}\rangle$ and $|f_{Pu}\rangle$ are plane waves (periodic boundary conditions can be introduced to quantize the global dynamics). Taking away the **u** free motion, one transforms (22) into a standard scattering differential equation with $|f_{Pu12}\rangle$ corresponding to a plane wave for the relative motion. Observe that all frame analysis is related to the α-space first.

The transformed equation (22) would describe elastic molecular scattering processes only. The reason is that $\langle ik|W_{R1R2}|ik'\rangle=\delta_{kk'}$. The inclusion of the nuclear part of the (V_u+V_{rm}) interaction operator permits describing inelastic scattering processes among rovibration states in the reactant molecular subspace.

3.3.2 Chemical conversion

The structure of the present model requires the quantum states of the QTS to produce a chemical conversion. For a chemical reaction the nuclear part is not sufficient to produce a transition since $\langle fk|W_{R1R2}|ik'\rangle= \delta_{fi}$ and the operator mediating conversion must be the electronic component of (V_u+V_{rm}).

Let $T_{3k\,1k'}$ be the rate of population of the QTS (Cf. eq.(17),(19) and (20)). Here, there is a structural factor given by the overlap integral $\langle 3k|1k'\rangle$. If the corresponding attractors (α-space) are too different at all intermolecular distances, the collision will not contribute to the probability $T_{3k\,1k'}$. The vibration k' must be a mode along the "reaction coordinate". Pictorially speaking, if the collision yields a pair where the nuclear wave functions occupy regions that are accessible to the QTS, then the overlap integral would have non-negligible value. This process can be referred to as molding of reactants into the "geometry" of the QTS. This is what one means by productive collision. The activation process is, therefore, not only a matter of energy but it includes excitation of appropriate vibration levels leading to dynamic molecular molding.

An important point to note is that in the R-BO scheme the QTS is a normal

molecule if it has the correct parity. Otherwise, it will sense the neighborhood in α-space where the reactive channels have minimal energy gaps. To open a reactive event from state |3k>, one of the accessible states in the product channel must be populated. Then,

$$T_{3k\,2k''} = \qquad (23)$$

$$4\{|A_o\,(\mathbf{n}.\,\mathbf{p}_e(\rho))_{2\,3}<3k|1k'>|^2\,/[(\,E_{3k}-E_{2k''}-\omega)^2]\}\,\sin^2[((E_{3k}-E_{2k''})/\hbar-\omega)\,t/2]$$

The transition probability involves a second overlap integral and a different electronic transition moment. If $(\mathbf{n}.\,\mathbf{p}_e(\rho))_{2\,3} << (\mathbf{n}.\,\mathbf{p}_e(\rho))_{1\,3}$ for instance, the system may attain a stationary regime with respect to the activation reaction. This model would correspond to the situation underlying the theory of absolute rate [23;24]. For now one can describe, with chemical nomenclature, the reaction as:

$$R1 + R2 \leftrightarrow QTS \rightarrow P1+P2$$

As time t becomes large, $T_{3k\,2k''}$ is only appreciably large for final states fulfilling the condition: $t \approx 2\pi\ \hbar/(E_{2k}-E_{3k'})$. If one calls Δt the time during which energy exchange can take place due to the perturbation, the transition probability will only yield appreciable values for $\Delta t\,\Delta E \approx h$ [25].

The selected vibration-rotation states {k'} of the QTS that contribute to the reaction are those having non-zero FC overlap integral. In the case where one sums over the k'-states, let us replace ΔE by the average thermal energy available to the system, namely, $k_B T$. T is the absolute temperature and k_B is the Boltzmann constant. The minimal time during which a transition is possible will be $\Delta t \approx h / k_B T$ and we take this as the measure of time (clock) for the conversion from QTS to P1+P2. Then, let $T_{3\,2}$ be the total probability to convert the QTS into P1+P2, so that the ratio $T_{3\,2}/\Delta t$ is the rate of conversion per QTS molecule. If [QTS] is the concentration of QTS molecules at time t, the rate measured in the laboratory will be proportional to [QTS] $T_{3\,2}/\Delta t$. A phenomenological rate is given by:

$$\text{Rate} = k_2\,[R1]\,[R2]$$

k_2 is the bimolecular rate constant. If the system is stationary with respect to the production of QTS, and we have the system in contact with a thermostat at temperature T, one can equate the rates and get

$$k_2 = (k_B T / h)\, T_{3\,2}\, [QTS] / [R1]\, [R2] = K\ddagger\, T_{3\,2} \qquad (24)$$

K‡ is Eyring's equilibrium constant in the transition state theory rate constant [23;24]. The derivation of equation (24) here is based upon quantum dynamical arguments. Compared to eq.(9.14) in reference [24], except for the derivation paths (that are totally different), both equations are formally identical.

3.3.3 $H+H_2$

A discussion of the most studied chemical reaction, $H+H_2$, would help in sensing some differences introduced by the R-BO approach. The QTS is well known. In the α-space it has a linear stationary geometry, $^2\Sigma_u$. The highest occupied orbital has a node between the extreme positions of the Coulomb sources. The point symmetry group can be $C_{\infty v}$. The molecule has one symmetric stretching and two degenerate bending modes which endow the system with a vibration-dependent rotation [26]. The α-space picture of bending-excited molecules would correspond to "instantaneous" triangle hydrogen disposition so that the shape of the system would depend upon the state of vibration excitation. The QTS has electronic parity −1 while the ingoing and outgoing molecular channels have the same parity. A direct conversion of $H+H_2$ into H_2+H cannot be a first order process. Therefore, QTS controls the reactive traffic. It is then sufficient to know its quantum state to determine the angular behavior by using the rules of angular momentum combination. For the system using only 1s-type basis, L=0 and the total angular momentum J=R+S, where R is the rotation angular momentum. Nuclear spin angular momentum can also be included. As there is no external magnetic field gradient, M_S is conserved. The reactive collision will be those for which the angular momentum rules produce an allowed state in the QTS. Pictorially speaking, the configuration of the products in α-space starts from one of the accessible conformations sustained by the rotation-vibration spectra of the QTS.

As an example, let us take the QTS translation-vibration-rotation (TVR) state wave function: $\exp(-i\,\mathbf{u}'.\mathbf{P}_{Ku}/\hbar)\; X_{ik}(R_1,R_2,R_3;\,^2\Sigma_u)$. The electronic state symbol is appended to the rotation-vibration wave function. For the sake of notation, these functions in the laboratory frame will be denoted as $\chi_{iku'}(Q_1,Q_2,Q_3;^2\Sigma_u)$. The reactant states are given by $\chi_{iku'}\,(Q_1,Q_2;\,H_2(^1\Sigma_g))\;\chi_{iku''}(Q_3;\,^2H(1s))$; the products by $\chi_{iku'}\,(Q_3,Q_2;\,H_2(^1\Sigma_g))\;\chi_{iku''}(Q_1;\,^2H(1s))$. The labels are derived from the α-space to help the discussion. The reactive cross section depends upon the Franck-Condon integral involving the QTS since the direct process has zero transition moment. The quantum states are all referred to the same frame. First, note that the anti symmetric vibration mode is excluded by symmetry. Only vibrations transforming according to the point symmetry group $C_{\infty v}$ are allowed. In solving eqs.(8) and (9), the energy (frequency) comes out imaginary for the antisymmetric vibration which is the usual reaction coordinate in the BO scheme. Here, only real energy solutions contribute to the system.

The probability to populate the QTS starting from the reactant collision pair states depend upon the product:

$$\chi_{iku'}(Q_1,Q_2,Q_3;^2\Sigma_u)\;\chi_{iku'}\,(Q_1,Q_2;\,H_2(^1\Sigma_g))\;\chi_{iku''}(Q_3;\,^2H(1s))$$

This is integrated over the $Q_1Q_2Q_3$-space. If the collision pair wave functions never overlap the vibration wave function $\chi_{iku'}(Q_1,Q_2,Q_3;^2\Sigma_u)$ of the QTS, there will be zero contribution to the cross section. In this case, the QTS defines the reaction domain. This is "quantized" by the corresponding vibration-rotation wave function. Therefore, from all possible collisions among the reactants, only those having a non-zero FC factor will contribute to the reaction rate. This is related to the steric factor, P, in elementary chemical kinetics theory. Selection rules for VR-transitions apply. The probability to find the system in one of the product channel states when starting from a QTS is controlled by the FC integral formed by the products of the type

$$\chi_{iku'}(Q_1,Q_2,Q_3;^2\Sigma_u)\;\chi_{iku''}(Q_3,Q_2;\,H_2(^1\Sigma_g))\;\chi_{iku'''}(Q_1;\,^2H(1s))$$

The FC integral can be different from zero if the collision product is "molded"

into the configuration space of the QTS. The "products" are released in those configuration space regions that are characteristic of the vibration states of the QTS.

The phenomenology related to the BO scheme, e.g. conic intersections, fades away. Instead, a physical process involving permutations of hydrogen labeling in the ingoing channel can be figured out. The channels are:

$$H^1+H^2\text{-}H^3;\ H^3+H^1\text{-}H^2;\ H^2+H^3\text{-}H^1$$

The corresponding transition structures open channels toward electronic excited states. The correlate with the conic intersection corresponds to highly vibration excitations of the QTS bending modes leading in the α-space to instantaneous triangular arrangements. The energy degenerate states correspond to the three ingoing channels having the same degree of vibration excitation. The non-stationary state would correspond to a coherent linear superposition. In that state, each channel has the same probability to be populated. Above this physical state, the excited H_3* is to be found together with Rydberg states.

4. Discussion

A rigged BO approach is developed and used to describe a chemical system calculated with present day advanced electronic methods. Chemical species are determined by electronic wave functions that are independent from the nuclear configuration space. This is the fundamental hypothesis [11]. Boundary conditions in the global electronic wave function are introduced via the solution of electronic Schrödinger equations for systems of external Coulomb sources (Cf. Eq.(8)). The associated stationary arrangement of external Coulomb sources allows for the introduction of molecular frames. This approach naturally leads to a state-to-state description particularly useful in gas phase reactions. A chemical reaction is described as if it were an electronic spectroscopy event or series of events.

The Hamiltonian H(r,Q) of the time independent Schrödinger eq.(1) is invariant under global symmetry operations. Since momentum and angular momentum are constant of motion [27], it was a common practice to separate the center of mass and rotations of the system as a whole. The problem was isomers and asymptotic subsystems; they are all related to the same global Hamiltonian. To solve the

problems, the BO separation procedure has been bypassed. The introduction of an auxiliary Coulomb Hamiltonian, eq.(8): $\{K_e+V_{ee}+V_{eN}(\rho,\alpha_{oi})+V_{NN}(\alpha_{oi})\}=H_e(\rho,\alpha_{oi})$ permits the introduction of point symmetry group properties and special boundary conditions. A class of chemical species is related to stationary electronic states tied to stationary arrangements of external Coulomb sources. The operator $H_e(\rho,\alpha_{oi})$ is always invariant to specific point symmetry groups. The electronic wave functions can hence be labeled with symmetry quantum numbers that are not necessarily symmetries of the global Hamiltonian. In the present theory, the electronic wave functions have hence local symmetry properties. The solutions to the nuclear Schrödinger equation (11) can be naturally separated into local rigid frame rotation invariance and the non-separable vibration-rotation problem. The product form of electronic and relative nuclear wave functions defines molecular species. The quantum nuclear states may be coherent or incoherent linear superposition of these vibration-rotation wave functions.

Henceforward, molecules appear from boundary conditions imposed to the electronic problem. A chemical species is not an eigenfunction of eq.(1). It is an eigenfunction of the local Schrödinger equation (8) and eq.(11). As shown in this work, the R-BO basis turns diagonal the global hamiltonian H(r,Q). The concept of molecular shape is then hidden in the global quantum mechanical problem. But it is there, and expresses as sets of electronic wave functions determining stationary arrangements of external sources of Coulomb potential. Note that the atomic nuclei are not considered as more or less "fixed". They are described by appropriate nuclear wave functions relative to particular electronic states (solutions to eq.(11)). Just as it is derived from molecular spectroscopy. Therefore, it seems hopeless to try to get such states as direct mathematical solutions derived from a many body Schrödinger equation [28] in an independent particle basis.

To date, analytic first and second derivatives of the electronic energy functional (eq.(7)) with respect to geometric parameters defining position of the external sources of Coulomb potential have been used to actually obtain models for both the electronic wave function and the geometry [2]. The art of obtaining saddle points [29] has been now fully developed.

The quantum mechanical rate process and mechanistic description calls for some comments.

i) Time scales. The time t appearing in the evolution operator $U(t,t_o)$ is not the time measuring conversion processes as they are derived from the transition amplitudes T_{ij}. The product of the energy exchanged between the molecular states, $\Delta E_{ij} = E_i - E_j$, during the time Δt, is bounded by the Planck constant $h/2\pi$. This is related to resonance conditions that make the amplitude of the transition moment significant. It is a generic clock of this kind that we used to derive the rate constant (24). It is expected that energy differences of the order of rotation energies to be involved in the population processes of the quantum transition-state starting from the reactant states. For a real reaction, a large band of electromagnetic modes are involved. If they are in thermal equilibrium, a Planck's blackbody radiation distribution will be obtained [30]. Experimentally, it is known that unimolecular reactions can be affected by ambient blackbody radiation [31].

ii) Symmetry rules. The point symmetry rules correlating asymptotic electronic states are valid for the Hamiltonian $H_e(\rho,\alpha_{oi})$. The symmetry operations leave invariant α_{oi}. The configuration space used for the nuclei has nothing to do with such operations. The reason lies in the fact that we are not considering a many-body-problem but a many-state-problem. Concepts such as crossing of potential energy surfaces can only be coined in the realm of α-space if at all. It is not a general quantum mechanical property. It is, however, extremely useful for many practical purposes such as the use of wave packet studies [32].

iii) The introduction of energy from external sources is essential to set up the real reaction and the theoretical description. Sound fields can be incorporated in the present approach. The introduction of local inertial frames does not alter the diagonal character in the R-BO base. The exchange of external energy can be seen as producing work on to the molecular system. The frames, however, are no longer inertial; they become "accelerated". The perturbing agent (force) acts at the **u**-coordinate level, the system changes the state; either via the momentum, if one uses a classical mechanical approximation and Newton's law with bounded products $\Delta p \Delta x \geq h$; or quantum dynamically by setting trap potentials for the **u**-mode. For example, ultrasound will produce chemical and/or luminescence effects that are related to the coupling between the external (**u**-modes) and electronic and nuclear modes via the operator V_u appearing in eq.(2). Some of the states are better described as wave packets; in this case such functions are no longer

eigenfunctions of the momentum operator. Sono-luminescence light emission [33] and sono-chemistry [34] can hence be rationalized in the R-BO scheme. Besides, new stationary **u**-states can be necessary to describe the phenomenology [35].

iv) Cross sections boil down to calculate integrals including terms such as eq.(20). Integration of the electronic part is totally independent from the nuclear coordinate space. The transition amplitude (Cf.eq.(19)) contain integrals covering the complete nuclear configuration space, Q. The Franck-Condon integral implicitly contains the **u**-variable when asymptotic states are required to describe the reaction. The molecular mechanisms are tied to the α-space and to the **u**-space. And, both spaces can be assigned to real space coordinates and thereby treated classically, semi classically or quantum mechanically. There is a paradox though. The time-dependent Schrödinger equation is used to treat rate processes via cross sections, but there is no clue as to how the chemistry is carried out: no mechanism can be obtained. But chemistry is concerned with mechanisms in the first place. In a molecular beam experiment, the reactants are prepared within a narrow domain in **u**-space. In the R-BO scheme we can calculate the energy of the product states and, as it is commonly the case, their **u**-space does not overlap with the one corresponding to reactants. The energy functional (Cf.eq.(7)) in α-space will tell us that the Boltzmann probability to populate it is nearly zero. There is a narrow region in **u**-space where the molecular energies (not the quantum energy eigenstates) are near resonance. This is the correlate of a bottle neck region. Such an effect is hidden in the quantum state wave function and an appropriate "time evolution" should take into account this state of affairs. In this paper we used the kinetic picture, R1 + R2 $\leftrightarrow$ QTS -> P1+P2, to bypass the orthodox quantum mechanical treatment. Reactions are what they are because they occur in "real space". This means, in non-inertial frames. The R-BO theory is fit to describe such processes.

v) The electronic excitation process is not of a "vertical" type. We should not mix up the model we use to calculate the rotation-vibration spectra with the very nature of a stationary state. It is nearly impossible to understand the novelty of the present approach if we retain the idea of point masses vibrating around a given α_{oi} configuration. A coherent superposition of quantum states cannot be represented classically. The chemical conversion implies a coherent superposition of all

relevant quantum states that an electromagnetic field (or sound field) can couple. Products and reactants are obtained after decoherence is set up and the chemical species measured. The "measurement" can be made by an observer or by an electromagnetic field of appropriate frequency so that the absorption or emission spectra is activated (not necessarily observed). The interaction of a given electromagnetic field with a chemical converting system leads to frequency signatures in the field that are characteristic of the reaction process; information concerning reaction processes can be extracted from correlation functions of the electromagnetic field. See for instance reference [36] for a theoretical description of ultrafast infrared pump-probe spectroscopy of water where real time variations of the average hydrogen bond distance lengths are extracted from correlation functions of the electromagnetic field.

The inclusion of the electromagnetic field in the description of chemical conversion is a necessity derived from the electrodynamics of charged systems. Let us consider a simple model to size the entropy effects. Prepare reactants with one mode in the electromagnetic field whose energy (frequency ω) is enough to overcome relevant barriers. After a lapse of time sufficiently long, in a real sample, the electromagnetic field will be populated with a huge number of frequencies smaller than ω. They will come up as a result of populations of all energy levels below the energy threshold. The entropy of the electromagnetic field increases. Irreversible chemical reactions may be correlated to entropy changes in the electromagnetic field.

In summary, the rigged Born-Oppenheimer framework permits a general description of chemical reactions. By retaining the stationary geometry structures determined with modern electronic wave function methods the relationship between quantum electronic state and molecular species is established. The relaxation processes involve serial changes of quantum states.

Acknowledgments

The author has benefited from many exciting discussions with Henk Fidder who contributed to a more definite picture of Franck-Condon excitations. NFR is thanked for continuous financial support.

References

[1] B. T. Sutcliffe, in *Potential energy surfaces*, A. F. Sax, Ed. (Springer, Berlin, 1999), pp. 61

[2] Y. Yamaguchi, Y. Osamura, J. D. Goddard and H. E. Schaefer III, *A new dimension to quantum chemistry: Analytic derivative methods in ab initio molecular electronic structure theory* (Oxford University Press, New York, 1994)

[3] J. J. Sakurai, *Modern Quantum Mechanics* (Benjamin/Cummings, Menlo Park, 1994)

[4] R. G. Woolley, J.Am.Chem.Soc. **100**, 1073 (1978)

[5] B. T. Sutcliffe, in *Theoretical models of chemical bonding*, Z. B. Maksic, Ed. (Springer-Verlag, Berlin, 1990), pp. 1

[6] M. Born and J. Oppenheimer, Ann. Physik **84**, 457 (1927)

[7] R. G. Woolley and B. T. Sutcliffe, Chem.Phys.Lett. **45**, 393 (1977)

[8] O. Goscinski and V. Mujica, in *Density matrices and density functionals*, R. Erdahl and V. H. Smith Jr, Eds. (Reidel, Dordrecht, 1987)

[9] M. Klein, in *Potential energy surfaces*, A. F. Sax, Ed. (Springer, Berlin, 1999), pp. 215

[10] Hunter, Int.J.Quantum Chem. **9**, 237 (1975)

[11] O. Tapia, in *Quantum systems in chemistry and physics, Vol II: Advanced problems and complex systems*, A. Hernandez-Laguna, J. Maruani, R. McWeeny and S. Wilson, Eds. (Kluwer, Dordrecht, 2000), pp. 193

[12] B. J. Roos, in *Lecture notes in quantum chemistry*, B. J. Roos, Ed. (Springer-Verlag, Berlin, 1992), pp. 179, B. O. Roos, (Ed.) *Lecture notes in quantum chemistry*, (Springer-Verlag, Berlin, 1992), B. O. Roos, Acc.Chem.Res. **32**, 137 (1999)

[13] O. Goscinski and A. Palma, Int.J.Quantum Chem. **15**, 197 (1979)

[14] G. Herzberg and E. Teller, Z.Physik.Chem. **B21**, 410 (1933)

[15] W. Siebrand, Chem.Phys.Lett. **51**, 5 (1977)

[16] O. Attabek, A. Hardisson and R. Lefebvre, Chem.Phys.Lett. **20**, 40 (1973)

[17] R. G. Woolley, Adv.Phys. **25**, 27 (1976)

[18] W. H. Miller, J.Chem.Phys. **61**, 1823 (1974)

[19] R. D. Levine and R. B. Bernstein, *Molecular reaction dynamics and chemical reactivity* (Oxford University Press, New York, 1987)

[20] W. H. Miller, J.Phys.Chem. **99**, 12387 (1995); M. S. Child, *Molecular collision theory* (Academic Press, London, 1974)

[21] J. A. Pople and J. W. Sidman, J.Chem.Phys. **27**, 1270 (1957)

[22] Kondrat'ev, *Chemical kinetics of gas reactions* (Pergamon Press, Oxford, 1964)

[23] H. Eyring, J. Chem. Phys. **3**, 107 (1935)

[24] D. Caldwell and H. Eyring, in *Perpectives in quantum theory*, W. Yourgrau and A. van der Merwe, Eds. (Dover Publications,Inc., New York, 1971), pp. 117

[25] E. Elbaz, *Quantum. The quantum theory of particles, fields, and cosmology* (Springer-Verlag, Berlin, 1998)

[26] H. W. Kroto, *Molecular rotation spectra* (Dover Publications Inc., New York, 1992)

[27] P. O. Löwdin, in *Quantum Chemistry-Basic Aspects, Actual Trends*, R. Carbó, Ed. (Elsevier Science Pub., Amsterdam, Netherland, 1989), pp. 605

[28] W. E. Thirring, in *Schrödinger*, C. W. Kilmister, Ed. (Cambridge University Press, Cambridge, 1987), pp. 65

[29] O. Tapia and J. Andres, Chem. Phys. Letters **109**, 471 (1984)

[30] O. Tapia, V. Moliner and J. Andres, I.J.Quantum Chem. **63**, 373 (1997)

[31] R. C. Dunbar and T. B. McMahon, Science, **279**, 194 (1998)

[32] J. A. Yeazell and T. Uzer, (Eds) *The physics and chemistry of wave packets*, (John Wiley & Sons, New York, 2000)

[33] S. Hilgenfeldt, S. Grossman and D. Lohse, Phys.Fluid **11**, 1318 (1999)

[34] T. J. Mason and J. P. Lorimer, *Sonochemistry* (Ellis Horwood Ltd, New York, 1988)

[35] V. N. Gheorghe and F. Vedel, Phys.Rev.A **45**, 4828 (1992)

[36] S. Bratos and J.-C. Leicknam, J.Chem.Phys. **101**, 4536 (1994)

Was H_2^- observed in solid H_2? A theoretical answer.

H.U. Suter, B. Engels
Institut für Physikalische und Theoretische Chemie,
Universität Bonn, Wegelerstrasse 12, D–53115 *Bonn*, Germany
and S. Lunell
Department of Quantum Chemistry,
University of Uppsala, S–75120 *Uppsala*, Sweden

Abstract

Density Funtional Theory (DFT) and ab initio CI cluster calculations were performed to simulate the hyperfine coupling constants of charged hydrogenic systems in solid hydrogen. Possible clusters are the complexated H_2^+ and H_2^- ions. The isotropic hyperfine coupling constant in a H_6^+ cluster was found to be around 572 MHz, in excellent agreement with the experimentally observed 569 MHz. The convergence upon the size of the clusters studied was investigated with two different $H_{14}^{\pm}$ clusters.

Contents

ADVANCES IN QUANTUM CHEMISTRY, VOLUME 40

0065-3276/01 $35.00

1 Introduction

The investigation of solid H_2 has been of growing interest in recent years. Solid H_2 exist in the two forms para–H_2 and ortho–H_2, corresponding to the spin states of the two nuclei. The percentage of p–H_2 varies from 99.8 % at 20 K to about 25 % at room temperature. The solid is a molecular crystal with strong covalent bonds and weak intermolecular bonds. The solid phase is hexagonal close packed with an a of about 3.6 Å , although a Pa3 structure is also known at very low temperatures [1].

Recently Miyazaki et al. [2] did electron spin resonance (e.s.r.) experiments on γ–irradiated solid H_2. They argued that the measured signal at 12.4 Gauss is due to an electron trapped at a distance of 13.8 Å with a p–H_2 molecule. The distance was obtained from a formula due to Gordy and Morehouse [3]. Their conclusion was challenged by Symons [4], who claimed that they indeed may have observed H_2^-. From the observed splitting of 12.4 Gauss he derived a hyperfine coupling constant (hfcc) of about 203 Gauss=568.9 MHz. He excluded H_2^+ whose hfcc is well known (both experimentally [5] as well as theoretically [6]) to be at 912.3 MHz. Symons claimed that the difference to this value could not be due to shielding effects of the matrix. The same naturally holds for free hydrogen atoms. This argument was adopted in the recent e.s.r. experiments of Miyazaki and coworkers [7, 8].

In a recent paper, however, Symons and Woolley [9] have reexamined the experimental evidence by Miyazaki et al. and have suggested that the observed e.s.r. spectra should be assigned to a H_2^+ radical centre rather than H_2^-. They also report electronic structure calculations on a variety of dihydrogen cluster radical species, that give strong, albeit indirect support to the revised interpretation.

It is well–known that free H_2^- is not stable [10]. Therefore, if H_2^- was observed it was due to the stabilisation of the surrounding environment and one may better speak of a H_{2n}^- species. The H_2^+ on the other hand will form H_{2n}^+ species. The question whether this kind of cluster remains stable as a free cluster is not the subject of this investigation. Instead, the aim of the present investigation is to directly verify or falsify the different suggested interpretations of the observed spectra by calculating the hfcc's of the possible clusters. The use of cluster models in the prediction of the hyperfine structure has turned out be highly successful, mainly due to the local nature of the hyperfine interaction. One example of such a correct prediction was the calculation of the hyperfine parameters of anomalous Muon [11] in diamond.

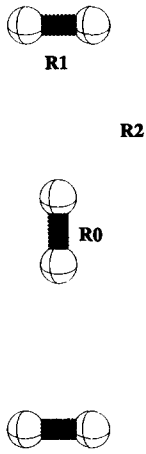

Figure 1: Structure of the cluster number 1.

2 Methods of Calculation

2.1 AO basis set dependence

Although the dependence of the hyperfine properties, such as the isotropic hfcc, on computational method and/or basis sets has been extensively studied in the literature [12], it is in the present connection instructive to examine specifically the performance of different types of hydrogen atom basis sets. This will also give us some insight in the possible errors of the reported calculations. H_2^+ has the advantage that the effect of electron correlation is not present in this system and hence the error of the Hartree–Fock calculation is identical with the error due to the AO basis set.

2.2 Model systems

Three H_2 clusters were used in this study. The first one was obtained by simply adding two hydrogen molecules normal to the ends of the central hydrogen molecule. This cluster is planar and depicted in Figure 1. Although this cluster seems inadequate to describe solid hydrogen, it will turn out that the hyperfine parameters are already described correctly with this model system. The next cluster is obtained by adding 4 additional hydrogen molecules normal to the axis defined by the central hydrogen molecule. The final cluster was inspired by the hexagonal–closed packed crystal structure, and represents one plane of the elementary cell. This cluster is depicted in Figure 2.

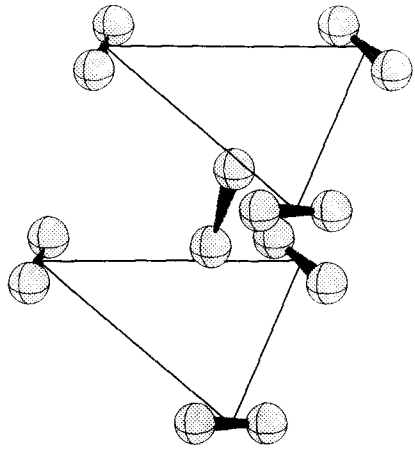

Figure 2: Structure of the cluster number 3 (hcp structure).

Due to the large flexibility of hydrogen molecules in the solid hydrogen, it was decided, contrary to the normal use of cluster models in solid state problems, to optimize the clusters fully, e.g. not to use the crystal parameters from X–ray or similar experiments.

2.3 Theoretical methods

Density functional calculations (DFT) using the B3LYP functional [13], and Møller–Plesset (MP) calculations were performed with the Gaussian94 program [14]. For some geometry optimizations the aug–cc–pVTZ basis set of Dunning and coworkers [15] was used. For the spin density calculations the AO basis set consists of the standard Chipman basis [16], augmented with a tight s function with an exponent of 85.087. To see the reasoning behind the use of the augmented Chipman AO basis set we have performed test calculations on the H_2^+ radical (cf. Table 1).
The CI calculations were performed with the MELDF–X series of programs [17]. The selection of the reference space was done as usual [18, 19]. For H_6^-, to quote one example, this resulted in 25 reference determinants and 79180 configurations. Due to this relatively small number the diagonalisation was done without selection. For H_{14}^- and H_{14}^+ only CIS (CI with singles) was done.

AO basis set	Fermi contact term
STO–3G	0.1641
STO–4G	0.1901
STO–5G	0.2063
STO–6G	0.2172
3–21G	0.1739
6–31G	0.2131
6–31G**	0.2109
STO–6G	0.2172
6–311++G**	0.1919
6–31++G**	0.2083
6–31++G(2df)	0.1906
DZ	0.2073
DZP	0.2048
Chipman	0.1965
Chipman+Peak	0.2063
cc–pVDZ	0.1800
aug–cc–pVDZ	0.1762
cc–pVTZ	0.1905
aug–cc–pVTZ	0.1906
cc–pVQZ	0.1954
aug–cc–pVQZ	0.1957
cc–pV5Z	0.2034
aug–cc–pV5Z	0.2034
exact [6]	0.2041

Table 1: The isotropic hfcc of H_2^+ for different AO basis sets at the bond distance of r=2 a.u. (0.2041 a.u. = 912.3 MHz).

Molecule	Method	R_2	R_0	R_1
H_6^-	MP2/aug-cc-pVTZ	2.955	0.739	0.744
H_6^-	QCISD/aug-cc-pVTZ	2.957	0.744	0.749
H_6^-	QCISD/Chipman+Peak	2.646	0.741	0.760
H_6^+	B3LYP/aug-cc-pVTZ	1.707	1.041	0.793
H_6^+	QCISD/Chipman+Peak	1.662	1.026	0.787
H_6^+	MP2/aug-cc-pVTZ	1.678	1.046	0.785

Table 2: Geometry of $H_6^{\pm}$

	$A_{iso}(H_0)$	$T_{iso}(H_0)$	$A_{iso}(H_1)$
B3LYP	562.13		288.24
CIS	564.90	69.07	255.42
CISD	574.62	68.09	246.61
MR–CISD	571.61	68.09	253.36

Table 3: Isotropic hfcc of hydrogen in H_6^+

3 Results

H_2^- is, as mentioned above, unstable with respect to ionisation. The calculated isotropic hfcc will tend to zero with increasing basis set size. (The actual value for the Chipman AO basis set is 22 MHz, due to the missing Rydberg type funtions.) To obtain a stabilisation of the charged H_2^-, cluster 1 consisting of 3 H_2 moleules in a row was investigated. The H_2 are thought to rotate freely in solid hydrogen. The cluster used is pictured in Figure 1. In Table 2 the optimized geometries of H_6^- and H_6^+ are depicted. The two outer H_2 molecules were forced to be normal to the H_2 chain, while the central H_2 was chosen to be horizontal to the chain, as shown in Figure 1.
The optimized geometry (with MP2/aug–cc–pVDZ) is more compact than expected from a comparison with solid hydrogen, where the center–center distance is around 3.5 Å [1]. For H_6^+, we found r=1.7 Å and for H_6^- we found r=3.0 Å. In the case of H_6^+, our calculated geometry is very close to those reported by Kurosaki and Takayanagi [21] and by Symons and Woolley [9]. The hyperfine structure of H_6^+ is depicted in Table 3. The value is converged to about 572 MHz, which is reasonably close to the experimental 569 MHz. The isotropic value of the hfcc for H_6^- is, on the other hand, close to zero for

atom	x	y	z
H0	±0.498201	0.0	0.0
H1	±1.378683	1.567917	±0.372264
H2	±1.378683	-0.461568	±1.543988
H3	±1.378683	-1.106349	±1.171724

Table 4: Coordinates in Ångström for the optimized hcp structure (MP2).

both the two lowest lying states.
We have further tested the effect of the size of the cluster by adding 4 more H_2 molecules to the H_6^- cluster and found essentially the same difference between the positive and negative clusters, already with the CIS calculations.
An attempt was also made to optimise $H_{14}^{\pm}$ clusters with a forced hcp structure (see Figure 2). The optimized geometry of the positive cluster is given in Table 4 and the hfcc's of both the positive and negative hcp clusters in Table 5.
H_2^- surrounded by H_2 in a hcp structure gave an A_{iso} of about 450 MHz, which is too small to account for the experimental observations. H_2^+ in the hcp structure has an isotropic hfcc of about 800 MHz, which is too large compared to experiment, but smaller than the 912 of free H_2^+. In this case, neither the positive nor the negative cluster gave a satisfactory agreement with experiment. It has, however, been found that an H_{14}^+ cluster which is optimized without constraints will distort to a configuration consisting of a central H_6^+ cluster and four outer H_2 weakly bound to the four corners of H_6^+ [22]. The assumption of a hcp cluster is therefore unrealistic, considering the high mobility of the H_2 molecules in the solid.
Considering the results for all clusters it is evident that the anion has in all cases a too small isotropic hfcc. This is physically quite easy to understand, since the H_2^- is not stable and therefore the electron will be distributed among many H_2 molecules. The cation on the other side has the tendency to build stable clusters which are more compact than the crystal structure. According to these calculations, the observed e.s.r. signals should be related to the cation instead of the suggested anion.

4 Summary and Conclusions

Density Functional Theory (DFT) and ab-initio CI calculations were performed on different ionized clusters of hydrogen (H_2), in order to explain

$H_2^-(H_2)_6$	H_{nn}	H
UHF	6.0	486.9
B3LYP	9.4	454.9
MP2	6.1	451.1
QCISD	7.3	435.1
CIS	5.3	448.7
$H_2^+(H_2)_6$		
UHF	12.9	755.8
B3LYP	86.1	588.3
MP2		747.5
UQCISD		659.7
CIS	60.7	821.3
CISD	57.3	809.8
MRDCI6	57.4	809.7
MRDCI7	61.2	800.9
MRDCI85	61.8	799.0

Table 5: Isotropic hfcc of hydrogen in hcp structure

the recent e.s.r. experiments of Miyazaki et al. [2]. These results could be explained by a small cluster containing H_2^+ surrounded by two H_2 molecules. The calculated A_{iso} of the H atoms in H_2^+ is found to be around 570 MHz, for both DFT and MR–CI methods. The A_{iso} of the anion is much smaller, and to obtain a hfcc which is in agreement with the experiment it would be necessary to elongate the H_2^- bond distance considerably. The conclusion that can be drawn from the present calculations is that the e.s.r. signals of Miyazaki et al. [2] can be assigned to a H_2^+ ion surrounded by H_2 molecules, of which two are more tightly bound to the central ion than the rest, forming a clearly identifiable H_6^+ unit, fully in accordance with the suggestion by Symons and Woolley [9].

5 Acknowledgment

H.U.S. wishes to thank the DAAD and for a travel grant under the Project 313/S-PPP-3/95. Some of the calculations were performed at the "Centro Svizzero di Calcolo Scientifico" (CSCS) in Manno (Switzerland).

References

[1] I. F. Silvera, Rev. Mod. Phys. **52** (1980) 393.

[2] T. Miyazaki, K. Yamamoto and Y. Aratono, Chem. Phys. Lett. **232** (1995) 229.

[3] W. Gordy and R. Morehouse, Phys. Rev. **151** (1966) 207.

[4] M. C. R. Symons, Chem. Phys. Lett. **247** (1995) 607.

[5] A. Carrington, T. R. McNab and C. A. Montgomerie, J. Phys. **B22** (1989) 3551.

[6] M. Cohen, R. P. McEachran and I. R. Schliefer, Chem.Phys.Lett. **10** (1971) 143; R.P. McEachran, C.J. Veentra and M. Cohen, Chem. Phys. Lett. **59** (1978) 275.

[7] T. Miyazaki, K. Yamamoto and Y. Aratono, Chem. Phys. Lett. **251** (1996) 219.

[8] T. Kumada, H. Imagaki, N. Kitagawa, K. Komaguchi, Y. Aratono and T. Miyazaki, J. Phys. Chem. **B 101** (1997) 1198.

[9] M. C. R. Symons and R. G. Woolley, Phys. Chem. Chem.Phys.**2** (2000) 217.

[10] C. W. Bauschlicher, J. Phys. **B 21** (1988) L413.

[11] N. Paschedag, H. U. Suter, D. M. Maric and P. F. Meier, Phys. Rev. Lett. **70** (1993) 154.

[12] See, e.g., B. Engels, L. A. Eriksson and S. Lunell, Adv. Quantum Chem. **27** (1996) 297 - 369.

[13] A. D. Becke, J. Chem. Phys. **98** (1993) 5648

[14] Gaussian 94, Revision B.3, M. J. Frisch, G. W. Trucks, H. B. Schlegel, P. M. W. Gill, B. G. Johnson, M. A. Robb, J. R. Cheeseman, T. Keith, G. A. Petersson, J. A. Montgomery, K. Raghavachari, M. A. Al-Laham, V. G. Zakrzewski, J. V. Ortiz, J. B. Foresman, C. Y. Peng, P. Y. Ayala, W. Chen, M. W. Wong, J. L. Andres, E. S. Replogle, R. Gomperts, R. L. Martin, D. J. Fox, J. S. Binkley, D. J. Defrees, J. Baker, J. P. Stewart, M. Head-Gordon, C. Gonzalez, and J. A. Pople, Gaussian, Inc., Pittsburgh PA, 1995.

[15] D. E. Woon and T. H. Dunning, J. Chem. Phys. **98** (1993) 1358; R. E. Kendall, T. H. Dunning, and R. J. Harrison, J. Chem. Phys. **96** (1992) 6796; T. H. Dunning, J. Chem. Phys. **90** (1989) 1007; D. E. Woon and T. H. Dunning, J. Chem. Phys. **103** (1995) 4572.

[16] D. M. Chipman, Theor. Chim. Acta **76** (1989) 73; J. Chem. Phys. **91** (1989) 5455.

[17] MELDF–X was originally written by L. McMurchie, S. Elbert, S. Langhoff, and E. R. Davidson. It has since been modified substantially by D. Feller, R. Cave, D. Rawlings, R. Frey, R. Daasch, L. Nitzche, P. Phillips, K. Iberle, C. Jackels, and E. R. Davidson.

[18] B. Engels, Chem. Phys. Lett. **179** (1991) 398; J. Chem. Phys. **100** (1994) 1380.

[19] H. U. Suter and B. Engels, J. Chem. Phys. **100** (1994) 2936.

[20] D. Feller and E. R. Davidson, Theor. Chim. Acta **68** (1985) 57.

[21] Y. Kurosaki and T. Takayanagi, Chem. Phys. Lett. **293** (1998) 59.

[22] Y. Kurosaki and T. Takayanagi, J. Chem. Phys. **109** (1998) 4327.

D PARAMETER OF THE MORSE POTENTIAL AS A NEW BOND INDEX FOR ESTIMATING BOND BREAKING ENERGY IN A MOLECULE

Elena S. Apostolova[1]

Department of Quantum Chemistry,
D.I. Mendeleev Russian University of Chemical Technology, Moscow, Russia

Usage of the D parameter of the Morse potential as a bond index is based on the effective Hamiltonian of the anharmonic vibrational problem. In CH_3Cl and CH_3F the D parameter and dissociation energy of localized bond (in parentheses) coincide with accuracy of: i) an experiment for C-Cl and C-F bonds 364.2 (351.5) and 471.9 (472) kJ/mol by calculations in minimal basis set; ii) precise quantum chemical calculations for C-H bonds 469 (422) and 451 (424) kJ/mol by calculations in extended basis set of vibrational states, respectively. A model atom approximation can be used in calculating the vibrational spectrum of CH_3Cl with all of the stretching vibrations in the local-mode limit, but not for those of CH_3F with C-F in the normal-mode limit. In this way, inaccuracy in the back spectral problem will be significantly reduced.

TABLE OF CONTENTS

[1] Electronic mail: elena@muctr.edu.ru

ADVANCES IN QUANTUM CHEMISTRY, VOLUME 40

0065-3276/01 $35.00

1. INTRODUCTION.

One of the major characteristics of the reactivity of molecules in a given electronic state is the bond breaking energy. At an adsorption of interest, there is also bond energy with a surface. Electronic quantum chemical theory permits the reception of these characteristics with high accuracy by ab initio calculations, as a rule, in view of electron correlation energy [1]. The complexity of this has created the basis for development of the phenomenological approaches, which will be easily realized in practice, but are not justified enough by the ab initio theory and seldom make a quantitative estimation of these properties possible [2]. Perspective direction is the development of an indexes reactivity method of compounds on paths of their usage in QSAR and QSPR. In this connection, the special interest is introduced with bond indexes and atomic charges, which are usually received as a result of the Mulliken and Löwdin electronic population analysis in molecular orbitals [3]. Therefore, we are seeing the development of new approaches permitting the extraction of chemical information from the solution of the vibrational quantum chemical problem, from the directly observed vibrational spectra of molecules.

A new method for estimating bond energy in a molecule using the effective Hamiltonian based on the Morse potentials with D_e and a parameters:

$$V_j(r_i) = D_e^j \left[1 - \exp(-a_j r_i) \right]^2 \qquad (1)$$

was formulated by this researcher and A.V. Tulub [4-9], and is advanced concerning YCX_3 molecules. Bonds limiting the applying of the method are:

- localized in quantum-chemical sense;
- where there is dissociation in which the symmetry of a system is conserved.

Parameter D:

$$D = D_e - E_0 \qquad (2)$$

(E_0 – zero-point vibration energy) of C-Y bond in $CHCl_3$ [4], $CDCl_3$, CHF_3 [5], CF_3Cl, CF_3I [6] well suits experimental bond energy even by isotope exchange $CHCl_3 \rightarrow CDCl_3$ (Table I). A model atom approximation permits replacement of C atom in $CF_3C{\equiv}CH$ by C-C or C≡C-C groups without an essential change in calculated C-H bond energy 462-469 kJ/mol and vibrational spectrum [7]. Using the method for localized adsorption problem has been discussed on CH_3F/NaCl (researched by Heidberg, et al.[10-12]).

D parameter is identified by the Arrhenius E_a parameter. In the absolute rate theory of chemical reactions, this is the activation energy. The path of a bond breaking reaction is estimated as a set of stretching vibrational transitions. Thus,

the dissociative electron attachment of CF_3Cl is accompanied by excitation of the ν_3 stretching mode of the C-Cl breaking bond [16]. Consequently, for separated and localized bonds, D parameter is a bond index for estimating bond breaking energy in a molecule.

Table I. D parameter [4-9] and D_{exp} bond breaking energy from experiment [13] of C-Y bond in YCX_3, kJ/mol

	D–CCl_3	H–CCl_3	H–CF_3	Cl–CF_3	I–CF_3	H-C≡CCF_3
D	374.5	349.2	444.2	361.7	230.0	462.5
D_{exp}	369 ± 7	358.2[1]	446.4±4.2	360.2±3.3	231.5[2]	-

[1] Reference [14]. [2] Reference [15].

1.1 Theoretical background of the effective Hamiltonian method.

The new method of estimating bond energy in a molecule is based on:

- Ability to transit to the localized orbitals basis set [17,18] and use the additive scheme to obtain the physicochemical properties of molecules (electrical dipole moment, tensor of polarizability), electrooptical characteristics of IR- and Raman spectra (derivative from the first on normal vibration coordinates) [19], and also bond length [20, 21].
- Success in solving a vibrational problem and attempts to estimate bond energy in a molecule with the use of the localized approach on the basis of the effective Hamiltonian. The effect of anharmonicity was accounted for by the third and fourth terms of factorization of potential energy in the Taylor series [22-26] or by the Morse potential [26-39].
- Results of the estimation of bond energy with a metal surface by a phenomenological Bond Order Correlation – Morse Potential method [2].

Of course, using the additive scheme rules out the possibility of calculating of the contribution of electron correlation component in bond energy. In fact, the difference between estimated from the Morse potential and experimental bond energies [40] decreases in HI, HBr, HCl, HF, H_2: 92.8 (31.4%), 81.8 (22.5 %), 59.5 (13.8 %), -25.8 (4.5 %), 30.4 (7.0 %) kJ/mol, respectively. Apparently, the accuracy of the calculation of bond energy in small molecules is usually low-level. Exceptions can be found with molecules containing atoms of inert gases. The enforced dissociation of NeOH was shown to be described by Morse-like potential [41].

1.1.1 Choice of the effective Hamiltonian.

To obtain the most precise results, the effective Hamiltonian should meet the following requirements:

- Predicting vibrational spectrum of a molecule with high accuracy;
- Allowing for the effect of anharmonicity;
- Containing probably smaller number of empirical parameters;
- Making estimation of bond energy possible.

The high accuracy of 10-20 cm^{-1} is achieved in calculation of the vibrational spectrum of hydrocarbons in harmonic approach [42]. But this decreases to the value of 100 cm^{-1} with the presence of heteroatoms, as, for example, is shown by calculation of the fundamentals of conjugated Schiff bases in 6-31G* basis set [43] and of K^+ ion complex with a single H_2O in the Hartree-Fock limit [44].

Accuracy increases if the effect of anharmonicity is allowed by the third and fourth terms of factorization of potential energy in the Taylor series. Thus, the fundamentals of the SiH_3^- anion were calculated by perturbation theory by TZ 2P + *diff*(Si) CISD method with the accuracy of 90 cm^{-1} [24]. The C-H overtones and combinations in H-CX_3, where X = D, F, Cl, CF_3, up to 6 quanta of excitation was predicted to within 2-15 cm^{-1} [22,23]. The same accuracy is achieved if the force constants are described as free parameters and obtained in the least-squares fit to observed data [23].

It is known [42] that this anharmonic potential is substituted by the Morse potential given by Eq. (1) without change in eigenvalues. In this case, the number of free parameters decreases per unity for every pair of interactions. The highest accuracy of 1-2 cm^{-1} was obtained in calculating the stretching overtone spectra of SF_6, WF_6, UF_6 [22,23,29,31], H_2O, D_2O, H_2S, SO_2, C_2H_2, C_2D_2 [27,34], CH_4, CD_4, SiH_4, GeH_4, GeD_4 [33] and C_6H_6 [32]. Properties of the Morse potential make it possible to predict decreasing overtone intensity [39], which is important for calculating the intensity of vibrations.

Thus, the Morse potential is the most appropriate for estimating bond energy in a molecule [4-9]. The C-X and C-Y bond stretching modes in YCX_3 molecules are treated as anharmonic Morse-like diatomic, non-linear coupled oscillators. The well-known [26-37] effective Hamiltonian of the local and normal mode model is used.

This effective Hamiltonian will improve the taking into account of deformation vibrations [15,26,29,30], all of degrees of freedom of the system, namely vibronic effects [38,45-47]. However, the action of these factors (including stretch-bend resonance interactions, that perturb overtone part of vibrational spectra most of YCX_3 molecules [15,26,29,30,48]) on vibrational

frequencies of systems is described as a small perturbation. The local and normal mode Hamiltonian is sufficient for estimating the bond energy in zero approach.

Parameters of the effective Hamiltonian for YCX_3 are calibrated on the observed C-Y and C-X stretching fundamentals, overtones and combinations at 2 quanta of excitation. At the highest excitations, describing the energy of anharmonic oscillator by the Morse potential can lead to significant error [49].

For estimating the separate C-Y bond energy as D parameter given by Eq. (2), the usage of spectral frequencies measured with accuracy of $\pm$ 0.5 cm^{-1} is desirable [5], as with IR absorption spectra of the solutions in liquid argon, used in previous works [5-7] for estimating C-Y bond energy in CHF_3 [48], CF_3Cl [30,50], CF_3I [15] and $CF_3C{\equiv}CH$ [25]. C-Y bond energy in $CHCl_3$ [4], $CDCl_3$ [5] was estimated using the IR spectra of solution in CCl_4, measured with accuracy of $\pm$ 3 cm^{-1} [51-53].

1.2 Formulation of the problem and test compounds.

YCX_3 molecules have been chosen as test compounds as in previous works [4-9]. Such compounds, especially Freons and methylhalides are also of interest for ecological problems [54,55]. The IR and photoacoustic absorption spectra measured by Law [26] and Smith, et al [56], in vapor CH_3F with accuracy of $\pm$ 0.5 cm^{-1} were used for estimating bond energy. The RMS error of IR spectrum measured by Duncan at al. [37] of vapor CH_3Cl was 2.6 cm^{-1} .

The C-Cl in CH_3Cl and C-F in CH_3F stretching vibrations will be shown to be related to the local- and normal-mode limit, respectively. The problem of the minimum number of free parameters of the model Hamiltonian [4-9] necessary for estimating bond energy in these two limit cases will be resolved below. The correlation between the D parameter and C-H bond energy in CH_3Y molecules and the possibility of considering this as a bond index depending on size of the basis set of vibrational states will be discussed below.

The back spectral problem (the inverse problem of a parameter set of the effective Hamiltonian determination) is inaccurate. The possibility of improving it, taking into account that the D parameter of separated C-F bond in CH_3F coincides with dissociation energy, will be discussed.

For the CH_3F, the possibility of a model atom approximation will be also discussed. The C-F group will be considered as a model atom. Stretching vibrational frequencies calculated in this work of up to 4 quanta of excitation will be compared with the predictions of the local-mode model for the CH_3 group only [26] and with the resonant perturbed spectrum of the molecule observed by Law [26].

2. MODEL HAMILTONIAN.

The effective local and normal mode model Hamiltonian is [4-9,26-29,33]:

$$\mathbf{H} = \mathbf{H_0} + \mathbf{H_1}, \tag{3}$$

where the local-mode model Hamiltonian $\mathbf{H_0}$ by neglect of rotation-vibration and also stretch-bend interaction for CH_3Y (Figure 1) is:

$$\mathbf{H_0} = \sum_{i=1}^{3} [(2\mu_1)^{-1}\mathbf{p_i}^2 + \mathbf{V_1}(r_i)] + (2\mu_2)^{-1}\mathbf{p_4}^2 + \mathbf{V_2}(r_4), \tag{4}$$

where $\mathbf{r_i}$-operators of the Cartesian displacement coordinates, $\mathbf{p_i}$ - conjugated momentum operators, $\mathbf{V_j}(r_i)$ – the Morse operators, $\mu_j = (m_j m_C) / (m_j + m_C)$, j = 1, 2 = H, Y; Y = F, Cl, m_C - mass of the central carbon atom. $\mathbf{H_1}$ - operator of the non-linear coupling, Morse-like oscillators by the elimination of the centre of mass motion is:

$$\mathbf{H_1} = (-2/m_C)\,(\mathbf{p_1p_2} - \mathbf{p_1p_3} - \mathbf{p_2p_3} + \sum_{i=1}^{3} \mathbf{p_ip_4}) + f_1 \sum_{i<j}^{3} \mathbf{r_ir_j} + f_2 \sum_{i=1}^{3} \mathbf{r_ir_4}, \tag{5}$$

where f_k - force constants are free parameters such as D_e^j and a_j.

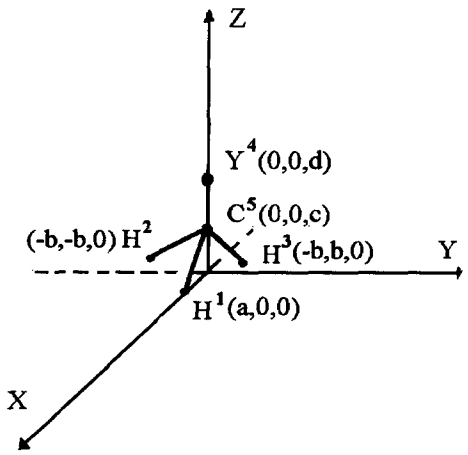

Figure 1. Cartesian coordinates of atoms in CH_3Y molecules.

A minimal basis set of vibrational states was used. The basis set functions $\langle v_1v_2v_3v_4|$ are given by product of eigenvectors $\langle v_i|$ of the four Morse operators, describing C-H and C-Y stretching modes, labeled by the vibrational quantum number v_i [28]. Diagonal elements of the local-mode Hamiltonian matrix are given by sums of eigenvalues of three equivalent C-H and C-Y Morse operators with harmonic frequencies ω_1, ω_2 and Morse anharmonicities ωx_1, ωx_2 :

$$\langle v_1v_2v_3v_4|H|v_1v_2v_3v_4\rangle = \sum_{i=1}^{3}[v_i\omega_1 - v_i(v_i+1)\,\omega x_1] + [v_4\omega_2 - v_4(v_4+1)\omega x_2], \quad (6)$$

$$\omega x_j = \hbar^2 a_j^2 (2\mu)^{-1} \quad , \quad \omega_j = 2(D_e^j\,\omega x_j)^{1/2} \quad (7)$$

and off-diagonal elements are subject to the selection rule:

$$\Delta v_i = \pm 1\,,\ \Delta v_j = \mp 1,\ \Delta v_k = 0\,,\ \Delta v_l = 0\,,\ k,l \neq i,j\,,$$

$$\langle (v_i+1)(v_j-1)v_kv_l|H|v_iv_jv_kv_l\rangle = \begin{cases} [(v_i+1)\,v_j]^{1/2}\,\lambda_1\,, & i=j=H \\ [(v_i+1)\,v_j]^{1/2}\,\lambda_2\,, & i=H, j=Y;\ i=Y, j=H \end{cases} \quad (8)$$

where λ_1, λ_2 are coupling stretches of the C-H and C-Y Morse-like oscillators.

All of vibrations of the molecule are ascribed [28] to:

- the local-mode limit, if: $\lambda_j \approx 0$ or $\omega x_j >> |\lambda_j|$, (9)
- the normal-mode limit, if: $\omega x_j \approx 0$ or $|\lambda_j| >> \omega x_j$ (10)

In the C_{3v} group symmetry adapted basis set (see Ref. [4] for details), the matrix of the effective Hamiltonian defined by Eqs. (3)-(5) is block-diagonal. The blocks and the diagonalized ones for two nearest vibrational levels are:

v = 1

$$\begin{matrix} \langle 1000;A_1| \\ \langle 0001;A_1| \end{matrix} \begin{bmatrix} \omega_1-2\omega x_1+2\lambda_1 & \sqrt{3}\lambda_2 \\ \sqrt{3}\lambda_2 & \omega_2-2\omega x_2 \end{bmatrix} = \begin{bmatrix} \nu_1 & 0 \\ 0 & \nu_3 \end{bmatrix} \quad (11)$$

$$\langle 1000;E|\ \omega_1-2\omega x_1-\lambda_1 = \nu_4 \quad (12)$$

v = 2

$$\begin{matrix} \langle 2000;A_1| \\ \langle 0110;A_1| \\ \langle 1001;A_1| \\ \langle 0002;A_1| \end{matrix} \begin{bmatrix} 2\omega_1-6\omega x_1 & 2\sqrt{2}\lambda_1 & \sqrt{2}\lambda_2 & 0 \\ 2\sqrt{2}\lambda_1 & 2\omega_1-4\omega x_1+2\lambda_1 & 2\lambda_2 & 0 \\ \sqrt{2}\lambda_2 & 2\lambda_2 & (\omega_2-2\omega x_2)+\omega_1-2\omega x_1+2\lambda_1 & \sqrt{6}\lambda_2 \\ 0 & 0 & \sqrt{6}\lambda_2 & 2\omega_2-6\omega x_2 \end{bmatrix} = \begin{bmatrix} 2\nu_1 & 0 & 0 & 0 \\ 0 & \nu_1+\nu_4 & 0 & 0 \\ 0 & 0 & \nu_1+\nu_3 & 0 \\ 0 & 0 & 0 & 2\nu_3 \end{bmatrix} \quad (13)$$

$$\begin{array}{l|ccc|} <2000;E| & 2\omega_1-6\omega x_1 & -\sqrt{2}\lambda_1 & \sqrt{2}\lambda_2 \\ <0110;E| & -\sqrt{2}\lambda_1 & 2\omega_1-4\omega x_1-\lambda_1 & -\lambda_2 \\ <1001;E| & \sqrt{2}\lambda_2 & -\lambda_2 & (\omega_2-2\omega x_2)+\omega_1-2\omega x_1-\lambda_1 \end{array} = \begin{vmatrix} 2\nu_4 & 0 & 0 \\ 0 & \nu_1+\nu_4 & 0 \\ 0 & 0 & \nu_3+\nu_4 \end{vmatrix} \quad (14)$$

3. BOND ENERGY AND OVERTONE SPECTRA OF CH_3F AND CH_3Cl.

In view of the small number of resonant unperturbed modes in the observed spectra of CH_3F [26,55] (Table II), usually used least-squares refinement of the six parameters of the model Hamiltonian for CX_3Y molecules [4,26,28] is impractical. For estimating C-F bond energy in CH_3F, only five parameters (ω_1 - ωx_1), ω_2, ωx_2, λ_1 and λ_2 are required. Furthermore, there are only five unperturbed stretching modes to calibrate it. Three of the five parameters are calculated with the equations obtained from Eqs. (11), (12), using the observed ν_1, ν_3, ν_4 [56] fundamentals:

$$(\omega_1 - 2\omega x_1) = 1/6\{(\nu_1 + \nu_3 + 4\nu_4) + [(\nu_1 - \nu_3)^2 - 12\lambda_2^2]^{1/2}\}, \quad (15)$$

$$\lambda_1 = (\omega_1 - 2\omega x_1) - \nu_4, \quad (16)$$

$$(\omega_2 - 2\omega x_2) = \nu_1 + \nu_3 - (\omega_1 - 2\omega x_1) - 2\lambda_1, \quad (17)$$

The ωx_2 and λ_2 parameters are calibrated on the $2\nu_3$ overtone [56] and the perpendicular band origin observed at 6000.8 cm^{-1} [26] using Eqs. (13), (14).

The ωx_1 was calibrated on the predicted center of the resonance multiplex at nearly degenerate A_1 and E bands each dominated by the $<3000|$ localized stretching state [26]. The complete parameter set so obtained and calculated stretching vibrational frequencies are given in Tables II, III. In Figure 2 are given predictions, such as stick spectra, of the six-parameter local and normal mode model are compared with similar predictions of the three-parameter local-mode model for the CH_3 group and with the observed spectra of CH_3F [26].

Obtaining such a parameter set for CH_3Cl was begun with $|\lambda_2|$ (λ_2 is obtained with accuracy of sign), which was calibrated with the feature observed at 3700.67 cm^{-1} and interpreted as $\nu_1+\nu_3$ [37]. The diagonal element, describing the localized $<1001;A_1|$ state at 2 quanta of excitation, given by Eq. (13) is equal to the Trace of the A_1 matrix given by Eq. (11):

$$<1001;A_1| = <1000;A_1| + <0001;A_1| = \nu_1 + \nu_3 \quad (18)$$

Table II. Stretching vibration frequencies (cm^{-1}) of CH_3Y (Y = F and Cl) from the zero-point vibrational level up to v=4 quanta of excitation.

N	Local (normal) mode[1]		Sym-metry	CH_3F		CH_3Cl	
				Calc.[2]	IR[3]	Calc.[2]	IR[4]
1		2	3	4	5	6	7
			Fundamentals, v=1				
1	<0001|	(ν_3)	A_1	1048.6	1048.6	732.8	732.84
2	<1000|	(ν_1)	A_1	2964.5	2964.5	2967.8	2967.78
3	<1000|	(ν_4)	E	3005.8	3005.8	3039.3	3039.29[5]
			Overtones and combinations, v=2 – 4				
4	<0002|	($2\nu_3$)	A_1	2081.4	2081.4	1456.8	1456.75
5	<1001|	($\nu_1+\nu_3$)	A_1	4003.9	-	3700.6	3700.67
6		($\nu_3+\nu_4$)	E	4046.9	-	3772.1	3773.52[5]
7	<2000|	($2\nu_1$)	A_1	5828.0	-	5875.0	5875.0
8		($2\nu_4$)	E	5835.5	-	5909.2	5923.4[5]
9	<1001|	($\nu_1+\nu_4$)	A_1	5965.5	-	6025.2	6015.3
10			E	5999.6	6000.8	6062.6	6062.7[5]
11	<0003|	($3\nu_3$)	A_1	3098	-	2171.7	-
12	<1002|	($\nu_1+2\nu_3$)	A_1	5028	-	4424.5	-
13		($2\nu_3+\nu_4$)	E	5076	-	4496.0	-
14	<2001|	($2\nu_1+\nu_3$)	A_1	6858	-	6607.9	-
15		($2\nu_4+\nu_3$)	E	6927	-	6642.1	-
16	<0111|	($\nu_1+\nu_3+\nu_4$)	A_1	6998	-	6758.1	-
17			E	7034	-	6795.4	-
18	<3000|	($3\nu_1$)	A_1	8535	8535[4]	8683.4	8632.1[5]
19		($3\nu_4$)	E	8536	-	8700.5	-
20	<0120|	($2\nu_1+\nu_4$)	A_1	8788	-	8849.8	8820.0
21		($\nu_1+2\nu_4$)	E	8816	-	8901.1	8856.0[5]
22			E	8835	-	8992.1	8976[5]
23			A_2	8863	-	9004.0	-
24	<1110|	($2\nu_1+\nu_4$)	A_1	8985	-	9079.0	9076.9
25	<0004|	($4\nu_3$)	A_1	4100	-	2878	-
26	<1003|	($\nu_1+3\nu_3$)	A_1	6036	-	5140	-
27		($3\nu_3+\nu_4$)	E_s	6092	-	5211	-
28	<2002|	($2\nu_1+2\nu_3$)	A_1	7872	-	7332	-
29		($2\nu_3+2\nu_4$)	E_s	7994	-	7366	-
30	<0112|	($\nu_1+2\nu_3+\nu_4$)	A_1	8014	-	7482	-
31			E_s	8058	-	7519	-
32	<3001|	($3\nu_1+\nu_3$)	A_1	9552	-	9416	-
33		($\nu_3+3\nu_4$)	E_s	9617	-	9433	-

1	2	3	4	5	6	7	8
34	<0211|	$(2\nu_1+\nu_3+\nu_4)$	A_1	9808	-	9583	-
35		$(\nu_1+\nu_3+2\nu_4)$	E_s	9838	-	9634	-
36			E_p	9859	-	9725	-
37			A_2	9887	-	9737	-
38	<1111|	$(2\nu_1+\nu_3+\nu_4)$	A_1	10011	-	9812	-
39	<4000|	$(4\nu_1)$	A_1	11094	11135[6]	11364	11268
40		$(4\nu_4)$	E_s	11094		11375	-
41	<0310|	$(3\nu_1+\nu_4)$	A_1	11508	11511[6]	11639	-
42		$(\nu_1+3\nu_4)$	E_s	11530	-	11683	-
43			E_p	11515	-	11732	-
44			A_2	11543	-	11744	-
45	<0220|	$(2\nu_1+2\nu_4)$	A_1	11671	-	11847	-
46			E_s	11678	-	11879	-
47	<2110|	$(2\nu_1+2\nu_4)$	A_1	11791	-	11912	-
48			E_s	11780	-	12003	-

[1] <1000| (ν_1), (ν_4) and <0001| (ν_3) – C-H and C-Y stretching vibration modes.
[2] This work. [3] Refs. [26,56]. [4] Ref. [37]. [5] Rotationally excited. [6] Center of band.

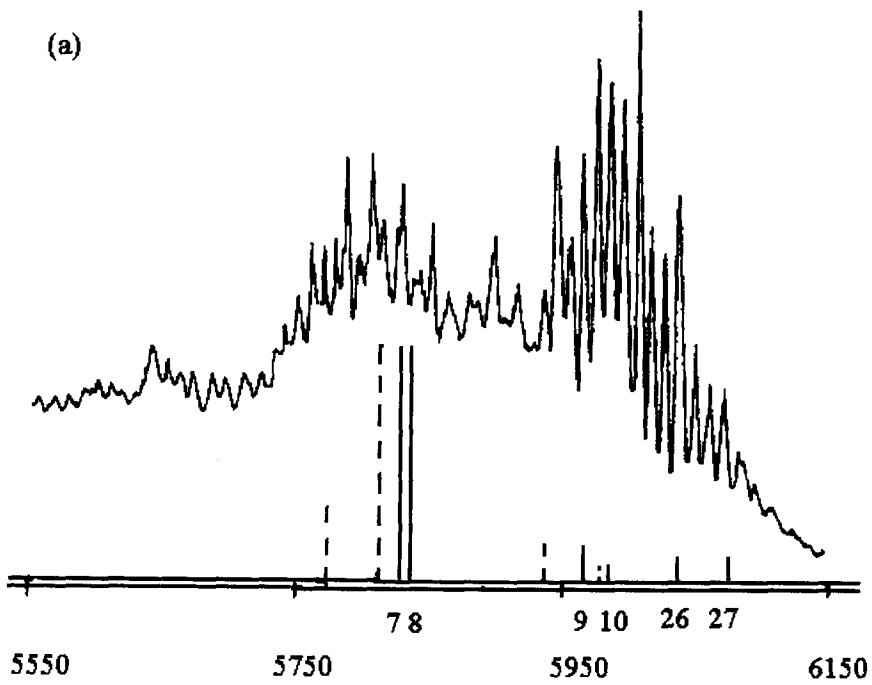

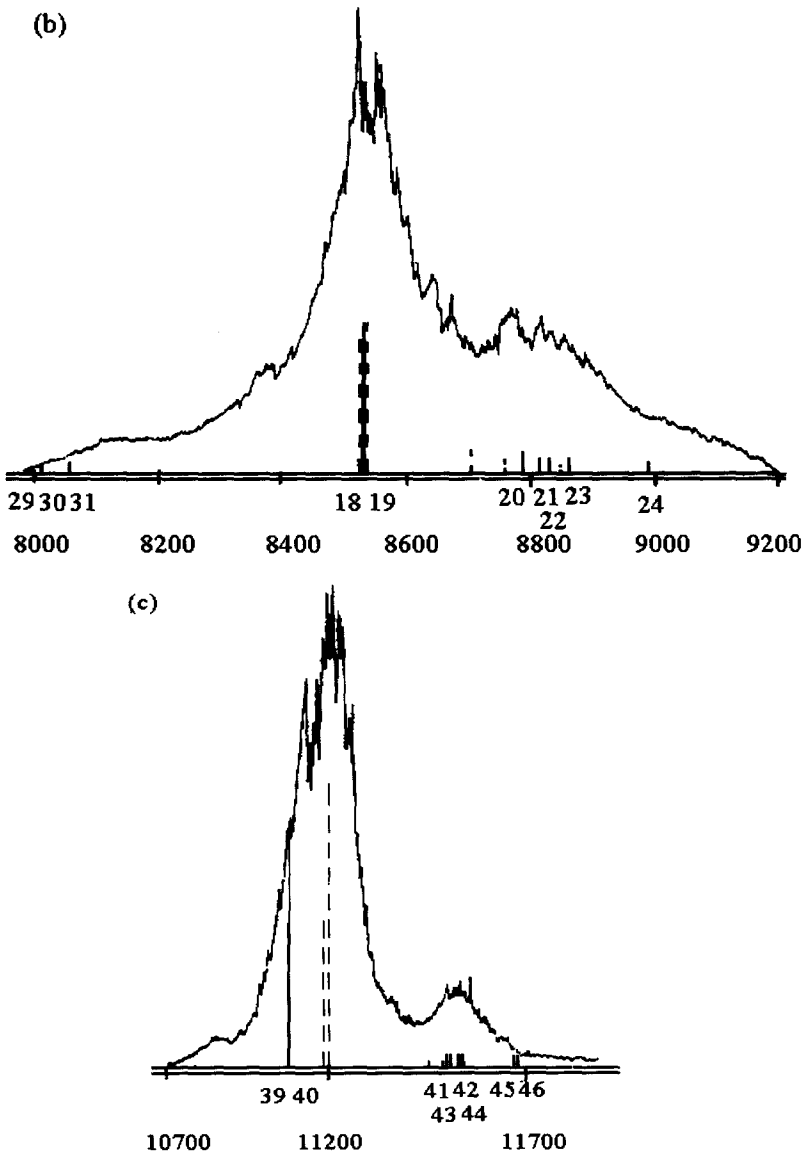

Figure 2. Predictions such as stick spectra of the six-parameter local and normal mode model (solid lines) and of the three-parameter local-mode model (Ref. [26]) for CH_3 group (broken lines) compared with the spectra of vapor CH_3F observed by Law [26] in the first v = 2 (a), second v = 3 (b) and third v = 4 (c) C-H stretching overtone regions. Numbers in the first rows are N given in Table II, in nearest row – wavenumbers/cm^{-1}.

For CH_3Cl this value 3700.62 cm^{-1} coincidences with the observed $\nu_1+\nu_3$ value with the accuracy of experiment (Table II). Thus, $|\lambda_2| = 0$ (being increased, it can only decrease the calculated energy of $<1001;A_1|$ state) (Table III).

Then C-Cl stretching vibrational modes are local according to Eq. (9). For estimating C-Cl bond energy in CH_3Cl only two parameters ω_2 and ωx_2 are required, which are easily obtained from Eqs. (11), (13):

$$(\omega_2 - 2\omega x_2) = <0001;A_1| = \nu_3, \quad (19)$$

$$(2\omega_2 - 6\omega x_2) = <0002;A_1| = 2\nu_3, \quad (20)$$

Three parameters describing local stretching vibrations of the CH_3 group λ_1, ω_1, ωx_1 given in Table III are obtained by Eqs. (13), (16) and (15):

$$(\omega_1 - 2\omega x_1) = 1/3(<1000;A_1| + 2<1000;E|) = 1/3(\nu_1 + 2\nu_4) \quad (21)$$

Table III. C-H and C-Y bond energies (kJ/mol) and parameters of local and normal mode model Hamiltonian (cm^{-1}) for CH_3Y at uncertainty ε (cm^{-1}) of calculating the stretching vibrational frequencies up to v quanta.

Parameter	$CDCl_3$	CH_3Cl	CH_3F	CHF_3	CF_3Cl	CF_3I
v	2	2	3	2	4	3
ε^1	5.0	10.	1.2	6.3	31	10.7
λ_1	-17.0	-23.8	-56.7	16.7	-53.8	-50.8
$\pm\lambda_2$	144.7	0	277.0	192.1	100.7	104.5
ω_1	747.5	3129.3	3103.4	1172.5	1172.8	1147.6
ω_2	2295.1	741.77	1195.2	3101.2	535.4	334.2
ωx_1	12.2	56.9	77.2	4.95	10.0	10.4
ωx_2	40.6	4.5	8.92	62.2	2.4	1.4
D_e^1	11424	43006	31203	69434	34383	31628
D_e^2	32437	30808	40039	38660	30500	19393
E_0^1	370.7	1550.4	1532.4	585.0	583.9	571.2
E_0^2	1137.4	369.8	595.4	1535.1	267.1	166.8
D^1	132.25^2	496.0^2	355.0^2	823.8^2	404.4^2	371.6^2
D^2	374.5^2	364.2^2	471.9^2	444.2^2	361.7^2	230.0^2
D_{exp}^1	-	421.7±4.2[3] 410.0[4]	423.8± ±4[3]	-	490± ±25[3]	431±8[3]
D_{exp}^2	369±7[3]	351.5[4]	472[3]	446.4± ±4.2[3]	360.2± ±3.3[3]	231.5[5] 223.8±2.9[3]

[1] ε - maximum absolute value of calculated minus observed frequency (Table II).
[2] 1 cm^{-1}=0.011964807 kJ/mol. [3] Ref. [13]. [4] Ref. [57]. [5] Ref. [15].

4. DISCUSSION.

The spectra of the stretching vibrations of CH_3F and CH_3Cl as given in Table II are calculated with the same high degree of accuracy (Table III) achieved earlier [4-9] for $CHCl_3$, $CDCl_3$, CHF_3, CF_3Cl, CF_3I, $CH{\equiv}CCF_3$. For $CHCl_3$ this accuracy is increased by the extension of the basis set of vibrational states [26]. For CH_3F the stretching vibrations frequencies up to 3 quanta of excitation are calculated in minimal basis set with the accuracy of extended ones (Figure 2 (a), (b)). At 4 quanta of excitation, the extended basis set [26] is more preferable (Figure 2 (c)). This is the result of another approach toward obtaining the parameter set.

D parameter of C-F bond in CH_3F coincides with the observed dissociation energy only in the case where the C-F stretching vibrations are ascribed to the normal-mode limit given by Eq. (10). In this way inaccuracy of the back spectral problem was significantly improved and the parameter set given in Table III was obtained. For CH_3Cl the parameter set is calibrated with the vibrational spectrum in the local-mode limit only, as was noted above. D parameter of C-Cl bond in CH_3Cl coincides with the bond breaking energy with the accuracy of experimental measurement. Thus, the effective Hamiltonian method is successful for estimating the separated C-F, C-Cl bond energy in CH_3F, CH_3Cl.

The effective Hamiltonian is two-parametric if the stretching vibrations of a separated bond are ascribed to the local-mode limit and minimum five-parametric in the normal-mode limit. Estimating C-H bond energy in $CHCl_3$, CHF_3 using the parameters of isotropic effective Hamiltonian for C-H group obtained by Quack, et al [22,23], in calculations with extended basis set results in values of low accuracy. The true symmetry of the effective Hamiltonian is the important factor for precisely estimating the separated C-Y bond energy, if its stretching vibrations are ascribed to the normal-mode limit. It is for the CX_3Y given in Table III, excepting CH_3Cl. There can be no substitution of the CX_3 group by model atom. The whole symmetric A_1 stretching vibration affects the bond breaking, such as the ν_3 mode in the dissociative electron attachment of CF_3Cl [16].

C-X bond energy in CX_3Y is estimated with a low degree of accuracy (Table III). Of higher accuracy are C-H bond energies estimated using the parameter set obtained earlier by Law [26] in calculations of CH_3Y in extended basis set (Table IV). All of the stretching vibrations in CH_3Cl are ascribed to the local-mode limit and ω_1, ωx_1, λ_1 parameters in minimal and extended basis sets are very similar. The substitution of the CCl group by model atom is possible. In CH_3F, stretching vibrations of the C-H bond are ascribed to the local-mode limit and of C-F bond to the normal-mode limit. The value of the ω_1 parameter closely approaches this calculated in extended basis set by substitution of the CF group by

model atom [26], but ωx_1, λ_1 are noticeably distinct. The distinctions are seen between parameters ω_2, ωx_2, λ_2 and ω_1, ωx_1, λ_1 in CH_3Cl and $CDCl_3$, CHF_3 and CH_3F (Table III). Thus, for example, non-separated C-X bond energy is estimated by the effective Hamiltonian method in calculations using extended vibrational basis set with a high degree of accuracy. The effective Hamiltonian is constructed for CX_3 group only, if its stretching vibrations can be ascribed to the local-mode limit and for the whole molecule in the case of the normal-mode limit.

Table IV. C-H bond energies (kJ/mol) in CH_3Y calculated using parameters of local-mode model Hamiltonian (cm^{-1}) for CH_3 group [26].

Parameter	CH_3Cl	CH_3F	CH_3Br	CD_3Br	CH_3I
λ_1	-27.8	-26.47	-31.2	-47.5	-30.7
ω_1	3131.8	3094.5	3143.9	2308.5	3149.6
ωx_1	60.2	61.0	60.0	31.8	60.6
D_e	40731.6	39245.6	41183.8	41896.0	40924.0
E_0	1550.8	1532.0	1557.0	1146.3	1559.6
D [1]	468.8	451.2	474.1	487.6	471.0
D_{exp} [2]	421.7±4.2	423.8±4	425.1±4.2	-	431±8

[1] 1 cm^{-1} = 0.011964807 kJ/mol. [2] Ref. [13].

The E stretching vibration affects C-X bond breaking in CX_3Y. The C_{3v} symmetry is broken. But D parameter is associated with the activation energy of a reaction, as was noted above. The effective Hamiltonian method is sufficient for estimating bond energy, if the transition state of the reaction is reagent-like, as for example with the radical oxidation of methane [58,59]. In electronic quantum chemical theory, small changes in electronic structure by bond breaking are accounted for by ab initio calculations in extended basis set, allowing for correlation. In the vibrational problem, the precise estimation of C-X bond energy in CX_3Y is possible in calculations using extended basis set, if the correlation component of the total energy of the molecule is minute.

5. CONCLUSIONS.

Prediction of the overtone vibrational spectra of the CX_3Y methylhalides can be based on the effective local and normal mode model Hamiltonian. D parameter, differs from D_e parameter of the Morse potential by E_0 energy of zero-point vibrations, coincides with dissociation energy of separated C-Y bond with experimental accuracy in calculations using minimal basis set, if the correlation

energy of the molecule is minute. For a non-separated C-X bond, this correlates with bond energy in calculations using extended basis set. Thus, D parameter is bond index for estimating localized bond energy in a molecule. The inaccuracy of back spectral problem thereby improves.

A model atom approximation is permitted if all of the stretching vibrations of the molecule are ascribed to the local-mode limit. In the normal-mode limit, using the effective Hamiltonian of the whole molecule is preferable, as was shown in the example of CH_3Cl and CH_3F.

REFERENCES.

[1] *Cluster Models for Surface and Bulk Phenomena*, edited by G. Pacchioni, P.G. Bagus and F. Parmigiani (NATO ASI Ser., New York, London, Toronto, 1992).

[2] *Metal-Surface Reaction Energetics. Theory and Applications to Heterogeneous Catalysis, Chemisorption und Surface Diffusion*, edited by E. Shustorovich (VCH Publishers Inc., New York, 1991).

[3] *Molecular Electrostatic Potentials Concepts and Applications. Theoretical and Computational Chemistry 3*, edited by J.S. Murray and K. Sen (Elsevier, Amsterdam, Lausanne, New York, Oxford, Shannon, Tokyo, 1996).

[4] E.S. Apostolova and A.V. Tulub, Opt. Spectrosk. **76** (11), 584 (1994).

[5] E.S. Apostolova and A.V. Tulub, Opt. Spectrosk. **78** (4), 622 (1995).

[6] E.S. Apostolova and A.V. Tulub, Russian J. Phys. Chem. **70** (9), 1517 (1996).

[7] E.S. Apostolova and A.V. Tulub, Zh. Strukt. Khim. **38** (2), 263 (1997).

[8] E.S. Apostolova and A.V. Tulub, in *Proceedings of XVI Mendeleev Congress on General and Applied Chemistry*, St. Petersburg, 1998 (Moscow, 1998), Vol. 1, p. 29.

[9] E.S. Apostolova and A.V. Tulub, in *Book of Abstracts of Fifth European Workshop on Quantum Systems in Chemistry and Physics,* Uppsala, Sweden, 2000 (Academic press, New York, 2000).

[10] J. Hedberg, H. Stein, and E. Riehl, Phys. Rev. Lett. **49** (9), 666 (1982).

[11] J. Hedberg, I. Hussla, and Z. Szilagy, in *Vibrations at Surfaces*, edited by C.R. Brundle and H. Morawitz (Elsevier, Amsterdam, Oxford, New York, 1983), p. 53.

[12] J. Hedberg, H. Stein, E. Riehl, Z. Szilagy, and H. Weiss, Surf. Sci. **158** (1-3), 553 (1985).

[13] *CRC Handbook of Chemistry and Physics*, 68th ed., edited by R.C.Ph.D. Weast (CRC, Boca Raton, 1987-1988), p. 9-64.
[14] *Handbook of Chemist* (Khimija, Leningrad, 1971), Vol. 1, p. 902.
[15] M.O. Bulanin, L.A. Zhigula, T.D. Kolomiitsova, and D.N. Shchepkin, Opt. Spectrosk. **36** (4), 663 (1984).
[16] L. Lehr and H. Miller, Chem. Phys. Lett. **250** (5,6), 515 (1996).
[17] I. V. Abarenkov, V. F. Bratsev, and A. V. Tulub, *The elements of quantum chemistry* (Visshaya Shkola, Moscow, 1989).
[18] S.G. Semenov, E.S. Apostolova, and S.M. Shevchenko, J. Mol. Struct. **251**, 389 (1991).
[19] L.A. Gribov and S.V. Kotov, J. Mol. Struct. **198**, 93 (1989).
[20] K. Jug, Theor. Chim. Acta. **51** (4), 331 (1979).
[21] E.S. Apostolova and S.G. Semenov, Vestnik St. Petersburg Gos. Univ., Pt. 4. Physic. Chemistry **4** (25), 39 (1993).
[22] R. Marquardt and M. Quack, J. Chem. Phys. **95** (7), 4854 (1991).
[23] H.-R. Dübal, T.K. Ha, M. Lewerenz, and M. Quack, J. Chem. Phys. **91** (11), 6698 (1989).
[24] M. Shen, Y. Xie, Y. Yamaguchi, and H.F. Shaefer III, J. Chem. Phys. **94** (12), 8112 (1991).
[25] G.V. Antonenko, T.D. Kolomiitsova, V.A. Kondaurov, and D.N. Shepkin, J. Mol. Struct. **275**, 183 (1992).
[26] M.M. Law, J. Chem. Phys. **111** (22), 10021 (1999).
[27] M.S. Child and R.T. Lawton, Faraday Disc. Chem. Soc. **71**, 273 (1981).
[28] L. Halonen and M.S. Child, J. Chem. Phys. **79** (2), 559 (1983).
[29] T.D. Kolomiitsova, S.M. Melikova, and G.P. Miroshnichenko, Opt. Spectrosk. **59** (6), 1226 (1985).
[30] L.A. Zhigula, T.D. Kolomiitsova, and S.M. Melikova, in *Molekulyarnaya Spektroskopiya* (*Molecular Spectroscopy*) (Leningr. Gos. Univ., Leningrad, 1990), Vyp. 8, p. 198.
[31] F. Iachello and S. Oss, Phys. Rev. Lett. **66** (23), 2976 (1991).
[32] F. Iachello and S. Oss, J. Chem. Phys. **99** (10), 7337 (1993).
[33] L. Halonen and M.S. Child, Mol. Phys. **4** (2), 239 (1982).
[34] F. Iachello and S. Oss, J. Mol. Spectr. **142** (1), 85 (1990).
[35] J.L. Duncan, Spectrochim. Acta. **45A** (10), 1067 (1989).
[36] J.L. Duncan, A.M. Ferguson, and S. Mathews, J. Chem. Phys. **91** (2), 783 (1989).
[37] J.L. Duncan and M.M. Law, J. Mol. Spectr. **140** (1), 13 (1990).
[38] A.I. Pavluchko, G.F. Lozenko, and L.A. Gribov, Opt. Spectrosk. **50** (3), 450 (1981).
[39] E.S. Medvedev, J. Chem. Phys. **108** (1), 81 (1998).

[40] K.S. Krasnov, N. V. Filippenko and V. A. Bobkova, *Molecular constants of inorganic compounds*, Hand-book (Khimiya, Leningrad, 1979).
[41] C.C. Chuang, P.M. Andrews and M.I. Lester, J. Chem. Phys. **103** (9), 3418 (1995).
[42] M.V. Wolkenstein, L.A. Gribov, M.A. Eljashevich and B.I. Stepanov *Vibrations of molecules*, Issue 2 (Nauka, Moscow, 1972).
[43] S. Masuda, H. Torii, and M. Tasumi J. Phys. Chem. **100** (38), 15335 (1996).
[44] H. Kistenmacher, H. Popkie, and E. Clementi, J. Chem. Phys. **59** (11), 5842 (1973).
[45] B.T. Sutcliffe in *Studies Phys. Theor. Chem.*, edited by R. Carbo (Elsevier Sci. Pub. Comp., Amsterdam, 1982), Vol. 21, p. 99.
[46] S. Curter and N.C. Handy, Comp. Phys. Rep. **5**, 117 (1986).
[47] A.S. Mahnev, N.F. Stepanov, and Ju.N. Panchenko, Vestnik Mosc. Univ., Pt. Chemistry. **18** (6), 644 (1977).
[48] T.D. Kolomiitsova, S.M. Melikova, and D.N. Shepkin, Opt. Spectrosk. **67** (3), 592 (1989).
[49] Z. Flügge, *Problems on Quantum Mechanic* (Mir, Moscow 1974), Vol. 1, p. 81.
[50] T.D. Kolomiitsova, V.A. Kondaurov, S.M. Melikova, and D.N. Shepkin, Zh. Prikl. Spektrosk. **43** (3), 427 (1985).
[51] B.E. Borisenko and D.N. Shepkin, Opt. Spectrosk. **29** (1), 46 (1970).
[52] G.M. Barrow and E. A. Yerger, J. Am. Chem. Soc. **76** (20), 5247 (1954).
[53] G. Herzberg, *Infrared and Raman Spectra of Polyatomic Molecules* (New York, 1945), p. 316.
[54] E.S. Apostolova, A.A. Pendin, S.V. Kholodkevich, and G.G. Jushina, Zh. Prikl. Khim. **68** (11), 1904 (1995).
[55] C.F. Mellot and A.K. Cheetham, J. Phys. Chem. B. **103** (19), 3864 (1999).
[56] W.L. Smith and I.M. Mills, J. Mol. Struct. **11**, 11 (1963).
[57] Landolt-Börnstein, *Zahlwerte und funktionen aus Physik, Chemie,Astronomy, Geophysik und Technik* (Springer-Verlag, Berliner-Göttingen, Heidelberg, 1951), Bd. 1, S. 353.
[58] C. Gozalez, J.W. McDouall, and H.B. Schlegel, J. Phys. Chem. **94** (6), 7467 (1990).
[59] E.S. Apostolova and A.V. Tulub, in *Problems of Advanced Koordination Chemistry* (St. Petersburg Gos. Univ., St. Petersburg, 1993), Vyp. 11, p. 156.

Effects of halogen substituents on the conformations of vinyl alcohol and vinyl thiol : a theoretical study

Y. GIRARD and P. CHAQUIN

Laboratoire de Chimie Théorique, Case 137, Université Pierre et Marie Curie, 4 place Jussieu, 75252 Paris CEDEX 05, France

ADVANCES IN QUANTUM CHEMISTRY, VOLUME 40

0065-3276/01 $35.00

1 Introduction

Proposed as far back as 1881 by Erlenmeyer [1], vinyl alcohol CH_2=CHOH remained hypothetical until the 70's [2]. It is present as traces in the equilibrium with acetaldehyde, because of its rather higher energy (11.2 kcal.mol^{-1}). The activation energy of the monomolecular transposition of these tautomeric molecules is also quite important (about 60 kcal.mol^{-1}) [3].

The enols are short-lived intermediates in various reactions (see bibliography in ref [4]) and have been the subjects of numerous theoretical studies.

The structure of vinyl alcohol has been investigated by both spectroscopic [2][5][6][7][8] and theoretical means [9][10][11], showing that the molecule exists mainly in a *syn* conformation (fig. 1).

The study of substituent effect has been focused on the tautomeric equilibrium between the acetaldehyde CH_3-COH and the *syn* vinyl alcohol CH_2=C(OH) [12][3][13][14]. It has been reported, without further comment [4] that for some substituted enols, the *anti* conformer is more stable, and is sometimes distorted in a staggered conformation (fig. 1). Nevertheless, as far as we know, no systematic study is available concerning the influence of substitution on (i) the relative energy of *syn* an *anti* conformers, (ii) the energy barrier between them and (iii) the existence of non-planar, staggered conformers. Such a study may allow a more comprehensive knowledge of small conjugated compounds and, from an experimental point of view, could be followed by spectroscopic studies. For instance, low temperatures matrices allow the trapping of various conformers and their study by IR spectroscopy.

Studies on vinyl thiol (or ethene thiol) are scarce. It has been detected experimentally, and its formation from ethylene and singlet sulfur atom has been predicted theoretically [15]. Its conformations have been studied both experimentally [16] and theoretically [17]. Using it, in a comparative way, in our study focused on vinyl alcohol seemed relevant.

We will present a conformational study of F, Cl, Br for mono, di and trisubstituted enols and thioenols of general formula $C_2X_nH_{3-n}OH$ and $C_2X_nH_{3-n}SH$, where X =F, Cl or Br,

2 Methodology

The potential energy curves of enols and thiols have been calculated as a function of a single parameter, θ, dihedral angle HOCC (resp. HSCC), all the remaining parameters being independantly optimized. The θ angle has been varied from 0° (*syn* conformation) to 180° (*anti* conformation) by 10° steps (fig. 1).

All calculations have been carried out with the Gaussian 98 series of programs [18]. The geometries of all species, were optimized using the hybrid density functional method B3LYP [19][20][21] with the standard 6-31G** basis set. Second-order Moller-Plesset theory calculations (MP2) , with a 6-311++G** basis set,

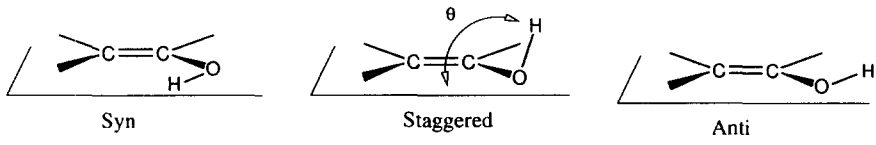

Figure 1: Definition of the θ angle.

were performed in different cases in order to ensure that similar results were obtained. MP2 results for fluorinated enols only are reported here, as an illustration of the good agreement between the two methods (table 3).

3 Results

The potential energy curves are reported (fig. 3-9) for all the mono, di and trihalogenated (F, Cl, Br) enols and thiols. For a sake of clarity the stereochemistry of substituents on carbon C_2 has been specified by their *cis* (c) or *trans* (t) position with respect to the functional group, OH or SH. In addition we noted (tables 1-9) the relative energies with the *syn* conformation taken as energy origin, of the rotational barrier (E_1), of the *anti* conformation (E_3), and of the staggered conformer whenever it is present (E_2) (see Fig.2). In addition we report the θ value corresponding to the *anti* planar ($\theta = 180^o$) or staggered ($\theta < 180^o$) conformers, and their main geometrical parameters. Units are kcal.mol^{-1} for energies, angströms for bond lengths and degrees for angles.

A large variety of situation is encountered. Some compounds follow the vinyl alcohol, with two planar conformations, and a more stable *syn* than *anti* (see for instance curve for *cis* CHBr=CHOH - #17 in fig. 6). In some other, a planar *anti* conformation is the more stable (for instance CH_2=CBrOH - #18 in fig. 6). In a number of compounds, the *anti* form is more or less staggered (for instance CCl_2=CHSH - #34 in fig. 8). There might even be neither *syn* nor *anti* planar conformations, but only a staggered *anti* one (for instance C_2F_3SH - #30 in fig. 7).

3.1 Vinyl alcohol and vinyl thiol

Structural parameters and relative energies for unsubstituted enol and thiol are reported in Table 1. Corresponding enegy curves are displayed in figure 1.

In agreement with previous results [9], the *syn* conformation of enol is more stable than the *anti* one by about 2 kcal.mol^{-1}, with a relatively high rotational barrier.

In vinyl thiol, we observe a very weak out of plane distortion of the *anti* conformer. Our results are in relatively good agreement with previous experimental

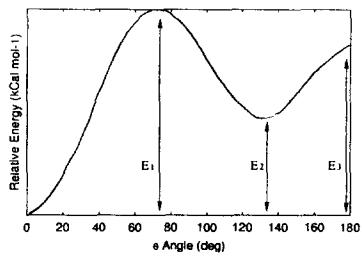

Figure 2: Definition of the energies E_1, E_2 and E_3 reported in tables 1-9.

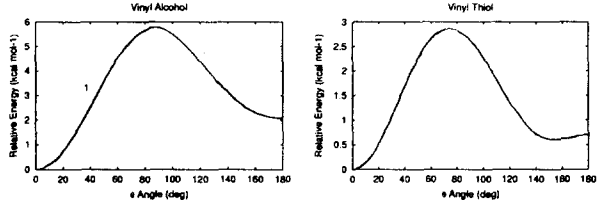

Figure 3: Potential energy curves of vinyl alcohol and vinyl thiol.

Compound	#	θAngle	E_1	E_2	E_3	r(C=C)	r(C-O)	r(O-H)
vinyl alcohol	1	180	+5.76		+2.06	1.331	1.369	0.964
vinyl thiol	23	152	+2.85	+0.61	+0.72	1.333	1.782	1.349

Table 1: Energy gaps of vinyl alcohol and vinyl thiol and main calculated parameters (B3LYP) of the stable *anti* conformers (see fig. 3).

and theoretical studies : E_1 and E_2 were estimated experimentally by Almond *et al.* [16] to be respectively 2.3 kcal.mol^{-1} and 0.3 kcal.mol^{-1}, and calculated by Plant *et al.* [17] to be respectively 2.27 kcal.mol^{-1} and 0.45 kcal.mol^{-1}, at RMP2/6-31G* level.

3.2 Substituted vinyl alcohols and thiols

Table 2 and 3, and figure 4 gather results for fluorinated enols. Chloroenols are displayed in table 4 / figure 5, bromoenols in table 5 / figure 6, fluorothiols in table 6 / figure 7, chlorothiols in table 7 / figure 8, and bromothiols in table 8 / figure 9.

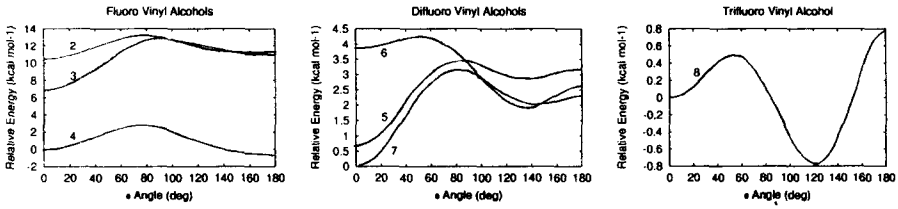

Figure 4: Potential energy curves of fluoroenols.

Compound	#	θAngle	E_1	E_2	E_3	r(C=C)	r(C-O)	r(O-H)
vinyl alcohol	1	180	+5.76		+2.06	1.331	1.369	0.964
(t)FHC=CHOH	2	180	+2.79		+0.88	1.330	1.371	0.963
(c)HFC=CHOH	3	180	+5.96		+4.20	1.331	1.367	0.963
HHC=CFOH	4	180	+2.77		-0.61	1.327	1.347	0.967
FFC=CHOH	5	136.5	+2.73	+2.16	+2.51	1.329	1.374	0.966
(t)FHC=CFOH	6	138	+0.40	-1.92	-1.22	1.330	1.347	0.969
(c)HFC=CFOH	7	143.2	+3.18	+2.04	+2.31	1.330	1.342	0.969
FFC=CFOH	8	121.2	+0.40	-0.77	+0.79	1.329	1.345	0.970

Table 2: Energy gaps of fluoroenols and main calculated parameters (B3LYP) of the stable *anti* conformers (see fig. 4).

Compound	#	θAngle	E_2	E_3	r(C=C)	r(C-O)	r(O-H)
vinyl alcohol	1	180		+1.56	1.337	1.370	0.959
(t)FHC=CHOH	2	180		+0.53	1.334	1.372	0.969
(c)HFC=CHOH	3	180		+3.53	1.336	1.365	0.959
HHC=CFOH	4	180		-0.11	1.331	1.345	0.963
FFC=CHOH	5	133.6	+1.18	+1.90	1.332	1.374	0.961
(t)FHC=CFOH	6	130.1	-2.18	-0.70	1.334	1.339	0.965
(c)HFC=CFOH	7	137.8	+1.08	+2.45	1.333	1.346	0.965
FFC=CFOH	8	121.3	-1.20	+0.99	1.332	1.343	0.965

Table 3: Energy gaps of fluoroenols and main calculated parameters (MP2) of the stable *anti* conformers (see fig. 4).

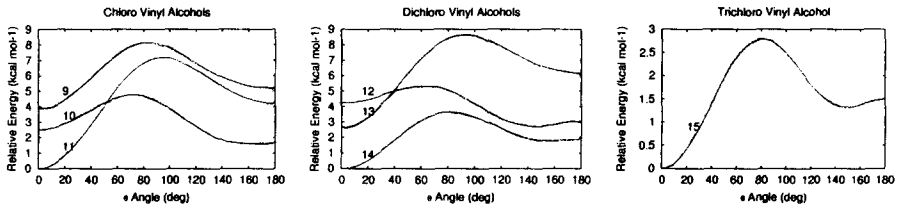

Figure 5: Potential energy curves of chloroenols.

Compound	#	θAngle	E_1	E_2	E_3	r(C=C)	r(C-O)	r(O-H)
vinyl alcohol	1	180	+5.76		+2.06	1.331	1.369	0.964
(t)ClHC=CHOH	9	180	+4.29		+1.38	1.333	1.365	0.964
(c)HClC=CHOH	10	180	+7.16		+4.24	1.333	1.359	0.964
HHC=CClOH	11	160	+2.25	-0.89	-0.82	1.330	1.351	0.967
ClClC=CHOH	12	180	+6.02		+3.55	1.338	1.358	0.964
(t)ClHC=CClOH	13	145	+1.13	-1.51	-1.14	1.336	1.353	0.969
(c)HClC=CClOH	14	180	+3.66		+1.84	1.335	1.344	0.967
ClClC=CClOH	15	145	+2.80	+1.31	+1.51	1.344	1.347	0.968

Table 4: Energy gaps of chloroenols and main calculated parameters (B3LYP) of the stable *anti* conformers (see fig. 5).

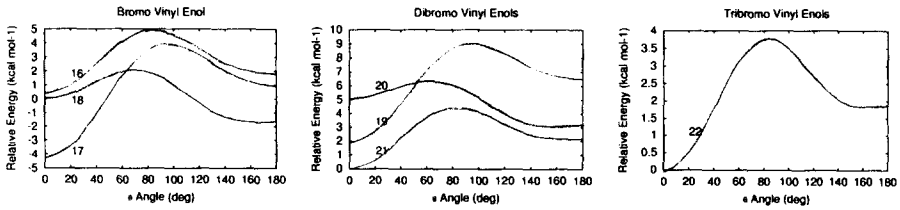

Figure 6: Potential energy curves of bromoenols.

Compound	#	θAngle	E_1	E_2	E_3	r(C=C)	r(C-O)	r(O-H)
vinyl alcohol	1	180	+5.76		+2.06	1.331	1.369	0.964
(t)BrHC=CHOH	16	180	+4.54		+1.46			
(c)HBrC=CHOH	17	180	+8.21		+5.24	1.332	1.358	0.964
(g)HHC=CBrOH	18	162	+1.95	-1.69	-1.58	1.328	1.351	0.966
(tc)BrBrC=CHOH	19	180	+7.16		+4.63	1.336	1.358	0.965
(tg)BrHC=CBrOH	20	150	+1.20	-2.04	-1.88	1.334	1.353	0.966
(cg)HBrC=CBrOH	21	180	+4.44		+2.18	1.332	1.344	0.966
(tcg)BrBrC=CBrOH	22	155	+3.77	+1.83	+1.87	1.341	1.348	0.967

Table 5: Energy gaps of bromoenols and main calculated parameters (B3LYP) of the stable *anti* conformers (see fig. 6).

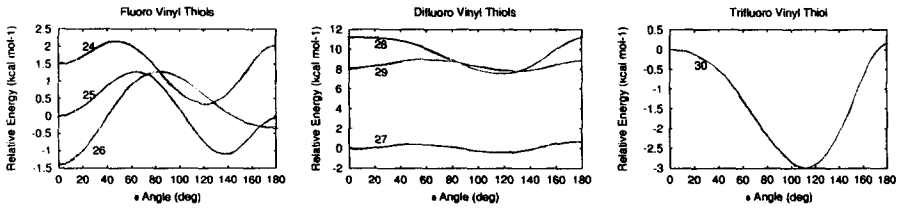

Figure 7: Potential energy curves of fluorothiols.

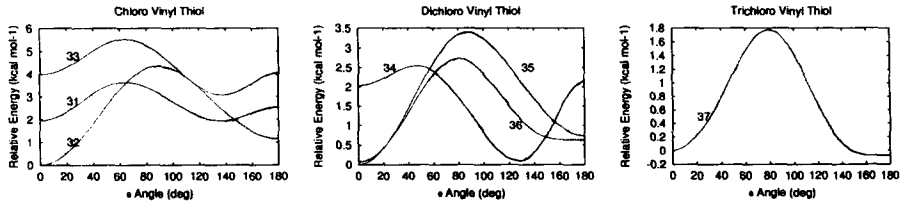

Figure 8: Potential energy curves of chlorothiols.

Compound	#	θAngle	E_1	E_2	E_3	r(C=C)	r(C-S)	r(S-H)
vinyl thiol	23	152	+2.85	+0.61	+0.72	1.333	1.782	1.349
(t)FHC=CHSH	24	121.1	+0.72	-1.12	+0.62	1.330	1.780	1.351
(c)HFC=CHSH	25	137.6	+1.27	-1.09	-0.02	1.329	1.777	1.350
HHC=CFSH	26	180	+2.68		+1.08	1.349	1.775	1.346
FFC=CHSH	27	115	+0.36	-0.36	+0.66	1.330	1.775	1.352
(t)FHC=CFSH	28	118.3		-3.71	-0.1	1.334	1.765	1.340
(c)HFC=CFSH	29	130	+0.83	-0.38	+0.68	1.333	1.344	1.351
FFC=CFSH	30	110		-2.98	+0.17	1.344	1.347	1.353

Table 6: Energy gaps of fluorothiols and main calculated parameters (B3LYP) of the stable *anti* conformers (see fig. 7).

Compound	#	θAngle	E_1	E_2	E_3	r(C=C)	r(C-S)	r(S-H)
vinyl thiol	23	152	+2.85	+0.61	+0.72	1.333	1.782	1.349
(t)ClHC=CHSH	31	140	+1.68	+0.01	+0.61	1.332	1.778	1.347
(c)HClC=CHSH	32	180	+4.37		+1.14	1.333	1.770	1.347
HHC=CClSH	33	140	+1.29	-0.95	+0.12	1.332	1.781	1.346
ClClC=CHSH	34	180	+3.39		+0.74	1.336	1.769	1.347
(t)ClHC=CClSH	35	130	+0.51	-1.93	+0.14	1.339	1.780	1.348
(c)HClC=CClSH	36	180	+2.67		+0.57	1.337	1.777	1.346
ClClC=CClSH	37	180	+1.81		-0.07	1.346	1.782	1.346

Table 7: Energy gaps of chlorothiols and main calculated parameters (B3LYP) of the stable *anti* conformers (see fig. 8).

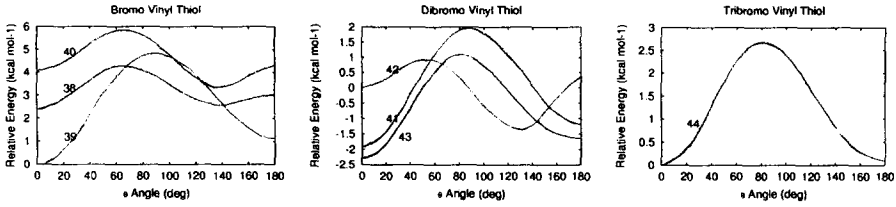

Figure 9: Potential energy curves of bromothiols.

Compound	#	θAngle	E_1	E_2	E_3	r(C=C)	r(C-S)	r(S-H)v
vinyl thiol	23	152	+2.85	+0.61	+0.72	1.333	1.782	1.349
(t)BrHC=CHSH	38	138	+1.88	+0.16	+0.66	1.331	1.781	1.350
(c)HBrC=CHSH	39	180	+4.85		+1.12	1.332	1.769	1.347
HHC=CBrSH	40	142	+1.80	-0.70	+0.29	1.332	1.774	1.349
BrBrC=CHSH	41	180	+3.86		+0.75	1.335	1.769	1.347
(t)BrHC=CBrSH	42	120	+0.90	-1.23	+0.39	1.337	1.776	1.349
(c)HBrC=CBrSH	43	180	+3.46		+0.66	1.334	1.772	1.334
BrBrC=CBrSH	44	180	+2.70		+0.10	1.351	1.771	1.345

Table 8: Energy gaps of bromothiols and main calculated parameters (B3LYP) of the stable *anti* conformers (see fig. 9).

4 Discussion

4.1 Main effects on conformations

The main features in the conformational analysis of these compounds, i.e. relative stabilities of *syn* and *anti* conformers, rotation energy barriers and eventually out of plane distortions of the *anti* conformers, result in manyfold weak interactions and it would be tedious and illusive to give their complete qualitative analysis. We can nevertheless display the most important of them and indicate the trends induced by the change of the nature of the substrate (enol or thioenol) or the position and the nature of substituents. Two interactions seems to be effective enough to be taken into account : electrostatic repulsions and attractions, and π orbital effects.

Electrostatic interactions

They are found between the OH (resp. SH) group and the most remote carbon (C_2), or a substituent in *cis* or *gem* position (fig. 10).

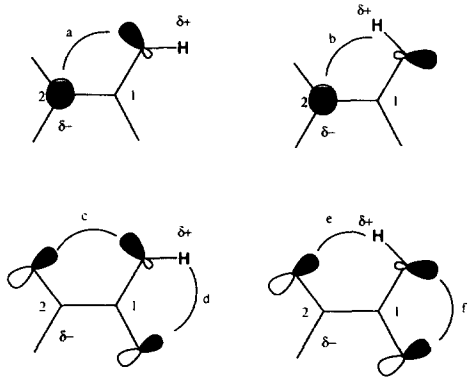

Figure 10: electrostatic interactions of OH or SH with C_2 (upper part) and with halogen substituents (lower part).

Six interactions are noteworthy. The first two, a and b occur in all the compounds, substituted or not :

- **Interaction a** : repulsion between the lone pair of oxygen and the π electron of carbon C_2.
- **Interaction b** : stabilizing interaction between the positive hydrogen and the negative carbon C_2.

The last four occur when a *trans* or *gem* halogen is present:

- **Interactions c and f** : halogen vs. oxygen lone pair repulsions.
- **Interactions d and e** : stabilizing interactions due to an hydrogen bond.

π molecular orbitals effect

They can ben rationalized using conjugated hydrocarbons as models (fig. 11). In this way, vinyl alcohol CH_2=CH-OH is seen as allyl anion CH_2=CH-CH_2^-. The π molecular orbitals system is then filled with not 3 but 4 electrons. In the similar way, for a substituted enol, for instance CFH=CHOH, the model will be a butadiene with 2 extra electrons. Additional electrons in formerly empty molecular orbitals are, in our model, grounds for the structural changes.

4.2 Vinyl alcohol vs. vinyl thiol

Vinyl alcohol

The model for both compounds is a 4 π electron allyl system (fig. 11 (I)). It exhibits a non bonding HOMO (π_2) and a bonding HOMO-1 (π_1). The π system of

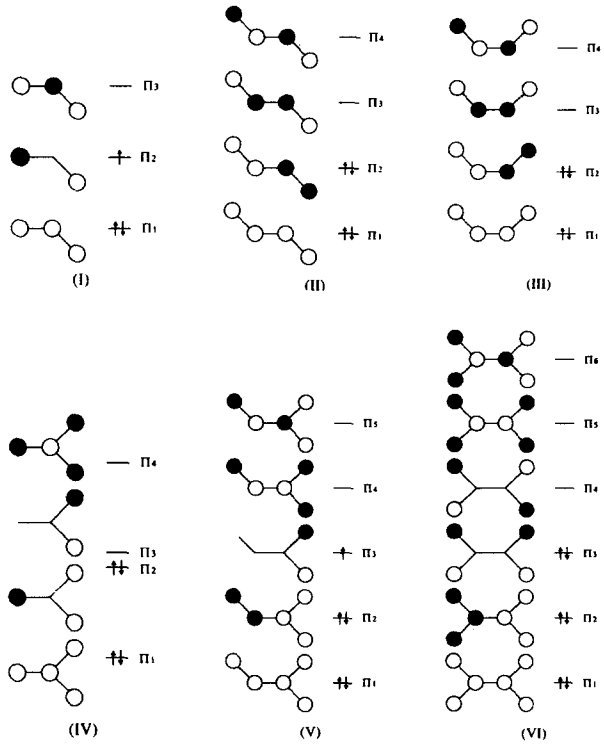

Figure 11: carbon models for π systems

enol is rather different from its prototype allyl's one. Indeed, because of the oxygen electronegativity, its actual π_2 MO is significantly antibonding along the C-O bond. This effect is nevertheless overcome by the strongest bonding character of the π_1 MO, wich is mainly located along the C-O bond. In addition, electrostatic effects should be considered : in the *anti* conformer, there is a strong electron repulsion (**interaction a** in fig. 10) between the lone pair of oxygen and the π electron of carbon C_2, which bears a negative charge partly due to the polarization of the C=C π bond. This interaction unfavors this structure and tends to repell the functional hydrogen out of the plane. In the *syn* conformer this interaction is nearly vanishing and the stabilizing **interaction b** occurs. The balance of these effects entails a rotationnal barrier (about 6 kcal.mol^{-1}) and a greater stability of the *syn* conformer with respect to the *anti* one of 2 kcal.mol^{-1}.

Vinyl thiol

In the thioenol, due to the smaller electronegativity of sulfur, the following changes in these interactions can be expected:

- the π_1 MO is less located on the sulfur and less bonding along the C-S bond.
- the polarization of the C=C bond, the absolute charge of C_2 and the charge of the SH hydrogene decrease, which lowers the importance of **interactions a and b**.
- the lone pair of the sulfur has less p character and is thus less directive, wich diminishes again **interaction a**.

As a result, the energy barrier drops to 3 kcal.mol^{-1} and the *syn/anti* energy difference drops to 0.5 kcal.mol^{-1} Moreover, at our level of calculation, the *anti* planar is no longer an energy minimum, in agreement with ref. [17].

4.3 Substituted compounds

The presence of substituents has as main effect a perturbation of the π system of the carbon net charges and, when in position *gem* or *cis*, brings new electrostatic interactions (**interactions d and e** in fig. 10).

Trans monohalogenated enols and thiols

With halogen substituents, the prototype molecule is still a 6-electron *trans* butadiene (fig. 11 (II)) but electronegativity of halogens leads to more complicated situations. The HOMO (π_3) is antibonding along the C-O bond, which favors out-of-plane distortion, whereas the π_1 and π_2 MOs are bonding and tend to keep the system planar. The most electronegative substituent, fluorine, brings the stronger effects :

- the lowest MOs are more located on the C-F bond wich weakens the CO π bonding.
- the C_2 carbon is less rich in electron, which weakens **interactions a and b**.

This results in a weaker rotational barrier (E_1 = 2.8 kcal.mol^{-1}) and nearer equal energies for *syn* and *anti* conformations (E_3 = +0.88 kcal.mol^{-1}).

Both preceding effects decrease along the series F, Cl and Br which exhibits an increasing rotational barrier and a *syn* conformation stabilization with respect to the *anti* one.

Subst.	F	Cl	Br	H
E_1	2.8	4.29	4.54	5.76
E_3	0.88	1.38	1.46	2.06

The thiol series follows the same trend :

Subst.	F	Cl	Br	H
E_1	0.72	1.68	1.88	2.85
E_3	0.62	0.61	0.66	0.72

Electronegative substituents leading to lower barriers, because of the weakening of the pro-planar effects, we should observe out-of-plane conformations. This is not the case for enols, even if the curves becomes more and more flat with Br, Cl and F. For thiols, we observe these staggered conformations. As expected, the F gives the more stable distorted conformation, relatively to the planar one. This is because all the factors stabilizing the planar conformations (both *syn* and *anti*) are weaker for thiols than for enols, the sulfur being less electronegative than the oxygen.

Trans monosubstituted enols : BH_2 and NH_2 substituents as probes

Using BH_2 and planar NH_2 as substituents in *trans* monosubstituted enols can be a very convenient way to probe the influence of the orbital effects, since they have a empty (for BH_2) or a full (for NH_2) p orbital, perpendicular to the BH_2 (resp. NH_2) plane. If BH_2, for instance, is kept in the molecular plane, there is a full conjugation between its empy p orbital and the π system. If BH_2 is rotated by 90°, the conjugation is turned off. The full p orbital of a planar NH_2 group can be used the same way.

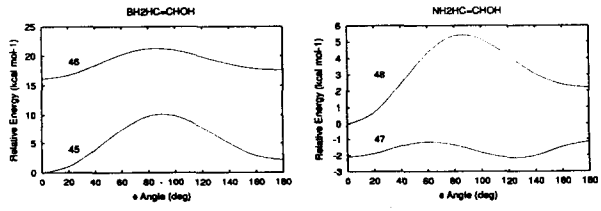

Figure 12: Potential energy curves of BH_2 and NH_2 substituted enols.

Compound		θAngle	E_1	E_2	E_3	r(C=C)	r(C-O)	r(O-H)
(t)BH2(plan)HC=CHOH	45	180	+10.2		+2.1	1.353	1.349	0.966
(t)BH2(per)HC=CHOH	46	180	+5.3		+1.5	1.335	1.373	0.964
(t)NH2(plan)H=CHOH	47	180	+0.93	-0.08	+0.95	1.338	1.391	0.962
(t)NH2(per)H=CHOH	48	125	+5.35		+2.21	1.337	1.370	0.963

Table 9: Energy gaps and main calculated parameters (B3LYP) of BH_2 and NH_2 substituted enols.

With BH_2 kept in the ethylene plane, we get a 4-electron trans-butadiene (fig. 11 (II)), and a large rotational barrier ($E_1 \approx 10$ kcal.mol^{-1}). This is not a surprise, because all the occupied MO's are bonding along CO. When the BH_2 group is frozen perpendicular to the conjugation plane, the empty p orbital cannot conjugates, and we obtain a potential energy curve very similar to the one of the parent enol ($E_1 \approx 5.3$ kcal.mol^{-1}).

With a planar NH_2 group in the molecular plane, the full p orbital conjugates, and the model is a 6-electron butadiene, with a doubly occupied anti-bonding-on-the-CO molecular orbital (π_3). The rotationnal barrier is thus lowered ($E_1 \approx$ 0.9 kcal.mol^{-1}). As expected, the barrier for the perpendicular NH_2 is close to the enol's one ($E_1 \approx 5.3$ kcal.mol^{-1}).

The stabilization of the *syn* conformer by the perpendicular NH_2 substituent, with respect to the corresponding BH_2 one can be attributed to **interaction a** in fig. 10 : the σ effect of N increases the polarization of the CC bond, which is on the contrary decreased by BH_2.

Interesting variations of the C-O distance are noticeable : when the conjugation occurs, the C=O bond is longer with the NH_2 than with the BH_2. When there is no conjugation, this distance is very close to the vinyl alcohol's one (1.369 Angstrom). This is coherent with our model : the π_3 orbital ((II) in fig. 11), filled with planar NH_2, is antibonding along the CO.

Cis and *gem* monosubstituted enols

The prototype π system of *cis* monosubstituted systems is a 6-electron butadiene (fig. 11 (III)). In addition to the effects observed for the corresponding *trans* molecules, we note a relative stabilization of the *syn* conformation due to a hydrogen bond **(interaction e)** and halogen-oxygen lone pair repulsion in the *anti* one. Despite the lone pair in-plane repulsion between oxygen and halogen, the *anti cis* compound is as stable as the corresponding *anti trans* with fluorine, and more stable with chlorine and the bromine. It could arise from the long range bonding interaction which takes place in the HOMO of these systems (π_3). The same effect is observed in the corresponding thioenols.

For the *gem* substituted compounds, the prototype is a 6-electron trimethylene

methane (fig. 11 (IV)), in which the only bonding MO is the low-lying π_1. It allows us to predict an easy deconjugation of oxygen and a stabilization of the *anti* conformation at the *syn* conformation expenses through **interactions d and f.** Thus barriers are rather low, especially for less electronegative halogen (**interaction d** is less important).

Subst.	F	Cl	Br
E_1	2.77	2.25	1.95
E_3	-0.61	-0.82	-1.58

Again, results for substituted thioenols can be roughly understood if one considers that the planar conformations (both *syn* and *anti*) are less stabilized than for enols.

Disubstituted enols

The prototype of the disubstituted enols and thiols, whatever the position of substituents, is V in fig. 11, with 8 electrons, in which the only bonding MOs are the low-lying $\pi_1$and π_2 orbitals. The bonding contribution along the C-O (resp. C-S) bond is thus very weak in fluorine compounds. For instance, starting from *syn* conformation, the rotational barrier is very weak in *trans* FHC=CFOH. Its *anti* conformer is stabilized by **interaction e.** All three *anti* fluorine molecules are slightly distorted.

The thioenols trends can still be derived from the enol one. There is practically no conformational preference for FFC=CHSH; this compound no longer exhibits a minimum for any planar conformation. The substituent effects decreases along the series F, Cl, Br. The planar conformations are again minima in the trichloroethinol but with a weak energy barrier (1.6 kcal.mol^{-1}).

Trisubstituted enols

The prototype of the trisubstituted compounds is (fig. 11 (VI)), with 10 electrons instead of 6. Once again, only the low lying π_1 and π_2 are bonding along C-O (C-S). As expected, the more electronegative the halogen, the higher barrier.

Subst.	F	Cl	Br
E_1	0.4	2.8	3.77
E_3	0.8	1.5	1.87

This is still true for the thiols, with lower barriers (and even no barrier for fluor).

Subst.	F	Cl	Br
E_1		1.81	2.7
E_3	-0.2	-0.1	0.1

5 Conclusion

These calculations show that, if vinyl alcohol and vinyl thiol indeed mainly exist in planar *syn* conformations, as previously stated, the situation can be very different when halogen substituents are present. In some cases, the *anti* conformation is more or less out-of-plane staggered and can become more stable than the *syn* one. The general trends of substituent effects can be discussed by molecular orbitals analysis and electrostatic interactions. The results are subject to experimental confirmation, at least in the case of enols since their conformers can be prepared by the action of singlet oxygen atom on substituted ethylen, and trapped in low temperature matrices.

Acknowledgements

The authors are greatly indebted to Professor B. Silvi for stimulating discussions.

References

[1] E. Erlenmeyer, Chem. Ber. **14** (1881) 320.

[2] S. Saito, Chem. Phys. Lett. **42** (1976) 399.

[3] J. B. Smith, M. T. Nguyen, W. J. Bouma, L. Radom, J. Am. Chem. Soc. **113** (1991) 6452.

[4] S. Sklena, Y. Apeloig, Z. Rappoport, J. Am. Chem. Soc. **120** (1998) 10359.

[5] M. Rodler, A. Bauder, J. Am. Chem. Soc. **106** (1984) 4025.

[6] M. Rodler, C. E. Blom, A. Bauder, J. Am. Chem. Soc. **106** (1984) 4029.

[7] M. Rodler, J. Mol. Spectrosc. **114** (1985) 23.

[8] M. Hawkins, L. Andrews, J. Am. Chem. Soc. **105** (1983) 2523.

[9] W. J. Bouma, L. Radom, J.Mol.Struct. **43** (1978) 2673

[10] J. B. Smith, L. Radom, J. Am. Chem. Soc. **112** (1990) 7525.

[11] J. B. Smith, D. Coffey Jr, L. Radom, J. Chem. Phys. **97** (1992) 6113.

[12] Y. Apeloig, D. Arad, Z. Rappoport, J. Am. Chem. Soc. **112** (1990) 9131.

[13] O. N. Ventura, A. Lledos, R. Bonaccorsi, J. Bertran, J. Tomasi, Theor. Chim. Acta **72** (1997) 175.

[14] J. Andres, L. R. Domingo, M. T. Picher, V. S. Safont, Int. J. of Quant. Chem. **66** (1998) 9.

[15] R. Hoffman, C. Wan, V. Neagu, Molecular Physics, **19** (1970) 113.

[16] V. Almond, R. Permanand, J. Macdonald, J.Mol.Struct **128** (1985) 337.

[17] C. Plant, J. Boggs, J. Macdonald, G. Williams, Structural Chemistry, **3** (1992) 3.

[18] Gaussian 98, Revision A.7, M. J. Frisch, G. W. Trucks, H. B. Schlegel, G. E. Scuseria, M. A. Robb, J. R. Cheeseman, V. G. Zakrzewski, J. A. Montgomery, Jr., R. E. Stratmann, J. C. Burant, S. Dapprich, J. M. Millam, A. D. Daniels, K. N. Kudin, M. C. Strain, O. Farkas, J. Tomasi, V. Barone, M. Cossi, R. Cammi, B. Mennucci, C. Pomelli, C. Adamo, S. Clifford, J. Ochterski, G. A. Petersson, P. Y. Ayala, Q. Cui, K. Morokuma, D. K. Malick, A. D. Rabuck, K. Raghavachari, J. B. Foresman, J. Cioslowski, J. V. Ortiz, A. G. Baboul, B. B. Stefanov, G. Liu, A. Liashenko, P. Piskorz, I. Komaromi, R. Gomperts, R. L. Martin, D. J. Fox, T. Keith, M. A. Al-Laham, C. Y. Peng, A. Nanayakkara, C. Gonzalez, M. Challacombe, P. M. W. Gill, B. Johnson, W. Chen, M. W. Wong, J. L. Andres, C. Gonzalez, M. Head-Gordon, E. S. Replogle, and J. A. Pople, Gaussian, Inc., Pittsburgh PA, 1998.

[19] C. Lee, W. Yang, R. G. Parr, Phys. Rev. B. **37** (1988) 785.

[20] B. Mielich, A. Savin,H. Stall, H. Preuss, Chem. Phys. Letters. **157** (1989) 200.

[21] A. D. Becke, J. Chem. Phys. **98** (1993) 5648.

Localization of energy exchanges in field-assisted double-barrier resonant tunneling

C. PEREZ del VALLE[1], R. LEFEBVRE[2,3] and O. ATABEK[2]

1 *Instituto de Ciencia de Materiales(CSIC), Cantoblanco, 28049 Madrid, Spain*

2 *Laboratoire de Photophysique Moléculaire, Campus d'Orsay, 91405 Orsay, France*

3 *U.F.R. de Physique Fondamentale et Appliquée, Université Pierre et Marie Curie, 75231 Paris, France*

Abstract

We analyze the situation where transmissivity through double barriers of the type met in semiconductor nanostructures is modified by the interaction of the incident particle with an oscillating electric field. Only a single resonance is present in the intermediate well, in order to avoid the effects due to induced transitions in the well. It is shown that when the particle needs to emit or absorb one or more quanta of the field to reach the resonant energy which favours transmissivity, the exchange of energy between field and particle takes place essentially at the two external discontinuities of the potential. This result could be submitted to an experimental test in the case where the field has a different origin, for instance when a surface phonon or plasmon in a double-barrier semiconductor device is created to reach the proper energy.

ADVANCES IN QUANTUM CHEMISTRY, VOLUME 40

0065-3276/01 $35.00

Contents

1 Introduction

There is a very rich literature on resonant transmissivity of a particle incident on a symmetric double-barrier. That the transmissivity can reach unity when the energy of the particle coincides with a quantized energy of the intermediate well has been known from the beginning of quantum mechanics and is treated in textbooks [1, 2]. When the double-barrier is not symmetrical, the transmissivity is still passing through a maximum when this coincidence takes place. This is the situation which is realized in double-barrier resonant tunneling (DBRT) semiconductor devices [3, 4, 5], where a bias static electric field is applied to induce a difference in the Fermi energies at the two contact electrodes. The bias potential affects the shape of the double-barrier. The current is measured as a function of this potential. Its evaluation involves an integral over the product of a supply function by the transmissivity [3].

We are concerned with a variant of this situation: the incident electrons are assumed to interact with an oscillating electric field. This adds a flexibility in the previous situation, since by absorption or emission of quanta of the field the electrons can reach the energy which favours transmissivity. This phenomenon has been experimentally confirmed when the change in energy of an electron incident on the double-barrier corresponds to the creation of a phonon [6] or a plasmon [7].

For an unbiased double-barrier, the electron can exchange energy with the field only at the discontinuities of the potential. The question we address ourselves is: are all discontinuities of equal importance in this exchange, or are certain

discontinuities more efficient than others? We make use of a method based on transfer matrices [8, 9] which allows even the consideration of potentials of arbitrary shapes. For the case of a stepwise potential the wavefunction is written in every region of constant potential as a linear combination of Gordon-Volkov waves [10] which take into account all possible photon exchanges compatible with the value chosen for the amplitude of the oscillating electric field. The wavefunctions and their derivatives are to be matched at all discontinuities of the potential and at all times [10]. This method solves completely the scattering problem: to an incident wave of unit amplitude it is possible to associate both reflected and transmitted waves displaying the absorption or emission of quanta of the field. Section II is devoted to a brief presentation of the method which allows for the calculation of the probabilities of transmission and reflection with an arbitrary number of absorbed or emitted quanta. Section III describes the technique which is used to impose energy exchanges at given potential discontinuities. Tests are made on two typical situations presenting only one discontinuity. In Section IV we point out that when the incident particle needs to exchange energy with the field to be at resonance, this exchange is primarily taking place at the external discontinuities of the potential. This observation could be subjected to a test, since in cases where surface phonons are involved, their frequencies may differ at the various interfaces in the material, so that the frequency which is relevant for the field-assisted phenomenon should be associated to particular interfaces.

Exchange localization was previously studied for a different model by Jauho [11], using a wavepacket propagation approach: a modulation of the well is more effective in producing a satellite resonance than a modulation of the barrier height. This was assigned to the fact that the particle spends more time in the well than in the barriers. The present localization has also a simple explanation: the wave must reach the well in a way similar to that operating in ordinary (field-free) resonant tunneling, that is by tunneling through the first barrier *before* reaching the well and tunneling through the second barrier *after* leaving the well.

We insist on the fact that the model under study presents only one resonance in the well. The conclusions are also valid with more than one resonance provided there is sufficient detuning between the frequency of the field and the transition frequencies. The situation where the frequency of the field matches with or is close to a transition frequency in the well has been analysed by Johansson and Wendin [12]. It is imperative in this case to consider energy exchanges in the region between the barriers.

2 Gordon-Volkov Wavefunctions for Field-Assisted Resonant Tunneling

The potentials which will be considered here are stepwise constant. In each region of these potentials the time-dependent wavefunction is a linear combination of solutions of the wave equation for a particle interacting with an electromagnetic field of vector potential with $A(t)$ [10]:

$$i\frac{\partial}{\partial t}\psi(x,t) = [-\frac{1}{2m}\frac{\partial^2}{\partial x^2} - \frac{A(t)p_x}{m} + V]\ \psi(x,t). \tag{1}$$

The equation is written in velocity gauge. Atomic units are used. The particle has charge unity and mass m in units of the free electron mass. V is the constant potential energy appropriate for the interval under consideration. The vector potential is supposed to be spatially constant at the length scale of the structure. With such a vector potential, the A^2 term contributes an irrelevant phase factor which can be omitted. For a one-mode field $A(t)$ is written as $A_0\ cos(\omega t)$. The associated electric field is $\mathcal{E}_0\ sin(\omega t)$, with $\mathcal{E}_0 = \omega A_0$. p_x is the linear momentum $i^{-1}\partial/\partial x$. For such a time-periodic Hamiltonian, a scattering approach can be developped, with a well-defined initial energy, and time-independent transition probabilities for reflection and transmission.

We note that going to the length gauge provides a coupling of the form $\mathcal{E}_0\ x\ cos(\omega t)$. This is to be contrasted with the form $V_0\ cos(\omega t)$ which is often assumed to investigate photon assisted tunneling [13, 14, 15]. However this is not of major consequence on the characterization of the different regimes which can be delineated in the phenomenon [9].

For a constant potential the solutions of the wave equation are Gordon-Volkov (G.V.) waves:

$$\psi(x,t) = exp\ [i(\pm kx - Et \pm \frac{A_0 k\ sin(\omega t)}{m\omega})], \tag{2}$$

with $k = [2m(E-V)]^{\frac{1}{2}}$. E is the energy of the incident particle.

When we take into account in a region of constant potential that the energy of the particle may have changed with respect to the incident energy E by absorption or emission of photons, with N being the maximum number retained for these photons, the general solution is written as:

$$\begin{aligned}\Psi(x,t) = \sum_{n=-N}^{n=N} & t_n\ \ exp\ [i(k_n x - E_n t + \frac{A_0 k_n\ sin(\omega t)}{m\omega})] \\ + & r_n\ \ exp\ [-i(k_n x + E_n t + \frac{A_0 k_n\ sin(\omega t)}{m\omega})]\end{aligned} \tag{3}$$

E_n is $E + n\omega$ and k_n is $[2m(E_n - V)]^{\frac{1}{2}}$.

These solutions given for each interval between two discontinuities must be continuous as well as their derivatives with respect to position. In addition, the matching is to be valid at all times. In previous work on this subject [8, 10, 16, 17] this was achieved by first Fourier expanding each function as a linear combination of time periodic exponentials $e^{in\omega t}$ and identifying the coefficients of the same exponential on each side of a given discontinuity. We have shown [18] that a much simpler, and as efficient, procedure consists in equaling the functions and their derivatives at a set of times uniformly distributed within a period of the field. The number of these times is to be chosen so that the amplitudes of all waves on one side can be related to the amplitudes of all waves on the other side by using a square matrix. This allows for the definition of a transfer matrix to propagate the solution all along the potential structure. The total number of amplitudes kept in the complete expression of the wavefunction on both sides of a potential discontinuity is $2(2N+1)$. The sampled times are $\tau_i = \frac{2\pi(i-1)}{(2N+1)\omega}$, with $i = 1, 2, .., 2N+1$. The number of equations is $2(2N+1)$ since both the functions and their derivatives with respect to position must match.

After imposing the usual scattering asymptotic conditions, reflection and transmission probabilities are given in terms of the r_n's in the region of the incident wave and of the t_n's in the region of the transmitted waves as:

$$R_n = |\frac{k_n^{in}}{k_0}|\ |r_n|^2, \quad T_n = |\frac{k_n^{out}}{k_0}|\ |t_n|^2 \tag{4}$$

where k_n^{in} and k_n^{out} are the wavenumbers of the open channels in the incoming and outgoing regions, k_0 being the wavenumber of the incident wave.

3 Localization of energy exchanges

A charged particle which is not submitted to an external force cannot exchange energy with the electromagnetic field. This means, in the case of a stepwise constant potential, that the exchange takes place only at the discontinuities of the potential, where the electron can be accelerated or decelerated. For a double-barrier potential, the discontinuities are of two types, external (on the outer edges of the barriers) or internal (on the inner edges of the barriers). We wish to design a procedure which ensures the control of the discontinuities which produce the exchanges. We attempt a very simple idea and we are going to test it in the simplest possible case, which is that of a one-step potential.

The wavefunctions given by Eq.(3) are linear combinations of G.V. waves which are modified whenever a discontinuity is met. The procedure to be used for the

double-barrier consists in (a) dropping the A_0 dependent terms in the exponents of the G.V waves on both sides of a discontinuity where exchange is to be prohibited; and (b) keeping A_0 dependent terms only on one side of a discontinuity where exchange is to be allowed. Rule (a) means that at such a discontinuity free waves and their derivatives are matched, just as in the field-free case, with however a multichannel representation. When rule (b) is applied to the external discontinuities the A_0 dependent terms are kept in the two asymptotic regions (both on the left and on the right of the device) so that free waves are propagating in the potential region. When it is applied to the internal discontinuities, these terms are maintained only in the well. In this way there is propagation of G.V. waves within the well.

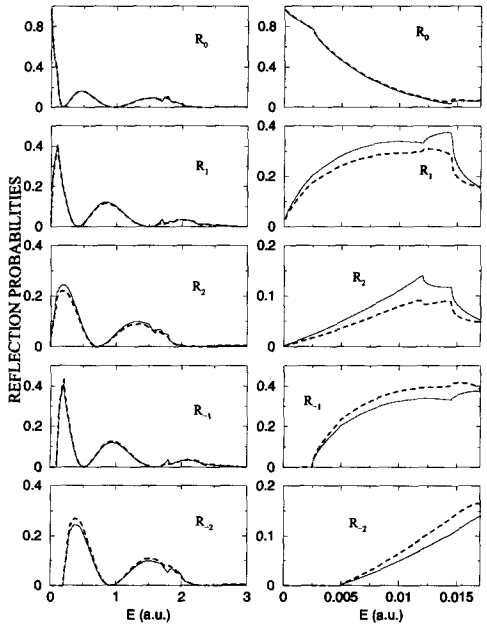

Figure 1: *Comparison of reflection probabilities calculated for two one-step potentials with two different procedures. Full curves: with matching of Gordon-Volkov waves on both sides of the discontinuity. R_n means reflection probability with absorption ($n > 0$) or emission ($n < 0$) of quanta. Dashed curves: matching of Gordon-Volkov waves with free waves. Left column: a one-step potential taken from [10]. The height of the step is* 2 *a.u.; the mass of the particle is that of a free electron. The frequency of the oscillating electric field is* 0.1 *a.u. and its peak amplitude* 0.02 *a.u.. The number of channels is* 27. *Right column: a one-step potential which is part of the potential studied in Section IV. Height:* 0.017 *a.u.; mass:* 0.07 m_0*; frequency:* 0.0025 *a.u.; peak field amplitude:* 1. 10^{-5} *a.u.; number of channels:* 11.

For a test on a single-step potential we compare the transition probabilities

obtained with either G.V. waves on both sides of the potential jump or with G.V. waves only on the side of the incident particle. We take first an example from the literature: Sacks and Szöke [10] have studied a single potential step of 2 a.u. with a field frequency $\omega = 0.1$ a.u.. The mass of the incident particle is the free electron mass ($m_0 = 1$ a.u.). They give graphs of various reflection and transmission probabilities for two peak electric field amplitudes: 0.01 and 0.02 a.u.. With the latter amplitude a comparison of the various reflection probabilities obtained with the two procedures is shown in the left column of Figure 1. Only the energy range below the step is considered. The mixed procedure (matching of G.V. waves with free waves) gives a very accurate account of the various multiphoton processes induced by the field.

Our next example is built after the parameters retained for the study of resonant tunneling presented in the next section. The height of the step is 0.017 a.u., the frequency 0.0025 a.u., and the mass 0.07 m_0. The electric field maximum amplitude is 1. 10^{-5} a.u.. A comparison along the same lines is made in the right column of Figure 1. We see that although there are some noticeable differences, the overall behaviour of the probabilities is very similar. We can conclude that the mixed procedure retains the essentials of the energy exchanges produced by a discontinuity.

4 Energy exchanges in resonant tunneling

If a particle incident on a double-barrier structure can have its energy modified through the interaction with an oscillating field, it is natural to expect that the transmissivity will exhibit a peak whenever the new energy is in coincidence with a quantized energy of the intermediate well. Before examining where the exchange has to take place for the process to be efficient, we recall the picture which can be given of double-barrier resonant tunneling in the absence of the field [19]. A particle in the well can escape by tunneling through the barriers. Consider one of these resonances. The lifetime of the particle in the well is the inverse of the width of this resonance. For a particle to be said incident on the structure at the energy of the resonance, its energy has to be within the window defined by the width. In particular, for thick barriers and therefore a narrow width, this means taking a very extended wavepacket to describe the particle. Even though very little of the wavepacket succeeds to tunnel into the well region, the process takes a very long time, long enough for the reflected wavelets coming from the multiple reflections in the well to interfere destructively with the primary reflected wave.

Our example is a double-barrier with equal barrier widths of 30 $\AA$, and a well of width 30 $\AA$ between them. The mass of the incident particle, the barrier heights, the frequency and the field amplitude have already been given.

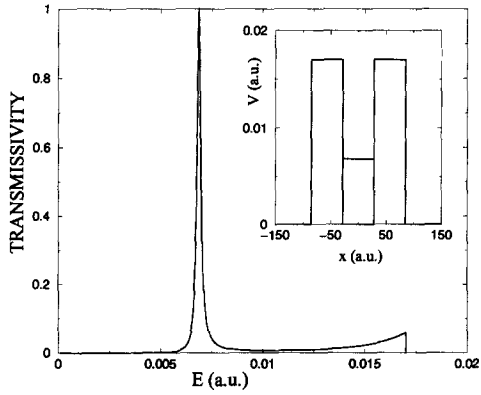

Figure 2: *Transmissivity of a symmetric double-barrier with a single resonance below the top of the barriers. The potential is shown in the inset. The widths of the barriers and of the well are* 30 $\AA$ *(*$\sim$ 56.7 *a.u.). The height of the barriers is* $\sim$ 0.46 *eV (*0.017 *a.u.) and the mass of the particle* $m = 0.07$ *in units of the free electron mass.*

Figure 2 shows the potential (inset) and the field-free transmissivity: there is only one resonance below the barriers, and as expected for a symmetrical structure, the transmissivity reaches value unity. We now couple the particle to the oscillating electric field.

Figure 3 gives the total transmissivity T. The main peak is at the resonance energy E_R, with now a reduced amplitude. The satellites are, as expected, at energies $E_R \pm \omega$ and $E_R \pm 2\omega$.

The transmissivities can be calculated in two other ways, labelled D_2 and D_1. D_2 restricts the exchanges at the two most external discontinuities, by applying rule (b) of the previous section at these two discontinuities and rule (a) at the two others. D_1 means that exchange is allowed only at the first discontinuity met by the particle by applying rule (b) at this position. When exchange of energy takes place at all four discontinuities as in Figure 3, the model is called D_4. When comparing all the probabilities calculated in the three different options, the following observations can be made:

(1) The total transmissivities of D_4, D_2 and D_1 are very similar.

(2) All transmissivities are similar in D_4 and D_2. This means that only the external discontinuities are involved in the energy exchange in this example.

Figure 4 displays for models D_4 (or D_2) and D_1 the probabilities T_n for net absorption ($n > 0$) or emission ($n < 0$) of n quanta, for $|n|$ up to 2. In the

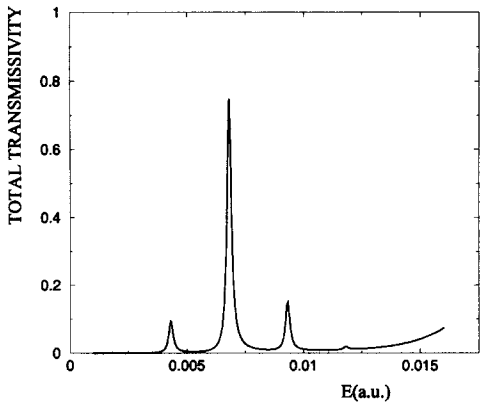

Figure 3: *Total transmissivity T of the double-barrier of Figure 1 with the particle coupled to an electric field of amplitude* 1. 10^{-5} *a.u. and frequency* $\omega = 0.0025$ *a.u.. The main peak is at the resonance energy* $E_R \sim 0.0068$ *a.u.. There are two satellites at energies* $E_R \pm \omega$ *and two (one is hardly discernable) at energies* $E_R \pm 2\omega$.

D_4 model (left column) the peaks in the different patterns have a very simple explanation. The main peak in T_0 is at the resonance energy E_R. This is ordinary resonant tunneling with no exchange involved, plus a small contribution with equal numbers of absorbed and emitted quanta. The peaks in T_1 are at energies $E_R - \omega$ and E_R. Since efficient tunneling takes place when the particle can reach the resonance energy, the left peak is to be assigned to a process where the absorption of a quantum occurs before the particle reaches the well, while the right peak corresponds to absorption after leaving the well. A similar explanation holds for the other probabilities.

For instance in T_{-1} the left peak is at energy E_R and the right peak at energy $E_R+\omega$. It is now the left peak which corresponds to an exchange after the particle has left the well, while the right peak is due to an exchange before reaching the well. This analysis classes the events in two categories, but does not tell us which of the two discontinuities before or after the well is most effective in producing the energy exchanges. The right column of Figure 4 gives the probabilities of the D_1 option. They show only one peak. We observe in a comparison of the two columns that all peaks of D_4 which are assigned to a process taking place *beyond* the well are missing in D_1. For instance in T_1 there is left only the peak at energy $E_R - \omega$, which is due to an absorption before reaching the well. We are now able to formulate a very simple hypothesis which can explain all the observations: the role of the first discontinuity is to produce a wave which reaches the well through the first barrier at the resonance energy. This is the situation prevailing to produce resonnant tunneling when no field is present. An emission or absorp-

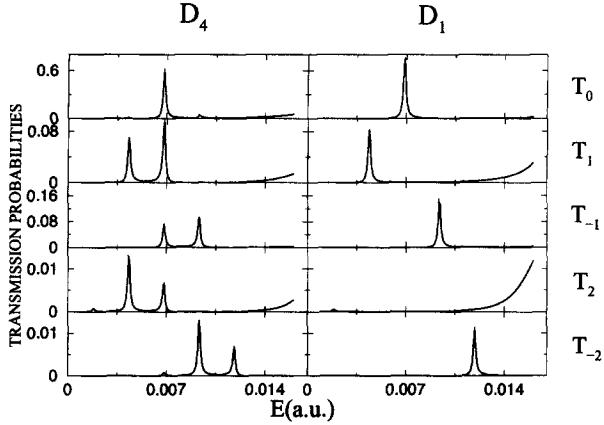

Figure 4: *Comparison of five probabilities of the double-barrier in the presence of an oscillating field, calculated either with energy exchanges at the four discontinuities of the potential (D_4) or only at the first discontinuity (D_1). The latter show only one peak (very weak in T_{-2}).*

	E	T	T_0	T_1	T_{-1}	T_2	T_{-2}
D_4	$E_R-\omega$	0.9411(-1)	0.1145(-1)	0.6906(-1)	0.1500(-3)	0.1259(-1)	0.0
	E_R	0.7497	0.5767	0.9503(-1)	0.7036(-1)	0.6580(-2)	0.7543(-3)
	$E_R+\omega$	0.1506	0.4443(-1)	0.8918(-3)	0.9314(-1)	0.7616(-4)	0.1257(-1)
D_2	$E_R-\omega$	0.8407(-1)	0.8393(-2)	0.6622(-1)	0.9383(-4)	0.9063(-2)	0.0
	E_R	0.7540	0.5850	0.8515(-1)	0.8192(-1)	0.4554(-2)	0.7606(-3)
	$E_R+\omega$	0.1552	0.1460(-1)	0.1783(-2)	0.1227	0.1570(-4)	0.1607(-1)
D_1	$E_R-\omega$	0.8347(-1)	bkg	0.8308(-1)	bkg	bkg	0.0
	E_R	0.7508	0.7498	bkg	bkg	bkg	bkg
	$E_R+\omega$	0.1512	bkg	bkg	0.1445	bkg	bkg

Table I. *Transmission probabilities at energies E_R and $E_R \pm \omega$ with the three options for energy exchange. D_4 means that all four discontinuities of the potential are taken into account. In the procedure D_2 only the most external discontinuities produce a change in the amplitudes of the multichannel wavefunction. Finally in D_1, only the first discontinuity is introduced. "bkg" in D_1 stands for background: no structure in the profile is observed at this energy. The results show the similarity of D_4 and D_2. In D_1 a single peak collects the transmission probabilities dispersed among several channels in the other two procedures.*

tion at the second discontinuity, although possibly producing the right energy, will fail to mimic the field-free situation. The wave must then proceed through the second barrier at the resonance energy, and only the last discontinuity can further affect the energy. In case D_1 there is no such modification of the energy. How is it then possible to explain that the total transmissivity is recovered? Table I shows that there is a splitting of the flux incident on the last discontinuity in

the cases D_4 and D_2. This table gives the peak transmissivities at energies close to E_R and $E_R \pm \omega$. The indication "bkg" for background in the part of the table devoted to D_1 means that there is no peak at these energies. The total transmissivities are very similar in all three calculations, this being due, as far as D_1 is concerned, to an enhancement of the transmissivity at the peak which persists, which collects, so to speak, the transmissivity of the missing peak.

We end with a word about possible inferences for an experimental study of field-assisted resonant tunneling. We have observed that essentially the same conclusions can be drawn if the double-barrier potential is affected by a bias field. The discussion is therefore applicable to situations similar to those mentioned in the Introduction[6, 7]. If the quanta are phonons or plasmons with different frequencies for the various interfaces in the sample, only the frequencies characteristic of the most external discontinuities should be involved.

Acknowledgments

We thank Professor Palma for useful discussions. CPV thanks the "Communidad de Madrid" for financial support. OA and RL acknowledge support from the "Comité Evaluation-Orientation de la Coopération Scientifique" (ECOS, contract no M98 P03) for financing a visit to the "Instituto de Física" of the University of Puebla, Mexico, where part of this work was done.

References

[1] D.Bohm, "Quantum Theory"; Prentice Hall:Englewoods Cliff, 1960.

[2] E. Merzbacher, "Quantum Mechanics"; Wiley:New York, 1970 (Chapt.6).

[3] R.Tsu and L. Esaki, Appl. Phys. Lett. **22** (1960) 562.

[4] L. L. Chang, L. Esaki and R. Tsu, Appl. Phys. Lett. **24** (1974) 593.

[5] T. C. L. G. Sollner, W. D. Goodhue, P. E. Tannenwald, C. D. Parker and D. D. Peck, Appl. Phys. Lett. **43** (1983) 588.

[6] V. J. Goldman, D. C. Tsui and J. E. Cunningham, Phys. Rev. B **36** (1987) 7635.

[7] C. Zhang, M. L. F. Lerch, A. D. Martin, P. E. Simmonds, and L. Eaves, Phys. Rev. Lett. **72** (1994) 72.

[8] J. Z. Kaminski, Z. Phys. D **16** (1990) 153.

[9] C. Pérez del Valle, R. Lefebvre and O. Atabek, Phys. Rev. A **59** (1999) 3701.

[10] R A. Sacks and A. Szöke, Phys. Rev. A **40** (1989) 5614.

[11] A.P. Jauho, Phys. Rev. B **41** (1990) 12327.

[12] P. Johansson and G. Wendin, Phys. Rev. B **46** (1992) 1451.

[13] P. K. Tien and J. P. Gordon, Phys. Rev. **129** (1963) 647.

[14] M. Büttiker and R. Landauer, Phys. Rev. Lett. **49** (1982) 1739.

[15] P. Johansson, Phys. Rev. B **41** (1990) 9892.

[16] S. Varró and F. Ehlotzky, J. Opt. Soc. B **7** (1990) 537.

[17] A. S. Fearnside, R. M. Potvliege and R. Shakeshaft Phys.Rev. A **51** (1995) 1471.

[18] R. Lefebvre, J. Mol. Struct. (THEOCHEM) **493** (1999) 117.

[19] A. P. Stamp and G. C. McIntosh, Am. J. of Phys. **64** (1996) 264.

SPIN UNCOUPLING IN CHEMICAL REACTIONS

BORIS F. MINAEV and HANS ÅGREN
The Royal Institute of Technology, SE-10044, Stockholm, Sweden

Abstract

Spin pairing is the main attribute of the covalent chemical bond. Exchange repulsion between closed shell molecules being responsible for activation barriers in bimolecular reactions can be explained by a high weight of the intermolecular triplet spin pairing. Intermolecular exchange interaction switches to a strong attraction when the molecules are in excited triplet states. This is the reason for that the thermal chemical reactivity often is coded by the triplet excited states of the reagents. Illustrations of such triplet state involvements in organic reactions are here presented in terms of canonic structures of the valence bond (VB) method. Reactions of the second-row transition metal atoms, clusters and complexes with small hydrocarbons are considered in a framework of the simple VB approximation. A qualitative analysis of the VB treatment demonstrates the importance of spin uncoupling through involvement of the triplet excited states of hydrocarbons in their chemical activation processes. The VB approximation indicates that the transition metal atom insertion into C-H bonds of a number of alkanes and alkenes is strongly determined by the "singlet-triplet" avoided crossing when the total spin of the reacting system is fixed by the low-spin term of the catalyst.

ADVANCES IN QUANTUM CHEMISTRY, VOLUME 40

0065-3276/01 $35.00

Contents

1 Introduction

From the pioneering studies of Woodward and Hoffmann [1] it is known that the activation barrier in chemical reactions, forbidden by orbital symmetry, arises from the avoided crossing of the ground state and an excited state. This was grounded on the orbital HOMO-LUMO crossing imposed by symmetry constraints [1]. State correlation diagrams [2, 3] made clear the importance of doubly excited states. Salem *at el.* [4, 5, 6] have classified numerous state crossings and avoided crossings of different types in photochemistry. Shaiks further elaboration indicated that avoided crossings could be a general mechanism whereby molecules rearrange their electrons, so that some bonds can be broken and others, new ones, formed [7]. From the VB method it follows that the spin-pairing scheme changes during a reaction and that it is also manifested by avoided crossings. Even in a classical reaction like H_2 + H, well-studied by the valence bond method [8, 9, 10], there is an avoided crossing of the ground state and the triplet excited state of the H_2 moiety. This spin-uncoupling, typical for many organic reactions, can be applied also for catalysis. The activation of the C-H bond in hydrocarbons will be considered in this paper.

The oxidative addition of hydrocarbons to a transition metal center is an important reaction for the development of catalytic processes involving for example the hydrogenation and hydroformylation of olefins [11]. The activation

of C-H bonds in alkanes by TM complexes and by bare TM atoms is a process which has been rather recently discovered [12, 13, 14, 15] and which has now attracted considerable attention of theoreticians [16, 17, 18, 19, 20, 21, 22, 23]. It should be stressed that the activation of unstrained alkanes is still a challenging problem. Systematic theoretical studies on the oxidative addition of hydrocarbons to the second-row TM atoms and complexes [17, 21, 24, 25, 26, 27, 22, 15] have led to the discovery of some trends in the electronic structure factors. These studies have mostly focussed on the requirements for the TM-species [17, 26, 27, 22]. At the same time a surprising trend in the activation of different types of hydrocarbons has not been convincingly explained, namely stronger C-H bonds are in general easier to activate than weaker C-H bonds [22]. Siegbahn [22] calculated metal-carbon (M-C) bond strengths for a number of M-C_nH_m compounds, like M-CH_3, M-C_2H_3, M-C_2H, M-C_2H_5, and explained all trends of M-C bond strengths by ionic contributions.

In the present work a simple London formula for application of the valence bond (VB) method to the tree-center problem [28] is used in order to stress the importance of triplet excited states of the activating molecule in the catalysis by TM atoms and complexes. Activation of the C-H bond in methane is considered as a conceivable example illustrating essential features of spin-uncoupling in catalysis. Theoretically studied reactions of hydrocarbons with the second-row TM atoms [15] are used for illustration of new features.

2 General discussion of spin-uncoupling in chemical reactions

It is well known that exchange repulsion between closed shell molecules is responsible for activation barriers in bimolecular reactions [6]. There are a few qualitative explanations of the exchange repulsion [6]; in order to stress spin effects and spin-uncoupling ideas we will in this work explain the exchange repulsion between closed shell molecules by the higher weight of the intermolecular triplet spin pairing. This is illustrated by Fig. 1 and can be explained as follows: Spins are singlet-coupled inside the molecules. Intermolecular pairing is arbitrary and all possible pairing schemes are equally probable. By statistics there are three triplets and one singlet state for each pair of electrons. Intermolecular interaction between two closed shell systems (two H_2 molecules as the simplest example) can be described in the valence bond method [6] by exchange integrals for two singlet-paired states and six triplet-paired states. For the singlets there is exchange stabilization, for the triplets - much stronger exchange destabilization. The total balance of the exchange inter-

molecular interaction is repulsion, which strongly depends on intermolecular overlap and is a reason for the activation barrier. The repulsion will be changed

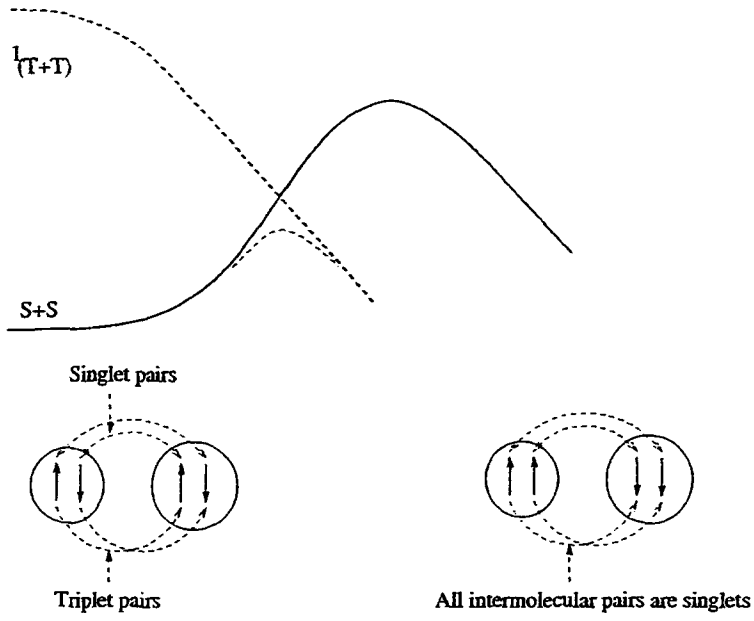

Figure 1. Exchange repulsion between two closed-shell molecules and the dependence of the activation barrier on the "double-triplet" excited state coupled to the singlet.

by strong intermolecular attraction when the triplet excited covalent states in each molecule are involved; simultaneous cleavage of each bond occurs and a new cyclization (or insertion) product will be formed. Two excited triplet states can be coupled into the total singlet state; the avoided crossing between two singlet states (the ground singlet state and the "double-triplet" singlet state) produces the activation barrier. The height of the barrier, the reaction path, the type of product and the reaction energy are thus determined to a large extent by the properties of the triplet states. The problem of catalysis is to activate in some way the triplet states of the molecules (to involve them into configuration mixing with smaller energetic expenditure).

Michl *et al.* [29] have calculated the H_4 system and shown that the doubly

excited singlet state S_2 which correlates with two H_2 molecules being excited to the triplet state $^3\Sigma_u^+$ is responsible for the avoided crossing with the ground state in the reaction $H_2 + H_2 = H_4 = H_2^{\cdot} + H_2$. The activation barrier at the transition state (H_4) is formed by the avoided crossing of these singlet states. Similar results have been obtained in other concerted chemical reactions like in disrotatory electro-cyclic reactions of polyenes [30] and in singlet oxygen cycloaddition to polyenes [31, 32]. In disrotatory closures of dienes the reacting singlet excited state is known to be produced by double excitations [3]. In *cis*-butadiene the second 2^1A_1 totally symmetric singlet excited state consists of two triplet excitations localized at each C=C moiety and coupled to the singlet [30, 6, 33]. The 2^1A_1 excited state is really prepared for the disrotating electro-cyclic photo reaction [33] and correlates with the ground state cyclobutene product. The avoided crossing between the ground state and the "double-triplet" singlet excited state is the reason for the activation barrier in disrotatory cyclization reactions [30].

The typical spin-uncoupling process can be illustrated also by the singlet oxygen $O_2(^1\Delta_g)$ cycloaddition to dienes [32]. The first triplet excited state of *cis*-butadiene combines with the ground triplet state of the O_2 molecule in order to create the singlet coupled excited term, which is responsible for the reactivity of singlet oxygen $O_2(^1\Delta_g)$. It correlates with the ground singlet state of the product and produces an avoided crossing with the ground singlet state of the reactants [32, 31, 34, 35]. The reason for that the singlet oxygen $O_2(^1\Delta_g)$ cycloaddition to dienes has smaller barrier than the Diels-Alder cycloaddition (alkene + diene) is connected with the fact that the oxygen molecule has a triplet ground state while the triplet state of alkenes is an excited state with high energy.

In the text above it is argued that the thermal chemical reactivity often is coded by the triplet excited states of the diamagnetic reagents. The crucial role of electron spin in the control of the reaction channels in the region of the activation complex is easily inferred from the general principles of chemical bonding. The radical-like (or diradical-like) moieties appear in the transition state wave functions [36].

Very often the catalyst (unsaturated TM complex) has a low-spin ground state with a high-spin state being very close in energy [23, 36, 37]. This situation is very useful for catalysis; it is not necessary to produce a spin-flip and a low barrier is achieved. The metal surface is an ideal catalyst in this sense, since any spin multiplicity can be realized at the local state of the surface, perturbed in the course of the chemisorption process. In other words, a metal cluster which simulates the surface in the course of the chemisorption process has a number of quasi-degenerate state with different spin-multiplicities.

The following requirement for catalysis can be inferred: In order to diminish the activation barrier one has to activate in some way the triplet states of the reacting molecules. For example, in the conceivable concerted isotope exchange reaction $H_2 + D_2 = HD + HD$, which proceeds through the square transition state, the activation energy would be strongly diminished if the reaction proceeds close to a transition metal atom, cluster or surface. Instead of the "double-triplet" singlet excited state (which correlates with the D_2 and H_2 molecules being excited to the triplet state $^3\Sigma_u^+$ in the reactants) one has to consider combinations of the $^3\Sigma_u^+$ term of one molecule with the triplet state of the TM atom (for example the ^3F ground state of the Ni atom), or the triplet ground state of Pd_n or Pt_n clusters [38, 39], which are coupled again to the singlet total-spin state. A number of such "double-triplet" singlet excited states will be mixed near the transition state and the barrier will be diminished significantly. In chemical terms it means that the mechanism of the isotope exchange reaction $H_2 + D_2 = HD + HD$ is altered; each molecule interacts with the metal and then the inter-ligand isotope exchange occurs before the dissociation of the catalytic complex. In terms of spin-uncoupling it means that only one $^3\Sigma_u^+$ excited state (instead of two) is involved in configuration interaction (CI), since the triplet state of the second counterpart, the catalyst, does not need (or needs very little) excitation energy. The "double-triplet" singlet states of this type have twice as low energy in comparison with the concerted $H_2 + D_2$ reaction. Their CI mixing and avoided crossing with the ground singlet state of the system could be the reason for a small barrier.

If the catalyst has a triplet ground state the lowest reactant state is a triplet; this state is non-reactive. The singlet potential energy surface (PES) is then slightly higher for the reactants, but has smaller barrier, so the reaction proceeds on the singlet PES. The reaction has to find a way to arrange a spin-flip in order produce a diamagnetic product. The other possibility could be realized if the high-spin and low-spin states of the catalyst are in thermodynamic equilibrium.

One can summarize that two types of spin-effects occur in chemical reactions; (i) alternation of the spin-pairing schemes during the reaction when the total spin is conserved (spin-uncoupling), and (ii); high-spin - low-spin transitions induced by spin-orbit coupling (SOC) [36]. The two effects become interconnected in a theoretical treatment. The first one (i) occurs on a very short time scale (femtoseconds), and thus not at a kinetic stage, but is rather a way of presentation of electronic rearrangement during the chemical reaction. The second effect (ii) occurs at a real kinetic stage, which could be measured experimentally.

Theoretical analysis of spin-uncoupling is a useful way to understand catalytic reactions, and to give an illustration of this we discuss how the TM species can

help an organic molecule to cleave the C-H bond. We first consider a simple oxidative addition reaction

$$CH_4 + M = H - M - CH_3. \quad (1)$$

With this well-studied process [15] as a model we apply a simple VB approximation in order to stress spin-uncoupling features which are not seen in a conventional MO approach. We then discuss hydrocarbon activation by transition metal complexes in general terms.

3 Methane activation by second-row transition-metal atoms

None of the neutral second-row transition metal atoms react with methane at 300 K, but some of them (Rh and Pd) react with ethane and larger alkanes [15]. *Ab initio* calculations [15] indicate that Y, Zr, Nb, Ru and Rh atoms produce very stable insertion products H-M-CH_3 in the reaction (1) with an activation barrier ($E_a \sim$ 4-20 kcal/mol), which is much lower than the C-H bond dissociation energy (103 kcal/mol). Some metals (Nb, Ru, Rh) have to change spin multiplicity [15] in the course of the reaction (1).

We shall start with the reaction presented by Eq.(1) for M = Y. The transition state (TS) is optimized by the restricted open shell Hartree-Fock (ROHF) method [6] with a 3-21 G basis set [40] using the GAMESS code [41]. The structure of the TS is similar to those presented in Ref. [24]. We also have calculated intrinsic reaction coordinates (IRC) and the configuration interaction (CI) at a few points along the IRC with 3-21G and STO-6G basis sets [42]. The minimal basis set was used deliberately in order to simplify the CI analysis and to estimate exchange integrals for AO's. These results are then used for the VB treatment. The Y atom has a doublet ground state (ds^2, ^2D). In a simple valence bond consideration only one d-AO will be taken into account. (The orbitals of the activated C-H bond will be denoted as c and h, respectively. The c orbital represents the corresponding sp^4-hybrid, h is the $1s$-AO on hydrogen atom). The ground doublet state wave function of the reagents in the valence bond (VB) method [6] is

$$\Psi_{1r} = 2^{-1/2}(|c\bar{h}d| - |\bar{c}hd|) \quad (2)$$

(Overlap integrals are neglected in the normalization factor. The usual notation of Slater determinants [6] is used here; the bar denotes a beta spin-orbit). This diabatic state represents the ground state singlet spin pairing in the covalent C-H bond. The third electron on the catalyst is decoupled from this pair.

The repulsive exchange interaction between the single electron of the catalyst and the covalent electron pair will grow for the reactant state, Eq. (2), when the system moves along the reaction path because of the dominant triplet coupling between the respective spins of the catalyst and catalysant [43]. This is shown schematically in Fig. 2.1, where the right-side determinant configuration from Eq. (2) is presented. There is one singlet and one triplet coupling between the Y atom and the atoms of the C-H bond. The triplet pairing is characterized by stronger exchange repulsion than the exchange attraction for the singlet pair. The exchange repulsion will predominate and increase while the system moves along the reaction coordinate; prolongation of the C-H bond will also destabilize the system because of the exchange energy loss in the singlet paired C-H covalent structure. The increase of energy of the ground state reagents is shown by a dashed line in Fig. 3. This diabatic state VB wave function, Eq. (2), correlates with the excited state of the product (Fig. 3).

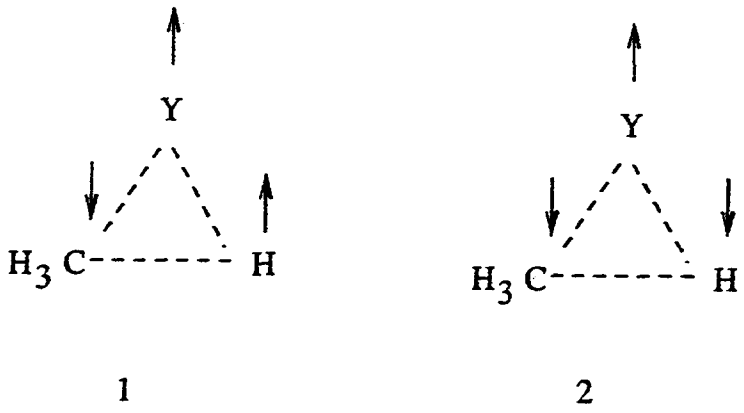

Figure 2. Spin pairing schemes for Y atom insertion reaction into methane.

In addition to this diabatic state the triplet excited covalent state localized on the activated C-H bond has to be taken into account [43]. Three electrons in three orbitals can be represented by the second doublet state wave function, Eq. (3). The coefficients in both expansions, Eq. (2) and Eq. (3), are obtained from the requirement $S^2\Psi = S(S+1)\Psi$, where the total spin quantum number, S=0.5, corresponds to the doublet state [44].

$$\Psi_{2r} = 6^{-1/2}(|c\bar{h}d| + |\bar{c}hd| - 2|ch\bar{d}|). \qquad (3)$$

This state is represented schematically in Fig. 2.2. The spins are paired up across the C-H linkage. A repulsive exchange interaction between two electrons of the C-H bond occurs. Movement along the reaction coordinate will lead to the strengthening of the growing Y-C or Y-H bonds and will make the C-H bond weaker for this type of valence bond structure. This VB diabatic state partly correlates with the ground state insertion product, at least until the transition state region. This part of the correlation diagram, Fig. 3, can be analyzed by a qualitative VB scheme based on the London formula [28]. In principle, modern valence bond (VB) methods can be used to construct the localized wave functions for specific diabatic states; however, *ab initio* valence bond theory is complicated and the VB calculations are extremely time consuming, something that prevents its application to catalytic systems. A simple VB approach has though advantages in that it can demonstrate in an explicit way some new features which are not seen in the Hartree-Fock-MO description.

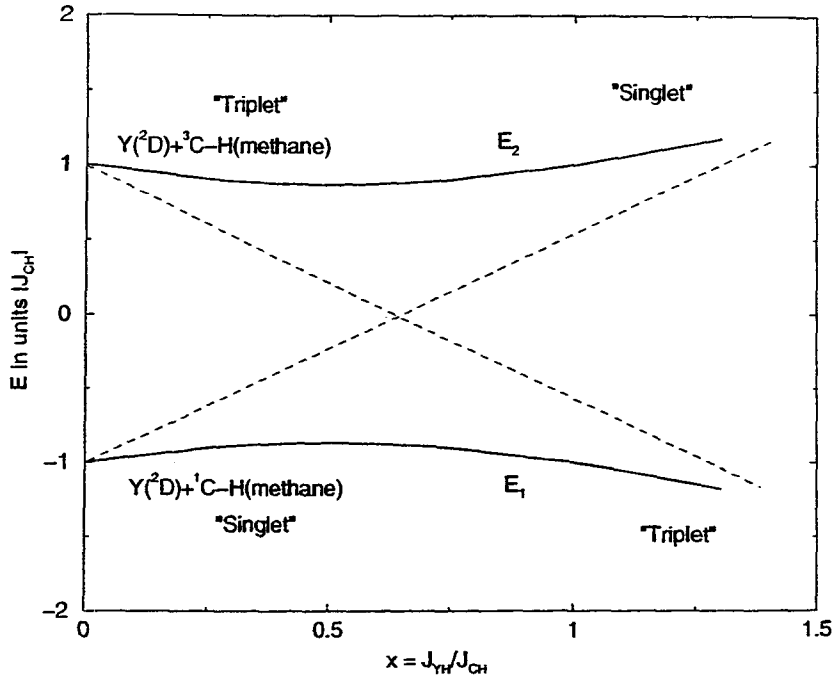

Figure 3. Potential energy curves for two doublet states in Y atom insertion into C-H bond of methane obtained by a simple VB approximation ($y \simeq 0$). The dashed lines correspond to the singlet and triplet spin pairing at the activated C-H bond.

At the beginning of the quantum chemistry era London proposed an approximate VB solution of the three-center, three-electron problem in the form [28]:

$$E_{1,2} = Q \pm \sqrt{J_{12}^2 + J_{13}^2 + J_{23}^2 - J_{12}J_{23} - J_{12}J_{13} - J_{13}J_{23}}. \quad (4)$$

Here "+" corresponds to the excited potential curve which correlates with the "triplet" C-H valence bond structure (Ψ_{2r} state, Eq. (3)), in the reactants; "-" corresponds to the ground state potential curve which correlates with the "singlet" methane in the reactants. J_{ij} is the exchange integral of the VB method, Q is predominantly the Coulomb term [6], and indices i, j denote the atomic centers, C, H, Y in our case, and run from 1 to 3. The same expression, but in a slightly different form, has been obtained in Ref. [45] by a general analysis of the energy for two VB structures, (Eq. 2) and (Eq. 3), of the three-center, three-electron problem with account of the traditional valence-bond approximations. Accounting for different ratios between the exchange integrals J_{ij} the authors of Ref. [45] have interpreted free radical reactions with olefins. A similar approach with a phenomenological Heisenberg spin-hamiltonian [46] has been applied for the activation of a covalent bond by a catalyst with one d-electron [43]. The qualitative conclusion was connected with the "triplet" state (Eq. 3) involvement in a catalytic process.

We consider now the insertion reaction, Eq. 1, for M=Y with the optimized transition state, where the Y-H distance is much longer than the C-H separation; both are shorter than the Y-C distance. The following ratios are introduced:

$$x = \frac{J_{HY}}{J_{CH}} = \frac{J_{13}}{J_{12}}, \quad (5)$$

$$y = \frac{J_{CY}}{J_{CH}} = \frac{J_{23}}{J_{12}}. \quad (6)$$

With these notations the energy expression of Eq. 4 can be rewritten in a form [45]:

$$E_{1,2} = Q \pm |J_{CH}| \sqrt{\frac{1}{2}[(1-x)^2 + (1-y)^2 + (x-y)^2]} \quad (7)$$

The ratio y is much smaller than the ratio x until the transition state is reached. Our calculations with 3-21 G and in STO-6G basis sets indicate that the exchange interactions at the beginning of the IRC and before the TS region are strongly non-equal; one can use $y \simeq 0$, which corresponds to $|J_{CY}| \ll |J_{CH}|$. Besides the distance arguments, an additional reason for this is connected with a strong orientation of the sp^3 hybrid along the C-H bond direction, which implies an approximate orthogonality to the d orbital of the metal at

the first stage of the reaction. Calculations of the intrinsic reaction coordinate (IRC) from the transition state by the ROHF method indicates that a weak precursor complex formation occurs first in the beginning of the reaction, Eq. 1, in agreement with other studies [15]. The precursor complex is mostly of electrostatic nature and exchange interactions $|J_{CY}|$, $|J_{HY}|$ are really much smaller than $|J_{CH}|$ at the beginning of the IRC. A movement along the IRC from the precursor complex to the transition state is determined by an increase of the H-Y-C angle and an increase of the x ratio. Accounting for that $y \simeq 0$, one can obtain from Eq. 7:

$$E_{1,2} = Q \pm |J_{CH}|\sqrt{1 - x + x^2} \tag{8}$$

Potential energy curves for these two states are presented in Fig. 3.

The simple approximations, Eqs. (5) - (8), have meaning until $x \leq 0.6$. After the transition state ($x = 0.5$) the J_{CH} exchange integral starts to decrease and y is not zero any more. In spite of the very crude approximations involved, the potential energy curves, Eq. 8, illustrate the conceptual importance of the triplet excited state of hydrocarbons in the process of their activation by metal atoms and by other TM species. The "singlet" and "triplet" potentials exhibit a strongly avoided crossing which produces a small activation barrier. For the lower potential curve, Eq. 8, the activation barrier is equal to

$$E_a = |J_{CH}|(1 - \frac{\sqrt{3}}{2}) \tag{9}$$

A similar approach can be applied for the Y atom insertion into the C-H bond of alkenes and other alkanes. Our calculation by the CI method in a 6-311++G(2d,2p) basis set with a complete active space for 8 electrons in 8 orbitals (1s orbital of carbon atom is frozen) predicts that the vertical S-T excitation energy in methane is around 11 eV (11.37 eV or 262 kcal/mol). Following the above approximation it is equal -$2J_{CH}$. From Eq. (9) the activation energy for the yttrium atom insertion reaction, Eq. (1) M=Y, should be 17.6 kcal/mol. This simple estimation is in a good agreement with very accurate *ab initio* calculations, E_a = 20.7 kcal/mol [15].

For alkenes the S-T excitation energy is in the range 3-4 eV [44]. This is a $\pi\pi^*$ excitation which transforms to the $\sigma\sigma^*$ excitation of the activating C-H bond when the system moves along the reaction path [47]. Estimations by previous formulas, Eqs. (8) - (9), give E_a ~4-6 kcal/mol; this is in a reasonable agreement with *ab initio* results for Y and Zr atoms (E_a ~2 kcal/mol) insertion into the C-H bond of ethene [15]. The $\pi - \sigma$ mixing in this reaction is very efficient because of the strong interaction between the 4*d*-AO's and the antibonding π^*-σ^* orbitals. Thus the vertical excitation energy to the $^3(\pi\pi^*)$ state can be used for the barrier estimation in reactions of Y atoms with ethene.

All of the 4*d*-series TM atoms (except Ag) react with linear alkenes of sufficient size [15]. The lowering of the excited triplet state energy in alkenes in comparison with alkanes is an obvious reason [47] for high reactivity with the former hydrocarbons; none of the metals react with methane at room temperature. The large difference in activation energy between alkenes and alkanes thus seems to be connected with the large difference in the S-T excitation energy for these hydrocarbons. The decrease of the excited triplet state energy with the size of linear alkenes correlates with the increase of the effective bimolecular rate constant for the second-row TM atoms measured by Carroll *at el.* [15].

For Zr and Nb atom insertion into methane the calculated activation energies are 16.9 and 15.6 kcal/mol [15], which are also in good agreement with a simple estimation using Eq. (9): E_a = 17.6 kcal/mol. These atoms have two and three *d*-electrons, respectively. The more detailed analysis indicates that the number of valence electrons (at least for n = 1-3) in catalysts is not important for estimation of the barrier, Eq. (9). The geometrical structure of the transition state is quite similar for all three atoms [24, 48] and the energetic behavior of the 30 low-lying excited states resemble each other (with a proper multiplicity account) until the transition state. All three atoms, Y, Zr and Nb, have non-zero spin in the ground state, which is sufficient in order to produce mixing and avoided crossing between the singlet and triplet states of the C-H bond.

The yttrium atom at room temperature does not react with methane but reacts slowly with cyclopropane [15]. The calculated barrier to the C-H bond insertion is 11 kcal/mol. The C-H bond in cyclopropane is stronger than in methane (calculated 108 vs 103 kcal/mol) [15]. Nevertheless, for all second-row TM atoms the barriers to C-H insertion are lower in cyclopropane than in methane. This was explained by a larger ionicity of the C-H bond in cyclopropane compared to the C-H bond in methane [15]. Behind this factor the new important argument follows from the above discussion and the VB correlation diagram; the triplet excited state in cyclopropane is lower than in methane (calculated 221 vs 262 kcal/mol by the CI method in 6-311++G(2d,2p) basis set in comparable complete active spaces). The delocalized and degenerate triplet excited state in cyclopropane and methane easily transforms to the local C-H excitation during the insertion reaction of the Y atom. The quantitative curve-crossing diagram, Fig. 3, where the transition state occurs by avoided crossing of the "singlet"- and "triplet"-coupled C-H valence bond structures is very useful not only to understand C-H bond activation by Y atoms but, in fact, to understand all catalytic processes with participation of TM species.

Actually, the odd number of electrons at the catalyst center is not of principal importance, as it follows from the simple three-electron picture, Eqs. 2 - 9. The

presence of low lying multiplets with nonzero total spin is the essential feature. The open shell state of the catalyst can mix the singlet and triplet states of the activating bond, so providing the spin uncoupling which is necessary for chemical activation. For example, the singlet ground state palladium atom ($^1S, d^{10}$) can also insert into the C-H bond of methane with a low activation barrier, E_a = 3.6 kcal/mol [15], because the excitation energy to the triplet ($^3D, d^9s^1$) state is only 0.81 eV [49]. This energy is very small in comparison with the S-T excitation in methane (11.37 eV), so the "double-triplet" $^1(^3\sigma\sigma^*, ^3D)$ singlet state can interact with the ground singlet state in the reaction Pd + CH_4.

The asymmetry of exchange interactions near the transition state is extremely important for the efficiency of the "S-T" avoiding crossing; If $x = y$, one obtains from Eq. (7) the following result $E_{1,2} = Q \pm |J_{CH}|(1 - x)$ in the whole range of the reaction. It means that a direct "S-T" crossing (not avoided) occurs at the point $x = 1$ and the activation energy is extremely high: $E_a = |J_{CH}|$. Thus it is just the half of the S-T excitation; for methane activation the E_a would be about 120 kcal/mol. The addition reactions of free radicals to olefins with a symmetric triangular approach ($x = y$) have been called "exchange forbidden" [45]. This extreme case can though not be realized in catalysis. Even in a symmetric reaction like Pd addition to ethylene [47] an account of 5s-excitation becomes important and leads to an efficient "S-T" avoided crossing. Thus the catalyst promotion energy is an additional factor which determines the activation barrier [15]. An important further complication is connected with the exchange energy loss upon metal atom excitation and bond formation [50, 16, 17].

Though the C-H bond is not strongly polar, the ionic contributions are very important in the transition state region [15, 47]. In general considerations of the three-center problem by the VB approach it was shown that ionic structures produce considerable lowering of the barrier even in the case of a symmetric triangular approach of the free radical to olefins [45]. The "S-T" crossing still occurs, but at lower energy. Thus additional arguments are connected with an account of the ionic structures, Fig. 4. The ground ^2D state of the Y atom is five-fold degenerate; though the degeneracy is lifted by interaction with methane there are a number of low lying excited states of different symmetries. The VB method provides mixing of all relevant states of proper symmetry. A number of ionic states, including a few CH_4^+ Y^-, CH_3^+Y H^- structures, participate in the CI mixing and contribute to the barrier height lowering. The charge-transfer configurations reach particularly low energies at the transition state geometry; Coulomb attraction between the ions reaches maximum before they begin to participate in covalent bonding. Effects of ionic contributions have been stressed by Carroll *et al.* using results from CI calculations [15].

For the Zr atom an electronic promotion energy from the ground triplet state $^3F_2(4d^25s^2)$ to the quintet state $^5F(4d^35s^1)$ has to be taken into account [49, 50] in order to produce the ground triplet state ($^3A''$) insertion product $HZrCH_3$. The lower barrier for Zr insertion in comparison with the Y atom reaction can be explained by the smaller excitation energy from the ground triplet state to the excited quintet $^5F(4d^35s^1)$ term. This promotion energy for the Zr atom is 0.6 eV, while for the Y atom the promotion ($^2D \rightarrow {}^4F$) energy is 1.36 eV [49]. The difference between the two values (0.76 eV = 17.5 kcal/mol) can not be compared with the difference between activation barriers for the two reactions (3.8 kcal/mol) since the promotion energy is only a minor factor in the activation barrier formation. To a great extent the barrier is determined by the S-T energy gap in methane as follows from a simple VB consideration (Eq. 9).

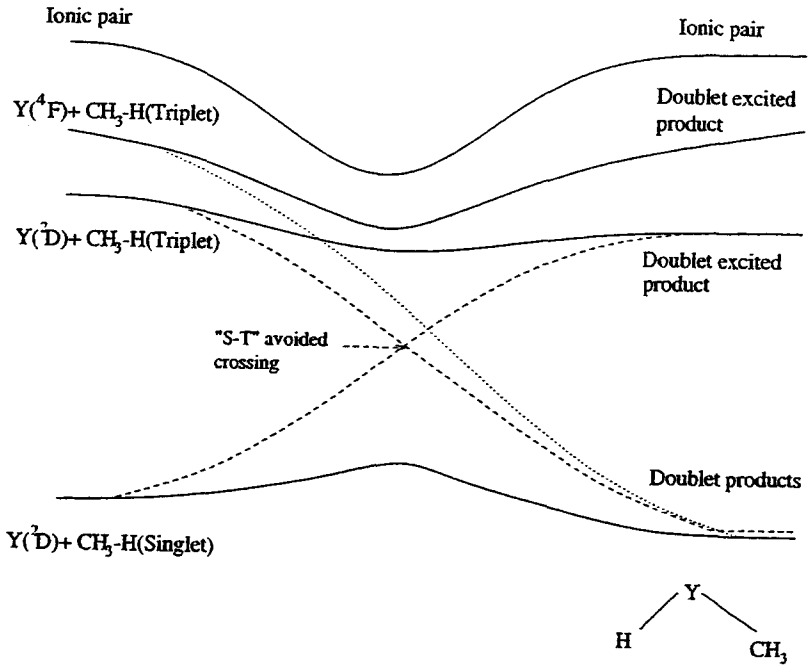

Figure 4. Qualitative potential energy surfaces cross sections along the reaction path of the Y atom insertion reaction into methane. Schematic correlation diagram for doublet states.

4 Hydrocarbon activation by transition metal complexes

The role of the promotion energy for barrier heights and reaction energies have been studied by Siegbahn *at el.* [50] not only for bare atoms but also for TM complexes with covalent ligands. Since the promotion energy to cleave the C-H bond, which correlates with the triplet excitation, is the same for methane activation by different metals and their complexes, all the trends mentioned in previous studies [50, 16, 17] can be applied to this analysis. The loss of exchange energy of unpaired $4d$ electrons when the two new bonds are formed in the product is important [16, 17]. The maximum number of open $4d$ orbitals occurs for the TM atoms in the middle of the row, molybdenum and technetium, and a minimum in the heat of product formation is therefore seen for these atoms [50, 15]. An account of promotion energy and exchange energy loss for the heat of product formation and for barrier heights are, however, not completely sufficient in the explanation of all trends [50].

Saturated TM complexes are usually unreactive with alkanes [51]. A reason for that can be obtained from the present VB analysis; the S-T gap is simply very high for such saturated TM species. However, the coordinatively unsaturated TM centers, like $C_5(CH_3)_5RhCO$, insert into the C-H bonds of many alkanes [14, 12, 13]. This and other complexes of the general formula MCpL(L=CO,PR_3) or $MClL_2$(L=PPh_3) have been found to activate C-H bonds (Cp is cyclopentanone) [12, 52, 13, 53]. The common feature of all these TM complexes (M=Rh, Ir) is a very low S-T energy gap [23]. The ground state of most of them is singlet; the involvement of the (high-spin) triplet state is necessary for combination with the triplet excited state of the C-H bond in order to produce the "double-triplet" singlet reactive state. The spin-uncoupling scheme discussed above has been applied recently [37] to reactions of the MCpCO complexes with methane (Cp = C_5H_5). Only the complexes with M=Rh,Ir activate C-H bonds of alkanes; most notably, the cobalt complexes were found to be inert, which is surprising for a metal belonging to the same group [23]. Siegbahn has shown that this is due to the triplet ground state for the $C_5H_5Co(CO)$ complex [23]. The insertion product has a singlet ground state so the triplet ground state cobalt complex has to change spin during the reaction [23]. It was shown that the S-T crossing occurs at the right side from the singlet transition state [37]; it means that SOC at the region of the S-T crossing seam is negligible in the CoCp(CO) complex insertion into the C-H bond [37]. From the VB correlation diagram it follows that the T-S transition occurs mostly on the C-H moiety and does not involve any orbital rotation (and hence no orbital angular momentum change during the T-S transition). At the same time the $C_5H_5Co(CO)$ complex efficiently reacts

with the CO molecule [12]. It is not necessary to cleave the bond during such a reaction and the triplet excitation in the reacting CO moiety is not involved in the reaction process. The T and S states differ by the orbital rotation within the $3d$-manifold of the Co atom; thus the SOC matrix element is comparatively large [37]. The spin flip is effectively allowed during the $C_5H_5Co(CO)$ complex reaction with CO and such an addition reaction proceeds very quickly [12].

Calculations of rhodium complexes with two ligands, RhLL' (L,L'=Cl, H, CO, NH_3), and their reactions with methane have lead Siegbahn and Svensson [27] to the following conclusions: Comparison between the molecular precursor complex and the transition state of the oxidative addition reaction has indicated different requirements for the TM complexes and their ligands. The authors of Ref. [27] have stressed that a ground singlet (or a low-lying singlet) state is required for the formation of a strongly bound molecular precursor complex, while for a low transition state barrier a ground triplet (or a low-lying triplet) state is an advantage. The authors of Ref. [27] come to the conclusion that the barrier from the precursor complex to the transition state is not expected to be a characteristic for the C-H dissociation reaction, but is dependent on the S-T splitting of the TM complexes being different for the different ligand combinations.

The spin-uncoupling scheme can easily explain the important findings of spin dependence from Ref. [27]. The molecular precursor complex formation does not need any bond cleavage. It occurs between two closed shell systems as a result of electrostatic polarization; this is actually a strongly bound van der Waals system. Its binding energy does not depend on the S-T splitting neither in the TM complex, nor in methane. From the VB correlation diagram it follows that the transition state barrier depends on the "double-triplet" state energy of the two reactants. Since only methane has been considered in Ref. [27] (the S-T energy gap in methane is constant), the barrier of the oxidative addition reactions between the TM complexes and methane depends only on the S-T energy gap in the TM complexes.

Finally, one has to mention that some models of hydrocarbon adsorption on cupper surfaces also illustrate the features of spin-uncoupling discussed above [54]. Geometry optimization of the adsorbed hydrocarbons indicates that their structures and energies are very close to the excited triplet state characteristics of the gas-phase molecules [54]. The Cu(110) and Cu(100) clusters consisting of 14 cupper atoms simulate the local state on the surface prepared for adsorption process; they have the triplet ground state. Any desirable spin state of the cluster can be easily achived in a sufficiently large metal compound and can so be involved in the spin-uncoupling process. Combination with the triplet excited state of the hydrocarbon can be accounted for in the VB correlation diagram and which then illustrates the involvement of the triplet excited

hydrocarbon in the adsorption process.

5 Conclusions

The involvement of the triplet state of hydrocarbons is a common feature of spin uncoupling in activation of hydrocarbons by transition metal species. This does, however, not mean that the triplet state of the hydrocarbon is involved in the reaction mechanism at the real kinetic stage (this is close to the case of alkene adsorption on cupper surfaces [54]). Instead it represents a way of analysis of the deformation of the wave function during the catalytic reaction in terms of VB structures.

Gas phase reactions of second-row TM atoms with small hydrocarbons [15] can be qualitatively interpreted by valence bond method correlation diagrams, which account for the "singlet-triplet" avoided crossing as the main reason for the lowering of the barrier heights. This VB scheme of spin-uncoupling illustrates, first of all, the crucial importance of the triplet excited state of the activated molecule. In the extended VB method an account of this state includes also the involvement of some excited states of the catalyst, which is in line with previous findings [16, 17, 55, 56, 48, 15]. In particular, the presence of a low-lying s^0 state is found to be of key importance for a low activation barrier [50]. This excited state should enter the qualitative analysis of all results, since this is the only possible reacting state, being anologous of the Ψ_{1r} (Eq. 2) reactant valence bond structure, which can participate as the lower branch in the "S-T" avoided crossing with the "triplet" counterpart valence bond structure Ψ_{2r} (Eq. 3). Entering this upper branch of reactants the metal atom has to be in the high-spin $d^{n+1}s^1$ state in order to be partly compensated by two non-paired spins of the triplet organic molecule. This is the reason that both the upper and lower branches of the VB diagram have the same low-spin multiplicity. This also explains that the low-spin state is always reactive in hydrocarbon activation by all TM species.

The energy of the low-spin $d^{n+1}s^1$ state of the TM atomi, found earlier as an important criterion for C-H bond activation [48, 50], can be accounted for by the VBCI treatment as well, since it naturally participates in the CI mixing of all low-spin states. Thus the VB treatment is compatible with the sd_σ hybridization and unshielding mechanism proposed by Blomberg *at el.* [48, 50].

The account of promotion and exchange-loss energies [50] can not explain all trends in the barrier heights for TM atoms and complexes. A reason for this is

that certain electronic states have not been accounted for in the analysis of the MO CI result [48, 50]; they get more important in the VB analysis. First of all this concerns the triplet excited state of the activating molecule. In the VB method an account of this state includes also the involvement of some other excited states of the catalyst. In particular, the presence of a low-lying s^0 state is very important for a low activation barrier. The low-lying $d^{n+2}s^0$ states are present, for example, in Rh and Pd atoms; these are the low-spin states ^2D and ^1S, respectively. As already mentioned above, these states are the only possible reacting states, being anologous to the Ψ_{1r} (Eq. 2) reactant valence bond structure, which can participate in the "S-T" avoided crossing with the "triplet" counterpart valence bond structure Ψ_{2r} (Eq. 3). The metal atom has to be in the high-spin $d^{n+1}s^1$ state in order to be partly compensated by two non-paired spins of the triplet organic molecule.

An important advantage of the VB approach to catalysis is that it is conceptually closely related to the traditional way in which chemists rationalize chemical structure and reactivity [6, 7, 45]. It is of considerable interest to construct diabatic electronic states representing specific resonance structures of a catalytic system. In this way the importance of the triplet excited state of organic substrates becomes immediately evident, and it is then easy to understand that only the low spin state of the catalyst is reactive.

6 Acknowledgements

This work was supported by Swedish Institute and by Swedish Royal Academy of Science.

References

[1] R.B. Woodward and R. Hoffmann. *J. Am. Chem. Soc.*, 87:2046, 1965.

[2] H.C. Longuet-Higgins and E.W. Abrahamson. *J. Am. Chem. Soc.*, 87:2045, 1965.

[3] W. Van der Lugt and L.J. Oosterhoff. *J. Am. Chem. Soc.*, 91:6042, 1969.

[4] L. Salem. *J. Am. Chem. Soc.*, 96:3486, 1974.

[5] W.G. Dauben, L. Salem, and N.Turro. *Acc. Chem. Res.*, 8:41, 1975.

[6] L. Salem. Electrons in chemical reactions : First principles. Wiley, New York, 1982.

[7] S.S Shaik. *J. Am. Chem. Soc.*, 103:3692, 1981.

[8] H. Eyring and M. Polani. page 445, 1932.

[9] H. Eyring, S.H. Lin, and S.M. Lin. *Basis chemical kinetics.* Wiley, New York, pp 27-36, 1980.

[10] A. Salikhov and H. Fischer. *Theor. Chim. Acta*, 96:114, 1997.

[11] N. Koga and K. Morokuma. *Chem. Rev.*, 91:823, 1991.

[12] E.P. Wasserman, C.B. Moore, and R.G. Bergman. *Science*, 255:315, 1992.

[13] A.A. Bengali, C.B. Moore, and R.G. Bergman. *J. Am. Chem. Soc.*, 117:3879, 1995.

[14] T.T. Wenzel and R.G. Bergman. *J. Am. Chem. Soc.*, 108:4856, 1986.

[15] J.J. Carroll, K.L. Haug, J.C. Weisshaar, M.R.A. Blomberg, P.E.M. Siegbahn, and M. Svensson. *J. Phys. Chem.*, 99:13955, 1995.

[16] J.J Low and W. A. Goddard III. *Organometallics*, 5:609, 1986.

[17] J.J Low and W. A. Goddard III. *J. Am. Chem. Soc.*, 108:6115, 1986.

[18] T. Ziegler, V. Tschinke, L. Fan, and A.D. Becke. *J. Am. Chem. Soc.*, 111:9177, 1989.

[19] N. Koga and K. Morokuma. *J. Phys. Chem.*, 94:5454, 1990.

[20] M.R.A. Blomberg, J. Schule, and P. Siegbahn. *J. Am. Chem. Soc.*, 111:6156, 1989.

[21] M.R.A. Blomberg, P. Siegbahn, and M. Svensson. *J. Phys. Chem.*, 96:9794, 1992.

[22] P.E.M. Siegbahn. *J. Phys. Chem.*, 99:12723, 1995.

[23] P.E.M. Siegbahn. *J. Am. Chem. Soc.*, 118:1487, 1996.

[24] M.R.A. Blomberg, P. Siegbahn, and M. Svensson. *J. Phys. Chem.*, 95:4313, 1991.

[25] P. Siegbahn, M.R.A. Blomberg, and M. Svensson. *J. Am. Chem. Soc.*, 115:1952, 1993.

[26] P. Siegbahn. *J. Am. Chem. Soc.*, 115:5803, 1993.

[27] P.E.M. Siegbahn and M. Svenson. *J. Am. Chem. Soc.*, 116:10124, 1994.

[28] F. London. *Zeitschr. Elektrochemie*, 35:352, 1929.

[29] W. Gerhartz, R.D. Poshusta, and J. Michl. *J. Am. Chem. Soc.*, 98:6427, 1976.

[30] D. Grimbert, G. Segal, and A. Devaquet. *J. Am. Chem. Soc.*, 97:6629, 1975.

[31] B.F. Minaev. *Rus. J. Struct. Chem.*, 23:170, 1982.

[32] B. F. Minaev. Theoretical analysis and prognostication of spin-orbit coupling effects in molecular spectroscopy and chemical kinetics. Dr. Sc. Thesis, N.N. Semenov Institute of Chemical Physics, Moscow. (in Rus.), 1983.

[33] B.F. Minaev, D. Jonsson, P. Norman, and H. Ågren. *Chem. Phys.*, 194:19, 1995.

[34] B.F. Minaev, I.S. Irgibaeva, and Z.M. Muldahmetov. *Theor. Exp. Chem. (USSR)*, 20:305, 1984.

[35] B.F. Minaev, V.A. Thihomirov, and Z.K. Dausheev. *Rus. Chem. Phys.*, 3:345, 1984.

[36] B.F. Minaev and H. Ågren. *Coll. Szechoslovak Chem. Commun.*, 60:339, 1995.

[37] B.F. Minaev. *Bulletin of the Polish Academy of Sciences. Chemistry*, 48:131, 2000.

[38] A. Fahmi and R.A. van Santen. *J. Phys. Chem.*, 100:5676, 1996.

[39] B.F. Minaev and H. Ågren. *J. Mol. Catalysis. A*, 149:179, 1999.

[40] M.M. Francl, W.J. Pietro, J.S. Binkley, W.J. Hehre, M.S. Gordon, D.J. DeFrees, and J.A. Pople. *J. Chem. Phys.*, 77:3654, 1982.

[41] M.W. Schmidt, K.K. Baldridge, J.A. Boats, S.T. Elbert, M.S. Gordon, J.H.Jensen, S. Koseki, N. Matsunaga, K.A. Nguyen, S.J. Su, and T.L. Windus. *J. Comput. Chem.*, 14:1347, 1993.

[42] W.J. Hehre, R. Ditchfield, and J.A. Pople. *J. Chem. Phys.*, 56:2257, 1972.

[43] B.F. Minaev. *Theor. Experimental Chem.*, 32:1, 1996.

[44] Z.M. Muldahmetov, B.F. Minaev, and G.A.Ketsle. Optical and magnetic properties of the triplet state. Nauka, Alma Ata (in Russ.), 1983.

[45] V. Bonacic-Koutecky, J. Koutecky, and L. Salem. *J. Am. Chem. Soc.*, 99:842, 1977.

[46] K. Yamaguchi. *Chem. Phys. Lett.*, 30:288, 1975.

[47] B.F. Minaev and H. Ågren. *Int. J. Quant. Chem.*, 72:581, 1999.

[48] M.R.A. Blomberg, P. Siegbahn, and M. Svensson. *J. Am. Chem. Soc.*, 114:6095, 1992.

[49] C.E. Moore. *Atomic Energy Levels. Volume III.* NBS, Washington, DC, 1958.

[50] P. Siegbahn, M.R.A. Blomberg, and M. Svensson. *J. Am. Chem. Soc.*, 115:4191, 1993.

[51] R.Z. Hinrichs, P.A. Willis, H.U. Stauffer, J.J. Schroden, and H.F. Davis. *J. Chem. Phys.*, 112:4634, 2000.

[52] W.D. Jones and F.J. Feher. *Acc. Chem. Res.*, 22:91, 1989.

[53] T. Fayet, A. Kaldor, and D.M. Cox. *J. Chem. Phys.*, 92:254, 1990.

[54] L. Triguero, L.G.M. Pettersson, B.F. Minaev, and H. Ågren. *J. Chem. Phys.*, 108:1193, 1998.

[55] E.A. Carter and W. A. Goddard III. *J. Phys. Chem.*, 92:2109, 1988.

[56] E.A. Carter and W. A. Goddard III. *J. Phys. Chem.*, 92:5679, 1988.

Assignment and Convergence of IR spectra for a sequence of polypyridine oligomers

by Peter Cronstrand and Hans Ågren

Theoretical Chemistry, The Royal Institute of Technology
S-10044 Stockholm, Sweden

Abstract

Vibrational modes and infrared spectra are studied computationally with B3LYP density functional theory for a sequence of oligomers - polypyridines up to four units - in order to explore the isomer dependence and convergence behavior with respect to the oligomer length. The infrared spectra of spin coated and bulk polypyridine are assigned and discussed on the basis of the computational results. A frequency region is identified with large dependence on isomer (1400 cm^{-1}) and one region with large dependence on sample (1000 cm^{-1}) and where any idealized polypyridine isomer fails to reproduce the experimental spectra.

Contents

ADVANCES IN QUANTUM CHEMISTRY, VOLUME 40

0065-3276/01 $35.00

1 Introduction

Infrared spectroscopy constitutes one out of several spectroscopic tools that can be useful for studies of structure-property relations and for orientational probing of technically important materials. For instance, infrared spectroscopy has recently been applied to study light emitting diodes (LED's) for the purpose of finding out about orientation and degradation for different sample preparations [1]. A prerequisite for such analysis is a proper assignment of spectral bands to modes with different dipolar directions. Oligomer modeling has become a viable option to systematically study how such properties evolve for the extended species. In this approach one considers a sequence of oligomers that models the full polymer, and studies the convergence of the infrared (IR) spectrum within this sequence. One thus attempts to find the limiting behavior by enlargements of the oligomer models, and study the smallest repeat unit up to a oligomer that it can be considered to represent the infinite system. A possible advantage thereby is that the spectra can easily be decomposed into local contributions and interpreted in terms of building blocks. A fundamental problem of this approach is, however, posed by the parameterizations of the oligomers; if the geometric and electronic structures of the oligomers should be considered as they appear for each particular oligomer or as they appear in the optimal bulk geometry, and if the bond-termination for the free oligomer has a special role. The purpose of the present paper is to make a convergence study of IR spectra with respect to an oligomer sequence. We choose polymers based on pyridine - polypyridine (PPY) - which have demonstrated large resistance to photo- and electrochemical oxidation in LED applications [2, 3, 4, 5]

2 Computational details

Several reports have recently demonstrated the utility of density functional theory for accurate predictions of IR spectra and vibrational modes of organic species [6, 7, 8]. This is further confirmed in this study, which gives vibrational frequencies of all major modes below 3000 cm^{-1} lying within 2-5 percent of experiment. The accuracy of Hartree-Fock calculations for the same modes are in the region of 10 percent. Above 3000 cm^{-1} the disagreement reaches 7 percent for DFT and 10 percent for Hartree-Fock. Multi-configurational (MCSCF) calculations for a few active orbitals improves the HF accuracy somewhat, however, for a significant improvement the amount of active orbitals needed leads to computational difficulties for any of the oligomers except pyridine. The calculations for polypyridine were carried out with the three parameter hybrid HF/DFT method using the LYP correlation functional (B3LYP) and employing the 4-31G basis set. A switch to larger basis sets, from 4-31G to

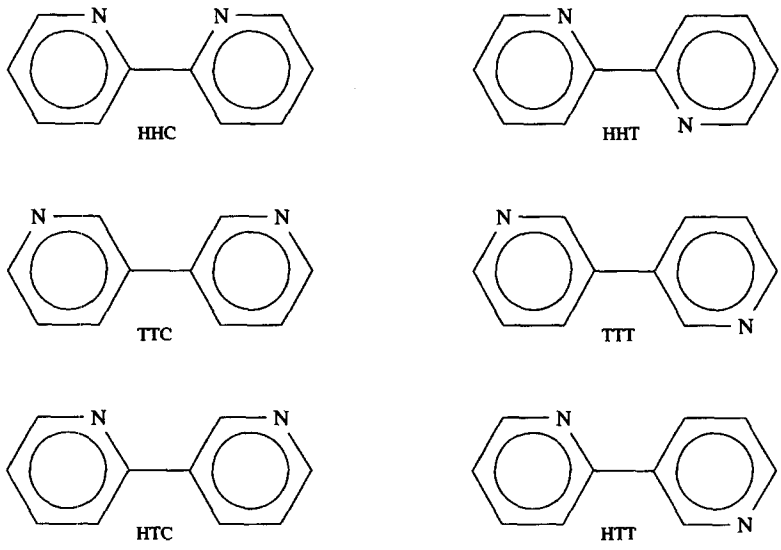

Fig. 1

Figure 1: The isomeric head-to-head, tail-to-tail and head-to-tail structures of PPY.

6-31G, 6-31G* and 6-31G+*, did not improve the results with any significance for pyridine, and we see from Fig. 2 that the same conclusion can be drawn also for larger oligomers when comparing 4-31G and 6-31G. Since the sample on which the experimental results [1] are based probably contains more than one isomer the results are somewhat harder to qualify for the oligomers of pyridine. The agreement among individual isomers with experiments is, with few exceptions, within 4 percent for all larger modes.

The DFT calculations were performed with the gaussian94 program on a Cray-T3E. For all cases complete geometry optimizations were carried out. Vibrational modes of a single small molecule are strongly dependent on the optimized geometry for the particular basis set. Choosing a geometry optimized with one larger basis set and calculating the IR spectra for another smaller basis set will in general not improve the result. We can expect the dependence of the optimized geometry to be weakened for longer oligomers since the modeling of the restoring force through the hessian of the nuclear potential surface will become less dependent on a specific nuclear coordinate but more on the overall structure. Geometry optimization is still an option,

Fig. 2

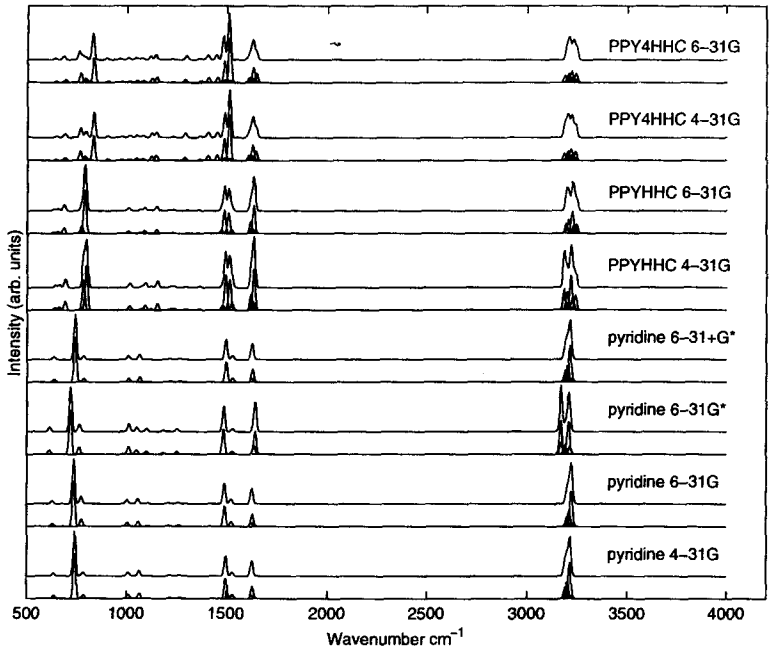

Figure 2: Theoretical IR spectra of pyridine, PPYHHC and PPY4HHC for the 4-31G and 6-31G basis sets. For all plots full width at half maximum (FWHM) is assumed to be 15 cm^{-1}.

since even for increased oligomer lengths the computational bottleneck lies in the time spent calculating the vibrational modes. The normal modes were analyzed with the aid of the program MOVIEMOL [9].

3 Results

Six isomers of PPY form possible unit cells for the polymer; the cis forms with head-to-head (PPYHHC), tail-to-tail (PPYTTC) and the head-to-tail (PPYHTC) isomers and the trans forms with head-to-head (PPYHHT), tail-to-tail (PPYTTT) and head-to-tail (PPYHTT) isomers. PPY4HHC, PPY4TTC, PPY4HTC, PPY4HHT, PPY4TTT and PPY4HTT will denote these isomers with the unit length 4 (that is with four pyridine rings). For an infinite oligomer will the head-to-head and tail-to-tail isomers be equal. Geometrical parameters are given in Fig. 1. In this paper the isomers will be treated separately even though mixed polymers are likely to occur in the experimental sample.

An increase of the length of the polymer affects the intensity of existing modes in pyridine, but does also split them and add several more, some of which correspond to the bonding between the pyridine rings. All effects are more or less sensitive to the actual location of the nitrogen atoms.

Figures 3-4 indicate convergence in all major modes when extending the oligomers. The difference between the head-to-head and the tail-to-tail isomers is most present in the dimer but strongly reduced for the oligomer with unit length 4. For all six isomers the stronger modes are already present in the pyridine monomer, but an extension tends to shift them slightly upwards. This overestimation increases with the wavenumber of the modes and is most significant for the mode at 3000 cm^{-1}. Note also that the calculations fail to properly reproduce the intensities in the region 800 - 1200 cm^{-1}, which perhaps is most apparent when comparing the proportions between the intensities of the modes around 800 cm^{-1}. Several factors must be considered in a comparison with the experimental results [1]. In the calculated spectra convoluting gaussians of the same width are assumed, and any broadening mechanism of the bands are therefore unaccounted for. Secondly, and as already commented, the measured samples do probably not represent one pure isomer, and one can therefore not expect that a single oligomer sequence simulates the experimental spectra perfectly. In order to facilitate the experimental comparison and the convergence behaviour we have plotted close lying modes separately as well as superposed them into a total spectrum.

The experimental data shown in Fig. 5 consist of IR absorption spectra of bulk PPY between two potassium bromide plates and infrared reflection absorption spectra (IRAS) of thin spin coated layers of PPY on gold. The reason for using a metal substrate in the latter case is that a well-defined reflection at a metal surface results in excitation of vibronic modes perpendicular to the plane of the film. Note that the wide band at 1200 cm^{-1} in the bulk spectra originates from the solvent [1].

The three major modes of pyridine as well as polypyridine are predicted for all isomers within a displacement of at maximum 60 cm^{-1}. From Fig. 7 we see that several features of the experimental spectra, such as the twofold modes at 800 cm^{-1} and 1500 cm^{-1}, are reproduced by the oligomers, perhaps most successfully by PPY4HTC which captures the mode at 1360 cm^{-1} in the experimental spectra. The modes at 1000 cm^{-1} are not successfully reproduced by any of the oligomers, however, all isomers have several minor modes located in this area. Similar to the weaker component of the twofold mode at 800 cm^{-1} in pyridine the intensities of these minor modes are underestimated.

The vibrational structure of the PPY is strongly dependent on which part of the molecule can be considered as rigid at a particular frequency. The vibrational modes can easily be separated into characteristic vibrations at certain

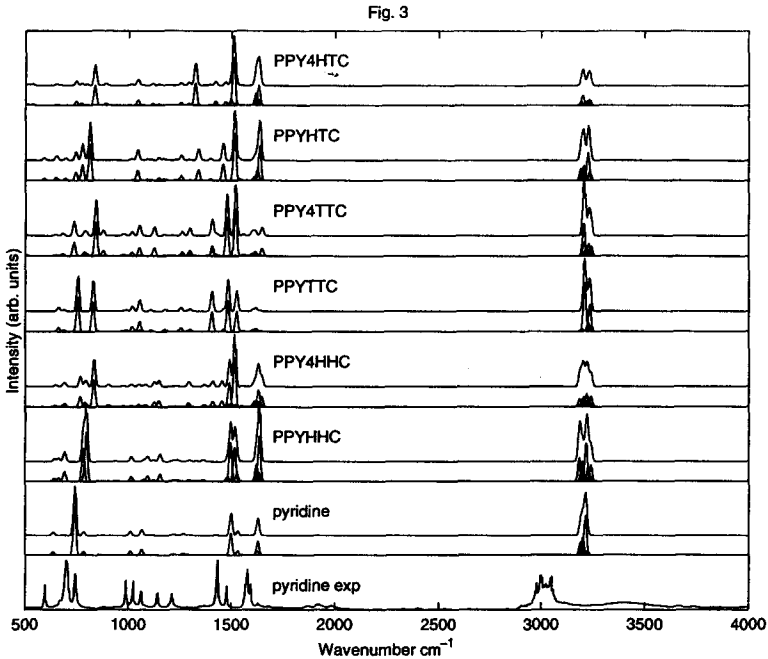

Figure 3: Theoretical IR spectra of PPYHHC, PPYTTC and PPYHTC.

frequency ranges. Below 400 cm^{-1} both the carbon-nitrogen skeleton which forms the pyridine ring itself and the C-H bonds can be considered as rigid and the new "external" vibrational modes are therefore restricted to bending and stretching of the bond joining the pyridine rings. However, in the region 400-700 cm^{-1} the pyridine ring is no longer rigid and a weak twisting motion is added to the former motions. From 600 cm^{-1} and up, the C-H bond tends to be more involved in the vibrational spectrum leading to a more complex behavior which in the region 700-1100 cm^{-1} mostly is based on stretching of the ring C-C bond and bending of the C-H bond. The latter vibrational mode is in the interval 1100-1600 cm^{-1} replaced by stretching of the C-H bond. Above 3000 cm^{-1} the pyridine rings have regained their rigidity and the modes include there only the rapidly stretching of the C-H bond.

In pyridine the calculated modes at 741 cm^{-1} and 784 cm^{-1} (corresponding to 704 cm^{-1} and 748 cm^{-1} in experimental spectra [10]) can be described as a symmetric bending out-of-plane (oop) of the molecule including all atoms. Since the calculated spectra fail to reproduce the proper relation between the intensities between these two modes of pyridine one can probably not expect the intensity relations of the isomers of PPY to be reliable in this region.

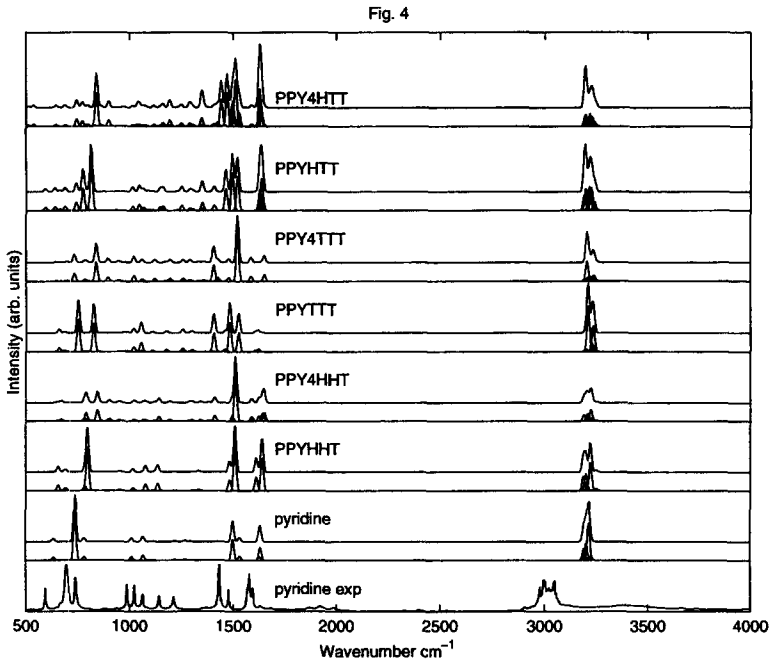

Figure 4: Theoretical IR spectra of PPYHHT, PPYTTT and PPYHTT.

However, for the 6 possible isomers only PPY4HHT shows modes with equal intensity, while the others show modes with significant differences in intensity. The modes with lower intensity are in those cases in general dominated by the bending of the hydrogen located at the end of the polymer, while the higher mode includes all hydrogens, which is a tendency that is repeated for other discussed modes as well.

The two modes around 1500 cm^{-1} for pyridine are characterized by bending in the plane (ip) of the molecule including all hydrogens. Opposite to the previously discussed mode the theoretical spectra more successfully reproduce the proportions between intensities of these modes, which also seems to be the case when comparing the spin coated spectra of PPY with the oligomer PPY4HHC. Extending the molecule to the oligomer produces similar results as for the previously discussed mode, that is, modes of lower intensity are localized to the hydrogens at the end of the molecule and modes of higher intensity involves all hydrogens and are more equally distributed over the molecule. For PPY4HTC and PPY4HHT only one mode survives, whereas PPY4HHC shows two modes of similar proportions as those in the PPY spin coated spectra (Fig. 5). The isomer PPY4HTT, on the other hand, differs from the other

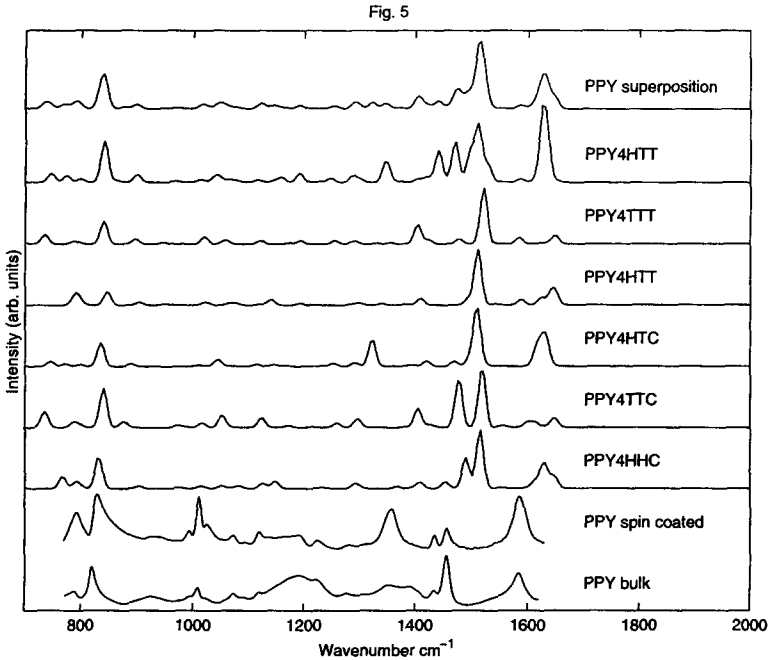

Figure 5: Theoretical and experimental [1] IR spectra of PPY. Note that the wide band at 1200 cm^{-1} in the bulk spectra originates from the solvent.

isomers by giving rise to several modes of equal order of intensity. The mode at 1629 cm^{-1} for pyridine can also be described as an in-plane bending of the molecule. Quite unlike the previous modes this mode leads to several minor modes indistinguishable in the superposed spectra when extending pyridine to PPY.

The most distinguishing mode between the six isomers of the polymer can be identified around 1340 cm^{-1} for the two head-to-tail (H-T) isomers, PPY-HTC and PPYHTT, which includes a weak symmetric stretching of the C-C bond joining the pyridine rings. Note, however, that it is not similar to a pure stretching mode with rigid pyridine rings as for the modes below 400 cm^{-1}. Modes of similar characteristics can not as easily be identified for PPYHHC or PPYHHT.

Wavenumber (cm^{-1})									
pyridine		PPY							
(exp) [10]	calc.	(exp) [1]	4HHC	4TTC	4HTC	4HHT	4TTT	4HTT	description
704	741	794	767~	735	745	791	735	746	oop
748	784	831	832	839	835	846	840	841	oop
–	–	1360	–	–	1323	–	–	1345	ip
1438	1498	1437	1489	1476	1496	1493	1404	1493	ip
1482	1531	1458	1514	1518	1508	1510	1519	1510	ip
1581	1629	1587	1631	1647	1630	1647	1647	1625	ip

Table 1: Theoretical and experimental vibrational modes for pyridine and the six isomers of PPY (oop means out of the molecularplane, ip in the molecular plane).

4 Discussion

An analysis based on the DFT technique demonstrates the oligomer convergence of the modes of vibration and IR spectra for polypyridine. The main features of the two cis isomers of polypyridine with head-to-head (PPYHHC) and the head-to-tail (PPYHTC) forms are shown to correspond to modes already active in pyridine, however, a mode characteristic for PPYHTC was calculated at 1323 cm^{-1}. We find good experimental comparison for modes above 1300 cm^{-1} corresponding to in-plane vibrations and beneath 900 cm^{-1} corresponding to out-of-plane vibrations, while agreement is absent in the intermediate region roughly at 1000 cm^{-1}. In this region we also find considerable disagreement between the experimental spectra corresponding to different preparations (c.f. PPY spin coated and PPY bulk spectra in Fig. 5). A reason for this disagreement can possibly be found in the fact that these modes occur in the transition region from out-of-plane to in-plane vibrations where the modes are mixed, and that this region could be most sensitive to conformational disruption. The underestimation of the intensities of these modes are though already present in the modeling of the spectra of pyridine (see Fig. 3-4).

Since the experimental spectra differ in modes with the same characterization it is still difficult to draw conclusions about the orientation of the film, but to exclude the possibility of a spin coated PPY consisting of flat lying pyridine rings. An interesting observation can be based on the fact that in these split modes, the lower mode is localized to hydrogens at the end of the oligomer whereas the higher modes include all hydrogens. If one simply weakens the modes that include all hydrogens in the bulk spectra much of the character of the spin coated spectra is regained. This procedure can unfortunately not explain the mode at 1360 cm^{-1} which in the calculated spectra only can be found for the PPYHTC and PPYHTT isomers. On the other hand, this might indicate that the H-T isomers are more frequent in the sample.

5 Acknowledgement

Computer time has generously been supported by NSC at the Swedish National Supercomputer center in Linköping. Dr. Leif Petterson is acknowledged for making the experimental spectra available to us and for useful discussions. We thank Prof. Umapathy for providing the program MOVIEMOL [9].

References

[1] L. A. A. Pettersson, H. Kariis, G. Greczynski, L. E. Horsburgh, A. P. Monkman *to be published*

[2] T. Yamamoto, T. Maruyama, Z.-H. Zhou, T. Ito, T. Fukuda, Y. Yoneda, F. Begum, T. Ikeda, S. Sasaki, H. Takezoe, A. Fukuda, K. Kubota *J. Am. Chem. Soc.*, 116 4832-45 (1994)

[3] D.D. Gebler,Y.Z. Wang, J. W. Blatchford, S. W. Jessen, L.-B Lin, T.L. Gustafson, H.L. Wang, T.M. Swager, A. G. MacDiarmid, A. J. Epstein *J. Appl. Phys.*, 78 4264-4266 (1995)

[4] S. Dailey, M Halim, E. Rebourt, L. E. Horsburgh, I. D. W. Samuel, A. P. Monkman *J. Phys. Condens. Matter*, 10 5171-5178 (1988)

[5] Y. Z. Wang, D. D. Gebler, D. J. Spry, D. K. Fu, T. M. Swager, A. G. MacDiarmid, A. J. Epstein *IEE Transactions on electron devices* vol. 44, no. 8 (1997)

[6] R. P. Mohandas, S. Umapathy, *J. Phys. Chem.*, A 101 4449-4459 (1997).

[7] R. N. Biswas, S. Umapathy, *J. Phys. Chem. A*, 101 5555-5566 (1997).

[8] C. W. Bauchlicher Jr, *Chem. Phys.* 233, 29 (1998).

[9] K. Hermansson, L. Ojamäe, University of Uppsala, Institute of Chemistry, Report UUIC-B19-500 (1994).

[10] The Aldrich Library of FT-IR Spectra, Edition I, Ed, Charles J. Rupert, Volume I.

D-wave Bipolaronic Condensate with Short Range Repulsive Electronic Correlations in an Extended Hubbard Model of High T_c Cuprate Superconductors

L.J DUNNE[b,c] and E.J BRÄNDAS[a]

[a]*Department of Quantum Chemistry*
University of Uppsala, Box 518, Uppsala, S-75120, Sweden

[b]*School of Applied Science*
South Bank University, London SE1 0AA, UK

[c]*School of Chemistry, Physics and Environmental Science*
University of Sussex, Falmer, Brighton, BN1 9QJ, UK

Abstract

The question as to whether Fermion pairs interacting with a short range Coulomb repulsion and longer range attractive tail can form a condensate is a key question for High Temperature Superconductivity [1-30]. If such a form of interaction can support a bound state it is commonly suggested that Bose-Einstein condensation of such pairs may occur, as in widely discussed Bipolaron models of High Temperature Cuprate superconductivity where the paired Fermions are holes. On the other hand it is frequently stated that strongly overlapping real-space pairing with a strong short range Coulomb repulsion is *a priori* implausible [4]. In this paper a review is made of our work on D-wave pairing [7-19] in real-space between electrons on a Cuprate lattice due to any effective interaction with a short range repulsive part and a longer range attractive tail such as might arise from Bipolaronic coupling.

Contents

ADVANCES IN QUANTUM CHEMISTRY, VOLUME 40

0065-3276/01 $35.00

1. Introduction

By adopting a set of plausible postulates it is possible to constuct a theory of high T_c cuprate superconductivity which displays much of the accepted behaviour of cuprate superconconductors. It is shown here that Yang's η-pairing scheme extended to embrace a D-wave condensate is favoured in the presence of an effective electron-electron interaction with a short range repulsion and a long range attractive tail. The tendency for pairs of electrons to evade the region of short range repulsion and to reside in the longer range attractive region of an effective potential can enable the system to adopt a low energy coherent electronic state with superconductive behaviour. For low hole doping levels we find that the condensate density is numerically close to the paired hole density. No Bosonisation of the pairs is invoked so that rigorous Fermion statistics of the particles is maintained throughout the calculation. The proposed theory accounts, in a simplified way, for many of the essential features of high T_c superconducting cuprates. The short range Coulomb repulsion is the driving force for the condensate D-wave symmetry. We will give particular attention to the heat capacity trends which allow us to make some inferences on localisation.

The fundamental structural characteristic of $n-$type or $p-$type cuprates are the cuprate layers depicted in Figure 1 where the square arrangement of lattice points is centred on a Cu atom depicted in black. We will assume that doping occurs from a band largely derived from oxygen orbitals and that the magnetic moments on the Cu ions, with phonons, dress the electrons in the oxygen band so that together with Friedel oscillations, the effective potential between such electrons may have a longer range attractive tail. The antiferromagnetic spin cloud around each Fermion quenches to a significant degree the oxygen band Fermion magnetic moments and we also suppose that such electrons can be pulled out of this spin dressing which is the 'spin gap' in our theory where, the C-axis conductivity will relate to the magnetic suscepibility in this stripping process releases pairs of electrons with a bare magnetic moment.

2. The Pair Condensate Wavefunction

There is a widely held view [1-17] that the pair condensate wavefunction has a dominant $d_{x^2-y^2}$symmetry. Recently, we presented a group theoretical analysis [7] of the pair condensate state function in real space for superconducting cuprates and studied the implications of the $d_{x^2-y^2}$ pairing symmetry for Fermions on a

cuprate lattice (shown in Figure 1) with local C_{4v} point group symmetry about the Cu atoms. A dominant pair of Wannier-type localized orbitals with e-symmetry on each unit cell, which seem very likely to be involved in the superconductivity of cuprates were identified. Furthermore, the essential features of the ARPES spectra discussed by Shen and co-workers [10] are reproduced within the experimental error which is roughly 0.1 eV in energy and 0.1 π in wavevector in a tight-binding model with orbital degeneracy. We will show that a pairing force between electrons pairs discussed above can tip the energy balance causing a phase coherent superposition of such pairs to cross over into the ground state and giving rise to the phenomenon of high temperature cuprate superconductivity.

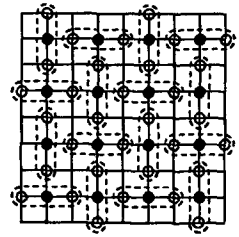

Figure 1 Copper/oxygen layer of Superconducting cuprates. Black and white circles represent copper and oxygen atoms respectively. A pair of e-basis Wannier functions, which are a linear combination of Cu and O atomic orbitals, transforming as (x, y) are localised on every lattice point at the centre of the unit cell.

It is pertinent to summarise our group theoretical argument on the important unresolved question in the chemistry of high temperature superconducting cuprates concerning the nature of the localized orbitals from which electrons are removed to create holes and discuss the chemical implications of the $d_{x^2-y^2}$ pairing symmetry for electrons on a cuprate lattice (shown in Figure 1) with local C_{4v} point group symmetry about the Cu atoms[1]. The group theoretical conclusion is that there is a degenerate pair of active bands in superconducting cuprates which are principally derived from localized e-orbitals and two possible singlet pairs formed from two different orbitals with symmetry classifications a_1, b_1 or a_2, b_2 and all three may contribute to the condensate state function to varying degrees. Hund's rule [36,40] and other energetic considerations and the experimental observation that singlet pairing [1-30] with a short coherence length occurs in superconducting cuprates

[1] The Cu atom is in an almost D_{4h} environment but there are small puckerings of the cuprate layer and external ions which lower the symmetry to C_{4v}

indicates that the first of these possibilities is likely to be dominant in these compounds. All three possibilities exclude models of cuprate superconductivity which are based on doping of a single band formed from linear combinations of one type of Wannier function centered on each unit cell. In identifying the most probable active localized orbital space we have not invoked any particular pairing mechanism but show below that localized e-orbitals are are well suited to obtain a superconductive state from short range repulsive electron correlations.

Following Gor'kov [23] and Yang [20,21] (for reviews see [18,41] and included references) the superconducting state is characterized by the existence of a thermal average, signified by the outer $\langle\rangle$, of the second order reduced electronic density matrix $\langle\rho(\mathbf{r}_1\sigma(1),\mathbf{r}_2\sigma(2)\,;\,\mathbf{r}'_1\sigma(1'),\mathbf{r}'_2\sigma(2'))\rangle$ which is anomalously large and which has the important property that when $\mathbf{r}_1 \approx \mathbf{r}_2$ and $\mathbf{r}'_1 \approx \mathbf{r}'_2$ and $|\mathbf{r}_1 - \mathbf{r}'_1|$ goes to infinity so that the pairs are well separated then the second order density matrix can be expressed as

$$\langle\rho(\mathbf{r}_1\sigma(1),\mathbf{r}_2\sigma(2);\mathbf{r}'_1\sigma(1'),\mathbf{r}'_2\sigma(2'))\rangle = \langle\psi^*(\mathbf{r}_1\sigma(1),\mathbf{r}_2\sigma(2))\rangle\,\langle\psi(\mathbf{r}'_1\sigma(1'),\mathbf{r}'_2\sigma(2'))\rangle \qquad (1)$$

where $\mathbf{r}$ and σ are space and spin variables. The range over which $\psi(\mathbf{r}_1\sigma(1),\mathbf{r}_2\sigma(2))$ remains finite as $|\mathbf{r}_1-\mathbf{r}_2|$ increases is a measure of the pair size or superconducting coherence length, which is known to be only a few Angstroms in superconducting cuprates and such a feature is widely accepted as indicating real space pairing of some type [8,9,18,20].

This factorization of the density matrix gives the condensate wavefunction $\psi(\mathbf{r}_1\sigma(1),\mathbf{r}_2\sigma(2))$ which when $\mathbf{r}_1 \approx \mathbf{r}_2 = \mathbf{r}$ is proportional to the Ginzburg-Landau wavefunction [23,36,41]. The condensate state function is isotropic for conventional superconductors but exhibits $d_{x^2-y^2}$ symmetry in real and momentum space for most superconducting cuprates, with the possibility of a small s-type component [10-16]. Yang [21] showed that the anomalous thermal average of the reduced density matrix discussed above can be identified for a many-electron state function from the reduced second order density matrix where the existence of a condensate is indicated by a macroscopically large eigenvalue and where the associated eigenvector is the pair condensate state function. Such a macroscopically large eigenvalue of the pair density matrix indicates a correspondingly large but bounded [20,21,25] population of pairs of electrons all with the same pair wavefunction which is analogous to a Bose-Einstein condensation of pairs into a single state. In superconducting cuprates the measured condensed electron pair

density [20,21,25] closely follows Yang's upper bound [21] for the eigenvalues of the pair density matrix. Whether one chooses to pair electrons or holes is irrelevant since pairing one type of carrier forces the pairing of the other and both the electron pair and hole pair have the same symmetry.

3. Group Theoretical Analysis

It is widely thought that in cuprate layers the Cu d-orbitals mix with oxygen $2p_x$, $2p_y$, $2p_z$ orbitals surrounding the Cu atom and that these orbitals play a dominant role in the superconductivity. We therefore consider a set of symmetry adapted orthogonalised [40] localized basis functions $\{\phi_i(r)\}$ formed principally from a linear combination of atomic orbitals centered on the Cu atoms in the cuprate layer. Such localized Wannier- type orbitals peak on the lattice point on which they are centered but spread out over neighbouring cells with gradually decreasing oscillations required to ensure orthogonality. Each localized orbital $\{\phi_i(r)\}$ or a degenerate pair of these centered on the same site, must transform as one of the irreducible representations (IRs) a_1, a_2, b_1, b_2 and e (for a degenerate pair) of the C_{4v} point group. Following Yang [21] (see eq A8) the condensate wavefunction which is an eigenfunction of the pair translation operator can be written as

$$\begin{aligned}\psi(r_1\sigma(1), r_2\sigma(2)) = {} & c_{12}[\Phi_1(1)\Phi_2(2) - \Phi_1(2)\Phi_2(1)] \\ & + c_{34}[\Phi_3(1)\Phi_4(2) - \Phi_3(2)\Phi_4(1)] \\ & + c_{56}[\Phi_5(1)\Phi_6(2) - \Phi_5(2)\Phi_6(1)] \\ & + \cdots \end{aligned} \tag{2}$$

where c_{ij} are a set of expansion coefficients and Φ_i are generalised spin orbitals. The pairwise occupation of the geminal states [19,22] in eqn(2) should be carefully noted as this is an essential characteristic of a superconducting condensate. Since the coherence length is short, it is reasonable to assume that the active orbitals $\{\phi_i(r)\}$ are strongly localized in space so that $\psi(\mathbf{r}_1\sigma(1), \mathbf{r}_2\sigma(2))$ decays to zero as $|\mathbf{r}_1 - \mathbf{r}_2|$ increases.

Eqn(2) may be decomposed into the form

$$\psi(\mathbf{r}_1\sigma(1), \mathbf{r}_2\sigma(2)) = \chi(\Gamma) + \sum_k \phi_k \tag{3}$$

where $\chi(\Gamma)$ represents the geminal functions localised on the principal axis transforming in the C_{4v} group as the irreducible representation Γ while the terms in

the sum are a linear combination of the remaining geminals transforming together as the same irreducible representation Γ [40]. If the condensate state function $\psi(\mathbf{r}_1\sigma(1), \mathbf{r}_2\sigma(2))$ has B_1 symmetry then both terms in the right hand side of eqn(3) above must have B_1 symmetry under the operations of the C_{4v} group. By reference to a direct product table for the C_{4v} group [40,42,43] we can enquire as to what pairs of irreducible representations make up $\chi(\Gamma)$ and have an antisymmetrised direct product with a B_1 component.

There are 3 possibilities given by

$$\begin{aligned} a_1 \otimes b_1 &= B_1 \\ a_2 \otimes b_2 &= B_1 \\ e \otimes e &= A_1 \oplus A_2 \oplus B_1 \oplus B_2 \end{aligned} \tag{4}$$

Thus, there may be (i) a degenerate pair of active e-orbitals and (ii) two possible hole pairs from two different orbitals a_1, b_1 and a_2 , b_2. The a_1, b_1 and a_2, b_2 pairs may be combined as singlets or triplets but only the singlet pairs are relevant here since experimentally the condensate state function in superconducting cuprates has singlet symmetry as shown from Knight shift and tunneling experiments [1-30]. The e-representation requires a degenerate pair of localized spin orbitals which we shall label as the pair (X,Y) on a lattice point. If two electrons are placed in these orbitals we obtain four pair functions which may be combined as follows

$$\begin{aligned} (X(1)Y(2) - Y(1)X(2)) &\quad - \quad {}^3A_2 \\ (X(1)X(2) + Y(1)Y(2)) &\quad - \quad {}^1A_1 \\ (X(1)Y(2) + Y(1)X(2)) &\quad - \quad {}^1B_2 \\ (X(1)X(2) - Y(1)Y(2)) &\quad - \quad {}^1B_1 \end{aligned} \tag{5}$$

The pair symmetry classifications in the C_{4v} group are given on the right and only the last pair function has $^1B_1$ symmetry. We are hence restricted to three possible singlet pair functions of $^1B_1$ symmetry of which one is likely to make a dominant contribution to the condensate state function.

It is a simple task [40,43,78] to construct symmetry adapted combinations of Cu(3d) and O(2p) orbitals which transform as a_1, b_1, a_2, b_2, e.

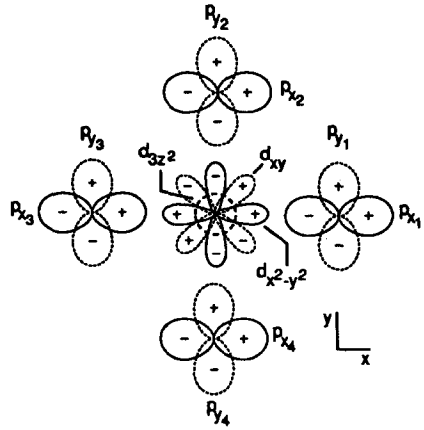

Figure 2 Orbitals used in the CuO_4 cluster, modified by Sawatsky *et al* [44]. The O $2p_z$ and Cu ($3d_{xz,yz}$) are not shown

Using the labeling scheme and cluster shown in Figure 2, the following combinations of the O(2p) and Cu(3d) basis functions have the irreducible representations indicated in the table below where the functions have been classified according to the u/g inversion symmetry in the near D_{4h} point group.

IR	Cu(3d)	O(2p)
$a_{1,g}$	d_z^2	$(p_{x1} + p_{y2} - p_{x3} - p_{y4})$
$a_{1,u}$	-	$(p_{z1} + p_{z2} + p_{z3} + p_{z4})$
$a_{2,g}$	-	$(p_{y1} - p_{x2} - p_{y3} + p_{x4})$
$b_{1,g}$	$d_{x^2-y^2}$	$(p_{x1} - p_{y2} - p_{x3} + p_{y4})$
$b_{1,u}$	-	$(p_{z1} - p_{z2} + p_{z3} - p_{z4})$
$b_{2,g}$	d_{xy}	$(p_{y1} + p_{x2} - p_{y3} - p_{x4})$
e_g	(d_{xz}, d_{yz})	$((p_{x1} - p_{x3}), (p_{x2} - p_{x4}))$
e_u	-	$((p_{x1} + p_{x3}), (p_{y2} + p_{y4}))$
		$((p_{y1} + p_{y3}), (p_{x2} + p_{x4}))$

This table has been previously published in part by Sawatzky et al [44]

There is no coupling between one-electron basis functions belonging to different irreducible representations so that the most significant hybridisation in the molecular orbitals of the CuO_4 cluster and hence in the Wannier type functions $\{\phi_i(r)\}$ can be inferred trivially from the above table. Most cluster calculations [44,45] put the antibonding b_1 single particle state as the highest energy occupied molecular orbital (HOMO) with the a_1, b_2 and e (all essentially gerade) antibonding orbitals

clustered together at about 1 eV below the b_1 orbital but other interactions may change this order somewhat.

Energetically, a condensate dominated by a_2, b_2 pairs is unlikely since the a_2 single particle state is essentially a non-bonding p-combination of O(2p) orbitals and is expected to lie well below the Fermi level. Similar conclusions can be made about all other non-bonding or weakly bonding orbitals. Therefore $a_1 b_1$ and e-pairs seem more likely.

Other things being equal, for repulsive electronic correlations the ground state of a_1, b_1 pairs is likely to be the triplet state, $^3B_1$, by Hund's rule. This principle energetically favours the most antisymmetrical space function and symmetrical spin function for a pair by minimising the short range Coulomb repulsion between electrons and is found to be widely applicable [40] in molecular systems.

On the other hand, with attractive forces, singlet a_1^2 or b_1^2, whichever is lower in energy, with $^1A_1$ symmetry is more favoured than a_1, b_1. Thus, a_1, b_1 pairs prepared in a singlet state would be unstable to the formation of a $^3B_1$ or $^1A_1$ pairs and it is hence improbable that singlet a_1, b_1 pairs make a dominant contribution to the condensate wavefunction in superconducting cuprates. Similar arguments can be made against the singlet a_2, b_2 pair. Thus, pairs derived from e-orbitals seem the most likely to dominate the condensate wavefunction and the highest antibonding of these is expected to be essentially from the (d_{xz}, d_{yz}) and ((p_{z1} - p_{z3}) , (p_{z2} - p_{z4}))$_g$ interaction as implied in the above table. Such e-orbitals have a significant oxygen $2p_z$ component and may also interact with e-combinations of apical $2p_x$ or $2p_y$ orbitals (the only analysis known to us which agrees with us is that due to Alexandrov [8]) and are not shown in the table above which agrees with spectroscopic indications that holes in doped cuprates have a primary oxygen 2p character [46]. The analysis above assumes a perfect lattice. Any deviation from this such as that caused by doping will allow mixing in of a range of other symmetry classifications into the condensate state function and this may account for the s-wave condensate component implicated in a wide range of experimental studies [3].

4. Energy Considerations

To derive a more detailed understanding of why e-pairs seem to be energetically preferred, we examine how such a condensate with $d_{x^2-y^2}$ symmetry may arise from repulsive electronic correlations of electrons on a cuprate lattice. We consider

N/2 cells centred on the Cu atom containing an orthonormal e-basis (in C_{4v} symmetry) of degenerate pairs of localized basis functions $\{\phi_{i,x}(r), \phi_{i,y}(r)\}$ formed principally from a linear combination of atomic orbitals centered on the Cu atoms in the cuprate layer giving N localised orbitals.

In the theory of conventional superconductivity with an attractive phonon-induced electron-electron interaction, it is common to find the stability of the superconducting state rationalised by the following argument. If n quasi-degenerate states with energy ε are coupled by an attractive matrix element $-V$ the Hamiltonian matrix has $(n-1)$ eigenvalues with energy ε and one which is identified as the superconducting state with energy $\varepsilon - nV$. However, a similar stabilisation may occur with repulsive off-diagonal matrix elements of the Hamiltonian matrix. An easy way to see this is to consider the real symmetric matrix eigenvalue problem of the form

$$\left(\begin{array}{cc|cc} \varepsilon & & \multicolumn{2}{c}{\multirow{2}{*}{$\mathbf{0}$}} & \\ & \ddots & & & \\ \hline \multicolumn{2}{c|}{\multirow{2}{*}{$\mathbf{0}$}} & \varepsilon & & \multirow{2}{*}{$\mathbf{v}$} \\ & & & \ddots & \\ \hline & & \multicolumn{2}{c|}{\multirow{2}{*}{$\mathbf{0}$}} & \varepsilon \\ \multicolumn{2}{c|}{\multirow{2}{*}{$\mathbf{v}^T$}} & & & \\ & & \multicolumn{2}{c}{} & \end{array}\right) \left(\begin{array}{c} \\ 1 \\ \hline \\ \pm 1 \\ \end{array}\right) = (\varepsilon \pm \kappa V) \left(\begin{array}{c} \\ 1 \\ \hline \\ \pm 1 \\ \end{array}\right) \tag{6}$$

where the submatrices $\mathbf{v}$ and $\mathbf{v}^T$ have the same number κ of elements equal to the repulsive two-electron matrix element V in each row and column. The extreme eigenvalues and eigenvectors are easily shown to be given by $\varepsilon \pm \kappa V$ and $(1, \pm 1)$. It may also be shown that when the submatrices $\mathbf{v}$ and $\mathbf{v}^T$ are full then all the other eigenvlues are at ε. Hence, despite the repulsive off diagonal matrix element, one state splits off from the others as in the case of attractive off-diagonal matrix elements.

To see the relevance of the above to cuprate superconductors consider an effective electronic Hamiltonian as the sum of one-body and two-body effective interactions. We adopt an extended Hubbard Hamiltonian postulated for the active space of the form

$$\mathcal{H} = \sum_{l,m} \langle l|\mathrm{h}|m\rangle a_l^+ a_m + \frac{1}{2} \sum_{k,l,m,n} \langle kl|\mathrm{g}|nm\rangle a_k^+ a_l^+ a_m a_n \tag{7}$$

where h and g are pertinent one and two body parts of the effective Hamiltonion and where the effective electron pair interaction, $g(i,j)$, is assumed to have a short

range repulsive hard core and a longer range attractive tail due to bipolaronic coupling. The summation in eq(7) is over cell orbitals and spins and where only on-cell and nearest neighbour matrix elements will be taken into account as significant in a localised basis.

If we suppose that there are N orbitals in the cuprate layer accessible to $2M$ electrons the fractional doping is given by $\rho = M/N$ where $1 \geq \rho \geq 0$ so that for hole doping a full set of cells with $\rho = 1$, and for electron doping $\rho = 0$, will be important. Cell orbitals in the cuprate layer can be occupied by a pair of singlet coupled electrons, a dimer ($\uparrow\downarrow$) or singly occupied by single unpaired electron with down ($\downarrow$) or up ($\uparrow$) spin. Every configuration of electrons arranged in the cuprate layer orbitals can be represented by a Slater determinant and an approximate many electron wavefunction obtained in principle from diagonalisation of the matrix representation of the Hamiltonian in the basis of Slater determinants.

Although an exact diagonalisation of such a Hamiltonian matrix is prohibitively arduous we are able to construct a mean-field theory. We assume, following the above arguments that there are a pair of localised Wannier type orbitals centred on each cell l of the form $\{\phi_{l,x}(\mathbf{r}), \phi_{l,y}(\mathbf{r})\}$ transforming together as the e degenerate irreducible representation in the C_{4v} point group. For mathematical expedience every pair of l, x orbitals is assigned a signature $(-1)^{l+1}$ and $(-1)^{l}$ for every pair of l, y orbitals. Hole doping is presumed to occur from a full valence band and electron doping into a vacant conduction band appropriate to the set of Wannier functions.

We consider first configurations in which $2M$ electrons giving M pairs of electrons are distributed over the lattice containing $N/2$ Cu atoms and N e-orbitals. Thus, there are $(N - M) = N_h$ hole pairs. Each of these is described by a Slater determinant ψ_k. The many electron state function is expanded in a basis of Slater determinants $\{\psi_k\}$ where each Slater determinant describing the configuration k of the filling of the e-basis orbitals on the cuprate lattice has an overall signature given by the product of all the signatures of the occupied orbitals in the configuration. The interaction between basis functions occurs in the off-diagonal blocks of the Hamiltonian matrix since matrix elements between two different Slater determinants basis functions are only finite when there is one Wannier pair different in the occupation numbers. In such a case the Hamiltonian matrix element is a two-electron integral of the type

$$V = \langle \phi_{i,x}(r_1)\phi_{i,x}(r_2)|g(1,2)|\phi_{j,x}(r_2)\phi_{j,x}(r_1)\rangle \tag{8}$$

for pair transfers between x-x orbitals, and similarly for y-y for different cells. Intracell x-y transfers have a corresponding matrix element V. Such matrix elements are non-zero only by virtue of some region of orbital overlap. Hence all integrals beyond nearest neighbour interactions are neglible in a localised basis and can be neglected. Only x-x and y-y nearest neighbour transfers and intracell x-y transfers which are significant energetically and these, remarkably, are between configurations having opposite signatures.

Every Slater determinant basis function, represented in the Hamiltonian matrix, corresponds to a unique arrangement of electrons on the cuprate layer and these can be grouped into $N!/(N-M_\uparrow-M_\downarrow)!M_\uparrow!M_\downarrow!$ sets corresponding to the possible ways of arranging the spin down ($\downarrow$) and up ($\uparrow$) spin monomers and to sub-classify the grouping of the remaining $(N-M_\uparrow-M_\downarrow)!/(N-M_\uparrow-M_\downarrow-M_D!)M_D!$ dimer ($\uparrow\downarrow$) configurations into 2 classes resolved by the $\pm$ sign of the product of the occupied dimer orbital signatures as described in detail in [18]. Thus collected, and neglecting the coupling between blocks the Hamiltonian matrix has a block form to be presented below. The off-diagonal coupling is most important for pair transfers between Slater determinant basis functions of opposite signature.

Every block j shown in the Hamiltonial matrix below has $g_j(M_\uparrow,M_\downarrow)=N!/(N-M_\uparrow-M_\downarrow)!M_\uparrow!M_\downarrow!$ quasi-degenerate states. If Δ is the diagonal cell interaction then pairs in the same cell will experience an interaction of roughly the magnitude of $\Delta\approx e^2\exp(-\gamma\xi)/d\xi$ where d is the background dielectric constant due to polarisable core electrons, ξ is the cell size (about 4Å) and γ is the Thomas-Fermi screening length given by $\gamma^2=[16\pi^2me^2(3\eta_c/\pi)^{1/3}]/dh^2$ where η_c is the carrier density given by $2M/\xi^3$ for electrons and $2N_h/\xi^3$ for holes [32,35,36]. Δ is then repulsive and dominated by the screened Coulomb repulsion at short range. This is the same appearance as presented in [19].

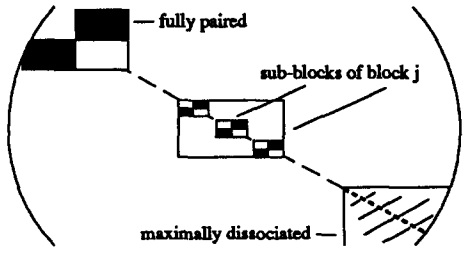

The ground state wavefunction is given by the geminal power

$$(N!/(N-M)!M!)^{-\frac{1}{2}}(1/M!)\left[\sum_l \exp(i\pi l)(a^+_{lx\uparrow}a^+_{lx\downarrow} - a^+_{ly\uparrow}a^+_{ly\downarrow})\right]^M |0) \qquad (9)$$

Following Dunne [19] relative to the completely dissociated state an estimate of the energy per orbital (relative to the normal state) for superconductive hole doping is $\Delta(1-\rho) - (2V+v)\rho(1-\rho)$. For electron doping the corresponding expression is $\Delta\rho - (2V+v)\rho(1-\rho)$. The first part of each term is the work required to bring electrons together while the second is the correlation energy.

To calculate thermal properties of the superconductor excited state energies and state functions are necessary and are obtained as follows. Every block j of the Hamiltonian matrix has $g_j(M_\uparrow, M_\downarrow)$ low-lying states with eigenvectors which are a linear combination of the sub-block degenerate states which may be mixed together to give excited state wavefunctions of the form

$$(N!/M_D!(N-M_\uparrow-M_\downarrow-M_D)!M_\uparrow!M_\downarrow!)^{-\frac{1}{2}}\sum_s c_s\psi_s \qquad (10)$$

where $|c_s| = 1$ and $s = 1,2,\ldots,g_j(M_\uparrow, M_\downarrow)$ refers to the sub-block s with eigenvector ψ_s of the block j of our concern. The above wavefunction describes a general state of the superconductor for any degree of pair dissociation up to T_c.

It is important to note that every sub-block in the Hamiltonian matrix has the form displayed in eq(6) above. If $X = M_D/N$ then $\Delta(X)$ will depend on the level of dimer dissociation. We will estimate $\Delta(X)$ by linearising in the density of condensed electrons derived below to give an average energy $X(1-2\rho+X)(\Delta/\rho - (2V+v))$ for hole doping and $X(1-2\rho+X)(\Delta/(1-\rho) - (2V+v))$ for electron doping relative to the completely dissociated normal state described by the lowest block on the right hand side of the Hamiltonian matrix. Δ is the screened diagonal Coulomb repulsion for bringing electrons into the same orbital when its neighbours are fully paired. The linearisation procedure adopted here to estimate the doping dependence of $\Delta(X)$ is likely to be reliable at low doping and can implicitly embrace a number of effects not considered here but we do not anticipate this to be a good semblance to reality at high doping.

The second order electronic density matrix can be constructed from the Hamiltonian matrix eigenvector given in eq(10) above to give

$$\begin{pmatrix} M_D/N & -\frac{M_D(N-2M+M_D)}{N(N-1)} & \cdots & \cdots \\ -\frac{M_D(N-2M+M_D)}{N(N-1)} & M_D/N & \cdots & \cdots \\ \vdots & \vdots & \ddots & \vdots \\ \cdots & \cdots & \cdots & M_D/N \end{pmatrix} \times \begin{pmatrix} 1 \\ -1 \\ \vdots \\ \cdots \end{pmatrix}$$

$$= [X + M_D(1 - 2\rho + X)] \begin{pmatrix} 1 \\ -1 \\ \vdots \\ \cdots \end{pmatrix} \tag{11}$$

This can be seen to have a macroscopically large eigenvalue signifying a condensate of pairs of electrons. All $g_j(M_\uparrow, M_\downarrow)$ low-lying states have the same density matrix eigenvector and eigenvalue.

Consequently the thermally averaged second order reduced electronic density matrix eigenvector is

$$\psi(\mathbf{r}_1\sigma_1, \mathbf{r}_2\sigma_2) = \lambda \sum_l (-1)^l [\phi_{lx}(\mathbf{r}_1)\phi_{lx}(\mathbf{r}_2) - \phi_{ly}(\mathbf{r}_2)\phi_{ly}(\mathbf{r}_1)](\uparrow(1)\downarrow(2) - \uparrow(2)\downarrow(1)) \tag{12}$$

which has $d_{x^2-y^2}$ pair symmetry in the C_{4v} group in conformity with experimental determinations of the condensate symmetry in high T_c superconducting cuprates. The function $\psi(\mathbf{r}_1\sigma_1, \mathbf{r}_2\sigma_2)$ transforms as the B_1 irreducible representation in the C_{4v} group. λ is the macroscopically large reduced second order electronic density matrix eigenvalue corresponding to a population $M_D(1 - 2\rho + X)$ condensed pairs of electrons where X is calculated by minimisation of the Helmholtz free energy F defined in section 5 below. The range over which $\psi(\mathbf{r}_1\sigma_1, \mathbf{r}_2\sigma_2)$ stays finite as $|\mathbf{r}_1 - \mathbf{r}_2|$ increases is a measure of the pair size or coherence length and in this theory, in view of the localised basis, this quantity is of the order of a few Angstroms in conformity with experimental observations [1-15].

The last term in eq(12) is the singlet spin function which multiplies the entire pair space state function which has $^1B_1$ symmetry in the C_{4v} group and where $\alpha(1), \beta(1)$ are spin eigenfunctions. If the above result is reliable we should be able to predict the electronic energy bands associated with the Wannier functions. Following Alexandrov [8] in the tight binding approximation we obtain an X-band and Y-band each with dispersion relations given by

$$E_x(k) = -2\beta_\sigma \cos(k_x) - 2\beta_\pi Cos(k_y)$$

and

$$E_y(k) = -2\beta_\sigma \cos(k_y) - 2\beta_\pi \cos(k_x) \tag{13}$$

where β_σ and β_π are the transfer integrals in the σ and π configurations for nearest neighbour Wannier functions and where we take, because of overlap anisotropy, $\beta_\sigma/\beta_\pi = 4$. The Fermi surface is constructed by taking the higher of the $E_x(k), E_y(k)$ for a given $\mathbf{k} = (k_x, k_y)$ where the lattice constant is set to 1. The resulting highest energy level dispersion relation for $\beta_\sigma = 0.2$ eV is shown in Figure 3.

The fundamental features of the ARPES spectra reported by Shen et al. are reproduced with the experimental error which is about 0.1 eV in energy and 0.1 π in wavevector.

5. Thermal Behaviour of Superconducting Cuprates

Following the arguments of ref [19] the Helmholtz free energy per orbital, F, is given up to T_c by

$$\begin{aligned} F = kT[(1-2\rho+2X)\ln(1-2\rho+2X) + 2(\rho - X)\ln(\rho - X)] \\ + (-2V - v + \Delta/t)(1-2\rho+X)X \end{aligned} \tag{14}$$

where $t = \rho$ when $\rho > 1/2$ and $t = (1-\rho)$ when $\rho < 1/2$. This is simply derived using the degeneracy factor $g_j(M_\uparrow, M_\downarrow)$ and energy relative to the normal state E_j for each block j given above and the formula $F = -(kT/N)\ln Q$ where $Q = \sum g_j \exp(-E_j/kT)$ is the canonical partition function and where the logarithm of the sum is evaluated by the method of the maximum term. Therefore minimisation of F with respect to X gives the equilibrium condition as a solution of the non-linear equation

$$2kT\ln[(1-2\rho+2X)/(\rho - X)] + (-2V - v + \Delta/t)(1-2\rho+2X) = 0 \tag{15}$$

The root of this non-linear equation gives the equilibrium value of X and for that reason the density of condensed electrons. The transition temperature can be located by noting that at T_c the equilibrium values of X are constrained by $X = 0$ for electron doping and $X = (2\rho - 1)$ for hole doping corresponding to zero density of condensed electrons. Insertion of these conditions into eq(15) gives the transition temperature T_c for both doping cases given by

$$kT_c = (2V + v - \Delta/(1-\rho))(1-2\rho)/2\ln[(1-2\rho)/\rho] \tag{16a}$$

for electron doping when $\rho < 1/2$ and

$$kT_c = (2V + v - \Delta/\rho)(2\rho - 1)/2\ln[(2\rho-1)/(1-\rho)] \tag{16b}$$

for hole doping when $\rho > 1/2$.

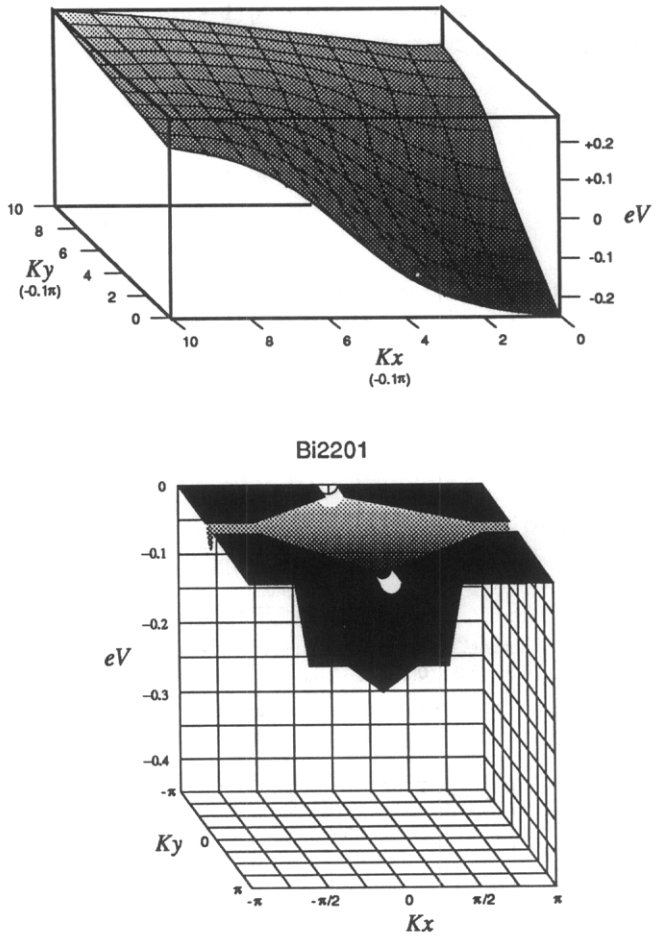

Figure 3 Dispersion relation for the uppermost energy levels for the $E_x(\mathbf{k})$, $E_y(\mathbf{k})$ bands discussed in the text for a given $\mathbf{k} = (k_x, k_y)$. The energy surface has fourfold symmetry about the origin. The result is compared with the photoemission data of Shen *et al* [7] also shown in the lower part of the figure.

The doping phase diagram implied by eqs(16a,16b) is shown in Figure 4 (which also demonstrates the well known electron-hole symmetry) and, for reasonable values of matrix elements and background dielectric constant given in the caption to Figure 4, our theory depicts superconductivity at high temperatures in the same doping range as for cuprates. The temperature and doping dependence of the energy gap can also be derived as follows. The energy to remove one electron

$$E_g(0) = 2V + v - \Delta/(1-\rho) \tag{17a}$$

for electron doping when $\rho < 1/2$ and

$$E_g(0) = 2V + v - \Delta/\rho \tag{17b}$$

for hole doping when $\rho > 1/2$.

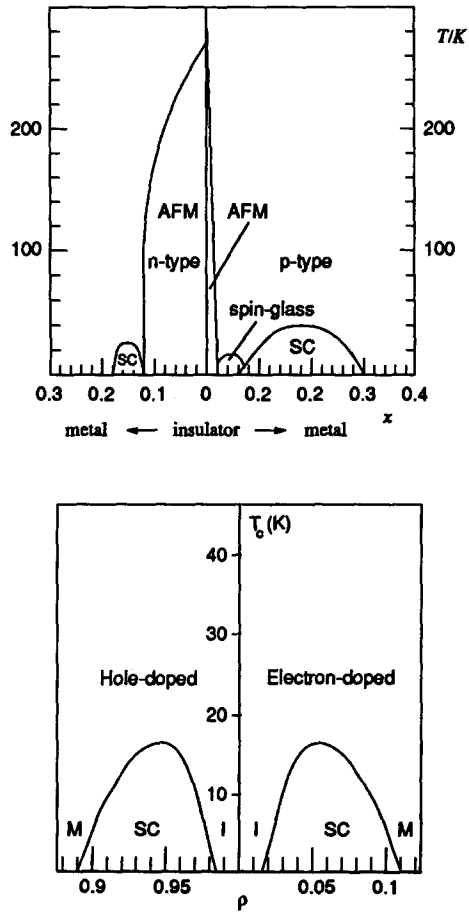

Figure 4 Theoretical doping dependence of the transition temperature predicted by our theory for the parameters $D = 5$, 2V+v= 0.564eV compared with the well known experimental doping T_c curve presented above.

This gives the ratio $E_g(0)/k\mathrm{T_c}$, given by

$$E_g(0)/k\mathrm{T_c} = 2\ln[(1-2\rho)/\rho]/(1-2\rho) \tag{18a}$$

for electron doping when $\rho < 1/2$ and

$$E_g(0)/k\mathrm{T_c} = 2\ln[(2\rho-1)/(1-\rho)]/(2\rho-1) \tag{18b}$$

for hole doping when $\rho > 1/2$.

These results represent an average of the energy gap over k-space.

It is worth remarking that the doping ranges shown in Figure 4 are relevant to cuprates. For example in $La_{2-x}Sr_xCuO_4$ the optimal doping is close x = 0.2 corresponding to 0.1 hole pairs/cell or 0.05 hole pairs per e-orbital.

At finite temperature the energy gap is the difference between the eigenvalues of two neighbouring blocks of the Hamiltonian matrix and given by

$$E_g(T) = (1-2\rho+2X)(2V+v-\Delta/(1-\rho)) \tag{19a}$$

for electron doping when $\rho < 1/2$ and

$$E_g(T) = (1-2\rho+2X)(2V+v-\Delta/\rho) \tag{19b}$$

for hole doping when $\rho > 1/2$.

The predictions of this for hole doping are shown in Figure 5. A comparison can be made with a recent collection of gap measurements given by Deutscher [3] where the above so-called strong coupling ratio varies from about 20 to 6 and falls with rising doping levels as predicted by our theory.

6. Temperature and Doping Dependence

The prediction that the zero temperature density of condensed electrons should be proportional to $\rho(1-\rho)$ is tested against experimental observations in Figure 6 where the hole concentration is estimated from the chemical formula.

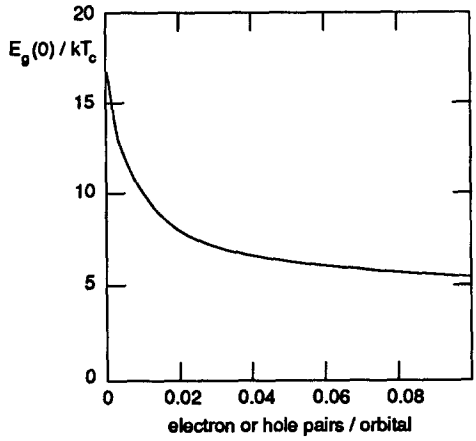

Figure 5 Theoretical gap ratios $E_g(0)/(kT_c)$ as a function of doping for superconducting cuprates.

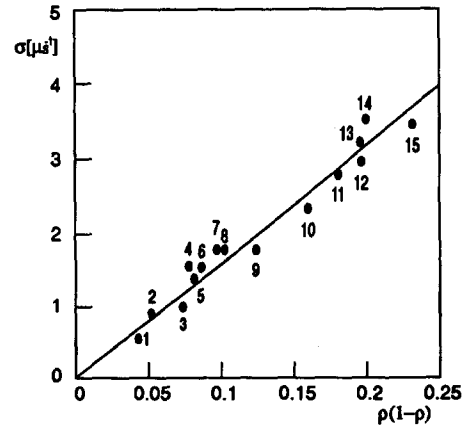

Figure 6 Plot of muon spin relaxation rate, ϕ, against $2\rho(1-\rho)$ for $La_{2-x}Sr_xCuO_4$ and $YBa_2Cu_3O_y$. The experimental measurements are from Uemura [33] and $2\rho(1-\rho)$ is estimated from the chemical formula of cuprates by valence counting.. There are 14 points starting from the left which correspond to the following x or y values. 1. $x = 0.08$, 2. $x = 0.1$, 3. $x = 0.15$, 4. $x = 0.15$, 5. $y = 6.66$ 6. $y = 6.67$, 7. $x = 0.20$, 8. $x = 0.21$, 9. $y = 6.67$, 10. $y = 6.86$, 11. $y = 6.95$, 12. $y = 6.95$, 13. $y = 7.0$, 14. $y = 7.0$, 15. $Y_{0.7}Ca^{2+}_{0.3}Ba_2Cu_3O_7$. The linear fit for this theory differs slightly from one given previously [26].

It can be seen that the prediction is in satisfactory agreement with experimental observations [33]. The temperature dependence of the density of condensed electrons is shown in Figure 7 which has utilised the thermal average of the density

of condensed electrons obtained as described above.

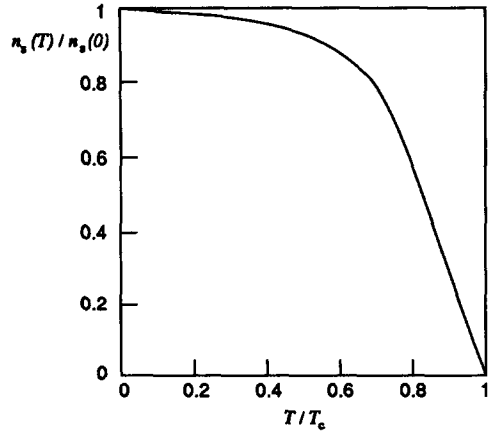

Figure 7 Theoretical temperature dependence of the condensate density.

The response for low doping closely follows a two-fluid type behaviour for low hole doping but which deviates from this at higher doping levels.

7. Condensation Energy and Heat Capacity

Heat capacity measurements on superconducting cuprates have been widely undertaken and recently Loram *et al* [29] reported condensation energies for a cuprate superconductor as a function of doping. In our theory the heat capacity per localised orbital (C_v/N_K) is given by

$$C_v/N_K = 2kT \ln[(\rho - X)(1 - 2\rho + 2X)] \frac{\mathrm{d}(X)}{\mathrm{d}(kT)} \tag{20}$$

which is obtained in the standard way from F given in eq(15). The condensation energy is given above in section 4. The trends shown by the theory are shown in Figure 8.

The heat capacity in the overdoped regime is predicted to be a few times larger than the underdoped. These unusual features seem to agree with experimental observations [29]. However to gain a reasonable agreement we must either suppose that a significant fraction of the paired holes remain localised and, perhaps due to the random potential introduced by doping, are inactive up to T_c. This may be due to stripe regions as introduced by Tranquada [39]. An alternative possibility is that this mean field theory overestimates the heat capacity by a factor of about

four as would, for example, be found in any mean field theory treatment of any system with reduced dimensionality. Note that Figure 9 shows the T_c doping curve for the parameters $2V + v = 0.592$ eV assuming that only ~1/4 of the holes are active in the superconductivity or that fluctations have severely broadened out the experimental heat capacity data.

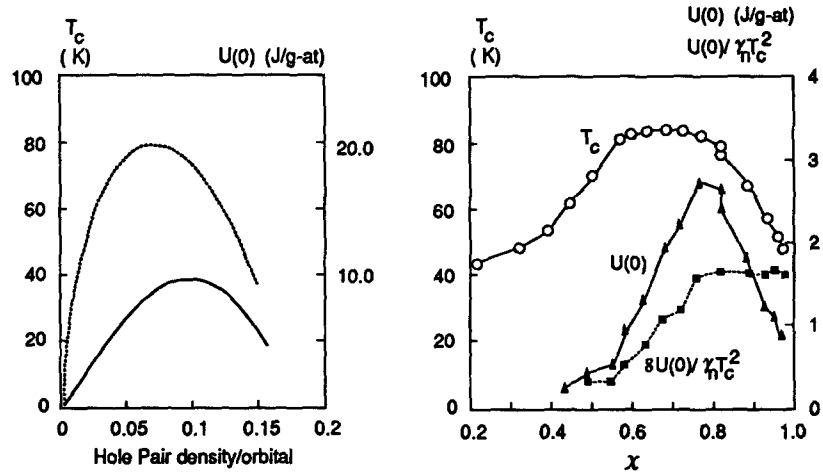

Figure 8 Theoretical T_c/doping behaviour and condensation energy shown on the left compared with experimental data from the Cambridge group (Cooper, Loram *et al* for YBCO(Ca 20%) shown on the right. The trends and relative peak positions are well described by the model.

Figures 9a, 9b, 9c show the trends in the heat capacity given by the model compared with the data measured by the Cambridge group.

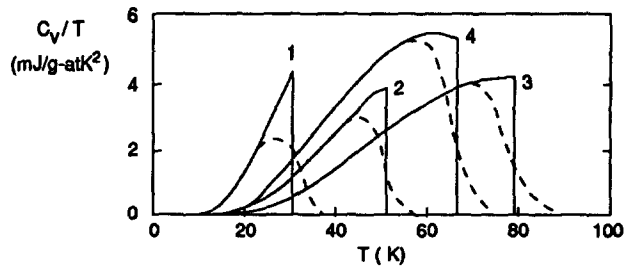

Figure 9a Theoretical predictions of γ. Peaks 1, 2, 3 relate to the under-doped regime (compare with Figure 9b) while peak 4 relates to the over-doped regime (compare with Figure 9c). The broken lines are the expected effect of fluctuations not included in our model.

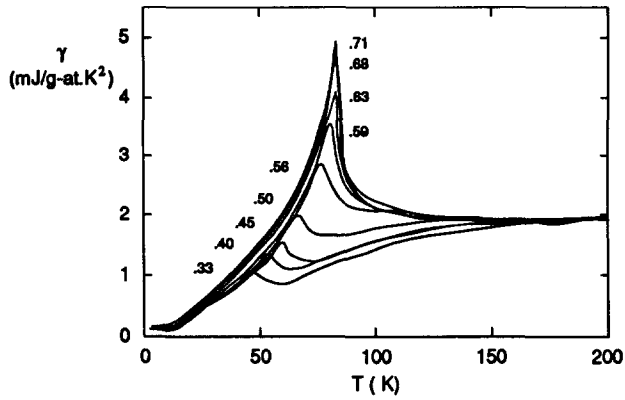

Figure 9b Experimental data from the Cambridge group (Cooper, Loram *et al* [29]) for YBCO(Ca 20%) for heat capacity in the under-doped regime

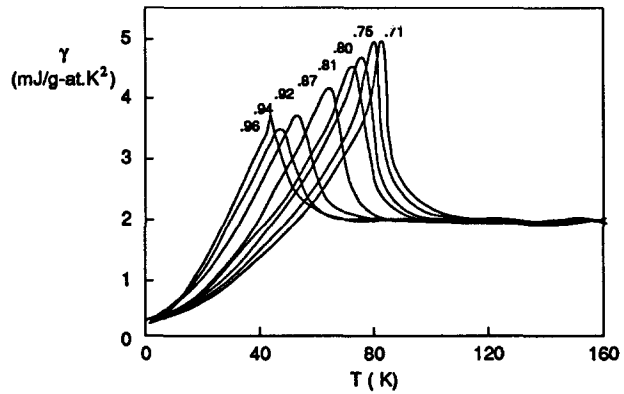

Figure 9c Experimental data from the Cambridge group (Cooper, Loram *et al* [29]) for YBCO(Ca 20%) for heat capacity in the over-doped regime

8. Summary and Conclusion

In summary, the theoretical model makes predictions for weakly doped cuprates for temperatures up to T_c where the trends are in remarkable agreement with experimentation. Our end conclusion is that high temperature superconductivity is primarily an electron correlation effect possibly supplemented by longer range polaronic attraction of the type discussed by Mott and Alexandrov (see [8,9] for other references). The 'spin gap', which is a widely recognised property of cuprates, and which is resposible for much of the magnetic susceptibility above T_c is possibly due to removal of the antiferromagnetic spin cloud which dresses layer electrons but a detailed theory remains to be worked out.

Acknowledgments

This paper is dedicated with gratitude and respect to the memory of Professor Per-Olov Löwdin.

References

[1] B. Batlogg (1997) *Physica C* **282-287**, xxiv-xxx
[2] T.M Rice (1997) *Physica C* **282-287**, xix-xxiii
[3] G. Deutscher (1999) *Nature* **397**, 410-412
[4] V.JEmery,S.A.Kivelson,O.Zachar (1997) *PhysicaC* **282-287**, 174
[5] D. Pines (1997) *Physica C* **282-287**, 273-278
[6] S. G Ovchinikov (1997) *Uspekhi (Physics)* **40**(10), 993-1017
[7] L.J Dunne,E.J Brändas, J. N Murrell and V. Coropceanu (1998) *Solid State Comm.* **108**, 410-412
[8] A.S Alexandrov (1996) *Phys Rev.* **53 B**, 2863-2869
[9] A.S Alexandrov and N. F Mott (1994) *Rep. Prog. Phys.* **57**,
[10] Z.X Shen, W.E Spicer, D.M King, D.S Dessau and B.O Wells (1995) *Science* **267**, 343-350
[11] M Sigrist and T.M Ricer (1995) *RevMod. Physics* **67**, 503-513
[12] D.A Wollman, D.J Van Harlingen, W.C Lee, D.M Ginsberg and A.J Leggett (1993) *Phys.RevLett.* **71**, 2134-2137
& D J Van Harlingen (1997) *Physica* C **282-287**, 128-131
[14] D.J Van Harlingen (1995) *RevMod. Physics* **67**, 503-513
[15] C.C Tsuei and J.R Kirtley (1997) *Physica* C **282-287**, 4-12
[16] J.F Annett, N. Goldenfeld, A.J Leggett, J.Low. (1996) *Temp. Phys.* **105**, 473-482
[17] L J Dunne (1997) *Physica* C **282-287**, 1787-1788
[18] L.J Dunne, J.N Murrell and E.J Brändas (1990) *Physica* C **169**, 501-507
[19] L.J Dunne (1994) *Physica* C **223**, 291-312
[20] C.N Yang (1989) *Phys. Rev. Lett.* **63**, 2144-2148
[21] C.N Yang (1962) *Rev. Mod. Phys.* **34**, 694-704
[22] A.J Coleman (1967) *Can. J. Phys.* **45**, 1271-1273
[23] L.P Gor'kov (1958) *J. Exp. Teoret. Phys.* **38**, 735-739
& L.P Gor'kov (1958) Translation of ref [23] *J. Exp. Teoret. Phys.* **7**, 505-509
& L.J Dunne and T.P Spiller (1993) *J.Phys: Condens. Matter* **5**, 145
[26] L.J Dunne and T.P Spiller (1992) *J.Phys: Condens. Matter* **4**, L563-L566

[27] P.P Edwards, T.V Ramakrishnan and C.N.R Rao (1995) *J. Phys.Chem.* **99**, 5228-5239
[28] L.Jansen and M. Boon (1967) *Theory of Finite Groups. Applications in Physics*, North-Holland Publishing Co., Amsterdam
[29] J.W Loram, K.A Mirza, J.R Cooper and J.L Tallon (1997) *Physica* C **282-287**, 1405-1406
[30] S.E Barrett, J.A Martindale, D.J Durand, C.P Pennington, C.P Slichter, T.A Friedman, J.P Rice, and D.M Ginsberg (1991) *Phys.RevLett* **66**, 108-111
[31] R. S Liu and P.P Edwards (1993) *Synthesis and Characterisation of High Temperature Superconductors*, Trans. Tech. Publ. Ltd., Switzerland
[32] N F Mott and E. A Davis (1971) *Electronic Processses in Non-Crystalline Materials*, Claerdon Press, Oxford
[33] Y.J Uemura *et al* (1989) *Phys. Rev. Lett.* **62**, 2317-2321
[34] T Schneider and H. Keller (1992) *Phys. Rev Lett.* **69**, 3374-3378
[35] P.P Edwards and M.J Sienko (1987) *Phys.Rev.* **B17**, 2575-2581
[36] C Kittel (1971) *An Introduction to Solid State Physics*, J. Wiley, New York
[37] L. Jansen and R. Block (1994) *Physica* **212**, 143
[38] E.J Brändas (1995) *Dynamics During Spectroscopic Transitions*, Eds E. Lippert and J.D Macomber, Springer-Verlag, Berlin
[39] J.M Tranquada (1997) *Physica* **282**, 166
[40] J.N Murrell, S.F.A Kettle, J.M Tedder (1965) *Valence Theory*, J.Wiley & Sons, London
[41] G Rickaysen (1971) *Essays In Physics* **3**, 1-34
[42] Atkins, P.W, Child, M.S and Philips, C.S.G (1970) *Tables for Group Theory*, Clarendon Press, Oxford
[43] L.Jansen, M. Boon (1967) *Theory of Finite Groups.Applications in Physics*, North-Holland Publishing Co., Amsterdam
[44] H. Eskes, L.H Tjeng and G.A Sawatzky (1990) *Phys.Rev* **41B**, 288-299
[45] H.U Suter, E.P Stoll, P.Hüsser, S. Schafroth and P.F Meier (1997) *Physica C* **282-287**, 1639-1640
[46] D.D Sarma and C.N.R Rao (1988) *Solid State Commun* **65**, 47-49

Orthogonalization of vectors and its relation to cognitive phenomena

Vipin Srivastava*
School of Physics, University of Hyderabad, Hyderabad 500 046, India

Abstract
A geometrical view of all known orthogonalization procedures is taken to understand their distinctive features and the inter-connections between them. Curious new information is gained which is also found useful to understand the basis of certain cognitive phenomena, like discrimination and categorisation. A spin-glass like neural network model has been introduced to understand the cognitive phenomena.

Contents

1. INTRODUCTION

The problem of conversion of a given set of linearly-independent vectors into a set of mutually orthogonal vectors has been studied for a long time. It finds wide applications in mathematics, physics and chemistry. The methods involve a straight forward and simple mathematics and differ in special conditions they satisfy. We present a simple analysis of the orthogonalization methods in terms of the projections of the given vectors on the orthogonalized bases vectors and find that the methods possess some powerful properties hitherto unknown. The discovered properties are not only curious but also have algorithmic value in that they enable geometrical constructions of the orthogonal basis sets and the eigenvalues of the metric matrix of the given vector-set. These properties also underline the scenarios where the different methods should be applicable.

We also discuss briefly the spin-glass like neural network model for memory [1] and show that orthogonalization of vectors could be intimately related with the brain's capability to discriminate among memories. We study Gram-Schmidt's orthogonalization in connection with sequential learning and find useful insight. We expect that the new understanding gained about the non-sequential orthogonalizations should provide clues to understand the memories based on non-sequential learning.

ADVANCES IN QUANTUM CHEMISTRY, VOLUME 40

0065-3276/01 $35.00

2. ORTHOGONALIZATION METHODS

The Gram-Schmidt orthogonalization procedure, the oldest and commonly used in mathematics (also applied to neural networks [1]), gives an orthonormal set depending on the *sequence* in which the given vectors are picked. The work on *sequence-independent* orthogonalization, in a particular context of physical problems, was started by Landshoff [2] and Wannier [3], and later developed comprehensively by Löwdin [4]. Two notable methods of this class are Löwdin's *Symmetric* [5] and *Canonical* [6] orthogonalizations. The Symmetric orthogonalization contains the results of Landshoff and Wannier [4]. The Canonical orthogonalization is generally known in the physics literature (see [7] for references) after Schweinler and Wigner [8] (hereafter referred to as S-W) who in fact introduced a versatile parameter "m" that highlighted an *extremal* property of Löwdin's Canonical orthogonalization. Earlier Löwdin [9] had talked about an *optimum-principle* obeyed by the Canonical orthogonalization which we find in a sense resembles the S-W extremal property. Recently Chaturvedi et al. [7] have given a new orthonormal basis that has another extremal property in terms of the S-W parameter m.

Let $\mathbf{V}$ represent a set of linearly independent vectors, $\vec{v}_1, \vec{v}_2, \vec{v}_3, \cdots, \vec{v}_N$, in a N- dimensional space which can in general be a complex vector space. We can define a general non-singular linear transformation $\mathbf{A}$ for the basis $\mathbf{V}$ to go to a new basis $\mathbf{Z}$:

$$\mathbf{Z} = \mathbf{VA}\,. \tag{1}$$

The set $\mathbf{Z}(\equiv \{\vec{z}_\kappa\})$ will be orthonormal if

$$< \mathbf{Z}|\mathbf{Z} >=< \mathbf{VA}|\mathbf{VA} >= \mathbf{A}^\dagger < \mathbf{V}|\mathbf{V} > \mathbf{A} = \mathbf{A}^\dagger\mathbf{MA} = \mathbf{I}\,, \tag{2}$$

where $\mathbf{M}$ is a Hermitian metric matrix of the given basis $\mathbf{V}$. The substitution

$$\mathbf{A} = \mathbf{M}^{-1/2}\mathbf{B}\,, \tag{3}$$

where $\mathbf{B}$ is an arbitrary unitary matrix, leads to the general solution of the orthogonalization problem. The specific choice $\mathbf{B} = \mathbf{I}$ gives the *Symmetric Orthogonalization*, $\mathbf{Z} \equiv \mathbf{\Phi} = \mathbf{VM}^{-1/2}$, while $\mathbf{B} = \mathbf{U}$, where $\mathbf{U}$ diagonalizes $\mathbf{M}$,

$$\mathbf{U}^\dagger\mathbf{MU} = \mathbf{d}\,, \tag{4}$$

gives the *Canonical Orthogonalization*, $\mathbf{Z} \equiv \mathbf{\Lambda} = \mathbf{VUd}^{-1/2}$. The orthonormal basis due to Chaturvedi et al., denoted here by $\mathbf{\Gamma}$, is related to $\mathbf{\Lambda}$ [7], and coincides with $\mathbf{\Phi}$ in a particular circumstance indicated below.

3. A GEOMETRICAL VIEW

Taking our cue from Schweinler and Wigner [8] we consider the matrix

$$\begin{pmatrix} |(\vec{v}_1,\vec{z}_1)|^2 & |(\vec{v}_1,\vec{z}_2)|^2 & \dots & |(\vec{v}_1,\vec{z}_N)|^2 \\ |(\vec{v}_2,\vec{z}_1)|^2 & |(\vec{v}_2,\vec{z}_2)|^2 & \dots & |(\vec{v}_2,\vec{z}_N)|^2 \\ \vdots & \vdots & & \vdots \\ |(\vec{v}_N,\vec{z}_1)|^2 & |(\vec{v}_N,\vec{z}_2)|^2 & \dots & |(\vec{v}_N,\vec{z}_N)|^2 \end{pmatrix}$$

of projection-squares of the given vectors $\{\vec{v}_k\}$ on a basis set $\{\vec{z}_\kappa\}$. The elements in a row corresponding to a particular $\vec{v}_k$ add up to $|\vec{v}_k|^2$:

$$\sum_\kappa |(\vec{v}_k,\vec{z}_\kappa)|^2 = |\vec{v}_k|^2\,,\quad k=1,...,N\,, \tag{5}$$

and the elements in a column for a particular $\vec{z}_\kappa$ add up to a real positive number c_κ:

$$\sum_k |(\vec{v}_k,\vec{z}_\kappa)|^2 = (\mathbf{AMMA}^\dagger)_{\kappa\kappa} = (\mathbf{BMB}^\dagger)_{\kappa\kappa} = c_\kappa\,,\quad \kappa=1,...,N\,. \tag{6}$$

Note that we have the identity

$$\sum_{\kappa=1}^{N} c_\kappa = \sum_{k=1}^{N} |\vec{v}_k|^2\,, \textit{a constant for a given set } \mathbf{V}\,. \tag{7a}$$

Further, we have

$$\sum_\kappa {c_\kappa}^2 = m,\ \textit{the } S-W \textit{ parameter.} \tag{7b}$$

A basis set $\mathbf{Z}$ will satisfy the set of simultaneous equations (6) with the positive real numbers c_κ's obeying the identity (7a). Specific bases will satisfy additional conditions on the values of c_κ's either through (7b) or otherwise. For instance, if $c_\kappa = |\vec{v}_k|^2$ with $\kappa = k$ (i.e. $\mathbf{B}$=$\mathbf{I}$ in (6)), we will get the *Symmetric* basis $\mathbf{Z} = \mathbf{\Phi}$; $m = m_{max}$, which will arise for the maximally lop-sided distribution of the c_κ's (satisfying (7a)), will give the *Canonical* basis $\mathbf{Z} = \mathbf{\Lambda}$; and $m = m_{min}$, which will correspond to an average distribution, $c_1 = c_2 = ... = c_N = (c_1 + c_2 + ... + c_N)/N$, will give the basis $\mathbf{Z} = \mathbf{\Gamma}$ of Chaturvedi et al. [7]. For normalized $\vec{v}_k$'s the basis $\mathbf{\Gamma}$ and the Symmetric basis $\mathbf{\Phi}$ become the same.

Following useful information is embedded in the above identification:

In the Symmetric case, where $\mathbf{Z} = \mathbf{\Phi}$, since the sum of squared-projections of all the $\vec{v_k}$'s on a $\vec{\phi}_\kappa$, say $\vec{\phi}_l$, is equal to the sum of squared-projections of all the $\vec{\phi}_\kappa$'s on the $\vec{v_k}$ with $k = l$, the symmetry properties of $\mathbf{V}$, if any, are preserved in $\mathbf{\Phi}$. This feature also ensures that $\mathbf{\Phi}$ resembles the original set $\mathbf{V}$ in that Löwdin's resemblance measure [4], $\langle \mathbf{Z}-\mathbf{V}|\mathbf{Z}-\mathbf{V}\rangle$, has its smallest value when $\mathbf{B}$=$\mathbf{I}$ or $\mathbf{Z} = \mathbf{\Phi}$. If seen slightly differently, the above symmetry interestingly implies that the squared-projections of all the $\vec{v_k}$'s on a $\vec{\phi}_l$ add up to the squared length of $\vec{v}_l$, the feature that can be used to geometrically generate the Symmetric basis set.

The last property above turns into a stricter condition in the case of $m = m_{min}$, where $\mathbf{Z} = \mathbf{\Gamma}$: the basis vectors $\vec{\gamma}_\kappa$ are arranged such that the sum of squared-projections of all the $\vec{v}_k$'s on each $\vec{\gamma}_\kappa$ is the *same* – equal to the average of $|\vec{v}_k|^2$ – irrespective of how the $\vec{v}_k$'s are arranged. In effect, the set $\mathbf{\Gamma}$ is arranged so as to cancel the effects of inhomogeneity in the distribution of $\vec{v}_k$'s.

On the other hand in the $m = m_{max}$ case, with $\mathbf{Z} = \mathbf{\Lambda}$, the basis vectors $\vec{\lambda}_\kappa$'s must be oriented such that they sample those directions in which bunches of $\vec{v}_k$'s tend to be oriented. In order to attain $m = m_{max}$ the Canonical basis set is arranged in such an optimal fashion that the sum of squared-projections of all the $\vec{v}_k$'s on one of the $\vec{\lambda}_\kappa$'s, say $\vec{\lambda}_1$ – *i.e.* c_1 – is the largest. After the $\vec{\lambda}_1$, is fixed, the rest of the set, orthogonal to $\vec{\lambda}_1$, is oriented such that another $\vec{\lambda}_\kappa$, say $\vec{\lambda}_2$, is able to maximise the *total* squared-projection of all the $\vec{v}_k$'s on it. This will be c_2 and will be smaller than c_1. All the $\vec{\lambda}_\kappa$'s are arranged according to this optimum-principle that ensures for the given set $\{\vec{v}_k\}$ the most lop-sided distribution of c_κ's with $c_1 > c_2 > ... > c_N$. This particular set of c_κ's in fact comprises the eigenvalues of $\mathbf{M}$ in the basis $\mathbf{\Lambda}$ (take $\mathbf{B}$=$\mathbf{U}$ in eqn.(6)) which are generically non-degenerate. The arrangement of $\vec{\lambda}_\kappa$'s that yields the S-W condition of $m = m_{max}$ manifests Löwdin's optimal property [4,9] of the Canonical orthogonalization. Note that just as the c_κ gains its largest values $(\mathbf{d})_{\kappa\kappa}$ for $\mathbf{B}$=$\mathbf{U}$, the quantity

$$\sum_\alpha |A_{\alpha\kappa}|^2 = (\mathbf{A}^\dagger\mathbf{A})_{\kappa\kappa} = (\mathbf{B}^\dagger\mathbf{M}^{-1}\mathbf{B})_{\kappa\kappa}\,, \tag{8}$$

has its smallest values for $\mathbf{B}$=$\mathbf{U}$, in which case it is $(\mathbf{d}^{-1})_{\kappa\kappa}$. If d_1^{-1} is the smallest value and the associated basis vector is $\vec{\lambda}_1$, Löwdin [9] showed that for all vectors orthogonal to $\vec{\lambda}_1$ the sum $\sum_\alpha |A_{\alpha\kappa}|^2$ has the smallest value $d_2^{-1}(> d_1^{-1})$ associated with $\vec{\lambda}_2$, and that one can go on in this manner to find the smallest d_κ^{-1}'s associated with the respective $\vec{\lambda}_\kappa$'s.

It should be noted that the value of m_{max} depends on the distribution of orientations of $\vec{v}_k$'s relative to each other, whereas the value of m_{min} is independent of this. There can be any number of $\mathbf{V}$'s satisfying a particular identity (7a) but differing in distributions of orientations of the vectors $\vec{v}_k$'s. Each of these will have a different m_{max} but the same m_{min}. The inhomogeneity in the distribution of directions of a given set of vectors will decide the value of m_{max} – the larger the inhomogeneity, the larger will be the value of m_{max}.

Now we will examine the Gram-Schmidt orthogonalization (represented by $\mathbf{Z}$=$\mathbf{\Omega}$) in the framework of eqns. (6). The bases $\mathbf{\Omega}$ (= $\{\vec{\omega}_\kappa\}$), where for a predetermined sequence of $\vec{v}_k$'s a sequence of $\vec{\omega}_\kappa$'s is generated such that a $\vec{v}_k$ has non-zero projections only on those $\vec{\omega}_\kappa$'s for which $\kappa \leq k$, satisfy the modified set of equations (6) with $|(\vec{v}_k, \vec{z}_\kappa)|^2$=0 for all $\kappa > k$ together with the identity (7a). It is clear at the outset that none of the $\mathbf{\Omega}$'s ($N!$ in number) can coincide with the Symmetric basis $\mathbf{\Phi}$, since for any $\mathbf{\Omega}$ at least c_1 is necessarily greater than $|\vec{v}_1|^2$. But, an $\mathbf{\Omega}$ corresponding to a certain sequence of $\vec{v}_k$'s can accidently coincide with the bases $\mathbf{\Gamma}$ or $\mathbf{\Lambda}$. The possibility of the coincidence with $\mathbf{\Gamma}$ will however be precluded if the $\vec{v}_k$'s are normalized for then $\mathbf{\Gamma}$ coincides with $\mathbf{\Phi}$ as seen above.

To conclude this section we summarise that it is easy to visualise all the orthogonalization methods in terms of the projections of the given vectors on the orthogonal bases and that this exercise elucidates interesting geometrical features of the orthogonalized bases hidden in their optimal, extremal and symmetry properties and also shows how these basis sets as well as the eigenvalues of the metric matrix of the given $\mathbf{V}$ can be constructed purely from geometrical considerations.

We will now review the neural network model for memory and study how the knowledge of orthogonalization methods can help us in understanding certain cognitive functions.

4. NEURAL NETWORK MODEL FOR MEMORY

All types of perceptions – due to sight, touch, hearing etc. – lead to neural activities and are translated into patterns of firing and quiescent neurons. In a system of N neurons such a pattern corresponding to (say) an object can be represented by an N-dimensional vector $\vec{\xi}$ whose N components ξ_i's are either $+1$ or -1 which respectively represent firing and quiescent neurons. Neurons tend to have either a high or a low activity level. So, the model treats them as binary objects which are either active or inactive. A configuration of $+1$ and -1 will represent a stable state of the neural system, and hence a memory, if the following function H representing the total energy of the system is minimised by it:

$$H = -\frac{1}{2}\sum_{i,j=1}^{N} J_{ij}\xi_i\xi_j \ . \tag{9}$$

Two neurons bearing values ξ_i and ξ_j (which can be $+1$ or -1) interact via J_{ij}, the synaptic connection between them, and contribute to the energy of the system. The total energy contributed by all the pairs of neurons in the course of exchange of electrochemical impulses comprises the Hamiltonian H. If the J_{ij} is compatible with ξ_i and ξ_j, the nature of the neurons i and j, in a given pattern then the exchange energy between them will contribute to the lowering of H (i.e. making it negative), otherwise H will be enhanced (i.e. made positive or less negative). For instance, for $\xi_i = \xi_j = 1$, $J_{ij} > 0$ will lower H while $J_{ij} < 0$ will enhance it. In this sense H can be viewed as a "discomfort" function which must be at its minimum for a stable state of the system. In the energy space the variation of H gives rise to a landscape with a large number of depressions; the memories correspond to the minima of these depressions. For simplicity one assumes $J_{ij} = J_{ji}$ and $J_{ii} = 0$.

The model represents learning in terms of the well known Hebb's hypothesis [10]. According to it 'learning' manifests itself in the modification of synaptic connections between all i's and j's as a new object (a pattern of $+1$ and -1) comes to be recorded. The effectiveness or the strength of a synapse – whether it is excitatory (i.e. $J_{ij} > 0$) or inhibitory (i.e. $J_{ij} < 0$) – is believed to be altered by the activities of the neurons it connects. This flexibility of the synapses is modelled in the following choice of J,

$$J_{ij} = \frac{1}{N}\sum_{\mu=1}^{p} \xi_i^{(\mu)}\xi_j^{(\mu)} \ , \tag{10}$$

and enables storage of information embodied in the patterns (or objects represented by index μ).

When one of the p memories of learnt patterns, say $\mu = \nu$, is presented to the brain for association, it generates local fields $h_i^{(\nu)}$ on all the neurons according to

$$h_i^{(\nu)} = \sum_{j \neq i} J_{ij} \xi_j^{(\nu)} \quad , \tag{11}$$

which is the collective influence produced by all the $\xi_j^{(\nu)}$'s on neuron i through the J_{ij}'s that are cumulatively modified in the course of learning of p patterns. The success of retrieval is measured by the sign of $h_i^{(\nu)}$ on all the sites i through the requirement: $h_i^{(\nu)} \xi_i^{(\nu)} > 0$. If the sign of $h_i^{(\nu)}$ turns out to be the same as that of $\xi_i^{(\nu)}$ for almost all i's then the presented $\vec{\xi}^{(\nu)}$ is supposed to associate well with the learnt ν^{th} pattern.

The above condition of associative memory fails for $p/N > 0.14$, i.e. the model gives a memory capacity of $0.14N$. If the number of patterns that come to be recorded exceeds $0.14N$ the retrieval process breaks down and a memory black-out results. The cause for this 'catastrophe' is the correlation among the memories. When the vectors $\vec{\xi}^{(\mu)}$ and $\vec{\xi}^{(\nu)}$ have some overlap, they have a non-vanishing scalar product, i.e. $\vec{\xi}^{(\mu)}.\vec{\xi}^{(\nu)} = \sum_i \xi_i^{(\mu)} \xi_i^{(\nu)} \neq 0$ and they represent correlated objects, while $\vec{\xi}^{(\mu)}.\vec{\xi}^{(\nu)} = 0$ defines them as uncorrelated or mutually *orthogonal* (i.e. perpendicular to each other). (Note that $\vec{\xi}^{(\mu)}.\vec{\xi}^{(\mu)} = N$ for all μ, which is square of length of a vector $\vec{\xi}$; all vectors are thus "normalized" to have the same length). The correlations make the system noisy as the number of stored memories increases until retrieval becomes minimal.

In the above treatment typically known as Hopfield model [11], in spite of correlations the memories are treated as independent. This is inconsistent. We argue that the very idea that a new memory should be lodged independently of (or without reference to) the previous memories is unrealistic and must be abandoned. For not only are the memories in general correlated, but the correlations are actually very much required to identify the fact that two objects, although different in some details, could belong to the same class of objects. So we must have a system that can deal with the correlations meaningfully and also circumvent the problem of noise arising out of them.

We have found [1] that orthogonalization of the correlated vectors not only takes care of the above problem very effectively but also gives vital insight into the phenomenon of memory storage in the brain. The orthogonalization process in fact acts like a decision making process wherein when a new object is compared with the stored ones, the nature of its correlation with them decides, in an efficient (or economical) manner, in what form it should be stored. The noise is also eliminated using this approach.

The proposal of orthogonalization amounts to the brain checking how much a particular pattern (or object) differs from those which it has seen before and

also how much similarities it possesses with them, and recording these similarities and differences in the synapses instead of recording the full information about the new object as is done in the Hopfield model. More interestingly the comparison process also involves detection of the extent to which the similarities and differences are present and enables the brain to lay relatively greater emphasis on the one that is present to a lesser extent. In other words it the model brain searches for similarities in predominantly different patterns, and for differences in predominantly similar patterns. This tendency of being selective in laying the emphasis either on similarities or on differences before storing the information is motivated by a *principle of economy*[12] apparently built into the orthogonalization scheme.

The above neural network model with orthogonalizing capability is very promising and it is apparent that Schmidt's orthogonalization is a plausible cognitive function the brain might be employing to discriminate an object from another. However the orthogonalization procedure's "*sequence-dependence*" imposes a constraint which makes it applicable only to phenomena like our thought process and use of language etc. that are sequential in time. One must realise that there are a host of cognitive phenomena that are not sequential in time. For instance, detection of changes in a visual array, categorization according to numerosities, etc. [13]. It is expected that the understanding developed for the sequence-independent orthogonalizations will prove valuable in exploring such phenomena.

Acknowledgements: The work on neural networks with Schmidt's orthogonalizing capability was done in collaboration with Professor S. F. Edwards. Thanks are due to Prof. P.-O. Löwdin for correspondence and encouragement.

REFERENCES

*E mail: vpssp@uohyd.ernet.in

1. Vipin Srivastava and S. F. Edwards, Physica A **276**, 352 (2000).
2. R. Z. Landshoff, Physik **102**, 201 (1936).
3. G. H. Wannier, Phys. Rev. **52**, 191 (1937).
4. See P.-O. Löwdin, Advn. Quant. Chem. no. 5, 185 (1990) for a review.
5. P.-O. Löwdin, Arkiv Mat. Astr. Fysik **35A**, 9 (1947).
6. P.-O. Löwdon, Advn. Phys. **5**, 1 (1956).
7. S. Chaturvedi et al., J. Phys. **A 31**, L367 (1998).
8. H. C. Schweinler and E. P. Wigner, J. Math. Phys. **97**, 1693 (1970).
9. P.-O. Löwdin, Phys. Rev. **97**, 1474 (1955).
10. D. O. Hebb, *The Organization of Behaviour* (Wiley, N.Y. 1949).
11. J. J. Hopfield, Proc. Natnl. Acad. Sc. **79**, 2554 (1982).
12. N. Chomsky, *Knowledge of Language* (Praeger, New York 1986).
13. B. Butterworth, Science **284**, 928 (1999);
    also S. Dehaene et al., *ibid* 970 (1999).

Binding in clusters with closed-subshell atoms (alkaline-earth elements)

I.G. Kaplan,[1,2] Szczepan Roszak,[2,3] and Jerzy Leszczynski[2]

[1]Instituto de Investigaciones en Materiales, UNAM, Apartado Postal 70-360, 04510 Mexico, D.F., MEXICO

[2]The Computational Center for Molecular Structure and Interactions, Department of Chemistry, Jackson State University, P.O. Box 17910 J.R. Lynch Street, Jackson, Mississippi 39217, USA

[3]Institute of Physical and Theoretical Chemistry, Wroclaw University of Technology, Wyb. Wyspianskiego 27, 50-370 Wroclaw, Poland

Abstract

The study of the binding in clusters with closed subshell atoms is performed. The study is based on the accurate calculations of the Be_n, Mg_n, and Ca_n (n =2, 3) clusters at the Møller-Plesset electron correlation level (MP4) and the SCF level, using a reasonably large basis set [6-311 + G(3df)]. The 2-and 3-body decompositions of the interaction energy at the MP4 and SCF levels, the NBO population analysis and the electron density difference maps allow to elucidate the nature of bonding in alkaline-earth clusters

Contents

ADVANCES IN QUANTUM CHEMISTRY, VOLUME 40

0065-3276/01 $35.00

1 Introduction

Many definitions of the phenomenon of chemical bonding are used. One appropiate definition can be formulated in the following way:

chemical bonding is the attraction between atoms due to the redistribution (collectivization, charge transfer) of their valence electron density.

According to this definition, a two-atom molecule can be bound by a covalent bond (collectivization of valence electrons), by an ionic bond (charge transfer between atoms), and by so-called polar bond (intermediate case: collectivization + charge transfer), see also Ref.[1].

Compounds, constructed with atoms having closed electronic shells or subshells have no valence electrons and do not fulfil the chemical bond definition. A well known example is the noble-gas atoms. They are stabilized by the van der Waals (dispersion) forces. The van der Waals bond is caused by the quantum mechanical fluctuations in the electron density of interacting atoms. On an average, the atomic electron density is not changed. Thus, according to the definition above, the van der Waals bond cannot be attributed to chemical bonding but rather to physical bonding. The binding by the van der Waals forces is very weak in comparison with the chemical bonding. The weakest measured bond was found in He_2: the dissociation energy is $D_0 = 1.2$ mK or 2.38 o10^{-6} kcal/mol [2] (the well depth is larger and equals 0.02 kcal/mol). Even in bulk, the noble gas atoms have such small cohesive energy that can form solids only at low temperature and He remains liquid at all temperatures. This is a consequence of the closed-shell electronic structure of the noble gas elements.

On the other hand, the alkaline earth elements Be, Mg, Ca, etc. have a closed electronic subshell, $(ns)^2$, but form solids with quite large cohesive energy, see Table I. The cohesive energy in solid Be equals 3.32 eV/atom which is larger than that in solids of open one-valence ns shell atoms: Li (1.63 eV/atom) and Na (1.10 eV/atom).

The dimers of Be, Mg and Ca are very weakly bound by the electron correlation effects, at the self-consistent field (SCF) level they are not stable. The binding energy of alkaline earth dimers is only 2-4 times larger than that in Kr_2 and Xe_2 dimers. Thus, alkaline dimers can be attributed to the van der Waals molecules. The situation is changed in many-atom clusters, even in trimers (Table II). This is evidently a manifestation of the many-body effects. The crucial role of the 3-body forces in the stabilization of the Be_n clusters was revealed at the SCF level previously [3-5], and more recently was established at the Møller-Plesset perturbation theory level up to the fourth order (MP4) [6,7]. The study of binding in the Be_n clusters [8-10] reveals that the 3-body exchange forces are attractive and give an important contribution to

the attractive 2-body dispersion forces. At equilibrium distances, the latter are almost completely compensated by the repulsive 2-body exchange forces. This makes the role of 3-body exchange attraction even more important. In alkaline earths we meet with a many-body binding.

Table I: Some properties of alkaline earth atoms and solids.

	ATOMS			SOLID	
	Polarizability 10^{-24} cm^3 [a]	ΔE_{at}, kcal/mol [b]	$\langle r_{nl} \rangle$ [c]	E_c kcal/mol [d]	T_m K [d]
Be	5.6	$2s^2 \longrightarrow 2s2p \ ^3P^0$	$\langle r_{2s} \rangle = 2.65$	76.5	1562
		62.84			
Mg	10.6	$3s^2 \longrightarrow 3s3p \ ^3P^0$	$\langle r_{3s} \rangle = 3.25$	34.7	922
		62.47			
Ca	22.8 - 25.0	$4s^2 \longrightarrow 4s4d \ ^3D$	$\langle r_{4s} \rangle = 4.22$	42.5	1113
		43.34			
		$4s^2 \longrightarrow 4s3d \ ^3D$			
		58.14			
	[a] Ref.23	[b] Ref.24	[c] Ref.25	[d] Ref.26	

In order to reveal the details of binding in alkaline-earth clusters, it is important to carry out a comparative study of binding in clusters of Be, Mg, and Ca. There are many publications, in addition to those cited above, devoted to calculations of alkaline-earth clusters (see Refs. [10-21] and references therein). But in most of these studies, different computational approaches were applied to calculate the geometry and binding energy.

Table II: Comparision of our calculations with literature data for the equilibrium geometry, distances are in Å, energies are in kcal/mol, $E_b = -E_{int}$.

Refs.	Methods of calculation	Be_2		Be_3		Mg_2		Mg_3		Ca_2		Ca_3	
		r_0	E_b	r_0	E_b	r_0	E_b	r_0	E_b	r_0	E_b	r_0	E_b
[12]	CASSCF/CI	2.50	1.86	2.23	19.02								
[14]	MRCI			2.22	22.4			3.37	6.3				
[19]	MP4(SDTQ)			2.23	21.6								
[18]	Best estimations based on MP2-R12			2.20	26.9			3.37	8.0				
[11]	CI											3.97	11.53
[17]	MRCI											4.16	12.10
[27]	Experiment	2.45	2.26										
[28,29]	Experiment					3.89	1.16						
[22]	MP4(SDTQ)	2.56	1.83	2.24	25.90	3.92	1.09	3.32	7.12	4.56	2.14	4.12	11.66

The nature of binding in these clusters was not studied. The only exception, to the best of our knowledge, are two works by Bauschlicher et al.[10,11]. In their study of alkaline-earth clusters, the authors came to the conclusion that the promotion of atomic electrons from ns to np vacant orbitals, leading to hybridization, is a major mechanism responsible for the binding in alkaline-earth compounds. As shown below, this is not the case. The binding in alkaline-earth clusters has more complicated nature and depends on many factors.

Our analysis is based on accurate calculations performed in Ref.[22] at the Møller-Plesset electron correlation level of the interaction energy and its many-body decomposition for Be_n, Mg_n, and Ca_n (n= 2 and 3) clusters using a reasonably large basis set [6-311 + G (3df)]. All calculations were also carried out at the SCF level which allowed to study separately the SCF and electron correlation contributions and give a physical analysis of each term in the dimer and trimer energy decompositions.

2 Calculation scheme and its check

In variational methods, the interaction energy is not calculated directly even if the Møller-Plesset perturbation theory is used. We have to calculate the interaction energy at all calculation levels as a difference

$$E_{int}(N) = E(N) - NE_a \tag{1}$$

where E(N) is the total energy of cluster A_N; E_a is the atomic energy calculated at the same level of accuracy as E(N). For taking into account the basis set superposition error (BSSE), the atomic energy in Eq. (1) was calculated using the dimer basis set for N = 2 and the trimer basis set for N = 3.

All calculations in Ref.[22] were performed utilizing the Gaussian-98 code [30]. The potential energy scan was performed by means of the Møller-Plesset perturbation theory up to the fourth order (MP4) in the frozen core approximation. The electronic density distribution was studied within the population analysis scheme based on the natural bond orbitals [31,32]. A population analysis was performed for the SCF density and MP4(SDQ) generalized density determined applying the Z-vector concept [33].

We tested the quality of the calculations [22] by applying several different approaches. Firstly, the calculations were compared with Møller-Plesset calculations with no frozen core, $1s^2$ frozen, and $1s^22s^22p^6$ frozen core electrons for Be, Mg, and Ca clusters, respectively. The inclusion of more electron in the correlation energy calculations slightly lowers two- as well as three-body

interaction energies. The largest frozen space in the case of Ca clusters leads to total energy changes around 10% and does not affect the qualitative picture of the studied interactions. Test calculations were also performed by the coupled cluster method with single and double substitutions from the Hartree-Fock determinant and with inclusion of triple excitations non-iteratively, CCSD(T) [34,35]. The calculated interaction energies are within a few percent of those of Møller-Plesset calculations, indicating that the choice of the MP4(SDTQ) approach is well justified as a basic tool for the presented analysis.

In Table II the results of our calculations [22] of the equilibrium geometry and binding energy together with the published data are presented. A comparison with literature data indicates a quite satisfactory agreement. The values of the binding energy for the trimers Be_3 and Mg_3 are very close to the best estimations in Ref. [18].

In order to check the convergence of the MP perturbation series, the perturbation contributions $\varepsilon_{MP}^{(n)}$ to the interaction energy in each order have to be calculated:

$$\begin{aligned} \varepsilon_{MP}^{(2)} &= E_{int}^{MP2} - E_{int}^{SCF} \ , \\ \varepsilon_{MP}^{(3)} &= E_{int}^{MP3} - E_{int}^{MP2} \ , \\ \varepsilon_{MP}^{(4)} &= E_{int}^{MP4} - E_{int}^{MP3} \ , \end{aligned} \tag{2}$$

According to its definition, the correlation energy at the MP4 level is equal to

$$\Delta E^{corr} = E_{int}^{MP4} - E_{int}^{SCF} = \sum_{n=2}^{4} \varepsilon_{MP}^{(n)} \ . \tag{3}$$

Let us express the MP series as the ratios to the second order contribution

$$\Delta E^{corr} = \varepsilon_{MP}^{(2)} \left(1 + \frac{\varepsilon_{MP}^{(3)}}{\varepsilon_{MP}^{(2)}} + \frac{\varepsilon_{MP}^{(4)}}{\varepsilon_{MP}^{(2)}} \right) \ . \tag{4}$$

At the equilibrium distance (Table III), the MP series (4) are the following:

$$\begin{aligned} Be_2 &: \ \varepsilon_{MP}^{(2)}(1 + 0.12 + 0.06) \ , \\ Mg_2 &: \ \varepsilon_{MP}^{(2)}(1 + 0.14 + 0.03) \ , \\ Ca_2 &: \ \varepsilon_{MP}^{(2)}(1 + 0.18 + 0.07) \ . \end{aligned} \tag{5}$$

Thus, the limitation of our calculation at the MP4 level looks quite justified. As shown in Ref. [22], the convergence is good at all calculated distances.

Table III: Interaction energy for dimers at the equilibrium distance at different levels of calculation, in kcal/mol.

Dimer	E_{int}^{SCF}	$\varepsilon_{MP}^{(2)}$	$\varepsilon_{MP}^{(3)}$	$\varepsilon_{MP}^{(4)}$	ΔE^{corr}	E_{int}^{MP4}
Be_2 $r_0 = 2.56$ Å	6.12	-6.71	-0.81	-0.43	-7.94	-1.83
Mg_2 $r_0 = 3.92$ Å	1.62	-2.34	-0.32	-0.06	-2.72	-1.09
Ca_2 $r_0 = 4.56$ Å	1.05	-2.56	-0.46	-0.17	-3.19	-2.14

The many-body decomposition of the interaction energy at different approximation is performed according to the general definitions, see Refs [36, 6]. For trimers we have only 2- and 3-body interaction energies. In the homoatomic case they are represented by the following formulae:

$$E_2(A_3) = \sum_{a<b} \varepsilon_{ab} \ , \tag{6}$$

$$\varepsilon_{ab} = E(ab) - 2E_a \tag{7}$$

where E(ab) is the total energy of two atoms at a particular distance they have in trimer abc. In the general case of a nonsymmetrical triangle, the sum (6) contains three different 2-body interaction energies.

The 3-body energy is defined as a difference

$$E_3(A_3) = E(A_3) - E_2(A_3) - 3E_a \tag{8}$$

where $E(A_3)$ is denoted as the total energy of trimer A_3.

The formulae (6)-(8) were applied for the calculations of the 2- and 3-body contributions to the interaction energy at the SCF and MP4 levels and for the decomposition of the electron correlation energy.

3 Discussion

3.1 Dimers

As was shown in Ref.[22], the interaction energy at the SCF level is positive for all three dimers at all distances. It is the electron correlation energy

that stabilizes the close-subshell-atoms dimers. The interaction energy at the equilibrium distances are presented in Table III. The equilibrium distance rises from $r_0 = 2.56$ Å for Be_2 to $r_0 = 4.56$ Å for Ca_2. The increase of the equilibrium distance in the row Be_2, Mg_2, and Ca_2 is well correlated with an increase in the average radius of the atomic valence shell (Table I). However, the binding energy does not have such monotonic behavior. The decrease of E_b from 1.83 kcal/mol for Be_2 to 1.09 kcal/mol for Mg_2 changes with an increase of E_b to 2.14 kcal/mol for Ca_2. The equilibrium distance for Ca_2 is very large (4.56 Å), and it could be expected that the bond will be weaker than in Mg_2. But this is not the case; the increase of the equilibrium distance compared with that in Mg_2 does not lead to weaker bond. It is explained by the smaller repulsive SCF energy and the larger correlation attraction at the equilibrium distances in the Ca_2 dimers, with respect to the Mg_2 dimer (see Table III). The same non-monotonic behavior takes place for the binding energy of the trimers: E_b = 25.9, 7.12, and 11.66 kcal/mol for Be_3, Mg_3, and Ca_3, respectively (Table II). It can be expected that this trend is also preserved in large clusters because in solid alkaline earths the cohesive energy and melting temperature show similar behavior (Table I).

The SCF interaction energy can be decomposed in different ways [36-38]. One possible decomposition is

$$E_{int}^{SCF} = \varepsilon_{el}^{(1)} + \varepsilon_{exch}^{(1)} + \Delta E_{ind.exch}^{def} \quad . \tag{9}$$

The electrostatics, $\varepsilon_{el}^{(1)}$, and exchange, $\varepsilon_{exch}^{(1)}$, energies correspond to the first order of the perturbation theory; so, they are defined in the undisturbed atomic wave functions. The third term, $\Delta E_{ind.exch}^{def}$, contains the induction interactions which cannot be separated from the exchange interactions. The induction forces polarize the SCF orbitals; accordingly, $\Delta E_{ind.exch}^{def}$ is defined on the deformed orbitals.

Atoms with closed subshells have no multipole moments and their electrostatic and induction interactions have a pure overlap origin; from which follows their short-range character. The main contribution to E_{int}^{SCF} gives the exchange interaction $\varepsilon_{exch}^{(1)}$. Between atoms with closed subshells, it is repulsive (as in the noble-gas atom systems). This determines the unstability of the alkaline earth dimers at the SCF approximation. They are stabilized by the attractive electron correlation forces.

At large distances, the electron correlation energy can be interpreted as a dispersion energy. At intermediate distances where the overlap of the atomic

Table IV: Comparison of E_2^{disp}, Eq. (10), with ΔE^{corr} for equilibrium and large distances, in kcal/mol.

	Be_2		Mg_2		Ca_2	
r,Å	E_2^{disp}	ΔE^{corr}	E_2^{disp}	ΔE^{corr}	E_2^{disp}	ΔE^{corr}
2.56	-79.62	-7.94				
3.92			-8.95	-2.27		
4.56					-14.40	-3.19
5.00	-0.35	-0.36	-1.29	-0.87	-6.85	-2.23
6.00	-0.10	-0.11	-0.35	-0.33	-1.68	-0.92
7.00	-0.03	-0.04	-0.11	-0.12	-0.55	-0.39
8.00			-0.04	-0.04	-0.22	-0.17
9.00					-0.10	-0.08
10.0					-0.05	-0.04

valence shells becomes essential, the dispersion forces cannot be defined without allowing for exchange effects. At these distances the multipole expansion is not valid [36]. It is instructive to compare the magnitudes of the pure dispersion energy and the electron correlation energy at different distances.

The energy of the dispersion interaction between two atoms can be presented with fine precision as a sum of three terms:

$$E_2^{disp} = -\left(\frac{C_6}{r^6} + \frac{C_8}{r^8} + \frac{C_{10}}{r^{10}}\right) \quad , \tag{10}$$

where the dipole-dipole (r^{-6}), dipole-quadrupole (r^{-8}), and dipole-octupole plus quadrupole-quadrupole (r^{-10}) dispersion interactions are taken into account. The dispersion coefficients C_n for the Be, Mg, and Ca atoms were estimated in Refs.[39] by the Padé approximant method. Using the values of C_n converted to $\left[\frac{\text{kcal}}{\text{mol}}\text{Å}^{\,n}\right]$ units, we have found the sum (10) at equilibrium

and at large distances and presented it in Table IV together with ΔE_{corr} calculated in Ref.[22]. As follows from Table IV, at large distances the electron correlation energy coincides with the pure dispersion energy with very good precision: for Be_2 at r $\geq$ 5 Å, for Mg_2 at r $\geq$6 Å, and for Ca_2 at r $\geq$9 Å. Note: this coincidence takes place for quantities calculated by different methods and at different approximations. From this follows that it is based on the physical ground: the dispersion forces have the electron correlation origin.

At equilibrium distances, the absolute value of the pure dispersion energy is much larger than ΔE_{corr} (in the case of Be_2, 10 times!). The exchange and overlap contributions to the electron correlation energy are repulsive and cause a decrease in dispersion attraction. At large distances, the dispersion energy in Ca_2 is about 5 times larger than that in Mg_2. This is correlated with the larger value of polarizability for the Ca atom compared with the Mg atom (Table I).

3.2 Trimers

In Table V we present the interaction energy at the SCF and MP4 levels for trimers Be_3, Mg_3, and Ca_3 in the equilateral triangle conformation. The trimers as well as dimers are not stable in the SCF approximation. According to Ref. [22], the SCF energy is positive at all calculated distances. On the other hand, the electron correlation corrections are negative and lead to stabilization of the alkaline-earth trimers. The binding in trimers is much stronger than in dimers. Especially in Be_3 where the value of E_b =25.9 kcal/mol is 14 times larger than the binding energy for Be_2 which has the van der Waals origin.

A more detailed analysis of the nature of binding is based on the many-body decomposition of the interaction energy

$$E_{int}^{MP4}(A_3) = E_2^{MP4}(A_3) + E_3^{MP4}(A_3) \tag{11}$$

which is also presented in Table V. The extremely large values of the ratio of the 3-body to 2-body energy for the equilibrium conformations of Be_3 and Mg_3 is connected with almost zero values of the 2-body interaction energies (the equilibrium distance in the Be_3 and Mg_3 equilateral triangle is located in the vicinity of the intersection of the $E_2(3)$ potential curve and the abscissa axis). Thus, in the frame of the many-body decomposition of the interaction energy, we have to conclude that for the Be_3 and Mg_3 trimers, the dominant factor of their stability are the 3-body forces. For the Ca_3 trimer the 2-body contribution to the interaction energy is non-negligible and amounts to 38%, although the 3-body interactions are a main contributor to the stability of the cluster.

Table V: Interaction energy and the many-body decomposition at the equilibrium geometry for the $C_{3\nu}$ symmetry, in kcal/mol.

Trimer	E_{int}^{MP4}	E_{int}^{SCF}	ΔE^{corr}	E_2^{MP4}	E_2^{SCF}	ΔE_2^{corr}	E_3^{MP4}	E_3^{SCF}	ΔE_3^{corr}	$\frac{E_3^{MP4}}{E_2^{MP4}}$
Be_3 $r_0 = 2.24$ Å	-25.90	0.60	-26.50	-0.79	35.45	-36.24	-25.11	-34.80	9.75	31.8
Mg_3 $r_0 = 3.32$ Å	-7.12	8.06	-15.18	-0.15	15.00	-15.15	-6.97	-6.94	-0.03	46.5
Ca_3 $r_0 = 4.12$ Å	-11.66	2.16	-13.82	-4.44	9.15	-13.59	-7.22	-6.98	-0.23	1.6

As discussed above, the equilibrium distances for the dimers are rather large, especially for Mg_2 and Ca_2. The addition of one more atom leads to a decrement in the equilibrium interatomic distance. In an equilateral triangle (the conformation which is the most stable conformation in the case of close-subshell-atom trimers) according to our calculations, the largest reduction 0.6 Å is revealed for Mg_3. However, for Be_3 and Ca_3, the reduction is also large enough: 0.32 Å and 0.44 Å, respectively. The explanation of this decrement is based on the interplay of the 2- and 3-body interactions in the cluster formation [6]: the attractive 3-body forces become larger with a decrease in the atom-atom distances while the 2-body forces undergo small changes because of the relative flatness of the 2-body potential curves.

In the same manner, as was done for the full interaction energy, the 2- and 3-body interaction energies can also be decomposed on the SCF and electron correlation parts:

$$E_n^{MP4} = E_n^{SCF} + \Delta E_n^{corr} \quad , n = 2, 3 \quad . \tag{12}$$

The 2-body SCF energy for an equilateral triangle is equal to

$$E_2^{SCF}(A_3) = 3E_{int}^{SCF}(A_2) \quad . \tag{13}$$

It indicates that, the physical sense of the 2-body SCF energy in trimers is the same as the SCF interaction energy in dimers: it is predominantly the exchange interactions which are repulsive for two interacting atoms with closed subshells. The attractive contributions from the electrostatic and induction energies are less than the repulsive exchange contribution. This is the reason that $E_2^{SCF}(A_3)$ is positive for the alkaline trimers in all calculated distance regions [22].

The situation is different in the case of the 3-body SCF energy. The main contribution to $E_3^{SCF}(A_3)$ is given by the 3-body exchange forces. These forces originate from the three-atomic electron exchange which mixes electrons of all three atoms. In closed-shell atom systems, contrary to the 2-body exchange forces, the 3-body exchange forces are attractive and make a contribution to the stabilization of trimers. Thus, for trimers there are two stabilization factors: ΔE_3^{SCF} and ΔE_2^{corr} .

The 2-body electron correlation energy, $\Delta E_2^{corr}(A_3)$, as in the case of dimers, is reduced at large distances to the dispersion energy. At intermediate distances, it contains both the exchange and dispersion contributions which cannot be separated. The exchange effects decrease the dispersion attraction; nevertheless, the 2-body electron correlation appears as a main factor of stabilization, especially for the Mg_3 and Ca_3 trimers.

The 3-body electron correlation energy, $\Delta E_3^{corr}(A_3)$, at large distances can be represented as the Axilrod-Teller 3-body dispersion energy [40]

$$E_3^{dis}(A_3)=\frac{C_9}{r_{ab}^3 r_{ac}^3 r_{bc}^3}(1+3Cos\theta_a Cos\theta_b Cos\theta_c) \quad . \tag{14}$$

For an equilateral triangle, Eq (14) is transformed to

$$E_3^{dis}(A_3) = \frac{11}{8}\frac{C_9}{r_{ab}^9} \tag{15}$$

According to Eq.(15), the 3-body dispersion energy is positive as is ΔE_3^{corr} at large distances. At intermediate distances, the negative contributions from the 3-body exchange and overlap effects can lead to negative values for ΔE_3^{corr}. This is what is revealed for Ca_3 and, close to the equilibrium distances, for Mg_3.

Note that the larger value of binding energy E_b (Ca_3) = 11.66 kcal/mol compared with E_b (Mg_3)=7.12 kcal/mol in spite of the greater equilibrium distance in the Ca_3 trimer is due to the smaller value of the repulsive SCF energy for Ca_3 : E_2^{SCF} (Ca_3)=9.15 kal/mol and E_2^{SCF} (Mg_3)=15 kcal/mol. This results in a greater stability of Ca_3 because the total attractive contribution for Ca_3 is smaller than for Mg_3 : $\Delta E_2^{corr} + E_3^{SCF} + \Delta E_3^{corr}$ = -20.8 and -22.12 kcal/mol for Ca_3 and Mg_3, respectively (see Table V).

3.3 Population of vacant atomic orbitals and electron density distribution

It is instructive to study the vacant atomic orbital population in dimers and trimers. As mentioned in the Introduction, in the 80's Bauschlicher et al. [10,11] came to the conclusion that the promotion of ns-electrons to np-orbitals leading to sp-hybridization is the main mechanism responsible for binding in alkaline-earth clusters. This conclusion was based on a study of the SCF Mulliken population analysis for tetramers, which are stable at the SCF level. At present, we can perform more precise analysis using the Natural Bond Orbital Analysis and calculate it at the electron correlation level.

In Table VI we present the net population of valence orbitals in dimers and trimers. We see that not only the p-population but even the d-population, especially for the Ca clusters, are not negligible. The latter is correlated with the experimental atomic excitation energies ΔE_{at} [24]. According to Table I, the energy of the 4s$\longrightarrow$3d excitation in the Ca atom is even smaller than the

Table VI: The net valence population, Δn_l^a, for the isolated atoms and clusters at the equilibrium geometry, obtained by the Natural Bond Orbital Analysis at the SCF and MP4 levels.

	SCF				MP			
A_n/l	ns	(n+1)s	np	nd	ns	(n+1)s	np	nd
Be	0.000	0.000	0.000	0.000	-0.135	0.004	0.130	0.001
Be_2	-0.044	0.006	0.037	0.001	-0.199	0.008	0.185	0.006
Be_3	-0.257	0.005	0.246	0.005	-0.315	0.009	0.288	0.016
Mg	0.000	0.000	0.000	0.000	-0.112	0.004	0.105	0.003
Mg_2	-0.007	0.001	0.005	0.000	-0.123	0.004	0.113	0.005
Mg_3	-0.045	0.002	0.040	0.002	-0.173	0.005	0.154	0.012
Ca	0.000	0.000	0.000	0.000	-0.138	0.003	0.124	0.011
Ca_2	-0.016	0.002	0.011	0.003	-0.161	0.005	0.139	0.018
Ca_3	-0.074	0.003	0.057	0.015	-0.229	0.006	0.184	0.039

[a]For atoms $\Delta n_l^{MP4}(A) = n_l^{MP4}(A) - n_l^{SCF}(A)$, for clusters $\Delta n_l^{MP4}(A_n) = n_l^{MP4}(A_n) - n_l^{SCF}(A)$, the similar definition is for n_l^{SCF}, therefore $n_l^{SCF}(A) = 0$.

ns⟶np excitation energies in Be and Mg atoms. On the other hand, there is no quantitative relation between ΔE_{at} and the net population numbers Δn_l in Table VI. The magnitude of ΔE_{at} (ns⟶np) in Be is larger than that in Ca; nevertheless, the np-population in the Be clusters is larger than in the Ca clusters.

We have also calculated the NBO valence population at the MP4 level for the isolated atoms. It could be expected that the inclusion of the electron correlation effects leads to some population of vacant (in the SCF approximation) atomic orbitals. But the values obtained are surprisingly large. The p-population in the Mg and Ca atoms are only slightly smaller than that in their dimers, and in the Be atom the population is 0.7 of the p-population in Be_2.

It is important to check: is the effect of a rather large population of vacant atomic orbitals at the electron correlation level specific for alkaline-earth atoms or it has a general character. In Table VII we present the results of net valence population calculations for noble-gas atoms performed by the Natural Bond Orbital Analysis at the MP4 level. We found non-negligible valence orbital population, especially for the d-orbitals. The results obtained for three different basis sets are quite close. Thus, the population of vacant orbitals in noble-gas atoms is not an artifact of the calculations. From this follows that elements traditionally assumed as closed-shell (noble gases) or closed-subshell (alkaline earths) atoms can to some extent manifest an anisotropic p- or d-symmetry behavior. It would be very interesting to obtain experimental evidence confirming this theoretical prediction.

Table VII: The net valence population, Δn_l^a, for isolated noble-gas atoms, obtained by the Natural Bond Orbital Analysis at the MP4 level.

atoms	ns	np	$\sum_m (n+m)s$	$\sum_m (n+m)p$	nd	nf
			a) The Sttutgart / Dresden basis set [41]			
Ne	-0.011	-0.062	0.009	0.040	0.023	0.002
Ar	-0.019	-0.129	0.007	0.028	0.105	0.008
Kr	-0.018	-0.119	0.006	0.024	0.095	0.012
Xe	-0.020	-0.131	0.006	0.021	0.106	0.019
			b) The Stevens et al. basis set [42,43]			
Ne	-0.010	-0.060	0.008	0.037	0.023	0.002
Ar	-0.019	-0.130	0.007	0.026	0.107	0.008
Kr	-0.018	-0.123	0.006	0.023	0.100	0.012
Xe	-0.020	-0.134	0.006	0.020	0.109	0.019
			c) 6-311+G (3df) basis set [44]			
Ne	-0.010	-0.061	0.008	0.039	0.022	0.002
Ar	-0.018	-0.126	0.007	0.027	0.101	0.009
Kr	-0.018	-0.119	0.006	0.024	0.095	0.012
Xe	no basis set available					

[a] $\Delta n_l(A) = n_l^{MP4}(A) - n_l^{SCF}(A)$

We have to take into consideration that some atom-atom interactions, which enhance the excited orbital population, do not lead to a bonding state. The last statement is confirmed by the valence orbital population in the alkaline-earth clusters at the SCF level. According to Table VI, at the SCF level there is a non-negligible p-population, especially for trimers. But in the

SCF approximation, the dimers and trimers are not stable. Thus, the repulsive SCF interactions also lead to the vacant orbitals population, although this kind of hybridization does not lead to binding.

The calculations in Ref. [10] were performed at the SCF level. In the frame of the latter, the isolated atoms do not have populated excited orbitals. The authors [10] found the ratio of p-population in different tetramers (which are stable at the SCF level) proportional to the ratio of their dissociation energies. However, at an election correlation level because of the p-population in the isolated atoms, we cannot expect such proportionality. It is evident for dimers: the p-population is largest in Be_2, although the bond strength is largest in Ca_2. For dimers, the p-population is not very different from that in the isolated atoms whereas for trimers the increase of the p-population is rather large. It is not directly proportional to the bond strength, but its amount qualitatively reflects a trend toward a more strong bond formation by the sp-hybridization.

More insight into the bonding comes from the density difference maps. The partitioning of the total density difference into 2- and 3- body terms was performed in the analogy to interaction energy expressions. In Figs. 1 and 2 we present the total density difference maps and its 2- and 3-body contributions in the Be_3 plane and in the perperdicular plane passing through the Be-Be bond. For 2-body density difference, we have positive values along the Be-Be bond which can be attributed to the σ-type bonding (the latter is more clear from the plot in the plane perpendicular to the Be_3 plane, Fig. 2a). The 2-body dispersion interactions do not change the density distribution. Thus, the σ-type redistribution originates from the SCF 2-body interactions, inside which there are two attractive interactions: electrostatic and induction. Because of the larger 2-body exchange repulsion, these attractions are not sufficient for the stabilization of Be_3, and we have to conclude that the σ-type redistribution of the 2-body density difference does not lead to a real bonding. This is analogical to the atomic p-population at the SCF level which also does not lead to trimer stability.

Figs. 1a and 2a also reveal a positive density difference in the nonbonding region (the area outside the atoms attached to the vertices of the triangle Be_3). This reflects the antibonding character of the 2-body exchange interactions. The 3-body interactions shift the electron density from nonbonding to bonding regions because in the total density difference plots, the electronic density gain is observed only in the bonding area (Fig. 1c).

As follows from Fig. 1b and 2b, the 3-body density difference is positive outside of the Be-Be line in a direction perpendicular to it, whereas it is negative beyond the Be_3 plane. So, the density difference has the π-in-plane character but is shifted outside the triangle Be3. The total density difference

plot (Fig 1c) resembles the interstitial orbital picture obtained in Li_N clusters by spin-coupled valence bond method [45,46]. This can also be connected with the rather large p-population of Be atoms in trimers.

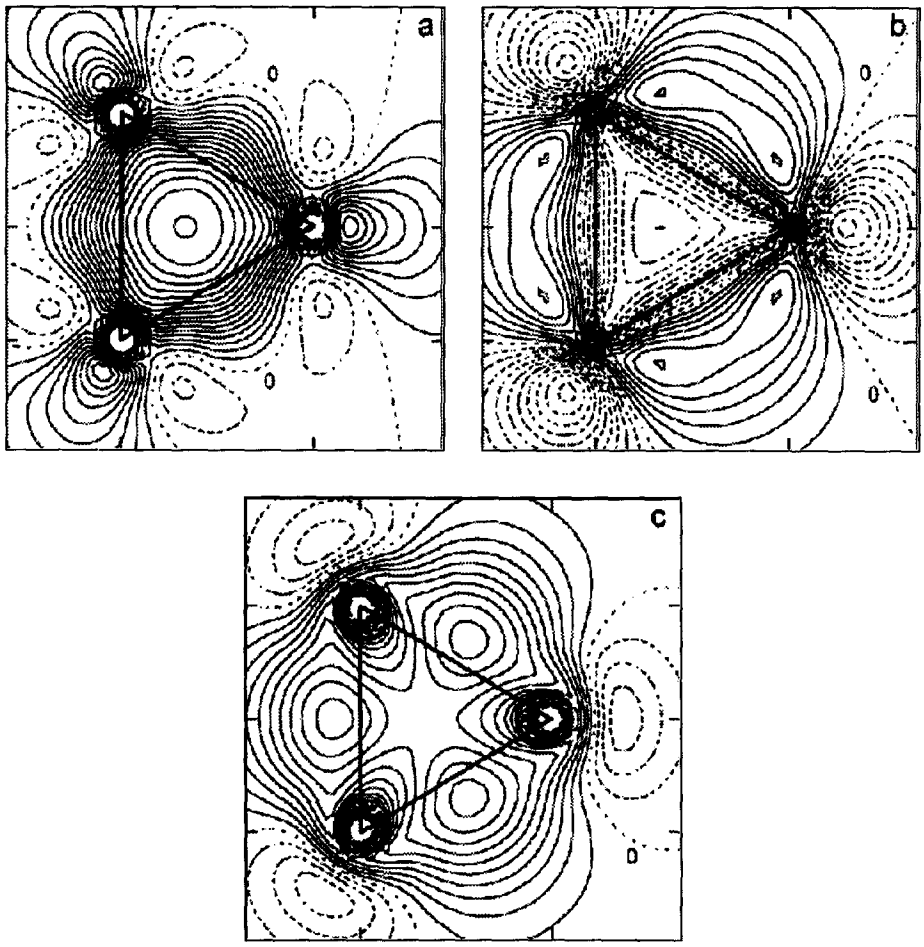

Figure 1: The electronic density difference maps for the Be_3 trimer partitioned for 2-body (a) and 3-body (b) contributions and the total difference density distribution (c). The plot is done in the plane of Be_3. The spacing between the contours is 0.001 electron/bohr. The contour with no density charge are labeled with zeros while solid lines indicate the enhancement of electronic density.

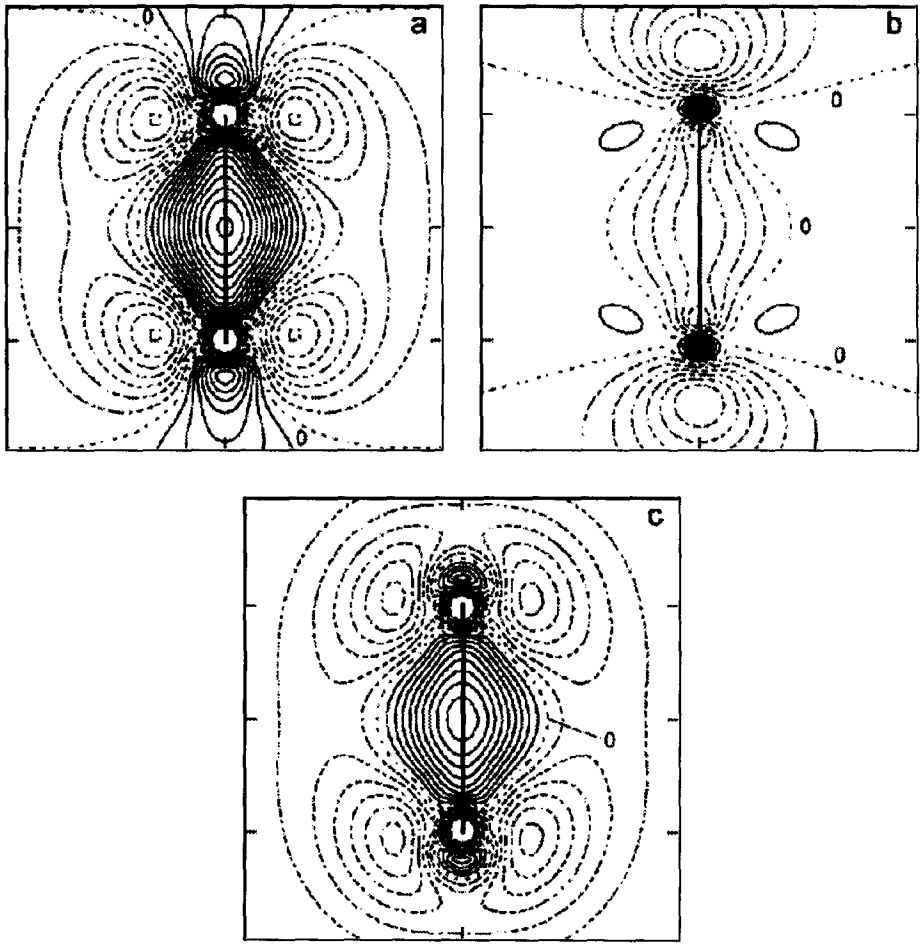

Figure 2: The electronic density difference maps for the Be_3 trimer partitioned for 2-body (a) and 3-body (b) contributions and the total difference density distribution (c). The plot is done in the plane perpendicular to the Be_3 plane and passing through the Be-Be bond. The spacing between the contours is 0.001 electron/borh. The contours with no density charge are labeled with zeros while solid lines indicate the enhancement of electronic density.

ACKNOWLEDGEMENT

This work was facilitated in part by the projects IN108697 of DGAPA UNAM and 32227- E of CONACYT (Mexico), the U.S. NSF grant 9805465, Wroclaw University of Technology Grant No. 341-831, and the U.S. Army High Performance Computing Research Center under the auspices of the Department of Army, Army Research Laboratory cooperative agreement number DAAH04-95-2-0003/contract number DAAH04-95-C-0008. This work does not necessarily reflect the policy of the USA government, and no official endorsement should be inferred. We would like to thank the Mississippi Center for Supercomputing Research, Poznan and Wroclaw Supercomputing and Networking Centers, and the Interdisciplinary Center for Mathematical and Computational Modeling of Warsaw University for a generous allotment of computer time.

References

[1] I.G. Kaplan, Int. J. Quant. Chem. **74**, 241, (1999).

[2] F. Luo, G. Kim, G.C. Mc Bane, C.F. Giese, and W.R. Gentry, J. Chem. Phys. **98**, 9687, 10086 (1993).

[3] W. Kolos, F. Nieves, and O. Novaro, Chem. Phys. Lett. **41**, 431 (1976).

[4] O. Novaro and W. Kolos, J. Chem. Phys. **67**, 5066 (1977).

[5] J.P. Daudey, O. Novaro, W. Kolos, and M. Berrondo, J. Chem. Phys. **71**, 4297 (1979).

[6] I.G. Kaplan, J. Hernández-Cobos, I. Ortega-Blake, and O. Novaro, Phys. Rev. **A53**, 2493 (1996).

[7] I.G. Kaplan, Adv. Quantum. Chem. **31**, 137 (1999).

[8] J. Hernández-Cobos, I.G. Kaplan, and J.N. Murrell, Mol. Phys. **92**,63 (1997).

[9] I.G. Kaplan, Polish J. Chem. **72**, 1454 (1998).

[10] C.W. Bauschlicher, V. Bagus, and B.N. Cox, J. Chem. Phys. **77**, 4032 (1982).

[11] S.P. Walch and C. W. Bauschlicher, J. Chem. Phys. **83**, 5735 (1985).

[12] R.J. Harrison and N.C. Handy, Chem. Phys. Lett. **123**, 321 (1986).

[13] V. Reuse, S. N. Khanna, V. De Coulon, and J. Buttet, Phys. Rev. **B39**, 12911 (1989); **B41**, 11743 (1990).

[14] T.J. Lee, A.P. Rendell, P. Rendell, and P.R. Taylor, J. Chem. Phys. **93**, 6636 (1990).

[15] T.J. Lee, A.P. Rendell, and P.R. Taylor, J. Chem. Phys. **92**, 489 (1990).

[16] J.D. Watts, I. Cernusak, J. Noga, R.J. Bartlett, C. W. Bauschlicher, Jr. T.J. Lee, A. P. Rendell, and P.R. Taylor, J. Chem. Phys. **93**, 8875 (1990).

[17] T.J.Lee, A.P. Rendell, and P.R. Taylor, Theor. Chim. Acta, **83**, 165 (1992).

[18] W. Klopper and J. Almlöf, J. Chem. Phys. **99**, 5167 (1993).

[19] P.V. Sudhakar and K. Lammertsmaa, J. Chem. Phys. **99**, 7929 (1993).

[20] L.A. Ericksson , J. Chem. Phys. **103**, 1050 (1995).

[21] E.R. Davidson and R.F. Frey, J. Chem. Phys. **106**, 2331 (1997).

[22] I.G. Kaplan, S. Roszak, and J. Leszczynski, J. Chem. Phys. **113**, 6245 (2000).

[23] CRC Handbook of Chemistry and Physics, Ed. D.R. Leed, 74th Edition CRC Press: Boca Raton 1993-1994.

[24] C.E. Moore, "Atomic Energy Levels," vol. I, Circular of the NBS 467, Washington, 1949.

[25] C. F. Bunge, J. A. Barrientos, and A. Vivier-Bunge, Atomic Data and Nuclear Data Tables **53**, 113 (1993).

[26] C. Kittel, "Introduction to Solid State Physics," Wiley & Sons: New York, 1996, 7th Edition, p. 57.

[27] V. E. Bondybey, Chem. Phys. Lett. **109**, 436, (1984).

[28] A. E. Balfour and A. E. Duglas, Can. J. Phys. **48**, 901 (1970).

[29] C.R. Vidal and H. Scheingraber, J. Mol. Spectr. **65**, 46 (1977).

[30] Gaussian 98, Revision A.6, M.J. Frisch, G. W. Trucks, H.B. Schlegel, G. E. Scuseria, M. A. Robb, J.R. Cheeseman, V. G. Zakrzewski, J. A. Montgomery, Jr. Stratmann, R. E., J. C. Burant, S. Dapprich, J.M. Millam, A.D. Daniels, K. N. Kudin, M.C. Strain, O. Farkas, J. Tomasi, V. Barone, M. Cossi, R. Cammi, B. Mennucci, C. Pomelli, C. Adamo, S. Clifford, J. Ochterski, G.A. Petersson, P. Y. Ayala, Q. Cui, K. Morokuma, D.K. Malick, A.D. Rabuck, K. Raghavachari, J.B. Foresman, Cioslowski, J. V. Ortiz, B.B. Stefanov, G. Lui, A. Liashenko, P. Piskorz, I.J. Komaromi, R. Gomperts, R.L. Martin, D.J. Fox, T. Keith, M.A. Al-Laham, C.Y. Peng, A. Nanayakkara, C. Gonzalez, M. Challacombe, P.M.W. Gill, B. Johonson, W. Chen, M. W. Wong, J.L. Andres, C. Gonzalez, M. Head-Gordon, E.S. Replogle, and J.A. Pople, Gaussian, Inc., Pittsburgh PA, 1998.

[31] F.W. Biegler-König, R.F.W. Bager, and T.H. Tang, J. Comput. Chem. **3**, 317 (1982).

[32] K.B. Wiberg, C.M. Hadad, T.J. Le Page, C.M. Breneman, and M.J. Frisch, J. Phys. Chem. **96**, 671 (1992).

[33] A.E. Reed, L.A. Curtiss, and F. Wienhold, Chem. Rev. **88**, 899 (1988).

[34] G.D. Purvis and R.J. Bartlett, J. Chem. Phys. **76**, 1910 (1982).

[35] J.A. Pople, M. Head-Gordon, and K. Raghavachari, J. Chem. Phys. **87**, 5968 (1987).

[36] I.G. Kaplan, Theory of Molecular Interactions (Elsevier, Amsterdam, 1986).

[37] K. Kitaura and K. Morokuma, Int. J. Quant. Chem. **10**, 325 (1976).

[38] G. Chalasinski, M.M. Szczesniak, and S.M. Cybulski, J. Chem. Phys. **92**, 2481 (1990).

[39] J.M. Standart and P.R. Certain, J. Chem. Phys. **83**, 3002 (1985).

[40] B.M. Axilrod and E. Teller, J. Chem. Phys. **11**, 299 (1943).

[41] A. Bergner, V.M. Dolg, W. Kuechle, H. Stall, and H. Preuss, Mol. Phys. **80**, 1431, (1993).

[42] W.J. Stevens, H. Basch, and M. J. Krauss , Chem. Phys. **81**, 6026, (1984).

[43] W.J. Stevens, M. Krauss, H. Basch, and P.G. Jasien , Canad. J. Chem. **70**, 612, (1992).

[44] L.A. Curtiss, M.P. Mc Grath, J-P. Blandeau, N.E. Davis, R.C. Binning, Jr, and L. J. Radom Chem. Phys. **103**, 6104, (1995).

[45] E. Tornaghi, D.L. Cooper, J. Gerratt, and M. Raimondi, J. Mol. Struct. (Theochem) **259**, 383, (1992).

[46] E. Tornaghi, D.L. Cooper, J. Gerratt, and M. Raimondi, J. Chem. Soc. Farad. Trans. **88**, 2309, (1992).

Reproduction of metal-cluster magic numbers using a q-deformed, 3-dimensional, harmonic oscillator model

A. I. KULEFF[†*], J. MARUANI[*] and P. P. RAYCHEV[†*]

[†] *Institute of Nuclear Research and Nuclear Energy, Bulgarian Academy of Sciences, 72 Tzarigradsko Chaussee, Sofia 1784, Bulgaria*

[*] *Laboratoire de Chimie Physique, CNRS and UPMC, 11 Rue Pierre et Marie Curie, 75005 Paris, France*

Abstract

In this paper we review the main properties of the q-deformed, 3-dimensional harmonic oscillator ($Q3O$) and show how this model can be used for the description of metal cluster properties. We recall that the $Q3O$ symmetry $u_q(3) \supset so_q(3)$, which is a non-linear deformation of the chain $u(3) \supset so(3)$, is a relevant symmetry for metal clusters. This is because the $Q3O$ potential gathers the main features of semi-empirical potentials (such as that of Nilsson and Clemenger) which have been successfully used in the description of metal clusters. The advantage of our model is that the class of q-deformed symmetries is richer than that of Lie symmetries, making the $Q3O$ potential more flexible than its classical analogs. We show how to derive potentials which, when put into the "standard" Schrödinger equation, provide a spectrum similar to the $Q3O$ model. We also introduce prescriptions for choosing the parameters τ and Δ of the model, thus closing the procedure for obtaining magic numbers. A good agreement is found between the magic numbers obtained through our model and the experimental results.

ADVANCES IN QUANTUM CHEMISTRY, VOLUME 40

0065-3276/01 $35.00

1 Introduction

Metal clusters have been the subject of both experimental and theoretical investigations for a long time (see, for example, review articles [1]-[3] and references therein). A new period in their study began with the discovery of magic numbers in cluster abundances [4]-[9], analogous to those appearing in the shell structure of atoms and nuclei [10]. This analogy led to the description of metal clusters in terms of the Nilsson–Clemenger model [11], which is a simplified version of the Nilsson model [12]-[15] used for atomic nuclei, in which spin-orbit interaction is neglected. The basic idea in these models is that free electrons in metal clusters move almost independently in the mean field created by uniformly distributed metal cations. Theoretical investigations in terms of the jellium model [16, 17] have shown that in the case of simple metal clusters the mean-field potential is similar to the Woods–Saxon potential for atomic nuclei [18] with a slight modification of a "wine bottle" type [19]. The Woods–Saxon potential itself looks like that of a harmonic oscillator truncated at a certain energy and flattened at the bottom. The "wine bottle" type correction takes into account a potential local maximum in the middle of the cluster.

It should be mentioned that the Nilsson-type potentials are implicitly non-local, since some of their parameters change slightly from shell to shell. On the other hand, a modified quantum theory based on the "deformation" of some standard symmetries used in quantum mechanics may describe the nonlinearity and non-locality of the interaction and take into account the deformability of the system as a whole. These symmetry "deformations" are usually referred to as q-deformations, and are described by the so-called q-deformed algebras (see, for instance, the review article [20]). In particular, a q-deformed version of

the 3-dimensional harmonic oscillator based on the "deformation" of the basic commutation relations [21] seems to be appropriate for the description of the non-locality of the mean field potential of the cluster and to take into account its intrinsic deformations.

Recently it has been shown [21] that the spectrum of this q-deformed, 3-dimensional harmonic oscillator ($Q3O$) reproduces very well that of the modified harmonic oscillator introduced by Nilsson [12, 15] without the spin-orbit coupling term. Since the Nilsson model without spin-orbit coupling is essentially the Nilsson–Clemenger model used for the description of metal clusters [11], it is worth examining whether the $Q3O$ model can be used to reproduce the magic numbers and some other properties of simple metal clusters.

Indeed it has been found [22] that $Q3O$ (which follows $u_q(3) \supset so_q(3)$ symmetry) yields correctly all magic numbers experimentally observed for alkali metal clusters up to 1500, the expected limit of validity for theories based on the filling of electronic shells [4]. This indicates that $u_q(3)$, which is a nonlinear deformation of the $u(3)$ symmetry describing the 3-dimensional isotropic (spherical) harmonic oscillator, is a good candidate for describing the symmetry of alkali metal clusters.

This paper discusses in greater detail those properties of the $Q3O$ that are needed for the description of metal clusters. We also calculate the full energy of the metal cluster and its second derivative as functions of the number of particles in the cluster and the deformation parameter of the oscillator.

2 A short overview of q-deformed algebras and some simple applications

It is well known that a set of observables $A_1, A_2, \ldots, A_f$ forms a Lie algebra if the commutator of every pair of observables can be expressed as a linear combination of observables in the set, i.e.:

$$[A_i, A_j] = \sum_k C_{ij}^k A_k. \tag{1}$$

In principle it is possible to replace the linear combination by an arbitrary (nonlinear) function $f_{ij}(q; A_1, \ldots, A_f)$ which depends on a parameter q, i.e.:

$$[A_i, A_j] = f_{ij}(q; A_1, \ldots, A_f). \tag{2}$$

If, in the limit $q \to 1$, one has

$$\lim_{q \to 1} f_{ij}(q; A_1, \ldots, A_f) = \sum_k C_{ij}^k A_k,$$

then one can say that (2) is a (nonlinear) q-deformation of the Lie algebra (1).

To avoid abstract definitions we shall give a simple example. As is well known, the angular momentum operators J_+, J_0, J_- satisfy the commutation relations

$$[J_\pm, J_0] = \pm J_\pm\,, \qquad [J_+, J_-] = 2J_0, \tag{3}$$

which thus close the Lie algebra $su(2)$ of angular momenta. Let us now introduce the function

$$[\mathcal{A}]_q \equiv \frac{q^{\mathcal{A}} - q^{-\mathcal{A}}}{q - q^{-1}}, \tag{4}$$

where $\mathcal{A}$ may be a number or an operator. Obviously, $\lim_{q\to 1}[\mathcal{A}]_q = \mathcal{A}$. We can then write a q-deformation of the algebra (3) in the form:

$$[L_\pm, L_0] = \pm L_\pm\,, \qquad [L_+, L_-] = [2L_0]_q. \tag{5}$$

The algebra (5) is known as a q-deformation of the $su(2)$-algebra, which is denoted as $su_q(2)$, while the operators that satisfy (5) are referred to as q-deformed angular momentum operators. Here the standard angular momentum operators are denoted by J_k, while we use the notation L_m for q-deformed ones.

In definition (4) q may be a real number, $q = e^\tau$, or a phase factor, $q = e^{i\tau}$. In these two cases one has, respectively:

$$[\mathcal{A}] = \begin{cases} \dfrac{\sin(\mathcal{A}\tau)}{\sin(\tau)} & \text{if } q = e^{i\tau}, \\ \dfrac{\sinh(\mathcal{A}\tau)}{\sinh(\tau)} & \text{if } q = e^{\tau}. \end{cases} \tag{6}$$

Here the subscript q in the bracket $[...]_q$ is omitted. In the case $q = e^{i\tau}$ the q-deformed angular momentum algebra takes the form:

$$[L_\pm, L_0] = \pm L_\pm\,,\ [L_+, L_-] = \frac{\sin(2L_0\tau)}{\sin(\tau)} \approx \left\{2L_0 + \left(\frac{1}{3}L_0 - \frac{4}{3}L_0^3\right)\tau^2 + \mathcal{O}(\tau^5)\right\}, \tag{7}$$

i.e., for small τ there is a small difference between standard and q-deformed angular momentum algebras.

From a mathematical viewpoint this small difference is essential, although there is a strong similarity between the representation theories of the standard and q-deformed $su(2)$-algebras. In the case of the standard algebra (3) one can define the following operator:

$$C_2[su(2)] \equiv \mathbf{L}^2 = \frac{1}{2}\left(J_+J_- + J_-J_+\right) + J_0^2, \tag{8}$$

known as the second-order Casimir operator (or angular momentum "length"), which commutes with all operators of the algebra. The eigenvalues of this Casimir operator are $l(l+1)$, where l is an integer or half-integer number that determines

the dimension of the representation space. The vectors in this space are labeled with the eigenvalues of J_0 (projection of the angular momentum operator), i.e., by the quantum number m which takes on the values $m = l, l-1, \ldots, -l$.

By analogy, in the $su_q(2)$-algebra one can find an operator (the q-deformed Casimir operator or q-deformed angular momentum "length") with the form:

$$C_2^q[su_q(2)] \equiv {}^q\mathbf{L}^2 = L_- L_+ [L_0][L_0 + 1], \tag{9}$$

which commutes with all operators of the q-deformed angular momentum algebra. Its eigenvalues are $[l][l+1]$, where l again is an integer or half-integer number that determines the dimension of the representation space, and the vectors in this space are labeled with the eigenvalues m of q-deformed L_0 which take on the values $m = l, l-1, \ldots, -l$.

The above example – in particular Eq. (7) – may give the wrong impression that q-deformations only yield small deviations from the standard symmetries used in quantum mechanics, which could be treated in a perturbative way. However, the q-deformation of an algebra changes drastically the mathematical structure of the theory, giving rise to a new kind of algebra known as Hopf algebra. In addition, from the physical viewpoint, it may be significant to make it possible to q-deform standard commutation relations and to reach in this manner a new quantum theory, more appropriate for the description of systems that are space-extended and / or deformable.

In order to illustrate this approach, we shall consider two simple quantum systems: the rigid rotator and the one-dimensional harmonic oscillator. Since the rotational and vibrational motions are incorporated in a natural way in the quantum behavior of the 3-dimensional harmonic oscillator, these examples will provide a good basis for understanding the properties of more general systems.

2.1 The q-deformed rigid rotator

The interest for possible applications of quantum algebras in physics has been awaken by the introduction of q-deformed boson creation and annihilation operators [23].

As is well known, in many problems of quantum mechanics it is useful to introduce the following operators:

$$a^\dagger = \sqrt{\frac{1}{2\hbar}}\,(q - ip)\,, \quad a = \sqrt{\frac{1}{2\hbar}}\,(q + ip)\,, \tag{10}$$

where q and p are the position and momentum operators, respectively. These operators, together with that representing the number of particles: $B = a^\dagger a$, close the algebra:

$$[B, a^\dagger] = a^\dagger, \quad [B, a] = -a, \tag{11}$$

$$[a, a^\dagger] = 1, \tag{12}$$

known as the Heisenberg-Weyl algebra.

This algebra can be deformed by introducing operators b and $b^\dagger$ together with a number operator N satisfying the commutation relations:

$$[N, b^\dagger] = b^\dagger, \quad [N, b] = -b, \tag{13}$$

$$bb^\dagger - q^{\pm 1} b^\dagger b = q^{\mp N}. \tag{14}$$

A consequence of these relations is that:

$$b^\dagger b = [N], \quad bb^\dagger = [N+1]. \tag{15}$$

In addition, the following conditions of Hermitian conjugation hold for q being a real number or a root of unity:

$$(b^\dagger)^\dagger = b, \quad N^\dagger = N. \tag{16}$$

Eq. (13) has the same form as Eq. (11) while Eq. (14) departs from Eq. (12) by the presence of a deformation parameter q. It should be noted that the number operator N is *not* equal to $b^\dagger b$ as in the standard formalism. Operators $b^\dagger$ and b are referred to as *q-deformed boson creation and annihilation operators*, respectively. The algebra defined by Eqs (13) and (14) is a q-deformation of the algebra (11, 12). It is clear that for $q \to 1$ Eq. (14) goes to the usual boson commutation relation (12).

In the case of the q-deformed angular momentum algebra $su_q(2)$ the generators can be mapped onto q-deformed bosons in the following way [23]:

$$L_+ = b_1^\dagger b_2, \quad L_- = b_2^\dagger b_1, \quad L_0 = \frac{1}{2}(N_1 - N_2), \tag{17}$$

where $b_i^\dagger$, b_i and N_i are q-deformed boson creation, annihilation and number operators. One can easily check that these boson images satisfy the commutation relations (5).

In the q-boson picture the normalized highest weight vector is:

$$|JJ\rangle = \frac{(b_1^\dagger)^{2J}}{\sqrt{[2J]!}}|0\rangle, \tag{18}$$

whereas the general vector $| JM >$ is given by:

$$|JM\rangle = \frac{(b_1^\dagger)^{J+M}}{\sqrt{[J+M]!}} \frac{(b_2^\dagger)^{J-M}}{\sqrt{[J-M]!}}|0\rangle. \tag{19}$$

The q-deformed rotator corresponds to the Hamiltonian:

$$H = \frac{1}{2I} C_2[su_q(2)] + E_0, \tag{20}$$

where I is the moment of inertia and E_0 the band head energy (for ground state bands $E_0 = 0$). For q being a real number, i.e., for $q = e^{\tau}$ with τ real, the energy levels of the q-rotator are:

$$E(J) = \frac{1}{2I}[J][J+1] + E_0 = \frac{1}{2I}\frac{\sinh(\tau J)\sinh[\tau(J+1)]}{\sinh^2(\tau)} + E_0, \qquad (21)$$

whereas for q being a phase factor, i.e., for $q = e^{i\tau}$ with τ real, one obtains:

$$E(J) = \frac{1}{2I}[J][J+1] + E_0 = \frac{1}{2I}\frac{\sin(\tau J)\sin[\tau(J+1)]}{\sin^2(\tau)} + E_0. \qquad (22)$$

Raychev *et al.* [24] have shown that good fits can be obtained for nuclear rotational spectra of "even–even" rare earths as well as actinide elements by using Eq. (22). Furthermore, it has been shown [25]-[28] that Eq. (22) may also give a good description of such effects as "backbending" and "staggering" in rotational spectra of superdeformed nuclei and diatomic molecules as well. It can be seen that Eq. (21) fails in describing such spectra.

It is empirically known that nuclear rotational spectra can be reproduced by using the following expansion for the rotational energy:

$$E(J) = AJ(J+1) + B[J(J+1)]^2 + C[J(J+1)]^3 + D[J(J+1)]^4 + \ldots, \qquad (23)$$

where the coefficients A, B, C, D, ...have alternating signs (starting with A positive) and decrease by about 3 orders of magnitude from one term to the next (see, e.g., [29]).

Making a Taylor expansion of the factors in the numerator of Eq. (21) / Eq. (22) and summing up the coefficients in front of the same powers of $J(J+1)$ one obtains, in both cases, expressions of the form (23), but for q real - Eq. (21) - it is impossible to get alternating signs while for q imaginary - Eq. (22) - the condition of alternating signs is fulfilled. This results in that the energy levels given by Eq. (21) increase more rapidly than those given by the simple $J(J+1)$ rule, while those given by Eq. (22) increase less rapidly than with the $J(J+1)$ rule (Fig. 1).

In order to check the order of magnitude of the coefficients for small values of τ, one may expand the spherical Bessel functions appearing in the Taylor expansions of Eq. (22) and keep only the lowest-order term in each expansion. The result is:

$$\begin{aligned} E(J) &= E_0 + \frac{1}{2I}\{J(J+1) - \frac{\tau^2}{3}[J(J+1)]^2 + \frac{2\tau^4}{45}[J(J+1)]^3 \\ &\quad - \frac{\tau^6}{315}[J(J+1)]^4 + \frac{2\tau^8}{14175}[J(J+1)]^5 - \ldots\}. \end{aligned} \qquad (24)$$

One notices that each term contains a factor τ^2 more than the previous term. For τ in the range about 0.03 [24], τ^2 is of the order of 10^{-3}, as expected.

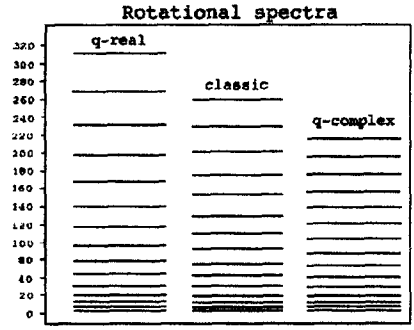

Figure 1: Comparison of the rotational spectra of the rigid rotator (center) and of the q-deformed system with q being a real number (left) or a phase factor (right).

It is worth noticing that in order to guarantee that $E(J)$ be an increasing function of J in Eq. (22), one must have

$$\tau(J+1) \leq \frac{\pi}{2}, \tag{25}$$

which defines a limit for the deformation parameter τ.

2.2 The q-deformed harmonic oscillator

The basis of the Fock space is defined by repeated action of the creation operator $b^\dagger$ on the vacuum state, which is annihilated by b:

$$b|0\rangle = 0, \qquad |n\rangle = \frac{(b^\dagger)^n}{\sqrt{[n]!}}|0\rangle. \tag{26}$$

The action of the q-deformed boson operators on the basis (26) is given by:

$$N|n\rangle = n|n\rangle, \qquad b^\dagger|n\rangle = \sqrt{[n+1]}|n+1\rangle, \qquad b|n\rangle = \sqrt{[n]}|n-1\rangle. \tag{27}$$

These equations are similar to those of the standard case, except there appear q-numbers instead of usual numbers under the square-root signs.

The Hamiltonian of the q-deformed harmonic oscillator can be written in terms of the q-deformed boson operators in the standard way:

$$H = \frac{\hbar\omega}{2}(bb^\dagger + b^\dagger b), \tag{28}$$

and its eigenvalues in the q-deformed basis (26) are:

$$E(n) = \frac{\hbar\omega}{2}([n] + [n+1]). \tag{29}$$

In particular, for q being a real number ($q = e^{\tau}$) the eigenvalues can be written in the form:

$$E(n) = \frac{\hbar\omega}{2} \frac{\sinh\left(\tau\left(n+\frac{1}{2}\right)\right)}{\sinh\frac{\tau}{2}}, \tag{30}$$

whereas for q being a phase factor ($q = e^{i\tau}$) one obtains:

$$E(n) = \frac{\hbar\omega}{2} \frac{\sin\left(\tau\left(n+\frac{1}{2}\right)\right)}{\sin\frac{\tau}{2}}. \tag{31}$$

In both cases, in the limit $q \to 1$ ($\tau \to 0$) one gets the standard expression for the energy of the one-dimensional harmonic oscillator:

$$E(n) = \hbar\omega\left(n+\frac{1}{2}\right). \tag{32}$$

One can easily see that for q real the energy eigenvalues increase more rapidly than in the ordinary case, in which the spectrum lines are equidistant (i.e., the spectrum gets "expanded"); whereas for q being a phase factor ($q = e^{i\tau}$ with τ real) the energy eigenvalues increase less rapidly than in the ordinary case (i.e., the spectrum gets "compressed"). In addition, when q is a phase factor there exist only a limited number of states, and the maximal value of n is given by the condition

$$\tau\left(n_{max}+\frac{1}{2}\right) \leq \frac{\pi}{2}. \tag{33}$$

The above condition allows one to determine the deformation parameter τ when the maximal number of states is known.

A comparison of the standard harmonic oscillator spectrum with the corresponding q-deformed oscillator spectra for q real and q complex is given in Fig. (2).

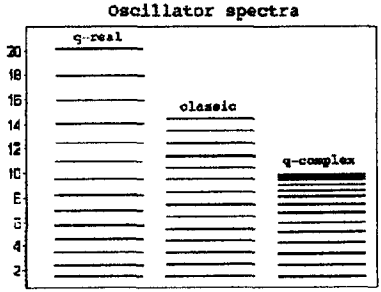

Figure 2: Comparison of the vibrational spectra of the harmonic oscillator (center) and of the q-deformed system with q being a real number (left) or a phase factor (right).

3 The q-deformed, 3-dimensional harmonic oscillator ($Q3O$)

As is well known, the standard 3-dimensional harmonic oscillator is a manifestation of the standard $u(3) \supset so(3)$ symmetry. It is instructive to see how a q-deformed version of the 3-dimensional harmonic oscillator is related to the $u_q(3)$ algebra and its $so_q(3)$ subalgebra. The construction of the Hamiltonian of the q-deformed, 3-dimensional harmonic oscillator is a non-trivial problem, because one has first to construct the square of the q-deformed angular momentum operator.

3.1 The $so_q(3)$ subalgebra of $u_q(3)$ and its basis states

Let us define three independent, q-deformed boson creation and annihilation operators, $b_i^\dagger$ and b_i ($i = +, 0, -$), and the corresponding number operators N_i, which satisfy the commutation relations:

$$[N_i, b_i^\dagger] = b_i^\dagger, \qquad [N_i, b_i] = -b_i, \qquad b_i b_i^\dagger - q^{\pm 1} b_i^\dagger b_i = q^{\mp N_i}. \tag{34}$$

It was shown in [30] that the $so_q(3)$ subalgebra of $u_q(3)$ can be defined only in the space of completely symmetric irreducible representations (SIRs) of $u_q(3)$, the basis states of which have the following form:

$$|n_+ n_0 n_-\rangle = \frac{(b_+^\dagger)^{n_+} (b_0^\dagger)^{n_0} (b_-^\dagger)^{n_-}}{\sqrt{[n_+]![n_0]![n_-]!}} |0\rangle, \tag{35}$$

the q-boson annihilation operators yielding $b_i|0\rangle = 0$ and the corresponding number operators yielding $N_i|n_+ n_0 n_-\rangle = n_i|n_+ n_0 n_-\rangle$, where i stands for $+, 0, -$. As usual, the q-numbers $[x]$ are defined as in Eq. (4).

The elements of the $so_q(3)$ algebra (the angular momentum operators) acting on the Fock space of the totally symmetric representations [N,0,0] of $u_q(3)$ (which is the space of the $Q3O$) have been obtained by van der Jeugt [30]. In the space defined by Eq. (35), the elements

$$\begin{aligned} L_+ &= q^{N_- - \frac{1}{2}N_0} \sqrt{q^{N_+} + q^{-N_+}}\, b_+^\dagger b_0 + b_0^\dagger b_-\, q^{N_+ - \frac{1}{2}N_0} \sqrt{q^{N_-} + q^{-N_-}}, \\ L_- &= b_0^\dagger b_+ q^{N_- - \frac{1}{2}N_0} \sqrt{q^{N_+} + q^{-N_+}} + q^{N_+ - \frac{1}{2}N_0} \sqrt{q^{N_-} + q^{-N_-}}\, b_-^\dagger b_0, \\ L_0 &= N_+ - N_-, \end{aligned} \tag{36}$$

which satisfy the commutation relations

$$[L_0, L_\pm] = \pm L_\pm, \quad [L_+, L_-] = [2L_0], \tag{37}$$

close the $so_q(3)$ algebra. Due to the fact that L_0 alone generates the $so_q(2)$ subalgebra, there stands the following chain of subalgebras:

$$su_q(3) \supset so_q(3) \supset so_q(2). \tag{38}$$

The $so_q(3)$ basis vectors can be written in terms of the basis vectors (35) as:

$$\begin{aligned} |N, L, M> \; &= q^{-[(L+M)(L+M-1)]/4} \sqrt{\frac{[N+L]!![2L+1][L+M]![L-M]!}{[N-L]!![N+L+1]!}} \\ &\times \sum_x q^{(2L-1)x/2} s^{(N-L)/2} \frac{|x, L+M-2x, x-M>}{\sqrt{[2x]!![L+M-2x]![2x-2M]!!}}, \end{aligned} \tag{39}$$

where the following notation is used:

$$s = (b_0^\dagger)^2 q^{N_+ + N_- + 1} - \sqrt{\frac{[2N_+][2N_-]}{[N_+][N_-]}} b_+^\dagger b_-^\dagger q^{-N_0 - \frac{1}{2}}, \tag{40}$$

and x takes on values from $max(0, M)$ to $[(L+M)/2]$ in steps of 1, L from N to 1 or 0 in steps of 2, M from $-L$ to $+L$ in steps of 1, and (e.g.) $[2x]!! = [2x][2x-2]\ldots[2]$. The action of the generators of $so_q(3)$ on the above defined states is given by:

$$L_0 \, |N, L, M> = M \, |N, L, M>, \tag{41}$$

$$L_\pm \, |N, L, M> = \sqrt{[L \mp M][L \pm M + 1]} \, |N, L, M \pm 1> . \tag{42}$$

The second-order Casimir operator of $so_q(3)$ takes the form

$$C_2[so_q(3)] = L^2 = L_- L_+ + [L_0][L_0 + 1], \tag{43}$$

and its action on the basis (39) is given by

$$C_2[so_q(3)] \, |N, L, M> = [L][L+1] \, |N, L, M> . \tag{44}$$

It can easily be seen that in the limit $q \to 1$, for which $[x] \to x$, the above equations yield their classical analogs.

A simplified form of the subalgebra $so_q(3)$ can be obtained by introducing the operators [31]

$$\begin{aligned} B_0 &= q^{-\frac{1}{2}N_0} b_0, & B_0^\dagger &= b_0^\dagger q^{-\frac{1}{2}N_0}, \\ B_i &= q^{N_i + \frac{1}{2}} b_i \sqrt{\frac{[2N_i]}{[N_i]}}, & B_i^\dagger &= \sqrt{\frac{[2N_i]}{[N_i]}} b_i^\dagger q^{N_i + \frac{1}{2}} \qquad (i = +, -). \end{aligned} \tag{45}$$

Here we shall consider only real values for the deformation parameter q (i.e., $q = e^\tau$ with τ real). The above-defined operators satisfy the usual commutation relations:

$$[N_i, B_i^\dagger] = B_i^\dagger, \qquad [N_i, B_i] = -B_i \, , \tag{46}$$

while in the Fock space, spanned by the normalized eigenvectors of the excitation number operators N_+, N_0, N_-, they satisfy the following commutation relations:

$$[B_0, B_0^\dagger] = q^{-2N_0}, \qquad [B_i, B_i^\dagger] = [2]q^{4N_i+1} \qquad (i = +, -). \tag{47}$$

It has been shown [31] that the angular momentum operators defined by Eqs (36), expressed in terms of the modified boson operators given by Eq. (45), take the simple form:

$$\begin{aligned} L_+ &= q^{-L_0+\frac{1}{2}} B_+^\dagger B_0 + q^{L_0-\frac{1}{2}} B_0^\dagger B_-, \\ L_- &= q^{-L_0-\frac{1}{2}} B_0^\dagger B_+ + q^{L_0+\frac{1}{2}} B_-^\dagger B_0, \\ L_0 &= N_+ - N_-, \end{aligned} \tag{48}$$

and satisfy the standard $so_q(3)$ commutation relations:

$$[L_0, L_\pm] = \pm L_\pm, \qquad [L_+, L_-] = [2L_0]. \tag{49}$$

Here we have restricted our considerations to real q because the operators L_+, L_-, L_0, given by Eqs (48), are not invariant with respect to the interchange $q \leftrightarrow q^{-1}$.

Using the definitions above, the Casimir operator corresponding to $so_q(3)$ can be written in the form [32]:

$$\begin{aligned} C_2^{(q)} &= \frac{1}{2}\left\{L_+L_- + L_-L_+ + [2][L_0]^2\right\} \\ &= L_-L_+ + [L_0][L_0+1] = L_+L_- + [L_0][L_0-1]. \end{aligned} \tag{50}$$

One can also define q-deformed states, $|n\ell m\rangle_q$, satisfying the following eigenvalue equations:

$$C_2^{(q)}|n\ell m\rangle_q = [\ell][\ell+1]|n\ell m\rangle_q, \quad L_0|n\ell m\rangle_q = m|n\ell m\rangle_q, \quad N|n\ell m\rangle_q = n|n\ell m\rangle_q. \tag{51}$$

Here $N = N_+ + N_0 + N_-$ is the total number operator for the q-deformed bosons, and the second-order Casimir operator is equal, by definition, to the square of the q-deformed angular momentum operator. These states have the following form [31]:

$$\begin{aligned} |n\ell m\rangle_q = {} & q^{\frac{1}{4}(n-\ell)(n+\ell+1)-\frac{1}{2}m^2} \sqrt{\frac{[n-\ell]!![\ell+m]![\ell-m]![2\ell+1]}{[n+\ell+1]!!}} \\ & \times \sum_{t=0}^{(n-\ell)/2} \sum_{p=\max(0,m)}^{\lfloor(\ell+m)/2\rfloor} \frac{(-1)^t q^{-(n+\ell+1)t}}{[2t]!![n-\ell-2t]!!} \frac{(B_+^\dagger)^{p+t}}{[2p]!!} \\ & \times \frac{(B_0^\dagger)^{n+m-2p-2t}}{[n+m-2p]!} \frac{(B_-^\dagger)^{p+t-m}}{[2p-2m]!!}|0\rangle, \end{aligned} \tag{52}$$

where $|0\rangle$ is the vacuum state, $[n]! = [n][n-1]\ldots[1]$, and $[n]!! = [n][n-2]\ldots[2]$ or $[1]$. The states (52) form a basis for the most symmetric representation $[n, 0, 0]$ of $u_q(3)$, corresponding to the chain $u_q(3) \supset so_q(3)$.

3.2 Irreducible tensor operators of the $so_q(3)$ subalgebra and construction of spherical vector operators

We shall first recall some definitions about q-deformed tensor operators within the framework of the $so_q(3)$ algebra.

Using the following definition of a q-commutator:

$$[A, B]_{q^\alpha} = AB - q^\alpha BA, \tag{53}$$

an irreducible tensor operator of rank j (with parameter q) within the $so_q(3)$ algebra is defined as a set of $2j+1$ operators $\mathcal{T}^{(q)}_{jm}$ satisfying the following relations:

$$[L_0, \mathcal{T}^{(q)}_{jm}] = m\,\mathcal{T}^{(q)}_{jm}, \qquad [L_\pm, \mathcal{T}^{(q)}_{jm}]_{q^m} q^{L_0} = \sqrt{[j \mp m][j \pm m + 1]}\,\mathcal{T}^{(q)}_{jm\pm 1}. \tag{54}$$

The conjugate irreducible q-tensor operator $\tilde{\mathcal{T}}^{(q)}_{jm}$ is then given by:

$$\tilde{\mathcal{T}}^{(q)}_{jm} = (-1)^{j-m} q^{-m} \mathcal{T}^{(q)}_{j,-m}, \tag{55}$$

and satisfies the following commutation relations:

$$[\tilde{\mathcal{T}}^{(q)}_{jm}, L_0] = m\,\tilde{\mathcal{T}}^{(q)}_{jm}, \qquad q^{L_0}[\tilde{\mathcal{T}}^{(q)}_{jm}, L_\pm]_{q^m} = \sqrt{[j \pm m][j \mp m + 1]}\,\tilde{\mathcal{T}}^{(q)}_{j,m\mp 1}. \tag{56}$$

It can be shown that the Hermitian conjugate of (55), i.e.:

$$\mathcal{P}^{(q)}_{jm} = (\tilde{\mathcal{T}}^{(q)}_{jm})^\dagger = (-1)^{j-m} q^{-m} (\mathcal{T}^{(q)}_{j,-m})^\dagger, \tag{57}$$

is also an irreducible q-tensor operator of rank j.

Following prescriptions from [32] for the tensor product of two irreducible tensor operators $\mathcal{A}^{(q_1)}_{j_1 m_1}$ and $\mathcal{B}^{(q_2)}_{j_2 m_2}$, one can write:

$$\left[\mathcal{A}^{(q_1)}_{j_1} \times \mathcal{B}^{(q_2)}_{j_2}\right]^{(q_3)}_{jm} = \sum_{m_1, m_2} {}^{q_3}C^{jm}_{j_1 m_1, j_2 m_2} \mathcal{A}^{(q_1)}_{j_1 m_1} \mathcal{B}^{(q_2)}_{j_2 m_2}, \tag{58}$$

where ${}^{q_3}C^{jm}_{j_1 m_1, j_2 m_2}$ designates the Clebsch-Gordan coefficients corresponding to the deformation parameter q_3. In general, the deformation parameters q_1, q_2 and q_3 can be arbitrary, but if one imposes the condition that the left hand side of Eq. (58) transforms as an irreducible q-tensor of rank j in such a way that the Wigner-Eckart theorem can be applied to Eq. (58) as a whole, then not all combinations of q_1, q_2 and q_3 are allowed.

Let us define the scalar product of two q-tensor operators depending on different variables (1) and (2) and acting on different vectors depending on these two variables. In this particular case the scalar product of the irreducible q and q^{-1}–tensor operators $\mathcal{A}^{(q)}_j(1)$ and $\mathcal{B}^{(1/q)}_j(2)$ of same rank, acting on the two vectors (1) and (2), is given by:

$$\begin{aligned} (\mathcal{A}^{(q)}_j(1) \cdot \mathcal{B}^{(1/q)}_j(2))^q &= (-1)^j \sqrt{[2j+1]}\left[\mathcal{A}^{(q)}_j(1) \times \mathcal{B}^{(1/q)}_j(2)\right]^{(q)}_{00} \\ &= \sum_m (-q)^m \mathcal{A}^{(q)}_{jm}(1)\, \mathcal{B}^{(1/q)}_{j-m}(2). \end{aligned} \tag{59}$$

It should be noted that the simplified angular momentum operators (48) satisfy the commutation relations (49) but are *not* tensor operators in that sense. However, one can use them to construct angular momentum operators that are first-rank tensors (i.e., $so_q(3)$ vectors) in the following way:

$$\begin{aligned}
\mathcal{L}^{(q)}_{\pm 1} &= \mp \frac{1}{\sqrt{[2]}} q^{-L_0} L_{\pm}, \\
\mathcal{L}^{(q)}_{0} &= \frac{1}{[2]} \left\{ q[2L_0] + (q - q^{-1}) L_- L_+ \right\} \\
&= \frac{1}{[2]} \left\{ q[2L_0] + (q - q^{-1}) \left(C_2^{(q)} - [L_0][L_0 + 1] \right) \right\}.
\end{aligned} \tag{60}$$

On the other hand, the modified boson operators B_i and $B_i^\dagger$ are *not* components of a tensor operator in the sense of the above definitions. However, as shown in [31], one can use them to define a vector operator $T^\dagger_m$ as:

$$\begin{aligned}
T^\dagger_{+1} &= \frac{1}{\sqrt{[2]}} B^\dagger_+ q^{-2N_+ + N - \frac{1}{2}}, \qquad T^\dagger_0 = B^\dagger_0 q^{-2N_+ + N}, \\
T^\dagger_{-1} &= \frac{1}{\sqrt{[2]}} \left\{ B^\dagger_- q^{2N_+ - N - \frac{1}{2}} - (q - q^{-1}) B_+ (B^\dagger_0)^2 q^{-2N_+ + N + \frac{3}{2}} \right\},
\end{aligned} \tag{61}$$

and the corresponding conjugate, $\tilde{T}_m = (-1)^m q^{-m} (T^\dagger_{-m})^\dagger$, as:

$$\begin{aligned}
\tilde{T}_{+1} &= -\frac{1}{\sqrt{[2]}} \left\{ q^{2N_+ - N - \frac{3}{2}} B_- - (q - q^{-1}) q^{-2N_+ + N + \frac{1}{2}} B^\dagger_+ (B_0)^2 \right\}, \\
\tilde{T}_0 &= q^{-2N_+ + N} B_0, \qquad \tilde{T}_{-1} = -\frac{1}{\sqrt{[2]}} q^{-2N_+ + N + \frac{1}{2}} B_+.
\end{aligned} \tag{62}$$

The operators T_i (and $T^\dagger$ as well) *do not commute* among themselves.

3.3 Choice of the angular momentum

Following the above argumentation, the angular momentum operator $\mathcal{L}^{(q)}_M$, considered as a vector operator in $so_q(3)$, can be represented in the form of a vector product:

$$\mathcal{L}^{(q)}_M = -\sqrt{\frac{[4]}{[2]}} \left[T^\dagger \times \tilde{T} \right]^{(1/q)}_{1M} = -\sqrt{\frac{[4]}{[2]}} \sum_{m,n} {}^{1/q}C^{1M}_{1m1n} T^\dagger_m \tilde{T}_n. \tag{63}$$

It can be shown [32] that its square can be written as:

$$(\mathcal{L}^{(q)})^2 \equiv \mathcal{L}^{(q)} \cdot \mathcal{L}^{(q)} = \sum (-q)^{-M} \mathcal{L}^{(q)}_M \mathcal{L}^{(q)}_{-M} = \frac{2}{[2]} C_2^{(q)} + \left(\frac{q - q^{-1}}{[2]} \right)^2 (C_2^{(q)})^2. \tag{64}$$

This expression differs from that of $C_2^{(q)}$ given above. However this difference is not essential, for if we take the expectation value of the operator $\mathcal{L}^{(q)} \cdot \mathcal{L}^{(q)}$ the result is:

$$ {}_q\langle \ell m | \mathcal{L}^{(q)} \cdot \mathcal{L}^{(q)} | \ell m \rangle_q = \frac{[2l][2l+2]}{[2]^2} = [l]_{q^2}[l+1]_{q^2}, \tag{65} $$

and therefore the replacement of ${}^q\mathbf{L}^2 \equiv C_2^{(q)}$ by $\mathcal{L}^{(q)} \cdot \mathcal{L}^{(q)}$ is equivalent to the replacement of q by q^2, which involves only the renormalization of some constant. For this reason we shall adopt as the square of the angular momentum operator the quantity ${}^q\mathbf{L}^2 \equiv C_2^{(q)}$, whose eigenvalues $[\ell][\ell+1]$ resemble the classical ones.

3.4 Choice of the $Q3O$ Hamiltonian and comparison with the Nilsson model

The Hamiltonian of the q-deformed, 3-dimensional harmonic oscillator must be defined in such a way as to satisfy the following requirements:

a) It is a scalar in $so_q(3)$, i.e., the energy is measurable simultaneously with the q-deformed angular momentum related to the $so_q(3)$ algebra and with its z-projection. Here $so_q(3)$ is the algebra corresponding to the 3-dimensional angular momenta "deformed" as a result of the q-deformation of the basic commutation relations.

b) It conserves the number of bosons in terms of which the quantum algebras $u_q(3)$ and $so_q(3)$ are represented.

c) In the limit $q \to 1$ (i.e., when the q-deformation disappears) it turns back to the Hamiltonian of the standard, 3-dimensional harmonic oscillator.

Let us now consider the following scalar operator, constructed in terms of $T_M^\dagger$ and $\tilde{T}_M$ as defined by Eqs (61) and (62):

$$ X_0^{(q)} = -\sqrt{[3]}[T^\dagger \times \tilde{T}]_{00}^{(1/q)} = -q^{-1}T_{+1}^\dagger \tilde{T}_{-1} + T_0^\dagger \tilde{T}_0 - qT_{-1}^\dagger \tilde{T}_{+1}. \tag{66} $$

We shall introduce the $Q3O$ Hamiltonian by the following expression:

$$ {}^qH_3 = \hbar\omega_0 X_0 = \hbar\omega_0 \left(-q^{-1}T_{+1}^\dagger \tilde{T}_{-1} + T_0^\dagger \tilde{T}_0 - qT_{-1}^\dagger \tilde{T}_{+1}\right). \tag{67} $$

This operator is a scalar in $so_q(3)$, it conserves the number of bosons, and in the limit $q \to 1$ it yields:

$$ \lim_{q\to 1} {}^qH_3 = \hbar\omega_0 \left(a_{+1}^\dagger a_{+1} + a_0^\dagger a_0 + a_{-1}^\dagger a_{-1}\right), \tag{68} $$

with $[a_m, a_n^\dagger] = \delta_{mn}$, which coincides with the Hamiltonian of the 3-dimensional harmonic oscillator, but for an additive constant.

It must be noted that the Hamiltonian defined by Eq. (67) does not commute with the square of the "classical" angular momentum $\mathbf{L}^2$, because of the space deformation of the q-deformed oscillator. Hence, the "standard" quantum

number l is not a good quantum number for the system. Nevertheless, the Hamiltonian ${}^qH_3$ commutes with ${}^q\mathbf{L}^2$ and then, the "quantum" momentum value ℓ is a good quantum number. We have no problem with the projection of the angular momentum on the z axis because the standard projection, l_z, coincides with the quantum projection, ℓ_z.

It is convenient to modify Eq. (67) so as to make it physically more significant. Using the third component of the q-deformed angular momentum:

$$\mathcal{L}_0^{(q)} = -\sqrt{\frac{[4]}{[2]}}\left[T^\dagger \times \tilde{T}\right]_{10}^{(1/q)} = -T_{+1}^\dagger \tilde{T}_{-1} + (q-q^{-1})T_0^\dagger \tilde{T}_0 + T_{-1}^\dagger \tilde{T}_0,$$

we obtain:

$$X_0^{(q)} + q\mathcal{L}_0^{(q)} = -[2]T_{+1}^\dagger \tilde{T}_{-1} + q^2 T_0^\dagger \tilde{T}_0. \tag{69}$$

As we have

$$T_{+1}^\dagger \tilde{T}_{-1} = \frac{[2N_+]}{[2]} q^{-2N_+ + 2N + 1} \text{ and } T_0^\dagger \tilde{T}_0 = [N_0] q^{-4N_+ - N_0 + 2N - 1}, \tag{70}$$

we obtain

$$X_0^{(q)} = -q\mathcal{L}_{10}^{(q)} + [N + L_0] q^{N - L_0 + 1}, \tag{71}$$

and after some algebraic manipulation we get:

$${}^qH_3 = \hbar\omega_0 X_0^{(q)} = \hbar\omega_0 \left\{ [N] q^{N+1} - \frac{q(q-q^{-1})}{[2]} C_2^{(q)} \right\}. \tag{72}$$

The energy eigenvalues of this q-deformed Hamiltonian are given by:

$${}^qE_3 = \hbar\omega_0 \left\{ [n] q^{n+1} - \frac{q(q-q^{-1})}{[2]} [\ell][\ell+1] \right\}, \tag{73}$$

where n is the vibrational quantum number and ℓ is the angular momentum value: $\ell = n, n-2, \ldots, 0$ or 1. It can easily be seen that in the limit $q \to 1$ one has $\lim_{q\to 1} E_q(n,l) = \hbar\omega_0 n$, which coincides with the classical result.

For small values of the deformation parameter τ in $q = e^\tau$, one may expand Eq. (73) in powers of τ, this yielding:

$$\begin{aligned} {}^qE_3 &= \hbar\omega_0 n - \hbar\omega_0 \tau \left[\ell(\ell+1) - n(n+1)\right] \\ &- \hbar\omega_0 \tau^2 \left[\ell(\ell+1) - \frac{1}{3} n(n+1)(2n+1)\right] + \mathcal{O}(\tau^3). \end{aligned} \tag{74}$$

Equation (74) bears a great similarity with that for the modified harmonic oscillator suggested by Nilsson and Clemenger [11, 12] where the spin-orbit coupling term is omitted:

$$V = \hbar\omega N - \hbar\omega\kappa'(\mathbf{L}^2 - < \mathbf{L}^2 >_N). \tag{75}$$

The energy eigenvalues of this modified harmonic oscillator are [21, 22]:

$$E_{nl} = \hbar\omega n - \hbar\omega\mu' \left[l(l+1) - n(n+3)/2\right], \tag{76}$$

where μ' is allowed to vary from shell to shell.

It has been proven [21] that the spectrum obtained with the $Q3O$ model closely resembles that of the modified harmonic oscillator of Nilsson and Clemenger. In both cases, the effect of the $l(l+1)$ term is to flatten the bottom of the harmonic oscillator potential, making it resemble the Woods–Saxon potential [18].

3.5 Determination of potentials for the $Q3O$ model

As shown in [22], the $Q3O$ model successfully describes the magic numbers of metal clusters. On the other hand, it is known that metal clusters are well described by Ekardt potentials [16] (for which analytical expressions are lacking), while these have recently been parameterized in terms of symmetrized Woods–Saxon and "wine-bottle" potentials [19] (for which analytical expressions are known).

Therefore the following question arises: in spite of the fact that the 3-dimension harmonic-oscillator potential is nonlocal and has specific properties, is it possible to derive potential forms which, put into the "standard" Schrödinger equation, will give about the same spectrum as the $Q3O$ model? This is a standard question in inverse scattering problems [33]. Classical potentials giving approximately the same spectrum as the q-deformed, one-dimensional harmonic oscillator have been obtained either through the use of standard perturbation theory [34], or within the WKB approximation [35].

In what follows we shall describe a procedure for determining potentials that give about the same spectrum as the $Q3O$ model, using perturbation theory [34]. According to this procedure, a potential may be chosen in the form:

$$V = V_0 + \kappa x^2 + \lambda x^4 + \mu x^6 + \xi x^8 + \cdots \tag{77}$$

Using first-order perturbation theory and keeping terms up to x^8 yields the spectrum:

$$\begin{aligned} E = {} & \epsilon_0 + \kappa + 3\lambda + 15\mu + 105\xi + (2\kappa + 6\lambda + 40\mu + 280\xi)n \\ & + (6\lambda + 30\mu + 350\xi)n^2 + (20\mu + 140\xi)n^3 + 70\xi n^4. \end{aligned} \tag{78}$$

The second term in Eq. (77) corresponds to the energy of the usual harmonic oscillator. For appropriate values of the numerical coefficients κ, λ, μ, ξ, the terms that follow can be considered as perturbations to this oscillator.

It is clear that this method can be applied to cases where the spectrum depends only on one quantum number n, the number of excitation quanta. For the $Q3O$, however, the spectrum (74) depends also on an additional quantum number ℓ, the angular momentum value. One way out is to search for an ℓ-dependent

equivalent potential, as is done in many branches of physics. In order to do so, for each possible value of ℓ one has to determine the energy as a function of n and then calculate the corresponding potential.

In the $Q3O$ model, the energy spectrum $E_q(n,\ell)$ for the various possible values of ℓ ($\ell = n,\ n-2,\ n-4,\ \ldots,\ 1$ or 0) can be put in the form [36]:

$$E_q(n,n) = \hbar\omega_0[n]_{q^2} \quad \text{for } \ell = n, \tag{79}$$

$$E_q(n,n-2) = \hbar\omega_0\left(q^2[n-1]_{q^2} + q^{2n}\right) \quad \text{for } \ell = n-2, \tag{80}$$

$$E_q(n,n-4) = \hbar\omega_0\left(q^4[n-2]_{q^2} + q^{2(n-1)}[2]_{q^2}\right) \quad \text{for } \ell = n-4, \quad \ldots \tag{81}$$

$$\begin{aligned} \ldots \quad E_q(n,2) &= \hbar\omega_0\left(q^6[[n-2]]_{q^2} + q^{-2}[[3]]_{q^2} - 1\right) = \\ &= E_q(n,0) - \hbar\omega_0(q^4 - q^{-2}) \quad \text{for } \ell = 2, \end{aligned} \tag{82}$$

$$E_q(n,1) = \hbar\omega_0\left(q^4[[n-1]]_{q^2} + 1\right) = E_q(n,0) - \hbar\omega_0(q^2 - 1) \quad \text{for } \ell = 1, \tag{83}$$

$$E_q(n,0) = \hbar\omega_0 q^2[[n]]_{q^2} \quad \text{for } \ell = 0, \tag{84}$$

where $[n]_q$ designates the q-numbers introduced in Eq. (4), which are symmetric under the exchange $q \leftrightarrow q^{-1}$, whereas $[[n]]_q$ designates the q-numbers:

$$[[n]]_q = \frac{q^n - 1}{q - 1}, \tag{85}$$

which are not symmetric under the exchange $q \leftrightarrow q^{-1}$. The formal difference between the expressions of types $E_q(n, n-p)$ and $E_q(n,q)$ arises from the double occurrence of n in the first type but not in the second, the two expressions yielding the same result, of course, for given values of n and $q = n - p$. All these expressions, as required, reduce to the classical expression $E(n) = \hbar\omega_0 n$ in the limit $q \to 1$.

We then consider the Taylor expansions of these energy expressions. By comparing them with Eq. (78) and equating the coefficients of the various powers of n (up to n^4), we determine the coefficients κ, λ, μ, ξ in each case. Substituting these coefficients in Eq. (77) and keeping the terms up to τ^4, we determine the corresponding potential in each case. We remark that for small values of τ the resulting potentials for $\ell = n,\ n-2,\ \ldots$ take the form:

$$V(x) = V_0 + ax^2 - bx^4 + cx^6 \quad (a,b,c > 0), \tag{86}$$

while the resulting potentials for $\ell = 0,\ 1,\ 2,\ \ldots$ take the form:

$$V(x) = V_0 + ax^2 + bx^4 + cx^6 + dx^8 \quad (a,b,c,d > 0), \tag{87}$$

where V_0 in both expansions and the coefficients in the first one are ℓ-dependent and all are polynomials of τ up to τ^4 [36].

The results of our analysis can be summarized as follows.

i) The Taylor expansions of the symmetrized Woods–Saxon and "wine-bottle" potentials, that have been used to fit the Ekardt potentials - which describe well metal clusters, have the same form as the potentials corresponding to the q-deformed, 3-dimensional harmonic oscillator. It is therefore not surprising that the $Q3O$ model gives a good description of the magic numbers of metal clusters.

ii) The potential expressions obtained through the use of perturbation theory are valid only near the origin ($x = 0$) and for relatively low values of n. They do not give information about the potential shape near the edge or for very large values of n. The determination of potential shapes accurate near the edges remains an open problem.

iii) For very large values of n the spectrum takes an exponential form. For example, Eq. (79) becomes (for $\tau > 0$):

$$E_q(n,n) = \hbar\omega_0 \frac{e^{2\tau n} - e^{-2\tau n}}{e^{2\tau} - e^{-2\tau}} \simeq \hbar\omega_0 \frac{e^{2\tau n}}{e^{2\tau} - e^{-2\tau}}. \tag{88}$$

Potentials with exponential spectra have been considered in Ref. [37], but there also the form of the potential could be determined only near the origin.

4 Energy expression for the metal cluster

The full energy of the metal cluster can be defined as:

$$E_{full} = \sum_{\bar{n}\bar{l}} E_{\bar{n}\bar{l}}, \tag{89}$$

where the sum is taken over all occupied states $\bar{n}\bar{l}$ and the single particle energies $E_{\bar{n}\bar{l}}$ are given by Eq. (73). As τ has the meaning of a deformation parameter, it is expected that this energy has a minimum for one or several values of τ, corresponding to cluster equilibrium. However, the expression for the energy given by Eq. (89) shows no peculiarities and increases monotonously with τ. On the other hand, the expression for the single particle energy (73) is not uniquely defined, in the sense that it can be the scalar expression of the Hamiltonian multiplied by an arbitrary scalar function of the deformation parameter, e.g. $q^{-n} = e^{-n\tau}$. Therefore it should be possible to find a suitable correction yielding the desired form for the energy E_{full}.

We found that a minimum in the full energy appears if we renormalize the energy expression by making the frequency factor $\hbar\omega_0$ in Eq. (73) depend on the deformation parameter τ, using the following prescription: $\hbar\omega_0 \to \hbar\omega_0(1+n\tau)^{-1}$, where n is the number of vibrational quanta. This form of the corrective factor is justified, for it results from the expansion of $q^{-n} = e^{-n\tau}$ for small τ:

$$e^{-n\tau} = 1 - n\tau + \ldots \approx \frac{1}{1+n\tau}.$$

At this stage of our research this renormalization seems a little bit intuitive, but we think that there exist deep physical reasons for its choice and this is the aim of our present investigation.

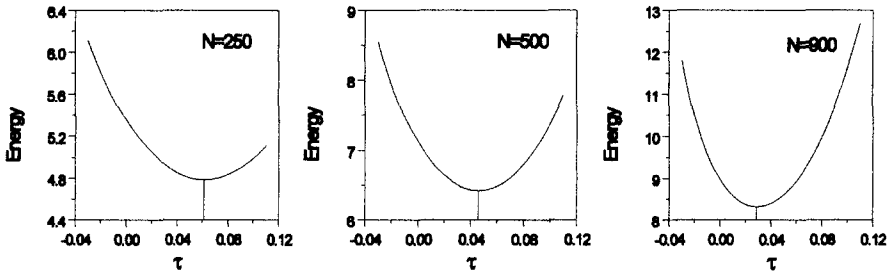

Figure 3: The full energy of the metal cluster as a function of the deformation parameter τ for three different values of the number of particles: $N = 250$ (left), $N = 500$ (center) and $N = 900$ (right). The minimum indicates the degree of q-deformation for which the cluster reaches an equilibrium shape.

Figure 3 displays the renormalized full energy of a few metal clusters, with different numbers of particles N, as a function of the deformation parameter τ. It can be seen that for every value of N the energy has a well pronounced minimum for a single value of τ, which determines the equilibrium shape of the cluster. It is worth noticing that the value of τ for which the energy achieves its minimum decreases with increasing size of the cluster. This means that small clusters are more deformed than larger ones, an expected result.

5 Results and Discussion

The calculations are performed in a standard way, the only critical point being the rearrangement of levels during the optimization procedure. This rearrangement is necessary for a correct treatment, because level crossing may impede a right counting of level degeneracies in the final summation.

The level scheme of the $Q3O$ for τ-dependent $\hbar\omega_0$ and $q = e^{\tau}$ with $\tau = 0.028$ is given in Table 1. Each level is characterized by the quantum numbers n (number of vibrational quanta) and l (eigenvalue of angular momentum). The maximal number of particles that a given level can accommodate is equal to $2(2\ell + 1)$.

Figure 4 displays the level scheme as a function of the deformation parameter τ. It is seen that, as in the Nilsson model, there exist level bunching areas followed by larger energy gaps separating different shells. Then, if the energy between two consecutive levels is larger than some characteristic value Δ it will be considered as a gap, and the number appearing above the gap will be recognized as a magic number (shown as $\star$ in Table 1).

Table 1: Energy spectrum of the q-deformed, 3-dimensional harmonic oscillator for τ-dependent $\hbar\omega_0$ and $q = e^{\tau}$ with $\tau = 0.028$. The magic numbers, marked $\star$, correspond to the energy gaps larger than 0.275, reported in boldface.

$n\ \ell$	Energy	$2(2\ell+1)$	Total	$n\ \ell$	Energy	$2(2\ell+1)$	Total
E[0 0] =	0.00000	(2)	[2] $\star$	E[7 5] =	6.64065	(22)	[220]
	0.97276			E[8 8] =	6.75325	(34)	[254] $\star$
E[1 1] =	0.97276	(6)	[8] $\star$		**0.32537**		
	0.92415			E[7 3] =	7.07862	(14)	[268]
E[2 2] =	1.89691	(10)	[18]	E[7 1] =	7.32017	(6)	[274]
E[2 0] =	2.06071	(2)	[20] $\star$	E[8 6] =	7.47995	(26)	[300]
	0.71840			E[9 9] =	7.49280	(38)	[338] $\star$
E[3 3] =	2.77911	(14)	[34]		**0.51293**		
E[3 1] =	3.04562	(6)	[40] $\star$	E[8 4] =	8.00573	(18)	[356]
	0.57977			E[10 10] =	8.22299	(42)	[398]
E[4 4] =	3.62538	(18)	[58] $\star$	E[9 7] =	8.30464	(30)	[428]
	0.36485			E[8 2] =	8.33720	(10)	[438]
E[4 2] =	3.99024	(10)	[68]	E[8 0] =	8.47852	(2)	[440] $\star$
E[4 0] =	4.14579	(2)	[70] $\star$		**0.43740**		
	0.29539			E[9 5] =	8.91592	(22)	[462]
E[5 5] =	4.44118	(22)	[92] $\star$	E[11 11] =	8.94715	(46)	[508]
	0.45949			E[10 8] =	9.11874	(34)	[542]
E[5 3] =	4.90066	(14)	[106]	E[9 3] =	9.33430	(14)	[556]
E[5 1] =	5.15408	(6)	[112]	E[9 1] =	9.56504	(6)	[562]
E[6 6] =	5.23146	(26)	[138] $\star$	E[12 12] =	9.66844	(50)	[612]
	0.55099			E[10 6] =	9.81364	(26)	[638]
E[6 4] =	5.78245	(18)	[156]	E[11 9] =	9.92597	(38)	[676] $\star$
E[7 7] =	6.00076	(30)	[186]		**0.39045**		
E[6 2] =	6.12981	(10)	[196]	E[10 4] =	10.31642	(18)	[694] $\star$
E[6 0] =	6.27790	(2)	[198] $\star$		**0.31697**		
	0.36275			E[10 2] =	10.63338	(10)	[704]

It was shown in Ref. [22] that the $Q3O$ model correctly reproduces all magic numbers observed for alkali metal clusters up to $N = 1500$, using for the model parameters the values $\tau = 0.038$, $\Delta = 0.39$. But there, these values were chosen more or less by trial and error, so as to fit the experimental data. With the renormalization of the energy expression described in the previous section, we now have a natural way for determining the deformation parameter τ, which is connected with the cluster stability.

In order to determine the other model parameter, the shell distance Δ, we take the second derivative of the full energy with respect to the number of particles N. This function has a physical meaning and can be interpreted as the separation energy of a particle pair. The result is shown in Fig. 5.

It is seen that this function has sharp maxima for those values of N for which shells and subshells are closed. Obviously this function involves rich information

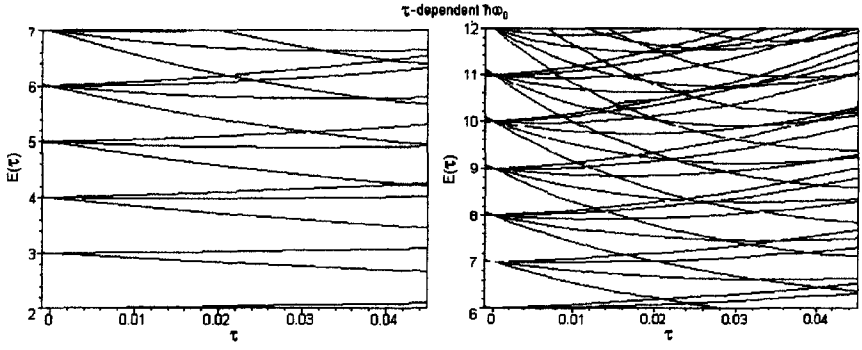

Figure 4: The energy spectrum of the q-deformed, 3-dimensional harmonic oscillator as a function of the deformation parameter τ. As in Nilsson model pictures, one observes level bunching areas at certain values of τ, separated by larger energy gaps.

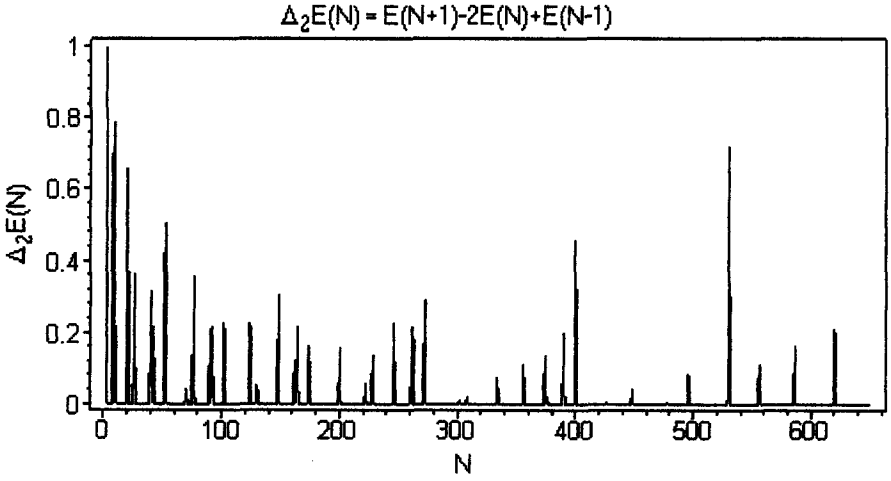

Figure 5: The second derivative of the full energy $E_{full}(N)$ as a function of the number of particles. One notices the well pronounced shell, subshell and supershell structure of the metal cluster. This pattern can be used to derive the characteristic distance Δ between shells (necessary to determine magic numbers), because the distance between peaks is proportional to that between shells.

about the shell and supershell structure of the metal cluster, and therefore it could be used for the determination of the characteristic distance Δ between the shells.

In Table 2 we compare the magic numbers predicted by this model with the experimental results from Martin *et al.* [4]. We see that there is very good

Table 2: Comparison between magic numbers derived using the $Q3O$ model with two different sets of parameters ([a] $\tau = 0.029$ and $\Delta = 0.275$; [b] $\tau = 0.025$ and $\Delta = 0.27$) with the experimental results from Martin *et al.* [4].

This work[a]	This work[b]	Experiment
2	2	2
8	8	8
20	20	20
34		34
40	40	40
58	58	58
	70	
92	92	90,92
138	138	138
198	198	198±2
254		
		263±5
338	338	341±5
440	440	443±5
	562	557±5
676	676	
694	694	700±5
778		
800		
854	832	840±15

agreement between theory and experiment, with very few exceptions. These are due to the τ-dependence of $\hbar\omega_0$ together with the connection between τ and N (Fig. 3). This means that, in spite of the small change of τ with increasing N, one must chose different values of the deformation parameter in different ranges of the particle number.

In conclusion, we may summarize as follows the main results of our application of the $Q3O$ model to the description of metal clusters. It was shown that the $Q3O$ symmetry $u_q(3) \supset so_q(3)$, which is a non-linear deformation of the chain $u(3) \supset so(3)$, is a relevant symmetry for metal clusters. This is because the $Q3O$ potential gathers the main features and bears great similarity with the Nilsson-Clemenger, symmetrized Woods–Saxon and "wine-bottle" potentials, which have been successfully used in the description of various metal cluster properties. The advantage of our q-deformed model lies in the fact that the class of quantum-algebra symmetries is richer than that of Lie-algebra symmetries, making the $Q3O$ potential more flexible than its classical analogs.

We have shown how to derive potentials which, when put into the "standard" Schrödinger equation, provide approximately the same spectrum as the q-deformed, 3-dimensional harmonic oscillator. In the present work, we have also found prescriptions for choosing the model parameters τ and Δ, thus closing the procedure for obtaining magic numbers. This could be very useful in further investigations on other properties of metal clusters.

Acknowledgments

This work was partly supported by a twinning convention between the Universities Pierre et Marie Curie (Paris) and Saint Kliment Ohridski (Sofia) and by the European project COST-D9 / 010 / 98. Professor Matey Mateev is gratefully acknowledged for his interest in this work. A. I. K. thanks the French Government for a PhD scholarship, and P. P. R. for a senior-scientist fellowship. The Bulgarian Ministry of Science and Education supported this work under contracts Φ-415 and Φ-547.

References

[1] W. A. de Heer, Rev. Mod. Phys. **65** (1993) 611.

[2] M. Brack, Rev. Mod. Phys. **65** (1993) 677.

[3] V. O. Nesterenko, Fiz. Elem. Chastits At. Yadra **23** (1992) 1665 [Sov. J. Part. Nucl. **23** (1992) 726].

[4] T. P. Martin, T. Bergmann, H. Göhlich and T. Lange, Chem. Phys. Lett. **172** (1990) 209; Z. Phys. D **19** (1991) 25.

[5] S. Bjrnholm, J. Borggreen, O. Echt, K. Hansen, J. Pedersen and H. D. Rasmussen, Phys. Rev. Lett. **65** (1990) 1627; Z. Phys. D **19** (1991) 47.

[6] W. D. Knight, K. Clemenger, W. A. de Heer, W. A. Saunders, M. Y. Chou and M. L. Cohen, Phys. Rev. Lett. **52** (1984) 2141; W. D. Knight, W. A. de Heer, K. Clemenger and W. A. Saunders, Solid State Commun. **53** (1985) 445.

[7] J. L. Persson, R. L. Whetten, H. P. Cheng and R. S. Berry, Chem. Phys. Lett. **186** (1991) 215.

[8] J. Pedersen, S. Bjrnholm, J. Borggreen, K. Hansen, T. P. Martin and H. D. Rasmussen, Nature **353** (1991) 733.

[9] C. Bréchignac, Ph. Cahuzac, M. de Frutos, J.-Ph. Roux and K. Bowen, in *Physics and Chemistry of Finite Systems: From Clusters to Crystals*, ed. P. Jena *et al.* (Kluwer, Dordrecht, 1992) Vol. 1 p. 369.

[10] M. G. Mayer and J. H. D. Jensen, *Elementary Theory of Nuclear Shell Structure* (Wiley, New York, 1955).

[11] K. Clemenger, Phys. Rev. B **32** (1985) 1359.

[12] S. G. Nilsson, Mat. Fys. Medd. Dan. Vid. Selsk. **29** (1955) no. 16.

[13] C. Gustafsson, I. L. Lamm, B. Nilsson and S. G. Nilsson, Ark. Fys. **36** (1967) 613.

[14] T. Bengtsson and I. Ragnarsson, Nucl. Phys. A **436** (1985) 14.

[15] S. G. Nilsson and I. Ragnarsson, *Shapes and Shells in Nuclear Structure* (Cambridge University Press, Cambridge, 1995).

[16] W. Ekardt, Phys. Rev. B **29** (1984) 1558.

[17] D. E. Beck, Solid State Commun. **49** (1984) 381; Phys. Rev. B **30** (1984) 6935.

[18] R. D. Woods and D. S. Saxon, Phys. Rev. **95** (1954) 577.

[19] B. A. Kotsos and M. E. Grypeos, in *Atomic and Nuclear Clusters*, ed. G. S. Anagnostatos and W. von Oertzen (Springer, Berlin, 1995) p. 242; Physica **229** (1997) 173.

[20] P. Raychev, Adv. Quant. Chem. **26** (1995) 239.

[21] P. P. Raychev, R. P. Roussev, N. Lo Iudice and P. A. Terziev, J. Phys. G **24** (1998) 1.

[22] D. Bonatsos, N. Karoussos, P. P. Raychev, R. P. Roussev and P. A. Terziev, Chem. Phys. Lett. **302** (1999) 392.

[23] L. C. Biedenharn, J. Phys. A **22** (1989) L873; A. J. Macfarlane, J. Phys. A **22** (1989) 4581.

[24] P. P. Raychev, R. P. Roussev and Yu. F. Smirnov, J. Phys. G **16** (1990) L137.

[25] L. P. Marinova, P. P. Raychev and J. Maruani, Mol. Phys. **82** (1994) 1115.

[26] P. P. Raychev, J. Maruani and S. Drenska, Phys. Rev. A **56** (1997) 2759.

[27] J. Maruani, S. B. Drenska, A. I. Kuleff, P. P. Raychev and P. A. Terziev, Phys. Rev. A **62** (2000) 022511.

[28] D. Bonatsos, N. Karoussos, C. Daskaloyannis, S. B. Drenska, N. Minkov, P. P. Raychev, R. P. Roussev and J. Maruani, Prog. Theor. Chem. Phys. B **6** (2000) 393.

[29] M. J. A. de Voigt, J. Dudek and Z. Szymánski, Rev. Mod. Phys. **55** (1983) 949.

[30] J. van der Jeugt, J. Phys. A **25** (1992) L213; J. Math. Phys. **34** (1993) 1799; Can. J. Phys. **72** (1994) 519.

[31] P. P. Raychev, R. P. Roussev, P. A. Terziev, D. Bonatsos and N. Lo Iudice, J. Phys. A **29** (1996) 6939.

[32] Yu. F. Smirnov, V. N. Tolstoy and Yu. I. Kharitonov, Yad. Fiz. **53** (1991) 959, 1746 [Sov. J. Nucl. Phys. **53** (1991) 593, 1068]; Yad. Fiz. **55** (1992) 2863 [Sov. J. Nucl. Phys. **55** (1992) 1599]; Yad. Fiz. **56** (1993) 223 [Phys. At. Nucl. **56** (1993) 690].

[33] K. Chadan and P. C. Sabatier, *Inverse Problems in Quantum Scattering Theory* (Springer, Heidelberg, 1977), Chap. XVI.

[34] D. Bonatsos, C. Daskaloyannis and K. Kokkotas, Phys. Rev. A **45** (1992) R6153.

[35] D. Bonatsos, C. Daskaloyannis and K. Kokkotas, J. Math. Phys. **33** (1992) 2958.

[36] D. Bonatsos, N. Karoussos, D. Lenis, P. P. Raychev, R. P. Roussev and P. A. Terziev, Phys. Rev. A **62** (2000) 013203.

[37] V. Spiridonov, Phys. Rev. Lett. **69** (1992) 398.

Reaction Dynamics of Metallic Clusters Colliding with Atoms

Ulf Saalmann

Atomfysik, Stockholms Universitet
Frescativägen 24, 10405 Stockholm, Sweden

Collisions of metallic clusters with atomic targets have been investigated theoretically within the microscopic framework of Non-adiabatic Quantum Molecular Dynamics. This approach combines self-consistently classical molecular dynamics for the atomic motion with time-dependent density functional theory for the electron dynamics. In a case study of atom-cluster collisions we examine the excitation mechanisms (electronic versus vibrational) and the related relaxation phenomena (phase transitions, fragmentation) for a wide range of impact energies. In addition, two studies of charge transfer competing with fragmentation in collisions with sodium clusters are presented. In the first study the influence of the cluster structure (size, isomers, temperature) on measured total cross sections is investigated for different charge transfer channels. In a second study of collisions with laser-excited targets the strong temperature dependence of the laser-enhanced charge transfer is discussed.

ADVANCES IN QUANTUM CHEMISTRY, VOLUME 40

0065-3276/01 $35.00

1 Introduction

Collisions with atomic clusters represent a relatively new branch of collision physics as compared to the well established fields of ion–atom collisions [1] and ion–solid interaction [2]. The study of cluster collisions is of particular interest and importance because it offers the possibility to tackle bridge–building questions (like the transition from individual excitations in the elementary ion–atom collision to the macroscopic stopping power in solids) as well as fundamental problems (like phase transitions in finite systems).

In general, the fundamental events accompanying these cluster collisions include the simultaneous occurrence and mutual coupling of electronic transitions (charge transfer, excitation, ionization) and atomic motion (vibration, rotation, fragmentation) in systems with a large but finite number of degrees of freedom (DOF). To cope with such situations we have recently developed a microscopic approach which treats electronic and atomic DOF in atomic systems *self–consistently* by combining time–dependent density functional theory with molecular dynamics: Non–Adiabatic Quantum Molecular Dynamics (NA-QMD) [3–5]. The respective coupled equations of motion will be discussed in Sect. 2.

From a case study [5], the different excitation mechanisms (electronic and vibrational) as well as related relaxation phenomena (phase transitions and fragmentation) in atom–cluster collisions will be presented in Sect. 3. We show the gradual change of these mechanisms as a function of the impact energy in a wide range for the collision system $Na_9^+ + Na$.

Charge transfer (CT) represents one of the most frequently studied phenomena in the field of ion–atom scattering [6] and has been intensively for ion–surface interactions [7] as well. In order to close this gap, there has been a great experimental effort on CT in cluster collisions [8–13]. Here in Sect. 4, we present two systematic investigations of recent experiments of CT measuring: 1) integral CT cross sections for various alkali clusters [14, 15], and 2) the laser–enhanced charge transfer for small sodium clusters [16].

2 Non–adiabatic quantum molecular dynamics

2.1 General equations of motion

Coupled equations of motions (EOM) for a mixed system of classical and quantum DOF can be derived by means of the Hamilton operator

$$\hat{H} = H_{\text{coll}}(\mathbf{R}, \mathbf{P}) + H_0(\hat{\mathbf{r}}, \hat{\mathbf{p}}) + H_{\text{int}}(\hat{\mathbf{r}}, \mathbf{R}) \tag{1}$$

with $\mathbf{R} \equiv \{\mathbf{R}_1, \ldots, \mathbf{R}_{N_n}\}$ and $\mathbf{P} \equiv \{\mathbf{P}_1, \ldots, \mathbf{P}_{N_n}\}$ the sets of positions and momenta of the N_n nuclei and $\hat{\mathbf{r}} \equiv \{\hat{\mathbf{r}}_1, \ldots, \hat{\mathbf{r}}_{N_e}\}$ and $\hat{\mathbf{p}} \equiv \{\hat{\mathbf{p}}_1, \ldots, \hat{\mathbf{p}}_{N_e}\}$ the sets of position and momentum operators of the N_e electrons [3]. Using total energy conservation and the Schrödinger equation for the time evolution of the electronic many–particle state (We use atomic units throughout the paper.)

$$\mathrm{i}\frac{\partial}{\partial t}\Psi(\mathbf{r},t) = \left\{\hat{H}_0 + \hat{H}_{\mathrm{int}}\right\}\Psi(\mathbf{r},t)\,, \tag{2}$$

one can derive classical Hamilton equations for the nuclei. The resulting force from the quantum system on the classical particles has been derived before starting from a full quantum–mechanical treatment [17–19]. Note, however, that the derivation used here guarantees total–energy conservation even if the many–particle wave–function is represented within a local, truncated basis: $\Psi(\mathbf{r},t) = \sum_\alpha \Phi_\alpha(\mathbf{r};\mathbf{R})a_\alpha(t)$. The forces ($A = 1 \ldots N_n$) are then given by

$$M_A\ddot{\mathbf{R}}_A = -\frac{\partial}{\partial \mathbf{R}_A}H_{\mathrm{coll}} - \sum_{\alpha\beta}\bar{a}_\alpha\left[\frac{\partial H_{\alpha\beta}}{\partial \mathbf{R}_A} - \sum_\gamma\left(\mathbf{R}^A_{\alpha\gamma}H_{\gamma\beta} + \mathrm{c.c.}\right)\right]a_\beta \tag{3}$$

with $H_{\alpha\beta} := \langle\Phi_\alpha|\hat{H}_0 + \hat{H}_{\mathrm{int}}|\Phi_\beta\rangle$ and $\mathbf{R}^A_{\alpha\gamma} := \langle\partial\Phi_\alpha/\partial\mathbf{R}_A|\Phi_\gamma\rangle$. The term $[\ldots]$ in Eq. (3) reduces only for a complete or for a fixed (i. e. independent of $\mathbf{R}$) basis set to a "Hellmann–Feynman–like" term.

It is known for a long time that such a mixed classical–quantum description may break down for the case that the kinetic energy of the classical motion is in the order the electronic transition energies ($\sim$eV). In the field of chemical reactions this problem has been handled by so–called surface–hopping approaches [20–22]. However, dealing with atomic clusters the large number of DOF prevents calculation of potential energy surfaces (and their couplings). Besides that we concentrate here on collision energies in the keV range, i. e. well above typical electronic energies [23].

2.2 Molecular dynamics combined with time–dependent density functional theory

Within the NA-QMD approach, electronic (quantum) and nuclear (classical) DOF are treated by combining time–dependent (TD) density functional theory (DFT) with molecular dynamics (MD). The basic theorem of TD DFT [24–26] states that for a system of interacting particles the many–particle state and, thus, any observable are *uniquely* determined by the time–dependent single–particle density $\rho(\mathbf{r},t)$ which can be written identically as the density

of a non–interacting reference system $\rho(\mathbf{r},t) = \sum_j^{N_e} \left|\psi^j(\mathbf{r},t)\right|^2$. The single–particle functions ψ^j are obtained from the time–dependent Kohn–Sham (KS) equations ($j = 1 \ldots N_e$)

$$\mathrm{i}\,\frac{\mathrm{d}}{\mathrm{d}t}\psi^j(\mathbf{r},t) = \left\{\hat{t} + V_{\text{eff}}(\mathbf{r},t)\right\}\psi^j(\mathbf{r},t)\,, \tag{4}$$

which result from the minimization of the electronic action integral [26]. The single–particle Hamilton operator in Eq. (4) contains besides the kinetic energy operator $\hat{t}$ a *local* effective potential

$$\begin{aligned} V_{\text{eff}}(\mathbf{r},t) &= V_{\text{eff}}[\rho](\mathbf{r},t) \\ &= V(\mathbf{r},\mathbf{R}) + \int \mathrm{d}^3r'\,\frac{\rho(\mathbf{r}',t)}{|\mathbf{r}-\mathbf{r}'|} + V_{\text{xc}}[\rho](\mathbf{r},t)\,. \end{aligned} \tag{5}$$

Note that here and later on $\mathbf{r}$ denotes the single–particle coordinate whereas $\mathbf{R}$ is still used as abbreviation for all nuclear positions as in Eq. (1). The potential (5) consists, on one hand, of an external potential $V(\mathbf{r},\mathbf{R})$, which in our case is time–dependent owing to the atomic motion $\mathbf{R}(t)$. On the other hand, there are electron–electron interaction terms, namely the Hartree and the exchange–correlation term, which depend both via the density ρ on the functions ψ^j. The exchange–correlation potential V_{xc} is defined within the so–called adiabatic local density approximation [25] which is the natural extension of the LDA from stationary DFT. It is assumed to give reliable results for problems where the time scale of the external potential (in our case typical collision times) is larger than the electronic time scale.

For the description of collision processes it is favorably to write the KS functions as linear combinations of atomic orbitals (LCAO) which move along the classical trajectories $\mathbf{R}_{A_\alpha}(t)$

$$\psi^j(\mathbf{r},t) = \sum_\alpha \phi_\alpha(\mathbf{r}-\mathbf{R}_{A_\alpha})\,a_\alpha^j(t)\,. \tag{6}$$

Here, A_α denotes the atom at which the atomic orbital ϕ_α is centered. By inserting the LCAO ansatz (6) into the KS equations (4) one arrives at

$$\dot{a}_\alpha^j(t) = -\sum_{\beta\gamma}\left(S^{-1}\right)_{\alpha\beta}\left\{\mathrm{i}H_{\beta\gamma} + \sum\nolimits_A^{N_n}\dot{\mathbf{R}}_A\mathbf{R}^A_{\beta\gamma}\right\}a_\gamma^j(t) \tag{7}$$

with the overlap matrix $S_{\alpha\beta} \equiv \langle\phi_\alpha\,|\phi_\beta\rangle$, the Hamilton matrix $H_{\alpha\beta} \equiv \langle\phi_\alpha|\,\hat{t}+V_{\text{eff}}\,|\phi_\beta\rangle$, and the coupling matrix $\mathbf{R}^A_{\alpha\beta} \equiv \langle\phi_\alpha\,|\partial\phi_\beta/\partial\mathbf{R}_A\rangle$. Note, that Eqs. (7) are highly non–linear owing to the density dependence of the effective potential V_{eff} of Eq. (5) which enters the Hamilton matrix $H_{\alpha\beta}$.

The corresponding Newton equations for the N_n ions can be derived by using the conservation of the total energy of the system leading to [3]

$$M_A\ddot{\mathbf{R}}_A = -\frac{\partial}{\partial R_A}\sum_B{}' \frac{Z_A Z_B}{|\mathbf{R}_A-\mathbf{R}_B|} \tag{8a}$$

$$-\sum_j^{N_e}\left\{\sum_{\alpha\beta}\overline{a}_\alpha^j\left(\frac{\partial H_{\alpha\beta}}{\partial R_A}-\left\langle\phi_\alpha\left|\frac{\partial(V_{\text{eff}}-V)}{\partial R_A}\right|\phi_\beta\right\rangle\right)a_\beta^j\right. \tag{8b}$$

$$\left.-\sum_{\alpha\beta\gamma\delta}\left[\overline{a}_\alpha^j H_{\alpha\beta}\left(S^{-1}\right)_{\beta\gamma}\mathbf{R}_{\gamma\delta}^A a_\delta^j+\text{c.c.}\right]\right\}\quad. \tag{8c}$$

The force on the right–hand side of Eq. (8) contains besides the collective term of the nucleus–nucleus repulsion (8a) and expectation values of gradients (8b) further terms (8c) which guarantee that the total energy of the system is conserved even for finite, local basis sets. These additional terms depend strongly on the applied basis set.

The TD KS equations (7) and the Newton equations (8) represent the coupled EOM of the NA-QMD approach and have to be solved simultaneously. In the following, subsequent approximations will be introduced which allow the systematic application of these EOM.

First of all, the core electrons are considered to be frozen. For further approximations the entire electronic density ρ is split

$$\rho(\mathbf{r},t)=\rho_0(\mathbf{r},\mathbf{R})+\Delta\rho(\mathbf{r},t)\,. \tag{9}$$

Here, ρ_0 corresponds to the adiabatic density of the neutral reference system, whereas the explicitly time–dependent term $\Delta\rho$ describes all non–adiabatic and charge effects. By means of the ansatz (9) two simplifying approximations can be introduced [3, 4]. First, the full density ρ in the exchange–correlation terms is replaced by the adiabatic part ρ_0. Second, the Hartree term in the total energy is decomposed with Eq. (9) into three terms with the structures $\rho_0\rho_0$, $\rho_0\Delta\rho$, and $\Delta\rho\Delta\rho$, where the first two are taken fully into account and the last one (which should be small in weakly charged systems) is neglected. This leads to *linear* KS equations which simplifies the numerical solution drastically. The resulting approximate EOM can be written as

$$\dot{a}_\alpha^j(t)=-\sum_{\beta\gamma}\left(S^{-1}\right)_{\alpha\beta}\left\{\mathrm{i}H_{\beta\gamma}^0+\sum_A^{N_n}\dot{\mathbf{R}}_A\mathbf{R}_{\beta\gamma}^A\right\}a_\gamma^j(t) \tag{10}$$

and

$$M_A\ddot{\mathbf{R}}_A = -\frac{\partial}{\partial R_A}U(\mathbf{R})$$

$$-\sum_{j}^{N_e}\left\{\sum_{\alpha\beta}\bar{a}_\alpha^j\left(\frac{\partial H^0_{\alpha\beta}}{\partial R_A}\right)a_\beta^j - \sum_{\alpha\beta\gamma\delta}\left[\bar{a}_\alpha^j H^0_{\alpha\beta}\left(S^{-1}\right)_{\beta\gamma}\mathbf{R}^A_{\gamma\delta}a_\delta^j + \text{c. c.}\right]\right\} \tag{11}$$

with the Hamilton matrix

$$H^0_{\alpha\beta} \equiv \left\langle \phi_\alpha \left| \hat{t} + V_{\text{eff}}[\rho_0](\mathbf{r},t)\right| \phi_\beta \right\rangle \,, \tag{12}$$

where the external potential in V_{eff} is to be understood as a sum of Coulomb and frozen–core potentials. This adiabatic Hamilton matrix $H^0_{\alpha\beta}$ is calculated in a two–center approximation [4] similar to the method used for adiabatic calculations [27]. The conservative potential $U(\mathbf{R})$ is defined by

$$U(\mathbf{R}) \equiv \frac{1}{2}\sum_{A}^{N_n}\sum_{B}^{N_n}{}' \frac{Z^0_A Z^0_B}{|\mathbf{R}_A-\mathbf{R}_B|} \tag{13a}$$

$$-\frac{1}{2}\int \mathrm{d}^3r \int \mathrm{d}^3r' \frac{\rho^0(\mathbf{r},\mathbf{R})\rho^0(\mathbf{r}',\mathbf{R})}{|\mathbf{r}-\mathbf{r}'|} \tag{13b}$$

$$-\int \mathrm{d}^3r \left[\rho^0(\mathbf{r},\mathbf{R},t)\right]^2 \frac{\delta\epsilon_{\text{xc}}[\rho^0]}{\delta\rho^0(\mathbf{r},\mathbf{R})} \tag{13c}$$

with Z^0_A the valence charge of atom A. Practically, $U(\mathbf{R})$ represents a short–range repulsive potential because the two large contributions (13a) and (13b) cancel each other to large extent. This is used to approximate $U(\mathbf{R})$ by a sum over pairwise interactions $U(R_{AB})$. These pair potentials are determined using *ab initio* calculations for diatomic molecules [4]. This approach has been tested against data of kinematically complete correlation experiments of collision induced dissociation [28].

3 Excitation and relaxation

We have studied the reaction dynamics of the collision $Na_9^+ + Na$ for a fixed collision geometry (with impact parameter b=0) but in a wide range of impact energies E_{cm}. In Fig. 1, the total kinetic energy loss (TKEL) $\Delta E := E_{\text{cm}} - E_{\text{cm}}(t\to+\infty)$, with $E_{\text{cm}}(t\to+\infty)$ the final kinetic energy of the relative motion between cluster–projectile and atomic target in the centre–of–mass system is shown for $E_{\text{cm}} = 0.2\,\text{eV}\ldots 1\,\text{MeV}$.

Besides the very low energy range $E_{\text{cm}} \lesssim 10\,\text{eV}$ (where maximal TKEL, i. e. ΔE=E_{cm}, is realized and connected with the formation of relatively long–living but in general unstable intermediate compounds Na_{10}^+), ΔE describes

the change of the internal energy of the system, i.e. excitations. In order to decide between electronic and vibrational contributions to ΔE the NA-QMD results are compared to those obtained from adiabatic calculations (denoted by QMD) performed with the same collision geometry. At impact energies below $E_{cm} \lesssim 200\,eV$, QMD and NA-QMD results are clearly seen to be identical and, thus, only vibrational excitations occur (adiabatic regime). Above $E_{cm} \gtrsim 5\,keV$ electronic transitions dominate (non–adiabatic regime). In the intermediate range of E_{cm} both mechanisms compete (transition regime).

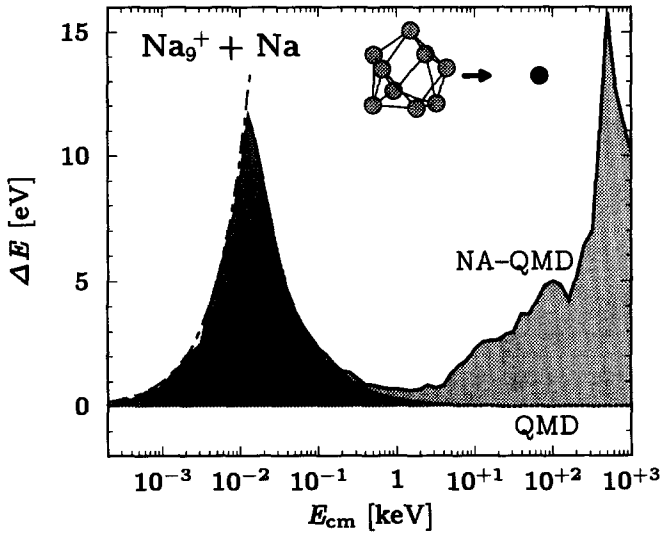

Figure 1: TKEL of relative motion ΔE in central $Na_9^+ + Na$ collisions for a fixed collision geometry *(insert)* as a function of the center–of–mass impact energy E_{cm} calculated with NA-QMD *(solid line)* and QMD *(dotted line)*. Vibrational and electronic contributions to ΔE are distinguished by grey and light–grey shaded areas, respectively.

The dynamics of the collision process and the subsequent cluster relaxation can be seen for characteristic impact energies in Fig. 2. It shows the time dependence of $\Delta E(t)=E_{cm}-E_{cm}(t)$, with $E_{cm}(t)$ the actual kinetic energy of the relative motion, and the displacement of the cluster atoms $d(t)$. The quantity $\Delta E(t)$ gives insight into the collision and excitation dynamics (forces, interaction time, TKEL). The displacement, defined as

$$d(t) := \frac{1}{NR}\sqrt{\sum_{A=1}^{N}\left[\mathbf{R}_A(t) - \mathbf{R}_A(0)\right]^2}$$

with $\mathbf{R}_A(0)$ the equilibrium positions of the N atoms in the ground–state geometry and R the cluster radius, characterizes quantitatively the relaxation:

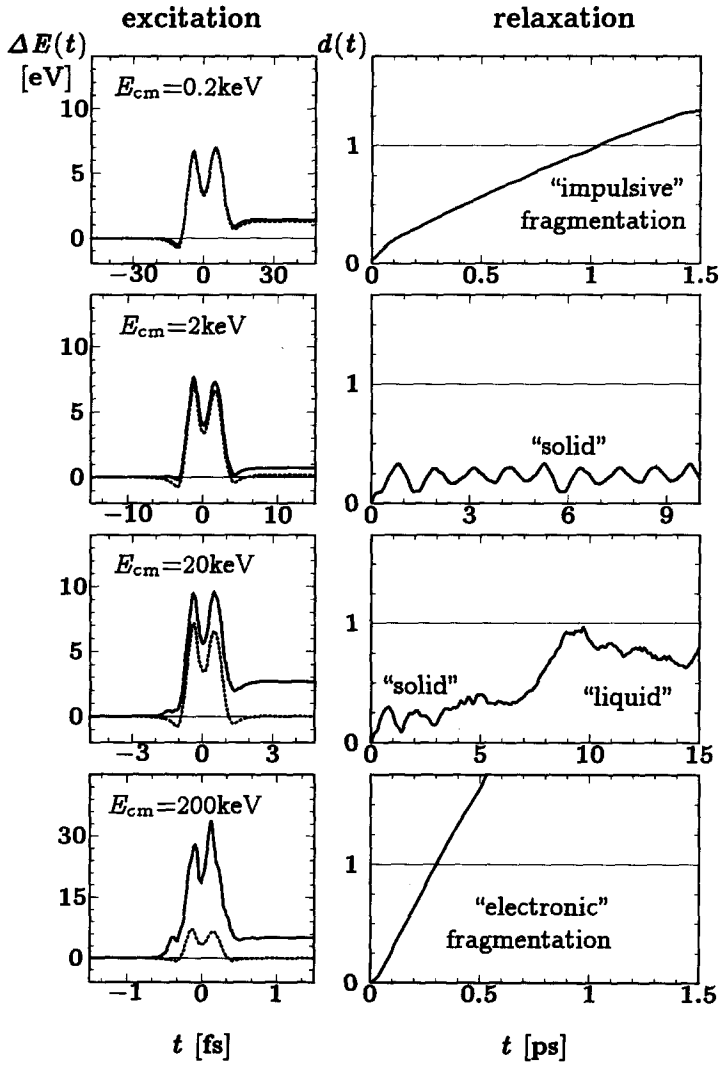

Figure 2: Difference of the impact energy and the actual kinetic energy $\Delta E(t)$ of relative motion *(left column)* and displacement $d(t)$ of the cluster atoms *(right)* as a function of time t for selected impact energies E_{cm} and the same collision geometry as in Fig. 1, calculated with NA-QMD *(dark solid lines)*. In the left column, the corresponding adiabatic QMD calculations *(dotted lines)* are also shown for comparison.

if $d \ll 1$ a "solid" configuration is described, if $d \sim 1$ a "liquid" state (atoms move throughout the cluster volume) is realized, and if $d \to \infty$ fragmentation

occurs.

Excitation and relaxation mechanisms and, in particular, the related time scales are basically different in all cases. In the pure adiabatic regime (E_{cm} = 200 eV), the vibrational excitation of the cluster is immediately connected with a fragmentation process which, in contrast to statistical evaporation, starts to proceed already during the interaction time of $\sim$ 40 fs (see left part of Fig. 2) as a consequence of sufficient momentum transfer between projectile and target atoms. Such non–statistical fragmentation has been experimentally verified only very recently [29] (called "impulsive" fragmentation mechanism). On the contrary, in the high–energetic non–adiabatic region E_{cm}=200 keV electronic excitation ($\sim$ 1 fs) and fragmentation ($\sim$ 300 fs) processes are separated by two orders of magnitude. Obviously, electron–vibration coupling needs time to become effective and to induce dissociation ("electronic" fragmentation).

At an impact energy of E_{cm}=2 keV the cluster remains stable after the collision with the excitation energy originally stored predominantly in electronic excitation. Electron–vibration coupling leads, however, to the excitation of collective surface vibrations indicated by the regular oscillating behavior of $d(t)$ well developed after about 1 ps. At E_{cm}=20 keV the first step of the relaxation phase is very similar to that observed at E_{cm}=2 keV. But, in this case electron–vibration coupling induces clearly a phase transition from "solid" to "liquid" in a second relaxation step coming about 10 ps after the collision (see right part of Fig. 2). Owing to the large TKEL one should expect statistical evaporation as the final decay channel. The excitation and relaxation mechanisms, summarized in Figs. 1 and 2, appear in a well defined order as a function of the impact energy due to the deliberately fixed collision geometry.

Finally we mention a quite interesting and unexpected phenomenon found in related studies: the occurrence of *cluster transparency* [5] in the closed shell system Na_9^+ + He. This mechanism is characterized by a practically undisturbed atom–cluster penetration in a certain, small range of E_{cm} within the transition regime. It turned out that for specific collision geometries in the range of $E_{cm} \sim 10 \ldots 100$ eV the relative velocity between projectile and target becomes, on one hand, too large to excite vibrational DOF and is, on the other hand, still too small to induce electronic transitions. As a consequence, the cluster appears to be transparent even in central collisions. More details including comparison with experimental data are published elsewhere [5].

4 Charge transfer versus fragmentation

4.1 Integral charge transfer cross section

We have made a detailed analysis of CT and fragmentation in $Na_n^+ + Cs$ collisions with $n = 4 \ldots 11$. The complexity of such cluster collisions can already be demonstrated by considering the smallest of these systems. All of the following reaction channels have to be considered:

$$\begin{aligned} Na_4^+(2.7\,\mathrm{keV}) + Cs &\rightarrow Na_4 + Cs^+ && (14a)\\ &\rightarrow Na_{4-m} + Na_m + Cs^+ && (14b)\\ &\rightarrow Na_4^+ + Cs && (14c)\\ &\rightarrow Na_{4-m}^+ + Na_m + Cs && (14d)\\ &\rightarrow Na_{4-m}^+ + Na_m^+ + Cs^- && (14e) \end{aligned}$$

taking into account in channel (14e) that Na_4^{++} is certainly unstable. In the experiment [8, 9] the CT cross section was determined by detecting the neutralized non–fragmented clusters, i. e. channel (14a) was measured *exclusively*. Therefore all other reactions, in particular (14b), have to be considered as competing channels. The fragmentation of the cluster, however, may result from secondary statistical decay processes initiated by collision–induced excitation on typical time scales of μs, cf. also discussion of Fig. 2. This represents a general problem for the comparison of results from microscopic simulations with experimental data influenced by such decay processes, because the relevant time scales cannot be covered by any molecular dynamics method. Consequently, the influence of these fragmentation processes has to be estimated based on the results from the simulation of the collision process (covering typically a few up to ~ 100 fs for collision energies in the keV range).

We start with a brief discussion of the system (14) in order to outline the procedure which gives us insight into the collision dynamics and finally absolute cross sections. (This method was applied in basically the same manner for the laser–enhanced CT presented in Sect. 4.2.) First the Na_4^+ projectile is prepared in its electronic and geometric ground state. Analyzing then the $Na_4^+ + Cs$ collisions event by event a strong dependence of the primary CT probability P_{prim} on the initial orientation of the cluster is observed, see upper panel of Fig. 3. There, P_{prim} represents the integral CT probability [30] to find Cs^+ in the exit channel without regard to the evolution of the cluster corresponding to an "integral" over channels (14a) and (14b). The b–weighted integration of the mean probability (thick line in the upper panel of Fig. 3) yields an integral CT cross section $\sigma_{\mathrm{prim}} = (38 \pm 2)$ Å^2, which is considerably larger than the experimental value [8] of $\sigma_{\mathrm{exp}} = (17 \pm 3)$ Å^2 due to the competing fragmentation channel (14b).

In the middle part of Fig. 3 the mean value of the TKEL ΔE, for the definition see Sect. 3, and of the actual kinetic energy of the vibrations E_{vib} calculated at the end of the simulation are shown as a function of the impact parameter b, where the average was taken over all those events, in which the cluster has not yet fragmented. ΔE represents in a given event the total excitation energy in the system, i. e. the reservoir of energy available for secondary processes. Whereas for small impact parameters $b \leq 5\,a_0$ certainly all clusters fragment, for larger impact parameters $b = 5 \ldots 10\,a_0$ the excitation energy is stored mainly in electronic DOF. The amount of electronic energy, which will

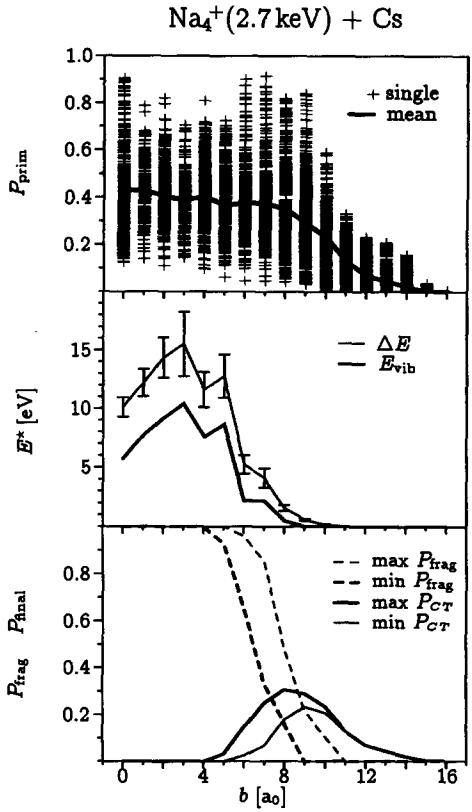

Figure 3: Calculated primary CT probability P_{prim} *(upper panel)* for all simulated events (+) and orientation-averaged *(thick line)*, mean TKEL ΔE and mean vibrational kinetic energy E_{vib} *(middle panel)*, as well as upper and lower limit for the final, i. e. exclusive CT probability obtained along with the limiting fragmentation probabilities *(lower panel)* as functions of the impact parameter b. The length of the error bars is given by two times the standard deviation of the orientation average.

actually be transferred into vibrational energy, can hardly be estimated without further calculation.

Therefore we calculate upper and lower limits for the fragmentation probability $P_{\text{frag}}(b)$ which are obtained by dividing the number of fragmentation events by the total number of simulated events, respectively, at a given impact parameter b. For the upper limit an event counts as fragmented when ΔE (i. e. the total excitation energy of the cluster) is larger than the dissociation threshold E_{diss} (0.44 eV for Na_4) whereas for the lower limit E_{vib} has to exceed E_{diss}. The "real" fragmentation probability, which has to be inbetween the limiting cases, is estimated simply by the average of the maximum and the minimum probability (both were drawn in the lower panel of Fig. 3). It comprises all relevant processes: direct or "impulsive" fragmentation, "electronic fragmentation", and also secondary statistical decay processes; cf. also Sect. 3. The final CT probabilities, obtained by an event–by–event combination of P_{prim} and P_{frag}, are also shown in terms of an upper and lower limit in the lower panel of Fig. 3. They will be used in the following to calculate cross sections for all measured cluster sizes.

First of all we have determined geometric structures and ionization potentials of the three most stable isomers [15], respectively, which are in reasonable agreement with *ab initio* structure calculations [31–33] and experimental ionization data [34]. For all isomeric structures the CT cross section σ_n corresponding to σ_{final} of channel (14a), i. e.

$$Na_n^+(2.7\,\text{keV}) + Cs \rightarrow Na_n + Cs^+\,, \tag{15}$$

has been plotted in the upper panel of Fig. 4 as a function of the cluster size n along with the measured data [8]. Large variations for different isomers at a given cluster size are found. An inspection of the corresponding occupation numbers indicates that the (valence) electron of the Cs atom is transferred preferably into an initially unoccupied orbital of the cluster in the energetic vicinity of the Cs(6s) level. These (comparatively high–lying) cluster levels reflect structural changes distinctly and, thus, vary the character of the CT process inbetween off–resonant and quasi–resonant resulting in the large differences found for σ_n. With the theoretical cross sections for the ground–state structures, i. e. assuming zero temperature in the projectile clusters, the variation of the experimental CT cross sections with the cluster size cannot be reproduced.

Calculations with "liquid" cluster ions in the initial state have been performed to take into account that the projectile clusters in the experiment are considerably heated by the laser ionization of the neutral ones. A fixed initial internal energy of about 0.1 eV below the respective dissociation limit [35] was chosen for all sizes n. (A more thorough investigation of the temperature

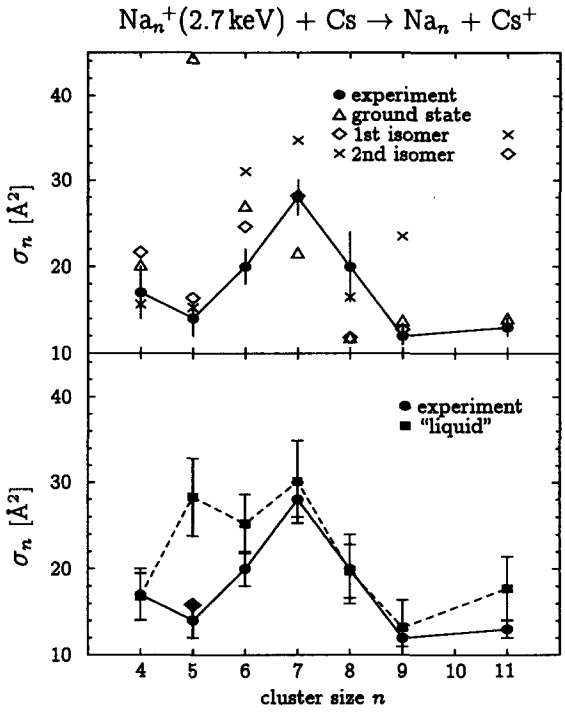

Figure 4: Calculated exclusive CT cross sections σ_n with zero initial temperature of the cluster *(upper panel)* for all the lowest three isomeric structures and for "liquid" cluster ions *(lower panel)* compared with the experimental data [8].

dependence has been performed for the laser–enhanced CT in Sect. 4.2.) The resulting CT cross sections σ_n are compared with the measured data in the lower panel of Fig. 4. Except for the case of $n = 5$, the theoretical cross sections calculated on an *absolute* scale are in agreement with the experimental data. The statistical error bars of the calculated cross sections reflects the large variations of the outcome of the collision with the initial configuration as illustrated in the upper panel of Fig. 3.

An experimental setup detecting the formed target ions Cs^+ or Cs^- after the collision with clusters could provide "pure" CT cross sections, i.e. without regard to the evolution of the cluster. The calculated integral CT cross sections $\sigma_+ \equiv \sigma(Cs^+)$ and $\sigma_- \equiv \sigma(Cs^-)$ in $Na_n^+(2.7\text{ keV}) + Cs$ are shown as a function of the cluster size n in Fig. 5. Note that the ground state $Cs^-(6s^2\,^1S)$ is expected to be bound [36]. Obviously, the cross sections for the "normal" CT process with Cs^+ in the exit channel are considerably larger (at least a factor of two) than for the "exotic" Cs^- formation, and the size dependences show

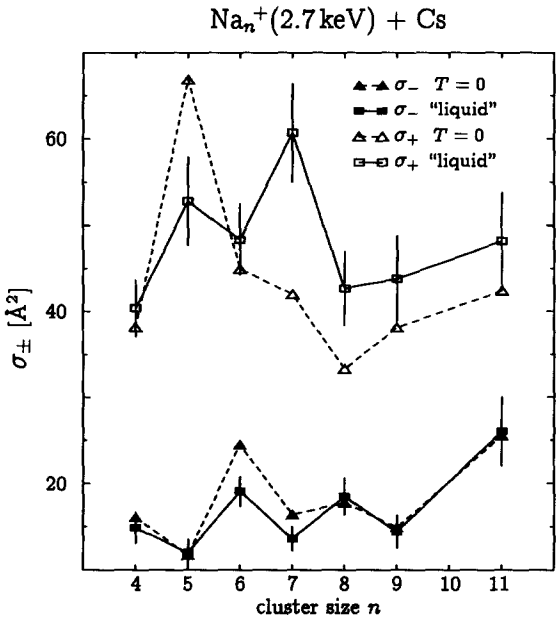

Figure 5: Calculated integral cross sections for the formation of Cs anions σ_- and cations σ_+ with zero initial temperature in the cluster for the ground state isomers as well as for "liquid" clusters as functions of the cluster size n.

up completely different.

The size dependence of σ_+ exhibits a strong similarity to that of the exclusive CT cross section σ_n for channel (15), which holds for $T = 0$ as well as for "liquid" projectile clusters. The absolute values of σ_+, however, are considerably larger than those of σ_n, because the fragmentation channels deplete the integral CT cross section.

In contrast to the findings for σ_+ (and σ_n), σ_- shows a conspicuous odd–even alternation as a function of size and a very weak temperature dependence. The latter results from the "robustness" of the initially occupied, low–lying levels in the cluster (where the electron producing Cs^- has to come from) against structural changes, whereas the orbitals involved in the "normal" CT process yielding Cs^+ reflect structural changes more distinctly.

4.2 Laser–enhanced charge transfer

In connection with the first experimental study of charge transfer in atom–cluster collisions with targets in a laser-excited state we have examined the interplay between electron transfer and cluster fragmentation. The experiment

measures the neutralization of the clusters ($n = 1 \ldots 4$) in

$$\begin{aligned} Na_n^+ + Na(3s) &\rightarrow Na_n + Na^+ \\ Na_n^+ + Na(3p) &\rightarrow Na_n + Na^+ \end{aligned} \qquad (16)$$

discriminating against collision–induced fragmentation of the neutralized clusters [16]. Applying the procedure described in detail in Sect. 4.1 we have calculated primary CT probabilities, fragmentation probabilities, and therefrom final, i. e. exclusive, CT probabilities for both types of collisions (16) at an energy of $E_{lab} = 5\,keV$ with the cluster projectiles in their respective ground–state geometries, i. e. $T = 0\,K$. Note, that electronic temperatures do not play any role for the small clusters studied here [37]. The integral cross section ratio σ_{3p}/σ_{3s} for this case, plotted in Fig. 6, shows a qualitative disagreement with the experimental data; for absolute values see Table 1. Therefore, we have repeated the analysis by taking into account and successively increasing the initial internal energies or temperatures T of the clusters. At a value of $T = 500\,K$ an overall agreement with the experimental ratios is obtained; see Fig. 6 and Table 1. Whereas the dimers are practically unaffected by the temperature T, we have found for the "real" clusters Na_3^+ and Na_4^+ that both processes — the charge transfer as well as the ensuing fragmentation — are very sensitive to it. Even though this temperature dependence is the result of a complex interplay of electron transfer and cluster fragmentation such a com-

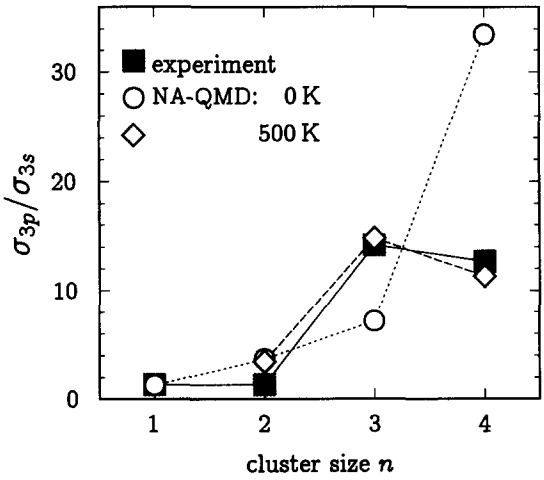

Figure 6: Ratio of total cross sections for the charge transfer in collisions (16) at an energy of $E_{lab} = 5\,keV$. The experimental data are compared with theoretical results obtained from NA-QMD calculations for two initial internal energies (temperatures) of the clusters.

Table 1: Total CT cross sections in $Å^2$ and laser–enhancement in collisions (16) with $E_{lab} = 5\,keV$ for two different cluster temperatures.

	$T = 0\,K$			$T = 500\,K$		
	σ_{3s}	σ_{3p}	σ_{3p}/σ_{3s}	σ_{3s}	σ_{3p}	σ_{3p}/σ_{3s}
Na_2^+	12	44	3.6	13	44	3.4
Na_3^+	7.0	50	7.1	3.6	52	14
Na_4^+	2.8	95	34	4.2	46	11

parison of experimental data and theoretical results may serve as a kind of a *"cluster thermometer"*.

5 Summary

Atom cluster collisions have been investigated by means of a self–consistent and simultaneous treatment of the atomic and electronic DOF involved. For the collision system $Na_9^+ + Na$ we have examined the excitation mechanisms as well as the relaxation scenarios which strongly depend on the impact energy. Three basically different fragmentation mechanisms — "impulsive" fragmentation, "electronic" fragmentation, and statistical decay — have been discussed.

The complexity of non–adiabatic cluster collisions has been illustrated by a detailed analysis of $Na_n^+ + Cs$ collisions. In particular, the interplay between CT and fragmentation or, more generally, the essential couplings between atomic and electronic DOF has been investigated carefully. The size and structure dependence of integral CT cross sections where compared with experiments. Furthermore, anion formation in cluster–atom collisions was predicted including cross sections for this exotic process. Finally, we have studied the temperature influence on the laser–enhanced CT in collisions $Na_n^+ + Na(3s/3p)$.

Acknowledgments

The author thanks Rüdiger Schmidt for the joint work on the formalism and the studies presented here, and Olaf Knospe for his cooperation on the CT project presented in Sect. 4.1. Financial support through a grant by the Deutscher Akademischer Austauschdienst (Germany) and the Kungliga Vetenskapsakademien (Sweden) is gratefully acknowledged.

References

[1] B. H. Bransden, *Atomic Collision Theory* (Benjamin–Cummings, Reading, 1983).

[2] M. Nastasi, J. Mayer, and J. K. Hirvonen, *Ion–Solid Interactions: Fundamentals and Applications* (Cambridge University Press, Cambridge, 1996).

[3] U. Saalmann and R. Schmidt, Z. Phys. D **38**, 153 (1996).

[4] U. Saalmann, *Nicht–adiabatische Quantenmolekulardynamik.*, Ph.D. thesis, Technische Universität Dresden (1997).

[5] U. Saalmann and R. Schmidt, Phys. Rev. Lett. **80**, 3213 (1998).

[6] B. H. Brandsen and M. R. C. McDowell, *Charge Exchange and the Theory of Ion–Atom Collisions* (Clarendon Press, Oxford, 1992).

[7] M. Kimura and N. F. Lane, Adv. At. Mol. Opt. Phys. **26**, 79 (1990).

[8] C. Bréchignac, P. Cahuzac, J. Leygnier, R. Pflaum, and J. Weiner, Phys. Rev. Lett. **61**, 314 (1988).

[9] C. Bréchignac, P. Cahuzac, F. Carlier, J. Leygnier, and I. V. Hertel, Z. Phys. D **17**, 61 (1990).

[10] B. Walch, C. L. Cocke, R. Voelpel, and E. Salzborn, Phys. Rev. Lett. **72**, 1439 (1994).

[11] H. Shen, P. Hvelplund, D. Mathur, A. Bárány, H. Cederquist, N. Selberg, and D. C. Lorents, Phys. Rev. A **52**, 3847 (1995).

[12] B. Farizon, M. Farizon, M. J. Gaillard, E. Gerlic, and S. Ouaskit, Int. J. Mass Spectrom. Ion Proc. **144**, 79 (1995).

[13] F. Rohmund and E. E. B. Campbell, Chem. Phys. Lett. **245**, 237 (1995).

[14] O. Knospe, J. Jellinek, U. Saalmann, and R. Schmidt, Eur. Phys. J. D **5**, 1 (1999).

[15] O. Knospe, J. Jellinek, U. Saalmann, and R. Schmidt, Phys. Rev. A **61**, 022715 (2000).

[16] Z. Roller-Lutz, Y. Wang, H. O. Lutz, U. Saalmann, and R. Schmidt, Phys. Rev. A **59**, R2555 (1999).

[17] P. Pechukas, Phys. Rev. **181**, 166, 174 (1969).

[18] D. J. Diestler, J. Chem. Phys. **78**, 2240 (1983).

[19] N. H. Kwong, J. Phys. B **20**, L647 (1987).

[20] J. C. Tully, in *Dynamics of Molecular Collisions*, edited by W. H. Miller (Plenum Press, New York, London, 1976).

[21] J. C. Tully, J. Chem. Phys. **93**, 1061 (1990).

[22] F. Webster, P. J. Rossky, and R. A. Friesner, Comp. Phys. Comm. **63**, 494 (1991).

[23] Note however, that the for the internal relaxation dynamics of the clusters this approach has to be used carefully as has been shown for the quantized fragmentation dynamics [28, 38] revealed in kinematically complete experiments of collision induced dissociation [29].

[24] E. Runge and E. K. U. Gross, Phys. Rev. Lett. **52**, 997 (1984).

[25] E. K. U. Gross and W. Kohn, Adv. Quant. Chem. **21**, 255 (1990).

[26] E. K. U. Gross, J. F. Dobson, and M. Petersilka, in *Topics in Current Chemistry (Density Functional Theory II)* (Springer, Berlin, 1996).

[27] D. Porezag, T. Frauenheim, T. Köhler, G. Seifert, and R. Kaschner, Phys. Rev. B **51**, 12947 (1995).

[28] J. A. Fayeton, M. Barat, J. C. Brenot, H. Dunet, Y. Picard, U. Saalmann, and R. Schmidt, Phys. Rev. A **57**, 1058 (1998).

[29] J. C. Brenot, H. Dunet, J. A. Fayeton, M. Barat, and M. Winter, Phys. Rev. Lett. **77**, 1246 (1996).

[30] The calculation of such (many–electron) transition probabilities is by no means trivial. It has been done in a statistical approach [15] similar to the one used for multiple ionization of sodium clusters [39].

[31] J. L. Martins, J. Buttet, and R. Car, Phys. Rev. B **31**, 1804 (1985).

[32] V. Bonačić-Koutecký, I. Boustani, M. Guest, and J. Koutecký, J. Chem. Phys. **89**, 4861 (1988).

[33] V. Bonačić-Koutecký, J. Pittner, C. Fuchs, P. Fantucci, and J. Koutecký, J. Chem. Phys. **104**, 1427 (1996).

[34] M. M. Kappes, M. Schär, U. Röthlisberger, C. Yeretzian, and E. Schumacher, Chem. Phys. Lett. **143**, 251 (1988).

[35] The "energetic distance" of 0.1 eV has been obtained from a detailed investigation of the tetramer in comparison with the experimental data [15].

[36] S. J. Buckman and C. W. Clark, Rev. Mod. Phys. **66**, 539 (1994).

[37] C. Yannouleas and U. Landman, Phys. Rev. Lett. **78**, 1424 (1997).

[38] F. Grossmann, U. Saalmann, and R. Schmidt, Ann. Phys. (Leipzig), submitted (2000).

[39] C. A. Ullrich, P.-G. Reinhard, and E. Suraud, J. Phys. B **30**, 5043 (1997).

Finite element three-body studies of bound and resonant states in atoms and molecules.

by

T. Alferova*, S. Andersson, N. Elander, S. Levin† and E. Yarevsky‡

Molecular Physics Group, Dept. of Physics, Stockholm Univ.

Box 6730, SE-113 85 Stockholm, Sweden.

Abstract

The development of a full angular momentum, three dimensional, smooth exterior complex dilated, finite element method for computing bound and resonant states in a wide class of quantum systems is described. Applications to the antiprotonic helium system, doubly excited states in the helium atom and to a model of a molecular van der Waals complex are discussed.

Contents

*On leave of absence from Department of Physics, Gomel state University, Gomel, Belarussia

†On leave of absence from Department of Mathematical and Computational Physics, Institute for Physics, St. Petersburg University, St. Petersburg, Russia.

‡International Solvay Institutes for Physics and Chemistry, Campus Plaine ULB C.P.231, Bd.du Triomphe, Brussels 1050, Belgium

ADVANCES IN QUANTUM CHEMISTRY, VOLUME 40

0065-3276/01 $35.00

3. A Numerical realization of three-body quantum mechanics.

   The finite element method applied to one-dimensional problems.

   The three-dimensional finite element problem in quantum mechanics.
4. Three applications

   The Antiprotonic helium system - a bound state application.

   Fragmenting levels for a known three-body problem - doubly excited states in the normal helium atom.

   A triatomic model problem - the $NeICl$ van der Waals complex.
5. Conclusions.

1 Introduction

Chemical reactions are believed to occur via a number of short-lived quantum states. We are interested in describing these states both in the free system (like a free molecule) as well as in a system imbedded in an environment (like a molecule in a solution). In order to describe these states we need not only to calculate their energies but also their fragmentation properties. The fact that two-body systems decay rates, described as a set of coupled forces (or more generally : coupled potential energy surfaces) vary with several orders of magnitude within the small energy range of around ten rotational quanta makes[1, 2] it necessary to have a very sharp theoretical and computational tool that is able to derive energies as well as decay rates and cross sections with very high accuracy.

Our goal is to obtain a general method for computing bound state as well as scattering properties of general few-body systems. The need for experimental (sometimes spectroscopic) accuracy requires us to be able to describe fundamental few-body systems in detail without making formal as well as uncontrollable numerical approximations.

Our current direction is to study dynamical processes in atomic and molecular two- and three-body systems. We use a technique which formally is based on the mathematical theory of dilation analytic functions. Numerically these results are realized though a fully three-dimensional finite element method applied to a total angular-momentum representation. We here show how generalizations of our previously published two-body methods to three-body systems are possible without formal approximations.

There are several reasons that makes it interesting to study three-body atomic and molecular systems. The recent experimental and theoretical studies on antiprotonic helium[3, 4] is an example of an exotic atomic system which was studied in order to find possible differences between antimatter and matter.

The antimatter is here represented by the antiproton which replaces one of the electrons in normal helium. The system was discovered when antiprotons were colliding with normal helium atoms in liquid phase. It was found that about 3% of the incoming antiprotons do not annihilate within the normal pico second range. These antiprotons are instead captured for some micro seconds before the annihilation takes place. Discrete optical transitions were observed to be emitted from the reaction and it was concluded that a collision complex with high angular momentum - the antiprotonic helium- was formed. The wave lengths of these radiative decay lines were later measured with high precision using laser fluorescence techniques. The fact that the interaction potentials in this system are pure coulombic made it possible for us to compute these transitions to experimental accuracy[5].

The role of electron-electron interaction is one of the main topics of atomic, molecular physics and quantum chemistry. The normal helium atom is then naturally one of the most fundamental systems. Doubly excited states are as almost bound states of special interest since the role of the electron-electron interaction is important in describing energies and also autoionization rates. Dielectronic recombination processes where one of the two excited electrons falls down to a lower level while the other is ejected appears to be a fundamental process where electron-electron interaction plays a dominant role[6]. The recently built electron-cooler storage rings[7] have made it possible to study dielectronic recombination and thereby doubly excited states with high experimental accuracy.

The role of resonances was in some sense verified by a study prototype three-body scattering reaction $F + H_2 \rightarrow HF(v, J) + H$ problem[8]. Recent experimental as well as theoretical results indicate that resonances play a very important role in this reaction[9]. We have previously developed methods by which scattering cross sections can be computed from the properties associated with resonant states[19, 28, 29, 30]. Problems like the fluorine hydrogen collision encourage us to come back and combine these methods with our current 3-D finite element method in order to study the influence of intermediate resonant states $FH_2\ (v, J, K)$ in

$$F + H_2 \rightarrow (\ FH_2\ (\tilde{v}, \tilde{J}, \tilde{K})\ ) \rightarrow HF(v, J) + H \qquad (1)$$

where $\tilde{v}, \tilde{J}$ and $\tilde{K}$ represent vibrational and rotational quantum numbers in the triatomic system while v and J are vibrational and rotational quantum numbers in the diatomic system. With this approach we hope to be able to assign resonant states in the complex energy plane, as described below and as illustrated in fig. 5 to structures in the cross section.

An overwhelming majority of the chemical reactions take place in the liquid solvated phase. In these environments, the statistical averaging of molecular

properties make the specificity of the outcome of chemical reactions dependent on the improbability of competing reactions. The coupling between the products and the reactants on the one side and the bath of solvent molecules on the other may greatly influence both the rate and the final outcome of the reaction and the study of its role in chemical reaction dynamics is of paramount importance [10]. Therefore, a presently rapidly growing field of research is that of coherent control of chemical reactions with laser fields[11]. Some of the more 'physical' projects considered are the study of solvation dynamics[12] and of primary photophysical processes. The principles for this, with the laser fields to "guide" the molecules along a specific reaction coordinate, have been proven to work in practice for small free molecules, but the question is how applicable they are to reactions in solutions. Accordingly, as the coherent control schemes are built on a detailed knowledge of the quantum mechanical properties of the reactants, it is essential to study the coupling to solvent molecules at the same level. This means that one, both in combined experimental and theoretical studies, needs to find model systems where the differences between the structural and dynamical properties of the free and loosely bound molecule (AB and $AB - X$ respectively) can be studied in detail.

It is known that the solution molecule interacts with the solute molecules via so called polarization or van der Waals forces. These forces are also active in the formation and binding of nobel-gas-diatom complexes. This kind of interaction is so weak that the vibrational and rotational motion of the diatomic in the van der Waals complex is similar to that of the free diatomic. A van der Waals system of the kind $AB - X$ is thus considered to be a good candidate as model system for these studies of solute - solvent interaction.

Summing up : Yes, there are many phenomena observed and to be observed which may be better understood with the help of accurate theoretical three-body methods.

2 Theory.

Earlier thee-body studies in our group were focused on zero angular momentum problems[13, 14, 15]. The relative motion and dynamics of a general three-body system is described by three coordinates. Jacobi coordinates (see fig. 1) are used in this work. One first connects two particles (2) and (3) using the coordinate x. The distance from the center of mass of particle (2) and (3) to particle (1) forms the next coordinate y. The angle between the vectors **x** and **y** then specifies the non-rotating three-body system completely. When we wanted to generalize these methods to non-zero angular momentum states it was natural to realize that a three-body system defines a plane and that

rotation of a three-body system is the rotation of a plane. This rotation is described by the Euler angles in classical mechanics[16] and illustrated in fig. 2.

2.1 The three-body Schrödinger problem

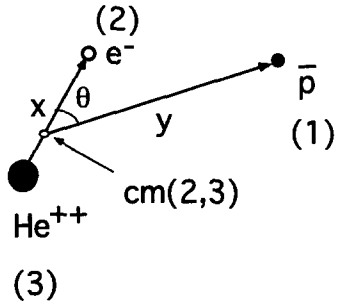

Figure 1: Definition of the Jacobi coordinates for the antiprotonic helium system.

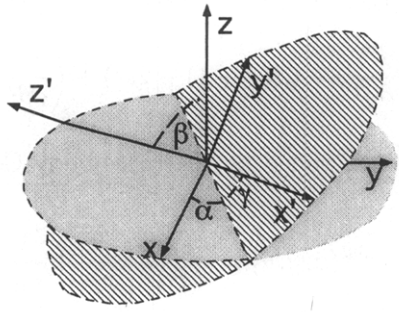

Figure 2: The Euler angles (α, β, γ) relate two sets of coordinates axis with respect to each other.

The total wave function Ψ^{JM} with angular momentum J and its projection M can be expanded in terms of Wigner D-functions [17, 18]:

$$^{\pm}\Psi^{JM} = \sum_{s=0,1}^{J} \frac{1}{\sqrt{2+2\delta_{s0}}} (D^{J}_{Ms}(\alpha,\beta,\gamma) \pm (-1)^{s} D^{J}_{M-s}(\alpha,\beta,\gamma)) \, ^{\pm}\psi^{(Js)}(\mathbf{R}). \quad (2)$$

Here '+' and '−' refer to states with normal and anomalous spatial parity, respectively. The Euler angles α, β and γ define a rotation of the body fixed

frame with respect to the laboratory fixed one and $\mathbf{R}$ is a three dimensional coordinate in the body fixed frame.

After substituting expansion (1) into the Schrödinger equation and using an orthogonality relation for D-function[17], one can derive the system of equations[18]:

$$-\imath\sqrt{1+\delta_{s1}}\,\frac{\lambda_-(J,s)}{2\mu_{1,23}y^2}\left(\frac{\partial}{\partial\theta}+(1-s)\cot\theta\right)\psi^{(Js-1)} \tag{3}$$

$$+\left(-\Delta_x^{(s)}-\Delta_y^{(s)}+V^{coul}(x,y,\theta)-E\right)\psi^{(Js)} \tag{4}$$

$$-\imath\sqrt{1+\delta_{s0}}\,\frac{\lambda_+(J,s)}{2\mu_{1,23}y^2}\left(\frac{\partial}{\partial\theta}+(1+s)\cot\theta\right)\psi^{(Js+1)}=0\,,\quad s=0\ldots J\,, \tag{5}$$

where $\lambda_\pm(J,s)=[J(J+1)-s(s\pm1)]^{1/2}$ and $\psi^{(J-1)}\equiv 0$.
The diagonal part $-\Delta_{x,y}^{(s)}$ of the kinetic energy operator is

$$-\Delta_x^{(s)}=-\frac{1}{2\mu_{23}x^2}\left(x\frac{\partial^2}{\partial x^2}x+\left(\frac{\partial^2}{\partial\theta^2}+\cot\theta\frac{\partial}{\partial\theta}-\frac{s^2}{\sin^2\theta}\right)\right)\,, \tag{6}$$

$$-\Delta_y^{(s)}=-\frac{1}{2\mu_{1,23}y^2}\left(y\frac{\partial^2}{\partial y^2}y-(J(J+1)-2s^2)+\left(\frac{\partial^2}{\partial\theta^2}+\cot\theta\frac{\partial}{\partial\theta}-\frac{s^2}{\sin^2\theta}\right)\right)\,, \tag{7}$$

The potential can be exemplified by the three-body Coulomb potential V^{coul} which is defined as :

$$V^{coul}(x,y,\theta)=-\frac{2}{r_{13}}-\frac{2}{r_{23}}+\frac{1}{r_{12}}\,. \tag{8}$$

The interparticle distances r_{ij} can be easily expressed in terms of Jacobi coordinates, and the reduced masses μ have been defined in terms of the particle masses m_i as $\mu_{23}=m_2m_3/(m_2+m_3)$, $\mu_{1,23}=m_1(m_2+m_3)/[m_1+(m_2+m_3)]$. A bound state in a quantum mechanical system is described by a real valued energy and the corresponding real valued eigenfunction. However we above set out to study fragmentation phenomena. We thus need to study complex energies and wavefunctions.

2.2 Resonant wavefunctions - asymptotically expanding Non-Integrable eigensolutions.

A resonant state has both an energy E_ν, a natural fragmentation decay width Γ_ν and a corresponding mean lifetime. Using the Breit-Wigner formalism[19,

20] we can assign the energy and the natural decay width of a resonant state to the real and the imaginary part of a complex valued energy. $\mathcal{E}_\nu = E_\nu - \imath\Gamma_\nu/2$. If the potential in the Schrödinger Hamiltonian is time-independent we can write the time-dependent wave function as a product

$$\psi_\nu(\mathbf{r},t) = \phi_\nu(\mathbf{r})\exp(-\imath E_\nu t)\exp(-\Gamma_\nu t/2) \quad \Rightarrow \quad |\psi_\nu(\mathbf{r},t)|^2 = |\phi(\mathbf{r})|^2\exp(-\Gamma_\nu t)$$

This implies that $\psi_\nu(\mathbf{r},t)$ can be used to describe an exponentially decaying probability distribution. The time-independent partial wave solutions above a threshold obey scattering boundary conditions. They are thus proportional to the regular solution $\varphi_\ell(E,r)$ a origin and tend to infinity like Jost solutions $f_\ell^+(E,r)$:

$$\lim_{r\to 0} \frac{\varphi_\ell(E,r)}{r^{\ell+1}} = 1 \tag{9}$$

$$\lim_{r\to\infty} \frac{f^+(E,r)}{\exp[\imath\sqrt{2\mu\mathcal{E}-V(\infty)}r]} = 1 \tag{10}$$

If the imaginary part of the energy $\mathcal{E}$ is negative and different from zero as it is for a resonant state we will have a solution with an exponentially growing amplitude. Such a state does not, as illustrated in fig. 3, have a square integrable wavefunction and it is only with great trouble that one in special cases may be able to compute it directly.

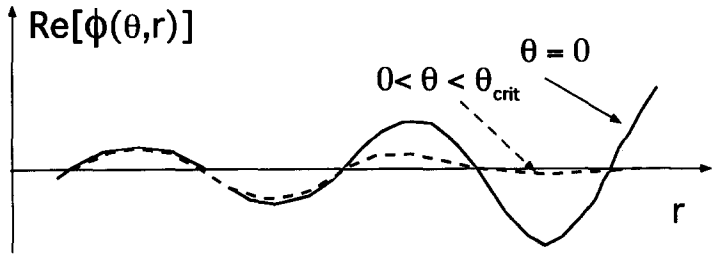

Figure 3: (a) An ordinary Gamow wave $\phi(r,0)$ and (b) a Gamow wave evaluated on the ray $r\exp[\imath\theta]$, where *theta* $\in \mathbf{R}$ and $\theta > 0$ in the first quadrant of the complex coordinate plane.

2.2.1 Complex Scaling

The eigenenergies and eigenfunctions of resonant eigenstates may be obtained by the complex dilation method[21, 22] which is illustrated in fig. 4. The

Hamiltonian H itself is continued to some operator $H(\theta)$, where the continuation is made with respect to the coordinates $\vec{r}$ instead of the energy E.

$$r \rightarrow r \exp(i\theta) \tag{11}$$

Then one looks for isolated zeroes of $H(\theta) - E$ of finite multiplicity, which correspond to poles of $(H(\theta) - E)^{-1}$.

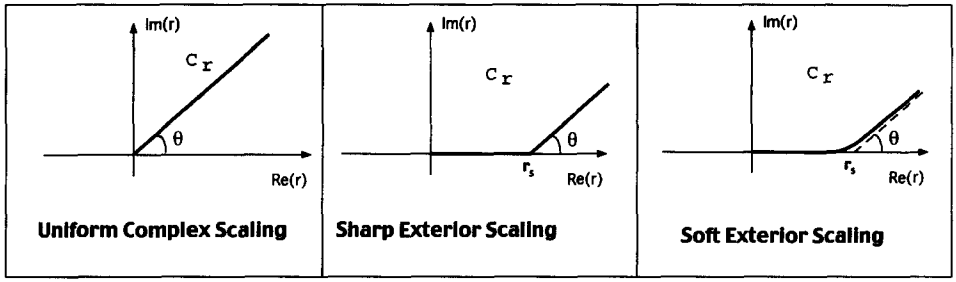

Figure 4: Complex scaling in three different forms : the original Uniform complex scaling of Balslev and Combes. The Exterior complex scaling proposed by Simon and the Smooth exterior complex scaling studied by Helffer are all discussed in the text.

Note that here we continued H to $H(\theta)$ first and then we find the poles of the resolvent of the continued operator.

Balslev and Combes[21] proved that this implies a similarity transformation of the Schrödinger problem yielding

- The isolated bound states of $H = H(0)$ are also eigenvalues of each $H(\theta)$.
- The continuous spectrum of the continued operator, $H(\theta)$ is $\sigma_{cont}(H(\theta)) = \cup_{E_i} \left\{ E_i + e^{-2i\theta}\mu,\ \mu \in \mathcal{R}^+ \right\}$
- $H(\theta)$ may have isolated complex eigenvalues some of which can be identified as resonances.

Exterior Complex Scaling[23]

$$r \rightarrow \xi(r) = \begin{cases} r & r < r_s \\ r_s + \exp(i\theta)(r - r_s) & r \geq r_s \end{cases} \tag{12}$$

has a wider applicability than the original uniform complex scaling because :

- it only requires the potentials to be asymptotically analytically defined functions.

- it allows us to threat problems where the potentials can be non-analytical outside a small region close to the real axis in the coordinate plane.

Although creating possibilities sharp exterior scaling also implies complications. The wave functions as well as their first derivatives are discontinuous at the exterior scaling point $r = r_s$. Formally this can be overcome by an introduction of a zero-range potential at this point[24]. In practical numerical applications using discretized grids Carlsund-Levin and Elander[25] found that sharp exterior scaling will introduce both distortions in the complex dilated continuum as well as a number of spurious eigenvalues.

Soft Exterior Scaling[26] avoids the discontinuity in the derivatives caused by the sharp bend in the integration path.

$$r \rightarrow \varphi(r) = r + \lambda g(r)\, \lambda = \exp(\imath\theta) - 1 \tag{13}$$

$$\text{with} \quad g(r) = \begin{cases} 0\,, & r \leq r_s \\ (r - r_s)(1 - \exp(-\sigma(r - r_s)^2))\,, & r > r_s \end{cases} . \tag{14}$$

Here r_s is the external radius and σ is the curvature parameter. Both the function and its derivative are continuous at r_s.

It is well-known that positions and widths of resonances are independent of the rotation angle θ. When a numerical approximation is used, resonances become θ-dependent. In this case, their positions E and widths Γ are defined by means of the complex variational principle[27]:

$$\left.\frac{dE}{d\theta}\right|_{\theta_r} = 0 \quad \text{and} \quad \left.\frac{d\Gamma}{d\theta}\right|_{\theta_i} = 0\,. \tag{15}$$

The two optimal angles θ_r and θ_i converge to one single angle as the accuracy of the calculation is increased.

2.3 Scattering cross sections from S-matrix poles through a Mittag-Leffler expansion.

Elander and collaborators, as well as other researchers, have shown that the eigenvalues and eigenfunctions of resonant states can be used to compute partial wave cross sections σ_ℓ and thereby also reaction rates in terms of a Laurent type expansion of the partial wave S-matrix[19, 28, 29, 30, 31]

$$S_\ell(E) = \sum_{\nu=1} \frac{\mathcal{R}es\ [\ S_\ell(E_\nu)\ ]}{(E - E_\nu)} + \mathcal{G}_{\ \ell}(E) \quad \text{yielding} \quad \sigma_\ell = |1 - S_\ell|^2. \tag{16}$$

This is illustrated in fig. 5. Our earlier model potential studies show that

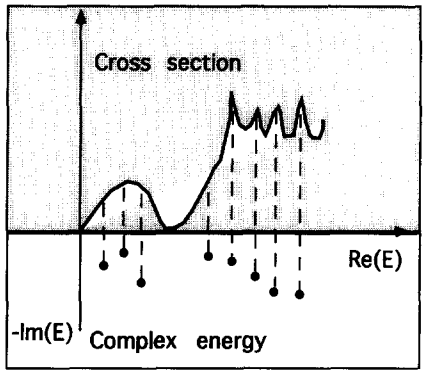

Figure 5: (A) Upper halfplane : A structured scattering cross section as a function of energy. (B) Complex S-matrix poles in the second Riemann sheet which, together with their residues, are used to describe the cross section.

only a few resonances may be sufficient to describe a reaction[28, 30, 29].We are currently studying how to extract the S-matrix residues from our finite element eigenvalues and eigenvectors. By combining the analysis of Rittby et al[28] and Krylstedt[29, 30] and the work of Newton[32] we believe that we have found a formal solution of how to compute the S-matrix residues from the corresponding complex dilated resonant wavefunctions. We believe that this tool will be useful in studying reactions both where resonances are dominant as in eq.(1) and where they are part of a background.

3 Numerical realization.

The results presented here were obtained by applying a three-dimensional finite element method (FEM) to eq.(4). However this formalism is to complicated and thus not pedagogical to be used directly in a review text like the present one. We thus first introduce a FEM-realization of the one-dimensional Schrödinger problem[33].

3.1 The Finite Element Method in one dimension

The finite element method is employed to solve the eigenvalue equation

$$\sum_{\beta} H_{\alpha\beta}\Psi_{\beta} = \Psi_{\alpha}$$

with Hamiltonians of the general form

$$H_{\alpha\beta} = -\frac{\delta_{\alpha\beta}}{2m}\left[\frac{d^2}{dr^2} + \frac{J(J+1)}{r^2}\right] + V_{\alpha\beta}(r)$$

One makes an ansatz for the eigenfunctions in the form

$$\tilde{\Psi}_c(r) = \sum_{im} c_{im} f_{im}(r)$$

where the f_{im} are non–zero only on finite intervals

$$f_{im}(r) \equiv 0 \quad r \notin [r_{i-1}, r_i], \quad i = 1, \ldots, N,$$

as illustrated in fig. 6. The best approximation to a given eigensolution within this ansatz is obtained by the solution of the finite–dimensional eigenproblem for the coefficients c_{im}

$$(\tilde{H} - \tilde{E}_k \tilde{S})c = 0 \quad \text{with matrices} \quad \begin{cases} (\tilde{H})_{im,jn} = \langle f_{im}|H|f_{jn}\rangle \\ (\tilde{S})_{im,jn} = \langle f_{im}|f_{jn}\rangle \end{cases}$$

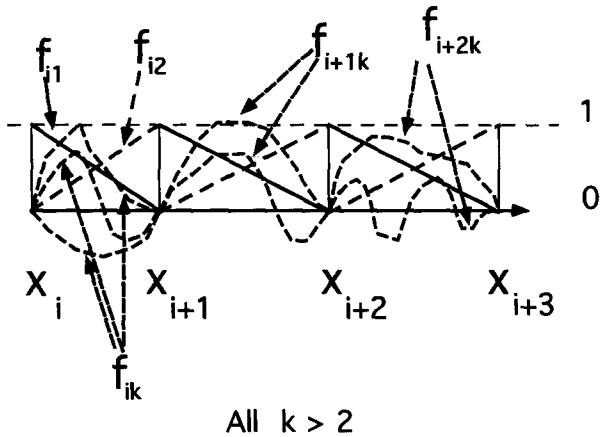

Figure 6: Finite Element basis functions in one dimension.

The matrix elements $\tilde{H}_{im,jn}$ and $\tilde{S}_{im,jn}$ are $\equiv 0$ when $i \neq j$. Therefore the matrices $\tilde{H}$ and $\tilde{S}$ are block–diagonal.

$$\tilde{H}_\theta \, \mathbf{c} = \begin{pmatrix} & \vdots & 0 & \cdots & \\ \ddots & H^{(i-1)}_{p+1,2} & 0 & 0 & 0 \\ H^{(i-1)}_{2,p+1} & H^{(i-1)}_{2,2} + H^{(i)}_{1,1} & \cdots & H^{(i)}_{1,2} & 0 \\ 0 & H^{(i)}_{3,1} & \cdots & H^{(i)}_{3,2} & 0 \\ \vdots & \vdots & \ddots & \vdots & 0 \\ 0 & H^{(i)}_{p+1,1} & \cdots & H^{(i)}_{p+1,2} & 0 \\ 0 & H^{(i)}_{2,1} & \cdots & H^{(i)}_{2,2} + H^{(i+1)}_{1,1} & \cdots \\ 0 & 0 & 0 & \vdots & \ddots \end{pmatrix} \begin{pmatrix} \vdots \\ c_{i-1,p+1} \\ c_{i,1} = c_{i-1,2} \\ c_{i,3} \\ \vdots \\ c_{i,p+1} \\ c_{i,2} = c_{i+1,1} \\ \vdots \end{pmatrix}$$

Due to the block–diagonal form of the matrices the method is fast and numerically stable.

3.2 The three-dimensional finite element problem.

We defined the elementary functions as functions, which are non–zero only inside a given element. On rectangular 3–dimensional elements this reads

$$f_{ik}(x, y, z) = 0 \quad \text{for} \quad (x, y, z) \notin [x_{l_i}, x_{u_i}] \times [y_{l_i}, y_{u_i}] \times [z_{l_i}, z_{u_i}].$$

Now we make another specific choice in our implementation, namely

$$f_{ik}(x, y, z) = u_{ik}(x) v_{ik}(y) w_{ik}(z),$$

There are essentially 3 major complications when going to 3 dimensions in a finite element calculation

- The number of functions required grows drastically. This problem is, of course, not as much a problem of the FEM, as it lies in the very nature of 3–dimensional calculations and it is shared by all methods.
- Every element has not only two, but many neighbors, typically of the order 26 in a rectangular grid. Moreover, the elements cannot be sorted in a linearly connected sequence. Therefore the matrices H and S, while remaining sparse, acquire a very broad band width with a large number of zeros within the band.
- The element boundaries are no longer simple points, but surfaces. The functions have to be continuous across these boundary surfaces.

Still we find that FEM has a number of advantages :

- FEM is more accurate than most global basis set methods.
- FEM is, as a basis set method, able to find close lying eigenvalues.
- FEM is able to give an accurate description of the wave function.

4 Three applications.

It is always dangerous to jump too high or to far in the beginning. Small steps lead to the results much faster. In order to be able to compute predissociating levels of a rotating triatomic molecule we thus started with studies of bound state model of a true three-body system - the antiprotonic helium. The next pilot case, the helium atom, is also well known. The nucleus is so much heavier that the two electrons in the helium atom but this system is still a good candidate for studies of fragmentation - in this case autoionization of doubly excited states. Both these systems have the advantage that the interaction is purely coulombic. This is not true for the third pilot case - the triatomic $NeICl$ van der Waals complex. Knowing that our method worked to high accuracy for the first two cases we were certain that we could get it to work for the triatomic.

4.1 The Antiprotonic helium system - a bound state application.

The antiprotonic helium system was used as a model when developing our non-zero angular momentum 3D finite element method. This is an example of a system for which the wave function cannot exactly be decomposed into an angular and a radial part. Besides the helium like atoms it is the experimentally most accurately known three-body system.

Antiprotonic helium is a quantum system which is similar to both an atom and a molecule. On one hand it resembles the helium atom in the sense that it has a heavy positive He^{2+} nucleus and two negative particles : the electron and the antiproton. On the other hand it resembles in some sense the hydrogen molecular ion since it has two heavy particles and one electron. Its specific property is that the two heavy particles are of opposite charge. Since it was first experimentally found at CERN in the early 1990'ies[3] one has been able to determine a number of transitions in the optical spectral region between different angular momentum levels with optical accuracy (4ppm) by using laser induced processes. The system has such properties that some of the levels, with $J \approx 30 - 40$, have radiative lifetimes of the order of a microsecond while the Auger lifetimes of these levels are considerably longer. Some other

observed levels have Auger lifetimes which are comparable or shorter than the radiative ones. Experimental results exists for both the $\overline{p} -^4 He^{2+} - e^-$ and the $\overline{p} -^3 He^{2+} - e^-$ systems.

The reasons we choose to study this system were : (1) The distance between the He^{2+} nucleus the electron and the antiproton are such that only pure Coulomb forces can be assumed in a few-body model. (2) The levels are known experimentally to high accuracy (3) Some levels with high angular momenta ($J \approx 30 - 40$) can to very good accuracy first be treated as bound levels. (4) Calculated radiative decay rates can thus be compared with experiment for some transitions without correcting for non-radiative processes. (5) The system is simple enough so that relativistic and QED contributions can be computed and the corrected transition wave lengths can be compared with experiments. (6) Isotope effects can be studied, both for the Schrödinger level results and for the relativistic and QED corrections. (7) The results of calculations using our theoretical methods for describing fragmentation - Auger type-decay rates- can be compared with experiments. The $\overline{p} - He^{2+} - e^-$ system is thus a good "guinea-pig" when one wants to develop a theoretical method to study the structure and state-specific decay dynamics of general three-body systems.

Energy levels for $\overline{p} - He^{2+} - e^-$ were computed by using a model based on the exact Hermitian Schrödinger Hamiltonian for a three-body problem and compared with the experimental data available at that time[34]. The discrepancy with experimental values was about 50ppm. The accuracy of the Schrödinger energy levels were increased by technical development and relativistic and QED corrections were calculated using the Schrödinger picture wave functions and perturbation theory to give almost experimental accuracy when relativistic corrections were added[5].

Terms to be calculated are relativistic mass correction terms for the electron and Darwin terms for the electron-antiproton and electron-helium interactions. They can be expressed in terms of the electron momentum $\mathbf{p}_e$ and $\delta-$functions of the corresponding distances :

$$\Delta E_{vJ}^{(rel)} = \alpha^2 \left\langle \psi^{(J0)} \left| -\frac{\mathbf{p}_e^4}{8} + \frac{\pi}{2}(2\delta(\mathbf{r}_{23}) - \delta(\mathbf{r}_{12})) \right| \psi^{(J0)} \right\rangle . \qquad (17)$$

Still the agreement was not satisfactory. We also noted that some QED corrections could be of the same order of magnitude as the relativistic corrections. Lamb shift for one electron in a helium-like atom with a nuclear charge Z can be expressed as:

$$\Delta E_{vJ}^{L} = \frac{8\alpha^3 Z}{3} \left\langle \psi^{(J0)} | \delta(\mathbf{r}_{23}) | \psi^{(J0)} \right\rangle \left(\frac{19}{30} + 2\log\frac{1}{\alpha Z} - \log\frac{K_0}{Z^2 Ry} \right) . \qquad (18)$$

Our problem was now that when QED corrections were added the agreement was reduced. However, an experimental pressure dependence of the measured transition wave lengths was found[35] which increases the uncertainty of the experimental data. Our theoretical transition energies do thus appear to be within the current experimental errorbars. The calculated radiative decay rates agree well with experimental work[5].

The isotopic $\overline{p} - {}^3He^{2+} - e^-$ system has the same general properties as the originally studied $\overline{p} - {}^4He^{2+} - e^-$ system[36]. While the isotope effect on the energy levels within the Schrödinger model shows, as can be expected, a scaling which goes as the square root of the respective reduced masses. However, we note that the relativistic and QED corrections scale in a different fashion. This latter scaling is not yet obvious from the formal theory[36].

We can at this stage state that we are now in possession of a very accurate theoretical and numerical tool to calculate properties of any three-body system where the interparticle forces may be expressed as a function of the three interparticle distances.

		$\Delta_{Exp-Calc}$
Original Experiment	597.36 nm	
Our non-relativistic results	597.224 nm	0.136 nm
With Rel. & Lamb shift corr.	597.258 nm	0.102 nm
Pressure corrected experiment	597.259 nm ($\pm$0.002nm)	
Final Experimental Deviation		< 0.001nm

Conclusion : Our method and its computational implementation is accurate for bound states and it works better than we originally had anticipated.

4.2 Fragmenting levels in a known three-body problem - doubly excited states in the normal helium atom.

At this stage we wanted to include fragmentation into our code using the complex scaling formalism. Very accurate theoretical results for energies and the corresponding widths of autoionizing states in $He-$like systems are available in the literature. In a paper [37] we show that we are able to calculate both energies and autoionization widths to a very high accuracy in good competition with other recently published work[6] using uniform complex scaling. Recently we have also generalized our methods to be able to compute decay properties of non-zero angular momentum systems. We have thus been able to calculate autoionization rates also for P levels in He. Also here, a comparison with previous studies[6] shows that our method is accurate and reliable. While

most other groups studying helium are limited to atomic systems we now have a general code which in principal is applicable for any three-body system.

	Present		Lindroth[6]			
	E	Γ	E	Γ	Δ_E	Δ_Γ
$^1S^e$	-0.777870	0.004535	-0.777868	0.004541	2×10^{-6}	-6×10^{-6}
$^1S^e$	-0.317457	6.66×10^{-3}	-0.31745	6.66×10^{-3}	7×10^{-6}	$>1\times10^{-6}$
$^1P^e$	-0.336088	4.49×10^{-3}	-0.33609	4.49×10^{-3}	2×10^{-6}	$>1\times10^{-6}$
$^1P^e$	-0.291157	7.41×10^{-5}	-0.29115	7.41×10^{-5}	7×10^{-6}	$>1\times10^{-7}$

Conclusion : Our method and its computational implementation is accurate also for resonant states.

4.3 A triatomic model problem - the $NeICl$ van der Waals complex

Having tested our formalism and code on the two coulomb interacting systems antiprotonic helium and doubly excited states in normal helium we were ready to attack a model of predissociating triatomic molecule. We choose the $NeICl$ van der Waals complex as our triatomic test molecule since a number of more and more accurate studies had been performed on zero-angular momentum levels of this system[38, 39, 40, 41, 42].

The $NeICl$ model potential is described by the total potential $V(x, y, \phi)$ as the sum of three atom-atom potentials of the Morse type

$$V(x, y, \phi) = V_{12}(r_{12}) + V_{13}(r_{13}) + V_{23}(r_{23}), \tag{19}$$

where

$$V_{ij}(r_{ij}) = D_{ij}\left[\exp(-\beta_{ij}(r_{ij} - r_{ij}^{eq})) - 1\right]^2. \tag{20}$$

The potential is highly asymmetric : $D_e^{I-Cl} \approx 1200\text{cm}^{-1}$ while $D_e^{Ne-ICl} \approx 60\text{cm}^{-1}$

An energy level in the upper $NeICl$ potential energy surface, cut along the $Ne---ICl$ coordinate (x), which corresponds to a $v = 2$ vibrational mode in the ICl diatomic subsystem, is imbedded in the rovibronic continua of the $NeICl$ levels for which the ICl diatom is in its vibrational levels $v = 0$ and 1 as illustrated inf fig. 7.

$$\Psi_{\text{total}} = \alpha\Psi_{Bv2} + \beta\Psi_{Cv1} + \gamma\Psi_{Cv0} \tag{21}$$

The total complex dlitated wave function of the $NeICl$ cluster is composed of a dominating part Ψ_{Bv2} where the Ne atom is bound to the ICl and parts where the Ne atom is moving free relative to the ICl diatom and the vibrational modes of this ICl diatom are $v = 1, 2$

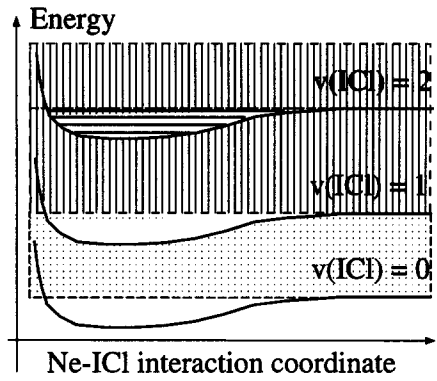

Figure 7: The three potential energy curves for the $Ne - ICl$ motion when the ICl diatomic sub-system has vibrational modes $v = 0, 1$ and 2.

Previous fully quantum mechanical studies of predissociation phenomena in triatomic molecules do not, to our knowledge, use a Hamiltonian that has a non-zero total angular momentum. Tennyson et al[43, 44, 45, 46, 47, 48, 49, 50, 51] solve the same equations as we do but have not yet, to our knowledge, treated any predissociation problems. The adiabatic rotation approximation method of Carter and Bowman[52] plus a complex $\mathcal{L}^2$ modification have, on the other hand, been used to compute rovibrational energies and widths in the HCO[53, 54] and $HOCl$[55, 56, 57] molecules. This method is based upon the the Wilson and Howard[58], Darling and Dennison[59] and Watson[60] formalism. It is less transparent but the exact formalism in refs.[58, 59, 60] is equivalent to the one presented here and in ref [43]. While both we and Tennyson et al[43] include the exact Hamiltonian in our formalism the latter authors[52] use an approximate method which they have analysed and motivated.

Using the present formalism we believe that we are able to report the first fully quantum mechanical calculation of predissociation widths for a triatomic molecule. Both exact and approximate results, in which Coriolis effects are neglected, have been calculated. The so far computed data includes rovibronic energies and predissociation widhts for the first three non-zero angular momenta (J= 0 - 3). For positive parity in eq.(4) we obtain $J + 1$ levels with different s values while negative partity yields J levels. The calculated energy spectrum resembles a normal asymmetric top molecule and in particular the variation in the computed widths albeit for a limited number of (J, s, τ) levels were found. However, the present set results is too small to give any general knowledge. Current work and future studies will hopefully be able to give such guidelines. The code has recently been ported on a IBM SP2 Nighthawk

8 node computer also using 64 bit arithmetics. While the total computer time for the earlier used DEC/Alpha 433a.u. workstation was of the order of 24 hours for obtaining a few eigenvalues, the IBM SP Nighthawk requires only about 3 hours for the same task.

5 Conclusions

We have in this contribution tried to give some insite in how predissociation phenomena in a triatomic system has been attached during the passed few years. We can now state that we do have a method and a code that allow us to calculate predissociation phenomena in triatomic systems described by a single potential energy surface. The concept of shape and Feshbach resonances does not seem to be so clear any more. In a diatomic system, described by an single potential energy curve, we would not have been able to have the interaction between different modes discussed above. Again, more studies need to be performed. Feshbach resonances in diatomic molecules are associated with more than one potential energy curve. The generalization of the present three-body formalism to Feshbach problems would in principle not have any formal complications. However, the size of the discretized matrix problem (the generalization of eq.(4)) is frightening. While we for the present single potential energy surface problem have banded matrices with dimensions of about 50.000 and bandwidhts of 3000 we would for a two potential energy surface crossing problems at least reach matrices four times as large. This is out of range for most applications. However, the current code does not have ways to optimize the finite element grid. Such methods are available in the literature and we may be able to find better and smaller grids that will give the same or even better accuracy on our present problems. We hope that we may be able to proceed along this route to treat Feshbach resonances in triatomic systems.

The Mittag-Leffler expansion methods described in section 2.3 is another challange. The idea and the detailed formalism should in principle be applicable to triatomic systems. If realized, we will have a very powerful tool helping us to describe collision cross sections in three-body systems in terms of the participating resonant states an their wavefunctions. I hope we by this contribution have shared with the reader the impression that the present work has just begun. Several new features may be included in the present theory yielding a way to describe three-body collisions in terms of quantized states with complex energies which are imbedded in or may be even constituting the continuum.

6 Acknowledgments.

The authors acknowledge the organizers of the Fifth European Workshop on Quantum Systems in Chemistry and Physics for encouraging us to present and complete this contribution. TA acknowleges support from the Swedish Institute. SA acknowleges from Physics Dept at Stochholm Univ.. SL and EY acknowleges support from the Royal Swedis Academy och Sciences and the Wenner Gren Foundations. The support by the Swedish Natural Science Council to this work is finally acknowleged.

References

[1] R. Mölenkamp and H.J. Korsch, Phys. Rev **A34**, 4716 (1986).

[2] E. Brändas M. Rittby and N. Elander In *Lecture Notes in Physics* **325**, *Ed. E. Brändas and N. Elander.* Springer Verlag, Heidelberg 1989. page 345.

[3] T. Yamazaki et al., Nature **361**, 238 (1993).

[4] V. I. Korobov, Phys. Rev. A **54**, R1749 (1996); Hyperfine Interactions, **101/102**, 479 (1996).

[5] N. Elander and E. Yarevsky, Phys. Rev. A**56**, 1855 (1997).
-. ibid Phys. Rev. A**57**, 2256 (1998).

[6] E. Lindroth, Phys. Rev. A**49**, 4473 (1994).

[7] R. Schuch, A. Barany, H. Danared, N. Elander and S. Mannervik, Nuclear Instr. and Methods **B43**,411 (1989).

[8] C.L. Russell and D.E. Manolopoulos, Chem. Phys. Lettr. **256**, 465 (1996).

[9] G.C. Schatz, Science, **288**, 1599 (2000) and references therein.

[10] J.T. Hynes, Nature **369**, 439 (1994).

[11] *"Chemical reactions in clusters"*, ed: E.R. Bernstein, Oxford Univ. Press, New York, 1996.

[12] M.L. Horng, J.A. Gardecki, A. Papazyan and M. Maroncelli, J. Phys. Chem. **99**, 17311 (1995).

[13] A. Scrinzi, N. Elander and B. Piraux, Phys. Rev. **A48**. Rapid Comm. R2527 (1993).

[14] A. Scrinzi, N. Elander and A. Wolf, Zeitschrift für Physik **D34**,185 (1995).

[15] A. Scrinzi, Computer Physics Comm., **86**, 67 (1995).

[16] H. Goldstein, Classical Mechanics, 2ed, Addison-Wesley Publ. Reading Mass, USA, 1980.

[17] D. A. Varshalovich, A. M. Moskalev, and V. K. Khersonskii, *Quantum Theory of Angular Momentum* (World Scientific, Singapore, New Jersey, Hong Kong, 1989).

[18] C. F. Curtiss, J. O. Hirschfelder, and F. T. Adler, J. Chem. Phys. **18**, 1638 (1950).

[19] N. Elander in **Multiple Quantum Scattering With Applications to Nuclear, Atomic and Molecular Physics**, *The IMA Volumes in Mathematics and its Applications* **89**, Editors : D. Thruhlar and B . Simon, Springer Verlag, New York, 1997, Page 283.

[20] *Lecture Notes in Physics* **325**, Editors. E. Brändas and N. Elander, Springer Verlag, Heidelberg 1989.

[21] E. Balslev and J.M. Combes, Comm. Math. Phys., **22**, 280 (1971).

[22] B. Simon, Ann. Math., **97**, 247 (1973).

[23] B. Simon, Phys. Lett. A **71**, 211 (1979).

[24] P.B. Kurasov, A. Scinzi and N.Elander, Phys. Rev.**A49**, 5095, (1994).

[25] C. Carlsund-Levin, Doctoral Thesis, Royal ,Institute of Technology, Stockholm, (2000).

[26] B. Helffer, In *Lecture Notes in Physics* **325**, *Ed. E. Brändas and N. Elander.* Springer Verlag, Heidelberg 1989. page 11.

[27] N. Moiseyev, P. R. Certain, and F. Weinhold, Molec. Phys. **36**, 1613 (1978).

[28] M. Rittby, N. Elander and E. Brändas, in *Lecture Notes in Physics* **325**, *Ed. E. Brändas and N. Elander.* Springer Verlag, Heidelberg 1989. page 129

[29] N. Elander, C. Carlsund, P. Krylstedt and P. Winkler, In *Lecture Notes in Physics* **325**, *Ed. E. Brändas and N. Elander.* Springer Verlag, Heidelberg 1989. page 384.

[30] P. Krylstedt, Ch. Carlsund and N. Elander, J. Phys. B. **22**, 1051 (1989).

[31] T.N. Rescigno, M.Baertschy, D. Byrum and C.W. McCurdy, Phys. Rev. **A55**, 4243 (1997).

[32] R. Newton, *Scattering theory of Paricles and Waves*, Springer Verlag, Second Ed., New York, 1982, Page 350 ff.

[33] A. Scrinzi and N. Elander, J. Chem . Phys.**98**, 3866 (1993).

[34] E. Yarevsky and N. Elander, Europhys. Lett., **37**, 453 (1997).

[35] R.S. Hayano et al. Phys. Rev. A. **55**, R1, (1997).

[36] S. Andersson, N. Elander and E. Yarevsky, J. Phys. **B31** (1998) 625.

[37] N. Elander and E. Yarevsky, Phys. Rev. A**57**, 3119 (1998).

[38] O. Roncero, J. A. Beswick, N. Halberstadt, P. Villarreal, and G. Delgano-Barrio, J. Chem. Phys. **92**, 3348 (1990).

[39] S. K. Gray, C. E. Wozny, J. Chem. Phys. **94**, 2817 (1991).

[40] N. Lipkin, N. Moiseyev, and C. Leforestier, J. Chem. Phys. **98**, 1888 (1993).

[41] V. Ryaboy, N. Moiseyev, V.A. Mandelshtam and H.S. Taylor, J. Chem. Phys. **101**, 5677 (1994).

[42] M. Monnerville and J.-M. Robe, J. Chem. Phys. **211**, 249 (1996).

[43] J. Tennyson, J.R. Henderson and N.G. Fulton, Comput. Phys. Commun. **86**, 175 (1995).

[44] I.N. Kozin, P. Jensen, J. Mol. Spectrosc **183**, 398 (1997).

[45] G.S. Yan, H. Xian, D.Q. Xie, Chem. Phys Lettr **271**, 157 (1997).

[46] O. L. Polyansky, N.F. Zobov, S. Viti, et al. Science **277**, 346 (1997).

[47] J.H. Schryber,O.L. Polyansky, P. Jensen, et al. J. Mol.Spectrosc **185**, 234 (1997).

[48] H.Y. Mussa, J. Tennyson, J. Chem. Phys. **109**, 10885 (1998).

[49] O. L. Polyansky, J. Tennyson and N.F. Zobov, Spectrochim Acta **A55**, 659 (1999).

[50] O. L. Polyansky, J. Tennyson, J. Chem. Phys. **110**, 5056 (1999).

[51] J.S. Kain, O.L. Polyansky and J. Tennyson, Chem. Phys Lettr. **317** 365 (2000)

[52] S. Carter and J.M. Bowman, J. Chem. Phys. **108**, 4397 (1998).

[53] D. Wang and J.M. Bowman, J. Phys. Chem. **100**, 1021 (1994).

[54] D. Wang and J.M. Bowman, Chem. Phys. Lettr. **235**, 277 (1995).

[55] S. Skokov, K.A. Peterson and J.M. Bowman, J. Phys. Chem. **109**, 2662 (1998).

[56] S. Skokov and J.M. Bowman, J. Phys. Chem. **110**,9789 (1999).

[57] S. Skokov and J.M. Bowman, J. Phys. Chem. **111**,4933 (1999).

[58] E.B. Jr. Wilson and J.B. Howard, J. Chem. Phys. **4**, 260 (1936).

[59] B.T. Darling and D.M. Dennison Phys. Rev. **57**, 128 (1940).

[60] J.M. Watson, Molec. Phys. **5**, 479 (1968).

A COMPUTER SIMULATION OF THE RING PUCKERING AND OXYGEN WAGGING DYNAMICS IN THE S_0 STATE OF CYCLOBUTANONE.

D.C. Moule[†], W. Fraessdorf[†], C. Muñoz-Caro[‡] and A. Niño[‡]
[†]*Department of Chemistry, Brock University, St Catharines, ON., L2S3A1, CANADA.*
and
[‡]*E.U. Informatica de Ciudad Real, Universidad de Castilla-LaMancha, 13071, Ciudad Real, SPAIN.*

Abstract

The satisfactory modelling of the ring puckering displacements in small ring molecules has been difficult to achieve since the equilibrium structure of the ring atoms depends on the balance between the ring strain and the torsional repulsion forces. Ring strain forces result from the compression of the C-C-C bond angles to 90 degrees to form the square ring and favour the planar conformation, whereas, the torsional repulsion forces between the C-H bonds prefer a puckered conformation. Information about the equilibrium structure and the balance between these forces comes from the sequence bands observed in the far infrared spectrum. A two dimensional study of the ring puckering and oxygen wagging vibrational modes was used to simulate the far infrared spectrum and test the balance between these forces.

Contents

ADVANCES IN QUANTUM CHEMISTRY, VOLUME 40

0065-3276/01 $35.00

1. INTRODUCTION

In 1945, Bell pointed out that the out-of-plane displacement of the diagonal atoms of a four membered system would result in a potential function that would be described by a single quartic term.[1] This prediction was based on a model where the puckering internal coordinate was assumed to be derived from a linear combination of bending coordinates of the ring atoms. With an out-of-plane displacement of the ring atoms, the quadratic force terms describing the bending displacements cancel each other, leaving a residual force constant term that is quartic in the ring displacements. In the case of cyclobutanone, C_4H_6O, the three ring carbons of nominally sp^3 hybridization (bond angle = 109.5°) and the sp^2 carbonyl atom (bond angle=120.0°) are compressed into a ring with angles close to 90.0°. The so-called ring strain generated by this compression stabilizes the ring into a planar conformation. The other major factor that determines the ring stability is the torsional repulsion between the four C-H bonds. In the planar conformation, these C-H bonds eclipse each other when viewed along the C-C bond direction and they create repulsions that distort the ring into a nonplanar conformation. In the prototype cyclobutanone system, CB, the torsional repulsions and the ring strain forces are closely balanced with the result that the equilibrium structure of the ring is pseudo-planar with the central barrier in the puckering potential lying well below the vibrational zero point energy.

It is possible to model the molecular potential for the puckering dynamics by a potential function containing two terms. The effect of the strain energy is represented by the quartic oscillator expression, $A(z)^4$ where z is an internal coordinate that measures the puckering displacement. The tendency towards nonplanarity can be measured by height of the central barrier that is described by a quadratic term $-B(z)^2$. While the resulting double minimum function, $V(z) = A(z)^4 - B(z)^2$ is too limited to model the dynamics at higher energies, it is useful for separating out the twin effects of ring strain and torsional repulsion.

Information about the Q_{20} ring puckering normal mode has been mainly drawn from the far-infrared region of the gas phase vibrational spectrum. Pioneering studies in this region were carried out with a grating spectrometer by Durig and Lord[2] and then in more detail by FTIR (Fourier transform infrared) interferometry

by Borgers and Strauss.[3] These latter authors were able to observe a sequence progression in the puckering mode up to 9 quanta of vibrational excitation. Of direct interest to the present study was their observation that the (v=8) 7 (v=7) and (v=9) 7 (v=8) sequence transitions resulted in infrared bands that were split into doublets. By an analyses of the hot band satellites in the microwave spectrum, Sharpen and Laurie[4] showed that this doublet splitting was the result of a localized perturbation. This study demonstrated that while the A, B, and C rotational constants showed a smooth increase with increasing puckering quantum number, for v=8 all three constants were displaced from their expected positions. This shift confirmed that the perturbation was restricted to a single v=8 level, at 560.45 cm^{-1}.

The other experimental data about the out-of-plane displacements comes from the hot band structure in the S_1 7 S_0 absorption that lies in the near ultraviolet region of the spectrum.[5-6] The intensities of the bands in an electronic system depend on Franck-Condon overlap factors that, in turn, depend on the structural differences between the states connected by the electronic transition. The major differences between the S_0 and S_1 states is an out-of-plane distortion of the C=O group in the upper S_1 electronic state. As a result, the spectrum displays long progressions in the wagging normal mode Q_{19}. At room temperature, the intervals between the hot bands at the red end of the spectrum establish the vibrational intervals in the wagging mode.

The present studies were undertaken as a prelude to an analyses of the electronic S_1 7 S_0 band spectrum of CB. A simulation of the vibronic fine structure in the jet-cooled ultraviolet system requires a knowledge of the puckering-wagging hypersurfaces of both the ground and excited electronic states as well as the molecular structures. This paper represents the first of a two part spectroscopic study of cyclobutanone and an extension to a recent calculation on the S_0 and S_1 states [7].

2. METHODS

The general procedure that is followed here is to use standard *ab initio* molecular orbital calculations to establish a set of potential and kinetic energy functions from which to determine an initial set of puckering - wagging vibrational energy levels. These energy levels are then fitted to the observed levels by adjusting the coefficients in the expansion that forms the potential function. This is the so-called morphing procedure whereby the *ab initio* potential surface is stretched and bent until the observed spectral features are reproduced in the calculations.

Both the ring puckering and the carbonyl wagging motions are needed for the description the low frequency modes of cyclobutanone. Energy points on a grid defined by selected values of the internal coordinates were obtained from fully optimized Hartree-Fock calculations with Møller Plesset corrections for electron correlation. These data points were fitted to the power series expansion

$$V = \sum_{k}^{N_V} V_k^0 \prod_{j}^{2} f_{kj} \qquad (1)$$

while the V are the coefficients in the expansion for the potential energy and are obtained from the fitting procedure while the f_{kj} represent the puckering and wagging internal coordinates. N_V is the number of terms on the series expansion. The kinetic energy contributions were generated in a somewhat similar way from the fully optimized geometry as elements of the rovibrational G matrix. The kinetic energy parameters were obtained by the inversion of the inertial matrix

$$\begin{pmatrix} I & X \\ X^t & I \end{pmatrix} \qquad (2)$$

where I is the inertial tensor corresponding to the overall rotation, Y is the vibration submatrix and X is the interaction term between the external and internal motions

$$X_i = \sum_a m_a \left(\vec{r}_a \times \frac{\partial \vec{r}_a}{\partial \alpha_i} \right)_i \qquad (3)$$

$$Y_{ij} = \sum_a m_a \left(\frac{\partial \vec{r}_a}{\partial \alpha_i} \times \frac{\partial \vec{r}_a}{\partial \alpha_j} \right) \qquad (4)$$

The mass of atom a is given by m_a and its displacement vector by r_a. The general Hamiltonian □ was used for the treatment of the multivibrational problem,

$$\hat{H} = \sum_{i}^{n}\sum_{j}^{n}\left(-B_{ij}\frac{\partial^2}{\partial q_i \partial q_j} - \frac{\partial B_{ij}\partial}{\partial q_i \partial q_j}\right) + \hat{V} \qquad (5)$$

where the number of vibrations, n, is two.

The two-dimensional Hamiltonian was solved variationally for the eigenvalues and eignenvectors using harmonic oscillator basis functions for the puckering and wagging coordinates. Nonrigid group theory was used for the labelling of the energy levels, factorization of the Hamiltonian matrix and the generation of the selection rules. The existence of the single plane of symmetry allows the wavefunctions to be classified according to the switch operator, √,

$$\hat{S}f(z,\theta) = f(-z,-\theta) \qquad (6)$$

where z and 2 are the two coordinates.

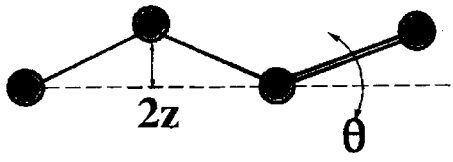

Figure 1. The ring puckering, z, and oxygen wagging, 2, coordinates in cyclobutanone.

3. CALCULATIONS

The model for the two low frequency modes, Q_{19} (wagging) and Q_{20} (puckering) was constructed from the two displacements that are illustrated in figure 1. The wagging internal coordinate is defined by the angle 2 between the C=O bond and the projection of the bisector of the carbonyl CCC angle. The ring puckering coordinate, z, is represented as the separation between the two imaginary diagonal lines that connect the opposite corners of the square ring in the out-of-plane direction. For a ring consisting of four identical atoms, this definition of z leads to a potential function that is governed by a single quartic term. The potential and kinetic energies for the joint puckering-wagging motions were evaluated as points on a grid defined by increments in the z and 2 coordinates. The data points for z ranged from ±0.32Å on either side of the plane, in steps of 0.08Å, whereas the angle 2 was incremented from -10 to +10° in steps of 5°.

Standard *ab initio* molecular orbital calculations were performed at a number of different levels of theory using the GAUSSIAN code.[8] Beyond the molecular orbital approximation of HF (Hartree-Fock) theory, the effect of electron correlation on the barrier to molecular inversion was investigated using Møller-Plesset many body perturbation theory, (MP2, MP3, MP4). The total energy evaluated at the grid points was transformed into the analytical form of equation (1) by a least squares fitting to a power series in the two coordinates. As the potential function for ring puckering contains a central barrier at 2=0°, it was necessary to employ a flexible function that consisted of quadratic, quartic and hexic terms, z^2, z^4 and z^6. At the other end of CB, the CCC=O group is planar and the potential for the C=O wagging is nearly quadratic in form. It is represented by the harmonic term 2^2 with a small anharmonic correction, 2^4. The coupling between these two internal coordinates that leads to the Q_{19} and Q_{20} normal coordinates was taken into account by the cross terms, z2, $z^3 2$ and $z2^3$. The expansion coefficients associated with these terms for two separate calculations, MP2/6-31G(d,p) and MP4/6-31G(2d,p) are collected together in Table 1. A plot of the two dimensional potential V(z,2) is given in fig. 2. The kinetic energy contributions were found to be relatively insensitive to displacements along the puckering and wagging coordinates. Reduced masses were determined for the optimized equilibrium geometry as elements of the inverse G matrix,[9], eqtn, (2). The B_{zz} and B_{22} constants for the puckering and wagging internal coordinates and the B_{z2} interaction term are also given in Table 1. The Schrödinger equation corresponding to the Hamiltonian operator, eqtn. (5), was solved variationally.[10] The symmmetry properties imposed by the $\sqrt{}$ operator were

taken into account by combining the harmonic oscillator basis functions into even and odd products.[11] It was found that 30 functions for both puckering and wagging were sufficient to reproduce the energy levels below 800 cm^{-1}. The results for the two *ab initio* calculations are given in Table 2.

4. RESULTS AND DISCUSSION

Table 1. The Calculated and Fitted Potential Energy Expansion Coefficients for the Ring-Puckering and Oxygen-Wagging Coordinates in Cyclobutanone , (z in Angstroms, 2 in radians and energy in cm^{-1}).

term	two-dimensions morphed	two-dimensions MP4/6-31G(2d,p)	two-dimensions MP2/6-31G(d,p)	puckering-only MP2/6-31G(d,p)
z^2	-640.459	-3019.23	-4752.02	-4394.605
z^4	58337.5	82231.5	88698.8	77562.78
z^6	-77033	-77033.6	-86115.8	
2^2	9923.69	10385.6	11534	
2^4	5181.97	-895.38	181.418	
z2	6354.81	-5593.06	-7492.83	
z^32	-32244.9	-16154.2	-11816.1	
$z2^3$	2354.81	-183.16	-2512.86	
cons.	0.1602	0.1602	1.3141	-1.232
B_{zz}	1.03	0.776	0.776	0.429
B_{z2}	1.354	1.278	1.278	
B_{22}	2.897	4.707	4.707	

The results of the two calculations are different and before any comparisons can be made, it is necessary to make a correlation with the experimental data. The most useful level data is found in the gas phase infrared spectra. In the 30 -100 cm^{-1} far infrared region of CB, the series of bands observed by Borgers and Strauss displayed a regular vibrational anharmonicity.[3] From the low frequencies it is clear that these bands can be attributed to the c-type central Q branches of a sequence series in the ring puckering mode. In terms of the ring puckering quantum number, v_z, the transitions to the hot bands have the designations: (v_z)7 (v_z -1). The sum of

the energies, cm^{-1}, of the band centres gives the ring puckering energy levels. These energy levels are given in Table 2. At the positions expected for the transitions terminating at v_z=8 and 9, the overall contours of the bands change abruptly and the bands split into doublets. Moreover, a microwave study by Scharpen and Laurie[4] of the hot satellite rotational lines shows a clear anomaly in the variation of the A, B and C rotational parameters at this level of vibrational excitation. Both Borgers and Strauss and Scharpen and Laurie suggest that a vibrational perturbation is operative at this energy. In their view, the pure puckering level v_z=8 interacts with the combination level (v_z=3) + (v_2=1). In terms of the joint two dimensional description for the two quantum numbers (v_z v_2), the perturbation for the first band would be described by (8,0) : (3,1) interaction.

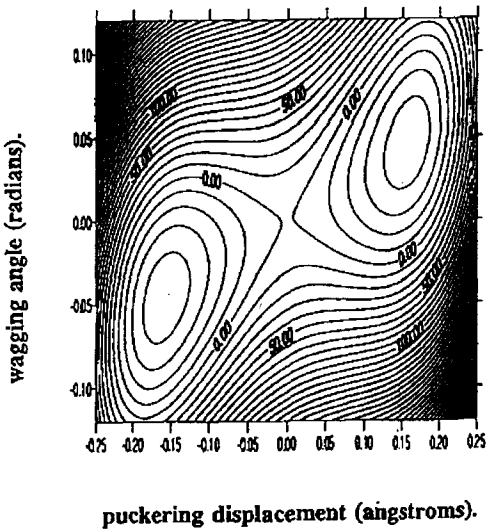

Figure 2. A plot of the two dimensional potential surface V(z,2) for the ring puckering, z, and oxygen wagging, 2, coordinates. Contour lines spaced at 10 cm^{-1} intervals.

Table 2. The Observed and Calculated Puckering + Wagging Vibrational Energy Levels in Cyclobutanone. Parameters from Table 1. (in cm^{-1})

v_z	v_2	sym.	obs.	fitted morphed	2 - D MP4	2 - D MP2	1- D MP2
0	0	aN	0	0	0	0	0
1	0	aO	35.85	36..09	31.37	13.36	20.76
2	0	aN	92.25	92.39	107.92	97.94	93.06
3	0	aO	156.85	156.85	191.88	168.23	168.06
4	0	aN	228.65	228.26	288.47	259.33	258.25
5	0	aO	305.65	305.13	393.62	359.18	358.25
6	0	aN	386.75	386.59	443.66	468.41	467.63
0	1	aO	394.2	394.12	409.01	428.81	
1	1	aN		435.94	507.63	444.59	
7	0	aO	471.55	472.07	521.56	583.32	584.5
2	1	aO		495.13	627.24	527.75	
8	0	aN	560.45	561.03	608.82	705.53	708.33
3	1	aN	561.65	562.73	753.36	603.11	
9	0	aO	653.75	653.78	708.82	833.73	838.51
4	1	aO		636.33	853.41	697.28	
0	2	aN	791.4	791.3	813.27	800.92	

The other necessary piece of information, the energy for the v_2 =1 first quantum of Q_{19} wagging, comes from the hot band intervals in the UV spectrum. The **n 6B*** electronic excitation in CB that leads to the first excited electronic state is accompanied by a planar to pyramidal structural distortion. Thus, on Franck-Condon grounds those modes that are most closely associated with the structural changes between the S_0 and S_1 electronic states will be those most active in the spectrum. In this case, it is the Q_{19} out-of-plane wagging mode that is expected to form the dominant progressions in the spectrum. The progression that originates from the first excited wagging level in the S_0 state has been measured to be 394.2 cm^{-1}. This information is collected together in Table 2 and is illustrated in fig. 3.

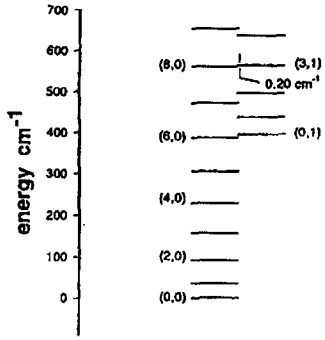

Figure 3. The ring puckering and oxygen wagging energy levels in the S_0 state of cyclobutanone.

The starting point for the fitting procedure was the potential surface derived from the MP4/6-31G(2d,p) energy points and the kinetic energy constants of Table 1. In the initial morphing of potential surface, only the levels up to the onset of the wagging fundamental at 394.2 cm^{-1} were considered. A fit of the first six levels in the puckering mode, (0,0) to (5,0), created a set of expansion parameters that were used as a starting point for an extrapolation to the higher (6,0) and (7,0) levels. At this point the wagging level (0,1) was introduced to complete the morphing of the uncoupled levels. For the final fitting, the levels directly involved in the perturbation, (8,0) : (3,1) were then added. The results of the fitting are given in Table 2 where excellent agreement is achieved. The conclusion that may be drawn from the nine parameter model potential is that the existing literature assignments are essentially correct and that the anomalies in the band positions at high quanta of ring puckering mode are indeed the result of a wagging - puckering vibrational perturbation.

A comparison between the MP4/6-31G(2d,p) and MP2/6-31(d,p) calculations (columns 6 and 7 of Table 2) that were used as a starting point for the refinement of the level positions reveals a number of trends. As the puckering

motion in CB is directed out of the molecular plane, it may be regarded as an inversion-interconversion of two equivalent nonplanar equilibrium conformations. The first two levels, $v_z(aN)=0$ and $v_z(aO)=1$ then form the 0+ and 0- components of the inversion manifold, (in the notation of the high barrier approximation). The first quantum of puckering, $v_z = 1$, observed at 35.85 cm^{-1} correlates to the inversion doubling splitting. The MP4 calculations place this value at 31.37 cm^{-1} in good agreement with the observed splitting, whereas the calculated separation for the MP2 calculation at 13.36 cm^{-1} is unreasonably small. As the inversion splitting is dependent on the curvature at the bottom of the potential well, it follows that the barrier heights for the MP2 case are simply too high. At higher energies the positions of the puckering levels are determined by the widths and the steepness of the potential well. In all cases, the calculated levels are greater than the observed levels and consequently the potential wells obtained from the *ab initio* procedure are too steep and too narrow. Along the wagging direction, the calculated value for the MP4 case at 409.01 cm^{-1} is in excellent agreement with the observed 394.2 cm^{-1} value.

Table 3. The One-Dimensional Ring Puckering Function for Cyclobutanone. Quartic and Quadratic Coefficients, Barrier Heights and Equilibrium Displacements, in cm^{-1} and Å.

no.	level of calculation	A	B	V_{max}	z_{min}
I	MP2/6-31G(d,p)	69752.2	4889.26	83.02	0.186
II	MP2/6-311++G(3df,2dp)	69516.1	5787.85	130.22	0.204
III	QCISD(T)/6-31G(d,p)	64269.4	2850.86	31.59	0.148
IV	QCISD(T)/6-311++G(3df,2dp)[a]	64033.3	3749.45	54.88	0.171
V	adiabatic correction	892.3	178.11	0.00	0.000
VI	effective vibrationally adiabatic	64292.6	2857.09	31.73	0.149
VII	experimental	24095.4	538.64	3.01	0.105

a) interpolated

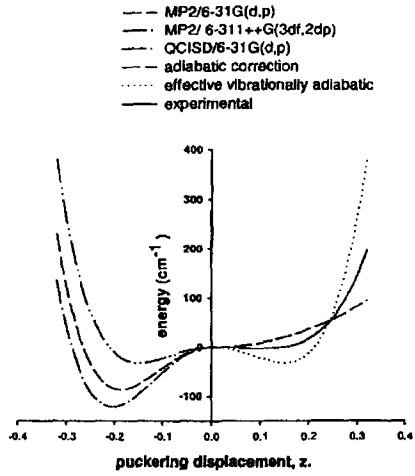

Figure 4. Calculated one - dimensional ring puckering potential functions with varying orbital basis sets and corrections for electron correlation. Only one half of each curve is illustrated.

5. IMPROVEMENTS TO THE POTENTIAL ENERGY

As the final part of this study we looked at the effects of improvements in the *ab initio* calculations on the ability of the one dimensional ring puckering function to reproduce the observed far infrared spectrum. Our intension here is not to make a systematic investigation of the effects of the corrections for electron correlation or the improvements that can be gained at the Hartree Fock level by expanding the number of basis functions. Rather we will follow a procedure that has been successfully applied by Schaefer and coworkers to calculate the shapes of the potential functions for a group of nonrigid molecules.[12] In essence, these workers showed that the improvements in the the *ab initio* methods on the heights of the barriers associated with inversion, torsion and puckering were additive. That is, they demonstrated that a calculation performed with at a modest basis set and high levels of correction for electron correlation could be combined with a similar calculation with a highly extended basis sets and low levels of electron correlation to yield a

potential function that contained both sets of improvements. Following their procedure, we generated a reference potential from optimized structures at the level MP2/6-31(d,p) and then converted the energy points into the two parameter puckering potential function, $V(z) = Az^4-Bz^2$. This function was found to have a central barrier of 83.02 cm^{-1} with minima at $z_{min} = \pm 0.186$ Å. A plot of this function is shown in fig. 4. The first correction, (electron correlation) was made at QCISD(T) and the 6-31G(d,p) reference, and reduced the barrier to 31.59 cm^{-1}. A plot of this QCISD(T)/6-31G(d,p) function is also shown in fig. 4. The final calculation at MP2/6-311++G(3df,2dp) had the reverse effect on the barrier and increased the height to 130.22 cm^{-1}. These three sets of calculations were combined to form an extrapolated QCISD(T)/6-311G(3df,2pd) potential. With a barrier of 54.88 cm^{-1} and out-of-plane displacement of $z_{min}= \pm 0.171$Å this "best" function is in disappointing agreement as the observed barrier is 3.01 cm^{-1}. It should be recognized that the potential is determined not only by electron and nuclear repulsion energies but by the zero point vibration energies, (ZPVE), of the remaining other 3N-7 vibrational modes. Their inclusion gives rise to an effective potential for the puckering mode with its own minima, z_{eff} and barrier height, V_{eff}. The corrections for ZPVE given in Table 3 and illustrated in fig. 4 are lacking a central barrier and consequently have the effect of depressing the barrier relative to the sides of the potential well. When all of the corrections are combined together the calculated effective, vibrationally adiabatic, potential has a barrier height of 31.73 cm^{-1}. Our final calculation may be regarded as disappointing as the barrier is still an order of magnitude greater than the 3.01 cm^{-1} observed value. From this somewhat limited analysis it is clear that even greater computational power will be required to produce a potential function that begins to approach the accuracy of the far-infrared data. Undoubtedly, the most successful improvements would be expected to come the incorporation of quadratic and quintic zeta extensions to the basis functions.

6. CONCLUSIONS

The dynamics of the ring puckering mode result from a balance between the ring strain forces that generate the quartic potential and strive to maintain the ring atoms in a planar conformation. Opposing the influences of the ring strain are the torsional repulsions between the bonds of the CH groups. When sighted along the carbon-carbon bonds, the CH groups totally eclipse each other and the torsional repulsion is maximized when he ring adopts the planar conformation.To reduce these repulsions it is necessary to stagger the dihedral angles between the CH groups by

bending the two halves of the ring through an out-of-plane distortion. If the torsional forces prevail over the ring strain forces, the equilibrium structure will be nonplanar and the corresponding potential function will contain a central maximum. The height of this barrier can then be related to the influence of the torsional repulsion forces. In the case of CB, the barrier height, at 3.01 cm^{-1}, is well below the vibrational zero point level and the ring structure is said to be pseudoplanar. The difficulty in modelling the bottom part of the puckering potential is thus a result of the near balance between the ring strain and the torsional repulsion forces.

It seems that the Møller - Plesset corrections for the effects of electron correlation are able to account for the through space influences of the CH repulsions and therby increase the height of the barrier to puckering. Increases in the number of basis functions are able to account for the changes in hybridization that result from the creation of the four membered ring and thus influence the ring strain energy. Thus, when both the electron correlation and the basis length corrections are improved to the same degree, the two influences tend to balance each other and only subtle differences occur in the shape of the potential function.

ACKNOWLEDGMENTS

L.M.B -T and D.C.M would like to thank the National Sciences and Engineering Council of Canada for financial support. C.M - C and A.N. acknowledge financial support from the Universidad de Castilla - LaMancha.

REFERENCES

1. R.P. Bell, Proc. Roy. Soc. (London) **A183**, 328 (1945).
2. J.R. Durig and R.C. Lord, J. Chem. Phys., **45**, 61 (1966).
3. T.R. Borgers and H.L. Strauss, J. Chem. Phys., **45**, 947 (1966).
4. L.H. Scharpen and V.W. Laurie, J. Chem. Phys., **49**, 221 (1968).
5. D.C. Moule, J. Chem. Phys., **64**, 3161 (1976).
6. J. Laane, in "Structure and Conformations of Non-Rigid Molecules" (J. Laane, M. Dakkouri, B. van der Veken and H. Oberhammer, Ed. Kluwer, Dortretch, 1993, NATO-ASI Vol. 410, pp 65-98.
7. Y.G. Smeyers, M. Belen-Ruiz and P. Otto, J. Mol. Struct. **390**, 91 (1997).
8. M.J. Frisch, G.W. Trucks, H.B. Schegel, P.M.W. Gill, B.G. Johnson, M.A. Robb, J.R. Cheeseman, T.A. Keith, G.A. Petersson, J.A. Montgomery, K. Raghavachari, M.A. Al-Laham, V.G. Zakzewski, J.V. Ortiz, J.B. Foresman, J. Ciolowski,B.B. Stefanov, A.Nanayakkara, M. Challacombe,C.Y. Peng, P.Y. Ayala, W. Chen, M.W.

Wong, J.L. Andres, E.S. Replogle, R. Gomperts, R.L. Martin, D.J. Fox, J.S. Brinkly, D.J. Defrees, J. Baker, J.P. Steward, M. Head-Gordon, C. Gonzalez, and J.A. Pople, Gaussian, Inc., Pittsburgh, PA, 1995.

9. A. Niño and C. Muñoz-Caro, Comput. Chem. **56**, 27 (1994).

10. H.M. Pickett, J. Chem. Phys. **56**, 1715 (1972)

11. Y.G. Smeyers, Advances in Quantum Chemistry, **24**,1 (1992).

12. A.G. Császár, W.D. Allen and H.F. Schaefer III, J. Chem. Phys. **108**,9751 (1998).

Finite-Difference Calculations for Atoms and Diatomic Molecules in Strong Magnetic and Static Electric Fields

by

Mikhail V. Ivanov[1] and Peter Schmelcher ,

Theoretische Chemie, Physikalisch–Chemisches Institut, Universität Heidelberg, INF 229, D-69120 Heidelberg, Federal Republic of Germany

Abstract. Fully numerical mesh solutions of 2D quantum equations of Schrödinger and Hartree-Fock type allow us to work with wavefunctions which possess a very flexible geometry. This flexibility is especially important for calculations of atoms and molecules in strong external fields where neither the external field nor the internal interactions can be considered as a perturbation. The applications of the present approach include calculations of atoms and diatomic molecules in strong static electric and magnetic fields. For the latter we have carried out Hartree-Fock calculations for He, Li, C and several other atoms. This yields in particular the first comprehensive investigation of the ground state configurations of the Li and C atoms in the whole range of magnetic fields ($0 < B < 10000$ a.u.) and a study of the ground state electronic configurations of all the atoms with $1 < Z \leq 10$ and their ions A^+ in the high-field fully spin-polarised regime. The results in a case of a strong electric field relate to single-electron systems including the correct solution of the Schrödinger equation for the H_2^+ ion (energies and decay rates) and the hydrogen atom in strong parallel electric and magnetic fields.

CONTENTS

[1] Current address: Institute of Precambrian Geology and Geochronology, Russian Academy of Sciences, Nab. Makarova 2, St. Petersburg 199034, Russia e-mail: MIvanov@MI1596.spb.edu

ADVANCES IN QUANTUM CHEMISTRY, VOLUME 40

0065-3276/01 $35.00

I INTRODUCTION

Theoretical studies of atoms and molecules in strong external fields are motivated by several applications. The latter are e.g. experiments with intense laser beams (electromagnetic fields with dominating electric component) and astronomical observations of white dwarfs and neutron stars (magnetic fields). The experimental availability of extremely strong electric fields in laser beams makes the theoretical study of various atomic and molecular species under such conditions very desirable. The properties of atomic and molecular systems in strong fields undergo dramatic changes in comparison with the field-free case. These changes are associated with the strong distortions of the spatial distributions of the electronic density and correspondingly the geometry of the electronic wavefunctions. This complex geometry is difficult for its description by means of traditional sets of basis functions and requires more flexible approaches which can, in particular, be provided by multidimensional mesh finite-difference methods.

Let us discuss the problem of atoms in a strong magnetic field in more detail. We start this consideration with the hydrogen atom which was the first atom whose behaviour in strong magnetic fields was investigated (for a list of references see [1–4]). In cylindrical coordinates (ρ, z) its non-relativistic Hamiltonian has the form (we use atomic units throughout our work)

$$H = -\frac{1}{2}\left(\frac{\partial^2}{\partial\rho^2} + \frac{1}{\rho}\frac{\partial}{\partial\rho} + \frac{\partial^2}{\partial z^2} - \frac{m^2}{\rho^2}\right) + s_z\gamma + \frac{m}{2}\gamma + \frac{\gamma^2}{8}\rho^2 - \frac{1}{r} \qquad (1)$$

where m is the magnetic quantum number, s_z is the spin z projection and $\gamma = B/B_0$, $B_0 = \hbar c/ea_0^2 = 2.3505{\cdot}10^5$T is the magnetic field strength in atomic units. The magnetic field is parallel to the z axis. The Hamiltonian (1) contains two potentials of different spatial symmetries: the spherical-symmetric Coulomb term $1/r$ and the cylindrically symmetric potential of the magnetic field $\gamma^2\rho^2/8$. When considering the impact of the competing Coulomb and diamagnetic interaction it is reasonable to distinguish the three different regimes of weak, strong and intermediate fields. In the latter case the magnetic and Coulomb forces are comparable. In the case of relatively weak fields the main features of the geometry of the wavefunction are determined by the dominating Coulomb term whereas the effect of the magnetic field can be consider as a perturbation of the Coulomb wavefunctions. For the opposite situation of very strong magnetic fields and dominating cylindrical

symmetry the adiabatic approximation [5–7] was the main theoretical tool during the last four decades. This approximation separately considers the fast motion of the electron across the field and its slow motion in a modified Coulomb potential along the field direction. Both early (see [8]) and more recent works [2,9–12] on the hydrogen atom have used different approaches for these regimes of the magnetic field. All these calculations had problems when considering the hydrogen atom in fields of intermediate strength. The detailed calculations of the hydrogen energy levels carried out by Rösner *et al* [2] also retained the separation into different regimes of the field strength by decomposing the electronic wave function either in terms of spherical (weak to intermediate fields) or cylindrical (intermediate to high fields) orbitals. A solution allowing to obtain comprehensive results on low-lying energy levels of the hydrogen atom for arbitrary field strengths including the intermediate field regime is provided by the multi-dimensional mesh solution of the Schrödinger equation [3].

For different electronic degrees of excitation of the atom the intermediate regime is met for different absolute values of the field strength. For the ground state this regime is roughly given by $\gamma = 0.2 - 20$. For atoms with several electrons there are two decisive factors which enrich the possible changes in the electronic structure with varying field strength compared to the one-electron system. First, we have a third competing interaction which is the electron-electron repulsion and, second, the different electrons feel very different Coulomb forces, i.e. possess different one particle energies, and consequently the regime of the intermediate field strengths appears to be the sum of the intermediate regimes for the separate electrons.

The fact that most methods have problems in the intermediate field region has consequences for the current state of the art of our knowledge on on multi-electron atoms in strong magnetic fields. There exist a number of such investigations in the literature [6,7,13–22]. The majority of them deals with the adiabatic regime in superstrong fields and the early works are mostly Hartree-Fock (HF) type calculations. There are also several early variational calculations for the low-field domain [15,23,24]. HF calculations for arbitrary field strengths have been carried out in refs. [2,19] by applying two different sets of basis functions in the high- and low-field regimes. As a result of the complicated geometry this approach suffers in the intermediate regime from very slow convergence and low accuracy of the calculated energy eigenvalues. Accurate HF calculations for arbitrary field strengths were carried out in refs. [18,20] by the 2D mesh HF method. Investigations on the ground state as well as a number of excited states of helium including the correlation energy have recently been performed via a Quantum Monte Carlo approach [22]. Very recently benchmark results with a precision of $10^{-4} - 10^{-6}$ for the energy levels have been obtained for a large number of excited states with different symmetries using a configuration interaction approach with an anisotropic Gaussian basis set [25,26]. Focusing on systems with more than two electrons however the number of investigations is very scarce [6,21,27]. In view of the above there is a need for further quantum mechanical investigations and for data on atoms with more than two electrons in a strong magnetic field. For the carbon atom there exist

two investigations [6,7] in the adiabatic approximation which give a few values for the binding energies in the high field regime and one more relevant recent work by Jones *et al* [21]. On the other hand, our two-dimensional Hartree-Fock approach allowed us recently to perform precise and reliable consideration of a series of multi-electron atoms for the whole range of the magnetic field strengths from $\gamma = 0$ up to ultrastrong fields $\gamma = 10^3 - 10^4$ [18,20,28–31].

II TWO-DIMENSIONAL MESH HARTREE-FOCK METHOD

Our calculations for multi-electron atoms in magnetic fields are carried out under the assumption of an infinitely heavy nucleus in the (unrestricted) Hartree-Fock approximation. The solution is established in the cylindrical coordinate system (ρ, ϕ, z) with the z-axis oriented along the magnetic field. We prescribe to each electron a definite value of the magnetic quantum number m_μ. Each single-electron wave function Ψ_μ depends on the variables ϕ and (ρ, z)

$$\Psi_\mu(\rho, \phi, z) = (2\pi)^{-1/2} e^{-im_\mu \phi} \psi_\mu(z, \rho) \tag{2}$$

where μ denotes the numbering of the electrons. The resulting partial differential equations for $\psi_\mu(z, \rho)$ have been presented in ref. [20].

The one-particle equations for the wave functions $\psi_\mu(z, \rho)$ are solved by means of the fully numerical mesh method described in refs. [3,18,20]. In our first works on the helium atom in magnetic fields [18,20] we calculated the Coulomb and exchange integrals by means of a direct summation over the mesh nodes. But this direct method is very expensive with respect to the computer time and due to this reason we obtained in the following works [28–31] these potentials as solutions of the corresponding Poisson equation. The problem of the boundary conditions for the Poisson equation as well as the problem of simultaneously solving Poisson equation on the same meshes with Schrödinger-like equations for the wave functions $\psi_\mu(z, \rho)$ have been discussed in ref. [20].

The simultaneous solution of the Poisson equations for the Coulomb and exchange potentials and Schrödinger-like equations for the wave functions $\psi_\mu(z, \rho)$ is a complicated computational problem, especially for atoms in strong magnetic fields. The problem consists in the different geometry of the spatial distribution of the electron density and the potentials correspondent to this density. In strong magnetic fields the distributions of the electronic densities are compressed towards the z axis and look like needles directed along the z axis. The equations for the wavefunctions can be solved in finite cylindrical domains as done in refs. [3,18,20]. For strong magnetic fields $\gamma >> 1$ these domains can be rather small in the ρ direction. On the other hand, the potentials created by these charge distributions cannot have such a strongly anisotropic form and the Poisson equations for them must be solved on meshes with the distribution of nodes not very different for the

z and ρ directions. This means some loss of the precision for the wavefunctions due to a decrease of the number of nodes in the area of a large electronic density. The most difficult problem, however, is the different asymptotic behaviour of the wavefunctions and potentials. The wavefunctions of the bound electrons decrease exponentially as $r \to \infty$ (r is the distance from the origin). This simplifies the problem of the solution of the corresponding equations in the infinite space because it is possible either to solve these equations in a finite domain Ω (with simple boundary conditions $\psi|_{\partial\Omega} = 0$ or $\partial\psi/\partial n|_{\partial\Omega} = 0$) with negligible errors for domains of reasonable dimensions or otherwise to solve these equations in the infinite space on meshes with exponentially growing distances between nodes as $r \to \infty$. The solutions of the Poisson equations for non-zero sums of charges decrease as $1/r$ as $r \to \infty$. In result, every spatial restriction of the domain Ω introduces a significant error into the final solution. In some other mesh Hartree-Fock approaches developed for diatomic molecules (e.g. see [32,33]) this problem has been solved for finite Ω by introducing special boundary conditions for the potentials obtained from the asymptotic behaviour of the potentials. This approach, being in principle approximate, requires additional calculations with different extensions of Ω to estimate the error.

In the present approach we address the above problems by using special forms of non-uniform meshes [28]. Solutions to the Poisson equation on separate meshes contain some errors δ_P associated with an inaccurate description of the potential far from the nucleus. However due to the special form of the function $\delta_P(h)$ for these meshes (where h is a formal mesh step) the errors do not show up in the final results for the energy and other physical quantities, which we obtain by means of the Richardson extrapolation procedure (polynomial extrapolation to $h = 0$ [3,41]). The main requirement for these meshes is not an exponential, but a polynomial increase of the mesh step h when $r \to \infty$. Moreover, this behaviour can be only linear one, i.e. $h^{-1} = O(1/r)$ as $r \to \infty$. The error of the mesh solution in this case has the form of a polynomial of the formal step of the mesh $\tilde{h} = 1/N$, where N is the number of nodes along one of the coordinates. In practical calculations these meshes are introduced by means of an orthogonal coordinate transformation from the physical coordinates x_p to the mathematical ones x_m made separately for ρ and z. And the numerical solution is, in fact, carried out on uniform meshes in the mathematical coordinates x_m. The characteristic feature of these meshes consists of rapidly increasing coordinates of several outermost nodes when increasing the total number of nodes and decreasing the actual mesh step in the vicinity of the origin. Due to this property we call these meshes "Run away" meshes. To be concrete we present here two such meshes:

1. The "Plain Poisson" mesh is generated by the coordinate transformation

$$x_\mathrm{p} = A\frac{x_\mathrm{m}}{1 - x_\mathrm{m}^2} \tag{3}$$

$-\infty < x_\mathrm{p} < +\infty$, $-1 < x_\mathrm{m} < +1$, A is a constant. This simplest mesh of this group is near to the uniform ones near the origin (i.e. a plot of the distance between the

neighbouring nodes contains a large horizontal section close to $x_p = 0$) and then this mesh smoothly transforms to the "run away" behaviour for $x_p \to \infty$.

2. The "Atomic Poisson" mesh

$$x_p = A\frac{(|x_m| + b)x_m}{1 - x_m^2} \tag{4}$$

($b > 0$) allows obtaining more precise results for atoms at reasonable values of $b < 1$ due to a more dense distribution of nodes near the origin. In fact, this formula provides three different types of behaviour in three different domains: (a) A uniform mesh in a small vicinity of $x_p = 0$. This behaviour provides absence of irregularities in the finite-difference representation of the Hamiltonian. (b) $|x_p| \approx A|x_m^2|$ - the quadratic expansion of the mesh. (c) $h^{-1} = O(1/r)$ as $r \to \infty$. The distribution of nodes for not too big distances from the origin (b) given by the simple formula (4) is similar to well known "Lagrange meshes" for atoms and provide similar precision of results. (See e.g. [34] for a definition of the "Laguerre mesh" (a mesh with nodes at zeros of the Laguerre polynomials) as a "Lagrange mesh" suitable for systems with the Coulomb potential and [35] (22.16.8) for approximate formulas for the zeros of the Laguerre polynomials).

The overall precision of our results depends, of course, on the number of mesh nodes and, if necessary, can be improved in calculations with denser meshes. The most dense meshes which we could use in the present calculations had 120×120 nodes. In most cases Richardson's sequences of meshes with maximal number 80×80 or 60×60 were sufficient.

III THE STRUCTURE OF THE ATOMIC GROUND STATE CONFIGURATIONS FOR THE LIMIT $\gamma \to \infty$

In this section we provide some qualitative considerations on the problem of the ground states of multi-electron atoms in the high field limit. These considerations along with the well known electronic structure of the ground states at $\gamma = 0$ present a starting point for the combined qualitative and numerical considerations given in the following section. At very high field strengths the nuclear attraction energies and HF potentials (which determine the motion along the z axis) are small compared to the interaction energies with the magnetic field (which determines the motion perpendicular to the magnetic field and is responsible for the Landau zone structure of the spectrum). Thus in the limit ($\gamma \to \infty$), all the one-electron wave functions of the ground state belong to the lowest Landau zones, i.e. $m_\mu \leq 0$ for all the electrons, and the system must be fully spin-polarised, i.e. $s_{z\mu} = -\frac{1}{2}$. For the Coulomb central field the one electron levels form quasi 1D Coulomb series with the binding energy $E_B = \frac{1}{2n_z^2}$ for $n_z > 0$, whereas $E_B(\gamma \to \infty) \to \infty$ for $n_z = 0$, where n_z is the number of nodal surfaces of the wave function crossing the z axis. In the

limit $\gamma \to \infty$ the ground state wave function must be formed of the tightly bound single-electron functions with $n_z = 0$. The one-particle binding energies of these functions decrease as $|m|$ increases and, thus, the electrons must occupy orbitals with increasing $|m|$ starting with $m = 0$.

In the language of the Hartree-Fock approximation the ground state wave function of an atom in the high-field limit is a fully spin-polarised set of single-electron orbitals with no nodal surfaces crossing the z axis and with non-positive magnetic quantum numbers decreasing from $m = 0$ to $m = -N + 1$, where N is the number of electrons. In result, we have for the first 10 atoms and positive ions in the limit $\gamma \to \infty$ the following structure of ground state configurations which is a simple substitute of the periodic law at very strong magnetic fields

H	He^+	$1s$	$M = 0$	$S_z = -1/2$
He	Li^+	$1s2p_{-1}$	$M = -1$	$S_z = -1$
Li	Be^+	$1s2p_{-1}3d_{-2}$	$M = -3$	$S_z = -3/2$
Be	B^+	$1s2p_{-1}3d_{-2}4f_{-3}$	$M = -6$	$S_z = -2$
B	C^+	$1s2p_{-1}3d_{-2}4f_{-3}5g_{-4}$	$M = -10$	$S_z = -5/2$
C	N^+	$1s2p_{-1}3d_{-2}4f_{-3}5g_{-4}6h_{-5}$	$M = -15$	$S_z = -3$
N	O^+	$1s2p_{-1}3d_{-2}4f_{-3}5g_{-4}6h_{-5}7i_{-6}$	$M = -21$	$S_z = -7/2$
O	F^+	$1s2p_{-1}3d_{-2}4f_{-3}5g_{-4}6h_{-5}7i_{-6}8j_{-7}$	$M = -28$	$S_z = -4$
F	Ne^+	$1s2p_{-1}3d_{-2}4f_{-3}5g_{-4}6h_{-5}7i_{-6}8j_{-7}9k_{-8}$	$M = -36$	$S_z = -9/2$
Ne	Na^+	$1s2p_{-1}3d_{-2}4f_{-3}5g_{-4}6h_{-5}7i_{-6}8j_{-7}9k_{-8}10l_{-9}$	$M = -45$	$S_z = -5$

We shall often refer in the following to these ground state configurations in the high-field limit as $|0_N\rangle$. The states $|0_N\rangle$ possess the complete spin polarisation $S_z = -N/2$. Decreasing the magnetic field strength, we can encounter a series of crossovers of the ground state configuration associated with transitions of one or several electrons from orbitals with the maximal values for $|m|$ to other orbitals with a different spatial geometry of the wave function but the same spin polarisation. This means the first few crossovers can take place within the space of fully spin polarised configurations. We shall refer to these configurations by noting only the difference with respect to the state $|0_N\rangle$. This notation can, of course, also be extended to non-fully spin polarised configurations. For instance the state $1s^2 2p_{-1}3d_{-2}4f_{-3}5g_{-4}$ with $S_z = -2$ of the carbon atom can be briefly referred to as $|1s^2\rangle$, since the default is the occupation of the hydrogenic series $1s, 2p_{-1}, 3d_{-2}, \ldots$ and only deviations from it are recorded by this notation.

IV GROUND STATE ELECTRONIC CONFIGURATIONS OF ATOMS AND POSITIVE IONS AT ARBITRARY FIELD STRENGTHS

Currently the carbon atom is the most complicated system with a thoroughly investigated structure of its electronic configurations for arbitrary magnetic fields and we start this section with a consideration of this atom.

In the case of decreasing the magnetic field strength from very large values to $\gamma = 0$ the fully spin-polarised ground state configuration of a multi-electron atom must undergo one or several crossovers to become finally the zero-field ground state configuration. This configuration for the carbon atom corresponds to the spectroscopic term ^3P. In the framework of the non-relativistic consideration this term consists of nine states degenerate due to three possible z-projections of the total spin $S_z = -1, 0, 1$ and three possible values of the total magnetic quantum number $M = -1, 0, 1$. For very weak magnetic fields it is reasonable to expect values $S_z = -1$ and $M = -1$ for the ground state which can be described in our notation as $1s^2 2s^2 2p_0 2p_{-1}$.

Thus the possible ground state configurations of the carbon atom can be divided into three groups according to their total spin projection S_z : the $S_z = -1$ group (low-field ground state configurations), the intermediate group $S_z = -2$ and the $S_z = -3$ group (the high-field ground state configurations). This grouping is required for the qualitative part of the following considerations which are based on the geometry of the spatial parts of the one electron wave functions.

We start our consideration for $\gamma \neq 0$ with the high-field ground state and subsequently consider other possible candidates in question for the electronic ground state for $S_z = -3$ (see Figure 1) *with decreasing field strength.* All the one electron wave functions of the high-field ground state $1s2p_{-1}3d_{-2}4f_{-3}5g_{-4}6h_{-5}$ possess no nodal surfaces crossing the z-axis and occupy the energetically lowest orbitals with magnetic quantum numbers ranging from $m = 0$ down to $m = -5$. We shall refer

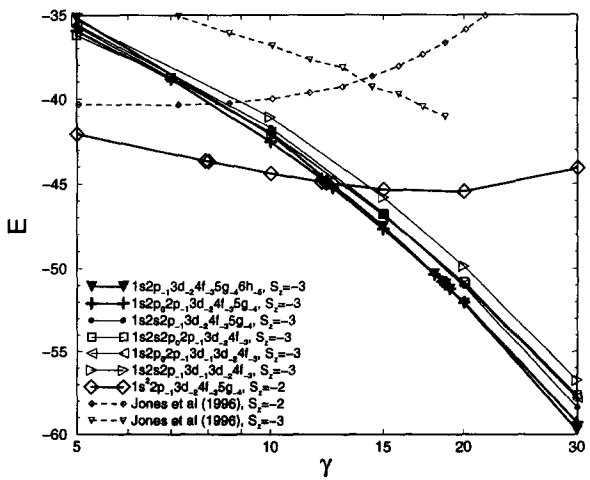

FIGURE 1. The total energies (in atomic units) of the states of the carbon atom as functions of the magnetic field strength considered for the extraction of the ground state electronic configurations with $S_z = -3$. Our results (solid lines) and data taken from ref.21 (broken lines). Energies and field strengths are given in atomic units.

TABLE 1. The Hartree-Fock ground state configurations of the carbon atom in external magnetic fields. The configurations presented in the table are the ground state configurations at $\gamma_{\min} \leq \gamma \leq \gamma_{\max}$.

no.	$\gamma_{\min}$	$\gamma_{\max}$	The ground state configuration	M	S_z	$E(\gamma_{\min})$
1	0	0.1862	$1s^2 2s^2 2p_0 2p_{-1}$	−1	−1	−37.69096
2	0.1862	0.4903	$1s^2 2s 2p_0 2p_{-1} 2p_{+1}$	0	−2	−37.9334
3	0.4903	4.207	$1s^2 2s 2p_0 2p_{-1} 3d_{-2}$	−3	−2	−38.3359
4	4.207	7.920	$1s^2 2p_0 2p_{-1} 3d_{-2} 4f_{-3}$	−6	−2	−41.7369
5	7.920	12.216	$1s^2 2p_{-1} 3d_{-2} 4f_{-3} 5g_{-4}$	−10	−2	−43.6397
6	12.216	18.664	$1s 2p_0 2p_{-1} 3d_{-2} 4f_{-3} 5g_{-4}$	−10	−3	−44.9341
7	18.664	∞	$1s 2p_{-1} 3d_{-2} 4f_{-3} 5g_{-4} 6h_{-5}$	−15	−3	−50.9257

to the number of the nodal surfaces crossing the z axis as n_z. The $6h_{-5}$ orbital possesses the smallest binding energy of all orbitals constituting the high-field ground state. Its binding energy decreases rapidly with decreasing field strength. Thus, we can expect that the first crossover of ground state configurations happens due to a change of the $6h_{-5}$ orbital into one possessing a higher binding energy at the corresponding lowered range of field strength. It is natural to suppose that the first transition while decreasing the magnetic field strength will involve a transition from an orbital possessing $n_z = 0$ to one for $n_z = 1$. The energetically lowest available one particle state with $n_z = 1$ is the $2p_0$ orbital. Another possible orbital into which the $6h_{-5}$ wave function could evolve is the $2s$ state. For the hydrogen atom or hydrogen-like ions in a magnetic field the $2p_0$ is stronger bound than the $2s$ orbital. On the other hand, owing to the electron screening in multi-electron

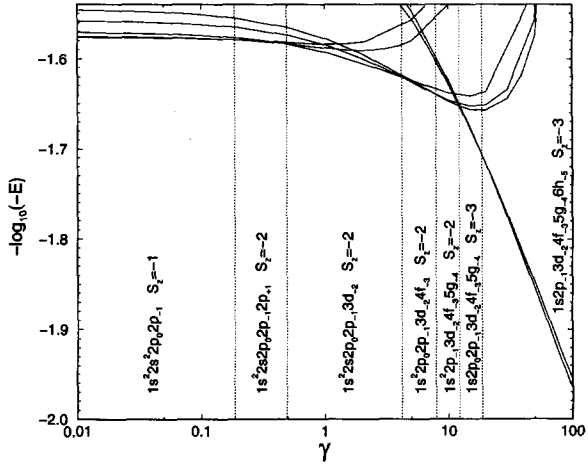

FIGURE 2. Energies of the ground state configurations as a function of the field strength. Vertical dotted lines divide regions belonging to different Hartree-Fock ground state configurations.

atoms in field-free space the $2s$ orbital tends to be more tightly bound than the $2p_0$ orbital. Thus, two states i.e. the $1s2p_02p_{-1}3d_{-2}4f_{-3}5g_{-4}$ state as well as the $1s2s2p_{-1}3d_{-2}4f_{-3}5g_{-4}$ configuration are candidates for becoming the ground state in the $S_z = -3$ set when we lower the field strength coming from the high field situation.

Analogous arguments lead to the three following candidates for the ground state in case of the second crossover in the $S_z = -3$ subset which takes place with decreasing field strength: $1s2s2p_02p_{-1}3d_{-2}4f_{-3}$, $1s2p_02p_{-1}3d_{-1}3d_{-2}4f_{-3}$ and $1s2s2p_{-1}3d_{-1}3d_{-2}4f_{-3}$. It is evident that the one particle energies for the $3d_{-1}$ and $2p_0$ obey $E_{3d_{-1}} > E_{2p_0}$ for all values of γ since they possess the same nodal structure with respect to the z-axis and only the $3d_{-1}$ possesses an additional node in the plane perpendicular to the z-axis. For this reason the configuration $1s2s2p_{-1}3d_{-1}3d_{-2}4f_{-3}$ can be excluded from our considerations of the ground state.

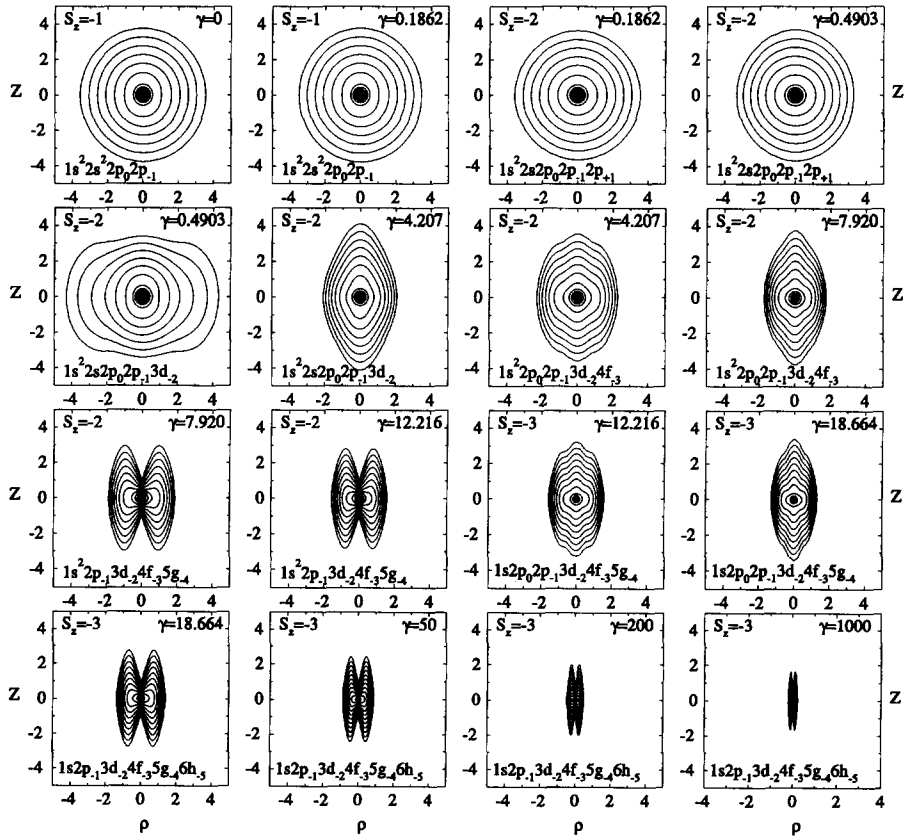

FIGURE 3. Contour plots of the total electronic densities for the ground state of the carbon atom. For neighbouring lines the densities are different by a factor of e. The coordinates z, ρ as well as the corresponding field strengths are given in atomic units.

TABLE 2. The Hartree-Fock ground state configurations of the lithium atom in external magnetic fields. The configurations, presented in the table are the ground state configurations at $\gamma_{\min} \leq \gamma \leq \gamma_{\max}$.

no.	$\gamma_{\min}$	$\gamma_{\max}$	The ground state configuration	M	S_z	$E(\gamma_{\min})$
1	0	0.17633	$1s^2 2s$	0	$-1/2$	-7.43275
2	0.17633	2.1530	$1s^2 2p_{-1}$	-1	$-1/2$	-7.48162
3	2.1530	∞	$1s2p_{-1}3d_{-2}$	-3	$-3/2$	-7.64785

This conclusion is fully confirmed by our calculations.

Similar reasoning given in detail in ref. [30] can be repeated for two other ($S_z = -2$ and $S_z = -1$) subsets of states and leads to the results presented in table 1 and in Figure 2.

Figure 3 allows us to add some more informations to the considerations of the previous section. This figure presents spatial distributions of the total electronic densities for the ground state configurations of the carbon atom. More precisely, it allows us to gain insights into the geometry of the distribution of the electron density in space and in particular its dependence on the magnetic quantum number and the total spin. Thereby we can understand the corresponding impact on the total energy of the atom. The first picture in this figure presents the distribution of the electron density of the ground state of the carbon atom at $\gamma = 0$. The following pictures show the distributions of the electronic densities at values of the field strength which mark the boundaries of the regimes of field strengths belonging to the different ground state configurations. For the high-field ground state we present the distribution of the electronic density at the crossover field strength $\gamma = 18.664$ and for three additional values of γ up to $\gamma = 1000$.

For each configuration the effect of the increasing field strength consists in compressing the electronic distribution towards the z axis. However most of the crossovers of ground state configurations involve the opposite effect which is due to the fact that they are associated with an increase of the total magnetic quantum number $M = \sum_{\mu=1}^{6} m_\mu$.

For the lithium atom the analogous arguments and calculations [29] lead to the scheme presented in table 2.

V GROUND STATE ELECTRONIC CONFIGURATIONS IN THE HIGH-FIELD REGIME

Let us consider now the series of neutral atoms and positive ions with $Z \leq 10$ in the high field domain which we define here as the one, where the ground state electronic configurations are fully spin polarised (Fully Spin Polarised (FSP) regime $S_z = -N/2$). The FSP regime supplies an additional advantage for calculations performed in the Hartree-Fock approach, because our one-determinant wave functions are eigenfunctions of the total spin operator $\mathbf{S}^2$. Starting from the high-field

TABLE 3. Total energies (a.u.) of the neutral atoms and ions A^+ at the crossover points of the ground state configurations.

Z	γ	Atomic state(s)	$-E$(Atomic)	Ionic state(s)	$-E(A^+)$
2	0.711	$\|0_N\rangle$, $\|1s^2\rangle$	2.76940	$\|0_N\rangle$	2.32488
3	2.153	$\|0_N\rangle$, $\|1s^2\rangle$	7.64785	$\|0_N\rangle$	7.00057
	2.0718	$\|1s^2\rangle$	7.65600	$\|0_N\rangle$, $\|1s^2\rangle$	6.94440
4	4.567	$\|0_N\rangle$, $\|1s^2\rangle$	15.9166	$\|0_N\rangle$	15.07309
	4.501	$\|1s^2\rangle$	15.91625	$\|0_N\rangle$, $\|1s^2\rangle$	15.01775
5	8.0251	$\|0_N\rangle$, $\|1s^2\rangle$	28.18667	$\|0_N\rangle$	27.16436
	7.957	$\|1s^2\rangle$	28.17996	$\|0_N\rangle$, $\|1s^2\rangle$	27.10004
6	18.664	$\|0_N\rangle$, $\|2p_0\rangle$	50.9257	$\|0_N\rangle$	49.50893
	14.536	$\|2p_0\rangle$	47.23836	$\|0_N\rangle$, $\|2p_0\rangle$	45.77150
	12.351	$\|2p_0\rangle$	45.07386	$\|2p_0\rangle$, $\|1s^2\rangle$	43.72095
	12.216	$\|2p_0\rangle$, $\|1s^2\rangle$	44.9341	$\|1s^2\rangle$	43.70075
7	36.849	$\|0_N\rangle$, $\|2p_0\rangle$	84.4186	$\|0_N\rangle$	82.58182
	30.509	$\|2p_0\rangle$	79.34493	$\|0_N\rangle$, $\|2p_0\rangle$	77.41246
	17.429	$\|2p_0\rangle$	66.72786	$\|2p_0\rangle$, $\|1s^2\rangle$	65.26170
	17.398	$\|2p_0\rangle$, $\|1s^22p_0\rangle$	66.69306	$\|1s^2\rangle$	65.25362
8	64.720	$\|0_N\rangle$, $\|2p_0\rangle$	130.6806	$\|0_N\rangle$	128.4054
	55.747	$\|2p_0\rangle$	124.1125	$\|0_N\rangle$, $\|2p_0\rangle$	121.69825
	23.985	$\|2p_0\rangle$, $\|1s^22p_0\rangle$	94.3773	$\|2p_0\rangle$	92.78308
	23.849	$\|1s^22p_0\rangle$	94.3336	$\|2p_0\rangle$, $\|1s^22p_0\rangle$	92.62502
9	104.650	$\|0_N\rangle$, $\|2p_0\rangle$	191.8770	$\|0_N\rangle$	189.1446
	92.624	$\|2p_0\rangle$	183.6944	$\|0_N\rangle$, $\|2p_0\rangle$	180.7819
	31.735	$\|2p_0\rangle$, $\|1s^22p_0\rangle$	128.1605	$\|2p_0\rangle$	126.4414
	31.612	$\|1s^22p_0\rangle$	128.1125	$\|2p_0\rangle$, $\|1s^22p_0\rangle$	126.2897
10	159.138	$\|0_N\rangle$, $\|2p_0\rangle$	270.220	$\|0_N\rangle$	267.0112
	143.604	$\|2p_0\rangle$	260.2740	$\|0_N\rangle$, $\|2p_0\rangle$	256.8459
	40.672	$\|2p_0\rangle$, $\|1s^22p_0\rangle$	168.4734	$\|2p_0\rangle$	166.6327
	40.559	$\|1s^22p_0\rangle$	168.4217	$\|2p_0\rangle$, $\|1s^22p_0\rangle$	166.4863

limit we investigate the electronic structure and properties of the ground states with decreasing field strength until we reach the first crossover to a partially spin polarised (PSP) configuration with $S_z = -N/2 + 1$.

The approach to this investigation is very similar to that described in the previous section and the picture of the crossovers associated with the ground states of atoms and positive ions A^+ is presented in table 3. It should be noted that, for atoms with $Z \leq 6$ and ions with $Z \leq 7$, the state $|1s^2\rangle$ becomes the ground state while lowering the spin polarisation from the maximal absolute value $S_z = -N/2$ to $S_z = -N/2 + 1$. For heavier atoms and ions we remark that the state $|1s^2\rangle$ is not the energetically lowest one in the PSP subset at magnetic field strengths for which its energy becomes equal to the energy of the lowest FSP state. For these atoms and ions the state $|1s^22p_0\rangle$ is energetically lower than $|1s^2\rangle$ at these field strengths. For atoms with $Z \geq 7$ and positive ions with $Z \geq 8$ the intersection points between the state $|1s^22p_0\rangle$ and the energetically lowest state in the FSP subspace have to be calculated. In result, the spin-flip crossover occurs at higher fields than this would

be in the case of $|1s^2\rangle$ being the lowest state in the PSP subspace. In particular, the spin-flip crossover for the neon atom is found to be slightly higher than the point of the crossover $|2p_0\rangle - |2p_0 3d_{-1}\rangle$, and, therefore, this atom has in the framework of the Hartree-Fock approximation only two fully spin polarised configurations likewise other neutral atoms and positive ions with $6 \leq Z \leq 10$. It should be noted that the situation with the neon atom can be regarded as a transient one due to closeness of the intersection $|2p_0\rangle - |2p_0 3d_{-1}\rangle$ to the intersection $|2p_0\rangle - |1s^2 2p_0\rangle$. This means that we can expect the configuration $|2p_0 3d_{-1}\rangle$ to be the global ground state for the sodium atom ($Z = 11$). In addition an investigation of the neon atom carried out on a more precise level than the Hartree-Fock method could also introduce some corrections to the picture described above for this atom.

Summarising our results we remark that the atoms and positive ions with $Z \leq 5$ have one FSP ground state configuration $|0_N\rangle$ whereas the atoms and ions with $6 \leq Z \leq 10$ possess two such configurations $|0_N\rangle$ and $|2p_0\rangle$.

Possessing total energies for all the atoms with $Z \leq 10$ we can compare these results with the adiabatic calculations [6,7]. Both our results (E_{2D}) and calculations [6,7] (E_{1D}) are carried out in the adiabatic approximation. The difference between E_{1D} and E_{2D} consists only in the usage of the adiabatic approximation for obtaining energies E_{1D} instead of exact solution of the Hartree-Fock equations for E_{2D}. Thus, the comparison of E_{1D} and E_{2D} allows us to evaluate the precision of the adiabatic approximation itself and obtain an idea of the degree of its applicability for multi-electron atoms for different field strengths and nuclear charges. All our values lie lower than the values of these adiabatic calculations. It is well known, that the precision of the adiabatic approximation decreases with decreasing field strength.

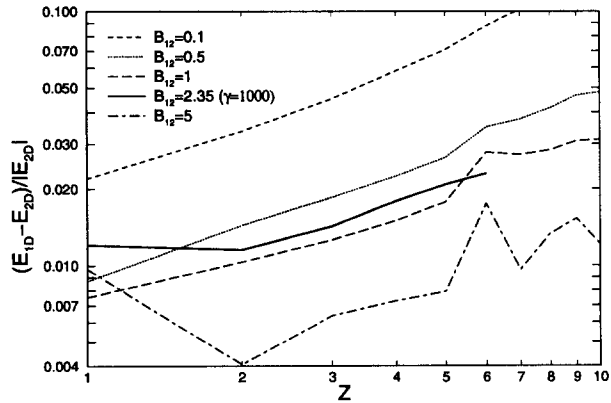

FIGURE 4. Relative errors of the total energy in the adiabatic approximation depending on the charge of the nucleus. E_{1D} – the total energies in the adiabatic approximation ($B_{12} = 0.1$, 0.5, 1, 5 [6], $B_{12} = 2.35$ [7]), E_{2D} – our two-dimensional mesh results. $B_{12} = B/10^{12}$G.

The increase of the relative errors with decreasing field strength is clearly visible in the table. On the other hand, the relative errors of the adiabatic approximation possess the tendency to increase with growing Z, which is manifested by the scaling transformation $E(Z,\gamma) = Z^2 E(1,\gamma/Z^2)$ (e.g. [36,20]) well known for hydrogen-like ions. The behaviour of the inner electrons is to some extent similar to the behaviour of the electrons in the corresponding hydrogen-like ions. Therefore their behaviour is to lowest order similar to the behaviour of the electron in the hydrogen atom at magnetic field strength γ/Z^2 i.e. this behaviour can be less accurately described by the adiabatic approximation at large Z values. The absolute values of the errors in the total energy associated with the adiabatic approximation are in many cases larger than the corresponding values of the ionisation energies.

VI MESH APPROACH FOR SINGLE-ELECTRON ATOMIC AND MOLECULAR SYSTEMS IN STRONG ELECTRIC FIELDS

In this section we present some features of our approach With respect to its application to systems in strong external electric fields and correspondingly some relevant physical results. In contrast to the situation discussed in the previous sections atoms and molecules in external uniform electric fields have no stationary states, because for every state there is a probability that one or several electrons leave the system. Thus, when switching on the external uniform electric field, all the stationary states turn into resonances. Using the complex form of the energy eigenvalues

$$E = E_0 - i\Gamma/2$$

one may consider quasi-stationary states of quantum systems similarly to the stationary ones. In this approach the real part of the energy E_0 is the centre of the band corresponding to the quasi-stationary state and the imaginary part $\Gamma/2$ is the half-width of the band which determines the lifetime of the state. In this communication we consider systems which can be described by two-dimensional one-electron Hamiltonians. These systems include the hydrogen atom and the H_2^+ molecular ion in an electric field [37–39] and the hydrogen atom in parallel electric and magnetic fields [39,40]. The only electron present in such a system can leave it under impact of the external electric field. ¿From the mathematical point of view the problem consists in obtaining solutions of the single-particle Schrödinger equation for this electron with the correct asymptotic behaviour of the wavefunction as an outgoing wave. Currently we have three different possibilities for fixing this asymptotics realised in our computational program:

1. Complex boundary condition method. This method is described in detail in ref. [38]. The method is based on the fact that the single-electron Schrödinger equation for a finite system can be solved with the arbitrary precision in a finite area both

for stationary and for quasi-stationary eigenstates. The case of stationary states is considered in [41,3]. The approach for the quasi-stationary states will be discussed following [38]. Figure 5 presents the potential curve for the simplest Hamiltonian of the hydrogen atom in an electric field

$$H = -\frac{1}{2}\left(\frac{\partial^2}{\partial\rho^2} + \frac{1}{\rho}\frac{\partial}{\partial\rho} + \frac{\partial^2}{\partial z^2} - \frac{m^2}{\rho^2}\right) - \frac{1}{r} - Fz \tag{5}$$

F is the electric field strength multiplied by the charge of the electron. Analogously to [40,3] the calculations can be carried out in an area Ω which is finite along the direction z. For this coordinate we used uniform meshes. The boundary of the area $z = -L_{z-}$ for $z < 0$ ($F \geq 0$) (Figure 5) is determined from the condition of small values of the wavefunction on the boundary and, therefore, small perturbations introduced by the corresponding boundary condition [3]. The values of the wavefunction on the opposite boundary of the area ($z = L_{z+}$) cannot be excluded from the consideration. We consider non-stationary states of the system decaying into continuum of free particles. In this process an electron leaves the system in direction $z \to +\infty$ and, thus, an outgoing wave boundary condition is to be established on $z = L_{z+}$. The form of this boundary condition can be derived from the asymptotic behaviour of the wavefunction for $z \to +\infty$ and has the form

$$\frac{\partial\psi}{\partial z} + \left(\frac{F}{2k^2} - ik\right)\psi\Big|_{z=L_{z+}} = 0 \tag{6}$$

where $k = [2(E+Fz)]^{1/2}$ is the wavenumber. Solving the Schrödinger equation with the Hamiltonian (5) and the boundary condition (6) established on a reasonable distance L_{z+} from the origin of the system we can obtain the complex eigenvalues of the energy and the wavefunctions of the type presented in the Figure 6.

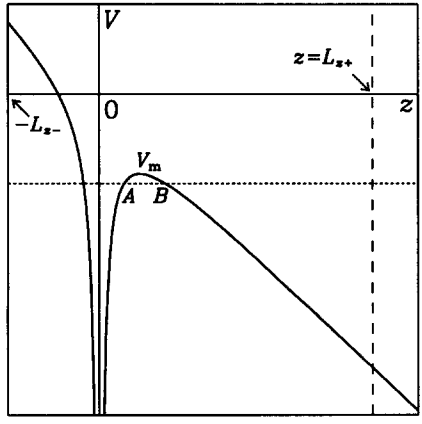

FIGURE 5. The potential energy for the hydrogen atom $V(\rho = 0, z)$ in the external uniform electric field.

This straightforward approach enables obtaining precise results both for atoms and molecules from weak to moderate strong fields (for instance for the ground state of the hydrogen atom up to $F = 0.20 - 0.25$ a.u.).

2. Classical complex rotation of the coordinate z in the form $z \to ze^{i\Theta}$. In this approach we have obtained precise results for atomic systems in strong fields from the lower bound of the over-barrier regime up to superstrong fields corresponding to regime $|\mathrm{Re}E| << |\mathrm{Im}E|$ [39]. On the other hand, this method cannot be immediately applied to molecular systems in our direct mesh approach [42,39].

3. Exterior complex transformation of the coordinate z. In our numerical approach we transform the real coordinate z into a curved path in the complex plane z. This transformation leaves intact the Hamiltonian in the internal part of the system, but supplies the complex rotation of z (and the possibility to use the zero asymptotic boundary conditions for the wavefunction) in the external part of the system. The transformation can be applied both for atoms and molecules and provides precise results for fields from weak up to superstrong with some decrease of the numerical precision in the regime $|\mathrm{Re}E| << |\mathrm{Im}E|$ [39].

The numerical results obtained by all three methods coincide And are in agreement with numerous published data on the hydrogen atom in electric fields (see e.g. [43–46] and references in [38]).

Some of our results for the hydrogen atom in parallel electric and magnetic fields [39] are shown in Table 4.

The second system which we present in this section is the hydrogen molecular ion H_2^+ in a strong longitudinal electric field. Our approach allowed us to carry out the first correct consideration of this system [37] and, in particular, to obtain the potential curves of its ground state, presented in Figure 7 (left). The minima in these curves give the equilibrium internuclear distances, presented in this Figure (right) as a function of the electric field strength. One can see that at a critical value of the electric field about 0.065 a.u. the minimum disappears and, thus, above

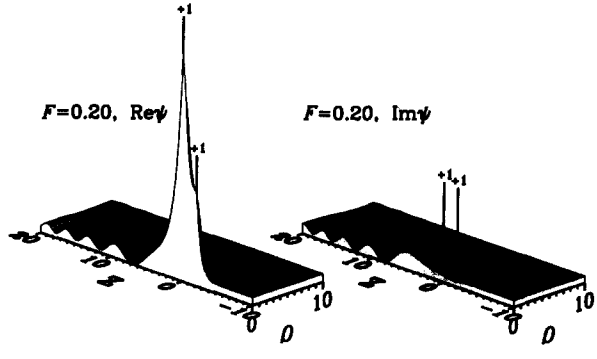

FIGURE 6. Real and imaginary parts of the wavefunction of the H_2^+ molecule in a longitudinal electric field F (a.u.).

TABLE 4. The ground state of the hydrogen atom in parallel electric and magnetic fields at $F = 0.1,\ 1,\ 5$.

	$F = 0.1$		$F = 1$		$F = 5$	
γ	E_0	$\Gamma/2$	E_0	$\Gamma/2$	E_0	$\Gamma/2$
0	−0.5274183	7.26904(−3)	−0.6243366	0.6468208	−0.1350071	3.083929
0.01	−0.532390	7.2624(−3)	−0.629329	0.646812	−0.140005	3.083925
0.1	−0.574600	6.6392(−3)	−0.673584	0.646053	−0.184739	3.083589
1	−0.8443098	9.5923(−5)	−1.0421379	0.577291	−0.6077008	3.050207
10	−1.7498730	—	−1.9579187	0.1173924	−2.375552	1.955678
100	−3.790110	—	−3.8219215	4.9988(−5)	−4.3806709	0.4909467
1000	−7.66247	—	−7.66807	—	−7.82561	1.04701(−2)

this critical value the hydrogen molecular ion cannot exist. This critical value of the maximal electric field $F_c = 0.065$a.u. $= 3.3$V/Å for the molecule H_2^+ is in a good agreement with experimental results by [47]. According this work H_2^+ molecule may exist in laser beam fields with intensity less than 10^{14}W/cm^2 which corresponds to 3V/Å, and does not exist in more intense fields.

VII CONCLUSIONS

In this communication we have presented a 2D fully numerical mesh solution method in its various applications to atoms and simple diatomic molecules in strong external electric and magnetic fields. Specifically these are calculations of atoms with $Z \leq 10$ and their positive ions in strong magnetic fields and the comprehensive investigation of the electronic structure of the ground states of the Li and C atoms

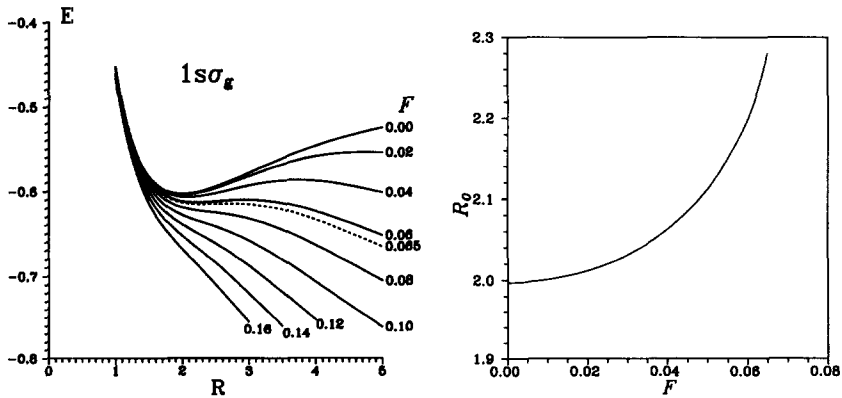

FIGURE 7. Left – Potential curves for the ground state of the H_2^+ molecule in longitudinal electric field F (a.u.). Right - The equilibrium internuclear distance of the molecule H_2^+ as a function of the applied electric field strength.

TABLE 5. Equilibrium internuclear distances and corresponding energies and half-widths of the energy of the ground state of H_2^+ molecule in longitudinal electric fields.

F	R_0	E_0	$\Gamma/2$	F	R_0	E_0	$\Gamma/2$
0.00	1.997	-0.60264	—	0.04	2.062	-0.60686	1.23(-19)
0.01	2.001	-0.60289	—	0.05	2.112	-0.60943	7.32(-15)
0.02	2.012	-0.60366	—	0.06	2.198	-0.61285	1.49(-11)
0.03	2.031	-0.60497	—	0.065	2.28	-0.61501	3.94(-10)

in arbitrary magnetic fields. For the carbon atom seven different electronic ground state configurations for different domains of the magnetic field strength have been found. The investigation of the series of atoms with $Z \leq 10$ in very strong magnetic fields enables us to evaluate the applicability of the adiabatic approximation and to show its decreasing precision for heavier atoms.

The mathematical technique developed for solving Schrödinger equations for quasi-steady states allowed us to obtain a series of results for the hydrogen atom in parallel electric and magnetic fields and for the H_2^+ ion in strong electric fields.

Thus, the method described above allows us to obtain a number of new physical results partially presented in this communication. These calculations are carried out in the Hartree-Fock approximation for multi-electron systems and are exact solutions of the Schrödinger equation for the single-electron case. As the following development of the method we plan to implement the configuration interaction approach in order to study correlation effects in multi-electron systems both in electric and magnetic fields.

REFERENCES

1. Friedrich, H.; Wintgen, D. *Phys.Rep.* **1989,** *183,* 37.
2. Rösner, W.; Wunner, G.; Herold, H.; Ruder, H. *J. Phys. B: At. Mol. Opt. Phys.* **1984,** *17,* 29.
3. Ivanov, M.V. *J. Phys. B: At. Mol. Opt. Phys.* **1988,** *21,* 447.
4. Kravchenko, Yu.P.; Liberman, M.A.; Johansson, B. *Phys.Rev.Lett.* **1996,** *77,* 619.
5. Elliott, R.J.; Loudon, R. *J. Phys. Chem. Sol.* **1960,** *15* 196.
6. Neuhauser, D.; Koonin, S.E.; Langanke, K. *Phys. Rev. A* **1986,** *33,* 2084; **1987,** *36,* 4163.
7. Demeur, M.; Heenen, P.-H.; Godefroid, M. *Phys. Rev. A* **1994,** *49,* 176.
8. Garstang, R.H. *Rep. Prog. Phys.* **1977,** *40,* 105.
9. Simola, J.; Virtamo, J. *J. Phys. B* **1978,** *11,* 3309.
10. Friedrich, H. *Phys. Rev. A* **1982,** *26,* 1827.
11. Fonte, G.; Falsaperla, P.; Schriffer, G.; Stanzial, D. *Phys. Rev. A* **1990,** *41,* 5807.
12. Schmidt, H.M. *J. Phys. B: At. Mol. Opt. Phys.* **1991,** *24,* 2947.
13. Mueller, R.O.; Rao, A.R.P.; Spruch, L. *Phys. Rev. A* **1975,** *11,* 789.
14. Virtamo, J. *J. Phys. B: At. Mol. Phys.* **1976,** *9,* 751.

15. Larsen, D.M. *Phys. Rev. B.* **1979,** *20,* 5217.
16. Gadiyak, G.V.; Lozovik, Yu.E.; Mashchenko, A.I.; Obrecht, M.S. *J. Phys. B: At. Mol. Phys.* **1982,** *15,* 2615.
17. Vincke, M.; Baye, D. *J. Phys. B: At. Mol. Opt. Phys.* **1989,** *22,* 2089.
18. Ivanov, M.V. *Opt. Spektrosk.* **1991,** *70,* 259; English transl.: *Opt. Spectrosc.* **1991,** *70,* 148.
19. Thurner, G.; Körbel, H.; Braun, M.; Herold, H.; Ruder, H.; Wunner G. *J. Phys. B: At. Mol. Opt. Phys.* **1993,** *26,* 4719.
20. Ivanov, M.V. *J. Phys. B: At. Mol. Opt. Phys.* **1994,** *27,* 4513.
21. Jones, M.D.; Ortiz, G.; Ceperley, D.M. *Phys. Rev. A.* **1996,** *54,* 219.
22. Jones, M.D.; Ortiz, G.; Ceperley, D.M. *Phys. Rev. E* **1997,** *55,* 6202; *Phys. Rev. A* **1999,** *59,* 2875.
23. Henry, R.J.; O'Connell, R.F.; Smith, E.R.; Chanmugam, G.; Rajagopal, A.K. *Phys. Rev. D* **1974,** *9,* 329.
24. Surmelian, G.L.; Henry, R.J.; O'Connell, R.F. *Phys. Lett. A* **1974,** *49,* 431.
25. Becken, W.; Schmelcher, P.; Diakonos, F.K. *J. Phys. B: At. Mol. Opt. Phys.* **1999,** *32,* 1557.
26. Becken, W.; Schmelcher, P. *J. Phys. B: At. Mol. Opt. Phys.* **2000,** *33,* 545.
27. Müller, E. *Astron. & Astrophys.* **1984,** *130,* 415.
28. Ivanov, M.V. *Phys. Lett. A* **1998,** *239,* 72.
29. Ivanov, M.V.; Schmelcher, P. *Phys. Rev. A* **1998,** *57,* 3793.
30. Ivanov, M.V.; Schmelcher, P. *Phys. Rev. A* **1999,** *60,* 3558.
31. Ivanov, M.V.; Schmelcher, P. *Phys. Rev. A* **2000,** *61,* 022505.
32. Laaksonen, L.; Pyykkö, P.; Sundholm, D. *Chem. Phys. Lett.* **1983,** *96,* 1.
33. Kobus, J. *Chem. Phys. Lett.* **1993,** *202,* 7.
34. Vincke, M.; Malegat, L.; Baye, D. *J. Phys. B: At. Mol. Opt. Phys.* **1993,** *26,* 811.
35. Abramowitz, M.; Stegun, I.A.; eds. "Handbook of Mathematical Functions"; Dover Publications: New York, 1972, 787.
36. Ruder, H.; Wunner, G.; Herold, H.; Geyer, F. "Atoms in Strong Magnetic Fields"; Springer-Verlag, 1994.
37. Ivanov, M.V. *Opt. Spektrosk.* **1994,** *76,* 711. English transl.: *Opt. Spectrosc.* **1994,** *76,* 631.
38. Ivanov, M.V. *J. Phys. B: At. Mol. Opt. Phys.* **1998,** *31,* 2833.
39. Ivanov, M.V. to be published.
40. Anokhin, S.B.; Ivanov, M.V. *Vestn. Leningr. Univ. Fiz. & Khim.* **1983,** *no.2,* 65.
41. Ivanov, M.V. *USSR Comput. Math. & Math. Phys.* **1986,** *26,* 140.
42. Simon, B. *Phys. Lett. A* **1979,** *71,* 211.
43. Kolosov, V.V. *J. Phys. B: At. Mol. Phys.* **1987,** *20,* 2359.
44. Kolosov, V.V. *J. Phys. B: At. Mol. Opt. Phys.* **1989,** *22,* 833.
45. Nicolaides, C.A.; Gotsis, H.J. *J. Phys. B: At. Mol. Opt. Phys.* **1992,** *25,* L171.
46. Nicolaides, C.A.; Themelis, S.I. *Phys. Rev. A* **1992,** *45,* 349.
47. Bucksbaum, P.H.; Zavriyev, A.; Muller, H.G.; Schumacher, D.W. *Phys. Rev. Lett.* **1990,** 1883.

Index

Boldface numerals indicate volume number

C

D

E

F

G

H

N

O

P

Q

R

S

T

U

V

W

Y

Z